NASA

Technical Memorandum 78104

PROCEEDINGS OF THE NINTH ANNUAL PRECISE TIME AND TIME INTERVAL (PTTI) APPLICATIONS AND PLANNING MEETING

MARCH 1978

National Aeronautics and Space Administration

Goddard Space Flight Center
Greenbelt, Maryland 20771

"NOTICE" TO BE PRINTED IN THE PROCEEDINGS

"All papers published in this proceeding which bear a copyright notice cannot be reproduced without the copyright owner's permission. All other papers published in this proceeding can be freely reproduced."

U. S. AIR FORCE

TM 78104

PROCEEDINGS
OF THE NINTH ANNUAL
PRECISE TIME AND TIME-INTERVAL
(PTTI)
APPLICATIONS AND PLANNING MEETING

Held at NASA Goddard Space Flight Center

November 29 – December 1, 1977

Sponsored by

Naval Electronic Systems Command
NASA Goddard Space Flight Center
Naval Research Laboratory
Naval Observatory
Defense Communications Agency

Prepared by
GODDARD SPACE FLIGHT CENTER
Greenbelt, Maryland 20771

Page intentionally left blank

Page intentionally left blank

EXECUTIVE COMMITTEE

Ralph T. Allen
Naval Electronic Systems Command

John A. Bowman
Naval Research Laboratory

Andrew R. Chi
NASA Goddard Space Flight Center

Laura C. Fisher
Naval Observatory

Andrew C. Johnson
Naval Observatory

James A. Murray, Jr.
Naval Research Laboratory

Dr. Harris A. Stover
Defense Communications Agency

Schuyler C. Wardrip
NASA Goddard Space Flight Center

GENERAL CHAIRMAN

DR. JAMES A. BARNES
National Bureau of Standards

TECHNICAL PROGRAM COMMITTEE

DR. HENRY F. FLIEGEL – CHAIRMAN
Jet Propulsion Laboratory

ANDREW R. CHI.
NASA Goddard Space Flight Center

DR. KENNETH J. JOHNSTON
Naval Research Laboratory

JAMES JESPERSEN
National Bureau of Standards

DR. WILLIAM J. KLEPCZYNSKI
Naval Observatory

EDITORIAL COMMITTEE

L. J. RUEGER – CHAIRMAN
John Hopkins University
Applied Physics Laboratory

FRANCIS MOORE – SECRETARY
Applied Physics Laboratory

RALPH T. ALLEN
Naval Electronic Systems Command

SANDRA L. HOWE
National Bureau of Standards

CHARLES A. BARTHOLOMEW
Naval Research Laboratory

DR. WILLIAM J. KLEPCZYNSKI
Naval Observatory

MIKE FISCHER
Hewlett Packard, Santa Clara

SCHUYLER C. WARDRIP
NASA Goddard Space Flight Center

SESSION CHAIRMEN

SESSION I
Dr. Henry F. Fliegel
Jet Propulsion Laboratory

SESSION II
Dr. William J. Klepczynski
Naval Observatory

SESSION III
Roger L. Easton
Naval Research Laboratory

SESSION IV
Dr. James A Barnes
National Bureau of Standards

SESSION V
Dr. Victor S. Reinhardt
NASA Goddard Space Flight Center

SESSION VI
Dr. Gernot M. R. Winkler
Naval Observatory

ARRANGEMENTS

Schuyler C. Wardrip, GSFC
Donald C. Kaufmann, GSFC
Shirley E. Darby, GSFC
William O'Leary, GSFC

FINANCE COMMITTEE

Laura C. Fisher, USNO
Schuyler C. Wardrip, GSFC

PUBLICATIONS

Virginia L. Walker, GSFC
Schuyler C. Wardrip, GSFC

PRINTING

Charles V. Hardesty, GSFC
Donald E. Ellis, GSFC

DISTRIBUTION

Susan A. Lehman, GSFC
James W. Edwards, GSFC

TECHNICAL ASSISTANCE

Donald C. Kaufmann, GSFC
Paul J. Kushmeider, GSFC
James C. Perry, GSFC
Joseph L. Soucy, Bendix

RECEPTIONISTS

Kathy McDonald, NRL
Dorothy Outlaw, USNO
Charlotte Prevost, APL
Emma K. Thomas, GSFC

BANQUET SPEAKER

Professor Franz Halberg
University of Minnesota Medical School
Subject: Human Periodic Phenomena

CALL TO SESSION

Dr. James A. Barnes
National Bureau of Standards, Boulder

WELCOME ADDRESS

Dr. Robert S. Cooper
Director, NASA Goddard Space Flight Center

OPENING COMMENTS

Rear Adm Earl B. Fowler, Jr.
Commander, Naval Electronic Systems Command

Capt Joseph C. Smith
Superintendent, U.S. Naval Observatory

Dr. Alan Berman
Director of Research, U.S. Naval Research Laboratory

Page intentionally left blank

Page intentionally left blank

CONTENTS

Page

SESSION I

Future Developments in U.S. Naval Observatory Time Services
Dr. Gart Westerhout, Scientific Director,
U.S. Naval Observatory 1

Atomic Frequency Standards: Survey and Forecast
Dr. Jacques Vanier, Laval University, Quebec, Canada 9

Criteria for the Selection of Atomic Clocks in Systems Application
Dr. Gernot M. R. Winkler, U.S. Naval Observatory. 59

Review of Methods for Measuring and Specifying Frequency Stability
Dr. James A. Barnes, National Bureau of Standards 61

SESSION II

VLBI and Its Current Applications within the Solar System
Dr. John L. Fanselow, Jet Propulsion Laboratory 85

Earth Rotation From Lunar Distances: Basis and Current Status
J. Derral Mulholland, University of Texas and Odile Calome,
Bureau International de l'Heure/Center d'Etudes et de Recherches
Geodynamiques et Astronomiques, Grasse, France. 97

Clock Rate Comparisons by Long Baseline Interferometry
W. H. Cannon, W. T. Petrachenko, and R. B. Langley,
Department of Physics and CRESS York University Toronto,
Ontario, Canada 113

Clock Synchronization Via Very Long Baseline Interferometry
A. E. E. Rogers, A. R. Whitney, H. F. Hinteregger, and C. A. Knight,
Haystack Observatory, T. A. Clark, NASA Goddard Space Flight
Center, W. J. Klepczynski, Naval Observatory, I. I. Shapiro and
C. C. Counselman, Massachusetts Institute of Technology and L. B.
Hanson, MIT/Lincoln Laboratory 127

Real-Time Accurate Time Transfer and Frequency Standards Evaluation Via Satellite Link Long Baseline Interferometry
S. H. Knowles and W. B. Waltman, Naval Research Laboratory, N. W. Broten and D. H. Fort, National Research Council, K. I. Kellermann and B. Rayhrer, National Radio Astronomy Observatory, G. W. Swenson, University of Illinois and J. L. Yen, University of Toronto 135

SESSION III

Time from NBS by Satellite
D. W. Hanson, D. D. Davis and J. V. Cateora, National Bureau of Standards, Boulder 139

A Transit Satellite Timing Receiver,
G. A. Hunt and R. E. Cashion, S. N., Inc. 153

Time Transfer Via GPS,
Leonard Schuchman and James Spilker, Stanford Telecommunications Inc. 167

Initial Results of the NAVSTAR GPS NTS-2 Satellite
James A. Buisson, Roger L. Easton and Thomas B. McCaskill, U.S. Naval Research Laboratory 177

Precise Time Transfer to the NASA Spaceflight Tracking and Data Network (STDN) Via the Tracking and Data Relay Satellite System (TDRSS),
G. P. Gafke and J. W. McIntyre, JHU Applied Physics Laboratory, S. C. Laios and S. C. Wardrip, NASA Goddard Space Flight Center . . . 201

SESSION IV

A Precision Microwave Frequency and Time Distribution System
John W. MacConnell and Richard L. Sydnor, Jet Propulsion Laboratory 227

Precise Time Transfer Unit (PTTU)
John J. Wilson and James E. Britt, U.S. Naval Ocean Systems Center and Philip A. Mitchell, U.S. Army Satellite Communications Station, Camp Roberts 239

Real Time Distribution Via Passive TV Transmissions
J. D. Lavanceau, U.S. Naval Observatory and L. F. Shepard, ILC Data Device Corporation 249

New Ways of Time and Standard Frequency Dissemination Over TV Networks
B. Kovacevic, Facility of Electrical Engineering University of Nis, Yugoslavia 277

International Time and Frequency Comparison for Long Term Via VLF and Loran-C
Yoshiyuki Yasuda, Kohsuke Akatsuka, Toyoshi Matsuura and Haruo Ohazawa, Radio Research Laboratories, Frequency Standard Division, Tokyo, Japan 289

Diurnal Variations in Loran-C Groundwave Propagation
Walter N. Dean, Magnavox Government & Industrial Electronics Co. . . 297

Nanosecond Time Transfer Via Shuttle Laser Ranging Experiment
Victor S. Reinhardt, Don A. Premo, Michael W. Fitzmaurice and S. Clark Wardrip, NASA Goddard Space Flight Center. 319

SESSION V

Some Recent Progress in Frequency Standards and Techniques
D. W. Allan, R. M. Garvey, H. Hellwig, D. A. Howe, S. Jarvis, A. Risley, S. R. Stein, H. Van de Stadt, F. L. Walls and D. J. Wineland, National Bureau of Standards 343

Analysis of Degraded Hydrogen Dissociator Envelopes by AES^{+}
Victor H. Ritz, Victor M. Bermudeg and Vincent J. Folen, U.S. Naval Research Laboratory 353

An Investigation of Polymer Coatings used in Hydrogen Maser Storage Bulbs
N. H. Turner, U.S. Naval Research Laboratory 371

An Investigation of the Shielding Properties of Molypermalloy Shields Designed for Use with a Hydrogen Maser
S. Wolf and J. Cox, U.S. Naval Research Laboratory. 381

A Spaceborne Hydrogen Maser Design
A. E. Popa, H. T. M. Wang, W. B. Bridges, J. E. Etter and D. Schnelker, Hugnes Research Laboratories and F. E. Goodwin, C. Lew, and M. Dials, Hughes Space and Communication Group 403

Operational Characteristics of a Prototype Spaceborne Hydrogen Maser
H. T. M. Wang, A. E. Popa, W. B. Bridges, and D. Schnelker, Hughes Research Laboratories 415

SESSION VI

The New State Time and Frequency Standard of the USSR and the Development of the System of Standard Frequency and Time Signal Emission
V. G. Ilyin, Tel'puchovskyi N. A. and V. V. Saxhin, USSR Gosstandart, Moscow 425

Steering of a Time Scale
M. Granveaud and J. Azoubıb, Bureau International de l'Heure, Paris, France 427

Development of an Atomic Rubidium Vapor Frequency Standard at NPL of India Using Indigenous Sources
V. R. Singh, G. M. Saxena and B. S. Mathur, National Physical Laboratory, New Delhi, India 437

Phase Noise Characteristics of Frequency Sources
A. L. Lance, W. D. Seal, F. G. Mendoza, and N. W. Hudson, TRW Defense and Space Systems Group 463

Increased Resolution for Beat-Period Based Frequency Stability Measurements
Eric Blomberg, MIT Lincoln Laboratory 485

Time Transfer Experiments for DCS Digital Network Timing and Synchronization
Peter Alexander and James W. Graham, CNR, Inc. 503

The Mechanics of Translation of Frequency Stability Measures Between Frequency and Time Domain Measurements
Andrew R. Chi, Goddard Space Flight Center. 523

Comparison of Theoretical and Observed Maser Stability Limitation Due to Thermal Noise and The Prospect of Improvement by Low Temperature Operation
R. F. C. Vessot, M. W. Levine, and E. M. Mattison, Smithsonian Astrophysical Observatory and Harvard College Observatory 549

A New Method to Eliminate Cavity Phase in Cesium Beam Standards
Stephen Jarvis, Jr., David J. Wineland, Helmut Hellwig, and R. Michael Garvey, National Bureau of Standards. 571

Page intentionally left blank

Page intentionally left blank

FOREWORD

The Proceedings contain the papers presented at the Ninth Annual Precise Time and Time Interval (PTTI) Applications and Planning Meeting. The questions and answers following the presentations are also included after each paper.

This meeting provided an opportunity to exchange information on precise time and frequency technology. The attendees came from various U. S. Government agencies, private industry, and universities. A number of foreign countries were also represented.

The meeting was divided into six sessions:

I. Topics of Special Interest
II. Very Long Baseline Interferometry (VLBI)
III. Time Transfer Techniques
IV. Time Distribution
V. Hydrogen Masers
VI. Frequency Standards

On behalf of the Executive Committee, I want to thank all those who contributed to the success of this year's meeting. Special credit should go to the Technical Program Chairman and his committee, the Editorial Chairman and his committee, the Session Chairmen, Speakers and Authors.

James A. Barnes
General Chairman

Page intentionally left blank

Page intentionally left blank

CALL TO SESSION

Dr. James A. Barnes
National Bureau of Standards

DR. BARNES: Good morning. I am Jim Barnes with the Time and Frequency Division of the National Bureau of Standards. It is my pleasure to call to session the Ninth Annual Precise Time and Time Interval Applications and Planning Meeting.

The main purpose of my opening remarks this morning is to handle a few housekeeping details and then introduce the speakers for the Welcoming Address and the Opening Comments. But first, I want to take this opportunity to call your attention to the banquet Wednesday evening. The speaker is Professor Franz Halberg, who will speak on "Human Periodic Phenomenon," which is a time and time interval problem and somewhat akin to what we are doing here. If not quite as precise as we will be talking about for the next three days, it should be at least interesting. I would heartily recommend that you consider the banquet.

I also want to bring up my personal indebtedness to the members of the organizing committee who are listed in the program, and I want to take this opportunity to publicly thank each and every one of them. I would like to give some special thanks to a few members of the group: in particular, Clark Wardrip of NASA, who has handled the many, many details of putting the meeting together; and Lauren Rueger, who was the General Chairman last year, for his guidance and assistance in helping me understand what needed to be done. Also, of course, I must thank Henry Fliegel of JPL, who is this year's Program Chairman, for putting together an excellent program for the meeting.

Now to a couple of housekeeping details. As I am sure most of you remember, the questions, answers, and comments that follow each of the technical papers are recorded and transcribed into the published proceedings of the meeting. It is important that you use a microphone so these comments get on tape and that you state your name and affiliation so they can be attributed to the right person. In this way, we can get the proper documentation and the proceedings will go much easier.

At this time, I would like to call on the representatives of the agencies who sponsor the PTTI meetings, and to start with, Dr. Robert S. Cooper, Director of NASA Goddard Space Flight Center, will present the Welcoming Address.

Page intentionally left blank

Page intentionally left blank

WELCOME ADDRESS

Dr. Robert S. Cooper
Director, Goddard Space Flight Center

Thank you Dr. Barnes and good morning ladies and gentlemen. It was my pleasure last year to welcome you to the PTTI Meeting hosted by the Naval Research Laboratory as a representative of one of the Sponsors. I am very pleased to welcome you here this morning to Goddard as the host. This is the fourth (4) time that Goddard has had the pleasure of hosting this annual meeting. As everyone has probably become aware of by now it has become traditional for Goddard and NRL to alternately host these important meetings.

Last year I talked briefly about some of our programs in the PTTI and related areas. We have made progress over the past year which is worthy to note.

To bring you up to date on our hydrogen maser frequency standard activity, the four (4) Goddard built (NASA Prototype) NP type masers continue to be the backbone of our frequency standard field work. These four (4) masers have impressive field operable records. They have accumulated a total of thirty-three (33) years of field operation and have traveled over one hundred and twenty thousand (120,000) miles to thirty-five (35) separate installations in support of various VLBI programs in the geodetic and astronomical work such as the ARIES, MJS (Mars-Jupiter-Saturn) and the Goddard VLBI validation program.

We hope that the second generation hydrogen masers that we are presently designing and constructing with support from the Applied Physics Lab will have an equally impressive record. These new masers which we call NASA Research or NR Hydrogen Masers have oscillated and are nearing final assembly and testing.

With the NR masers, we hope to achieve the performance of our latest experimental masers in a rugged package designed to simplify field set up and maintenance. These masers will have a microprocessor based electronics package which among other things will monitor its own performance and perform self-diagnosis.

Work on our variable volume hydrogen masers and a new mercury ion frequency standard is continuing. As you have heard us mention in the past, we hope to achieve 10^{-14} frequency accuracy with these devices. I might mention that because of some recent measurements we made with our Concertina Maser and a new capillary bulb collimator developed at Williams College under a NASA grant, we think we can develop field operable hydrogen masers with a line of 6.5

times ten to the ninth. This maser is presently being designed and promises to yield parts in 10^{16} frequency stability.

Our new Frequency Standard Test Facility will at last be complete early in 1978. We have long awaited the completion of this separate isolated building. This new facility, in addition to housing hydrogen masers of various designs and configurations for our R&D programs, will contain an automatic data acquisition system capable of intercomparing up to 16 frequency standards with picosecond resolution. The facility will basically be used to study the long term stability, environmental performance and accuracy of hydrogen masers under controlled conditions.

As I mentioned we use hydrogen masers in support of VLBI work. Goddard, with collaborators at MIT, Haystack Observatory and colleagues at JPL, pioneered in applying hydrogen maser techniques to VLBI measurements in the geodetic and astronomical work. Kydrogen masers of various designs are currently at use in tracking stations, and radio astronomy stations in Massachusetts, California, West Virginia and Sweden, to study polar motion, the structure and kinematics of quasars and to develop VLBI techniques for subdecimeter accuracies necessary to measure continental drift.

The VLBI activity at Goddard in FY-78 will include the completion of the development of the wideband, centimeter accuracy Mark-III VLBI system. Breadboard Mark-III system tests were successfully completed in September and the implementation of the final system is underway. This Mark-III system will be used in the planned operational polar motion/UT.1 network of the National Geodetic Survey.

Starting next month, Goddard and JPL will jointly construct an interim intercomparison between the satellite laser ranging and the older Mark-I and Mark-II VLBI systems for measuring transcontinental baselines between Haystack Observatory, Massachusetts, Goldstone, California, and Owens Valley Radio Observatory, California. This is part of the NASA validation program to prove the capability of laser ranging and VLBI for measuring small crustal motions.

Since VLBI utilizes hydrogen masers and correlates the received signals from widely separated stations, VLBI has the potential of very accurate time synchronization between these stations. In March 1977 the GSFC/Haystack Observatory/MIT VLBI group and the U. S. Naval Observatory conducted a VLBI time synchronization experiment between stations at Haystack Observatory (Westford, Massachusetts) and the National Radio Astronomy Observatory (Greenbank, West Virginia). The synchronizaton was found to agree to within 25 nanoseconds with an independent synchronization by USNO traveling cesium clocks.

In addition to our frequency standard work and VLBI activity, Goddard also has requirements for very precise global clock synchronization, and we are continually looking to new techniques to meet our timing needs. As I reported last year, in cooperation with the Applied Physics Lab and the Naval Surface Weapons Center we were developing a time transfer receiver which would utilize the NRL developed Navigational Technology Satellites for world wide sub-microsecond clodk synchronization. I am very happy to report that these time transfer receivers are being implemented into our eight (8) transportable laser tracking vans. One of the NTS time transfer receivers is on display at the rear of the auditorium. I would like to congratulate Roger Easton's group at NRL and others for the successful launch of NTS-2 this past summer. I know that the paper scheduled for presentation on the preliminary results of the NTS-2 satellite should be very interesting.

During the early to mid 1980's there will be two U.S. satellite systems that can be used for sub-microsecond clock synchronization. These two systems are the DOD Global Positioning System (GPS) and our own NASA Tracking Data Relay Satellite Systems (TDRSS). I see from the program that papers will also be presented on the use of these two systems for tens of nanoseconds global timing.

Among our guests today from the other PTTI sponsoring agencies are Rear Admiral Earl B. Fowler, Jr., Commander of the Naval Electronic Systems Command, Captain Joseph C. Smith, Superintendent of the Naval Observatory, Dr. Gart Westerhout, Scientific Director of the Naval Observatory and Dr. Alan Berman, Director of Research of the Naval Research Laboratory.

I would also like to welcome and acknowledge the attendance of the many foreign nationals. Your presence here makes the PTTI Meetings that much more meaningful. Goddard looks forward to continued cooperation with each of you and this includes our friends here at home.

I think that it is significant to note that of the 34 papers scheduled for presentation, ten (10) will be presented by authors from other countries. This world wide participation is evidence of the importance that the PTTI community and you the attendees place on these annual meetings. I encourage to you to continue your efforts.

I look forward to participating in the Sessions as my schedule permits and I hope to get a chance to talk with many of you during the sessions. I thank you for coming and hope that you have a rewarding three days here at Goddard.

Thank you.

Page intentionally left blank

Page intentionally left blank

OPENING COMMENTS

RAdm. Earl B. Fowler, Jr.
Commander, Naval Electronic Systems Command

RADM. FOWLER: Thank you very much, Dr. Barnes, and good morning, ladies and gentlemen. It is my pleasure to be here at Goddard Space Flight Center this morning as one of the co-sponsors of this meeting. I welcome each of you and especially our distinguished foreign visitors. The Naval Observatory, the Naval Research Laboratory, the Naval Electronic Systems Command, the Defense Communications Agency and the National Aeronautics and Space Administration, Goddard Space Flight Center, are co-sponsoring this event which bring together many of the national and international agencies with responsibilities and interests in PTTI.

It is quite appropriate that three Navy organizations participate in this co-sponsorship. It was the increasing speed of ships as sail gave way to steam and their need for improved timing to improve navigation that placed the United States Navy in an early leading international position in PTTI.

Our illustrious Naval Observatory has from early time been the timekeeper of the world, and much later our very renowned Naval Research Laboratory began to play a key scientific and engineering role as the use of PTTI became important to communication and then later to almost all electronic systems.

The Naval Electronic Systems Command is a late arrival on the PTTI scene, but we now have a key role also. It among other things contains the Navy project management for the newest navigation system, the Global Positioning System which Dr. Cooper mentioned, so now PTTI has come full circle.

We need your best PTTI efforts to improve navigation once again. Just as our forefathers saw sail give way to steam, we modern naval officers are seeing the most exciting and revolutionary changes in our ships and airplanes, spacecraft, weapons, and command systems. Your best PTTI efforts are needed now in more ways and in more places for more uses than ever before. For the scientists here I challenge you to put forth your best ideas, and for my colleagues the

engineers here we must do substantially more to make communicators and navigators, the data processing specialists, and so on, the designers of these systems, understand better the fundamental place for PTTI in their design concepts.

Since the last time I addressed this meeting, the Naval Electronic Systems Command has grown and matured in its assignment as the Navy manager for PTTI. We have developed a master plan, which has provided the Navy's PTTI program with a new system concept and program direction which will meet the current and future PTTI requirements of the Navy and also be in accordance with the Naval Observatory's plan for the Department of Defense PTTI program.

The new concept for a PTTI system will provide the communication and navigation systems on Navy ships and aircraft and stations with PTTI information from the Naval Observatory to the required accuracy on a continuous worldwide near real time basis via two major subsystems. These are a primary worldwide PTTI dissemination subsystem and a standardized local distribution subsystem.

Today the technology is satisfying the current Navy PTTI requirements. However, it appears that we must continue to improve on that technology in order to meet the needs of tomorrow. This does not negate the need I outlined the last time I addressed this planning meeting to encourage maximum usage of existing capabilities, to minimize the proliferation of PTTI equipment and systems. This need to improve technology and to maximize the use of existing systems emphasizes the need for exchange of ideas and the dissemination of information, which these meetings provide.

I encourage each of you to take full advantage of this forum to increase your knowledge and understanding of the problems, techniques, and capabilities. The work you are doing is so very, very important.

I am certain that our NASA hosts will provide once again an enjoyable and informative meeting, and I certainly thank each of you for your participation. And I wish you the very best for this session. Thank you very much.

OPENING COMMENTS

Captain Joseph C. Smith
Superintendent, U. S. Naval Observatory

CAPT. SMITH: Dr. Barnes, Ladies and Gentlemen. It is indeed a pleasure to have the opportunity to address the 9th Annual PTTI Planning Meeting. I thought it would be appropriate today to give a status report of where we have been this past year and where we intend to go this next year in PTTI and timing matters. I have found this past year at the United States Naval Observatory most enjoyable and stimulating working in this important field. During this past year we have made advances in at least 10 separate timing matters:

1. The West Coast Loran-C chain has been synchronized and is now directly traceable to the U. S. Naval Observatory Master Clock.

2. The U. S. Naval Observatory Master Clock is now automatically updated by computer to provisional U. S. Naval Observatory mean time. This additionally includes a new computer system which was put into operation in Richmond, Florida.

3. Our publications have expanded in order to better service the many users of PTTI worldwide. There are over 1200 different organizations and individuals on our mailing list for various Time Service Announcements of which 300 are foreign. Series 4, 7, and 17, which are published weekly, go to about 800 different subscribers. Times of coincidence tables for the new Loran-C chain are sent out to over 400 subcribers. The new experimental series precise time transfer report is sent out to over 200 subscribers. It contains results of satellite and television timing transfers, portable clock trips, and Loran-C monitoring. The experimental series 6 publication is now sent to over 100 subscribers. This series contains time and latitude observations at Washington and Richmond and other data.

4. In the astronomical area, we are now determining UTO using new and different PZT's. The 65-centimeter PZT number 7 has become operational in Washington, and the 20-centimeter PZT number 6 has become operational in Richmond, Florida, along with a microdensitometer to measure plates there.

5. We have expanded our telephone service to include daily TV, Loran-C, and VLF phase values. The telephone series 4 is now available on both commercial and autovon numbers.

6. In the area of satellite usage for time transfer, the U. S. Naval Observatory has worked with the Transit Satellite Office on the commercial development of a transit time recovery receiver, which will

allow worldwide 25-microsecond time synchronization traceable to the U. S. Naval Observatory Master Clock. Additionally, the Naval Observatory was the prime mover in obtaining the funds necessary to build the first GPS timing receiver.

7. In the area of TV, our time work has expanded to now include Channel 11, KTTV, in Los Angeles. This station is used for distribution of absolute time traceable to the U. S. Naval Observatory Master Clock.

8. Our portable clock trips this year have visited 5 continents. They have gone from north of the Arctic Circle to south of the Tropic of Capricorn. They have traveled halfway around the world, east and west, visiting some 70 installations worldwide.

9. We have not neglected international cooperation and assistance in monitoring various timing systems. We are currently working with 10 different countries at 11 different sites on timing matters worldwide.

10. In the area of VLBI time transfers, we have had the opportunity to work closely with NRL and NRAO in setting up time transfer experiments. These experiments, conducted with Haystack and Algonquin Park as well as Green Bank, West Virginia, have proven most useful in setting the course for future VLBI work.

During the coming year, we intend to continue these areas as well as push forward in 10 other areas of concern.

1. We will be working on the synchronization of the Canadian West Coast and Alaska Loran-C chains.

2. We will develop an algorithm to compute UTC (USNO) in real time.

3. We are constructing an additional clock vault which will house the special clock boxes developed by the University of Maryland, and we plan to continue the applied research using the University of Maryland team working in close conjunction with our scientists.

4. The series 16 publications will be expanded from 4 to 6 pages in order to contain more Precise Time Reference Stations (PTRS).

5. Construction of PZT number 8 has started and will be part of our overall astronomical instrumentation system to better observe time.

6. We will begin observations with NRAO utilizing their 35-kilometer interferometer.

7. The GPS time transfer unit will continue to be developed and the first operational test will take place at the Naval Observatory upon

receipt of the unit.

8. The Washington local distribution of time utilizing TV will be further improved with a goal of 1 nanosecond precision.

9. We shall continue VLBI experimentation in conjunction with the Max-Planck-Institute (West Germany) and the NRL Maryland Point facility for time transfer.

10. We shall continue work with the Department of Defense on time details in order to strengthen the timing capabilities and procedures so necessary for the DoD to meet the future challenges of improved and rapidly-increasing technology requiring precise time.

It is our sincere desire at the U. S. Naval Observatory to continue to support the important role of timing in DoD and in the Navy. Obviously, these efforts carry over both nationally and internationally. It has indeed been a pleasure for me to have had the opportunity to meet many of you during this past year, and I look forward to meeting many more of you during the coming one. Please do not hesitate to call us on timing matters at any time. We are happy to be a part of this most important undertaking. I am sure this meeting will once more point out new avenues to explore and new challenges to conquer. We of the Naval Observatory wish you well in this important collective endeavor.

Page intentionally left blank

Page intentionally left blank

WELCOME ADDRESS

Dr. Alan Berman, Director of Research
Naval Research Laboratory

On behalf of the Naval Research Laboratory, I would like to welcome you to the Ninth Annual Precise Time and Time Interval Application and Planning Meeting. It is a pleasure for NRL to act as one of the Co-hosts and Sponsors of this meeting. As Director of Research of NRL, it has been my privilege to welcome five or six previous meetings in this series. I have noted that the PTTI meeting has grown in prestige each year. From rather small beginnings, attendance has expanded remarkably and each year has seen more and more foreign attendance.

In the course of writing welcoming addresses over a period of years, I have run out of anecdotal information to use as filler material. Therefore, I think it is appropriate that I look somewhat seriously at the progress which has been made by the PTTI community over the span of the last nine meetings.

I am impressed with the progress that has been made in the availability of frequency sources since the first meeting. While rubidium and cesium sources were generally available nine years ago, they have been made extremely compact, highly reliable, radiation hardened, and space qualified. Indeed at this moment, there are cesium sources in space in the NTS-2 satellite. Ten years ago a hydrogen maser was a large ungainly installation that required a team of PhD's to act as baby sitters. There are some who claim that this is still the situation. Actually, I think considerable progress has been made and we are developing hydrogen masers which will be space qualified, physically compact, and relatively light. For those of you who get a chance to visit Roger Easton over at NRL, I think he can show you some space qualified hardware that has been functioning for several years and is yielding excellent performance.

Above and beyond the development of hardware in the last nine or ten years, I am impressed by the broad recognition that has come about of the importance of precise time and time interval. The application of precise time and time sources to navigation is well understood and is based on the pioneering work of your community. The US will launch the GPS series of satellites. These birds will allow unprecedented navigational accuracy with all the attendance benefits to the military and civilian components of our society that you know well. The application of PTTI technology in the area of communications has allowed better and faster synchronization of communication links and the use of more sophisticated cryptological techniques. Geodesy, geophysics, long base line radio astronomy, and interferometry have certainly blossomed in the last ten years. Ultimately, all of the advances in these fields stemmed from the general availability of precise time sources and from our improved ability to transfer time. A possible breakthrough for society is the application of the long base line interferometry for detection of strains in the earth's crust. It is possible that this will provide earthquake warnings with great savings of life and possibly property. Missile and satellite tracking systems, meterology generally, and a wide variety of maser application are subjects that are the substance of this meeting and areas where your community can generally be quite proud.

We at NRL are proud of the part we have played in the time and frequency field since we first opened our doors in 1923. We have been keenly interested in most of the developments in the field from that day to this. It is quite evident that the requirements of frequency stability and time precision will continue to increase in the future as they have in the past. It is therefore, with great pleasure that I join the other hosts in welcoming you to this conference.

FUTURE DEVELOPMENTS IN U.S. NAVAL OBSERVATORY TIME SERVICE

Gart Westerhout
U. S. Naval Observatory
Washington, D. C.

ABSTRACT

During the next 10 years, the U. S. Naval Observatory will be embarking on several new programs. These programs are intended to improve the U. S. Naval Observatory clock system in order to meet the stringent requirements of future systems and to improve time transfer and monitoring techniques. A descriptive review of these programs and their implementation will be given. They include radio astrometry methods to determine UTO and polar motion and to do VLBI time transfer, incorporation of hydrogen massers in the clock system, development of GPS monitoring equipment, and additional smaller programs.

INTRODUCTION

The U.S. Naval Observatory (NAVOBSY) is charged, by DoD directive, with sole responsibility for establishing, coordinating and maintaining PTTI capabilities. Increasingly accurate time information is needed for both navigation and communication. Since the development of capabilities for better accuracy takes time, the Naval Observatory must, of necessity, always be many years ahead of deployment of new systems requiring accurate time. This paper will review some of the plans to implement new and more accurate methods of time determination and time transfer.

THE RADIO ASTROMETRY PROGRAM

The Naval Observatory plans to utilize the inherently more accurate information obtainable through radio interferometry in its overall effort of obtaining more accurate positional reference frames. Of interest at this meeting, of course, is the determination of UTO. The main task of the NAVOBSY Time Service is operational: providing daily values of time and Earth rotation parameters. In Table 1, various methods of determining these data are compared. The first part lists the optical determinations for four different instruments, visual zenith telescope, photographic zenith telescope, astrolabe, and the NAVOBSY 65-cm photographic zenith telescope. The internal mean errors listed in the second column are averages over one night using the observations of approximately 20 to 40 stars. The third column, giving external mean errors, providing averages over many nights. Note that

Table 1

OPTICAL DETERMINATIONS OF UT0 AND POLAR MOTION

	m.e. (internal)	m.e. (external)
VZT	± 0".20 (PM)	± 0".13 (PM)
PZT	0".04 (PM) 4 ms (UT0)	0".09 (PM) 7 ms (UT0)
Astrolabe	0".06 4 ms	0".10 10 ms
65-cm PZT	0".03 3 ms	
	Average over one night, 20-40 stars	Average over many nights

RADIO DETERMINATIONS OF UT0 AND POLAR MOTION

	m.e. (internal)
35-km Interfer.	± 0".01 expected 1 ms
VLBI	0".002 expected 0.1 ms

AVERAGE CURRENT DETERMINATIONS

	m.e. (internal)	
IPMS	± 0".01	(40 observatories)
BIH	0".015 1.2 ms	(50 observatories, one month)
Doppler	0".012	(10-20 stations, 2 days)

in a number of cases the external mean error is larger than the internal mean error. This is due to systematic errors caused bv refraction effects of a local nature which cannot be corrected for by the standard methods. Another cause for systematic errors is the fact that on different nights and in different seasons of the year different groups of stars are used; these stars are tied to a reference svstem which has errors that can amount to 0.1 to 0.2 arc seconds, and the errors are caused to a large extent by the poor knowledge of the proper motions of the stars. Methods are being developed to better determine atmospheric refraction and there are extensive efforts underway to considerably improve the internal consistency of the stellar reference frame. It is especially in this latter effort that radio interferometry, as well as optical interferometric methods, might eventually play a very important role.

In the second part of Table 1 are listed the expected mean errors using two different types of radio determinations of UTO and polar motion. The 35-km interferometer referred to is the connected-link interferometer of the National Radio Astronomy Observatory in Green Bank, WV. The expected mean errors are based on a limited series of observations of a few days each of a small number of radio sources. Similarly, the expected very long baseline interferometric values are based on a few experiments that have taken place in the last few years. "Expected", in this context, means that, with proper care and with extended observations, it is hoped that eventually such accuracies will be obtained on a routine basis. In particular, it is hoped that development of equipment especially geared to polar motion and UTO will increase the accuracies considerably.

In the third part of Table 1 are listed the average mean errors of polar motion and time published bv the International Polar Motion Service (IPMS) and the Bureau International de l'Heure (BIH). It will be noted that averages over a month's observations using many different observatories provide approximately the same accuracy that a radio interferometer can reach in a few hours of observation. Doppler and laser ranging techniques provide approximately the same kind of accuracies as expected from the 35-km interferometer. Daily values of UT and polar motion to this precision are basically unknown. It should be noted that 1 millisecond of time is equivalent to 1½ feet. Obviously the improved accuracy is needed for geodesy, surveying, and the physics of the interior of the Earth.

The NAVOBSY, in collaboration with the Naval Research Laboratory, hopes to acquire and operate the Green Bank 35-km interferometer for daily measurement of UTO and polar motion starting in FY79.

TIME TRANSFER VIA VERY LONG BASELINE INTERFEROMETRY (VLBI)

The inherent capability of a VLBI system to synchronize two oscillators at each end of a network is better than 1 nanosecond. This is an inherent capability - it has not been proven that this accuracy can be realistically utilized. No system yet exists to calibrate or check this value.

It is important to realize that the most accurate time transfers with portable clocks have accuracies of approximately 25 nanoseconds. In very special cases, using multiple trips, it is possible to obtain 10 nanoseconds accuracy. One experiment, which used an entire clock ensemble and provided extremely carefully controlled pressure and temperature surroundings, claims to have maintained an accuracy, during transport of the clocks over a period of 15 hours, of the order of 1 nanosecond. Transportation of a clock ensemble in this manner may make it possible to verify the VLBI accuracies.

In order to reach such accuracies with VLBI, all antenna system delays have to be very carefully calibrated on each end. It seems possible to set up an internal VLBI system with sub-nanosecond accuracy, but eventually the system will have to be tied to other time systems. It is dependent, therefore, on currently existing time transfer mechanisms, such as Loran-C, which presently provides accuracies of, at most, 100 to 150 nanoseconds. Hopefully, more accurate continuous time transfer techniques will be developed in the course of the next few years.

The advantage of VLBI time transfer is, of course, its great inherent precision. There are many possible locations for VLBI stations using existing antennas; it is relatively inexpensive to construct new stations at the existing antennas if such are required; and the system spans intercontinental baselines with ease. Another great advantage is that there is no direct reliance for time transfer on vulnerable satellites. A disadvantage is that clocks get synchronized ex post facto; the digital tapes acquired at each of the VLBI stations have to be transported to a central location for processing. Experiments have been run where the data has been transferred via satellites and these will be reported on elsewhere in this volume. This technique, of course, does give instantaneous results but depends, again, on satellite availability which is expensive.

Requirements now demand an accuracy of 10 nanoseconds for time synchronization around the globe. It is clear that in order to reach that type of accuracy, the Naval Observatory needs to be able to transfer time to approximately an order of magnitude better. So in order to even reach the current requirements for communication and navigation we already are required to transfer time to the order of 1 nanosecond.

It is especially for these reasons, and because the NAVOBSY is responsible for this work as far as the DoD is concerned, that we are pushing so hard towards making systems like this operational. We simply cannot afford to remain in an experimental state for too long.

MASTER CLOCK IMPROVEMENT

The requirement exists for an improved operational master clock system. The current Naval Observatory Master Clock is an ensemble of more than 20 cesium clocks interrelated via a computer. Presently, the computer calculates a provisional mean and controls a real-time clock which differs from the provisional mean by 5 nanoseconds, on the average. A final mean is later calculated, and the difference of the provisional mean from the final mean can sometimes be as high as 40 nanoseconds. The noise of the final mean is only a few nanoseconds. Obviously, correcting the time provided by the real-time clock a few days later is a very cumbersome method. NAVOBSY's goal is the calculation of a real-time final mean and to have a real-time clock which differs from this mean by no more than 1 nanosecond. Two things are required in order to reach this: (a) improved algorithms in the calculations and, (b) improved oscillators in order to eliminate noise and to obtain greater inherent stability. The NAVOBSY is in the process of studying: (a) the acquisition of a clock ensemble consisting of hydrogen masers and, (b) the feasibility of using super-conducting cavity oscillators or other high performance cryogenic oscillators. Again it should be noted that accuracy of a real-time clock of 1 nanosecond is a requirement that is here now. Users come to the NAVOBSY with their portable clock and expect accuracies of better than 10 nanoseconds; they do not want to later correct their time transfer from provisional to final mean time. We need an operational system with 1 nanosecond accuracy.

DEVELOPMENT OF GLOBAL POSITIONING SYSTEM (GPS) TIME TRANSFER UNIT

In order to utilize the GPS system for time transfer and clock synchronization, a single channel time transfer unit is now being developed and will be tested at the NAVOBSY. The unit will be available commercially. The NAVOBSY will monitor on a regular basis the GPS satellite clocks for comparison with the improved master clock system which, hopefully, will be stable enough as a comparison standard.

Comparable work has been done using the Transit Satellite system, in conjunction with the Navy Astronautics Group. To improve time distribution around the world, a timing receiver was developed that can provide time anywhere with an accuracy of a few microseconds. This receiver is commercially available at nominal cost. It is hoped that the GPS receiver now under construction will allow time distribution several orders of magnitude better.

IMPROVEMENT OF TV TIME TRANSFER

Details concerning NAVOBSY's efforts in this area are published elsewhere in this volume. The TV Time Transfer system which has been operational in the Washington, D. C. area for some time is now being implemented in the Los Angeles area as well. Currently, work is underway to use this system for very precise navigation in local areas.

INCREASED LORAN-C COVERAGE

Due to the expansion of the Loran-C system, the NAVOBSY, which monitors the Loran-C timing, will have to increase its monitoring capabilities. Improvement in the 100 to 150 nanoseconds accuracy of Loran-C is not expected as efforts for improving accuracies are going into other systems. The very large area of coverage of the Loran-C system is its major benefit.

LASER TIME TRANSFER

A program is underway, in collaboration with NASA, to perform an experiment using the space shuttle. This system is the reverse of the normal laser timing experiments in that the laser will be on-board the space shuttle and the retro-reflectors will be on the ground. The ground stations record the time of arrival and, using the on-board clock on the space shuttle it is possible to transfer time with extremely high accuracy. In fact the accuracy expected is such that the only method we see of checking it is by VLBI techniques and, therefore, it is planned to mount ground stations at various VLBI sites. Of course this will work only if we already have proven the inherent accuracy of the VLBI system.

CONCLUSION

The NAVOBSY continues to improve its determination of the Earth's rotational parameters as well as its master atomic clock and time transfer techniques. It is important to point out that the various efforts in these directions should be coordinated as closely as possible. All factors, whether they be astronomical, technological, or geodetic, influencing time and time transfer should be considered. It is hoped that the efforts being made for closer coordination will continue.

QUESTIONS AND ANSWERS

MR. LAUREN RUEGER, Johns Hopkins University, Applied Physics Lab:

You indicated Doppler measurements were only integrated for a couple of days and you take your interferometer measurements for a month. Is there some reason you discriminate against the Doppler?

DR. WESTERHOUT:

No, I didn't discriminate against the Doppler at all. I was simply saying that typically the Doppler values that are published are averages over 10 or 20 stations over a few days, and they have the same accuracy as what one expects to get out of the 35-kilometer interferometer.

MR. RUEGER:

Our experience has been that we get a substantially better mean for month averages.

DR. WESTERHOUT:

Thank you.

Page intentionally left blank

Page intentionally left blank

ATOMIC FREQUENCY STANDARDS: SURVEY AND FORECAST

by

Jacques Vanier
Laboratoire d'Electronique Quantique
Département de Génie Electrique
Université Laval
Québec, Canada

The present paper is a concise survey giving the characteristics (mainly stability and accuracy) of state of the art Atomic Frequency Standards. A modest attempt is made at a projection in the future on improvements that could be accomplished with major research and development efforts. The reader will find well documented information on Atomic Frequency Standards in several review papers which have been published within the last ten years (1-7). The present paper is based on some of these articles, and owes much to some other publications more closely related to the question of forecast (8-10). It is also based on private communications with various scientists working actively in this field.

The Basis of Atomic Frequency Standards.

Basic concepts

An atomic frequency standard is a frequency generator in which the essential harmonic motion is produced by an atomic resonance. This resonance originates in a transition between two specific energy levels of the atom in question. The resonance frequency is given by

$$\nu_o = \frac{E_2 - E_1}{h} \qquad (1)$$

where E_2 and E_1 are the energy of the two levels involved and h is Planck's constant. The main reasons behind the idea of using such an atomic resonance for producing an harmonic motion are:

a) The energy difference $\Delta E = E_2 - E_1$ giving rise to ν_o is primarily a function of fields internal to the atoms and, within some specific conditions and limits, is only slightly affected by external fields or perturbations. Furthermore these perturbations in many cases can be well controlled and calculated, and corrections can be applied to the frequency observed experimentally. When the corrections are well known, one can retrace back from the frequency measured to the actual resonance frequency ν_o of the free atom at rest. This consideration is related to the accuracy of the particular standard. Here accuracy is defined as the cumulative uncertainty on the frequency corrections which must be applied to the observed frequency in order to obtain the transition frequency of the free atom at rest, divided by the nominal frequency. In practice it amounts to a measure of innacuracy. The smallest numbers give the highest accuracy.

b) With some ensembles of atoms it is possible to obtain very narrow resonance lines. This is in fact related to the actual life time of the atoms in a particular state. The longer the lifetime of the atoms, the narrower the resonance is and one defines a line quality factor as

$$Q_\ell = \frac{\nu_o}{\Delta \nu} \qquad (2)$$

where $\Delta \nu$ is the width of resonance line. Although, in principle the lifetime of atoms in a given state may be years, in practice the simple process of probing the resonance limits this lifetime and a compromise must be made between signal amplitude and linewidth. Furthermore, as

will be discussed below, other perturbations which broaden the line are always present in actual devices. However, the line Q's possible in practice for some atoms are still much higher than those obtained in the best standard mechanical devices such as quartz crystals used in precision oscillators. The line quality factor relates to the precision with which the line center can be determined experimentally. The line quality factor relates also to the stability of the frequency standard. Here frequency stability is a measure of the degree to which the frequency will stay constant after the oscillator has been set in operation. In the present article we will characterize the stability either through the spectral density $S_y(f)$ of fractional frequency fluctuations or $\sigma_y(\tau)$, the two sample variance. (11)

c) It is also believed that $\nu_o = \frac{E_2 - E_1}{h}$, for a given pair of levels in a specific atom, is a constant independent of time. This is in contrast with the actual rotation rate of the earth which is known to fluctuate and quartz crystals whose frequency is known to change with time. The idea is fundamental and drifts observed in actual frequency standards are assumed at present to be entirely inherent to the practical realization of the standard. The second is currently defined in terms of a particular transition in cesium, whose frequency is 9, 192, 631, 770 Hz.

Practical realization.

In order to realize an actual device based on the concepts discussed above, several practical considerations must be examined. These considerations actually dictate the choice of atoms which is of course a main point in the whole discussion.

The problem can be best situated with a block diagram showing the two possible approaches. In general one wants an oscillator

at a given nominal frequency of, say, 10 MHz to represent as well as possible the characteristics of the atomic resonance line. It thus amounts to a question of locking a frequency generator, generally a quartz oscillator to the atomic resonance line. This can be done in the two modes illustrated in figure 1. In the active mode, the atomic ensemble, well prepared in a given state, emits energy at its resonance frequency. The quartz oscillator is locked in phase to the coherent signal emitted by the atomic ensemble; one has what is called a phase lock loop. In the passive mode, the ensemble of atoms also well prepared in a given state is questionned or interrogated with a signal derived from the crystal oscillator as to what its frequency is; we then have a frequency lock loop. Figures 2 and 3 give more details on the two approaches.

From figure 1, it is seen that one must consider as essential processes: a) the choice of the atomic ensemble, b) its storage, c) its preparation, d) its interrogation and e) the detection of the atomic signal. These points have been discussed in some details by several authors in various ways. (9, 10). It is clear that the processes are not completly independent and that interaction can exist between them. For exemple the choice of the atomic ensemble is dictated by practical considerations such as obtaining a decent vapor pressure at a moderate temperature, the possibility of storing it in some enclosure or forming a beam of these atoms.

a) Choice of the atomic ensembles: As a general rule and added to constraints of practicality, the ΔE of the atomic ensemble chosen should be affected as little as possible by external force fields and by the experimental set up used to detect the resonance. Another consideration, of course, is also that the line width should not be affected to a too great extent by the same mechanisms used to detect the resonance.

For the purpose of the discussion it is best to look at the requirements for active and passive devices separatly. However on a general basis, for practical reasons, a first criterion should be fulfilled: the atomic resonance frequency should be in a usefull range in order that its detection is not too difficult and that it can be used, for example, for locking a crystal oscillator. This constraint has greatly limited the choice of atoms for practical frequency standards. Of course, frequency standards exist at very high frequencies (stabilized lasers). However their signal frequency cannot be processed as easily as in the case of basic standards in the microwave region. These standards exist as a class almost by themselves and until, reliable, low cost, low complexity synthesis techniques are developed they will stay that way. This in no way, however, has inhibited research as such in this particular sector.

In active devices, such as the hydrogen and rubidium masers, where the storage principle in a bulb is used, other requirements are low atomic polarizability, in order that upon collisions ΔE and $\Delta \nu$ are not altered too drastically, as well as absence of reaction with other atoms used as buffer gas or wall coating of the container.

In passive devices using beam techniques, the detection of particles requires a low ionization potential if the hot wire technique is used for particle detection. On the other hand if selective optical absorption is used to detect the state of the ensemble, the transition probability at the photon wavelength should be high.

Noble gases are chemically inert but they have a ground state ^1S_o, thus have no magnetic moment, have no hyperfine structure and do not possess a resonance frequency in the microwave range which

is a range of frequencies easily treated with present technology. On the other hand, hydrogen and alkali atoms (Li, K, Na, Rb, Cs, Fr) have a $^2S_{\frac{1}{2}}$ ground state and thus have a strong magnetic moment. Their hyperfine frequency is in a usefull range where present day technology permits easy experimental signal processing. However they are far from being chemically inert. A compromise is thus made. They are either used as a beam or under the form of a vapor pressure contained in an enclosure coated internally with an inert film or imbedded in an inert gaseous matrix such as a buffer gas. The atoms that have been most studied for the purpose of atomic frequency standard applications are H, Rb, and Cs. Presently they form the core of the most documented atomic frequency standards. They have been used in different types of arrangements either active or passive. Unfortunatly their frequency depends quite a lot on the magnetic field present and serious precautions must be taken to shield these atomic ensembles from environmental fluctuations.

Of course other atoms or molecules have been used for frequency standards applications or have been tried. For example NH_3 and Tℓ have interesting characteristics and have been used for implementing particular frequency standards. These will be discussed below. Other atoms have also been proposed and are presently under investigation. These are, Mg, Ca, Ag, Ba, Hg, Bi and others. However the implementation of these atoms in a given system, forms, for each one, a particular case and must be discussed on an individual basis. For frequency standard applications, they generally suffer from one of the requirements mentioned above: generally it is the frequency which is not in a usefull range. Some other atoms suffer from the signal detection point of view. However, this is related to the actual experimental technique used.

Thus the main point to remember here is that the choice of the atomic ensemble for practical frequency standard applications depends largely on considerations related to the problem of "usable frequency" and this will stay true until reliable frequency synthesis from microwave to optical frequencies becomes routine work in the laboratory. On the other hand, intrinsic atomic particularities will dictate the experimental arrangement to be used.

b) The storage of the atomic ensemble: The atom must be stored somewhere to be examined as to what is its resonance frequency. Here, storage is taken in its most general sense. The most conventional storage processes are the following:

- Storage in a bulb under the form of a vapor.

  . The inside of the bulb may be coated with an inert film. In that case the atom is free to move inside the bulb and makes collision with the wall. This permits long observation times; for hydrogen a lifetime in excess of one second is possible. However collisions with the wall create perturbations in the atomic wave function, causing relaxation and an average frequency shift.

  . The bulb is not coated, but an inert gas is introduced by which the motion of the studied atoms is inhibited to some extent and can take place mainly through diffusion. This technique is used presently in Rb and Cs vapor frequency standards (passive and active). The buffer gases commonly used are N_2, Ar, Ne, CH_4. The atom has a lifetime limited by collision processes with the buffer gas atoms and diffusion to the wall.

  . In some cases, it is preferable to use both techniques at the same time: wall coating and buffer gas. In this case the lifetime is

limited mostly by collision processes with the buffer gas.

- Storage through drift in a beam.

In this case the storage region is the atomic beam and the interrogation or observation of the atomic ensemble is done at very specific regions in the path of the beam. A typical example is the case of the NH_3 maser in which the beam of molecules passes through a microwave cavity and emits its energy inside this same cavity. The average storage time τ is simply the length of the cavity divided by the average speed of the molecules. The line width is thus of the order of $1/\tau$. Another typical example is the Cs beam tube whose observation is done at two different regions of the beam path in two microwave cavities. In this case although the observation time in each region is short, the drift time between the two regions is of fundamental importance. If L is the distance between these regions the effective time of storage is $\sim L/v$ (v=atomic speed). It should be realized that this technique can be applied at any frequencies up to the visible. Since the line width, v/L, is in principle a constant for a given L, the line Q increases with the frequency. It is also clear that this type of storage is the one that is closest to that in which the atom is observed as a "free atom". However secondary effects are always present which affect either the stability or the accuracy of a particular device.

- Other storage techniques.

There are other storage, techniques possible like those used in ion traps, in which the ion is kept in a region of space by alternating electric fields.

Associated with storage the main effects on frequency affecting stability or accuracy can be, collisions with the buffer gas or the

vessell wall, storage time, (line Q), electric and magnetic fields, first and second order Doppler effects. The first order Doppler effect is mostly a design problem and is generally eliminated through a suitable experimental arrangement.

c) Preparation of the ensemble: Atoms are distributed among the energy levels according to the Boltzmann distribution law. This means that for temperatures above $300^{o}K$, where the frequency standards normally operate, all levels are equally populated even for energy differences corresponding to the microwave region. This is of fundamental importance for the following reason. The detection of the resonance signal is done through the excitation of transitions among a pair of levels. It is clear that if the levels are equally populated, the excitation of transitions has no effect on the populations themselves as well as on the excitation field itself. Consequently no effect is observed. However if there is a difference of population between the levels, the excitation field may either be enhanced or decreased, depending on the sign of the population difference. On the other hand the atomic distribution among the levels may be altered by the excitation and this effect, in a beam for example, may be detected through proper techniques like the counting of particles.

There are several methods that can be used to alter the population of the levels. Among those, the most common are spatial selection through magnetic field gradients (electric field gradients in the case of molecules with electric dipole moments) and optical pumping. Other mechanisms that can be used for state selection are also spin exchange, chemical reaction, electronic collisions, temporal decay from on state to another along a beam. However they are not used in the traditional frequency standards as such, and will be mentionned at the time of discussion of some particular devices.

The process of preparation or state selection, has in some cases profound influence on the frequency of the atomic ensemble. For example we may mention light shifts in the case of optical pumping and creation of magnetic field inhomogeneities in the system where spatial state selection is done with magnets.

d) Interrogation of the ensemble: In order to know the actual atomic resonance frequency, a signal at that frequency is used. In the case of masers, a signal is generated inside the device which, in a sense, interrogates itself. This is the case of the H, Rb and NH_3 masers for example. Lasers fall also in this class. It should be noted that in all these cases the signal is affected by various effects inherent to the process of emission in the resonance structure which is necessary to obtain maser action. This is the so-called cavity pulling effect and it affects both accuracy and stability.

In the case of passive devices the interrogation of the ensemble is done also at the resonance frequency. The atomic resonance signal, however, is observed through particular techniques which will be discussed below. However, here again the process of ensemble interrogation has very profound effects on the resonance signal. It can affect its frequency (stability or accuracy) through unsymmetrical interrogating spectrum, power shift through an unsymmetrical resonance line, a phase shift associated with cavity construction in the case of separated interrogating regions and cavity pulling. The interrogating signal used may also cause broadening of the line which may decrease the ability to find its center and consequently influence the accuracy and stability of the system.

e) Detection: In the case of masers, and some passive devices the signal to be detected is in the microwave range and normally a

superheterodyne technique is used. Although very efficient and sensitive, the technique adds noise to the signal and decreases the observed stability of the device. In passive devices the population difference of the particles having made a transition is monitored. These techniques are also very efficient but, of course, noise limits their sensitivity. In optically pumped devices, the noise comes from the photovoltaic device itself or the detected light. In some beam devices the counting of particles creates shot noise. Thus, detection in general is plagued with the problem of noise inherent either to the detector itself or the signal being detected and it is a major subject of research. Improvements in noise levels associated with detection means generally improvements in short term stability.

Survey.

Traditional frequency standards.

Three atomic frequency standards have known a rather intensive development phase. Those are the Hydrogen Maser, the Rubidium Gas Cell Frequency Standard and the Cesium Beam Frequency Standard . Their physical characteristics are given in table I.

Hydrogen Maser: (13, 14, 15)

An energy level diagram of the $^2S_{\frac{1}{2}}$ ground state of H is shown in figure 4 along with a schematic diagram showing the principles of operation of the device. The maser operates between levels $F = 1$, $m_F = 0$ and $F = 0$, $m_F = 0$. Atomic hydrogen is produced in a dissociator and sent through a selector (hexapole magnet) under the form of a beam. Atoms in the upper state tend to focus on the axis of symmetry of the magnet while those in the lower states have a trajectory which

diverges from the axis. Thus, atoms in state $F = 1$ and $m_F = 0$ enter the storage bulb which is coated internally with teflon and placed inside a high Q cavity. When the flux is strong enough oscillation takes place and the signal is observed with a small loop inside the cavity coupled to a superheterodyne receiver. Thus the preparation of the states is a spatial selection, the storage is done in a coated cell and the interrogation is done in a microwave cavity (self oscillation). The detection of the signal is done with a superheterodyne receiver.

The principal characteristics of such a device are its unsurpassed short, medium and long term stability. The spectral purity of a typical H maser is approximatly:

$$Sy(f) = 5 \times 10^{-25} f^2 + 10^{-27}/f^2 \qquad (3)$$

with a flicker floor probably well below $10^{-30} f^{-1}$. Its stability $\sigma(\tau)$ in the time domain is shown in figure 7. The characteristics given here are those of the maser itself. The stability is limited by temperature fluctuations through cavity pulling, magnetic field fluctuations, effects of load fluctuations on the cavity tuning and by the low power output which limits the short term stability. It is believed that the flicker floor has not been observed yet. The accuracy of the device is limited to about 2×10^{-12} due to uncertainties in the wall shift (16). The tuning accuracy through classical spin exchange broadening is of the order of a few parts in 10^{14} (17). Other secondary effects are also present, but they can be calculated or measured to a precision that is not a limiting factor (18, 17).

The device is not available commercially but is fabricated in various institutions, research laboratories and universities.

Cesium Beam Frequency Standard: (19, 20, 21, 22, 23)

A diagram showing the principles of operation of the cesium beam frequency standard is shown in figure 5 along with an energy level diagram of the atom. The drift region between the two cavities acts as the storage region. In the diagram shown, atoms in the $F = 3$, $m_F = 0$ state are those which strike the detector. Thus when the atoms, which are selected by magnet A, are induced to make a transition from the level $F = 4$, $m_F = 0$ to $F = 3$, $m_F = 0$ in the microwave cavity, the beam becomes populated with atoms in the $F = 3$, $m_F = 0$ level at the exit of region C. The flux of atoms reaching the detector is then a critical function of the frequency applied. The signal observed is also shown in figure 5. The application of r.f. radiation at two separate interrogation regions allows a considerable reduction in line width. It is in fact a function of the distance L between the two arms of the cavity: $\Delta\nu = 0.65\ {}^{v_p}/_{L}$, where v_p is the most probable velocity.

The cesium beam tube, is a frequency discriminator and must be incorporated in an electronic servo system which locks a crystal oscillator to the resonance line. The spectral purity of a typical laboratory frequency standard is given by:

$$S_y(H) = 5 \times 10^{-29}/f \pm 10^{-24} \qquad (4)$$

Its stability $\sigma(\tau)$ in the time domain is given in figure 7. In the short term region the stability is limited by shot noise at the detector. In laboratory devices, a flicker floor is observed at a level of the order of 10^{-14} or lower. The accuracy is about 1×10^{-13} in long laboratory models and is limited by magnetic field, cavity phase shift and 2nd order Doppler effects.

The cesium beam frequency standard exists as a primary standard in several laboratories and small units are available commercially.

Rubidium vapor frequency standard: (24, 25, 26, 27, 28, 29)

Figure 6 shows a diagram of the passive, optically pumped, rubidium 87 frequency standard (optical package). The basic principles are the following. Light from a rubidium 87 lamp is filtered by a so called hyperfine filter made of an ampoule containing rubidium 85 and a buffer gas such as argon. This arrangement shapes the spectrum of the light in such a way that a population inversion is obtained in the cell which follows and which contains rubidium 87 and a buffer gas. This cell becomes transparent through this optical pumping effect. If it is exposed to radiation at the proper frequency, corresponding to that which is necessary to excite transitions between the states $F = 3$, $m_f = 0$ and $F = 2$, $m_f = 0$ of the ground state, this same cell becomes opaque again and this effect can be detected through a decrease in light intensity reaching the silicon solar cell detector. Thus, in this present case, storage is done in a cell with a buffer gas, interrogation is done in the same region, preparation is accomplished through optical pumping and the detection of the signal is done with a solar cell.

This optical package is used as a frequency discrimator to lock a crystal oscillator to the resonance frequency. The spectral purity of the system is typically

$$S_y(f) = 10^{-26}/f + 5 \times 10^{-23}, \qquad (5)$$

and its stability in the time domain is shown in figure 7. The principal factors limiting its stability are magnetic field, 2nd order Doppler effects, buffer gas and light shifts. All these effects may vary in time depending on the environmental conditions. Furthermore, there is generally a drift associated with the absorption cell which can be due to a reaction of rubidium with the glass of the enclosure. The accuracy of this device is not competitive with the two previous standards, mainly because of the very large buffer gas shift present.

The rubidium vapor frequency standard is available commercially under various models.

Other well documented frequency standards.

The physical characteristics of some other well documented frequency standards are summarized in table 2.

$^{15}NH_3$ maser: (30, 31)

In this maser the storage is accomplished through a single passage of a beam in a microwave cavity. The preparation is spatial electrostatic deflection. Interrogation is, as in the hydrogen maser, in a cavity, and the detection is done with a superheterodyne receiver. The short interaction time limits the stability of the maser to about 5×10^{-11} (cavity pulling). The accuracy is limited to the same value by collisions between molecules in the beam (32). The amonia maser has played a very important role in the history of the development of presently available frequency standards.

Rb maser: (33, 34, 35, 36, 37).

Masers using either of the two isotopes Rb^{85} or Rb^{87}

have been realized. Figure 8 is a block diagram of a Rb^{87} maser. The principles of operation are the same as in the passive Rb gas cell, but the cavity is designed to have a very high quality factor and self oscillation is obtained. Thus the storage is done in a cell with a buffer gas, the preparation is done through optical pumping, the interrogation is made in a microwave cavity (self oscillation), and the detection is done with a superheterodyne receiver. The main advantage of the rubidium maser is its small size and its unsurpassed short term stability. However its long term stability is limited by cavity pulling effects and by the same factors as in the passive rubidium gas cell. The short term stability in present devices, is described by

$$\sigma(\tau) = 1 \times 10^{-13} \tau^{-1},$$

and it is not believed that the flicker floor has been observed yet.

Tl beam: (38, 39, 40, 41)

This device works essentially in the same way as the Cs beam tube, the only difference being the atom used and the frequency involved. The main problem in its realization has been a detection problem. The advantage over Cs would be a low magnetic field sensitivity. No work is presently being done on the device.

Rb^{87} beam: (42, 43)

The implementation that has been studied in some detail is shown in figure 9. Here the only difference from the cesium beam is the method of preparation and of detection. This is done through optical pumping. One advantage of this method over the magnetic selection could be the realization of a better homogeneity of velocities accross the beam. This could make cavity phase shift evaluation more

rigorous. This selection method could also be used with a Cs beam.

Saturated absorption stabilized lasers. (44, 45, 46, 47, 48, 49, 50, 51, 87)

This class of frequency standards falls in the passive type, the laser radiation being used as the interrogation signal generator and thus being slaved to a resonance appearing in an absorption cell. These frequency standards form a class by themselves operating at very high frequencies, in the terahertz region, where frequency comparisons are still an art. A schematic diagram of the device is shown in figure 10. Here the storage is done in a cell and actual preparation is not necessary. Due to the high frequency involved, the Maxwell Boltzmann law provides sufficient population difference between the levels of interest. The molecules commonly used are CH_4, I_2 and CO_2, with the proper laser providing the power for interrogation. The main particularity of the device resides in the method of interrogation called saturated absorption. The beam of light traverses the absorption cell twice in opposite directions, produces transitions and creates saturation only for those atoms having no first order Doppler effect or in other words crossing the beam at right angle. Thus, at the resonance frequency a slight increase in transmission is observed and this is the signal used to lock the laser to this same resonance frequency. The detector can be a PIN photodiode or an infrared device such as an In Sb detector. The stability $\sigma(\tau)$ of the methane stabilized He Ne laser is shown in figure 7 along with the traditional frequency standards. The accuracy of stabilized lasers is in the range of 10^{-11} to 10^{-12} and is limited by hyperfine structure, pressure shift, wave front curvature, 2nd order Doppler effect and recoil effect. (52).

Proposed atomic frequency standards.

Several other atomic frequency standards have been proposed. Their principal physical characteristics are shown in table 3.

Cs maser (53, 54)

This device works on the same principles as the Rb maser. Figure 8 in which rubidium is replaced by cesium applies in principle. The main advantage would be its good short term stability due to its expected high power output.

H beam tube (55, 56) and Ag beam device (57).

These devices work on the same principles as the Cs and Tℓ beam tubes. It is not evident that there are definite, theoritical or practical advantages in the proposed devices.

Cs cell (optically pumped) (58, 59, 60, 61)

This device works on the same principles as the Rb passive gas cell. The main advantage would lie in the weak interaction of Cs with glass, probably improving long term stability. However a bulky hyperfine filter must be used to filter the light for efficient optical pumping.

Magnesium and calcium beam. (62, 63, 64)

This proposal is based on temporal state selection in a beam. Magnesium and calcium show a metastable ^3P level with fine structure. The ^3P states are populated through electron collisions and a beam is formed. The $^3P_1$ level then decay to the ground state by emitting visible light with a lifetime of the order of 1 ms. A

submillimeter wavelenght radiation exciting the transition ^3P_o to $^3P_1$, for instance, replenishes the $^3P_1$ level. Its decay to the ground state gives an added emission of light which allows the detection of the transition. The main advantage would reside in a very high line Q, due to the long lifetime involved and the high frequency of the transition. Major problems reside in the generation of the submillimetre wave for interrogating the resonance.

Ion storage (65, 66, 67, 68, 69, 88)

This device is based on the storage of ions in a trap formed by non uniform alternating electric fields without the need of any applied magnetic fields. The stored ions do not collide with any surfaces and storage times longer than several hours have been reported for sufficiently low background pressures. If the stored ions possess a hyperfine structure, one could then think of state preparation, interrogation and detection in the same way as in conventional passive frequency standards. The hyperfine splitting of $^3He^+$ has been precisely measured and the sources of frequency offsets analysed (65). However light ions have a large second order Doppler frequency shift and are not suited for frequency standard applications. Heavy ions such as mercury appear to be more convenient. The hyperfine splitting of $^{199}Hg^+$ has been observed with a fractional linewidth of 2×10^{-10} and has been precisely measured. This result is attractive for frequency standards application. The proposed scheme for detection of the resonance is similar to what is used in the passive optically pumped standard. Light from a $^{202}Hg^+$ lamp is selectively absorbed by one of the hyperfine components of the $^{199}Hg^+$ ions. The hyperfine transition at 40.5 GHz is thus detected by the change in the intensity of the resonance fluorescence. One main difficulty in this technique resides in the low signal to noise ratio available due to the low ion density at which the trap operates.

H beam storage (70, 71)

The basic idea behind the operation of this device is the same as in the operation of the hydrogen maser, except that it is operated in the passive mode. A microwave signal is used to interrogate the atoms stored in a coated bulb and the effect of the atomic transitions on the interrogation signal is used to lock a crystal oscillator to the atomic resonance. In one version, the modulation technique used is one in which the intensity of the beam is altered. Otherwise the system works in a way similar to passive frequency standards. The main advantage is the reduction of the effect of cavity pulling through the possibility of using very low Q cavities since the oscillation condition does not need to be satisfied. However the wall shift problems remains and should be the principal limit to the accuracy of the device.

NH_3 absorption cell (72, 73)

This is one of the simplest versions of an atomic frequency standard and is based on one of the oldest ideas. The storage is done in a cell and the full Doppler broadened absorption line is interrogated. The states are not prepared and for the absorption, one relies on the Maxwell Boltzman distribution law of the populations among the levels. The microwave absorption is detected through standard techniques and a crystal oscillator is locked to the atomic resonance signal. The accuracy is low ($\sim 10^{-9}$) and the stability is given by

$$\sigma(\tau) = 6\times 10^{-10}\tau^{-\frac{1}{2}} ,$$

with a flicker floor in the 10^{-10} range. The main purpose is the realization of a small, rugged, fast warm up device.

Atomic beam stabilized lasers (74, 75, 76, 77)

This is a class of devices in which a laser is stabilized through its interaction with a resonance frequency that can exist in an atomic beam as shown in Fig. 11. In this case the atoms which are used as a reference for stabilizing the laser can be considered free in the same sense as in the passive cesium frequency standard. Several implementations are possible. In the simplest approach the absorption of the laser light by the atomic beam is detected and is used as the resonance signal for locking the laser. More recently the technique of separated Ramsey interrogation regions has been proposed for the optical range. In principle it should provide extremely high line Q ($10^{11} \sim 10^{12}$). This proposal coupled with the two photon absorption technique (78, 79) shows promises in stability and accuracy. Atomic beams which appear to attract much attention are calcium, bismuth and iodine.

Forecast

Traditional devices

Figure 7 and equations 3, 4 and 5 give the present state of the art stability of the three most documented and most utilized frequency standards: H maser, Cs beam tube, Rb gas cell. An analysis over the past years shows that the stability of these devices, especially in the long term region has been increasing continuously. Better understanding of the physical processes involved and of the sources of noise has provided a basis for a better design of the devices themselves. The H maser has now passed the 10^{-15} level in the 10,000 second region and it appears that the limitation is still a question of cavity temperature control and magnetic shielding. It is thus probable that with some reasonable effort, further improvements will be realized. It should be mentionned that the order of magnitude of

stability mentionned here is not common laboratory practice. Care should be taken in the transfer of this kind of stability to quartz crystal oscillators. It appears that one must be extremely cautious about time varying phase shifts being generated in the detection components. However it is not unlikely that through better cavity design and magnetic shielding and through improved detection systems a flicker floor below the 10^{-15} level would be observed. The laboratory Cs beam tube has reached a level of flicker floor of the order of 7×10^{-14}. In the short term region, better stability could be achieved with more intense beams but this could affect the lifetime of the device.

The accuracy of the hydrogen maser is still limited at the time of writing by the wall shift, to about 2×10^{-12}. This is two orders of magnitude worse than any other uncertainties related, for exemple, to the magnetic field determination or cavity tuning. It is not possible at this time to tell exactly what kind of improvement we can hope for. However there is intensive work being done on wall coatings and bulbs with variable geometries. It appears that operation at a temperature close to the point where the wall shift goes to zero may be a proper avenue of research. The accuracy of the laboratory cesium beam device has passed the 10^{-13} level. The main uncertainties are originating in the magnetic field and the cavity phase shifts. One problem lies on the non-uniform distribution of velocities across the beam. This makes the actual evaluation of the cavity phase shift difficult. It is possible that through homogeneous state preparation a better evaluation of the cavity phase shift could be done. People working in this field believe that an accuracy of 1×10^{-14} can effectively be achieved. These comments are summarized in table 4 along with some projections on the rubidium gas cell device. The numbers in circles are the author's evaluation of the possibility that the projection will be realized, 0 meaning no confidence at all and 5 meaning

certainty. This evaluation is based on many intangible factors and is entirely subjective.

Weight and size: The hydrogen maser has been reduced considerably in size during the last several years and it appears that further reduction could be realized by using cavities in the TE111 mode (80). Present state of the art masers occupy a volume of the order of 100 liters and weigh 45 kg. In the case of commercial cesium beam frequency standards it appears that further progress in size and weight could be gained through a reduction in size of the tube but with a parallel degradation in stability and accuracy. On the other hand it appears that further improvements are possible in the field of passive rubidium frequency standards. The optical package is gaining more and more in simplicity and the use of integrated circuits and modern technology has made possible real gain in size. At present, units 2 liters in volume and weighing 2 kg are available commercially.

Other devices.

The other devices or techniques which appear most promising are the hydrogen beam device, the ion storage technique, the magnesium beam device and atomic beam stabilized lasers using optical Ramsey resonance techniques. The hydrogen beam storage technique has proven to be feasable and reports on its stability are most encouraging. The technique will also allow an easier determination of the wall shift than in an actual maser. The ion storage technique has made some progress but it appears that serious problems are still encountered at the S/N level. Work is in progress to solve this problem (81). In the case of the magnesium beam proposal, the problem of generating an interrogating signal at the resonance frequency appears to be important. However efforts are being made with infrared lasers in this direction and we

ACKNOWLEDGEMENT

I would like to thank the following persons which through private communications have helped me in the task of writing this paper: A.O. McCoubrey, R. Hall, K. Shimoda, A.G. Mungall, R.F.C. Vessot, H.E. Peters, H.A. Schuessler, D. Morris, C. Audoin, D.S. Sutcliffe, A. Risley, H. Hellwig, V. Reinhardt, E. Haffner, F. L. Walls, S. Hahn, K. Radecki.

REFERENCES

(1) McCoubrey A O 1967 Proc. IEEE 55 805-14

(2) Baugh R A and Cutler L S 1970 Microwave J. 43-56

(3) Ramsey N F 1972 IEEE Trans. Instrum. Meas. IM-21 90-8

(4) Cook A H 1972 Rep. Prog. Phys. 35 463-528

(5) Kartaschoff P and Barnes J A 1972 Proc. IEEE 60 493-501

(6) Hellwig H 1975 Proc. IEEE 63-212-29

(7) Audoin C, Vanier J 1976 J. Phys. E Sc. Inst. 9 697-720

(8) Hellwig H 1973 National Bureau of Standards Technical Note 646

(9) Hellwig H 1970 Metrologia 6 118-26

(10) Hellwig H, Halford D, 1974. NBS Monograph 140-137

(11) Barnes J A et al 1971 IEEE Trans. Instrum. Meas. IM-20 105-20

(12) Risley A S 1971 NBS Tech. Note 399

(13) Goldenberg H M, Kleppner D and Ramsey N F 1960 Phys. Rev. Lett. 5 361-2

(14) Kleppner D, Goldenberg H M and Ramsey N F 1962 Phys. Rev. 126 603-15

(15) Kleppner D, Berg H C, Crampton S B, Ramsey N F, Vessot R F C, Peters H E and Vanier J 1965 Phys. Rev. A 138 972-83

(16) Vanier J, Larouche R and Audoin C 1975 Proc. 29th A. Symp. on Frequency Control, USAEC Fort Monmouth, NJ (Washington DC: Electronic Industries Association) pp 371-82

(17) Petit P, Viennet J, Barillet R, Desaintfuscien M and Audoin C 1974 Metrologia 10 61-7

(18) Crampton S B and Wang H T M 1975 Phys. Rev. A 12 1305-12

(19) Essen L, Donaldson R W, Hope E G and Bangham M J 1973 Metrologia 9 128-37

(20) Ramsey N F 1956b Molecular Beams (Oxford: Clarendon) pp 115-44

(21) Mungall A G et al 1976 Metrologia 12 129-139

(22) Glaze D J, Hellwig H, Allan D W, Jarvis S and Wainwright A E 1974 IEEE Trans. Instrum. Meas. IM-23 489-501

(23) Becker G 1976 2nd Frequency Standards and Metrology Symposium Copper Mountain Co. (unpublished)

(24) Bender P, Beaty E and Chi A R 1958 Phys. Rev. Lett. 1 311-3

(25) Carpenter R J, Beaty E G, Bender P L, Saito S and Stone R O 1960 IRE Trans. Instrum. 1-9 132-5

(26) Packard M E and Swartz B E 1962 Proc. IRE 1-22 215-23

(27) Gourber J P 1965 Ann. Radioélect. 20 191-211

(28) Missout G and Vanier J 1975b IEEE Trans. Instrum. Meas. 24 180-4

(29) Jechart E 1973 Proc. 27th A. Symp. on Frequency Control, USAEC Fort Monmouth, NJ (Springfield, Virginia: National Technical Information Service) pp 387-9

(30) Basov N G and Prokhorov A M 1954 Sov. Phys.-JETP 27 282

(31) Gordon J P, Zeiger H J and Townes C H 1954 Phys. Rev. 95 282-4

(32) De Prins 1962 IRE Trans. Instrum. I-11 200-3

(33) Davidovits P and Knabble N 1964 J. Appl. Phys. 35 3042

(34) Davidovits P and Novick R 1966 Proc. IEEE 54 155-70

(35) Vanier J 1968 Phys. Rev. 168 129-49

(36) Têtu M, Busca G and Vanier J 1973 IEEE Trans. Instrum. Meas. IM-22 250-7

(37) Khaplanov G M, Biketov V D, Volkova N I, Lukoshkova G I, Basarov Ye N, Yukhvidin Ya A and Gubin V P 1968 Radio Engng Electron. Phys. 13 137

(38) Kush P 1957 Proc. 11th A. Symp. on Frequency Control, USAEC Fort Monmouth, NJ (Springfield, Virginia: National Technical Information Service) pp 373-84

(39) Bonanomi J 1962 IRE Trans. Instrum. I-11 212-5

(40) Beehler R E and Glaze D J 1966 IEEE Trans. Instrum. Meas. IM-15 55-8

(41) Lacey R F 1967 Metrologia 3 70-8

(42) Arditi M and Cérez P 1972 IEEE Trans. Instrum. Meas. IM-21 391-5

(43) Cérez P, Hartmann F, 1977 IEEE J of Quantum Electronics QE 13 344-351

(44) Hafner E 7th PTTE Conf. 1975

(45) Barger R L and Hall J L 1969b Proc. 23rd A. Symp. on Frequency Control, USAEC Fort Monmouth, NJ (Springfield, Virginia: National Technical Information Service) p 306

(46) Hellwig H, Bell H E, Kartaschoff P and Bergquist J C 1972 J. Appl. Phys. 43 450-2

(47) Bagaev S N and Chebotaev V P 1972 JETP Lett. 16 433-5

(48) Brillet A, Cérez P, Hajdukovic S and Hartmann F 1975 Proc. Amco-5 Conf., Paris, ed J H Sanders and A H Wapstra (New York: Plenum) pp 350-6

(49) Cérez P, Brillet A and Hartmann F 1974 IEEE Trans. Instrum. Meas. IM-23 526-8

(50) Helmcke J and Bayer-Helms F 1974 IEEE Trans. Instrum. Meas. IM-23 529-31

(51) Baird K 1976 2nd Frequency Standards and Metrology Symposium Copper Mountain Co. (unpublished)

(52) Hall J L, Bordé C 1976 2nd Frequency Standards and Metrology Symposium Copper Mountain Co. (unpublished)

(53) Strumia F 1976 Private Communication

(54) Vanier J, Strumia F 1976 Can J. Phys. 54 2355-66

(55) Peters H E 1971 Proc. Frequency Standards and Metrology Seminar (Quebec: Laval University) pp 29-64 (unpublished)

(56) Peters H E 1972 Proc. 26th A. Symp. on Frequency Control, USAEC Fort Monmouth, NJ (Springfield, Virginia: National Technical Information Service)

(57) Hahn S L and Radecki K W 1974 Conf. on Precision Electromagnetic Measurements, London unpublished

(58) Arditi M and Carver T R 1958 Phys. Rev. 109 1012-3

(59) Beaty E, Bender P and Chi A R 1958 Phys. Rev. 112 450-1

(60) Bava E, de Marchi A, Rovera G, Beverini N and Strumia F 1975 Alta Freq. 44 574-8

(61) Rovera G, De Marchi A, Vanier J 1976 IEEE Trans. IM-25 203-10

(62) Strumia F 1972 Metrologia 8 85-90

(63) Giusfredi G, Minguzzi P, Strumia F and Tonneli M 1975 Z. Phys. A 274 279-87

(64) Strumia F, Minguzzi 1976 2nd Frequency Standards and Metrology Symposium Copper Mountain Col. (unpublished)

(65) Schuessler H A, Fortson E N and Dehmelt H G 1969 Phys. Rev. 187 5-38

(66) Schuessler H A 1971 Metrologia 7 103-7

(67) Major F G and Werth G 1973 Phys. Rev. Lett. 30 1155-8

(68) Duchêne J, Audoin C, Schermann J 1976 2nd Frequency Standards and Metrology Symposium Copper Mountain Col. (unpublished)

(69) Iffländer R, Werth G 1976 2nd Frequency Standards and Metrology Symposium Copper Mountain Col. (unpublished)

(70) Hellwig H 1970a Metrologia 6 56-60

(71) Walls F.L, Hellwig H 1976 Proc. of the 30th Annual Symp. on Freq. Control 473 80

(72) Townes C H and Schawlow A L 1955 Microwave Spectroscopy (New York: McGraw-Hill) pp 300-35

(73) Hellwig H (private communication)

(74) Ezekiel S and Weiss R 1968 Phys. Rev. Lett. 20 91-3

(75) Hackel L, Hackel R, Ezekiel S-1976 2nd Frequency Standards and Metrology Symposium Copper Mountain Col. (unpublished)

(76) Bergquist J.C, Lee SA, Hall J.L Phys. Rev. Letters 1977 38 159-162

(77) Barger R, West J, English T 1976 2nd Frequency Standards and Metrology Symposium Copper Mountain Col. (unpublished)

(78) Vasilenko L S, Chebotaev V P and Shishaev A V 1970 JETP Lett. 12 113-6

(79) Cagnac B, Grynberg G and Biraben F 1973 J. Physique 34 845-53

(80) Mattison E, Vessot R and Levine M 1976 2nd Frequency Standards and Metrology Symposium Copper Mountain Col. (unpublished)

(81) Audoin C (private communication)

(82) Strumia F (private communication)

(83) Hall J.L (private communication)

(84) Knight D, Edwards G, Blaney T 1976 2nd Frequency Standards and Metrology Symposium Copper Mountain Col. (unpublished)

(85) Kramer G 1976 2nd Frequency Standards and Metrology Symposium Copper Mountain Col. (unpublished)

(86) Evenson K M (private communication)

(87) Freed C Proc. 31^{rst} A. Symp. on Frequency Control USAEC Fort Monmouth N.J. p 592 (Electronic Industries Ass. Washington D.C.)

(88) Mc Guire M.D. Proc. 31^{rst} A. Symp. on Frequency Control USAEC Fort Monmouth N.J. p 612 (Electronic Industries Ass. Washington D.C.)

FIGURE CAPTIONS

Figure 1. The two basic versions of atomic frequency standards. The continuous paths apply to the passive mode, while the dotted paths apply to the active mode.

Figure 2. Block diagram of the phase lock loop commonly used to lock a crystal oscillator to a maser signal.

Figure 3. Block diagram of the frequency lock loop normally used to lock a crystal oscillator to the atomic resonance line.

Figure 4. Schematic diagram of a hydrogen maser.

Figure 5. Schematic diagram of the cesium beam tube used in passive cesium frequency standards and using the separated Ramsey cavity technique.

Figure 6. Schematic diagram of the optical package used in the passive rubidium 87 frequency standard. In some practical devices the isotopic filter is removed and natural rubidium is used in the storage cell. Mixtures of isotopes can be used in the lamp to reduce the light shift.

Figure 7. Time domain frequency stability of the three traditional frequency standards: H maser, Cs beam frequency standard and passive Rb gas cell. The stability of the methane stabilized laser is also shown for comparison.

Figure 8. Schematic diagram of the optical package of the Rb maser. This is similar to the diagram of figure 6 except for the detection of the resonance signal. Here the cavity Q is high enough to permit oscillation and the signal is detected with a superheterodyne receiver.

Figure 9. Passive rubidium beam frequency standard using optical pumping for state selection and detection.

Figure 10. Schematic diagram of a saturated absorption stabilized laser.

Figure 11. Basic concepts used in the stabilization of a laser with an atomic beam. (One version is shown and several other implementations can be thought of.)

TABLE I

PRINCIPLES OF OPERATION OF THE TRADITIONAL ATOMIC FREQUENCY STANDARDS

Frequency standards (Atomic ensemble)	Transition frequency (Hz)	Basic principles (Storage + interrogation	State selection (Preparation)	Detection system (Detection)	Atomic line Q	Main sources of frequency offset
Cs beam	9 192 631 770 by definition of the second	Passive Atomic beam Ramsey cavities	Magnetic deflection	Hot wire ionizer	7×10^6 to 3×10^8	Magnetic field Doppler (2nd order) Cavity phase shift
H maser	1 420 405 751.768 $\pm$ 0.002	Active maser Atomic beam Teflon coated storage cell	Magnetic deflection	Superheterodyne receiver 10^{-13} W	2×10^9	Magnetic field Doppler (2nd order) wall shift
Rb cell	6 834 682 612.8 $\pm$ 0.5	Passive Storage cell Buffer gas	Optical pumping	Silicon solar cell	5×10^7	Magnetic field Doppler (2nd order) Buffer gas and light shifts

TABLE 2

PRINCIPLES OF OPERATION OF WELL DOCUMENTED ATOMIC FREQUENCY STANDARDS

Frequency standards (Atomic ensemble)	Transition frequency (Hz)	Basic principles (Storage + interrogation)	State selection	Detection system (Detection)	Atomic line Q	Main sources of frequency offset
$^{15}NH_3$ maser	22 789 421 701 ± 1	Active maser Atomic beam Single passage in a cavity	Electrostatic deflection	Superheterodyne receiver 10^{-10} W	5×10^6	Collisions in an intense beam
Rb maser	^{87}Rb: 6 834 682 612.8 ± 0.5 ^{85}Rb: 3 035 732 439 ± 5	Active maser Storage cell buffer gas	Optical pumping	Superheterodyne receiver 10^{-10} W	5×10^7	Magnetic field Doppler (2nd order) Buffer gas and light shifts
^{87}Rb beam	6 834 682 612.8 ± 0.5	Passive Atomic beam Ramsey cavities	Optical pumping	Photomultiplier	6×10^6	Magnetic field Doppler (2nd order) Cavity phase shift
Tl beam	21 310 833 946.6 ± 0.2	Passive Atomic beam Ramsey cavities	Magnetic deflection	Oxidized hot wire ionizer	10^8	Magnetic field Doppler (2nd order) Cavity phase shift

TABLE 2 (cont'd)

PRINCIPLES OF OPERATION OF WELL DOCUMENTED ATOMIC FREQUENCY STANDARDS

Frequency standards (Atomic ensemble)	Transition frequency (Hz)	Basic principles (Storage + interrogation)	State selection	Detection system (Detection)	Atomic line Q	Main sources of frequency offset
Saturated absorption stabilized lasers	Iodine 127 R(127) 11-5 band, a component (473 612 214.1 ± 1.9) 10^6	Passive Saturated absorption in a storage cell	Not needed (Maxwell-Boltzmann law)	Silicon PIN Photodiode	2×10^8	At present: hyperfine structure or pressure shift
	Methane P(7)ν_3 band (88 376 181 627 ± 50) 10^3			InAs or cooled InSb detector	4×10^8 to 1.5×10^{10}	In future: wavefront curvature
	Carbon dioxide R(30) (29 442 483 315 ± 25) 10^3			Cooled InSb detector	5×10^7	Doppler (2nd order) Recoil effect

TABLE 3

PRINCIPLES OF OPERATION OF PROPOSED ATOMIC FREQUENCY STANDARDS

Proposed devices (Atomic ensemble)	Transition frequency (Hz)	Basic principles (Storage + interrogation)	State selection	Detection system (Detection)	Atomic line Q	Main sources of frequency offset
H beam tube	1 420 405 751.768 ± 0.002	Passive Atomic beam Ramsey cavities	Magnetic deflection	Penning gauge	10^6	Magnetic field Doppler (2nd order) Cavity phase shift
H beam storage	1 420 405 751.768 ± 0.002	Passive Atomic beam Teflon coated Storage cell	Magnetic deflection	Superheterodyne receiver	2×10^9	Magnetic field Doppler (2nd order) Wall shift
Silver beam	^{107}Ag: 1 712 512 111 ± 18 ^{109}Ag: 1 976 932 075 ± 17	Passive Atomic beam Ramsey cavities	Magnetic deflection	Electron bombardment ionizer	10^6	Magnetic field Doppler (2nd order) Cavity phase shift
Stored ^{199}Hg	40 507 348 050 ± 50	Passive Storage of ions in an electric field	Optical pumping	Photomultiplier	5×10^9	Magnetic field Light shift Doppler (2nd order).

TABLE 3 (cont'd)

PRINCIPLES OF OPERATION OF PROPOSED ATOMIC FREQUENCY STANDARDS

Proposed devices (Atomic ensemble)	Transition frequency (Hz)	Basic principles (Storage + interrogation)	State selection	Detection system (Detection)	Atomic line Q	Main sources of frequency offset
Calcium beam	$(1563.6) \times 10^9$	Passive Atomic beam Two interaction regions	Decay along the beam	Photomultiplier	10^9	Doppler effects
Magnesium beam	$(601.32) \times 10^9$	Passive Atomic beam Two interaction regions	Decay along the beam	Photomultiplier	10^9	Doppler effects residual 1st order and 2nd order
Caesium cell	9 192 631 770	Passive Storage cell Buffer gas	Optical pumping	Silicon solar cell	5×10^7	Magnetic field Doppler (2nd order) Buffer gas and light shifts
Cs maser	9 192 631 770	Active maser Storage cell Buffer gas	Optical pumping	Superheterodyne receiver	5×10^7	Magnetic field Doppler (2nd order) Buffer gas and light shifts
Atomic beam Stabilized Laser (Ca, Bi, I_2.)		Passive 2 Photon transitions Saturated absorption Ramsey Interaction Regions	Decay along the beam Magnetic selection	Hot wire detector Photomultiplier	$10^8 - 10^9$ (one interaction region)	Light shifts 2nd order Doppler effects

TABLE 4

TRADITIONAL ATOMIC FREQUENCY STANDARDS. STABILITY AND ACCURACY. STATE OF THE ART AND PROJECTION

Frequency Standard	Stability				Accuracy	
	Present		Projected		Present	Projected
	Short term	Flicker Floor	Short term	Flicker Floor		
Cs beam						
Laboratory type	$7 \times 10^{-14} \tau^{-\frac{1}{2}}$	7×10^{-15}	same	1×10^{-15} (3)	8×10^{-14}	10^{-14} (1)
Commercial (H.P.)	$5 \times 10^{-12} \tau^{-\frac{1}{2}}$	5×10^{-14}	----	----	7×10^{-12}	----
H maser	$4 \times 10^{-13} \tau^{-1}$	not observed	----	$< 10^{-15}$ (4)	2×10^{-12}	1×10^{-13} (2)
Rb gas cell	$5 \times 10^{-12} \tau^{-\frac{1}{2}}$	1×10^{-13}	$1 \times 10^{-12} \tau^{-\frac{1}{2}}$ (3)	1×10^{-14} (2)	----	----

TABLE 5

PROMISING ATOMIC FREQUENCY STANDARDS. STABILITY AND ACCURACY. STATE OF THE ART AND PROJECTION

Type of device	Stability				Accuracy	
	Present		Projected		Present	Projected
	Short term	Flicker Floor	Short term	Flicker Floor		
Saturated absorption stabilized Laser (I_2)	$2.5 \times 10^{-11} \tau^{-\frac{1}{2}}$	8×10^{-13}	$2.5 \times 10^{-12} \tau^{-\frac{1}{2}}$ (4)	----	$\sim 2 \times 10^{-12}$	----
(CH_4)	$3 \times 10^{-13} \tau^{-\frac{1}{2}}$	3×10^{-14}	----	----	10^{-11}	----
Mg, Ca beams	Projected $Q_\ell = 5 \times 10^9$		$10^{-14} \tau^{-\frac{1}{2}}$ (2)	----	----	10^{-14} (?)
Rb Maser	$1 \times 10^{-13} \tau^{-1}$	not observed	4×10^{-14} (3)	$\sim 10^{-14}$ (4)	----	----
Ion Storage (Hg, Ba)	Present $Q_\ell = 3 \times 10^9$ Projected $Q_\ell = 3 \times 10^{10}$		$3 \times 10^{-12} \tau^{-\frac{1}{2}}$ (1)	----	----	10^{-13} (1)
Atomic Beam stabilized Laser 2 photon absorption and separated Ramsey Interrogation Regions (Ca, Bi, I_2...)	5×10^{-12} for $\tau = 0.1$ S	Present $Q_\ell = 2 \times 10^8$: one interaction region Projected $Q_\ell = 10^{12}$: Ramsey interrogation technique (3)				
H Maser (passive)	$1.5 \times 10^{-12} \tau^{-\frac{1}{2}}$		$7 \times 10^{-13} \tau^{-\frac{1}{2}}$ (4)	$\sim 10^{-15}$ (3)	10^{-12}	10^{-13} (1)
NH_3 cell (passive)	$6 \times 10^{-10} \tau^{-\frac{1}{2}}$	2×10^{-10}	$1 \times 10^{-10} \tau^{-\frac{1}{2}}$ (3)	2×10^{-11} (3)	2×10^{-9}	5×10^{-10} (2)

FL 2827
WSMC/PMET TECHNICAL LIBRARY
VANDENBERG AFB CA 93437-6021

should expect results soon (82). Finally the two photon absorption technique coupled with the separated Ramsey interrogation technique appears to be extremely promising. In fact a line Q of the order of 10^{12} is projected and appears realistic (83). These projections are summarized in table 5 along with projections on some other devices which were examined in this paper.

Frequency synthesis.

As was mentioned earlier, stabilized lasers form a class by themselves which has no easy connection with the traditional frequency standards such as the Cs beam frequency standards. Until reliable synthesis, up to the frequencies encountered in the laser stabilization field, becomes a common laboratory technique, a gap will exist between the traditional standards and the stabilized lasers, and these last devices will have limited use. However research on this subject is being done in some laboratories. (84, 85). Presently it is possible through the use of several lasers and point contact metal diodes, to mix up and synthesize frequencies up to a corresponding wavelenght of 1.5 μ. (86) However, this still remains somewhat of an art and intensive work is required in this direction if substantial results are wanted.

ATOMIC FREQUENCY STANDARDS : BASIC PRINCIPLE

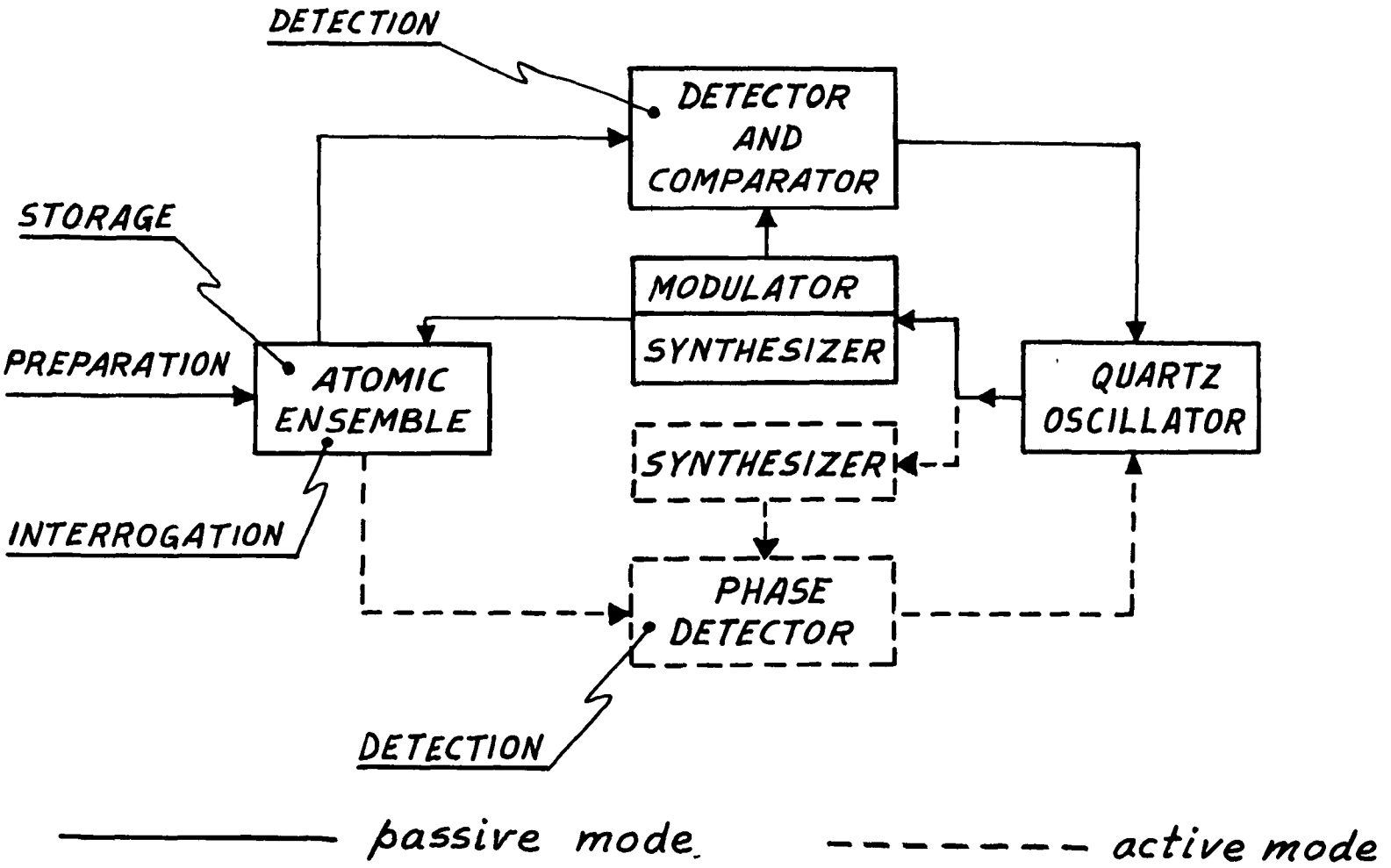


FIGURE 1

ACTIVE CRYSTAL OSCILLATOR MASER PHASE LOCK LOOP

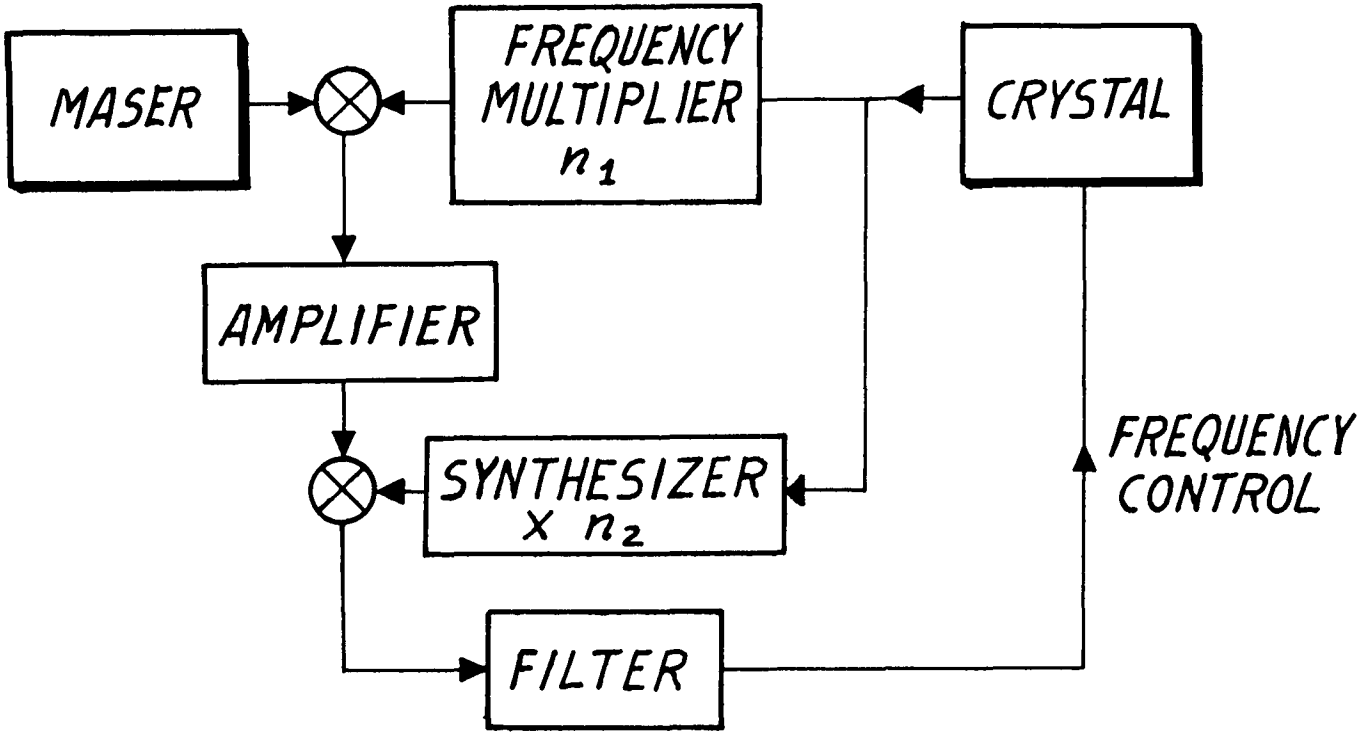


FIGURE 2

CRYSTAL OSCILLATOR PASSIVE REFERENCE FREQUENCY LOCK LOOP

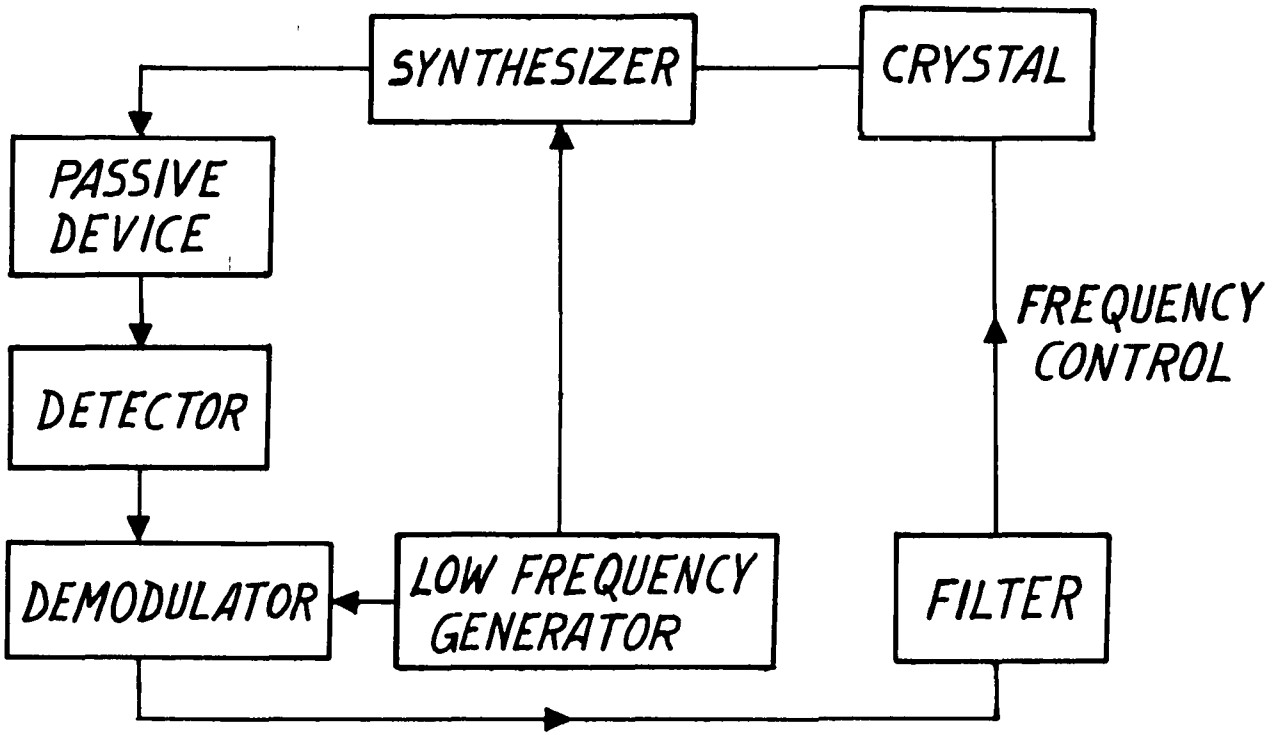


FIGURE 3

H MASER

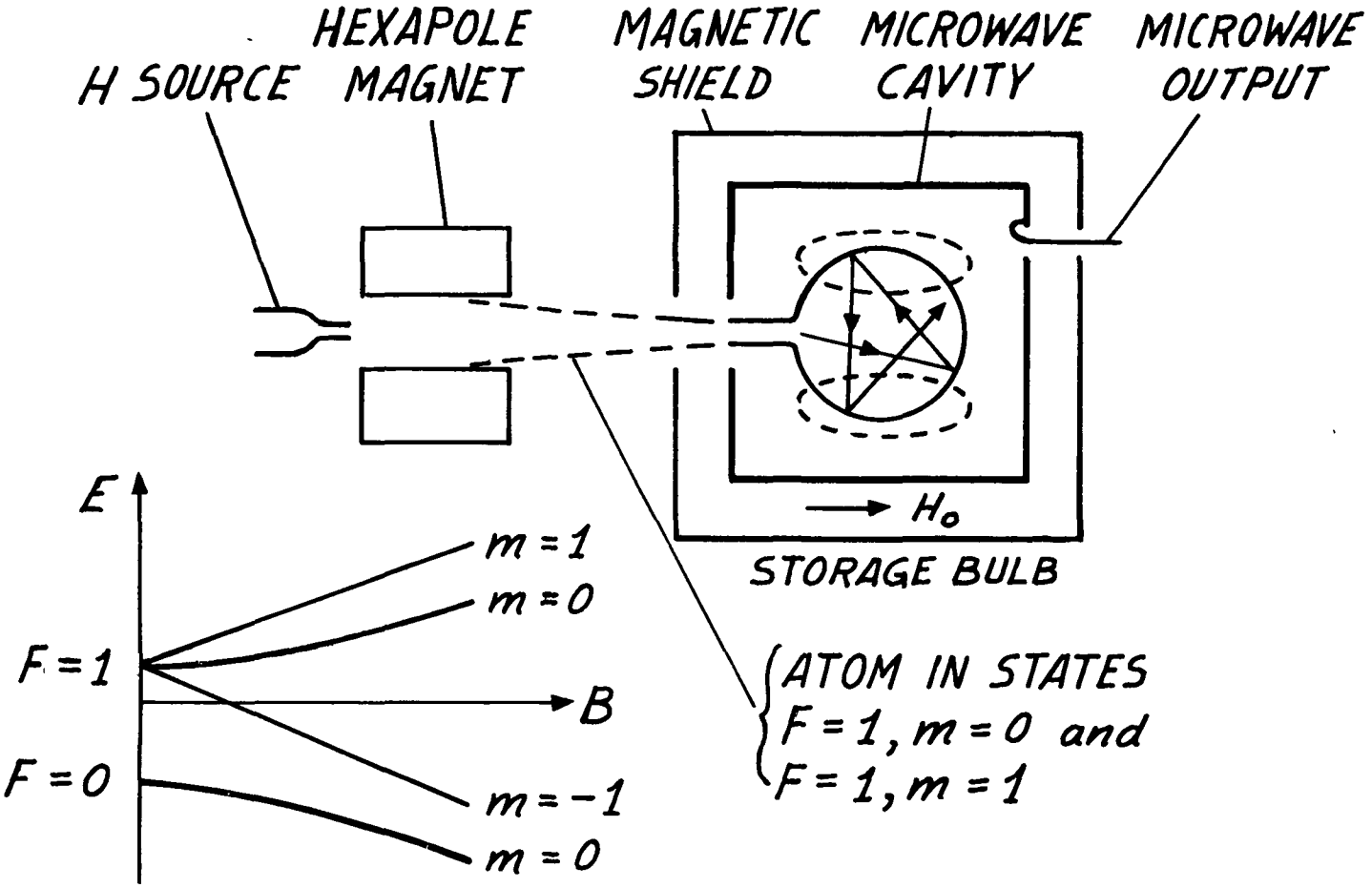
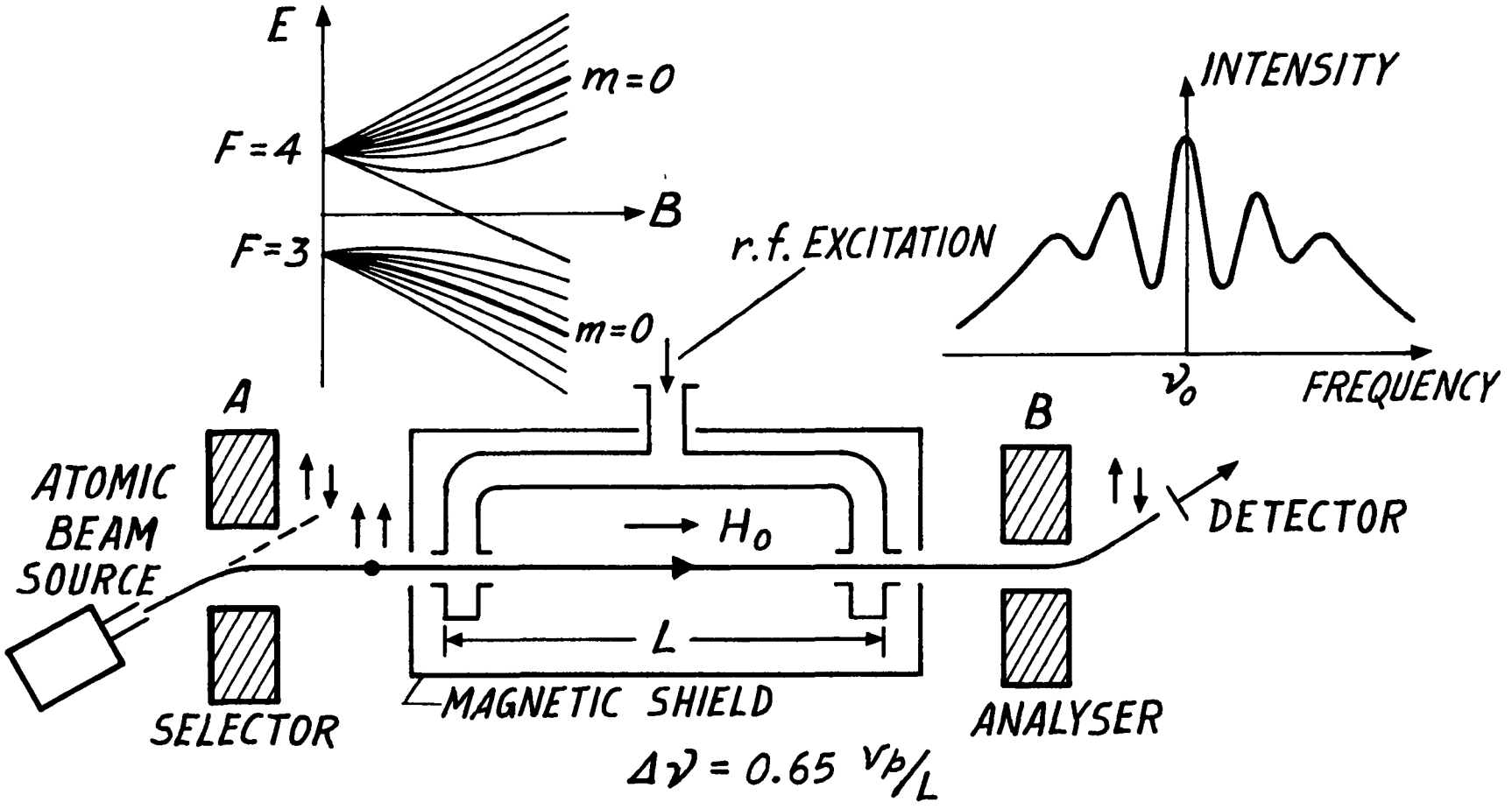


FIGURE 4



PASSIVE CESIUM BEAM FREQUENCY STANDARD

FIGURE 5

PASSIVE RUBIDIUM GAS CELL FREQUENCY STANDARD

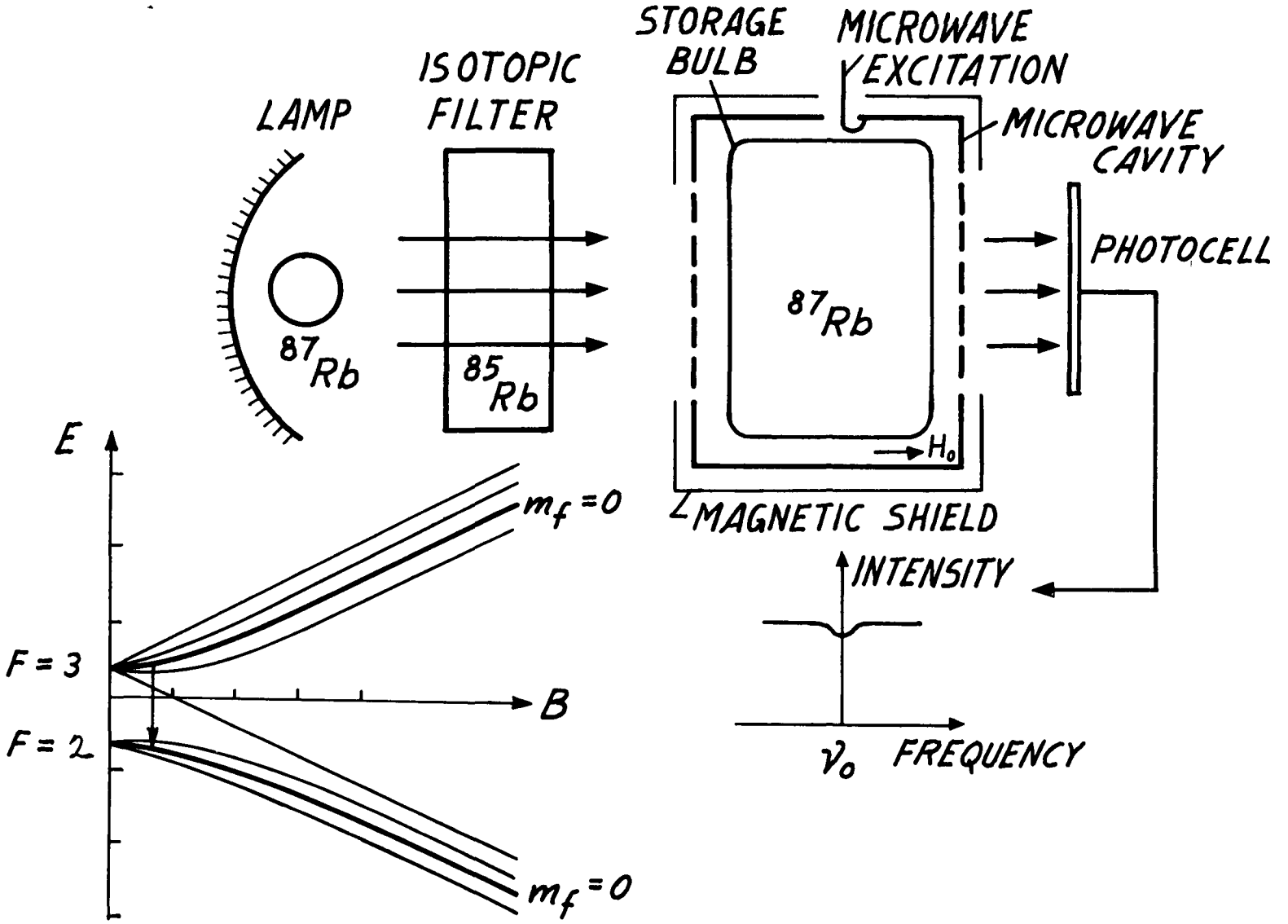
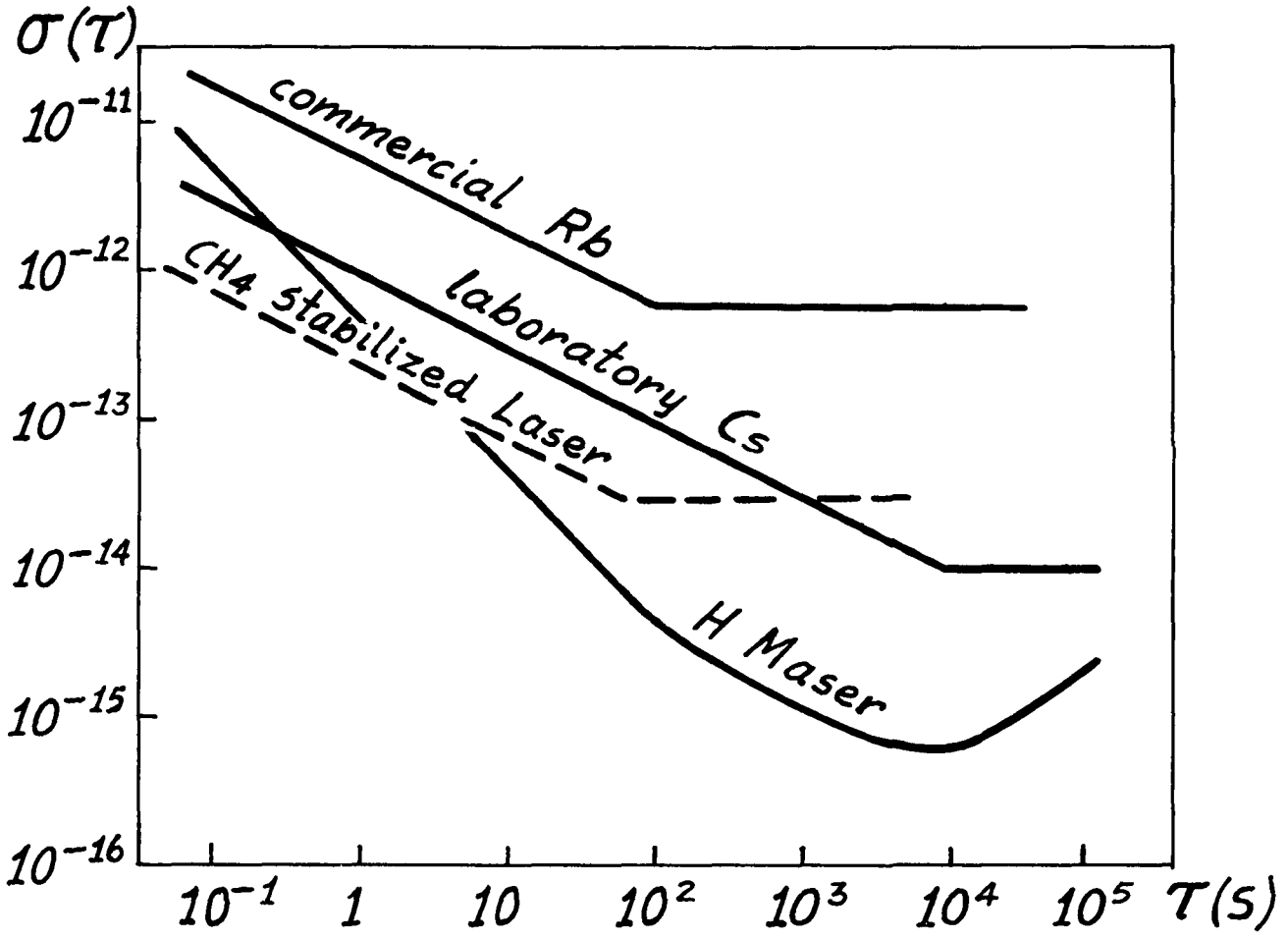


FIGURE 6



STABILITY OF ATOMIC FREQUENCY STANDARDS.

FIGURE 7

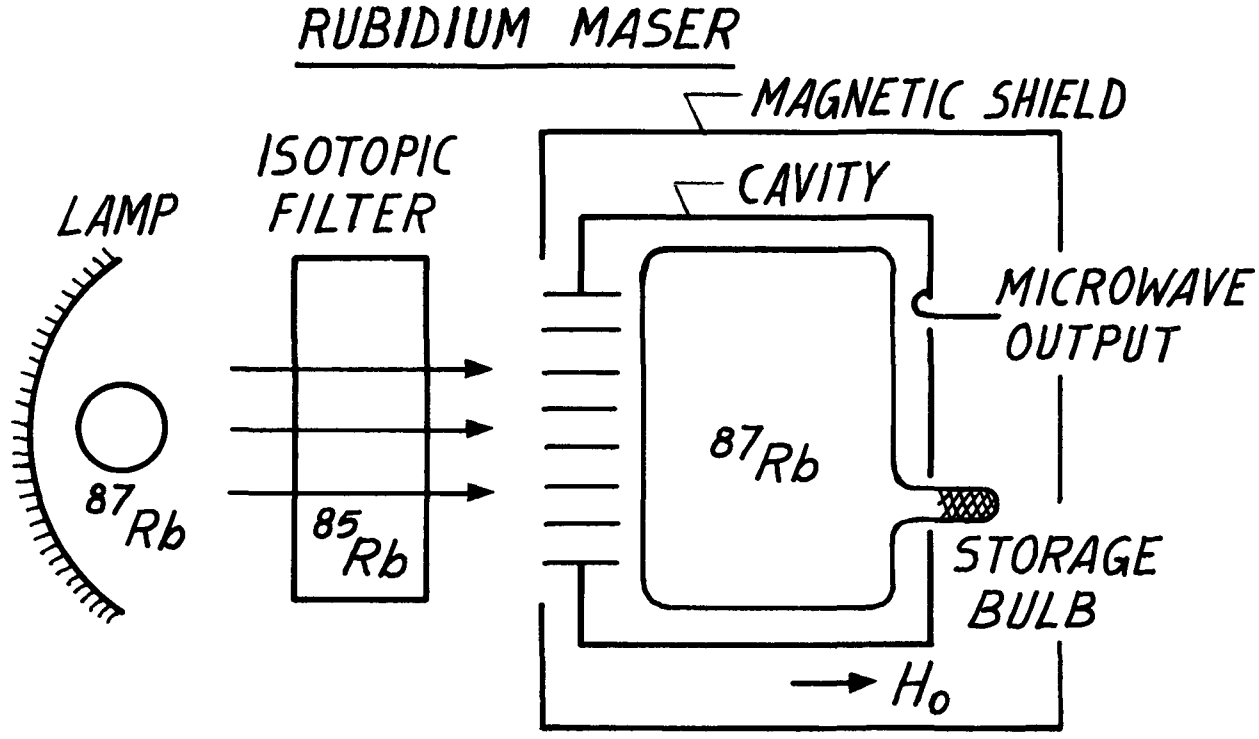

RUBIDIUM MASER
MAGNETIC SHIELD
ISOTOPIC FILTER
CAVITY
LAMP
MICROWAVE OUTPUT
87Rb
85Rb
87Rb
STORAGE BULB
Ho

FIGURE 8

PASSIVE RUBIDIUM ATOMIC BEAM FREQUENCY STANDARD
(optically pumped)

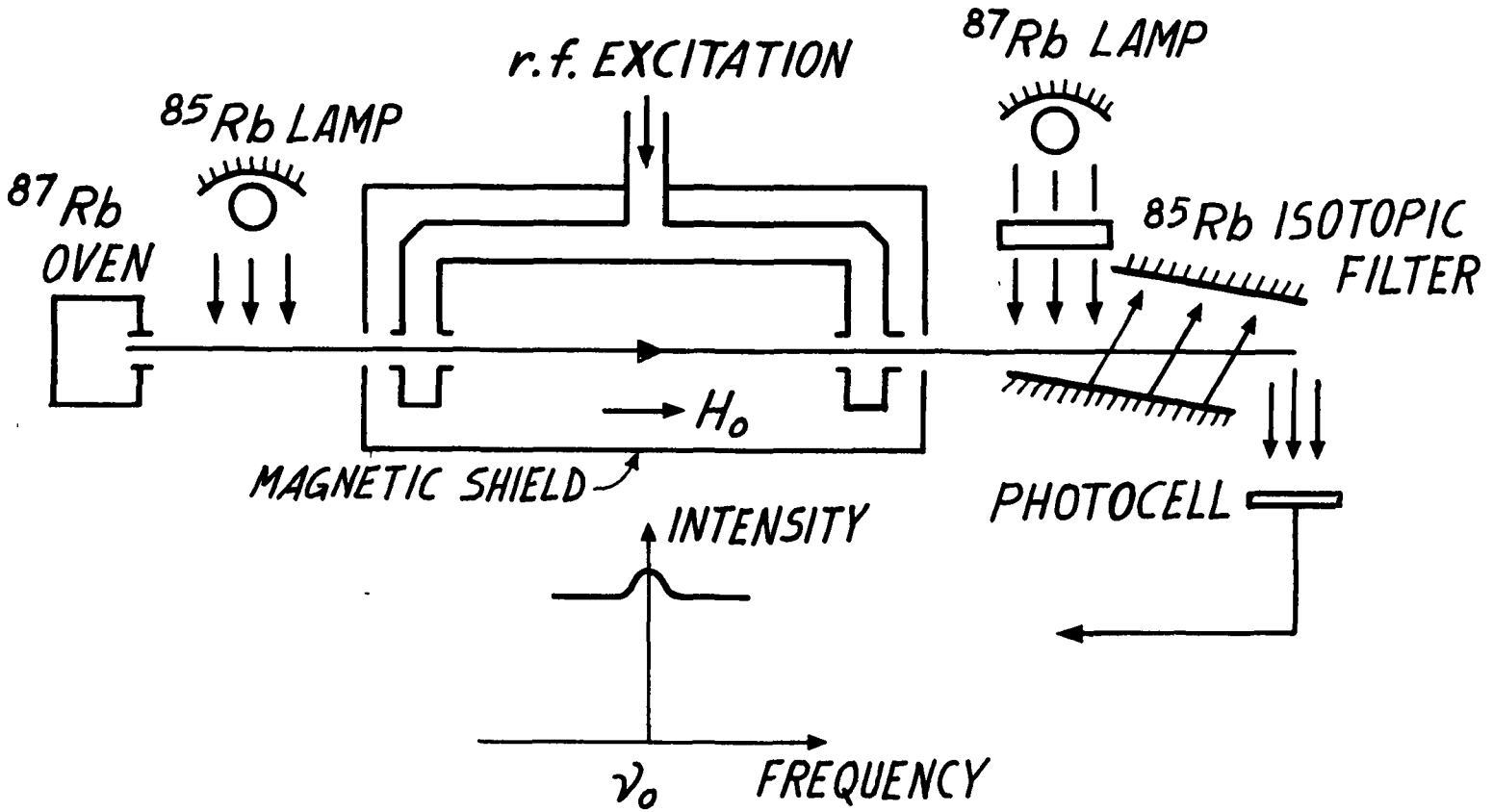


FIGURE 9

SATURATED ABSORPTION STABILIZED LASER

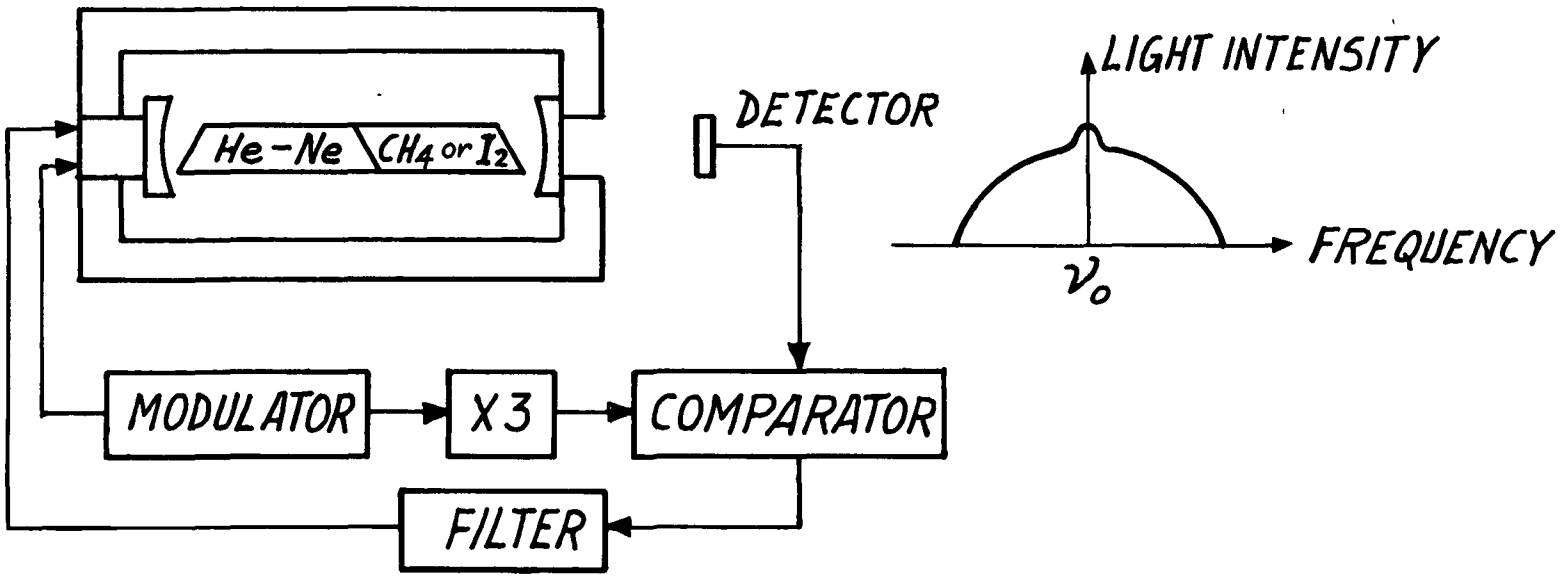


FIGURE 10

ATOMIC BEAM STABILIZED LASER (one version)

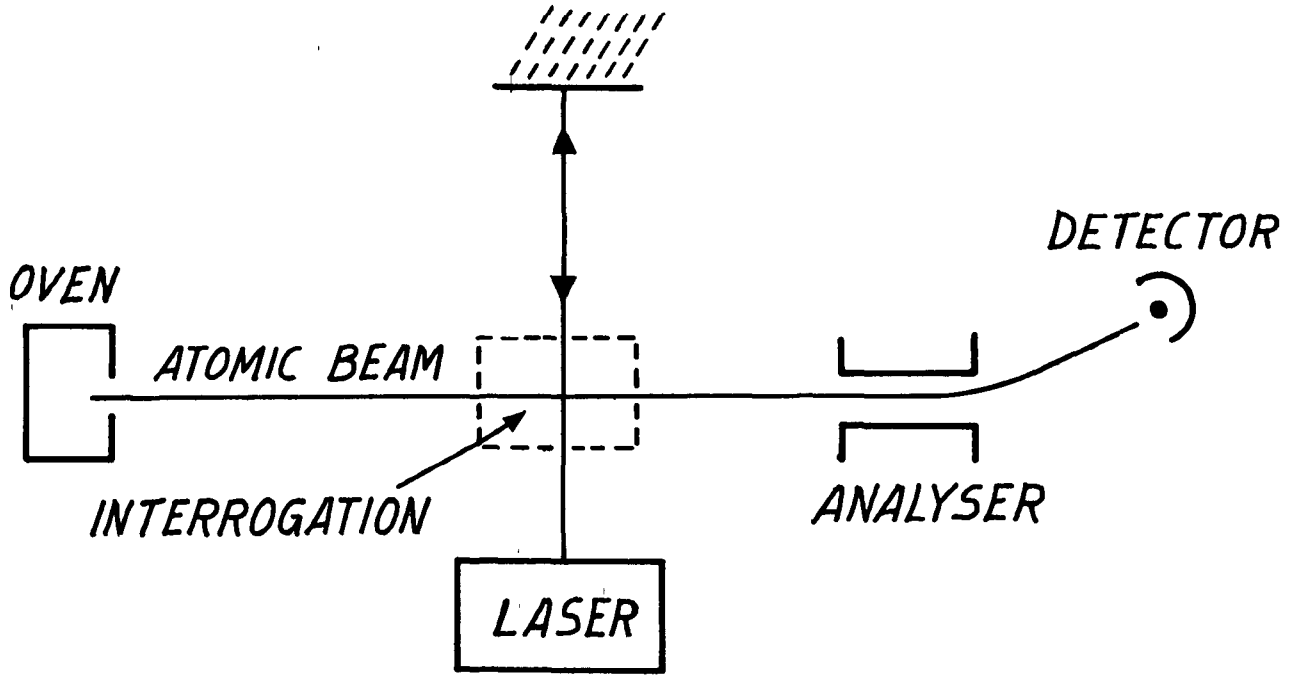


FIGURE 11

Page intentionally left blank

Page intentionally left blank

CRITERIA FOR THE SELECTION OF ATOMIC CLOCKS IN SYSTEMS APPLICATIONS

Gernot M. R. Winkler
U. S. Naval Observatory
Washington, DC

ABSTRACT

Increasing numbers of time ordered electronic systems envision the use of atomic clocks as their central or remote station time-frequency (T/F) reference. The selection of one of the commercially available devices is not often a clear and simple matter but requires a good compromise between performance (given as spectral purity of the output signal or as frequency stability in one of the accepted measures), environmental sensitivity (magnetic field, temperature, pressure, etc.), reliability, maintenance requirements and price. After a brief discussion of the fundamental concepts, as pertinent, the specifications of the different types of clocks will be reviewed and examples for actual selection and rationales discussed.

LITERATURE

Hellwig, H., "Frequency Standards and Clocks", NBS TN 616, March 1974.

Hellwig, H., "A Review of Precision Oscillators", NBS TN 662, February 1975.

CCIR Study Group VII Document Number US - 7/107, 1978.

(Informal Remarks – Paper not Published)

Page intentionally left blank

Page intentionally left blank

A REVIEW OF METHODS OF ANALYZING FREQUENCY STABILITY

James A. Barnes

ABSTRACT

Extensive research over the past years has provided a model for the description of frequency instabilities of clocks and oscillators. This model consists of the superposition of three distinct parts: (1) random, non-deterministic fluctuations described as noise; (2) long-term, systematic trends or aging; and (3) fluctuations induced by environmental sensitivities of the oscillator or clock. The random part of the model includes noises which have presented certain mathematical problems. These mathematical problems are partly responsible for the creation of numerous techniques of analysis, but these techniques have neither produced substantively new models nor have they added insight into the physical origins of the random fluctuations--some of which remain obscure. The purpose of the measurement process is to estimate the levels and kinds of instabilities present in a given device--that is, to quantify the model. The mathematical analysis used is merely a means toward this end, and it is important to retain this perspective. Fortunately, there are relatively simple means of analysis which are also commonly used--the two-sample variance and the power spectral density.

Crucial to any measurement are the intended uses of the result. This includes the levels of accuracy and precision needed, as well as the intended application. For example, one may wish only a relative comparison between two oscillators; and, thus, absolute accuracy (as opposed to precision) is of no interest. The specific application intended for the measurement will often influence the form in which the final quantified model is reported.

I. INTRODUCTION

It appears to be a custom, nowadays, to have a paper reviewing the concepts of the measurement of frequency stability at conferences dealing with time and frequency. Consistent with this trend, this paper has been prepared at the request of the program committee.

Perhaps one of the most useful aspects of review papers is to provide an entrance into the literature of the field being reviewed. In the case of frequency stability, there is really a great deal published; and it is with some difficulty, now, that anything new can be added--especially in review papers. In order to provide entrance into the literature, four specific papers are cited here. The first two reasonably cover the technical subject prior to about 1973. The next two papers are excellent review papers on the subject and are more current:

[1] Barnes et al., "Characterization of Frequency Stability," IEEE Trans. on I&M, Vol. IM-20, No. 2, May 1971, pp. 105-120.

[2] Lesage and Audoin, "Estimation of the Two-Sample Variance with a Limited Number of Data," Proceedings of the 31st Annual Symposium on Frequency Control, 1977, pp. 311-318.

[3] Rutman, "Oscillator Specifications: A Review of Classical and New Ideas," Proceedings of the 31st Annual Symposium on Frequency Control, June 1977, pp. 291-301.

[4] Winkler, "A Brief Review of Frequency Stability Measures," Proceedings of the 8th Annual Precise Time and Time Interval (PTTI) Applications and Planning Meeting, Nov. 1976, pp. 489-527.

Not only are the last two excellent review papers, but they also provide rather extensive bibliographies covering the more important publications in the field.

The present paper attempts (in a rather tutorial vein) to review the subject of frequency stability mainly from the viewpoint of Operations Research (OR), with the hope of developing an intuitive understanding of the concepts and operations. Those who prefer the more mathematical approach are referred to the above-cited references. Thus, it is by intent that detailed mathematical calculations are avoided as far as possible in this paper.

II. MEASUREMENT AS AN OPERATION

Figure 1 is a somewhat simplified diagram of measurement operations. In any measurement, one begins with some idea about what one wants to measure. That is, one has a <u>model</u> in mind.

In the case of a measurement of the acceleration due to gravity, for example, one assumes Newton's laws and assumes that g is reasonably constant. In the case of a voltage measurement, as another example, one assumes that a volt meter will not unduly load the source and that the meter covers the range of expected voltages. All of these underlying assumptions are part of the modeling process, and it is important not only to make the assumptions but also to document them.

In the case of frequency fluctuations of clocks and oscillators, rather comprehensive models already exist and are discussed below to some significant extent. Thus, it is not necessary to invent new models to begin the measurement process--they are already well documented. On the other hand, a researcher might be able to improve our understanding substantially with new models, but research is often a separate field from straightforward measurements. The emphasis of this paper is to review present measurements and not to discuss the opportunities for research to produce or evaluate new models.

Based on the model assumed and the equipment available, one designs an experiment to evaluate the model. If the experimenter is wise, he will also design his analysis of the data at the beginning.

If one is performing a measurement, there is some aspect of the model which is unknown. In the above-mentioned example, concerning the measurement of the acceleration due to gravity, the parameter g of the equation $S = 1/2\ gt^2$ was to be determined by experiment. It was assumed that the object accelerated uniformly, and only the constant g was to be determined. That is, g was an undetermined parameter of the model.

In the case of the measurement of frequency fluctuations, the typical models consist (among other things) of the superposition of several different noises. The levels of each of these noises are not normally known in advance. That is, the noise levels are undetermined parameters to be estimated in the measurement operation.

This leads us to what I think is an important definition: A measurement is an operation designed to estimate the numerical value of a model parameter. Thus, without a model, no meaningful measurment is possible. Given a model, many measurements often suggest themselves. For example, when Newton suggested that every particle in the universe attracts every other particle in the universe with a force that is proportional to etc., etc., one can immediately set about measuring that constant of proportionality, big-G. Without the model, the experiments don't make sense.

Based on the experimental design, one next actually performs the experiment and obtains data. The data are subjected to the analysis routines which had been previously designed, and the unknown parameters of the model are "fitted" to the results. One typically designs test experiments to verify the functioning of the equipment and to ensure that

one is actually fitting parameters to the oscillator being measured and not the measuring system. For example, if the noise level of the measuring system is higher than that of the oscillators under test, one might get good model fits to the data; however, the results will not be applicable to the oscillator but rather to the measurement system.

It is at this point that the researcher and the engineer part company. The researcher into frequency fluctuations will be interested in perfecting and refining the models or gaining insight into more fundamental models. The specific levels of noise might not be of particular interest to him, but rather the adequacy of the model in reflecting "reality might be more important. For example, he might be interested in whether other models might provide a better fit. On the other hand, the engineer who just wanted to know how bad the oscillator was in order to decide whether or not it was useful in his particular application has his measurement, and he can leave the operations of Figure 1.

Fortunately, researchers have produced some rather comprehensive and useful models which seem quite adequate to describe present-day oscillators rather completely. This is a sign of a mature field of study. Even though the physical origins of some of the noise components of oscillator models remain obscure, one really doesn't expect significant revisions in the models themselves. We may gain added insight into their origins or get small refinements; but, overall, no great changes are expected in the mathematical form of the models.

III. MODELS OF FREQUENCY FLUCTUATIONS

The conventional models [1] of an oscillator begin by assuming that the output signal, V(t), is approximately sinusoidal and can be represented by the equation

$$V(t) = [V_0 + \varepsilon(t)] \sin \Phi(t) \qquad (1)$$

where V_0 is the nominal (constant) amplitude; $\varepsilon(t)$ represents the fluctuations in amplitude; and $\Phi(t)$ is the instantaneous phase of the oscillator. In particular, the phase is assumed to be represented in the form

$$\Phi(t) = 2\pi\nu_0 t + \phi(t), \qquad (2)$$

where ν_0 is the nominal frequency of the oscillator and $\phi(t)$ represents the instantaneous phase deviation from the nominal phase, $2\pi\nu_0 t$.

For the sake of completeness and utility, it should be noted that there are certain restrictions on eq. (1) and (2). Stated in a qualitative way, these restrictions are (a) that the fluctuations in amplitude, $\varepsilon(t)$, are small compared to the nominal amplitude, V_o; and (b) that the fluctuations in instantaneous frequency, $\frac{1}{2\pi}\frac{d\phi}{dt}$, are small compared to the nominal frequency, ν_o. Mathematically, these can be expressed in the form

$$\varepsilon(t) << V_o,$$

$$\frac{1}{2\pi}\frac{d\phi(t)}{dt} << \nu_o.$$

Normally, high-quality oscillators easily meet these conditions.

It is of value, also, to introduce certain terms which are commonly used throughout the literature on frequency stability. The instantaneous (angular) frequency of an oscillator is defined to be the time rate of change of the phase. Expressed as a cycle frequency, $\nu(t)$,

$$\nu(t) \equiv \frac{1}{2\pi}\frac{d}{dt}\Phi(t), \qquad (4)$$

where $\nu(r)$ is expressed in Hertz.

Also, the instantaneous, fractional frequency fluctuations about the nominal are commonly defined by the expression [1]

$$y(t) \equiv \frac{1}{2\pi\nu_o}\frac{d\phi(t)}{dt}\ ; \qquad (5)$$

which, with the aid of equations (2) and (4) can be expressed in the form

$$y(t) \approx \frac{\nu(\tau) - \nu_o}{\nu_o} \qquad (6)$$

Most models are concerned with the quantity y(t). Occasionally, however, one sees in the literature the time error, x(t), being used. This quantity, x(t) is defined by the relation

$$x(t) \equiv \frac{1}{2\pi\nu_o}\phi(t), \qquad (7)$$

and clearly satisfies the relation

$$y(t) = \frac{dx(t)}{dt} . \qquad (8)$$

In words, $x(t)$ is the instantaneous time error of a clock run from the oscillator. It is thus expected that frequency stability measurements will be concerned with various statistical functions of both $x(t)$ and $y(t)$ such as power spectral densities, e.g., $S_y(f)$.

The conventional model used to describe frequency fluctuations, $y(t)$, has three main subdivisions (see table 1): (1) random, non-deterministic fluctuations described as noise; (2) long-term, systematic trends or aging; and (3) fluctuations induced by environmental sensitivities of the oscillator or clock.

The treatment of environmental sensitivities is a rather special case and (although extremely important) will not be covered here. In general, one wants to minimize environmental sensitivities. The separation of environmentally induced fluctuations from intrinsic fluctuations is normally done by correlation techniques. Toward this end the transfer function models of Box & Jenkins [5] are of value.

The treatment of systematic trends is often given short shrift. In principle, a linear drift in frequency of an oscillator with time can be measured with arbitrarily high accuracy. In practice, however, one might not have the time to evaluate the model parameter with sufficient accuracy to relegate it to the status of an adequately well-known constant. This is especially true when one realizes that the random parts of the model disturb the accuracy with which the systematic parts can be determined, and that an error in the frequency drift term, for example, becomes a quadratic error with running time in the indicated time (or phase) of a clock. Indeed, when one is attempting to predict clock performance for the future, errors in estimating the systematic terms almost always predominate for very long prediction intervals (months to years). Percival [15] has proposed using prediction errors directly as a measure of frequency stability because the important contribution of the systematic terms is automatically incorporated.

The random, non-deterministic parts of the model have received a great deal of attention with primary emphasis on the continuous, Gaussian elements.

Generally, experiments have revealed five different noise types that might be needed to model an oscillator. Typically, only two or three of the terms are necessary to describe the noise elements of an individual oscillator over a large range of time intervals. The five terms of the Gaussian noise elements listed in table 1 have names and are listed in table 2.

The sporadic elements constitute a special problem. The objective documentation of their existence is limited [7,8], and no clear consensus exists on how to handle them [4,6,8]. However, it does appear, in general, that no great errors are committed if one simply ignores these elements entirely. The reasons behind this are twofold. First, the step sizes are normally small (of the order of other noises); and second, they tend to be infrequent (perhaps less than once per day). For the remainder of this paper, the sporadic elements will be ignored--a subject more appropriate to research on oscillator models than to practical measurements of frequency stability. It is acknowledged, however, that in some applications the sporadic parts could be quite important.

III. EXPERIMENT AND ANALYSIS

To this point in the paper everything has been reasonably straightforward and without much controversy. Indeed, there is amazing consensus on the model elements. In the areas of analysis and (to a lesser extent) experimentation, there is not such close agreement. One can find numerous analytical techniques designed to fit the model parameters (noise levels, drift rate, etc.) to the data.

Each of the analytical techniques has its own advantages. Typically, these advantages either favor a certain method of analysis of the data as derived from special equipment (e.g., frequency counters or spectrum analyzers), or they have the value of being useful for richer models than those considered here. (For example, if one were to consider a model with a frequency spectral density ($S_y(f)$) varying as $|f|^{\alpha}$ for $\alpha < -3$, then very special analysis techniques would be needed. However, such models are almost never needed in practice.)

There are two general considerations which should guide the design of the experiments and the analysis. Basically, these two considerations are (a) the resources available and (b) the intended use of the results.

The resources available which limit the measurements include equipment, mathematical and computational sophistication, and time. In the absence of elaborate equipment it may well be necessary to fill in with more mathematical and computational skills. Time constraints limit both the precision and range of the results and hence the range over which a model can be verified.

The intended use of the results is equally important. For example, if an experimenter has a requirement for an oscillator to remain stable in frequency to, say, a part in 10^6 for sample times from 1 to 10 seconds, and he discovers that his oscillator is, say, about 100 times better than this, then that experimenter would be foolish to pursue his measurements to a 1 percent accuracy tolerance--he can be sure that it's adequate with a very rough experiment. Also, of course, one has greater confidence in results which require less mathematical manipulation. Thus,

one gains in designing experiments which come closest to reflecting the intended use of the oscillator or clock when that use is known.

In the absence of overriding reasons to choose one analytical technique or data-acquisition system over another, it clearly makes sense to choose the simplest and easiest. Of course, with the simpler techniques there are fewer opportunities for errors, and one can obtain reasonable confidence in a short period of time. In keeping with the above, this paper is confined to two analytical techniques as recommended in [1]: the power spectral density of the fractional frequency fluctuations, $S_y(f)$, and the two-sample variance, $\sigma_y^2(\tau)$. (The two-sample variance is sometimes referred to as the "Allan variance." Certainly there are values in other techniques, but they are adequately covered in the literature and will not be covered here. In particular, Rutman [3] provides an especially lucid comparison of the various analytical techniques.

Power Spectral Density of y(t)

Since the noise models suggested above were expressed directly in terms of the spectral density, $S_y(f)$, of the fractional frequency fluctuations, y(t), an obvious approach is to estimate directly $S_y(f)$. This is typically done either with analog techniques or by sampling y(t) at regular intervals and converting to a spectral density with the aid of a computer [9]. Systems also exist which perform the sampling automatically and convert to spectral estimates without the need to transfer the data to a computer.

Of course, the spectral estimates will not automatically be provided in the same form as the model elements given in Tables 1 and 2. One must "fit" the parameters or noise levels to, say, a graphical representation of the spectral density. In such a display, the periodic elements of the model are revealed in an especially lucid form. The presence of the other systematic elements, however, is not so obvious and will probably require special treatment to resolve.

With any of the measurement schemes there is often a problem in obtaining reliable values of y(t) or an analog signal of y(t) not contaminated by the noise of associated circuitry. For very high-quality signal sources this is a major problem. Often one takes two or more comparable oscillators and "beats" their signals together to obtain the difference frequency between the two oscillators. This difference signal can be amplified and analyzed by fairly conventional techniques provided this difference signal also satisfies the constraints of (3), above. However, the data are representative of both oscillators, and one must make some model assumptions about how to divide the results between the two oscillators. If three oscillators are intercompared in all possible combinations, one can make a statistical separation of the results if one makes use of a model assumption that the fluctuations of each oscillator are

statistically uncorrelated with the others [10]. Various techniques for acquiring data on very stable oscillators have been devised and can be found in the literature [11,12,13].

Two-Sample Variance, $\sigma_y^2(\tau)$

One of the most common ways of acquiring frequency data is by means of a frequency counter which totals the number of cycles, n, of the signal in a specified interval of time, τ. The sample frequency is then just n/τ, and large volumes of data are easily generated.

The quantity n/τ can be related to y(t) by some straightforward mathematical manipulation. One can define the average fractional frequency, $\bar{y}_k$, over the interval t_k to $t_k + \tau$ by the relation

$$\bar{y}_k \equiv \frac{1}{\tau} \int_{t_k}^{t_k+\tau} y(t)dt. \tag{9}$$

where $t_{k+1} = t_k + T$, and T is the interval between the beginnings of successive averages. With the aid of (4) and (6) this can be written in the form

$$\begin{aligned} y_k &= \frac{1}{\tau} \int_{t_k}^{t_k+\tau} \frac{\nu(t) - \nu_o}{\nu_o} \, dt \\ &= \frac{1}{2\pi\nu_o\tau} \int_{t_k}^{t_k+\tau} \frac{d\Phi}{dt} \, dt - 1 \\ &= \frac{1}{\nu_o\tau} \left[\frac{\Phi(\tau_k+\tau) - \Phi(\tau_k)}{2\pi} \right] - 1. \end{aligned} \tag{10}$$

However, the quantity in the brackets is just the accumulated phase (in radians) during the interval, divided by 2π. That is, it is the number of cycles, n_k. Thus, (10) becomes

$$\bar{y}_k = \frac{1}{\nu_o} \cdot \frac{n_k}{\tau} - 1, \tag{11}$$

and n_k is just the k-th counter reading.

At this point one might be tempted to do some simple and conventional statistics on the $\bar{y}_k$. For example, one might compute a mean and a variance for the set or perform a linear regression. However, this is fraught with difficulty. The problem arises from the model elements of $S_y(f)$ which are proportional to $|f|^{-1}$ and $|f|^{-2}$; that is, flicker frequency noise and random walk frequency noise. These types of noise do not have convergent variances. That is, as more and more data are taken and the variance is estimated with more and more data, the variance itself grows, seemingly without bound.*

Clearly, some other statistical tool is necessary to analyze the data for practical applications. Since the problem arises with adding too much data to the variance estimate, the obvious solution is administratively to limit the data used for each estimate and then average all of the individual estimates. By convention the data limit has been taken at only two values of $\bar{y}_k$ for each variance estimate [1]. In order to gain confidence in this estimate, one averages many estimates of the variance. Lesage and Audoin [2] have derived expressions for the confidence intervals for the estimates of the two-sample variance estimated in this way for the model elements listed in Table 2.

It is of value to explicitly state the computations involved with the two-sample variance. Normally, statisticians estimate a mean of a set of N values of a random variable, u_i, by the equation

$$\bar{u} = \frac{1}{N} \sum_{i=1}^{N} u_i . \tag{12}$$

The variance, σ^2, is estimated by the equation

$$\sigma^2 = \frac{1}{N-1} \sum_{i=1}^{N} (u_i - \bar{u})^2 . \tag{13}$$

For the case N = 2, equations (12) and (13) can be combined in the simple form

$$\sigma^2(N = 2) = \frac{(u_2 - u_1)^2}{2} . \tag{14}$$

*One is not suggesting here that the frequency fluctuations of real devices are actually unbounded. Rather, in a practical sense one is unlikely to have the time (perhaps many, many years) to take enough data to see convergence in fact. See ref. [8].

At this point, we can define the two-sample variance, $\sigma_y^2(\tau)$, as the (infinite) average of estimates of the variance for two samples. That is, mathematically,

$$\sigma_y^2(\tau) = \lim_{m \to \infty} \frac{1}{m-1} \sum_{k=1}^{m-1} \frac{(\bar{y}_{k+1} - \bar{y}_k)^2}{2} . \qquad (15)$$

In practice, of course, one estimates $\sigma_y^2(\tau)$ from a finite set of m values of $\bar{y}_k$ and cannot pass to the limit.

An additional restriction must be added. In equation (9), above, $\bar{y}_k$ was the average from t_k to $t_k + \tau$, but the next average began at $t_{k+1} = t_k + T$. The two-sample variance, $\sigma_y^2(\tau)$, is defined to be restricted to those cases for which $T = \tau$. That is, in words, each sample of $\bar{y}_k$ must be exactly adjacent in time to $\bar{y}_{k+1}$ with no "dead time" between measurements. There are times when this condition is difficult to meet, and corrections must be made. Again, for the model elements of Table 2, the corrections can be found in the literature [14].

A final point on $\sigma_y^2(\tau)$ is to note that there is a bandwidth, f_h, to the measuring system, and this can influence the results. Again, it is a matter of convention to specify f_h with the measurement and to require $2\pi f_h \tau >> 1$ for all measurements.

In practice one can determine a set of $\bar{y}_k$-values, each of which is an average of the fractional frequency fluctuations from nominal. One can then form an estimate, $\hat{\sigma}_y^2(\tau)$, of $\sigma_y^2(\tau)$ with the equation

$$\hat{\sigma}_y^2(\tau) = \frac{1}{m-1} \sum_{k=1}^{m-1} \frac{(\bar{y}_{k+1} - \bar{y}_k)^2}{2} . \qquad (16)$$

For $\tau' = 2\tau$, one can average adjacent values of $\bar{y}_k$ and obtain a new list, $\bar{y}_k'$, where

$$\bar{y}_k' = \frac{\bar{y}_{2k} + \bar{y}_{2k-1}}{2} \qquad (17)$$

and hence determine $\hat{\sigma}_y^2(2\tau)$ based on $m' = \frac{m}{2}$ values.

This process can be repeated for integer multiples of τ out to half of the total data length.

It is then normal to plot $\sqrt{\hat{\sigma}_y^2(\tau)}$ versus τ on log-log graph paper. Typically, regions of the plot can be approximated with straight line segments (see Fig. 2). Since straight lines on log-log paper can be represented by equations of the form $\sigma_y^2(\tau) = A\tau^{\mu}$, one is fitting this form of a model to the $\sigma_y^2(\tau)$ estimates. However, this is essentially equivalent to the models of Table 2 [1]. In fact, Table 3 shows that the models of Table 2 translate into $\sigma_y^2(\tau)$ values varying as τ to some power. With the aid of Table 3, then one can estimate the levels, h_α, of the various noise terms; and, with the aid of the uncertainties listed, obtain confidence intervals for the $\sigma_y(\tau)$ estimates plotted. Thus, the analysis by the use of the two-sample variance allows one to quantify the model parameters (i.e., to measure the stability of the oscillator) and evaluate the adequacy of the model fit.

Although the two-sample variance has required a fair amount of space to explain here, it is really one of the easiest analysis techniques to use. Probably for this reason it is one of the most common techniques used, also. The price one pays for this ease in analysis is some loss in confidence in the results. If one is interested in the spectrum of the frequency fluctuations, then it is probably true that direct spectral estimates are slightly more precise for the measurement process than the two-sample variance, but often this is not a critical issue. Often, "final" results are simply reported as values of the two-sample variance or its square root, since they can be readily translated into the spectral densities via Table 3.

Spectral Density of Phase Fluctuations

One can estimate the power spectral densities of various quantities. Two interesting quantities in addition to $y(t)$ are $V(t)$ and $\phi(t)$ as defined in equations (1) and (2). The rf power spectral density, $S_V(f)$, is just the spectral density one would obtain if he were to analyze directly the output voltage, $V(t)$, of the oscillator. Of course, it is important whenever the rf spectral purity is important (e.g., in communications systems). Included in $S_V(f)$ are effects from the amplitude fluctuations, $\varepsilon(t)$, as well as the phase (frequency) fluctuations, $\phi(t)$. Typically, direct estimates of $S_V(f)$ are limited in resolution to a few Hertz of bandwidth and, thus, are not particularly useful for evaluating long-term performance of the oscillator.

For short-term fluctuations, one often sees estimates of the power spectral density of the phase fluctuations, $S_\phi(f)$. Often it occurs for precision oscillators that $\varepsilon(t)$ is sufficiently small that [1]

$$S_\phi(f) \approx \frac{4}{V_o^2} \; S_V(\nu_o \pm f), \tag{18}$$

where $f > 0$. That is, the sideband power at $\pm f$ removed from the carrier frequency, ν_o, is proportional to the phase power spectral density.

There is another useful equation relating $S_\phi(f)$ with $S_y(f)$. Reference [1] shows that

$$S_y(f) = \left(\frac{f}{\nu_o}\right)^2 \; S_\phi(f). \tag{19}$$

Often one measures the sideband power of the rf spectrum, $S_V(\nu_o \pm f)$, and uses (18) to estimate $S_\phi(f)$. Occasionally, one devises a circuit to obtain a voltage analog of $\phi(t)$ and spectrum analyzes it directly [13]. Equation (19) provides a link of $S_\phi(f)$ with $S_y(f)$ and hence the rest of the oscillator model.

Systematics

The power spectrum and the two-sample variance are useful tools for the analysis of the random, non-deterministic elements of the model. Their use in the presence of the systematic elements can cause problems [4,15], and for this reason it is often important to remove the systematic elements before the noise analysis. It is important to emphasize that "removal for analysis" does not imply that these elements are discarded--they are recognized, evaluated, and remembered to be reported in the final accounting of the model parameters. Thus, the overall analysis operations are shown in Figure 3.

The methods of separation of the systematics will vary with particular applications. For example, some oscillators display a nearly linear drift in frequency (i.e., $\bar{y}_k$) with running time. For analysis by the two-sample variance technique it is often important to "remove" this first. This can be done by means of a linear least squares regression to the $\bar{y}_k$, but the drift which is removed should be reported in the final accounting of the model. Again in the presence of periodic terms, the two-sample variance will be very difficult to interpret. Thus, one should either use direct spectrum estimation or devise an appropriate technique to remove periodicities before a two-sample variance is used. Some of the difficulties associated with removing systematics are discussed by Winkler [4].

IV. USES OF THE VARIOUS MEASURES OF FREQUENCY STABILITY

The estimates of the frequency stability of an oscillator or clock have many uses, spanning the range from research to procurement specifications. As mentioned above, the form in which the model is expressed should be influenced by the intended use. For example, if the noise model for a given oscillator included flicker frequency noise as an element, this could be equivalently expressed as a power spectral density varying as $|f|^{-1}$ or a constant $\sigma_y(\tau)$ with varying τ. Which mode of expression one uses is just a matter of convenience.

It is probably true that theoreticians and researchers in the field of frequency instabilities normally use the power spectral densities. It is probably this historical fact which is the source of the mode of expression of the random parts of the model in Tables 1 and 2. That is, the random model elements were expressed in terms of power spectral densities. Also, for diagnostics of oscillators, the use of power spectral densities is very common. A spectrum analyzer can be a very powerful tool in the design, construction, and evaluation of precision signal sources.

Table 4 lists some uses of the measures of frequency instabilities with the commonly used method of analysis. Included in the methods of analysis are references to ARIMA models [5]. ARIMA models provide a powerful and convenient method of analysis, computer simulation, and prediction for random processes and deserve special mention in addition to $S_y(f)$ and $\sigma_y(\tau)$. Although they are not used to any great extent in the measurement of frequency stability, they provide the only practical approach to computer simulation of oscillator performance. It is possible to translate from models based on Table 2 to ARIMA models directly [8,15].

V. SUMMARY

The measurement of frequency stability is the process of evaluating (i.e., quantifying) a set of model parameters. The typical model elements found to be adequate to model the frequency instabilities include (a) random, non-deterministic elements expressed in terms of power-law-types of power spectral densities; (b) systematic terms like linear frequency drift; and (c) environmental sensitivities.

Various mathematical techniques exist to fit these model elements to a particular oscillator, but the most common are power spectrum analysis and the computation of the two-sample variance. Other analysis techniques have been studied and have important advantages for special situations. For example, ARIMA models [5] provide the only practical approach to computer simulation of oscillator performance.

A measurement of the frequency stability of an oscillator includes the values and uncertainties of the model parameters, the range of applicability of the model, and a description of the experiment and analytical techniques.

TABLE 1

Model Elements

1. Random (Noise) Elements

   - Gaussian Noise Elements

     $$S_y(f) = h_{-2}|f|^{-2} + h_{-1}|f|^{-1} + h_0 + h_1|f| + h_2|f|^2$$

   - Sporadic Elements

     Sudden steps in frequency and/or time (phase)

2. Systematic Elements

   - Linear frequency drift
   - Frequency offset
   - Time (phase) offset
   - Periodic terms

3. Environmental Elements

TABLE 2

Names of Noise Types

Name	Frequency Dependence* Power Spectral Density of Frequency	Power Spectral Density of Phase
White Phase Noise	$\|f\|^2$	$\|f\|^0$
Flicker Phase Noise	$\|f\|^1$	$\|f\|^{-1}$
White Frequency Noise	$\|f\|^0$	$\|f\|^{-2}$
Flicker Frequency Noise	$\|f\|^{-1}$	$\|f\|^{-3}$
Random Walk Frequency Noise	$\|f\|^{-2}$	$\|f\|^{-4}$

*where

$$\frac{1}{N\tau_o} \leq |f| \leq \frac{1}{2\tau_o};\ \tau_o = \text{sampling}$$

interval, and N = total number of data points.

TABLE 3. Translation between $S_y(f)$ and $\sigma_y^2(\tau)$.

Noise Type (Model)	$S_y(f)$	$\sigma_y^2(\tau)$ [1]	Uncertainty [2] in $\sqrt{\sigma_y^2(\tau)}$ for m values of y where $m > 5$
White Phase Noise*	$h_2 \lvert f \rvert^2$	$h_2 \frac{3f_h}{(2\pi)^2\tau^2}$	$\pm \frac{0.99}{\sqrt{m}} \cdot \sigma_y(\tau)$
Flicker Phase Noise*	$h_1 \lvert f \rvert$	$h_1 \frac{1}{(2\pi\tau)^2}$ 3 γ + ln $(2\pi f_h \tau)$ - ln 2 $\gamma = 0.577$	$\pm \frac{0.99}{\sqrt{m}} \cdot \sigma_y(\tau)$
White Frequency Noise	h_0	$\frac{h_0}{2\tau}$	$\pm \frac{0.87}{\sqrt{m}} \cdot \sigma_y(\tau)$
Flicker Frequency Noise	$h_{-1} \lvert f \rvert^{-1}$	h_{-1} 2 ln 2	$\pm \frac{0.77}{\sqrt{m}} \cdot \sigma_y(\tau)$
Random Walk Frequency Noise	$h_{-2} \lvert f \rvert^{-2}$	$h_{-2} \frac{(2\pi)^2\tau}{6}$	$\pm \frac{0.75}{\sqrt{m}} \cdot \sigma_y(\tau)$

*The quality f_h is the high-frequency cutoff of the noise; $2\pi\tau f_h >> 1$.

TABLE 4

Uses of Measures of Frequency Stability

Use	Generally Preferred Method of Analysis
Theory/Research	Power Spectral Densities, $S_y(f)$ & $S_\phi(f)$
Diagnostics	Power Spectral Densities, $S_y(f)$ & $S_\phi(f)$
Overall Performance Prediction	Power Spectral Densities, $S_y(f)$ & $S_\phi(f)$
Simple Comparisons	Two-Sample Variances
Simple Estimate of PSD	Two-Sample Variances
Procurement Specs.	Two-Sample Variances
Computer Simulation	ARIMA Models [5]
Prediction	ARIMA Models [5]
Environmental Correlations (Diagnostics)	ARIMA Models [5]

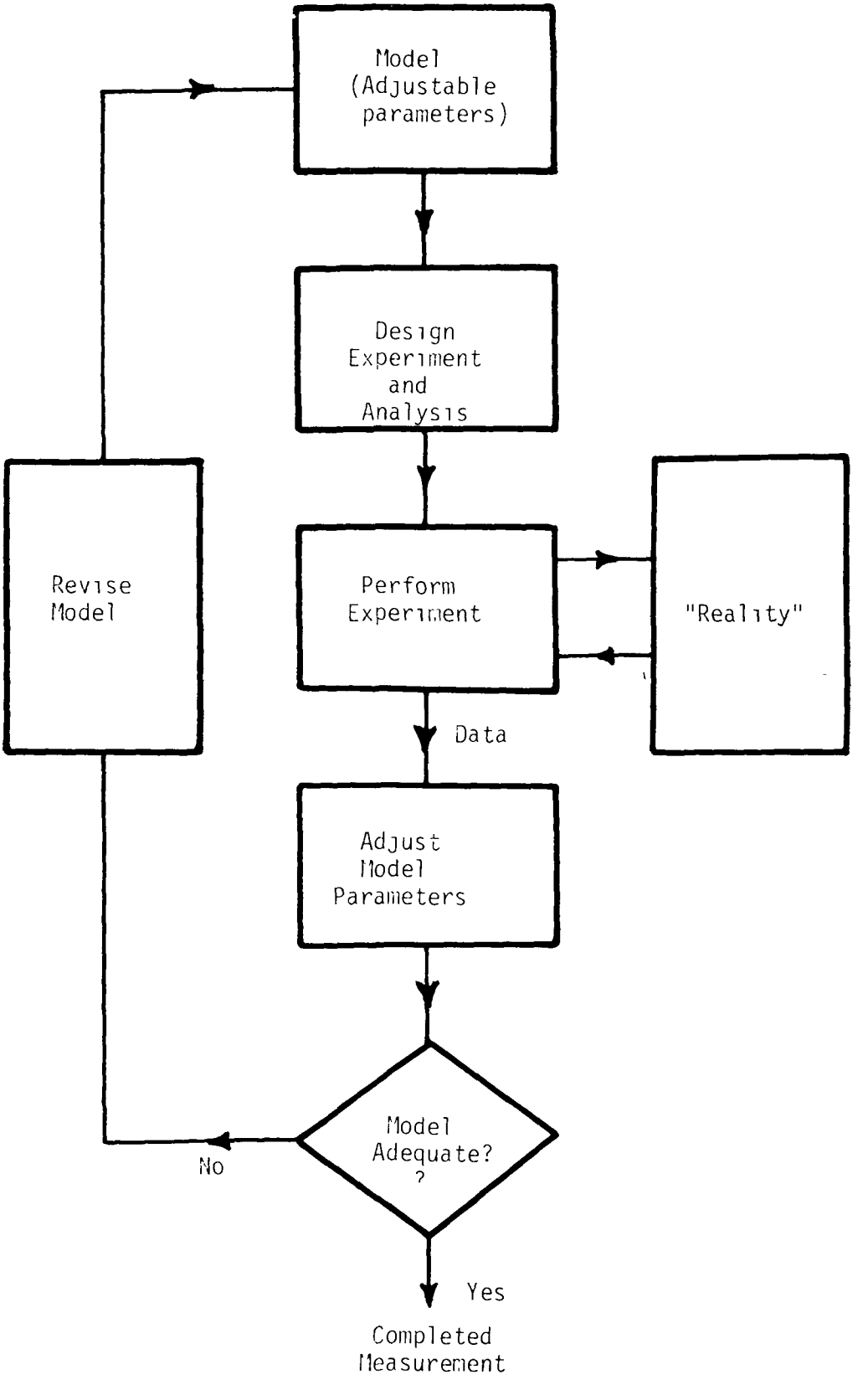


Figure 1. A Model of the Measurement Process.

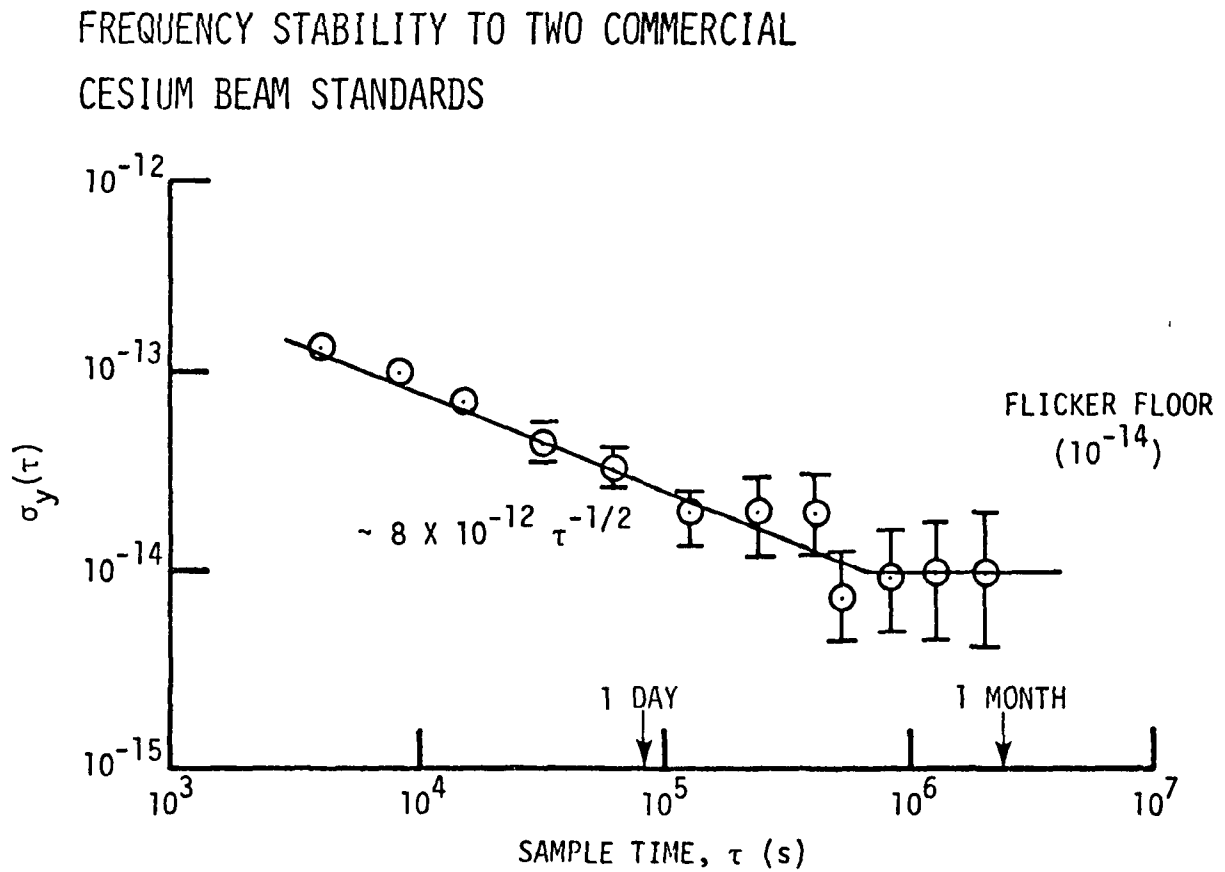


Figure 2. Frequency stability as measured between two state-of-the art commercial cesium frequency standards.

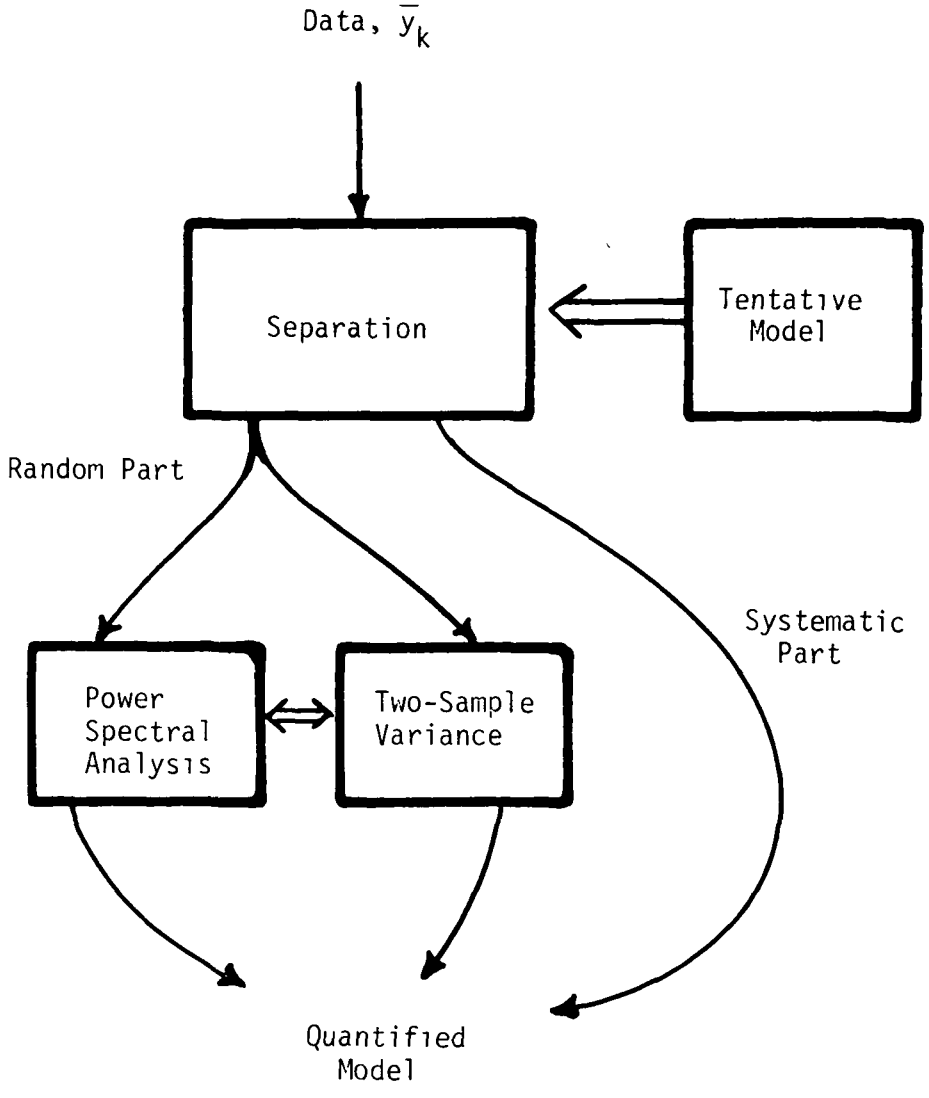


Figure 3. Analysis Techniques.

REFERENCES

[1] J. A. Barnes et al., "Characterization of Frequency Stability," IEEE Trans. on I&M, Vol. IM-20, No. 2, May 1971, pp. 105-120.

[2] Lesage and Audoin, "Estimation of the Two-Sample Variance with a Limited Number of Data," Proceedings of the 31st Annual Symposium on Frequency Control, 1977, pp. 311-318.

[3] J. Rutman, "Oscillator Specifications: A Review of Classical and New Ideas," Proceedings of the 31st Annual Symposium on Frequency Control, June 1977, pp. 291-301.

[4] G.M.R. Winkler, "A Brief Review of Frequency Stability Measures," Proceedings of the 8th Annual Precise Time and Time Interval (PTTI) Applications and Planning Meeting, Nov. 1976, pp. 489-527.

[5] G.E.P. Box and G. M. Jenkins, Time Series Analysis, Holden-Day, San Francisco, Calif. (1970).

[6] D. Percival, "A Heuristic Model of Long-Term Clock Behavior," Proc. 30th Annual Symposium on Frequency Control, June 1976, pp. 414-419.

[7] D. W. Allan, et al., "Performance, Modeling, and Simulation of Some Cesium Beam Clocks," Proc. 27th Annual Symposium on Frequency Control, May 1973, pp. 334-346.

[8] J. A. Barnes, "Models for the Interpretation of Frequency Stability Measurements," NBS Technical Note 683, August 1976.

[9] G. M. Jenkins and D. G. Watts, Spectral Analysis and its Applications, Holden-Day, San Francisco, 1968.

[10] J. E. Gray and D. W. Allan, "A Method for Estimating the Frequency Stability of an Individual Oscillator," Proc., 28th Annual Symposium on Frequency Control, May 1974, pp. 243-247.

[11] D. W. Allan, "The Measurement of Frequency and Frequency Stability of Precision Oscillators," NBS Technical Note 669, July 1975; Proceedings of the 6th Annual Precise Time and Time Interval (PTTI) Applications and Planning Meeting, Dec. 3-5, 1974, pp. 109-141.

[12] D. A. Howe, "Frequency Domain Stability Measurements: A Tutorial Introduction," NBS Technical Note 679, March 1976.

[13] F. L. Walls and S. R. Stein, "Accurate Measurements of Spectral Density of Phase Noise in Devices," Proc. 31st Annual Symposium on Frequency Control, June 1977, pp. 335-343.

[14] J. A. Barnes, "Tables of Bias Functions, B_1 and B_2, for Variance Based on Finite Samples of Processes with Power Law Spectral Densities," NBS Technical Note 375, January 1979.

[15] D. Percival, "Prediction Error Analysis of Atomic Frequency Standards," Proc. 31st Annual Symposium on Frequency Control, June 1977, pp. 319-326.

VLBI AND ITS CURRENT APPLICATIONS WITHIN THE SOLAR SYSTEM

Dr. John L. Fanselow
Jet Propulsion Laboratory
Pasadena, California 91103

ABSTRACT

This paper outlines the general theory of VLBI, and discusses its sensitivity as a measurement tool. Specific applications of the technique currently in use or in advanced planning stages will be summarized.

Independent station radio interferometry, more commonly known as VLBI (Very Long Baseline Interferometry) is a technique that was pioneered in 1967 by radio astronomers to study the structure of compact natural radio sources. Since then its applications have expanded to geodesy, spacecraft navigation, astrometry, and to time and frequency synchronization.

Figure 1 illustrates the underlying physical principles of interferometry. Two points, separated by a baseline $\vec{B}$, receive a signal from a very distant point source by way of the ray paths shown with the solid lines. In the particular case shown the signal received at R2 will be the same signal received at R1, but at a time interval, τ, later. Thus there is a constant phase difference, $\tau c/\lambda$, between the signals received at these two points.

Changing the angle between the baseline and the source by $\delta\theta = \frac{\lambda}{2B}$ causes the phase difference in the received signals at R1 and R2 to be altered by one half cycle. This angle increment is thus the interferometer angular resolution, which can be subarcsecond on rather modest baselines at typical microwave frequencies. (See the table in Fig. 1.) At transcontinental and intercontinental baselines this resolution becomes milliarcseconds or less (1 milliarcsecond subtends a distance of 750 meters at the sun as viewed from the earth). It is this excellent angular resolution which first attracted the radio astronomers in their quest to understand the small scale structure of radio sources.

Couple this sensitivity to small changes in angle with the passive, nearly all-weather capability of a microwave receiving system. You will then understand radio interferometry's potential for spacecraft navigation and for its use in the definition of a fundamental celestial

coordinate system, a coordinate system tied to the most distant objects in the known universe, the quasars. Further, add to this the experimental fact that the time delay, τ, can be measured with accuracies of 0.5-5 cm on most baselines, and you will appreciate that the technique has great potential for geodetic measurements. Geodetic measurements of a few centimeters, obtained with only a few hours of data, will provide a new era in the geometric measurement of the crustal deformations of the earth.

In this talk I want to limit myself to applications of VLBI within the Solar System. While the astrophysical applications are equally exciting, my time limit of one half hour permits me to cover only a portion of the field. However, before discussing the specific applications, I would like to outline the data acquisition, and reduction processes for VLBI.

Fig. 2 schematically shows the earth-fixed geometry of two antennas receiving the radio noise from a natural radio source at infinity. If the source is nearby, such as a spacecraft in the solar system, the curvature of the wave front must also be taken into account. For natural sources, the signal is usually white noise, while for artificial sources the signal is not usually purely random. (Spacecraft transmitting band-limited white noise, and natural radio sources, emitting spectral lines are important exceptions). Note also, that as the earth rotates "under" the source, the time delay between the arrival of the signal at station #1, and at #2 changes.

A typical data acquisition and processing flow is outlined in Figure 3. Each of the two stations receives the r.f. signal, digitizes and time tags it, and then records that data on magnetic tape. In this acquisition process independent frequency standards are used. For certain applications, standards with a $\Delta f/f \sim 5 \times 10^{-13}$ performance over hours are adequate. However, standards with a $\Delta f/f$ performance of $\sim 10^{-15}$ over nearly 24 hours are required for the most demanding of geodetic applications, i.e. measurements of intercontinental baselines with centimeter accuracy.

Variations on this acquisition process do exist. For example, one group does not digitize. Another group has also succeeded in transmitting the data back to a central correlation site by way of a wide band satellite link, thereby eliminating tapes.

By whatever means the data is brought to the central correlation site, at that site the two data streams are reconstructed such that the data transmission process is transparent. Since in the acquisition process the signal arrived at station #1 at an interval, τ, ahead of its arrival at station #2, it is necessary in the correlation process to delay the data stream from station #1 by some estimate, τ_m, of the actual

delay interval, τ. Otherwise, there would be no correlation between the bits.

In Figure 3 one can intuitively see that inserting a delay in the bit stream coming from the tape obtained at the left hand station, #1, is equivalent to moving that station along the incoming ray path until the signal received at that station is in time coincidence with the signal received at the other station. Since the correlator is free to vary this model delay, any unknown τ_g, can thus be determined. The best estimate of τ_g is that model delay, τ_m, which gives the maximum correlation between the signals received at the two stations.

One further complication, however, is that the actual delay, τ, is changing with time as the earth rotates. Thus, the correlation process must be driven by a computer capable of constantly updating the model for τ_m. Since we are often dealing with signals whose correlated power is 0.1 - 1% of the total received power, it is necessary to integrate for many million bits in order to develop an adequate signal to noise to detect the signal. Thus, the model for τ, must be sufficiently good such that the residual, $\tau_g - \tau_m$, is very nearly independent of time.

Once this is done, the output of the correlation is a time sequence of correlation sums, each sum being the sum of 10^6 - 10^7 single bit correlations. The time history of these correlation sums is the fundamental output of the interferometer, and up through this output all VLBI users have common data flow requirements.

Application dependent processing starts branching out at this point. However, for the applications I will review some sort of least squares estimation process is usually involved. In general, the apriori models of τ are not optimal. However, by estimation techniques applied over an ensemble of observations, both the geometric and hardware parameters in the model for τ can be refined from their apriori values. For example, relative station locations, and source positions may be improved. Clock differences, UT1, and Polar Motion are other parameters which are regularly refined from their apriori values.

Figure 4 presents the sensitivity of the derived VLBI observables τ, and $\dot{\tau}$ (more commonly $\nu\dot{\tau}$, or fringe frequency, where ν is the observing frequency), to two typical VLBI geometric parameters, an angle, and a baseline length. The second column refers to the time delay observable, τ. Typically it can be measured with an accuracy of better than 0.1 nsec (3 cm). The sensitivity of this observable to changes in angle is proportional to baseline length and has a maximum of 150 nsec/arcsec for a 10,000 km baseline. The sensitivity of observed time delay to changes in baseline length is 3.3 nsec/meter and is independent of baseline length.

With such sensitivities, and with the observable accuracy of 0.1 ηsec it should not be surprising that VLBI has the potential accuracy for centimeter level geodesy and for milliarcsec level astrometry.

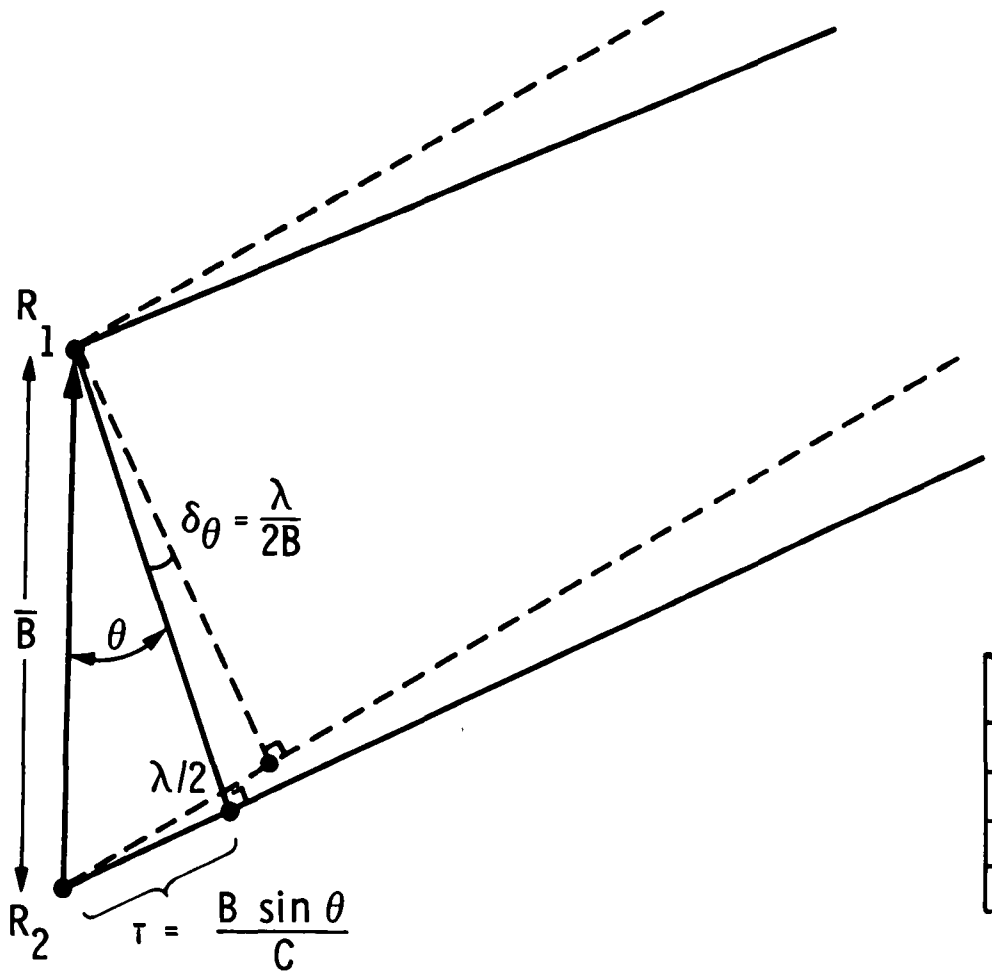
The time rate of change of time delay, while not quite so powerful in practice, does aid in the least squares parameter adjustments used for long baseline observations. Inclusion of that observable in the estimation processes decouples parameter correlations that would otherwise degrade the parameter estimates. Column 3 provides typical measurement accuracies and sensitivities on long baselines for the time derivative of delay (fringe frequency).

Despite the great promise of radio interferometry, I do not want to make obtaining this potential accuracy appear trivial. Calibrations of the receiving system, of the atmosphere, ionosphere, and space plasma are necessary along with a great deal of care in the data processing. The calibrations include simultaneous observations at S- and X-Band to remove the ionosphere and space plasma contributions, as well as water vapor radiometer measurements of the atmospheric water vapor along the line of sight to remove the differential delay contribution of the water vapor. Surface weather data, particularly atmospheric pressure, and receiver phase calibrations are also required.

However, these calibrations now appear feasible at the 0.5 - 2 cm level with current technology, meticulously applied. Actually, as some of the other speakers will discuss in more detail later, significant demonstrations of some aspects of this VLBI potential are already finished or are underway.

This concludes the outline of VLBI data acquisition, processing, and sensitivity. In the time remaining, I would like very briefly to outline the current and anticipated programs which apply radio interferometry within the Solar System. Table I provides such a summary for programs within the United States. Each entry in this table gives the program name, the institutions responsible for its implementation, the sponsoring agencies, the primary goal of the program, and the status. Other countries, such as Canada (one of the founders of the VLBI technique), Norway, and Australia have embryonic programs in these applications areas also. Since this table is self explanatory, I wish to finish my talk with a guided study of this table.

INTERFEROMETER ANGULAR RESOLUTION



$\frac{\lambda}{2B}$ arc sec (1 arc sec $\simeq$ 5 μrad)

B (km) \ ν Hz	10^9	10^{10}
10	3	0.3
100	0.3	0.03
1000	0.03	0.003
10000	0.003	0.0003

FIGURE 1

GEOMETRY OF RADIO INTERFEROMETRY EXPERIMENTS

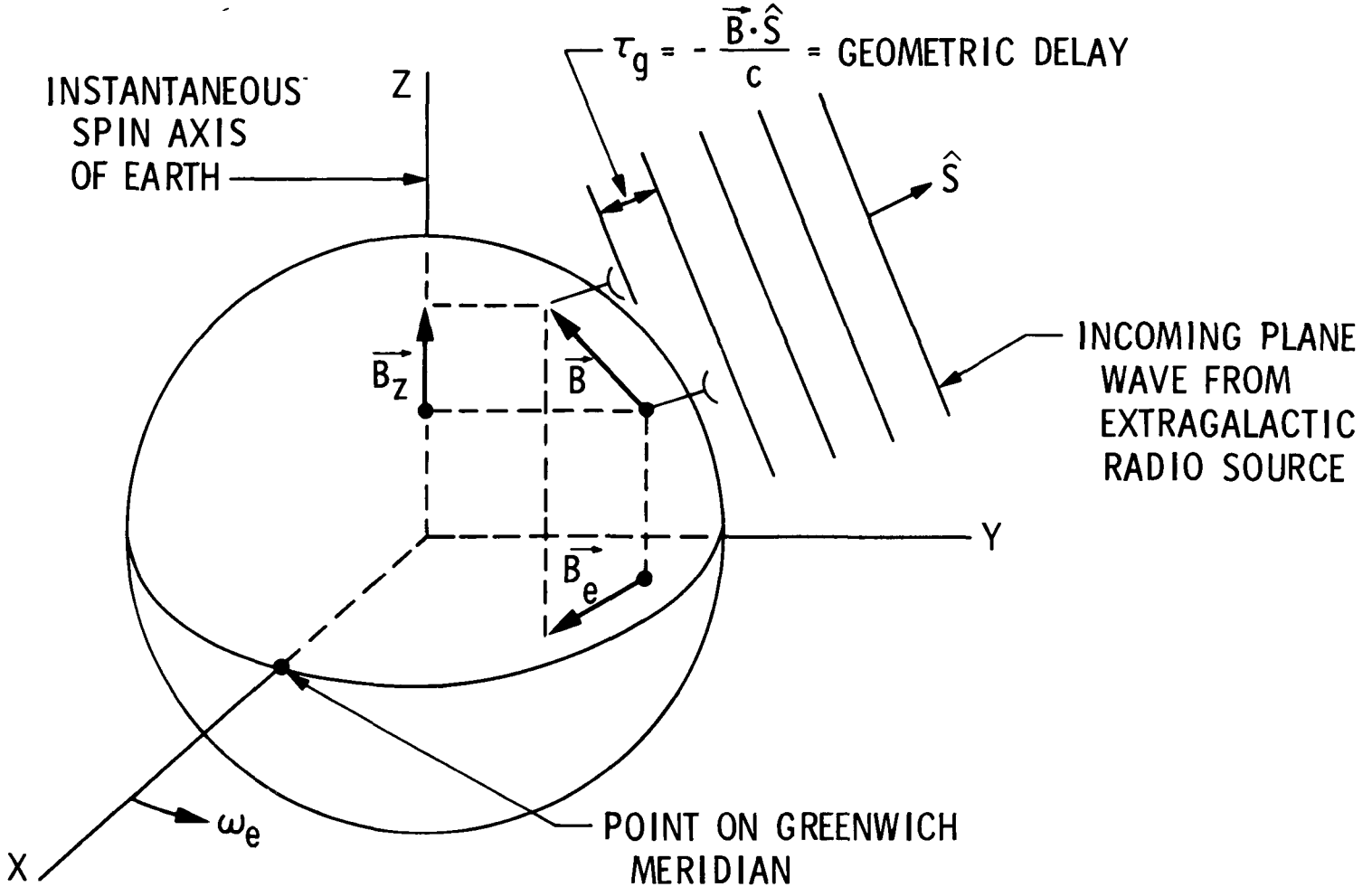


FIGURE 2

DATA ACQUISITION AND PROCESSING FLOW FOR VLBI

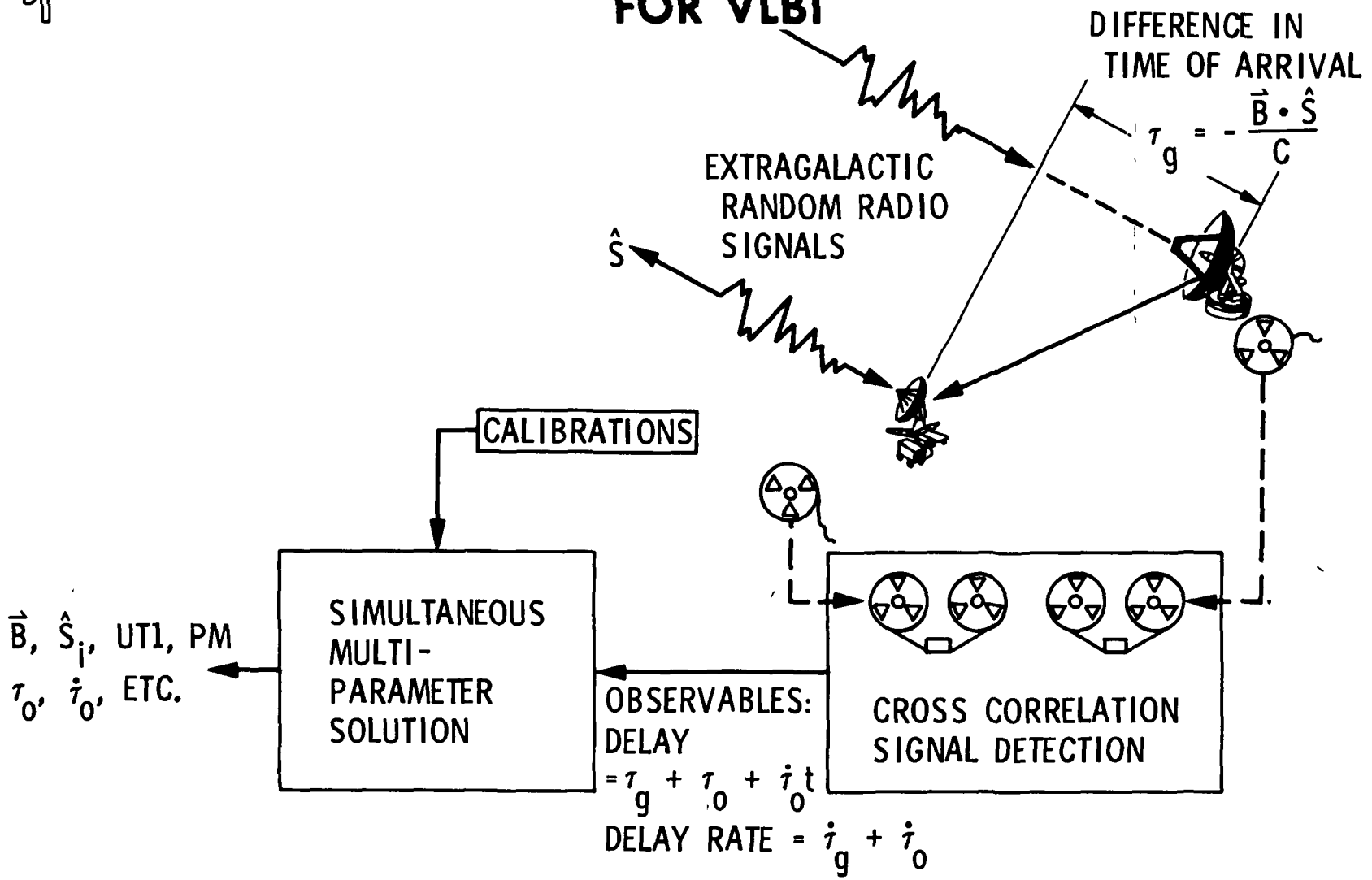


FIGURE 3

MAXIMUM SENSITIVITY OF VLBI FOR ANGULAR AND METRIC MEASUREMENTS ON 10000 km BASELINE

PARAMETER \ OBSERVABLE	DELAY (τ) ($\sigma \leqslant$ 0.1nsec)	FRINGE FREQUENCY ($\nu\dot{\tau}$) (X-BAND $\sigma \leqslant$ 1 mHz)
ANGLE	150 $\frac{\text{nsec}}{\text{arcsec}}$	98 $\frac{\text{mHz}}{\text{arcsec}}$
BASELINE	3.3 $\frac{\text{nsec}}{\text{meter}}$	2 $\frac{\text{mHz}}{\text{meter}}$

FIGURE 4

SPECIFIC APPLICATIONS OF VLBI

PROGRAM NAME	INSTITUTIONS (SPONSORS)	PRIMARY GOAL	COMPLETE✓ OR DATE EXPECTED	SPECIFIC RESULTS
HAYSTACK/OVRO/ FAIRBANKS TRIANGLE	MIT/HO/GSFC (DOD-ARPA)	TECHNIQUE DEVELOPMENT FOR GEODESY	✓	1-3 meter VECTOR CLOSURE OF BASELINES
QUASAR PATROL	GSFC/MIT/HO/ NRAO/JPL (NASA-OA NASA-OTDA NSF)	RADIO ASTRONOMY	✓	a) CROSS COUNTRY BASELINE LENGTH REPEATABILITY ~20 cm
DSN VLBI DEVELOPMENT	JPL (NASA-OTDA)	TECHNIQUE DEVELOPMENT FOR SPACECRAFT NAVIGATION SUPPORT	✓ 7/79 1980	a) 50 cm ACCURACY CALIFORNIA/SPAIN BASELINE b) UT1 ~2 msec DEVELOP SOURCE CATALOG AND OBTAIN STATION LOCATIONS FOR OPERATIONAL VLBI DEMONSTRATE 5-10 cm VECTOR ACCURACY ON INTERCONTINENTAL BASELINES

FIGURE 5

SPECIFIC APPLICATIONS OF VLBI

PROGRAM NAME	INSTITUTIONS (SPONSORS)	PRIMARY GOAL	COMPLETE√ OR DATE EXPECTED	SPECIFIC RESULTS
ARIES (ASTRONOMICAL RADIO INTER-FEROMETRY EARTH SURVEYING)	JPL (NASA-OA)	PORTABLE ANTENNA TECHNIQUE DEVELOPMENT FOR GEODESY	√	a) 3 cm VECTOR REPEATABILITY ON 16 km BASELINE USING 64/26 meter STATIONS
			√	b) OCCUPIED 11 SITES IN 2 YEARS WITH 9 meter ANTENNA ~10 cm ACCURACY
			√	c) 3 cm VECTOR AGREEMENT WITH SURVEY ON 300 meter BASE-LINE
			√	d) 6 cm LENGTH AGREEMENT WITH NGS SURVEY ON 30 km BASELINE
			1978	e) 1-5 cm ACCURACY WITH 9 meter
			1978	f) 5-10 cm ACCURACY WITH 4 meter HIGH MOBILITY STATION
ALSEP ΔVLBI	JPL (NASA-OA)	LUNAR EPHEMERIS REFINEMENT	1978	TIE LUNAR EPHEMERIS TO RADIO SOURCE REFERENCE FRAME
PPME (PACIFIC PLATE MOTION EXPERIMENT)	GSFC/HO/MIT (NASA-OA)	GEODESY	√	a) HO/OVRO/NRAO 8 cm LENGTH REPEATABILITY
			√	b) POLAR MOTION CONSISTENT WITH SATELLITE DOPPLER MEASUREMENTS AT ~30 cm
			√	c) 20-50 cm VECTOR CLOSURE ON VARIOUS CONTINENTAL TRIANGLES
			√	d) 0.3 cm REPEATABILITY ON 1.2 km BASELINE
			√	e) STATION LOCATION MEASUREMENTS CONSISTENT WITH GEOCEIVERS AT 20-30 cm
			√	f) CLOCK SYNCH vs TRAVELING CLOCK COMPARISON AGREES WITHIN 10 nsec
			1978	g) DEVELOP 100 MBS DATA SYSTEM

FIGURE 6

SPECIFIC APPLICATIONS OF VLBI

PROGRAM NAME	INSTITUTIONS (SPONSORS)	PRIMARY GOAL	COMPLETE ✓ OR DATE EXPECTED	SPECIFIC RESULTS
VLBI VALIDATION	JPL/GSFC (NASA-OTDA) NASA-OA	TECHNIQUE VALIDATION	1980 1981	"VALIDATE" ACCURACY OF VLBI ON TRANSCONTINENTAL BASELINES AT 5 cm OR BETTER LEVEL COMPARE BASELINE MEASUREMENTS WITH COMPETING TECHNIQUES - LUNAR LASER, SATELLITE LASER
DSN OPERATIONAL VLBI	JPL (NASA-OTDA)	SUPPORT FOR SPACECRAFT NAVIGATION	7/79	OPERATIONAL INTERCONTINENTAL VLBI SYSTEM WITH WEEKLY OBSERVATIONS a) UT1/PM AT 50 cm LEVEL b) CLOCK SYNCH AT 10 nsec, FREQ SYNCH AT 10^{-13} c) 24 hour TURNAROUND
DSN ΔVLBI	JPL (NASA-OTDA)	TECHNIQUE DEVELOPMENT FOR SPACECRAFT NAVIGATION	1980	DEVELOP TECHNIQUE WHICH DIFFERENTIALLY MEASURES SPACECRAFT CELESTIAL POSITION RELATIVE TO FIXED NATURAL RADIO SOURCES (ACCURACY ~0".001). USE IN JOP MISSION

FIGURE 7

DR. TOM CLARK, NASA Goddard Space Flight Center:

Another group that has participated with Goddard, Haystack, MIT, et al, on an international front in many of our experiments, has been the group at Chalmers Institute of Technology at their observatory in Uppsala, Sweden. They have been very active in all of this and should have been included in the last list.

DR. FANSELOW:

Okay, fine.

EARTH ROTATION FROM LUNAR DISTANCES: BASIS AND CURRENT STATUS

J. Derral Mulholland (University of Texas at Austin) and
Odile Calame (Bureau International de l'Heure/Centre
d'Etudes et de Recherches Geodynamiques et Astronomiques
Grasse, France)

ABSTRACT

The observing campaign Earth Rotation from Lunar Distances (EROLD) was organized to provide an initial test of the applicability of lunar ranging to the determination of Universal Time and polar motion in a service bureau mode. Current plans call for a two-year campaign, overlapping with similar efforts using other techniques. The first year is largely concerned with making the network of observing stations operational, with the prospect that some 5-7 stations may be participating in 1978. This paper discusses the lunar laser technique, the EROLD organization and goals, and the present status of the observing campaign.

INTRODUCTION

It has been recognized for the past several years that the presently-used techniques for routine determination of the rotational position of the Earth's crust are no longer adequate for the scientific and practical applications for which these data are required. Many of the classical instruments are now of questionable utility and will surely have to be retired from service within one or two decades. The pertinent question, then, is not *whether* they will be replaced, but with *what* will they be replaced.

There begins to be an impressive number of potential candidates for the next-generation Earth rotation service. One can, for

example, imagine a network of instruments conceptually related to the classical method, such as the new giant photographic zenith tube (PZT) at the U. S. Naval Observatory, or the photoelectric astrolabes under development in France and China. It seems more likely, however, that the new network will rely primarily on completely new techniques. The present possibilities include various techniques for radio tracking of artificial satellites, radio interferometry of celestial radio sources, and laser ranging to the Moon or to artificial satellites. In principle, each of these systems presents unique advantages and capabilities not totally shared by the others; in practical application to the needs of an Earth rotation service, each of them also shows important drawbacks. We have tried to summarize both sides of this situation in Tables 1-4.

It is important to note that none of these systems was invented for the purpose of Universal Time and polar motion. Each of them had other motivations that seemed to be more important, and most of them have demonstrated in practice that they are capable of important scientific or technical tasks. But our present subject is their applicability to the daily needs of a service bureau function. The Doppler Polar Motion Service (DPMS) has shown that it can operate in this mode, but with severe disadvantages. Episodic determinations of UTO and/or the variation in latitude have been obtained by VLBI, artificial satellite ranging, and LLR, but we believe that (excepting DPMS) *none* of the new techniques have demonstrated their utility in a daily service network mode, nor at what real cost. True, there are sensitivity studies and projections for several of them, but most of these are believed at most by their authors. It seems undeniable that the only real way to discover the utility of the new techniques as potential next-generation Earth rotation networks is to perform realistic pilot demonstrations for each one, unless there are obvious grounds on which to exclude it. If this is done, we may suspect that the resulting "best buy" will be (as now) a hybrid system incorporating two or more of the new techniques whose advantages and disadvantages are in some way complementary.

The observing campaign called Earth Rotation from Lunar Distances (EROLD) is intended to be just such a pilot demonstration. The concept was developed in discussions between us in 1974, and was proposed first to the NASA Lunar Laser Ranging Team and then to COSPAR Working Group 1 that same year. COSPAR responded by recommending that the campaign be undertaken, and the Working Group appointed a Steering Committee to work out the details and provide coordination at the international level, recognizing that no one country is capable of determining the three-dimensional rotation of Earth from entirely within its own boundaries.

BASIS OF THE TECHNIQUE

The laser ranging technique provides measures of a nature very different from classical astronomical observations. It is an *active* process, in which the observer illuminates a target and observes the illumination that he himself has provided. It is also unlike at least some of the other new techniques, in that the observed object is entirely passive, and thus is not subject to technological failure nor administrative shutdown. (The often-mentioned fact that the target *might* be destroyed by a chance collision is in fact shared with *all* techniques, and the probabilities are quite infinitesimal for all of them.) With the laser, a pulse of light is transmitted by a terrestrial station towards a reflector on the lunar surface. Because of the cube-corner design of the reflector, the light that strikes it is retransmitted towards Earth in the same direction from which it came (Figure 1). Thus, the signal is detected by a photomultiplier at the same station from which it came. The observation recorded is the time delay between the transmission of the laser pulse and the detection of the reflected signal. For convenience, one often refers to this as a distance measurement, but it is essential to understand that it is really an aberration time, more commonly called "light time". The time delay cannot be symmetric about the reflection time, because of the relative motions of the Earth and Moon during the interval of about 2.6 seconds (1).

Since 1969, five laser reflectors have been placed on the lunar surface. The reflector on Lunakhod I has been observed only a few times by the French and Soviet teams, with relatively poor accuracy. Those carried by Apollo 11, Apollo 14, Apollo 15, and Luna 21 (Lunakhod II) have been observed regularly from the McDonald Observatory since they were deposited. The typical accuracy of these ranges, expressed as an equivalent one-way distance, is now 10-15 cm, and 5-cm ranges are no longer rare. We should note here that, at least in principle, only one reflector is required for Earth rotation determinations, so there seems to be a reserve that is more than adequate to render the meteorite "problem" truly insignificant.

It does not seem necessary to give the details about the process used to analyze these data to obtain improved estimates of the physical parameters of the Earth-Moon system, as this information is already published (e.g. 2,3). The two questions that do seem to be important here are: a) are the Earth rotation parameters separable from the other parts of the physical model, and b) can the geocentric motion of the reflector be modelled with sufficient accuracy to permit meaningful Earth rotation results?

Imagine a simplified problem in which the Moon does not move, but is fixed like a star in distant inertial space. In that case, the laser time delays measured from a point fixed on the surface of Earth would vary only as a function of the Earth's motion. Neglecting the

Earth's orbital motion for the moment, the delays would vary only as a function of the local hour angle of the reflector and its minimum (i.e. meridian) zenith distance. If the rotational axis of the Earth's crust were also fixed in inertial space, then the range could be described as exactly a simple harmonic function of time, and the determination of the geocentric coordinates of the station would consist of finding the amplitude, phase and zero offset of that sine function. True enough, that is not the real world. Suppose we approach the real world a little more closely and imagine that the Moon *does* move about the Earth, that the Earth *does* move about the Sun, and that the Earth's rotational axis *does* move in inertial space, *but* that we know these motions perfectly. Then the range is no longer a sinusoid, but the residuals of the observations with respect to the perfectly-known prediction model will be, with the amplitude, phase and zero offset depending on the station coordinates. If, however, our world includes the one imperfection of a plastic, inhomogeneous, poorly-understood Earth, then problems begin to arise. The rotation axis of the crust is no longer fixed with respect to the crust itself, and the rotation rate of the crust is no longer constant or even perfectly predictable. In other words, there will be variations in the apparent longitude and latitude of an observing station. The sinusoid concept can still be used with long observation series to give some sort of mean or nominal coordinates for the station, which can then be entered into the prediction model. The slippage of the Earth's crust will then be exhibited as quasi-sinusoidal residuals, a function that is locally harmonic, but with variable amplitude and phase. If the period of these modulations is long compared with one day, as suggested by Stolz et al (4), then the sinusoid model can be applied daily to obtain an estimate of the mean values of the apparent variations in longitude (UT0) and latitude (meridian component of polar motion) for that station and that day. The data from several stations can be combined to give an estimate of UT1, x and y for that day.

How does this idealized determination of Earth rotation fit into the realities? Of course, we do not have a perfect model. Nobody has a perfect model, not for the Moon, not for optical or radio star positions, not for TRANSIT nor for LAGEOS. And as with all systems, anything that introduces an error into the predicted hour angle or meridian zenith distance of the observed object *can* be largely absorbed (rightly or wrongly) into an estimate of UT0 and variation of latitude. In *all* methods, the hope is that the physical model can be made sufficiently complete by the addition of other solution parameters that the contamination of Earth rotation results will be small compared to the values obtained. We repeat, because it is often ignored, that *no* technique for modelling a phenomenon for which there is no theory can hope to do more. What we perceive to be an advantage for LLR is that there is no known non-gravitational phenomenon that is important in the orbital motion, and the only one that exists in the lunar rotation has well-defined periods separable from the other factors. The modelling of gravity fields seems not to be a serious problem, either. That is

not to say that there are no problems. The statement made five years ago by one of our colleagues that "we know every factor that could influence the lunar orbit at the few-centimeter level" was not justified then and probably is not now. The best indication that there are still things to discover is the fact that, with 15-cm data, the best global solutions without determination of the Earth rotation parameters give 40-cm residuals, and including the Earth rotation parameters only reduces the rms residual to about 30 cm. The disparities between different studies are still too high (about the same level as the rumored differences between different LAGEOS results), but they are at least within the BIH uncertainties. It is easy to overemphasize these problems, however, because the uncertainties in the present classical results are much smaller than the mean errors of single observations.

The conclusion that we continue to draw from this is that the best, perhaps the only, way to draw clearly justified conclusions as to the relative merits of the various techniques is to perform realistic and extended tests of each one in a service mode of operation, preferably with temporal overlap between the different methods, to detect systematic error within each.

EROLD ORGANIZATION PLAN

In recognition of the necessity that EROLD be a collaboration between observing groups and the Earth rotation services, the Steering Committee appointed by COSPAR Working Group 1 consisted of one representative from each national observing team then existing, the Bureau International de l'Heure (BIH), the International Polar Motion Service (IPMS), plus the chairman of COSPAR Panel 1D on Lunar Laser Ranging, *ex officio*. Since that time, one new observing team has been represented, as well as the group responsible for pre-processing the data from the three stations nearest operational status.

The first meeting of the Steering Committee was held at the IUGG General Assembly in 1975. As a result of strong urgings from non-members present, the BIH accepted (somewhat reluctantly) the responsibility to act experimentally as the central agency for combining results from the individual stations for the determination of UT1, x and y. This seemed a natural extension of one of the agency's fundamental activities, but it did pose a problem: the reduction of LLR data requires significantly different analysis capability and computing technique from that then existing at BIH. This problem was solved by a collaboration between personnel at the Observatoire de Paris (BIH/OP) and the Centre d'Etudes et de Recherches Geodynamiques et Astronomiques (BIH/CERGA). A plan for the BIH participation in EROLD was presented to the Steering Committee at its June 1976 Meeting

at Austin (5). The BIH activity was defined to consist of:
--- Collection of normal points from participating observatories;
--- Calculation of residuals with respect to a uniform model;
--- Preliminary reduction of the raw residuals;
--- Calculation of UT1, x and y;
--- Regular distribution of results;
--- Study modes of combining LLR with other data types.
The *regular* distribution of results is a key factor in service bureau operations. The proposed schedule is given in Table 5. This will provide important feedback to the observing crews, as well as valuable data to the various users of LLR (and other) observations. This is, after all, the prime function of an Earth rotation service.

PRESENT RESULTS OF EROLD AND FUTURE PROSPECTS

At what stage does November 1977 find EROLD? Not a very satisfying one, unfortunately. In principle, the observing campaign was to have begun on 1 January 1977, a date chosen because it seemed likely that three stations would be fully operational at that time. The planned duration was two years, which would include one year for the stations and the BIH to "shake down" their operations, to uncover and solve the startup problems, and then another year of "production" operations. In fact, at this moment, the only station producing real observations of usable quality on a near-daily basis is the same one that has been doing so for about eight years, the McDonald Observatory. The BIH computation system, which *was* ready for experimental use last January, has never yet been tested on real data, because there have been essentially no multi-station data. The current status of the prospective stations in the LLR network is as follows:
AUSTRALIA --- Of the new stations, Orroral appears to be the closest to operation, which is a happy circumstance in view of its southern latitude. They have been firing regularly for several months and gradually isolating and fixing various problems. There have been several successful echo detections, but they are not yet obtained consistently. Experienced LLR people estimate that Orroral could become operational at almost any instant.
FRANCE --- The station at Pic-du-Midi was closed in 1974 and a new one begun on the Calern Plateau; it was to have been finished in 1976, but they have experienced severe budget delays. The 1.5 m telescope was mounted in June 1977, and optical/mechanical testing is now underway. The refurbished and upgraded laser will be installed early next year. Ranging tests *could* begin (optimistically) as early as June 1978. Lunar acquisition may be attempted with the second-generation artificial satellite station at Calern before that time.
GERMANY (Federal Republic) --- Approval and funding have been received

to upgrade the operational second-generation artificial satellite station at Wettzell to lunar capability. Equipment modifications are expected to be delivered on site next June. Lunar tests might begin as early as September 1978.
JAPAN --- Considerable difficulty has been experienced in bringing the Dodaira station to operational status. Many equipment and optical problems have been found and corrected. Further attempts at lunar ranging are scheduled for November and December 1977.
USA --- The McDonald station has recently been upgraded to the point that 5-cm normal points are common, even if not yet the rule. The Haleakala station is continuing to experience great difficulty is becoming operational. Some very high-quality echos have been received, but system debugging continues to be a full-time occupation.
USSR --- Ranging operations on the 2.6 m telescope at Crimea are still permitted only 20-25 days per year, which is inadequate for full EROLD participation. The proposed new dedicated station is still several years in the future.
Thus, the situation can be summarized in the following way:
--- The data analysis and distribution system is ready;
--- One station demonstrates that near-daily operations are possible;
--- Three-station operation may become a reality at any moment;
--- Full network operation (5-6 stations) cannot be expected before late 1978 or early 1979.

Everyone will likely agree that this is not very satisfying. Is this equivalent to saying that it is a failure, or that it should not have been tried? We think that the answer to both questions is "no". Certainly, EROLD is not yet a success, but it is also not yet a failure; it still has prospects for success. It has not yet been demonstrated that LLR can serve as a cornerstone for the next-generation Earth rotation service, but no *other* high-precision technique has yet demonstrated this capacity either. Yes, it is true that satellite ranging and VLBI have been used to determine Earth rotation parameters on a few isolated days and much after the fact, just as LLR has done. What must be demonstrated is the capability for, and the cost of, daily or near-daily operations with quick turn-around of results. EROLD was the first of the formally-organized campaigns to adopt this as its prime goal. Such campaigns are now organized or in process of being organized for the other techniques, and we are pleased to see this. We hope that our own efforts have been among the stimuli for assuring that all of the new techniques receive an adequate test. We do not know which technique or combination of techniques will prove to be the most viable for an Earth rotation service, although we *do* have private opinions. Opinions are not important; we must all try to assure that each technique is tested in a realistic mode, so that the best decisions may be made. In that way, one does not seek that a *technique* "wins", but that science and technology win.

REFERENCES

1. Calame, O.: "Etude des mouvements libratoires lunaires et localisation des stations terrestres, a partir des mesures laser de distance" Dissertation, Université de Paris VI, 1975.
2. Calame, O.: *Manuscripta Geodaetica* 1, 173, 1976.
3. Mulholland, J. D.: in *Scientific Applications of Lunar Laser Ranging* (J. D. Mulholland, ed.) Reidel, Dordrecht, 1977, p. 9.
4. Stolz, A., Bender, P. L., Faller, J. E., Silverberg, E. C., Mulholland, J. D., Shelus, P. J., Williams, J. G., Carter, W. E., Currie, D. G., and Kaula, W. M.: *Science* 193, 997, 1976.
5. Calame, O., Chollet, F., and Guinot, B.: *COSPAR Bull.* 77, 43, 1976.

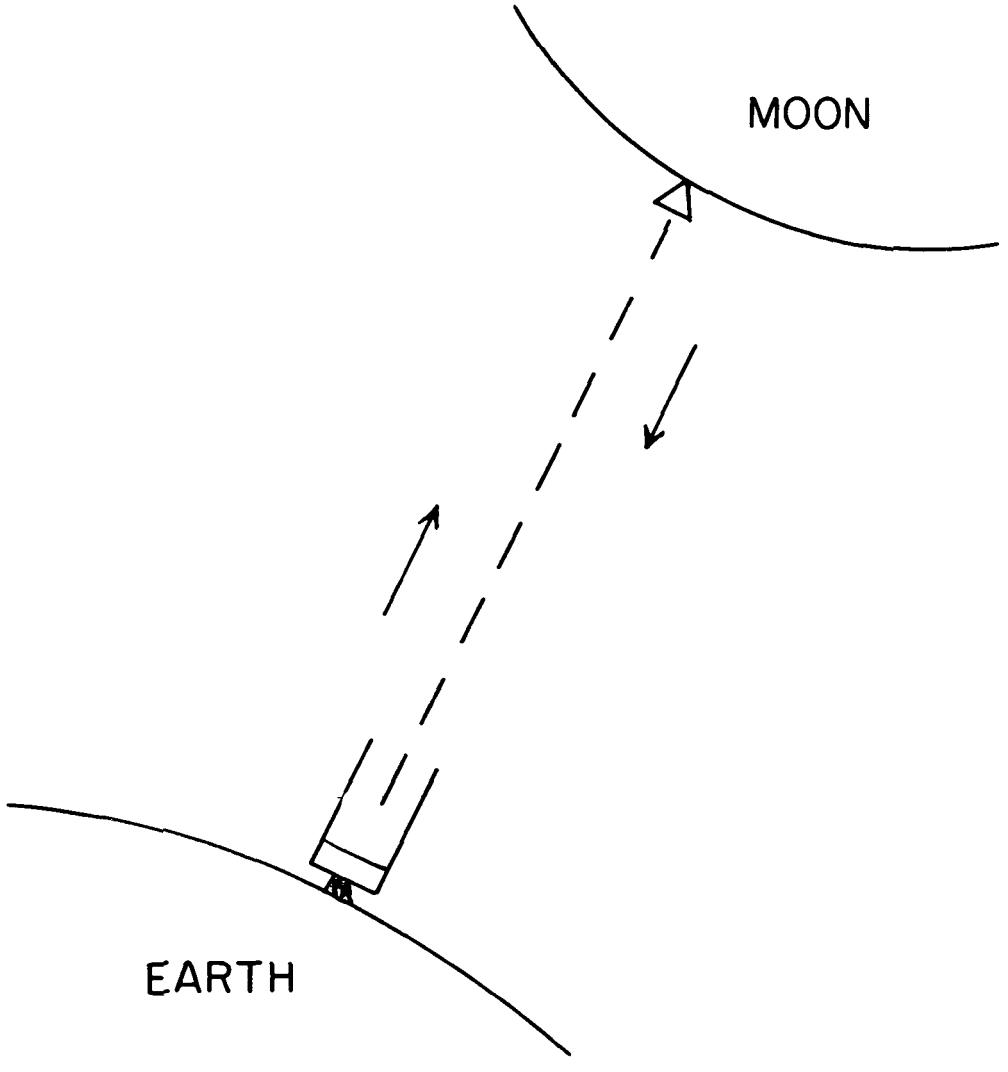


Figure 1: A schematic representation of lunar laser ranging

Table 1: Radio Tracking of Artificial Satellites

A. "Classical" doppler tracking
B. Global Positioning System (GPS), high-density network of 12-hr satellites

	A	B
Advantages		
All-weather capability	x	x
One observation requires only a few minutes	x	x
Low operational cost	x	?
High technical level not required of operations personnel	x	x
Operational network has demonstrated daily operations	x	
Disadvantages		
No tie to inertial reference system	x	x
Currently relies on data and models under military security	x	x
Produces pole position only, not Universal time	x	?
Inherent accuracy limit poorer than with other new techniques	x	?
Currently relies on TRANSIT satellites, which may be discontinued	x	

Table 2: Radio Interferometry of Celestial Radio Sources

A. Connected-element, phase-coherent interferometry
B. Very-long-baseline Interferometry (VLBI)
C. Phase-linked VLBI using satellite communications link

	A	B	C
Advantages			
Weather limit due only to extremely high humidity	x	x	x
Gives direct tie to inertial reference frame	x	x	x
Uses natural (and near-inertial) targets, not subject to failure	x	x	x
Near real-time data processing	x		x
Disadvantages			
Long integration times, each observation is several hours continuous	x	x	x
Two stations (two telescopes) required for each observation	x	x	
Four telescopes required for each observation			x
Inherent accuracy limit poorer than for other new techniques	x		
Little real-time indication of successful observation		x	
Requires large fraction of a communications satellite			x

Table 3: Laser Ranging to Artificial Satellites (LAGEOS and STARLETTE)

Advantages

- Observed object is passive, not subject to failure or shutdown
- One observation requires only about one hour (one complete pass)
- Observing network exists, largely operational
- Pointing requirements less stringent than for LLR
- Perhaps less costly per station than LLR (???)

Disadvantages

- Must have clear sky and good transparency
- No tie to inertial reference system
- Partial passes not useful for Earth rotation
- More stations required than for other techniques
- Requires highly accurate modelling of Earth's gravity field and non-gravitational forces
- Orbit rectification introduces discontinuities into Earth rotation results
- Uses limit of current technology; requires highly-skilled, dedicated personnel

Table 4: Lunar Laser Ranging (LLR)

Advantages

- Observed object is passive, not subject to failure or shutdown
- One observation requires only a few minutes
- Gives tie to inertial reference system through lunar and planetary orbits
- Low-order modelling of gravity fields sufficient, and no non-gravitational forces
- Oldest reflector shows no degradation after 8 years' use

Disadvantages

- Must have clear sky and good transparency
- Several observations required each day at each station
- New Moon gap in present data (not inherent to technique)
- Requires accurate gravitational modelling of entire planetary system
- Uses limit of current technology; requires highly-skilled, dedicated personnel

Table 5: Proposed Schedule for BIH Reduction of EROLD Data

Day j	Beginning of an observing interval
j + a	End of that observing interval
j + b	Reception of the normal points at BIH/CERGA
j + c	Reception of the residuals at BIH/OP
j + d	Transmission of the results for Universal Time and pole coordinates from BIH/OP to participating observing groups

The tentative values are: a = 7 days, (b - a) = 10-15 days, (c - b) = 3-4 days, (d - c) = 2-3 days

ACKNOWLEDGEMENT

One of the authors has received partial support from the U. S. Office of Naval Research, under contract N00014-76-C-0641.

QUESTIONS AND ANSWERS

DR. WILLIAM KLEPCZYNSKI, U. S. Naval Observatory:

You indicated that a study showed that you could not determine all the earth rotation parameters within any one country. Was that with just lunar laser ranging?

DR. MULHOLLAND:

No, with anything.

DR. KLEPCZYNSKI:

Even VLBI?

DR. MULHOLLAND:

I think so.

DR. TOM CLARK, NASA Goddard Space Flight Center:

I would think that the Hawaiians and Texans would certainly want to be thought of as being in the same country. In terms of the lunar laser, those are nearly orthogonal on the earth, which I think does meet the criteria. And certainly also in the case of the VLBI situation, if you regard Alaska, Hawaii, and the continental United States as all members of the same country, I believe the job can be done quite admirably on baselines involving combinations geographically deposed that way.

DR. MULHOLLAND:

I agree. I would be interested in seeing that done. I am reminded of the idea that one can model the moon's gravitational field by observations of one site only. Orthogonality is perhaps not enough. I could say very distinctly that McDonald and Hawaii are not enough. Hawaii has too low a latitude.

DR. KLEPCZYNSKI:

I believe you really must qualify to what precision you wish your quantities so that you could then determine them within one country.

DR. MULHOLLAND:

All right, that's fair enough. But I think implicit in everything we are talking about here today is the determination of all three components of the rotational position, all to a consistently and extremely high accuracy.

DR. KLEPCZYNSKI:

Next Monday, the Naval Observatory will begin observing on a monthly basis at the Greenbank interferometer to determine earth rotation parameters.

DR. MULHOLLAND:

I was under the impression, however, that the daily operation is somewhat in the future. It is the daily operation that one has to do eventually.

DR. KLEPCZYNSKI:

Well, if we can do it monthly, regularly, I think we will be ahead of the game.

DR. MULHOLLAND:

If you can do it monthly, regularly, you will be ahead of us.

CLOCK RATE COMPARISONS BY LONG BASELINE INTERFEROMETRY

W. H. Cannon, R. B. Langley, W. T. Petrachenko
Department of Physics and CRESS, York University, Toronto, Canada.

ABSTRACT

We report a comparison of the determination of the frequency difference between remotely sited frequency standards by: (a) the technique of long baseline interferometry (b) the use of Loran-C/Time Service transmissions. In the long baseline interferometer technique the frequency difference between the local oscillators at each antenna site was modelled as a polynomial in time whose coefficients were estimated from the interferometer fringe frequencies simultaneously with other parameters of the interferometer.

The agreement between the two techniques ranged from 5 parts in 10^{13} r.m.s. for a 5 day continuous interval in March 1973 to 6 parts in 10^{12} r.m.s. for a 2 day continuous interval in June 1973. A number of experimental difficulties degraded the results of the June 1973 experiment and the former figure of 5 parts in 10^{13} is regarded as being representative of the expected agreement between the two techniques.

I INTRODUCTION

We report the results of some relative clock rate measurements accomplished by remote comparison using the technique of long baseline interferometry (LBI). The interferometer was made up of the 25 m. antenna at Chilbolton, England now known as the Chilbolton Observatory (CRO) operated by the Appleton Laboratory facility of the U. K. Science Research Council, and the 46 m. antenna of the Algonquin Radio Observatory (ARO) at Algonquin Park, Ontario, Canada operated by the National Research Council of Canada. The interferometer which has a baseline of 5265 km. was operated at 10,680 MHz (2.8 cm. wavelength). The antenna sites were equipped with cooled parametric amplifiers, local oscillators phase locked to Hewlett Packard H-10A atomic hydrogen masers, and IVC 800 series video tape recorders recording an IF bandwidth of about 5 MHz on standard one inch wide video tape.

The three experiments in March, May and June of 1973 were originally intended only to reveal the structure of a number of extra galactic radio sources (Legg et al., 1973; Legg et al., 1977). However the

structure and operation of the interferometer were of a sufficiently high quality that the interferometer output, particularly the fringe frequencies, held the potential of yielding useful geodetic and astrometric results as well (Cannon et al., 1977).

The model used in the geodetic and astrometric analysis of the LBI fringe frequencies included a polynomial in time representing the relative frequency offset of the two on-site local oscillators , the coefficients of which were to be estimated simultaneously with the geodetic and astrometric parameters. In the results of the LBI parameter estimation procedure the coefficients of the local oscillator polynomial were correlated (in certain cases with correlation coefficients in excess of 0.90) with the solutions for the other parameters of the model. In order to assess the significance of these correlations and to test the reliability of the LBI geodetic and astrometric solutions it was decided to attempt an independent estimate, using Loran-C transmissions, of the local oscillator frequency offset for comparison with the LBI solution.

The data necessary to make such a comparison wereavailable from the station logs for the March and June experiments. For the most part this data consisted of a record at each site, maintained throughout the experiment, of the drift of the "station clock" (driven by the hydrogen maser in each case) relative to the time of arrival of a given Loran-C pulse. The "Daily Phase Values" published in USNO Time Service Publication Series 4 would allow a determination of the relative drift of the two Loran-C pulses and thus a determination of the relative drift of the two "station clocks".

A schematic diagram depicting that portion of the experimental arrangement relevant to this study is shown in FIGURE 1. The frequency standard for the "station clock" at ARO is a hydrogen maser H.P.-10A Ser. 9 maintaining a time scale designated UTC[ARO-H9] while at CRO the frequency standard for the "station clock" is a hydrogen maser H.P.-10A Ser. 11 maintaining a time scale designated UTC[CRO-H11]. The Loran-C pulses received at ARO and CRO during these experiments were emitted from the Nantucket slave station (designated 9930Y) of the U.S. East Coast chain and from the Sylt slave station (designated 7970W) of the Norwegian Sea chain respectively. The reception of the Loran-C pulses at ARO and CRO is used to materialize a time scale designated UTC Loran-C [ARO 9930Y] and UTC Loran-C[CRO 7970W] respectively.

The correlator for the interferometer used in these experiments was an analogue device for which the amplitude of a zero frequency fringe becomes indeterminate. The interferometer was also operating in a double side band mode which, while increasing the signal-to-noise ratio of the correlation function has the disadvantage of being unable to distinguish positive and negative fringe frequencies. In an effort to avoid experimental difficulties arising as a result of these two

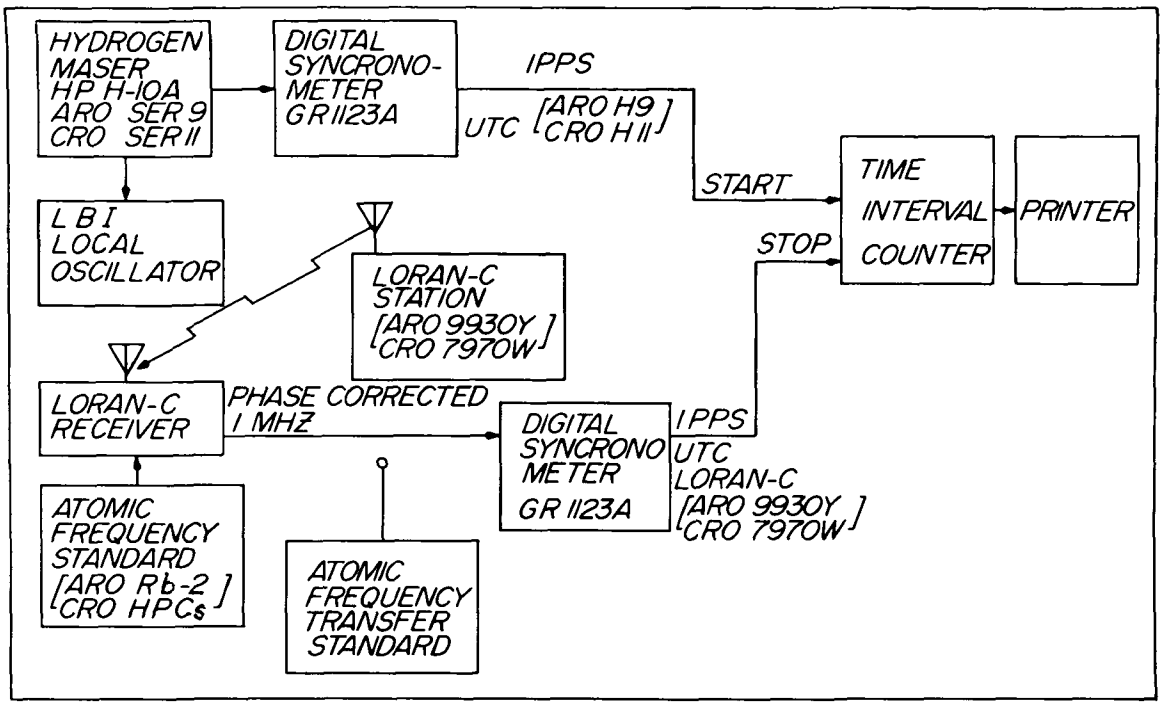


FIGURE 1. Schematic of experimental arrangement for comparing LBI local oscillators.

factors it was decided to deliberately offset the local oscillator at ARO from the local oscillator at CRO by a fixed frequency increment. This "nominal local oscillator offset" was 300 mHz in the March 1973 experiment and 500 mHz in the June 1973 experiment.

II MARCH 1973 EXPERIMENTAL RESULTS

The analysis of the experimental data for March 1973 proceeded as follows.

Defining $\tau_{ARO}(t)$ as

$$\tau_{ARO}(t) = \text{UTC[ARO H9]} - \text{UTC Loran-C[ARO 9930Y]} \qquad (1)$$

and $\tau_{CRO}(t)$ as

$$\tau_{CRO}(t) = \text{UTC[CRO H11]} - \text{UTC Loran-C[CRO 7970W]} \qquad (2)$$

and defining $\tau_{9930}(t)$ as

$$\tau_{9930}(t) = \text{UTC[USNO-M.C.]} - \text{UTC[Loran-C 9930]} \qquad (3)$$

and $\tau_{7970}(t)$ as

$$\tau_{7970}(t) = \text{UTC[USNO M.C.]} - \text{UTC[LORAN-C 7970]} \quad (4)$$

then the drift of the station clocks relative to each other is $\Delta\tau_{ARO/CRO}(t)$ where

$$\Delta\tau_{ARO/CRO}(t) = [\tau_{ARO}(t) - \tau_{9930}(t)] - [\tau_{CRO}(t) - \tau_{7970}(t)] \quad (5)$$

The data for the determination of $\tau_{ARO}(t)$ and $\tau_{CRO}(t)$ were logged during the experiment of March 1973 at each antenna site and are shown together with a maximum likelihood polynomial fit for ARO and CRO in FIGURES 2a and 2b respectively. The error bars shown are $\pm$ 0.2 μs which we have taken as a measure of the standard deviation of a single determination of $\tau_{ARO}(t)$, $\tau_{CRO}(t)$. The order of the polynomial (which in this case is 3rd order) was chosen as the lowest order polynomial from which a further increase in order produced no significant reduction of variance.

The data for the determination of $\tau_{9930}(t)$ and $\tau_{7970}(t)$ are published as "Daily Phase Values and Time Differences" in USNO Time Service Publication Series 4 (USNO Time Service Publications 1973). In determining $\tau_{9930}(t)$ and $\tau_{7970}(t)$ from the "Daily Phase Values" for March 1973 maximum likelihood first order polynomials were fitted to the U. S. East Coast Chain data for February 14, 1973 to May 30, 1973 inclusive to give $\tau_{9930}(t)$ and to the Norwegian Sea Chain data for January 1, 1973 to June 4, 1973 inclusive to give $\tau_{7970}(t)$.

The local oscillator frequency offset between ARO and CRO is $\Delta f_o(t)$ where

$$\Delta f_o(t) = f_{o_{ARO}}(t) - f_{o_{CRO}}(t) \quad (6)$$

and where $f_{o_{ARO}}, f_{o_{CRO}}$ are the local oscillator frequencies, nominally 10,680 MHz, at ARO and CRO respectively. The local oscillator frequency offset as determined by the Loran-C/USNO M.C. data is $\Delta f_{o_{Loran}}(t)$ where

$$\Delta f_{o_{Loran}}(t) = f_o \cdot \frac{d}{dt}[\Delta\tau_{ARO/CRO}(t)] \quad (7)$$

and where f_o is the nominal local oscillator frequency.
The local oscillator frequency offset as determined by inversion of the LBI fringe frequency data is $\Delta f_{o_{LBI}}(t)$.

FIGURE 3 shows a comparison of $\Delta f_{o_{Loran}}(t)$ and $\Delta f_{o_{LBI}}(t)$. The LBI fringe frequency model for $\Delta f_{o_{LBI}}(t)$ includes small relativistic effects

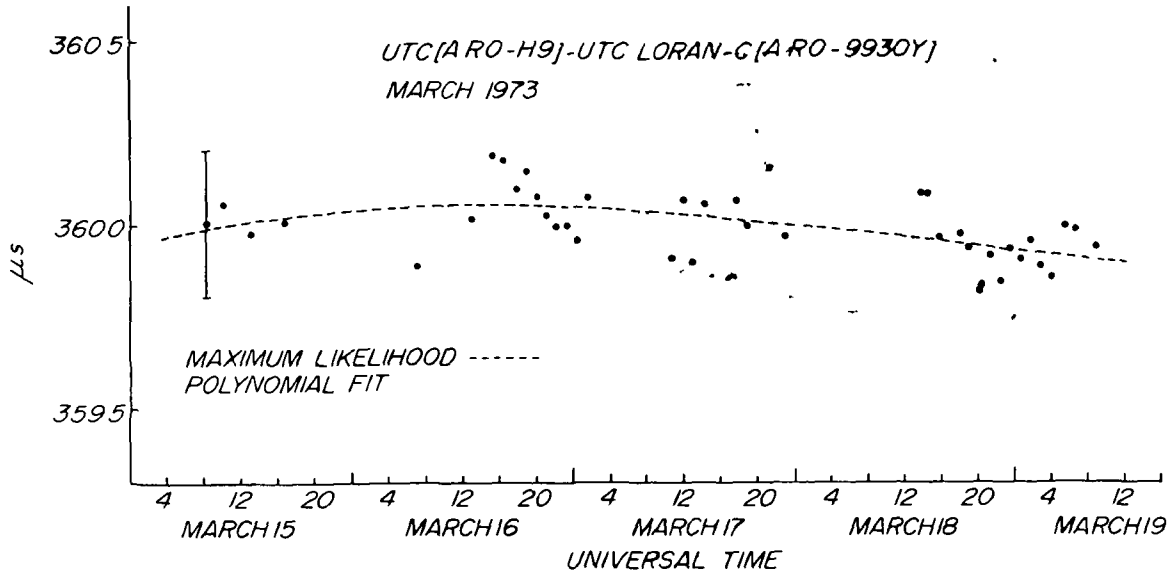


FIGURE 2a

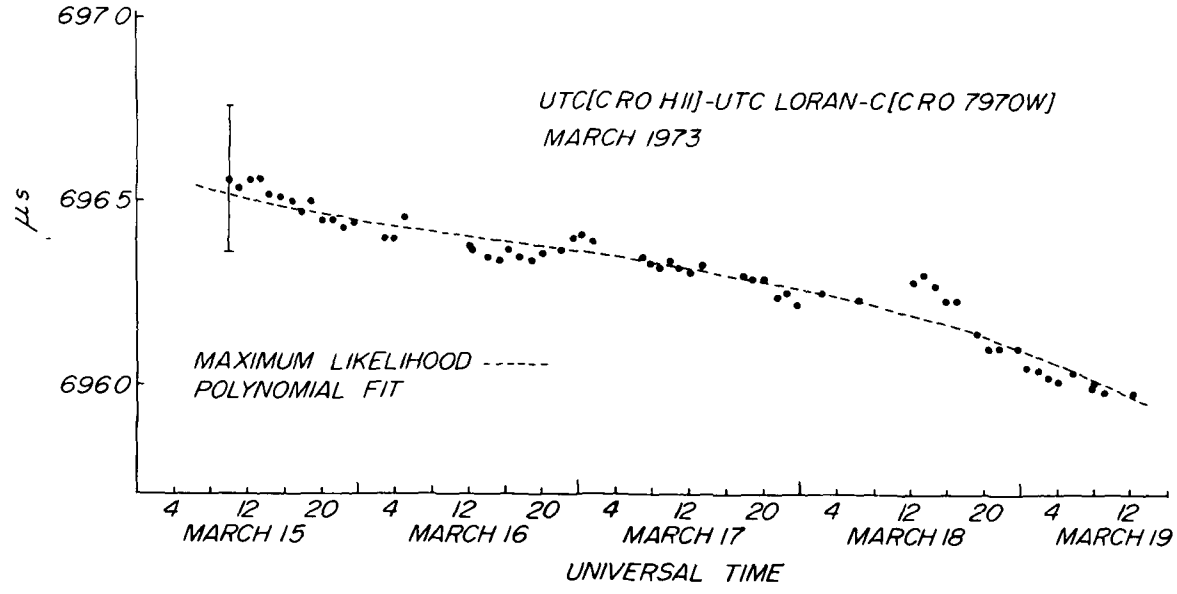


FIGURE 2b

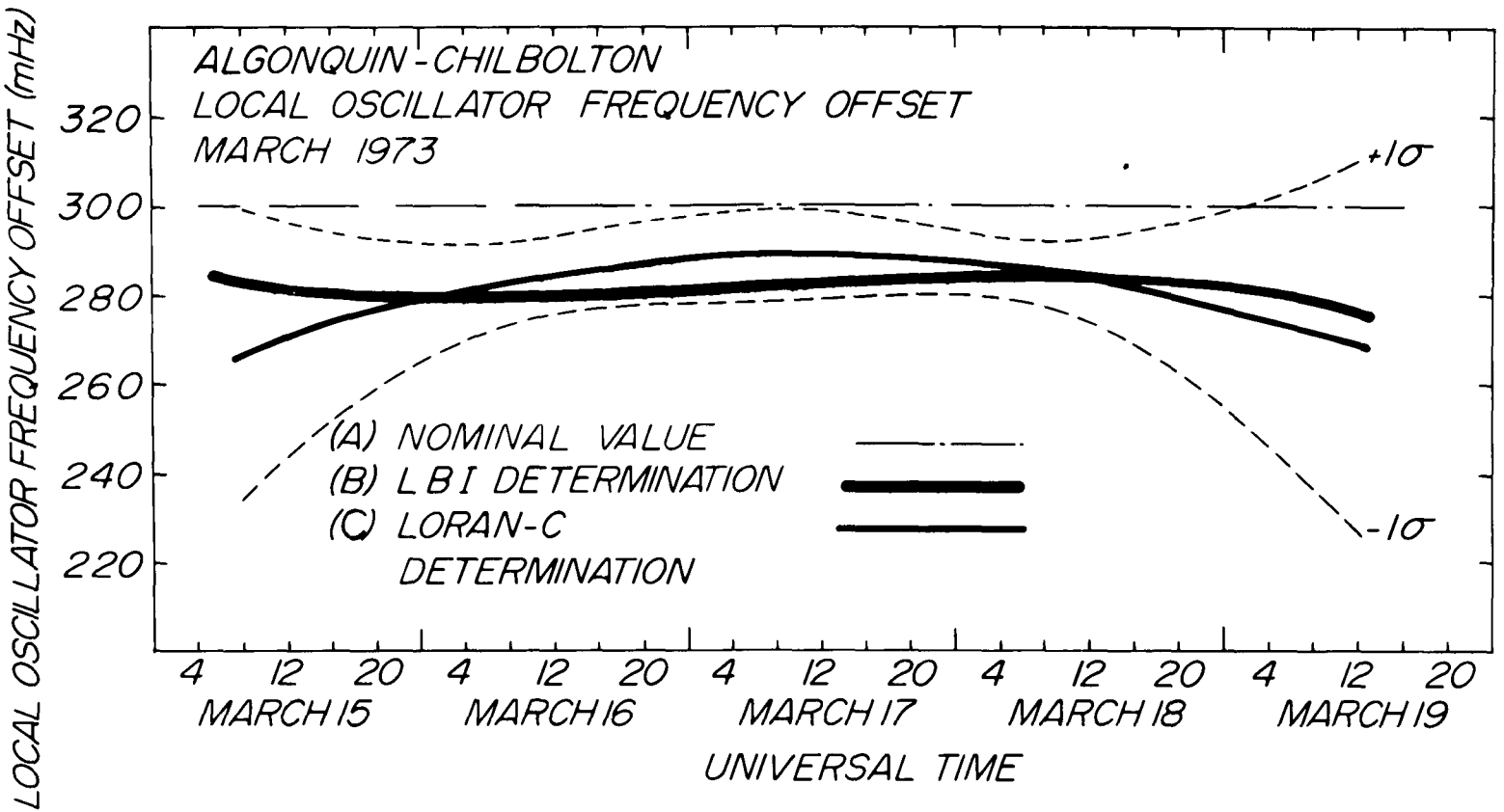


FIGURE 3. Long baseline interferometer local oscillator offset, $\Delta f_o(t)$, as determined by (a) Nominal Setting (b) LBI fringe frequency analysis (c) Loran-C/Time Service data. March 1973.

of the order of a few milliHertz as indicated by Robertson (1975). Also shown in FIGURE 3 are the $\pm$ 1σ standard deviations on $\Delta f_{o_{Loran}}(t)$ indicated by dashed lines and computed by the usual techniques of propagation of error assuming $\pm$ 0.2 μs standard deviation on the individual Loran-C timing measurements. The width of the $\pm$ 1σ region surrounding $\Delta f_{o_{Loran}}(t)$ should probably be somewhat larger as the authors have subsequently been informed (Lavanceau,1976) that the standard deviation on Loran-C timing measurements for the Norwegian Sea Chain is more typically $\pm$ 0.5 μs. In spite of this it is seen that the two methods of estimating the local oscillator offset agree rather well for the experiment of March 1973. Both estimates are seen from FIGURE 3 to disagree with the "expected" or nominal local oscillator offset of 300 mHz by about 20 mHz r.m.s. The disagreement of 20 mHz r.m.s. in 10 GHz between the two independent determinations of $\Delta f_o(t)$ on the one hand and the nominal value of $\Delta f_o(t)$ on the other hand is of the order of 2 parts in 10^{12} and is of the order of the reproducibility or "setability" of "commerical" hydrogen maser frequency standards (Audoin and Vanier, 1976). The disagreement between the two independent determinations of $\Delta f_o(t)$ by Loran-C on the one hand and by LBI on the other hand is of the order of 5 mHz r.m.s. or of the order of 5 parts in 10^{13} and is comparable to the reproducibility or setability of "laboratory" Cs beam frequency standards (Audoin and Vanier, 1976).

III JUNE 1973 EXPERIMENTAL RESULTS

The data for the experiment of June 1973 were much poorer than those of March 1973. In the first place due to a receiver malfunction at Chilbolton it was not possible to monitor the drift of the station clock, UTC[CRO-H11], against UTC Loran-C[CRO 7970 W]. Instead, a transfer frequency standard, Rb-340, was transported from the National Physical Laboratory (NPL) Teddington and the time difference UTC[CRO-H11] - UTC[Rb-340] was logged at Chilbolton during the experiment. At Algonquin Park the Loran receiver was functioning and the time difference UTC[ARO-H9]-UTC Loran-C[ARO 9930Y] was logged as in March 1973. Trouble with the local oscillator phase lock loop, once at Algonquin Park ($\sim$0930 U.T. June 17, 1973) and twice at Chilbolton (0430 U.T. and 1300 U.T. June 17, 1973) produced large discontinuities in these two data sets as is indicated by FIGURES 4a and 4b. An attempt was made to estimate the magnitude of the "time glitches" by piecewise fitting curves to the continuous segments of the data and matching their first derivatives at the times of local oscillator phase lock failure. The resulting "deglitched" clock data are shown in FIGURES 5a and 5b.

In order to obtain a measure of the drift of the station clocks relative to each other, $\Delta\tau_{ARO/CRO}(t)$, it was necessary to refer UTC[CRO H11] back to UTC[USNO M.C.] in spite of the absence of the Loran-C timing data. This was accomplished through the use of the transfer standard Rb-340

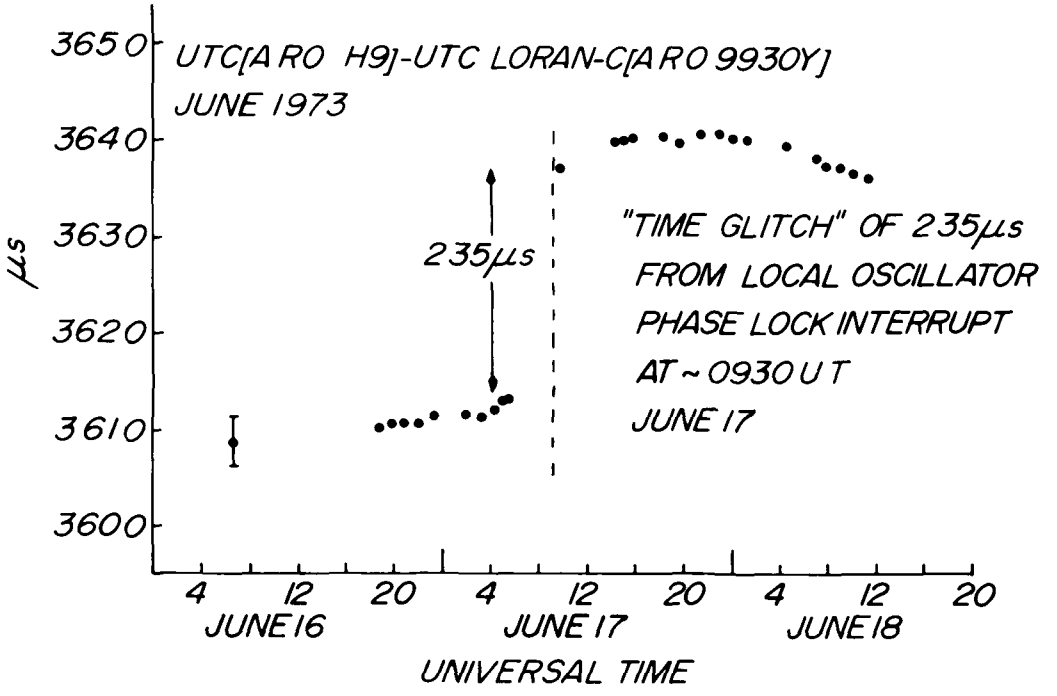


FIGURE 4a

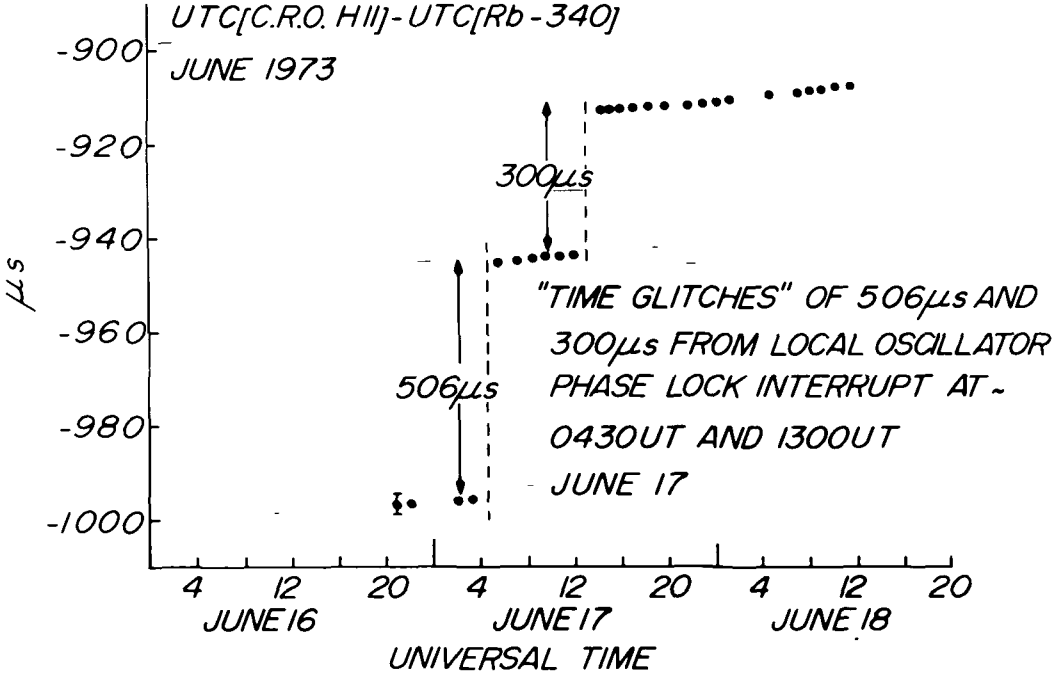


FIGURE 4b

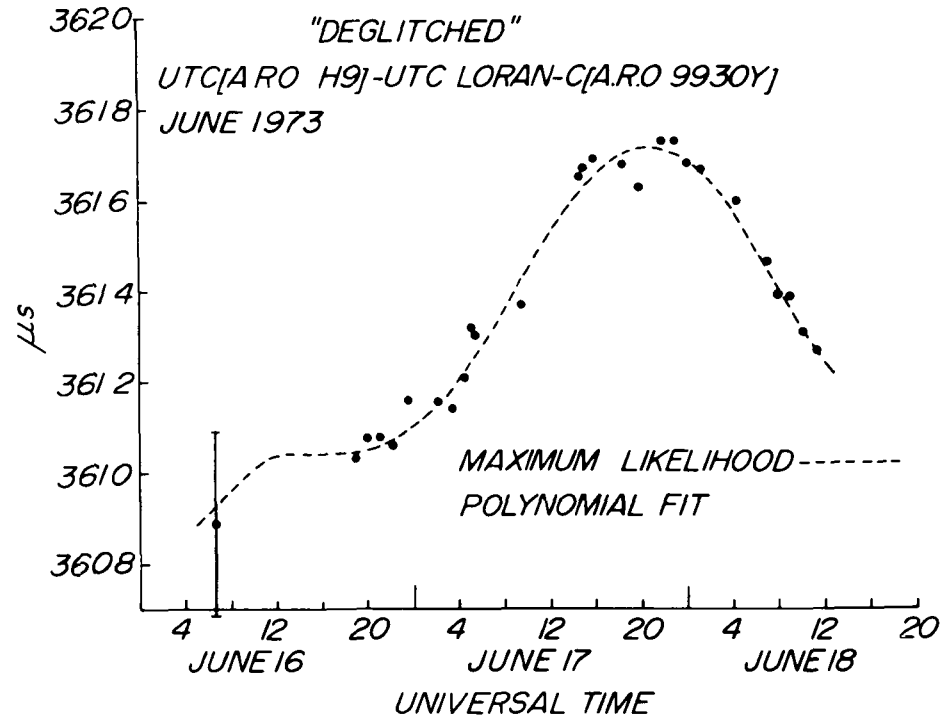


FIGURE 5a

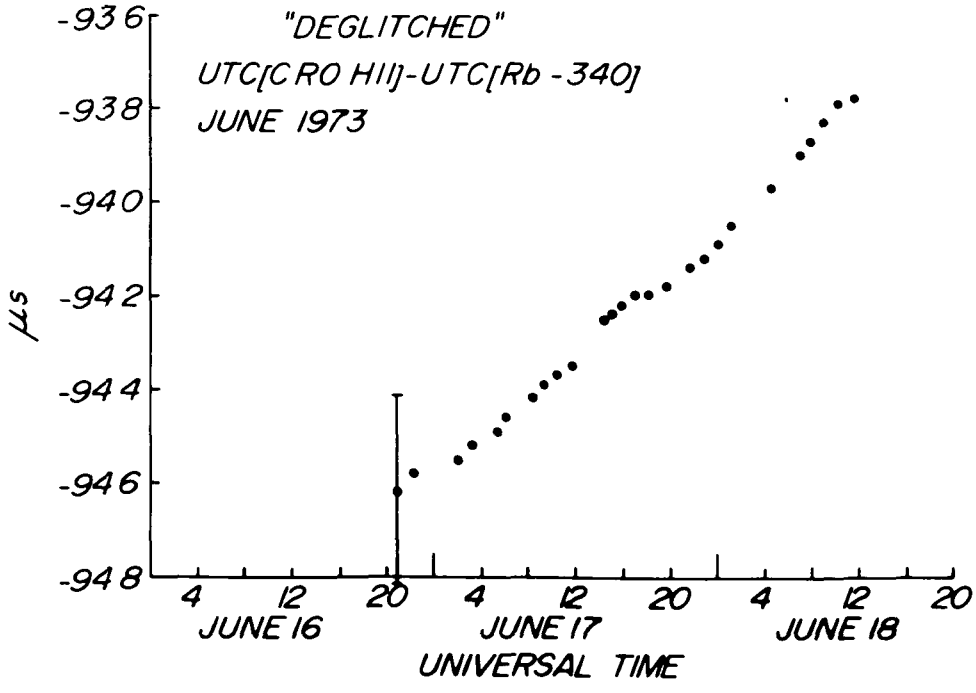


FIGURE 5b

and the laboratory frequency standard Cs-418 at NPL which provides time scale UTC[NPL]. The difference UTC[USNO-M.C.] - UTC[NPL] at ten day intervals, was then obtained from the Annual Report of the BIH (1974).

A comparison of the frequency standard Rb-340 against Cs-418 yielded

(i) ∿10:00 U.T. June 12 1973
UTC[NPL] - UTC[Rb-340] = 43.31 μs

(ii) ∿10:00 U.T. June 19 1973
UTC[NPL] - UTC[Rb-340] = 48.44 μs

It was necessary to assume that Rb-340 had drifted linearly relative to Cs-340 had drifted linearly relative to Cs-418 at the constant rate of -0.733 μs per day for the duration of the experiment. With this assumption the drift of the "station clock" UTC[CRO HII] relative to UTC[NPL] could be established. The results of this calculation together with a maximum likelihood polynomial fit to the data are shown in FIGURE 6.

The rate of Cs-418 relative to USNO M.C. was established by a linear fit to the BIH data for UTC[USNO M.C.] - UTC[NPL] obtained from the

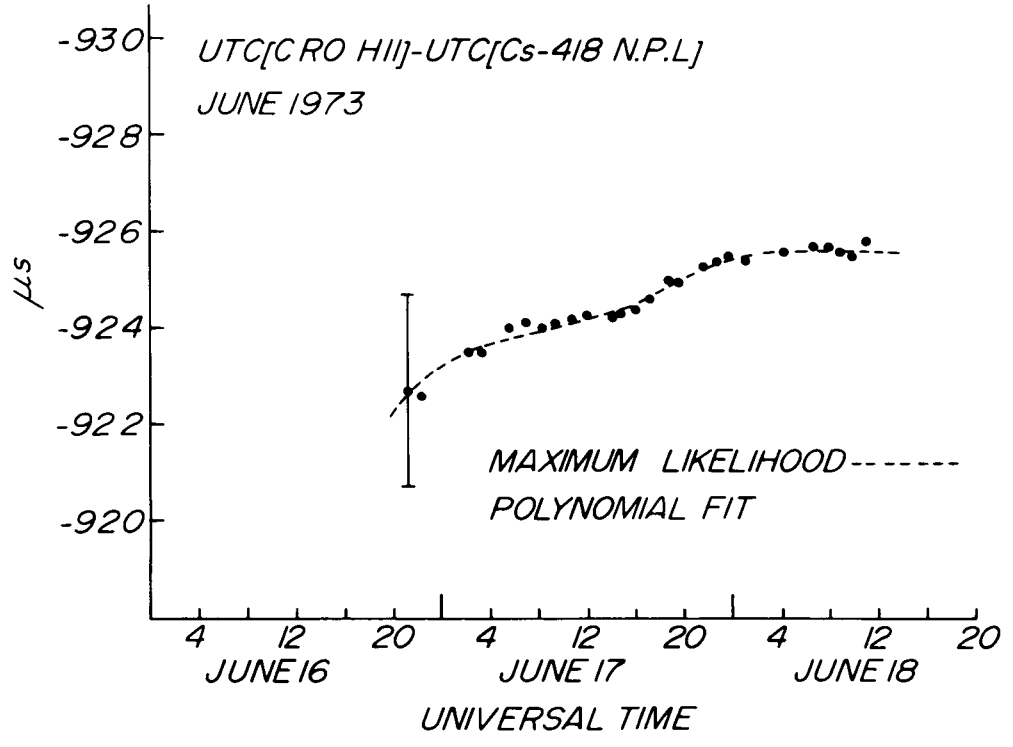


FIGURE 6

BIH Annual Report for 1973 pp 30-33 (1974). Since NPL readjusted the C field, beam current, and loop gain on Cs-418 on June 25, 1973 (Swabey, 1976) the rate of UTC[NPL] relative to UTC[USNO M.C.] for the June experiment was obtained on the basis of BIH data covering the interval January 7, 1973 - June 16, 1973. During this interval UTC [USNO M.C.] - UTC[NPL] was changing at the rate of -0.050 μs per day.

The results of this analysis are shown in FIGURE 7. The heavy curve indicates $\Delta f_{o_{LBI}}(t)$, the LBI determination of the local oscillator frequency offset including small relativistic corrections (Robertson, 1976) and the lighter curve indicates $\Delta f_{o_{Loran}}(t)$, the Loran-C/Time

Service determination of the local oscillator frequency offset. The disagreement between the two solutions is quite large, ∿60 mHz r.m.s., or roughly 6 parts in 10^{12} compared to the results for the March experiment which were ∿5mHz r.m.s. or 5 parts in 10^{13} respectively.

The experimental procedure for June 1973 was clearly inferior to that of March 1973. The experimental procedure for March 1973 allowed (subject to the limitations on precision inherent in Loran-C timing measurements) a more or less continuous, independent monitoring of the relative rate of the two station clocks for comparison with the LBI solution. This was not the case in the June 1973 experiment which required interpolation of clock rates over 5 and 10 day intervals. Considering the large number of assumptions and corrections (each of them with their attendant errors) required to analyse the June 1973 data, even these somewhat poorer results should perhaps be seen as encouraging.

Again in June 1973 as in March 1973 the two independant solutions to the local oscillator frequency offset disagree with the nominal value of 500 mHz by significantly greater amounts than that by which they disagree with each other.

IV CONCLUSIONS

This study appears to indicate that the technique of LBI compares favourably with the use of the Loran-C/Time Service method as a means of monitoring frequency differences between remotely sited frequency standards.

The practical limitations on the precision with which this can be achieved by the Loran-C/Time Service technique are imposed by the variations in the propagation delays of the Loran-C pulses which are the order of ± 0.2 μs - ± 1.0 μs. Even assuming favourable conditions this effect appears to produce a ± 1σ standard deviation of the order of 10-20 mHz relative oscillator frequency difference for oscillators whose frequencies are in the 10 GHz range. Thus it would appear that the Loran-C/Time Service technique allows a comparison of remote

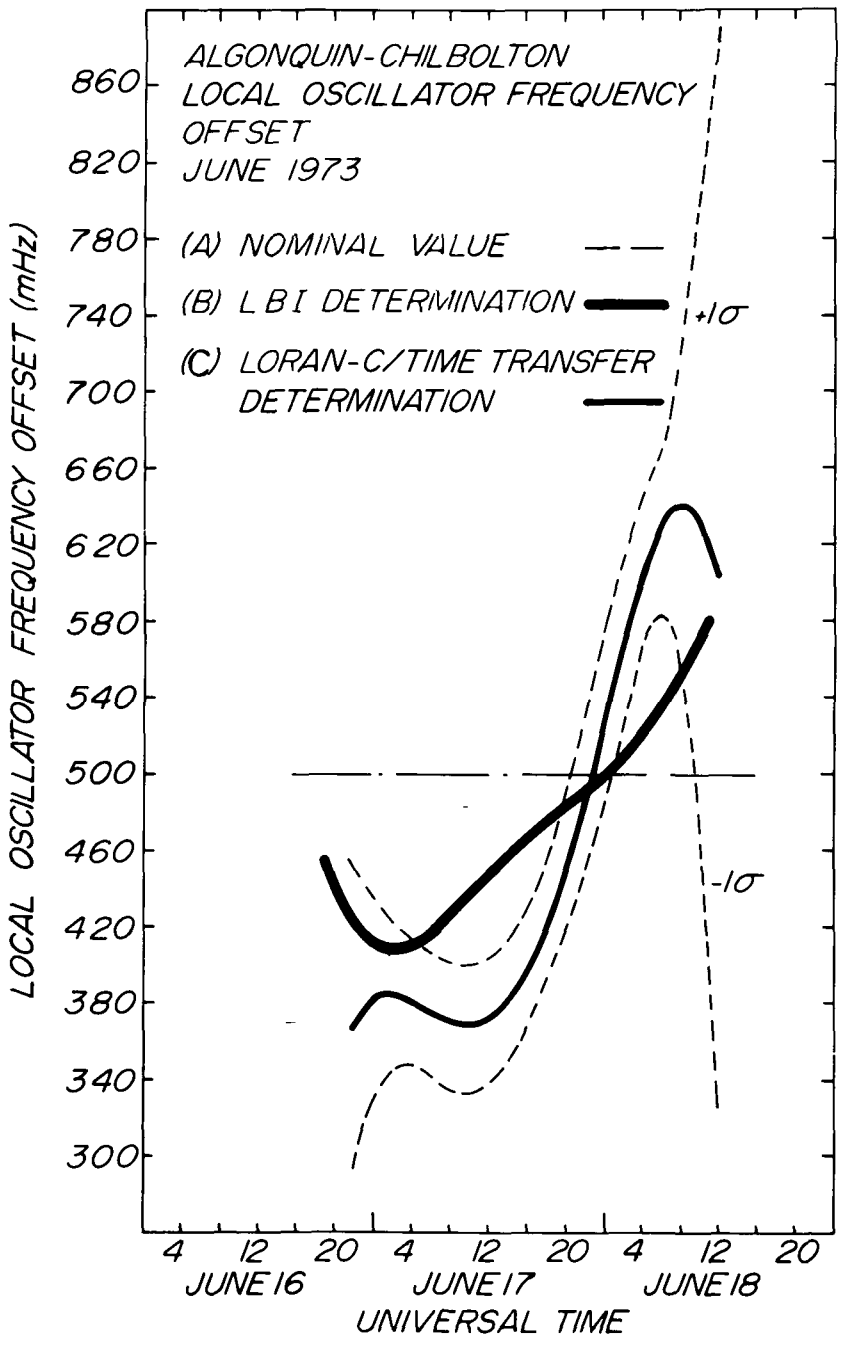


FIGURE 7. Long baseline interferometer local oscillator offset, $\Delta f_o(t)$, as determined by (a) Nominal setting (b) LBI fringe frequency analysis (c) Loran-C/Time Service data June 1973.

frequency standards with a maximum precision of roughly one part in 10^{12} for ground wave Loran-C reception averaged over a few days.

The practical limitations on the LBI technique are imposed by:

(a) uncertainties in the baseline length and orientation

(b) uncertainties in the source coordinates

(c) uncertainties in the atmospheric transmission effects on the received RF signal

(d) uncertainties in the short term rotation rate of the earth.

Estimates of the magnitudes of these effects can be made by combining typical values of the partial derivative of fringe frequency with respect to these various parameters with typical values of their uncertainties. For an interferometer baseline ∿5000 km and observing frequency ∿10 GHz these calculations are summarized in TABLE 1.

TABLE 1.

Uncertain quantity	Typical uncertainty	Typical contribution to fringe frequency
vector baseline	± 1 m. each coordinate	± 1 mHz
source coordinates	± 0".1 each coordinate	± 3 mHz
atmospheric phase delay rate	phase delay fluctuations ∿6 cm. Time scale ∿15 minutes	± 2 mHz
short term rotation rate of earth	l.o.d. known to ± 3 ms on a single night	± 3 mHz

These various effects all combine to produce an uncertainty of ± 5 mHz in the LBI determination of the relative frequency of remotely sited oscillators in the 10 GHz range. This corresponds to a precision of roughly five parts in 10^{13} or comparable to the precision of the Loran-C/Time Service technique. This is confirmed by the experimental results reported here.

ACKNOWLEDGEMENTS

We would like to acknowledge the work of N. W. Broten, T. H. Legg, D. N. Fort of the Herzberg Institute of Astrophysics, Ottawa, Canada; J. L. Yen of the University of Toronto, Toronto, Canada; P. C. Barber and M.J.S. Quigley of the Appleton Laboratory, Slough, England; as well as B. R. Swabey of the National Physical Laboratory, Middlesex, England all of whom assisted with the observations and the correlation of the recorded data.

REFERENCES

Audoin, C., Vanier, J., "Atomic Frequency Standards and Clocks", J. Phys.(E), Scientific Instruments, 9, 697-720, 1976.

Bureau International de l'Heure, "Rapport Annuel pour 1973", Conseil International des Unions Scientifiques, Paris, 1974.

Cannon, W. H., Langley, R. B., Petrachenko, W. T., Kouba, J. "Geodesy and Astrometry by Transatlantic Long Baseline Interferometry", submitted to J.G.R. September 1977.

Lavanceau, J. D., Personal Communication, September 1976.

Legg, T. H., Broten, N. W., Fort, D. N., Yen, J. L., Bale, F. V., Barber, P. C., Quigley, M.J.S., "Long Baseline Interferometry of the Seyfert Galaxy 3C84", Nature, 244, 18-19, 1973.

Legg, T. H., Broten, N. W., Fort, D. N., Quigley, M.J.S., Bale, F. V., Barber, P. C., Yen, J. L., "The Small Scale Structure and Variability of 3C273B", Astrophys. J., 211, 21-30, 1977.

Robertson, D. S., "Special Relativity and Very Long Baseline Interferometers", Nature 257, 467-468, 1975.

Swabey, B. R., Personal Communication, September 1976.

USNO Time Service Publication Series 4, January-December, 1973.

PRECISE CLOCK SYNCHRONIZATION VIA VERY-LONG-BASELINE INTERFEROMETRY

T.A. Clark (NASA-GSFC), C.C. Counselman (MIT),
P.G. Ford (MIT), L.B. Hanson (Lincoln Laboratory),
H.F. Hinteregger (Haystack Obs.), W. Klepczynski (USNO),
C.A. Knight (Haystack Obs.), D.S. Robertson (NGS),
A.E.E. Rogers (Haystack Obs.), J. Ryan (NASA-GSFC),
I.I. Shapiro (MIT), and A.R. Whitney (Haystack Obs.)

ABSTRACT

Hydrogen-maser clocks at the 37-meter-diameter radio telescope of the Haystack Observatory in Westford, Massachusetts, and the 43-meter-diameter radio telescope of the National Radio Astronomy Observatory in Green Bank, West Virginia, were synchronized by very-long-baseline interferometry on 28 March 1977 and on 23 September 1977. The synchronization was also accomplished independently on each of these occasions by means of traveling Cesium clocks. The clock data, fully analyzed in each case only after the completion of the corresponding VLBI data analysis, confirmed the VLBI results to within 19 and 13 nanoseconds for the first and second experiments, respectively.

Accurate clock synchronization via very-long-baseline interferometry (VLBI) has been possible for several years, and has been a byproduct of many precision astrometric and geodetic experiments (1,2). However, most past synchronization results have been limited in absolute accuracy by certain constant, but poorly known, instrumental delays. Accurate absolute synchronization by VLBI was only recently (3) demonstrated in a short (~1 km) baseline experiment, in which, for the first time, care was taken to estimate or to measure all instrumental delays. Here we report the first absolute synchronization results from relatively long, 845-km, baseline experiments. These experiments are also the first in which the synchronization by interferometry was checked subsequently by an independent agency [the U. S. Naval Observatory (USNO)].

The synchronization experiments involved the hydrogen-maser clocks at the 37-m-diameter radio telescope of the Haystack Observatory in Westford, Massachusetts, and the 43-m-diameter radio telescope of the National Radio Astronomy Observatory (NRAO) in Green Bank, West Virginia. In the first experiment, on 28 March 1977, the synchronization via VLBI was checked by transporting two Cesium clocks from the USNO in Washington, D.C., one to each of the telescopes, and both back to Washington. In the second experiment, on 23 September 1977, the two Cesium clocks were transported together from the USNO to Haystack, then to NRAO, and finally back to the USNO.

Figure 1 shows a block diagram of the interferometer terminals used in the experiments. A fast rise time (<30 ps) pulse generator was used to calibrate delays in the receiver and recording electronics. The calibration pulse was also returned from the pulse generator, which was located close

to the telescope feed, to the control room for easy comparison with the clock which controlled the VLBI recording. A hydrogen-maser frequency standard controlled both the calibration pulse generator and the recording clock both at Haystack and at NRAO.

In our VLBI system the delay of a signal arriving from a distant quasi-stellar radio source is measured using a bandwidth synthesis technique (4) involving the sequential sampling of 360-kHz bands spaced over a much wider spanned bandwidth of 100 MHz, centered at 8441 MHz. The multiband delay measurement has a 1 microsecond ambiguity imposed by a minimum spacing of 1 MHz between the narrow, 360-kHz band samples. However, the ambiguity is eliminated by using the less precise, but unambiguous, delay measurement obtained from the crosscorrelation of signals within a single 360-kHz band.

The difference between the readings of the independent clocks controlling the two interferometer terminals is derived from the analysis of a set of VLBI observations of several radio sources, by simultaneous estimation of baseline vectors, radio source positions, and clock parameters (5). The results from the experiment performed on 28 March 1977 are given in Table 1, where line 16 shows the estimated difference between the VLBI clocks after correction for the instrumental delays. An instrumental delay correction for the antenna geometry (line 1) is needed to correct for the difference in signal delay between the baseline vector termination point (6) and the antenna feed point. Line 21 shows the difference between the VLBI terminal clocks as estimated from the traveling clocks, after correction for the linearly-interpolated relative drift between the portable clocks, based on pre-trip and post-trip comparisons made at the USNO in Washington.

Table 2 shows the results of the experiment performed on 23 September 1977. In this experiment, since Haystack was visited by the traveling clocks approximately seven hours later than NRAO, it was necessary to account for the estimated drifts, over this interval, of the traveling clocks relative to Haystack's clock. (See line 24 of Table 2.) The latter's rate was already accurately known relative to that of the USNO Master Clock, through long-term comparisons via Loran C. The rates of the traveling clocks were determined from direct comparisons with the Master Clock in Washington, before and after the trip.

The accuracy of the VLBI clock synchronization is not limited by the uncertainty of the estimate of the radio signal (group) delay, which is much less than 1 nanosecond, but rather by the accuracy of the determination of the various instrumental delays. The cumulative error arising from these estimates of instrumental delays is thought to be less than ±10 nanoseconds. The error of the synchronization via traveling clocks is limited by clock drifts and is estimated to be under ±20 nanoseconds.

Acknowledgements. The Massachusetts Institute of Technology experimenters were supported in part by the National Aeronautics and Space Administration (NASA) under grant NGR22-009-839 and in part by the National Science Foundation (NSF) under grant EAR76-22615.

The Haystack experimenters were supported by NASA contract NAS5-22843. All NASA support is derived from the Office of Space and Terrestrial Applications (OSTA) under the Tectonic Plate Motion Project of the Earth and Ocean Dynamics Applications Program. Radio astronomy programs at the Haystack Observatory are conducted with support from the NSF, grant GP-25865.

The National Radio Astronomy Observatory is operated by Associated Universities, Inc., under contract with the NSF.

References and Notes

1. H. F. Hinteregger, et al., Science 178, 396 (1972).

2. I. I. Shapiro, et al., Science 186, 920 (1974); 191, 451.

3. C. C. Counselman, et al., Proc. IEEE 65, 1622 (1977).

4. A. R. Whitney, et al., Radio Science 11, 421, (1976).

5. I. I. Shapiro in Methods of Experimental Physics, Vol. 12, Part C, M. L. Meeks, Editor (Academic Press, 1976).

6. The baseline termination point at Haystack is the intersection of azimuth and elevation axes and at NRAO it is the intersection of the polar axis and the perpendicular plane that contains the declination axis.

Table 1 Comparison Between VLBI Clock Synchronization and Traveling Clock Synchronization for the 28 March 1977 Experiment

Line No.		Haystack (μsec)	NRAO (μsec)	Comments
1	Antenna geometrical delay	0.06977	0.05167	Estimated from antenna geometry
2	Feed delay	0.00920	0.00175	Estimated from feed geometry
3	Calibration cable delay	0.60500	0.59090	Measured with a time domain reflectometer
4	Calibration injection delay	0.00800	0.00900	Estimated from cable lengths
5	(Clock-cal. pulse)	0.77800	0.76310	Measured using electronic counter (HP5345A)
6	Instrumental delay	-0.10203	-0.12778	Lines (1)+(2)+(3)-(4)-(5)
7	Receiver delay	0.01	0.01	Estimate
8	IF cable delay	0.61	0.63	Measured with time domain reflectometer
9	IF to video converter delay	5.60	5.00	Estimated from impulse response
10	Recording system delay	-21.01	-22.14	Measured by test signal injection
11	Single band instrumental delay	-14.71	-16.45	Lines (1)+(2)+(7)+(8)+(9)+(10)
12	Clock solution from single-band VLBI data	20.208	Clock solution for an epoch of 1920 UT, 28 March 77	
13	Line 12 corrected for single-band instrumental delays	21.948	Lines $(12)+(11)_H-(11)_N$	
14	Clock solution from multi-band VLBI data	xx.8133	Clock solution for an epoch of 1920 UT, 28 March 77	
15	Line 14 corrected for inst. delays	xx.8390	Lines $(14)+(6)_H-(6)_N$	
16	(NRAO VLBI Clock-Haystack VLBI Clock)	21.8390	1 μsec ambiguity resolved by line (13)	
17	(USNO PC653-USNO PC1255)	1.813	Measured at 1310 UT, 28 March 77 before departure for each VLBI site	
18	(USNO PC653-USNO PC1255)	1.839	Measured at 0310 UT, 29 March 77 after return of traveling clocks to Washington, D.C.	
19	(Haystack VLBI Clock-USNO PC1255)	13.120	Measured at 1911 UT, 28 March 1977	
20	(NRAO VLBI Clock-USNO PC653)	33.114	Measured at 1928 UT, 28 March 1977	
21	(NRAO VLBI Clock-Haystack VLBI Clock)	21.820	Lines (20)-(19)+((17)+(18))/2	
22	(VLBI Clock Sync.-Trav. Clock Sync.)	0.019	Difference of results from two methods of clock synchronization Lines (16)-(21)	

Table 2 Comparison Between VLBI Clock Synchronization and Traveling Clock Synchronization for the 23 September 1977 Experiment

Line No.		Haystack (μsec)	NRAO (μsec)	Comments
1	Antenna geometrical delay	0.06977	0.05167	Estimated from antenna geometry
2	Feed delay	0.00920	0.00175	Estimated from feed geometry
3	Calibration cable delay	0.60500	0.58740	Measured with a time domain reflectometer
4	Calibration injection delay	0.00800	0.00900	Estimated from cable lengths
5	(Clock-cal. pulse)	0.75800	0 13070	Measured using electronic counter (HP5345A)
6	Instrumental delay	-0 08203	0.50112	Lines (1)+(2)+(3)-(4)-(5)
7	Receiver delay	0.01	0.01	Estimate
8	IF cable delay	0.61	0.63	Measured with time domain reflectometer
9	IF to video converter delay	5 60	5 00	Estimated from impulse response
10	Recording system delay	-21.01	-22.14	Measured by test signal injection
11	Single band instrumental delay	-14.71	-16.45	Lines (1)+(2)+(7)+(8)+(9)+(10)
12	Clock solution from single-band VLBI data	15.530	Clock solution for an epoch of 1520 UT 23 Sept 77	
13	Line 12 corrected for single-band inst. delays	17.270	Lines $(12)+(11)_H-(11)_N$	
14	Clock solution from multi-band VLBI data	xx.8202	Clock solution for an epoch of 1520 UT 23 Sept 77	
15	Line 14 corrected for inst. delays	xx.2370	Lines (14) and $(6)_H-(6)_N$	
16	(NRAO VLBI Clock-Haystack VLBI Clock)	17.2370	1 μsec ambiguity resolved by line (13)	
17	(Haystack VLBI Clock - Cs 1117)	16.4350	2227 UT, 23 Sept 77 (measured with 48" cable on Cs)	
18	(Haystack VLBI Clock - Cs 1368)	17.1890	2227 UT, 23 Sept 77 (measured with 48" cable on Cs)	
19	(Haystack VLBI Clock - Mean of Cs)	16 8066	Line ((17)+(18))/2 corrected for 48" of cable	
20	(NRAO VLBI Clock - Cs 1117)	33.6580	1519 UT, 23 Sept 1977	
21	(NRAO VLBI Clock - Cs 1368)	34.4260	1519 UT, 23 Sept 1977	
22	(NRAO VLBI Clock - Mean of Cs)	34.0420	Lines ((20)+(21))/2	
23	(NRAO VLBI Clock - Haystack VLBI Clock)	17.2354	Lines (22)-(19)	
24	(NRAO VLBI Clock - Haystack VLBI Clock) corrected for drifts over 7 hrs to Haystack	17.2238	Corrected for Cs drift rate of 3.05 ns/hour and for a Haystack maser drift rate of 1.39 ns/hour, both measured relative to USN Master Clock	
25	(VLBI Clock Sync. - Trav. Clock Sync)	0.0132	Difference of results from two methods of clock synchronization, lines (16)-(24)	

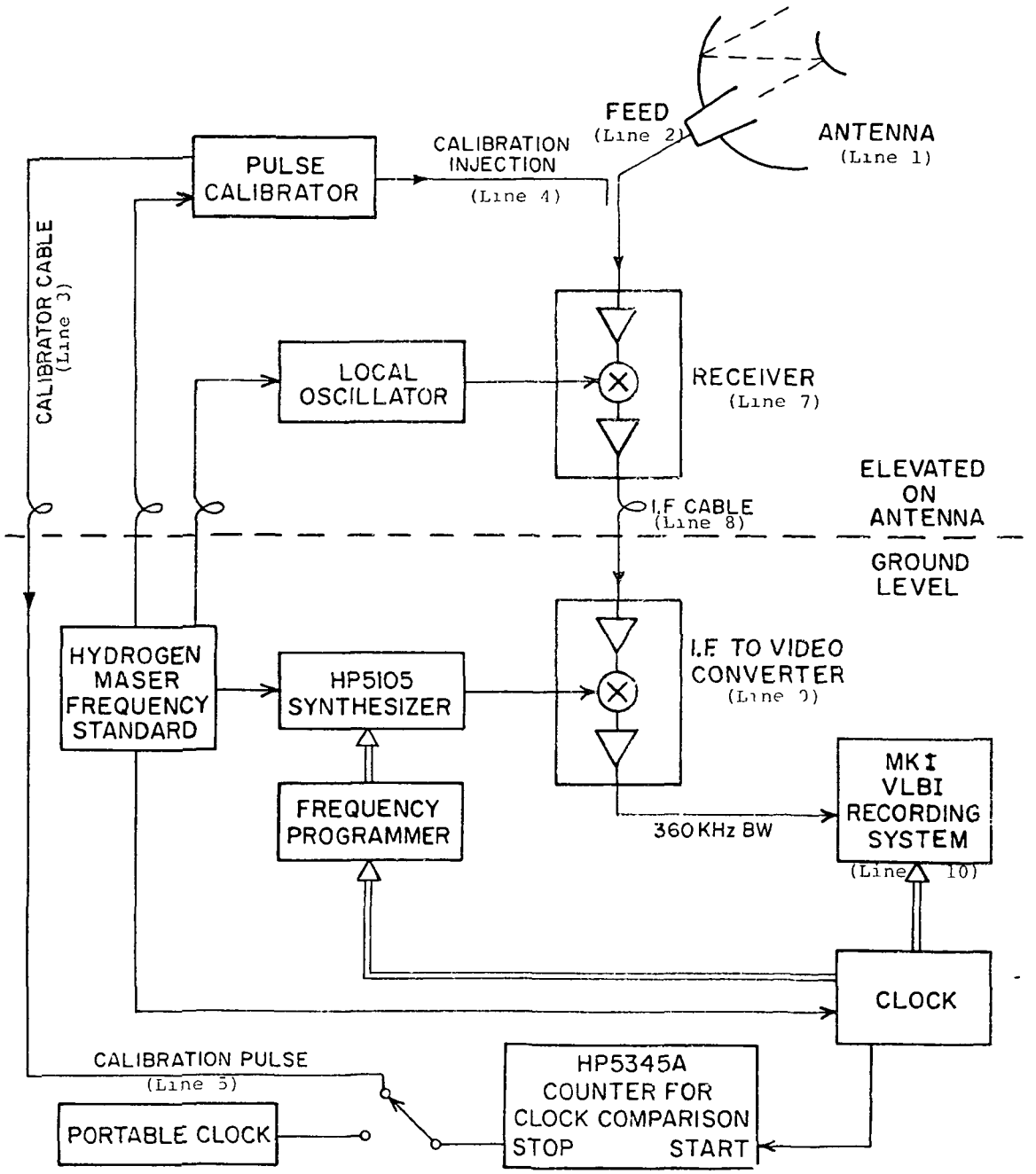


Figure 1 Block Diagram of VLBI Terminal (Line numbers in parentheses refer to Tables 1 and 2.)

Page intentionally left blank

Page intentionally left blank

REAL-TIME ACCURATE TIME TRANSFER AND FREQUENCY STANDARDS EVALUATION VIA SATELLITE LINK LONG BASELINE INTERFEROMETRY

S.H. Knowles, W.B. Waltman (E.O. Hulburt Center for Space Research, NRL, Washington, D.C. 20375)

W. B. Klepczynski (USNO, Washington, D. C. 20390)

N.W. Broten, D.H. Fort (National Research Council, Ottawa, Canada)

K. I. Kellermann, B. Rayhrer (NRAO, Green Bank, West Virginia 24944)

G. W. Swenson, (University of Illinois, Urbana, Illinois)

and

J.L. Yen (University of Toronto, Toronto, Canada)

Radio interferometry on natural sources which has been an important radio astronomy technique, requires two connections between the antennas; a data link and a local oscillator synchronization link. For baselines of up to a few kilometers, these connections are made by cables, and for up to about 50 kilometers by direct microwave link. Radio interferometry over longer distances has used the "VLBI" technique, which records the two data streams on magnetic tape for later correlation and uses independent atomic frequency standards at each station. An alternative method for long-baseline interferometers is to use an artificial satellite as a real-time link between the two antennas. This method was first successfully demonstrated by our group in November 1976, and reported on at the 8th PTTI Conference. This report records the results of an experiment by our group conducted in February 1977 to demonstrate the feasibility of a real-time accurate time transfer. Observing sites at Green Bank, West Virginia (National Radio Astronomy Observatory) and Lake Traverse, Ontario (Algonquin Radio observatory) were used for the experiment. A communications satellite known variously as Hermes or CTS-1 was made available courtesy of the Canadian Ministry of Communications. Cesium beam time standards belonging to the U. S. Naval Observatory were transported to each site as an independent check on the accuracy of the time transfer; they were calibrated at the beginning and end of each trip. The actual experiment was performed on 20 February 1977 at 1955 UT, observing the natural radio source 3C84 at 2.8 cm wavelength. The measured delay was observed in real time at the master

station in Ontario by looking at the observed correlation on a cathode-ray display. The correlation output was also recorded on magnetic tape for later analysis. The raw measured time difference was ARO-GB = +470 nanoseconds. With our system bandwidth of 10 MHz, the correlation function was 100 nanoseconds wide, and its centroid could be determined with a precision of about 10 nanoseconds. This measurement was then corrected for the cable delays at each station, and agreed with that predicted from the cesium clocks to within 70 nanoseconds. This error could have been accounted for, e.g., by a 25 meter error in baselines or the relatively coarse cable delay measurements at Algonquin Radio Observatory. Bandwidth synthesis and accurate calibration techniques as described in Counselman et al. (1977) could be applied to yield real-time comparisons with an accuracy of a few nanoseconds. It should be noted that by transmitting sampled and clocked data the delay time of the satellite link does not enter into the measurement.

As an additional demonstration of the versatility of a real-time interferometer link, the stability of several different samples of atomic frequency standards was compared by substituting them in turn as master oscillators for the local oscillator at one station and observing the apparent dispersion in frequency of the interferometer fringes. This is known to be a very sensitive test of frequency standards because of the high multiplication involved. The results are displayed in figure 1. In each case a one minute averaging time was used. Resolution is 0.016 MHz, or about 6×10^{-13}. It will be seen that the H-P 5065A rubidium standard is close to the stability of a hydrogen maser over this period, while a cesium standard, even the "supertube" version, is appreciably poorer. These measurements did not test long-term stability. Also illustrated is an attempt to improve a cesium standard by using an external crystal idler instead of its internal crystal. This did not result in noticeable improvement; the same is true when the time constant of the servo loop was changed in a cesium standard equipped with this adjustment. We are continuing our satellite-link VLBI experiments. Our current objective is to use the satellite to provide a local oscillator link as well as a real-time data link. A two way path is required to correct for changes in the satellite position. Since the translation oscillator in the Hermes satellite is not phase coherent, the beacon signal from the satellite must also be used at each station to correct for the satellite oscillator phase. The use of the satellite link to correct the L.O. phase will provide much higher phase accuracy then previous VLBI techniques and should greatly ease the requirements on

the frequency standards used.

1. S. H. Knowles, W. B. Waltman, N. W. Broten D. H. Fort, K. I. Kellermann, B. Rayhrer, J. L. Yen, and G. W. Swenson, "First Results from a Satellite Data Link Radio Interferometer", Proceedings of the 8th Annual PTTI Meetıng, p. 529, November 30-December 2, 1976, NASA Doc. No. X-814-77-149.

2. C. C. Counselman, I. I. Shapiro, A. E. E. Rogers, H. F. Hinteregger, C. A. Knight, A. R. Whitney, and T. A. Clark, "VLBI Clock Synchronization", Proceedings IEEE, 65, 1622 (1977).

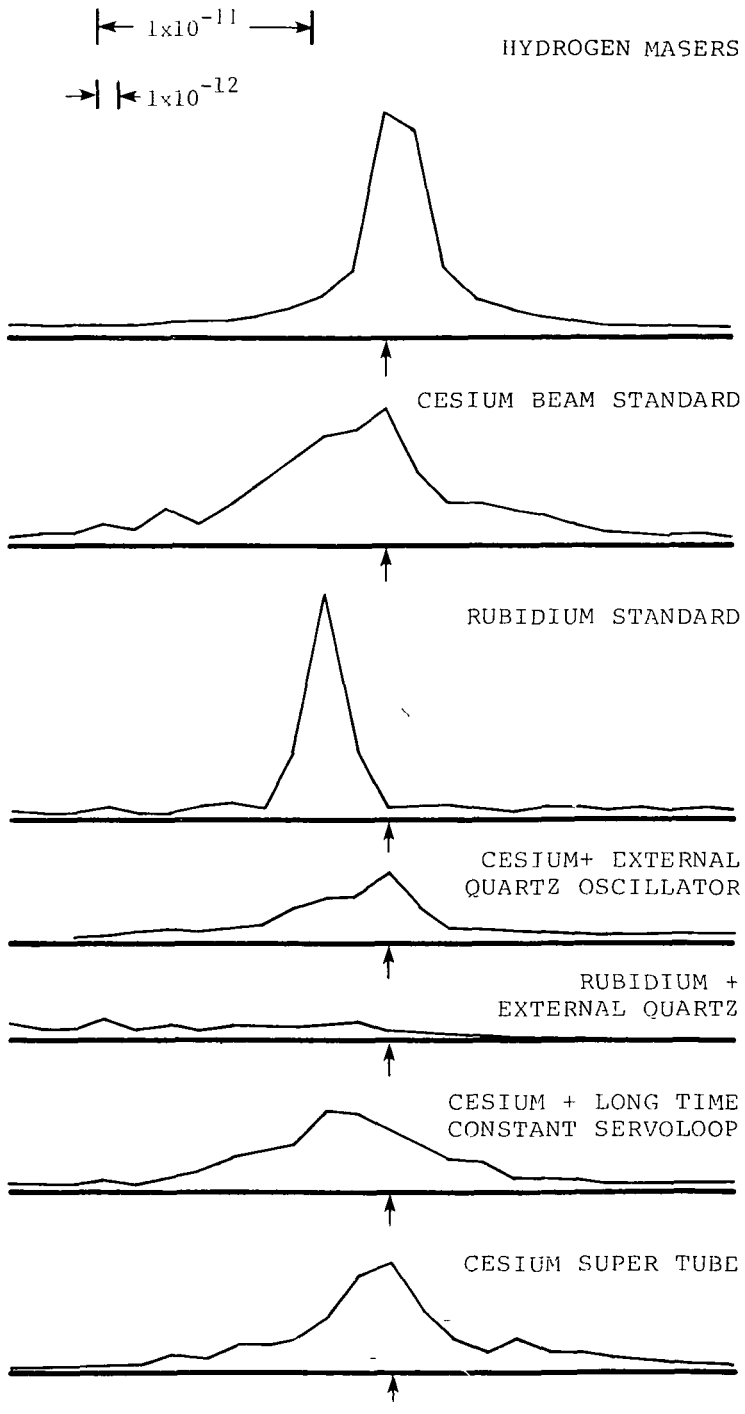


Figure 1. Comparison of frequency spread of various oscillators; 1 minute averaging time. In all cases a hydrogen maser was used for the other local oscillator.

TIME FROM NBS BY SATELLITE

D. W. Hanson, D. D. Davis, and J. V. Cateora National Bureau of Standards, Boulder, Colorado

ABSTRACT

As a complement to the present time and frequency services of WWV, WWVH, and WWVB, the National Bureau of Standards (NBS) is now sponsoring a satellite-disseminated time code using the GOES[1] satellites of the National Oceanic and Atmospheric Administration. The time code is referenced to the UTC(NBS) time scale, giving Coordinated Universal Time. It is considered by NOAA to be a permanent feature of the GOES satellites intended to serve the GOES users. It may, however, be used by others requiring a general purpose time reference. The time code is available to the entire Western Hemisphere from two satellites on a near full-time basis.

This paper is basically an update of last year's PTTI paper on the GOES time code. The time-code generation system is being improved to include a continuous update of its ephemeris message in place of the present 30-minute updated message; triple redundancy is being designed into the generation equipment at the Wallops Island, Virginia, ground station; and monthly status reports will be included in the NBS Time and Frequency Services Bulletin; e.g., scheduled outages, solar eclipses, and past performances. This paper includes comments on NBS experience with the reception of the signals, possible sources of interference, and how to obtain best results.

INTRODUCTION

In May 1974, NBS began an experiment of time-code broadcasts from the National Oceanic and Atmospheric Administration's (NOAA's) Geostationary Operational Environmental Satellites (GOES). Based upon subsequent successful performance and useful application for the users of the GOES

[1] GOES is the acronym for Geostationary Operational Environmental Satellite.

satellites, NOAA now considers the time code to be a permanent feature. In March 1977, NBS and NOAA formally agreed to continue the time code broadcasts, with NBS operating the code and providing the time and frequency reference.

There are now three satellites in orbit; two are operational and the third is an "in-orbit" "hot" spare ready to replace either satellite in case of failure. There is another satellite ready for launch when needed and three more satellites are under construction. This complement of GOES satellites is expected to insure two satellites in continuous operation until the late 1980's. Plans to continue the program beyond the year 2000 are being made.

Considering the long life, the important mission[2] of the GOES program, and the wide geographical coverage of the satellites, the GOES time signals are finding many applications where reliability, automatic signal recovery, and accuracy are desirable. Being geostationary, GOES is a source of continuous synchronization, offering a significant advantage over non-geostationary satellites which can only provide exposure to the user during brief periods of time at intervals ranging from about one hour to many hours or even days.

TIME CODE SYSTEM

The time code is part of the interrogation channel of the GOES satellites. The interrogation channel is used to command remote sensors to send their collected data to the GOES satellites. The satellites relay these data to the Command and Data Acquisition (CDA) facility at Wallops Island, Virginia, for processing and dissemination to users. Interrogation messages are continuously being sent through the GOES satellites. The format of the messages is shown in figure 1.

The interrogation message is exactly one-half second in length or 50 bits. The data rate, provided by atomic oscillators, is 100 bits per second (b/s). The interrogation message is binary and phase modulates a carrier ± 60 degrees after being Manchester-encoded; i.e., data and data clock are modulo-two added before modulating the carrier. An interrogation message consists of four bits representing a BCD word of time code beginning

---

[2]The GOES satellites provide meteorological observations for:
- -Continuous storm tracking through cloud photography
- -Cloud analysis-density, temperature, height, wind velocity
- -Surface temperature mapping
- -Space environment sun/earth interaction
- -Remote sensing of floods, rain, snow, Tsunamis, earthquakes, air/water pollution, etc.

on the half-second of UTC, followed by a maximum length sequence (MLS) 15 bits in length for message synchronization, and ending with 31 bits as an address for a particular remote sensor. Sixty interrogation messages are required to send the 60 BCD time-code words constituting a time-code frame. The time-code frame begins on the half minute of UTC and repeats every 30 seconds (see figure 2). The time code frame contains a synchronization word, a time message (UTC), the UT1 correction, and the satellite's position in terms of its longitude, latitude, and height above the surface of the earth minus a bias of 119,300 microseconds. The position information is presently updated on the half hour.

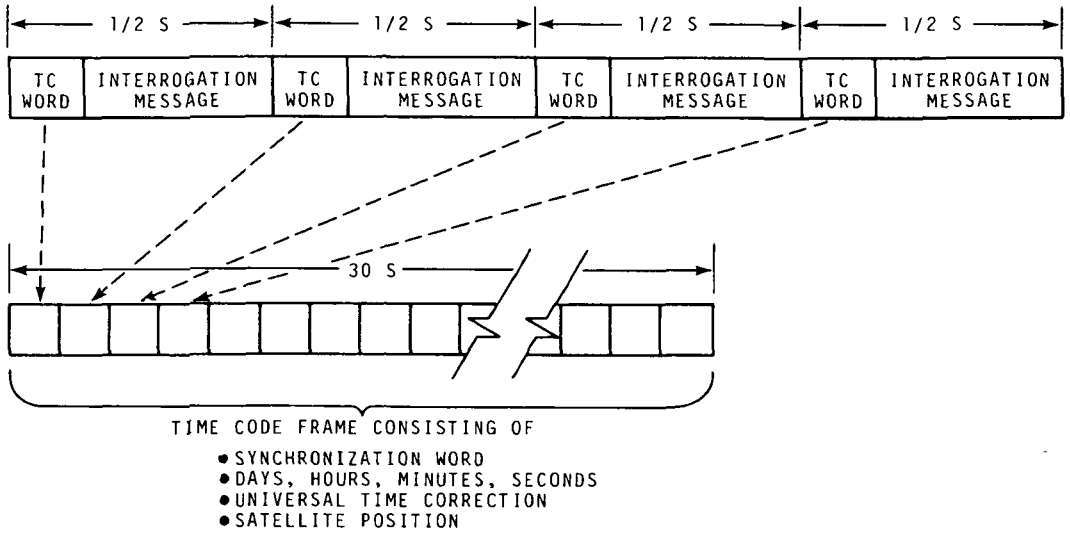


Fig. 1-Interrogation-message format

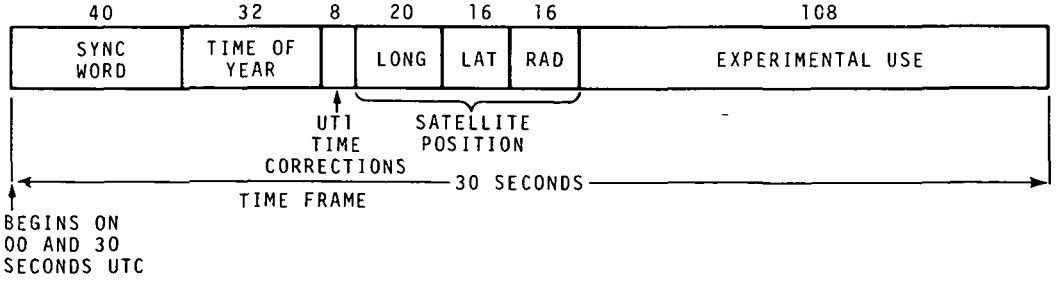


Fig. 2-Time code format

NBS maintains an ensemble of three clocks at NOAA's CDA facility, Wallops Island, Virginia. These clocks provide the time and frequency reference for the time code. The time-code generation system, partly shown in figure 3, is completely redundant and fully supported by an uninterruptable power supply. There is a communication interface between the equipment and NBS/Boulder using a telephone line. Over the telephone line, satellite position information is sent to the CDA and stored in memory for eventual incorporation into the time code and interrogation message.

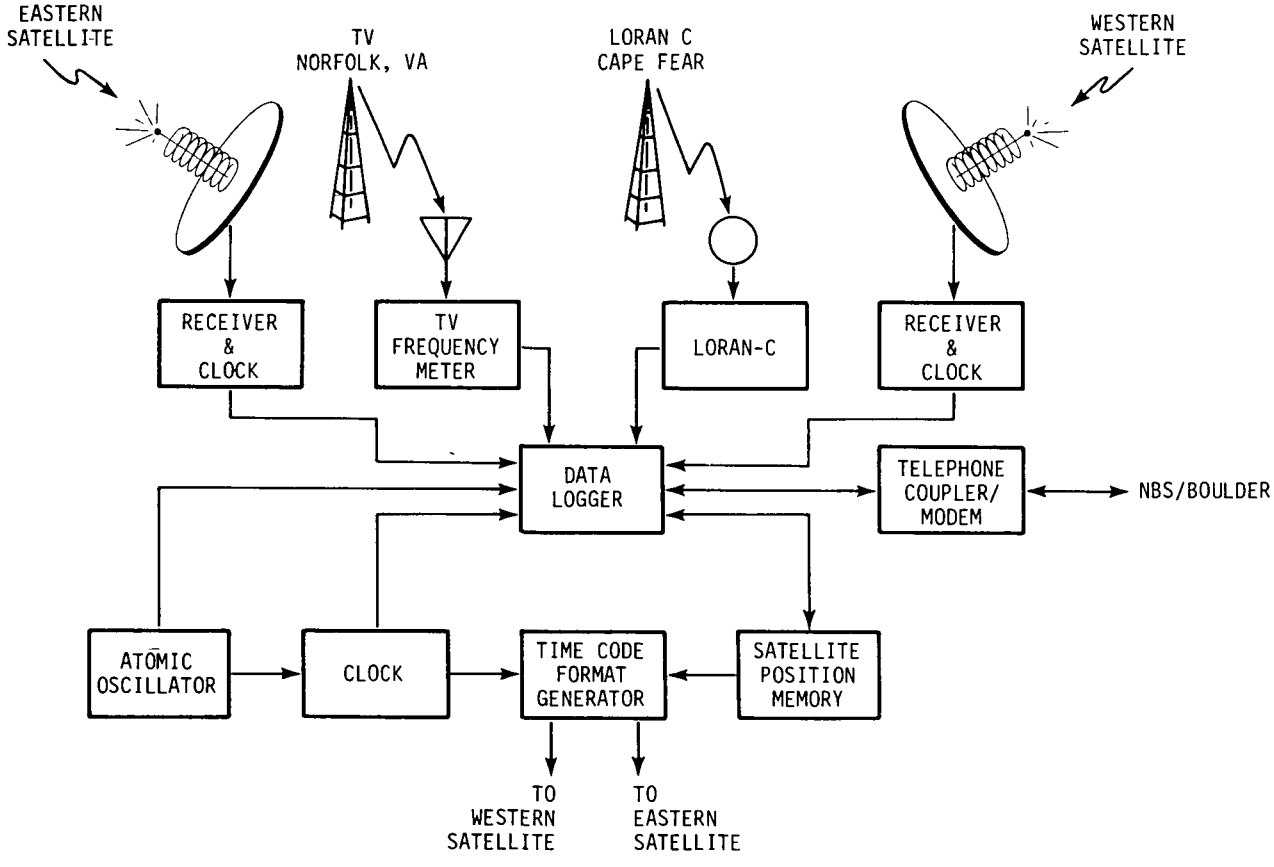


Fig. 3-Time code generation at CDA

Data are also retrieved from the CDA via the telephone line to Boulder. These data include the frequency of the atomic oscillators and the time of the clocks relative to UTC as compared to TV transmissions from Norfolk, Virginia, and to Loran-C transmissions from Cape Fear, North Carolina. The Data Logger also measures and stores the time of arrival of the signals from both the Western and Eastern GOES satellites as received at the CDA. Besides the time and frequency monitoring functions, the Data Logger provides the information necessary for NBS staff at Boulder to remotely determine if and where malfunctions exist and how to correct them by switching in redundant system components.

The satellite position information is generated at Boulder using a CDC 6600 computer and orbital elements furnished by NOAA's National Environmental Satellite Service (NESS). NESS generates these orbital elements weekly using data obtained from their trilateration range and range rate (R&RR) tracking network. The tracking data are obtained by measuring the R&RR to the Western satellite from the CDA, and sites in the states of Washington and Hawaii. The Eastern satellite is observed from the CDA, Santiago, Chile, and Ascension Island in the South Atlantic.

	WESTERN SATELLITE	EASTERN SATELLITE
FREQUENCY	468.8250 MHz	468.8375 MHz
POLARIZATION	RHCP	RHCP
MODULATION	CPSK (± 60°)	CPSK (± 60°)
DATA RATE	100 BPS	100 BPS
SATELLITE LOCATION	135° W	75° W
SIGNAL STRENGTH (OUTPUT FROM ISOTROPIC ANTENNA)	-139 dBm	-139 dBm
CODING	MANCHESTER	MANCHESTER
BANDWIDTH	400 Hz	400 Hz

Fig. 4-Interrogation channel signal characteristics

The GOES time signals for both satellites are summarized in figure 4. The signals are right-hand circularly polarized and separated in frequency by 12.5 kHz. The data rate is 100 b/s requiring 400 Hz of bandwidth. The data are Manchester coded and phase modulate the carrier ± 60 degrees, thus providing a carrier for the application of conventional phase lock demodulation techniques. The geographical coverage of the two satellites is shown in figure 5.

Figure 6 shows equipment designed for automatic time recovery from the GOES satellites. The antenna uses microstrip construction and provides 5 dB of gain right circularly polarized. It has a low noise preamplifier attached to its back plane. The receiver contains a microprocessor to determine and automatically compensate for net propagation delay of the time signals.

RESULTS

Data have been collected at NBS in Boulder, Colorado, using a receiver designed for automatic time recovery. Figure 7 shows the results of measurements taken every half hour for one day. These results have been repeated every day for more than one year. The results have shown the GOES system to provide a time reference to easily within ± 20 microseconds.

An equation relating the time recovered from the satellite to the master clock at Wallops Island is given below. Term 1 is known to better than 1 μs using the data logger which compares the CDA clocks to Loran-C and TV Line-10. This term will be controlled in the next generation system to be installed at Wallops Island early next year at this level or better. Terms 2, 4, 5, and 6 are expected to remain constant at the few microseconds level and can for the most part be calibrated out of a user's system. Term 3 is computed and compensated for by the user or his receiver with microprocessor capabilities.

$$\text{UTC(NBS)} - \text{SATELLITE RECEIVER} = \underset{1}{(\text{UTC} - \text{CDA})} + \underset{2}{(\text{CDA EQUIP DELAY})} +$$

$$\underset{3}{\left(\begin{array}{c}\text{FREE SPACE}\\ \text{PROPAGATION}\\ \text{DELAY}\end{array}\right)} + \underset{4}{\left(\begin{array}{c}\text{SATELLITE}\\ \text{TRANSPONDER}\\ \text{DELAY}\end{array}\right)} +$$

$$\underset{5}{\left(\begin{array}{c}\text{IONOSPHERE \&}\\ \text{TROPOSPHERE}\\ \text{DELAY}\end{array}\right)} + \underset{6}{\left(\begin{array}{c}\text{RECEIVER}\\ \text{AND CLOCK}\\ \text{DELAY}\end{array}\right)}$$

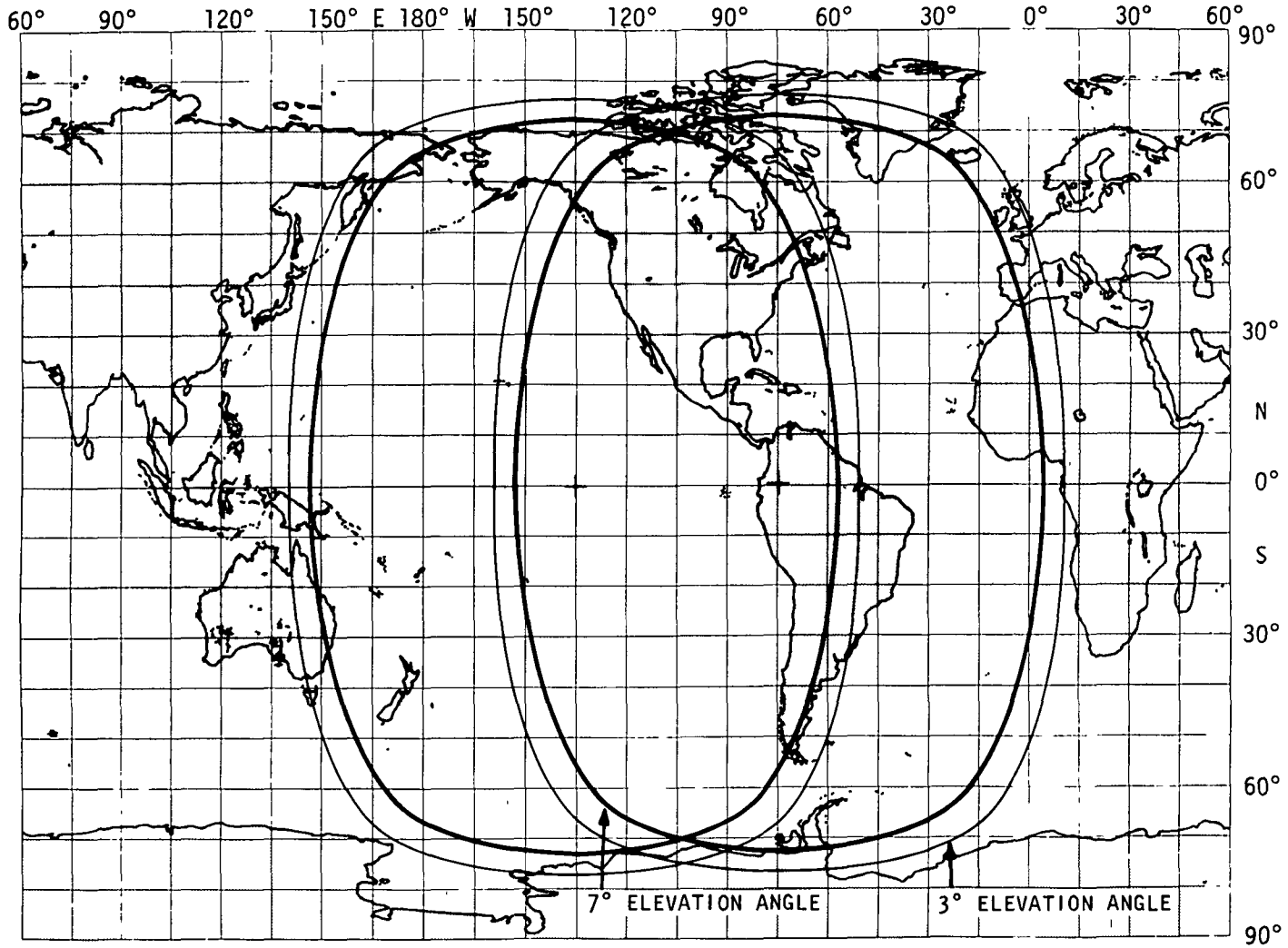


Fig. 5-Coverage of GOES satellites



Fig. 6a-GOES time receiving equipment

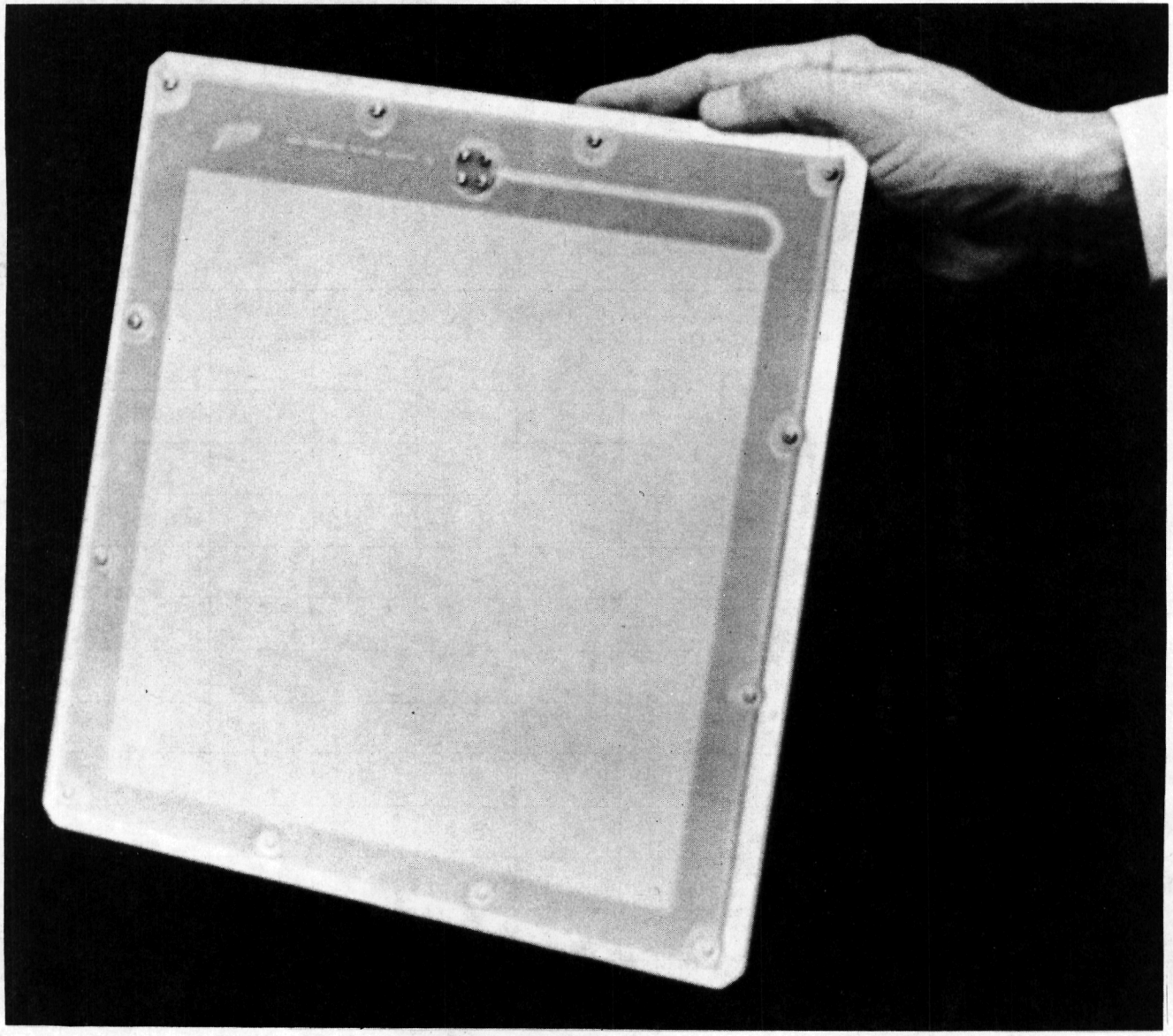


Fig. 6b-GOES time receiving equipment

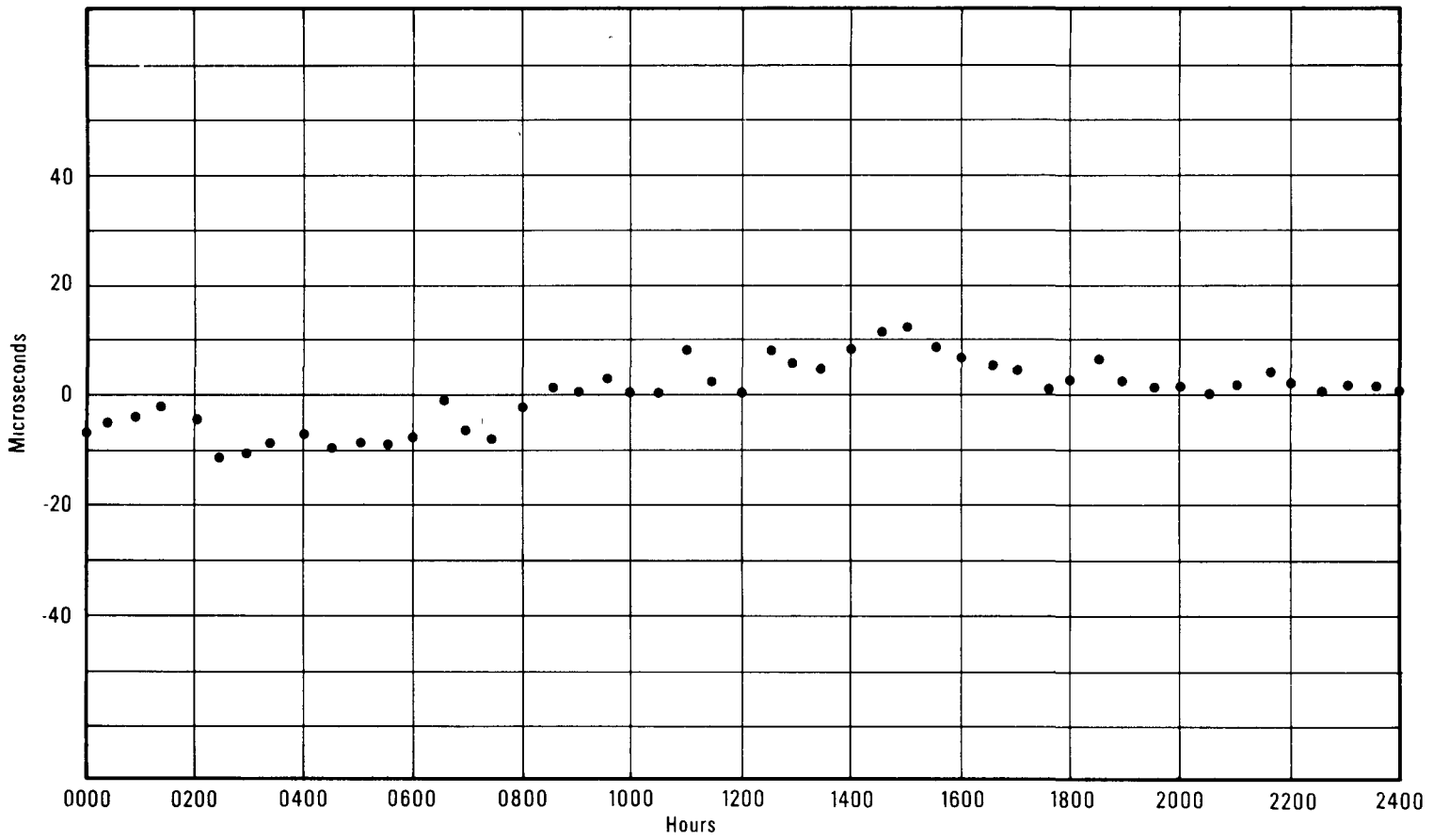


Fig. 7-UTC(NBS)-GOES receiver (NBS manufactured)

Since the GOES time code is transmitted outside the spectrum reserved exclusively for time and frequency broadcasts, it cannot be considered an NBS service in the same sense that WWV, WWVH, and WWVB are services. The "land-mobile" services and the GOES interrogation channels use the same frequency allocations (468.8250 and 468.8375 MHz), which means the time code may suffer interference from land-mobile transmissions. This is particularly true in urban areas where there is a high density of land-mobile activity. The satellite frequency allocations are secondary to the land-mobile services. Therefore, any such interference must be accepted by the time signal users. Complaints to the FCC will not result in any adjustments in favor of such users. The spectrum use by satellite and land-mobile is illustrated in figure 8.

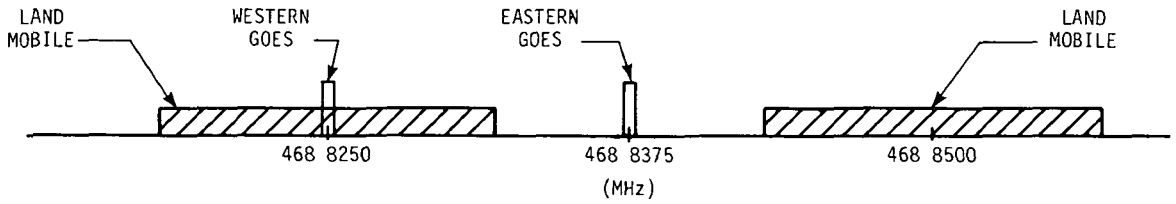


Fig. 8-Frequency use

Because of the spacing of frequency assignments to the land-mobile users, there is far less interference to the eastern satellite signals than to the western satellite. Therefore, the eastern satellite should be used by those users situated in large urban areas.

Although the GOES satellites transmit continuously, there may be interruptions during the periods of solar eclipses. The GOES satellites undergo spring and autumn eclipses during a 46-day interval at the vernal and autumnal equinoxes. The eclipses vary from a few minutes at the beginning and end of eclipse periods to a maximum of approximately 72 minutes at the equinox. The eclipses begin 23 days prior to equinox and end 23 days after equinox; i.e., March 1 to April 15 and September 1 to October 15. The outages occur during local midnight for the satellites' mean meridian (see figure 9).

There will also be shutdowns for periodic maintenance at the Wallops Island ground station. These scheduled outages will be reduced in the future as redundancy is added to the system.

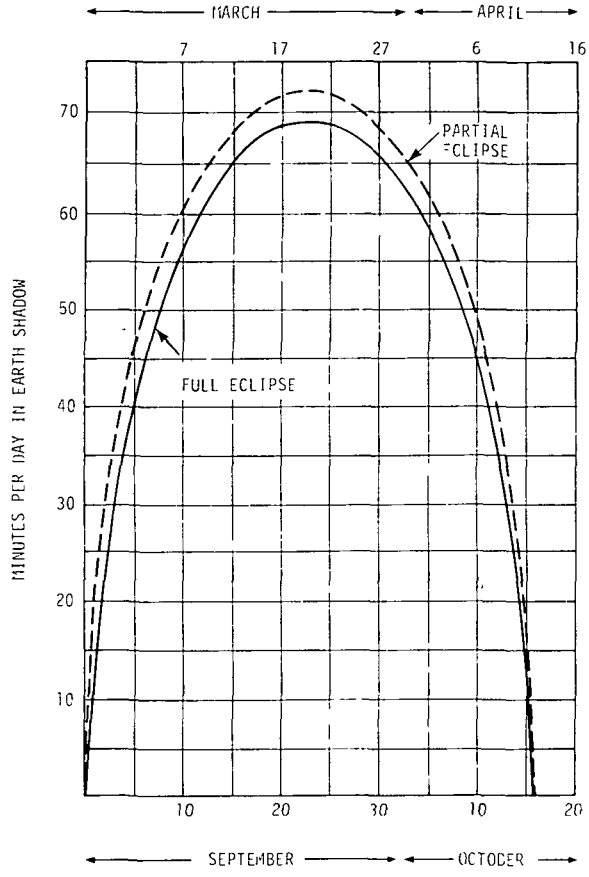


Fig. 9-Solar eclipse time

FUTURE PLANS AND IMPROVEMENTS

The satellites now under construction will have a 3 dB increase in radiated power and an improved antenna system. The time-code generation system at Wallops Island will be replaced with one of an improved design which reduces parts count by a factor of four. The system will be triple redundant. The satellite position data will be compressed using Chebychev polynomials to reduce storage requirements at the CDA and allow more frequent updates in the time-code message. By early 1978, the satellite position data will be updated every five minutes rather than at the present thirty-minute intervals.

Early in 1978, NBS will begin to report on the status of the GOES time system, including expected outages and improvements, in the NBS Time and Frequency Services Bulletin issued monthly.

QUESTIONS AND ANSWERS

MR. ELLIS BRYANT, Weatherchron Company:

Our company uses the WWV code to update telephone time announcements for the public. Are there any plans to put a daylight savings marker of some sort in the time code so we can generate local time?

MR. DAVIS:

We do have quite a number of bits that are designated for experimental use at present, and this could certainly be easily done. Frankly, we haven't finalized what all of those bits will be. There are over a hundred of them in the 30 second time code messages that are presently unused. Some will be used for system checking, but certainly I think it is a good idea to include the daylight saving time marker.

MR. ROGER EASTON, Naval Research Laboratory:

What sort of accuracy do you advertise?

MR. DAVIS:

The stability is on the order of less than $\pm$ 20 microseconds. Now, we haven't done enough clock carries from Wallops to NBS/Boulder to other locations to verify just what the level would be for taking a unit out in the field, setting it up, and saying, "Yes, we guarantee it at such and such accuracy." I am sure it is well below 100 microseconds, but how much below I can't say at this time.

Page intentionally left blank

Page intentionally left blank

A TRANSIT SATELLITE TIMING RECEIVER

G. A. Hunt and R. E. Cashion
S. N., Inc., Silver Spring, Maryland

ABSTRACT

The development of a time transfer instrument employing a TRANSIT satellite receiver and a microprocessor based computer is described. This instrument has been tested at the U. S. Naval Observatory measuring the time difference between the USNO Master Clock and the timing receiver. Data from these tests are presented which show the system can provide time referenced to UTC accurate to 25 microseconds or better.

The paper treats principles of operation, time transfer capabilities of the satellite system, projected system capabilities, system errors, and features of the timing receiver.

INTRODUCTION

The T-200 Satellite Timing Receiver uses signals from the Navy Navigation Satellite System (NNSS) or TRANSIT. Time marks in the satellite signal are referenced to UTC (USNO). This allows an earth station to derive accurate time from NNSS if the following functions are implemented:

1. Recover the satellite time
2. Reference a local clock to the received time
3. Correct the local clock for offset

The Satellite Timing Receiver was developed to accomplish these tasks and to provide a synchronized 1 pulse/second output and UTC in hours-minutes-seconds format.

The time-keeping ability of the operational NNSS is superior to that required for the navigation function, but up to the present time no instrument has been available to make full use of this fact. NNSS can provide unique and desirable features for time transfer. For example, the system is fully operational now and has been since 1964. The system is fully funded and maintained by the U. S. Navy. A polar orbit satellite configuration provides world-wide coverage. Transmission from the satellites is at VHF with essentially no unpredictable signal propagation effects.

THE NAVY NAVIGATION SATELLITE SYSTEM

TRANSIT (NNSS) is an operational system of five satellites and associated ground support stations. The satellites are in almost circular polar orbits of approximately 7500 km radius. The system was funded by and is supported by the U. S. Navy, and although the system continues to have widespread military use, the U. S. Government released details of the system for uncontrolled use world-wide in 1967.

Conventional (i.e., navigational) use of the NNSS is accomplished by a passive earth station receiving the signals from a single satellite with an omnidirectional antenna. The received messages describe the satellite orbit to an accuracy of approximately ±5 meters. Included in the message is a digital signal called the fiducial time mark (FTM) that delimits two-minute periods in the satellite transmission. Ground stations monitor each satellite and uplink new orbital data and clock adjustments to keep the onboard satellite clock FTM synchronized to the USNO master clock. Integration of the frequency difference between received signals and a stable internal oscillator frequency (doppler) between FTMs provides a measure of the change in slant range between the satellite and the earth station.

Using an assumed position on Earth and the received orbital data, a theoretical change in slant range can be computed. Using several such calculations and their measured analog from the doppler, the error in the assumed position can be deduced. This yields the "satellite fix".

RECOVERY OF TIME

Major functional elements of the timing receiver are shown in block diagram form in Fig. 1. The key elements are:

1. NNSS receiver
2. FTM detector
3. Microsecond clock
4. Microcomputer

The receiver gives orbital information from the satellite message to the microcomputer and, in turn, is controlled by the microcomputer. The receiver also drives the fiducial time mark detector from its phase detector output.

Precise time (to 1 microsecond) is kept in a 6 digit decade counter driven by 1 MHz derived from the precision local oscillator. The overflow from this counter generates a 1 pps signal - the primary output from the timing receiver. This microsecond register can be advanced or retarded by the computer in increments of 1 microsecond. Hours-minutes-seconds time is kept by the computer and displayed in a seven segment LED display on the front panel.

Transfer of the microsecond clock to the microcomputer is done by a latch which the microcomputer can read at any time. The microsecond clock continues to run when the latch is strobed.

Every two minutes the satellite transmits a sync word of 23 "ones" followed by a "zero" and 400 Hz modulation. The FTM is defined to be that transition between the final binary zero in the sync word and the beginning of the 400 Hz "beep". Fig. 2a shows the end of one two-minute message and the beginning of the next showing the FTM. The microprocessor generates an enable signal for the FTM detection circuitry that allows detection of the first zero crossing after the last bit of the message. This zero crossing occurs 1/16 of a bit time (1229 microsecond) after the FTM at the detector. The FTM is delayed through the receiver by 435 microseconds. Timing relationships of the derived FTM (FTM') are shown in Fig. 2b.

FTM' is used to latch the microsecond clock during the satellite pass. The latch reading is transferred to the microprocessor after each FTM (i.e., every two minutes). Data stored in the microcomputer memory represent the clock reading at each FTM' during the pass.

To detect any microsecond clock offset, it is necessary to modify these readings so they are referenced to the transmitted FTM. The two sources of difference between the transmitted FTM and FTM' are propagation path (a function of slant range) and detection delay (a constant). Corrections to the latched clock readings are therefore of the form:

$$\text{Corr} = A_0 + A_1 S \qquad \text{(Equation 1.)}$$

$$A_0 = 1664\ \mu s$$

$$A_1 = 3.3356405\ \mu s/km$$

Where S = slant range in km

Using orbital information transmitted by the satellite and location of the instrument read from internal registers, the slant range to the satellite is computed for each point. Microsecond clock readings are adjusted backwards by a number of microseconds indicated by Equation 1. Because the FTM was transmitted on a second mark (every two minutes UTC), the difference between corrected clock readings and zero (ahead or behind) is the clock error indicated by that FTM reception. Between 3 and 9 of these corrections are available for each usable satellite pass.

After data have been reduced to form a single clock correction amount, the microsecond clock can be advanced or retarded accordingly.

SOURCES OF ERROR

The primary sources of error are caused by (1) time jitter in FTM detection and (2) offset in the FTM transmitted by the satellite. The user has no control over the latter except to average clock corrections over several satellites. The limiting factor in satellite FTM error is the ability of the controlling agency to monitor satellite performance. Corrections to satellite clock are straightforward once the offset is determined. Summaries of offset data published by USNO show FTM accuracies in the ±30 μs range. The T-200 allows averaging over several satellites to reduce time-keeping error at the expense of correction response time. Filtering algorithms are discussed in the next section.

Reduction of time jitter in the FTM detection was an important part of the development of this instrument. A combination of careful hardware design and microcomputer control permits detection with very low jitter considering the narrow bandwidth and low signal to noise ratio (S/N) of the receiver. Fig. 3 shows the jitter as a function of signal strength. These data were obtained in the laboratory by using a NNSS Test Set.

Using an omnidirectional antenna, full limiting signals are not always possible. However, the 20 μs peak-to-peak jitter for satellite elevations above 10° allows good performance for most of an average satellite pass. Editing of FTM detection for elevation angle is done by using corresponding slant ranges as described in the next section.

EDITING, AVERAGING, AND FILTERING

Although the clock correction corresponding to one FTM detection could be used, the mean of an edited ensemble of the corrections from a single pass yields significantly superior accuracy.

Editing of the points corresponding to a pass of a single satellite is done after satellite set time and is a two-step process. The first step removes clock corrections corresponding to slant ranges greater than 2800 km (elevation angles less than 10°). The mean and variance of the remainder of the clock error points are computed. If the standard deviation does not exceed 24 μs, the ensemble is accepted. Otherwise, all points more than 1 standard deviation from the mean are deleted. If the ensemble has 3 or more points after all editing, a clock correction is computed as the mean ("best estimate") of the points.

Fig. 4a shows a computer printout of data from the T-200 for a single pass of satellite 30120 on 23 October at 1648 UT. These data were taken with intrapass editing disabled. The clock correcting subroutine was disabled to permit data acquisition of the indicated corrections under a variety of conditions.

As can be seen, the data have a high standard deviation primarily due to two data points (#0, #6). The mean clock error was -445 μs, and would have caused a 445 μs clock advance if it had been used.

Fig. 4b shows the same pass processed using the intrapass editing algorithm described. Point #0 was eliminated because slant range was greater than 2800 km, and point #6 was eliminated because it differed from the mean by 1391 μs (2.27 σ). The new mean, -74 μs, was computed from the remaining points and the standard deviation improved to 15 μs.

The T-200 permits the net clock correction at each pass to be filtered over a number of satellite passes that is user selectable. Filtering the correction over a number of satellites smooths the offset and improves instrument performance at the expense of response time. Using a filter time constant of one satellite average period will allow a correction at every satellite that produces an acceptable result. Using a larger time constant places more emphasis on the correction of the satellite constellation and less on any one satellite. Also, a large error in one satellite would not grossly effect the instrument error if filtering was used.

SYSTEM PERFORMANCE

Transmission accuracy of the satellite FTM determines timing accuracy in the T-200 receiver. Currently, NNSS satellites are controlled by the U. S. Navy Astronautics Group (NAG), Point Mugu, California. Under NAG control, FTM measurements are made at five different ground stations. All stations receive data from each satellite for at least four passes per day. Each pass contains an average of seven FTM measurements, or a total number of about 150 data points per day, thus, statistics on FTM measurements are very good.

TRANSIT SAT.

Synchronization between NAG and USNO is maintained to within 5 microseconds by portable clock trips. Under present time-keeping procedures, satellite time is maintained within about ±30 microseconds of UTC, but it should be emphasized that satellite navigation does not require time with greater accuracy. A change in operating procedures can yield time-keeping within ±15 microseconds at little or no additional expense, and a joint program between NAG and USNO is now underway to implement this improvement.

Tests on the prototype T-200 receiver were performed at the U. S. Naval Observatory during May and June, 1977, with results given in Fig. 5. The receiver reference clock during these tests was an atomic source and all measurements were relative to the USNO Master Clock. The results of these tests were used to improve the correction algorithm and to determine the exact equipment delays. The value used for equipment delay during these tests was 1702 μs, whereas the correct value is

actually 1664 μs. This caused the 38 μs bias shown in the receiver performance of Fig. 5c and 5d.

Fig. 5a shows USNO published time differences[1] for the period May 20, 1977 through June 7, 1977. Fig. 5b shows raw T-200 Satellite Timing Receiver measurements (T-200 clock - USNO Master Clock) for the same time period. Fig. 5c and Fig. 5d show the T-200 and USNO time difference after application of computed filter corrections during this test period.

From Fig. 5a it can be seen that satellite clock differences are randomly distributed with mean zero. Since T-200 clock corrections can be filtered over all satellites in the constellation, the satellite clock errors are integrated such that the receiver clock at any given time may be closer to UTC than any individual satellite time. This result is shown in Fig. 5c and Fig. 5d. Improvements in control of satellite time would, of course, improve the T-200 receiver clock.

OPERATOR CONTROLS

Two inputs are required to start the receiver: receiver location and initial clock time. An internal receiver printed circuit contains decimal switches for the input of latitude, longitude, and antenna height. Once set, these switches need not be changed unless the receiver is moved to a new site.

The UTC clock must be set, but initial clock error may be up to 15 minutes without effecting the T-200 accuracy after its first satellite correction. At completion of the first satellite pass, hours, minutes, and seconds are corrected to actual UTC, and the microseconds clock is corrected for the computed error without filtering. This should place the 1 pps output to within 50 microseconds of UTC. Each succeeding satellite correction will have filtering applied if this has been selected.

The microprocessor in the receiver design has made the T-200 automatic for most operations. The microcomputer (1) sets initial parameters at turn-on, (2) controls receiver message recovery, (3) edits FTM data based on quality criteria, (4) computes and applies clock corrections, and (5) automatically self-tests once each hour.

Although the receiver can operate without attention, features are incorporated in the design to permit operator adjustment of the clock

---

(1) Average values for time difference between NNSS satellites and USNO are published by USNO in "TRANSIT Satellite Report, Series 17". Data shown are from Reports No. 265, 26 May 1977; No. 266, 2 June 1977; No. 267, 9 June 1977, and No. 268, 16 June 1977.

(prior to the first satellite only), to delete corrections from specific satellites, and to change the filter function.

An optional feature for the T-200 is a module which determines receiver position. This design is useful on ships at sea or on vehicles which are expected to move between locations. Another option provides a summary printout of correction data at each satellite pass. Optional internal oscillators are available with accuracies of 1 x 10^{-9}/24 hours or 5 x 10^{-11}/24 hours.

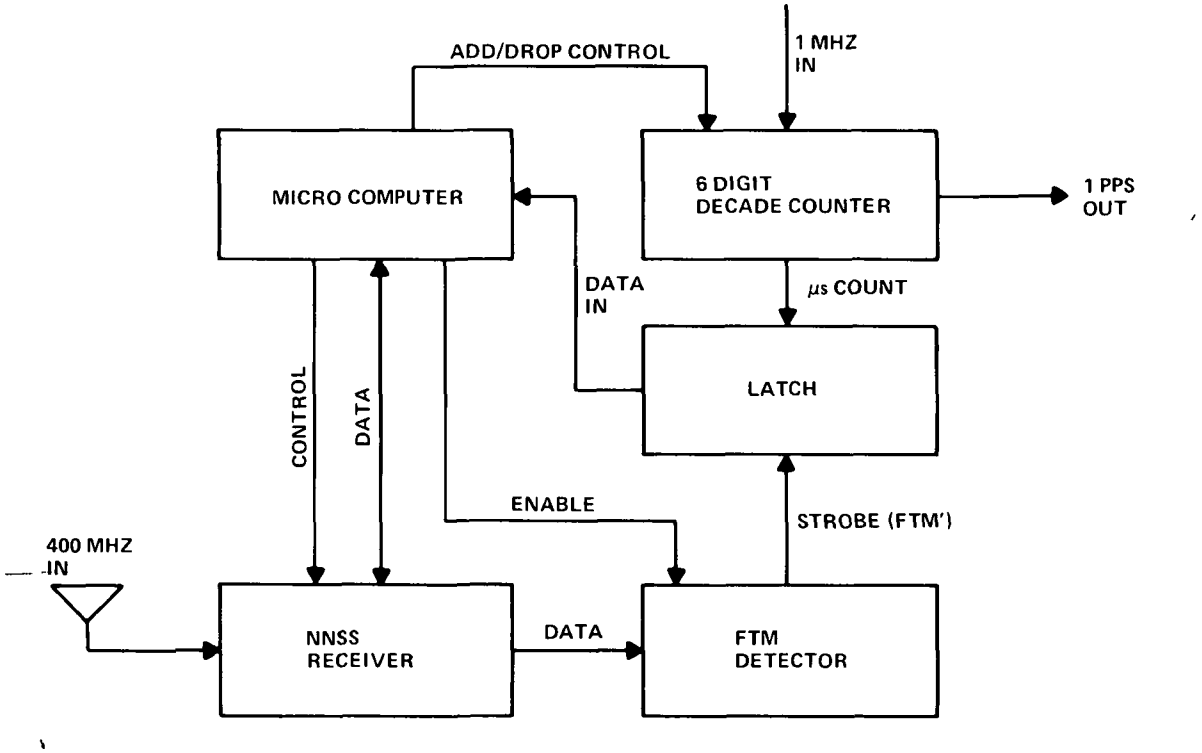


Fig 1 Timing Receiver Block Diagram

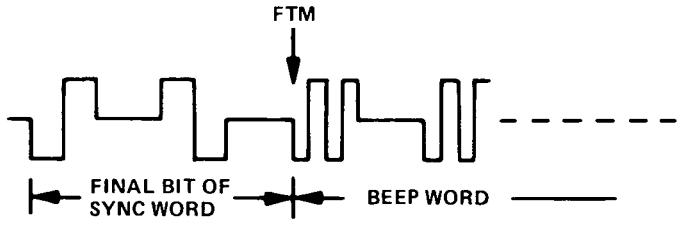


Fig 2a Data Pattern at FTM

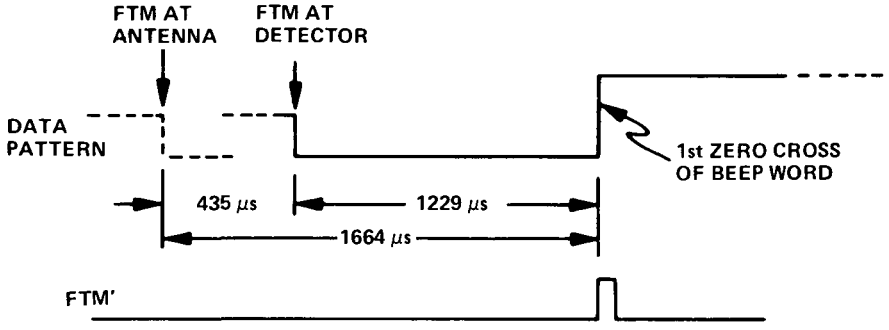


Fig 2b FTM' Derivation

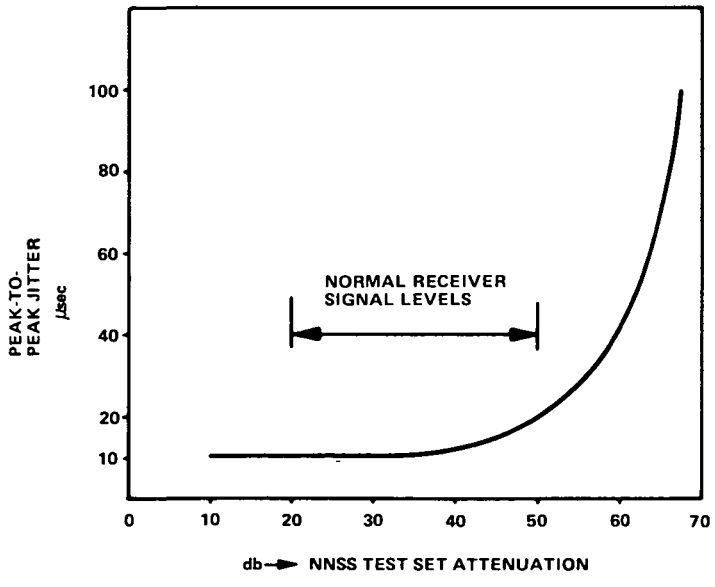


Fig 3 FTM Detection Jitter

SAT #30120
LOCK 1008 MIN UT

INDEX	SLANT RANGE KM	CLOCK CORREC USEC
0	2832	– 160
1	2186	– 92
2	1673	– 77
3	1451	– 74
4	1648	– 78
5	2149	– 52
6	2792	–2299
7	3494	
8	4217	
MEAN	–405 USEC	
STD DEV	836 USEC	

Fig 4a T-200 Pass Without Editing

SAT #30120
LOCK 1008 MIN UT

INDEX	SLANT RANGE KM	CLOCK CORREC USEC
0	2832	
1	2186	– 92
2	1673	– 77
3	1451	– 74
4	1648	– 78
5	2149	– 52
6	2792	
7	3494	
8	4217	
MEAN	– 75 USEC	
STD DEV	14 USEC	

Fig 4b T-200 Pass After Editing

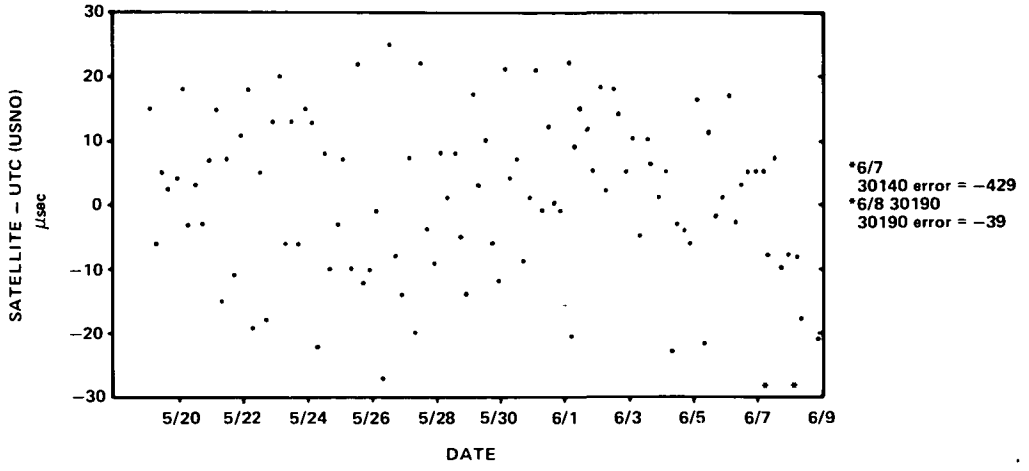


Fig 5a Average Satellite Error

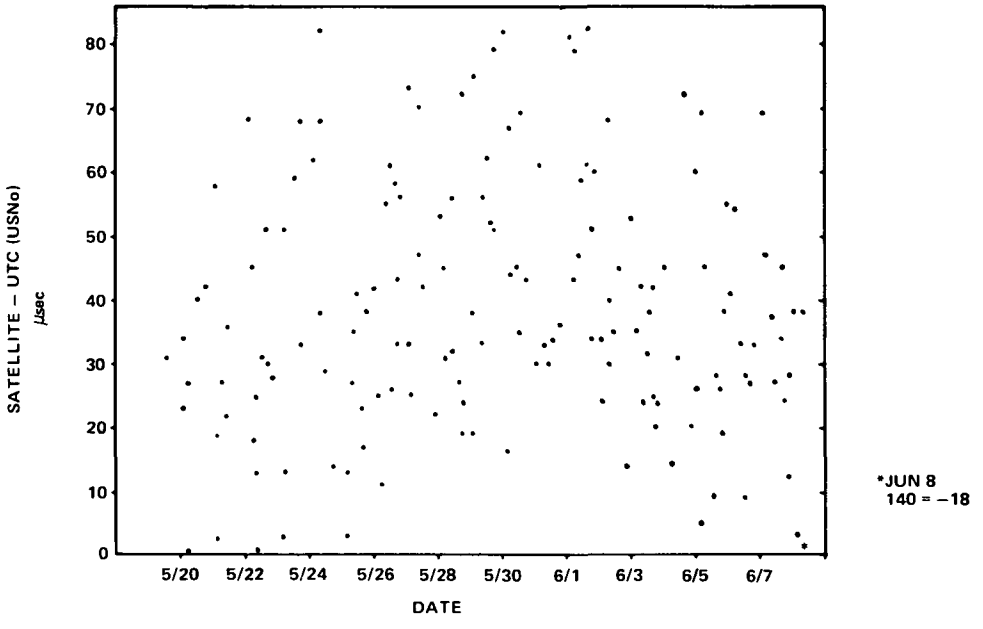


Fig 5b T-200 Raw Clock Error

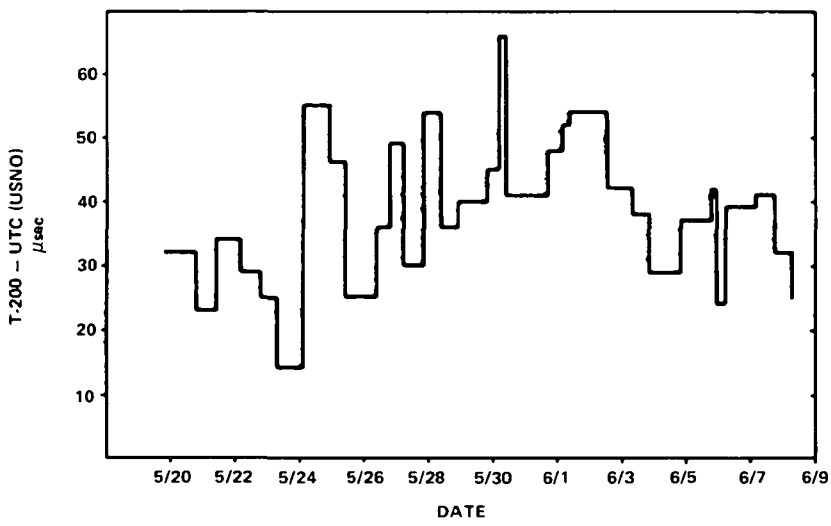


Fig 5c T-200 Computed Clock Error (Filter Factor = 5)

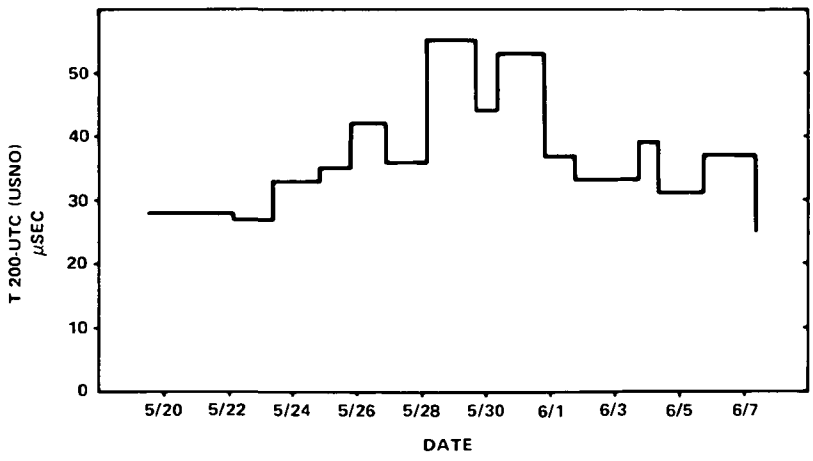


Fig 5d T-200 Computed Clock Error (Filter Factor = 10)

QUESTIONS AND ANSWERS

MR. GEORGE OJA, U. S. Naval Representative Office:

For the maximum interval between satellite passes, what would you expect the accumulated error to be into the internal oscillator?

MR. HUNT:

Knowing the precision and stability of your reference clock, it can be computed directly. It is a function only of the clock. The timing receiver removes the offset from the time. The precision of time between satellite fixes is a function of the accuracy of the clock, obviously, so it depends on how good your oscillator is. If you work on a microsecond-a-day clock, which is very common, your maximum error due to the non-continuous operation of the satellite system would be 1 microsecond if it were a day. The Constellation, as I understand it, is in a particularly bad phase right now. It is working its way out. We are getting satellite passes one after the other for a few times and then go several hours without them. So given the maximum time of several hours, what is your oscillator stability? You can answer your own question.

MR. OJA:

Yes, that's what I mean. What oscillator are you using?

MR. HUNT:

We provide no oscillator. I am sorry I didn't make this point clear. You use your own oscillator. Or, there are two optional oscillators, both of which offer microsecond-a-day type stability.

MR. LAUREN RUEGER, Johns Hopkins University Applied Physics Lab:

Have you tried reconciling the published excursions of the satellite system time with the data that you have presented?

MR. HUNT:

Yes. We see some correlation, but not a whole lot. Frankly, the controlling agency has the same problem we do in measuring the offset to the USNO master clock. We can see some correlation, however. When the satellite indicates it is very far off in one direction--20 or 30 microseconds one way or the other--we can see that in our data also, although we can't measure it precisely to that. Removing the satellite offset from our data after the fact using USNO Publication 17 improves it somewhat but doesn't remove all that we think it could.

MR. RUEGER:

Is there a limitation in the resolution if the satellite system does get control down to $\pm$ 5 microseconds? Will you be able to see it?

MR. HUNT:

That I don't know. Perhaps the gentleman from NAJ or the Navy can tell us. On one pass, we are looking at, typically, between 8 and 12 microseconds standard deviation. The slide I made showed 14. We are doing better than that now because we have improved our fiducial time mark detector. We are computing the position of the satellite to well within 25 meters, which obviously is down in the noise as far as microseconds are concerned. So, I think the resolution available ultimately goes back to how well the satellite system can be controlled down to a floor in the 10-microsecond region.

MR. RUEGER:

You would be able to see 1 microsecond if we were holding the mean to that value?

MR. HUNT:

If you were holding the mean to that value and we filtered, we would be in our floor of around 10 microseconds due to the jitter in the fiducial time mark detector, although some of that could be removed with additional filtering. How much we don't know yet because we don't have the Navy satellite system correctable to that point. Hopefully, this new procedure will improve it enough so that we can see these factors.

DR. GERNOT M. R. WINKLER, U. S. Naval Observatory:

I would like to comment. The Naval Astronautics operations and the timing control of the satellite system, as it is executed now, is more than sufficient to satisfy navigational requirements. The use which we see here represents additional potential of a national resource. It is now up to us to tighten these operational procedures, to tighten up the timing. I am confident that we will be able to do that to make that national resource more readily available.

MR. ROGER EASTON, Naval Research Laboratory:

What is the cost of the receiver?

MR. HUNT:

I don't know the price. I can give a range. It is on the GSA schedule, and the price depends, of course, on quantity. I believe the price for quantity one is in the vicinity of $13,000 to $14,000.

A TIME TRANSFER UNIT FOR GPS

Jackson T. Witherspoon, Leonard Schuchman
Stanford Telecommunications, Inc., Sunnyvale, CA & McLean, VA

ABSTRACT

A Time Transfer Unit (TTU) for use with NAVSTAR satellites of the Global Positioning System (GPS) is described. The unit can provide world-wide time transfer with an accuracy of better than 100 nanoseconds relative to GPS system time. Techniques used for GPS signal processing and data reduction are summarized, and potential applications discussed.

INTRODUCTION

Satellites have been used for a number of years for transfer of time and frequency between primary standards and users of precise time [1]. NAVSTAR satellites of the Global Positioning System (GPS) will soon provide world-wide access to precise timing signals which will permit a properly equipped user to calibrate a local time source relative to a primary standard to within fractions of a microsecond. The minimum user configuration consists of an omni-directional antenna and preamp, a Time Transfer Receiver, a teletype or equivalent alphanumeric printer, and a scientific hand calculator. Users with existing computers can eliminate the manual computation by connecting the receiver directly to a host processor.

For users without existing processing capability, an integrated receiver/processor or Time Transfer Unit (TTU) is available which is completely self-contained and fully automated. For users who do not have atomic frequency standards but who wish to improve the accuracy of their local time reference to better than 1 microsecond, the TTU can be operated in an automatic time correction mode in which the local time reference is periodically corrected.

This paper describes the operation and design of a prototype unit now under development.

OPERATION

The basic configuration of the TTU is shown in Figure 1. The unit accepts stable reference time (1 pps) and frequency (5 MHz) signals from the local time standard or unit to be calibrated, and the L1 signal at 1575 MHz from any GPS NAVSTAR satellite. Ephemeris data from the NAVSTAR satellite is detected and processed to determine satellite position and to estimate the time of arrival of the satellite signal

epoch. The actual time of arrival is recorded and compared with the expected value after correction for ionospheric, tropospheric, and relativistic errors, and the difference is displayed as the local time error. Sequential time error measurements are filtered to provide minimum variance time and frequency error data for display to the user or for logging with other user applications data. Time error is displayed as a nine digit plus sign decimal number in units of seconds with a range of $\pm$ six seconds and a resolution of 10 nanoseconds. Frequency error is computed from the rate of change of the filtered time error and displayed as a six digit plus sign decimal number in parts per 10^9 with a range of $\pm$ one part 10^6 and a resolution of one part in 10^{12}. The output data is updated every six seconds; the normal smoothing interval is two minutes but can be adjusted to a particular user's requirements. The smoothing filter also generates an estimate of the variance of the output data.

Several optional modes of operation are available to match different user requirements. For the user who needs a corrected 1 pps time reference, a time synthesizer can be added to the basic configuration which generates a 1 pps which is advanced or retarded relative to the reference 1 pps by an amount equal to the computed time error.

Time Transfer Technique

The time transfer technique used is illustrated in Figure 2 which shows typical satellite, user and received time epochs relative to system (GPS) time. GPS satellites transmit continuous navigation signals with readily identified epochs every 6 seconds. The satellite transmission is determined by an atomic standard which will in general differ by some amount (Parameter A in Figure 2) from system time. An estimate of A is contained in the navigation data and is available to the TTU. The satellite epoch arrives at the TTU and is detected by the receiver at some later time and is measured by reference to the local station time reference (Parameter C in Figure 2). The transit time (sum of A + B + C in Figure 2) can be estimated from satellite ephemeris and ionospheric error available in the navigation data, and from known user location and equipment bias calibrations. The station time error is taken as the difference between expected and measured time of arrival. Table 1 summarizes the major sources of error in the technique described. Note that these errors are associated with a single measurement and do not include potential improvement from smoothing over multiple samples or combining measurements from multiple satellites. The reader is referred to [2] for a more complete discussion of the GPS Navigation Data Message and its contents.

TABLE 1

TTU ERROR BUDGET

Satellite Ephemeris	10 ns
Satellite Clock Drift	10 ns
Ionosphere/Troposphere	30 ns
User Location/Calibration	15 ns
Receiver Noise	20 ns
RSS Error	41 ns

Satellite Availability

NTS-2, the first of six NAVSTAR satellites planned for Phase I system deployment was launched in 1977 and is undergoing test and evaluation. This satellite can be seen for an average of six hours per day anywhere in the world. Figure 3 illustrates expected times in view for the six satellite constellation from San Francisco. Note that at least one satellite is in view about 18 out of 24 hours each day.

RECEIVER DESCRIPTION

The Time Transfer Receiver is contained in a standard 19" wide rack mounted chassis. A remotable L-band preamp and omni-directional antenna are provided for external or roof top mounting.

RF Antenna/Preamp

The RF antenna/preamp assembly is designed to ensure a carrier-to-noise-density ratio for the L1 signal under worst case conditions of 37 dB/Hz. The antenna is a narrowband, circularly polarized unit providing unity gain over the L1 frequency band everywhere above 20 degrees elevation. The preamplifier is of conventional design, preceded by a narrowband preselector, providing a noise figure of better than 5 dB and a gain of more than 40 dB. The entire assembly is designed for operation in an unprotected environment over a temperature range of $-25^{o}C$ to $+65^{o}C$.

Time Transfer Receiver

The heart of the TTU is the Time Transfer Receiver (TTR). The TTR receives and tracks the PRN coded GPS signal at 1575 MHz, demodulates the carrier and detects the 50 bps Navigation data which bi-phase modulates the carrier. Navigation data, code epochs, and receiver status are provided as outputs for processing or printing via an IEEE-488-1975 compatible interface bus every six seconds. Figure 4 illustrates the TTR front panel controls. The receiver may be operated manually from this panel or remotely via the processor interface. GPS time-of-week is continuously displayed in the center display. Figure 5 illustrates the major functional elements of the receiver.

Downconverter

The downconverter preselects, downconverts, amplifies, filters, and levels the input L-band signal. Single downconversion is used to an IF of 81.84 MHz where signal distribution and correlation is performed. All conversion signals are synthesized from the local frequency standard. Provisions are included for injection of test RF or IF signals from a NAVSTAR test transmitter such as STI Model 5001.

Code Tracking Loop

The code tracking loop is a conventional early-late delay-locked loop employing a single code channel which is switched between early and late code references. An early-late discriminator accepts the early and late codes, correlates the received and reference codes, and demultiplexes the switched error signals to produce a digital error signal proportional to the received code offset. The code loop filter and number-controlled-oscillator circuits which generate the corrected code clock are all digital designs which retain the phase noise purity of the reference oscillator so as to achieve a very narrow band tracking loop. The code generator generates any one of 37 Gold codes used for the GPS C/A signals, the proper code selectable by satellite ID.

Navigation Data Detection

This module accepts video 50 Hz navigation data from the carrier loop, synchronizes and detects the data and subframe synchronization, and generates data, timing and synchronization signals for the external processor. The received HOW word is also extracted for panel display.

Frequency Synthesizer

This module plus an internal 10 MHz frequency reference provides for generation of all internally used frequencies from an internal or external frequency standard.

Interface and Control

This module provides control of receiver operating modes, front panel controls, local HOW generation and external control and status interfaces with the processor via the IEEE Interface Bus.

Data Processing Configuration

As indicated earlier, the data processing configuration required for the TTU will depend on the particular host user's application. For the development model of the TTU, a time-shared 16-bit mini-processor/CRT keyboard will be used. This configuration was selected to provide flexibility of test and evaluation, particularly with respect to evalua-

tion of time-transfer algorithms. An extended precision time interval counter is included in the processor configuration to process the receiver generated code epochs measurements with 10 nanosecond resolution.

The software provided with the TTU includes, in addition to standard vendor operating systems and library routines, nine applications peculiar modules which provide operator initiation, control, data acquisition, data reduction, display, and diagnostic capability, all at the CRT/keyboard which acts as the control station for the system. Figure 6 illustrates the processing sequence.

Upon initialization, the system verifies proper program loading, checks all Input/Output operations, and requests operator inputs for satellite ID, initial doppler offset and verification of proper system time. The receiver is then interrogated, and if status is valid, a navigation data frame is read in and checked for validity. When a valid frame of data is available, navigation data processing begins. This process produces an estimate of transit-time once every six seconds which is then compared to the measured time-of-arrival as determined from the time interval between received and local code epochs. Consecutive differences are then smoothed over a two minute interval to produce refined estimates of both time and frequency error in the local user's clock. These data are displayed to the operator as illustrated in Figure 7.

SUMMARY

A Time Transfer Unit capable of providing 100 nanosecond world-wide time synchronization via RF signals transmitted by GPS NAVSTAR satellites has been described. Such units can provide more frequent and improved calibration of existing atomic clocks at remote locations, and upgrading of time and frequency accuracy available from conventional crystal frequency standards.

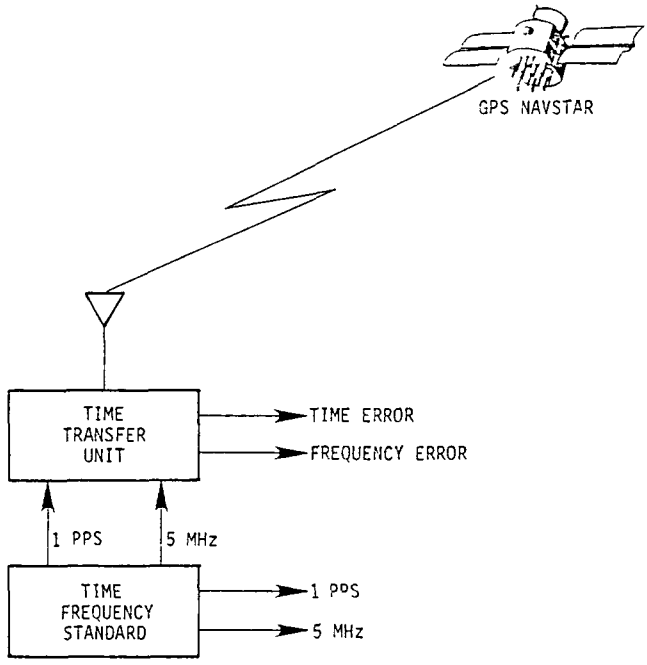


FIGURE 1 GPS TIME TRANSFER UNIT

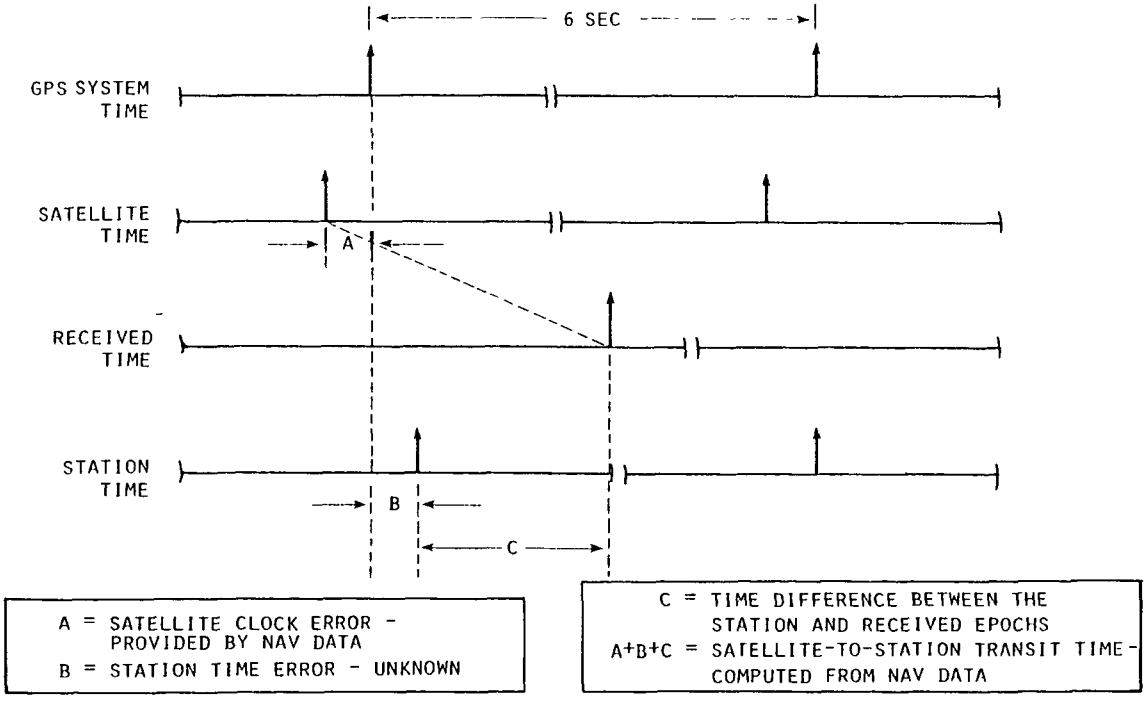


FIGURE 2 SYSTEM TIME RELATIONSHIPS

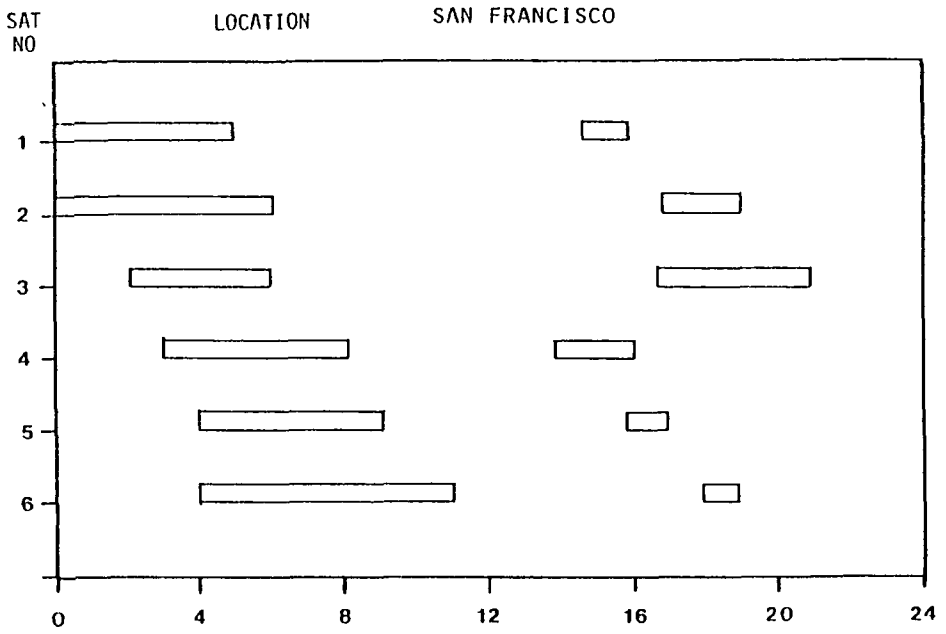


FIGURE 3 GPS PHASE I SATELLITE IN VIEW TIME

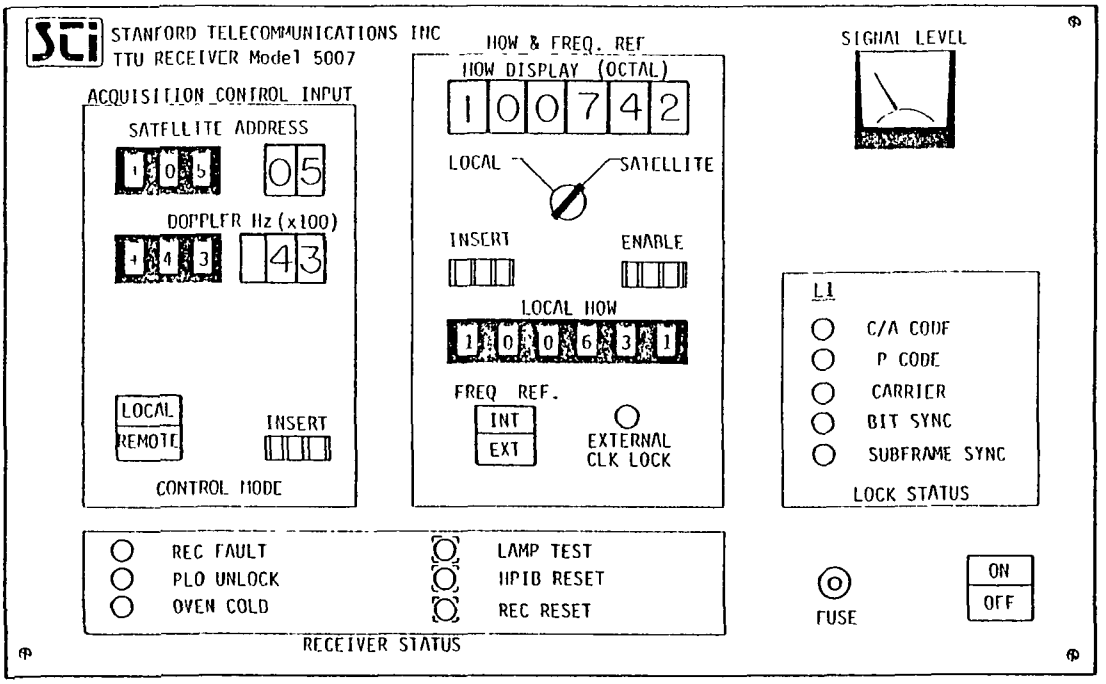


FIGURE 4 FRONT PANEL FROM PROPOSAL

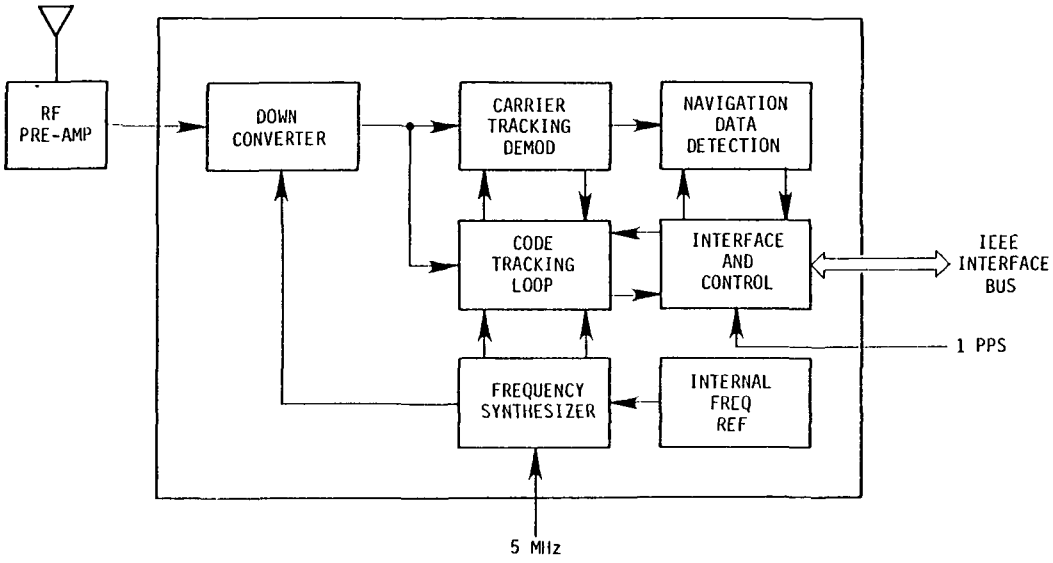


FIGURE 5 TIME TRANSFER RECEIVER

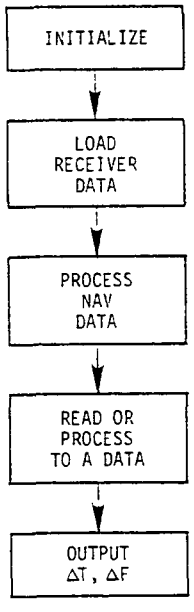


FIGURE 6 TTU PROCESSING SEQUENCE

GMT TIME DAY:HR:MI:SE	GPS TIME OF WEEK	TIME ERROR SECONDS	FREQ ERROR PARTS
123:12:23:40	12394	+5.11891E-07	+4.35179E-09
123:12:23:46	12395	+5.12510E-07	+4.26892E-09
123:12:23:52	12396	+5.16636E-07	+4.16312E-09
123:12:23:58	12397	+5.19073E-07	+4.06891E-09
123:12:24: 0	12398	+5.17294E-07	+4.00627E-09
123:12:24: 6	12399	+5.13459E-07	+3.93368E-09
123:12:24:12	12400	+5.14403E-07	+3.83309E-09
123:12:24:18	12401	+5.14089E-07	+3.72197E-09
123:12:24:24	12402	+5.15032E-07	+3.64947E-09
123:12:24:30	12403	+5.13194E-07	+3.57126E-09
123:12:24:36	12404	+5.18841E-07	+3.50480E-09
123:12:24:42	12405	+5.19879E-07	+3.42245E-09
123:12:24:48	12406	+5.20146E-07	+3.39225E-09
123:12:24:54	12407	+5.23184E-07	+3.33367E-09
123:12:25: 0	12408	+5.25976E-07	+3.27245E-09
123:12:25: 6	12409	+5.21148E-07	+3.23060E-09
123:12:25:12	12410	+5.20144E-07	+3.18878E-09
123:12:25:18	12411	+5.23869E-07	+3.10310E-09
123:12:25:24	12412	+5.23300E-07	+3.04279E-09
123:12:25:30	12413	+5.20568E-07	+3.01173E-09
123:12:25:36	12414	+5.21002E-07	+2.95748E-09
123:12:25:42	12415	+5.22653E-07	+2.89300E-09
123:12:25:48	12416	+5.19774E-07	+2.84795E-09
123:12:25:54	12417	+5.18780E-07	+2.81089E-09
123:12:26: 0	12418	+5.21168E-07	+2.75104E-09
123:12:26: 6	12419	+5.23914E-07	+2.70288E-09
123:12:26:12	12420	+5.19829E-07	+2.67354E-09
123:12:26:18	12421	+5.20343E-07	+2.64690E-09

FIGURE 7 TYPICAL TTU DISPLAY

REFERENCES

[1] Easton, R.L., Fisher, L. C., Hanson, D. W., Hellwig, H. W., Rueger, L. J., "Dissemination of Time and Frequency by Satellite," Proc. IEEE, Oct. 1976, Vol. 64, pp. 1482.

[2] Van Dierendonck, A. J., Russell, S. S., Kopitske, E. R., Birnbaum, M., "The GPS Navigation Message," AIAA Guidance and Control Conference, San Diego, CA, August 1976.

INITIAL RESULTS OF THE NAVSTAR GPS NTS-2 SATELLITE

James A. Buisson, Roger L. Easton, Thomas B. McCaskill
U.S. Naval Research Laboratory (NRL)
Washington, D.C.

ABSTRACT

NTS-2 was successfully launched on 23 June 1977 into a near 12-hour circular orbit. Precise frequency and timing signals are derived from the two cesium frequency standards. This paper discusses the launch and preliminary results which include verification of the relativistic clock effect.

INTRODUCTION

The successful launch of the Navigation Technology Satellite No. 2 (NTS-2) marks the beginning of a new era in navigation and time-keeping history. NTS-2 (Fig. 1) is the first NAVSTAR GPS (1) Phase I Satellite, which will provide near-instantaneous navigation and time-synchronization service on a worldwide, continuous basis to the DOD community and a wide variety of commercial users. NTS-2 technological features encompass the world's first orbiting cesium frequency standards, built by Frequency and Time Systems (FTS); nickel-hydrogen batteries (developed by COMSAT); three axis gravity gradient stabilization with momentum wheel unloading; control of the spacecraft orbit; verification of Einstein's relativistic clock shift; time interval measurement precision of 3 nanoseconds; and a worldwide network (GE International Time Sharing) for data acquisition.

NTS-2 is also the fourth in a series of NRL technology satellites (Fig. 2) which have carried quartz (2), rubidium (3) and cesium (4) oscillators into orbit. The NTS-3 spacecraft, now under development at NRL, is scheduled to carry the first orbiting hydrogen maser (5) frequency standard(s). The primary data type for all of the technology satellites has been precise time difference measurements, which have been used for time transfer (6), navigation (7, 8) and orbit determination.

GPS LAUNCH PROCEDURE

The GPS launch procedure (Fig. 3) requires that the spacecraft be inserted into a pre-assigned position in the GPS constellation; first into a high eccentricity transfer orbit (Fig. 4), then into a low eccentricity drift orbit (Fig. 5), followed by final constellation placement. A set of orbital values and tolerances was specified; the most critical tolerance was for orbital period which was required to be within an accuracy of 1 second of the specified value of 717.973 minutes (nearly 12 sidereal hours).

The NRL built spacecraft was launched into the transfer orbit from Vandenberg Air Force Base on June 23, 1977, at 0817UTC. First acquisition of signal (AOS) was made by the NTS tracking station in Panama. NTS-2 was then acquired and tracked from Blossom Point, Md. Calculations of measurement residuals indicated a nominal transfer orbit. The scheduled apogee kick motor (AKM) burn at the first apogee was deferred in order to allow processing of measurements from the launch tracking network (Fig. 6). The launch tracking network consisted of two of the NTS tracking stations (Panama and Chesapeake Bay, Md.) complemented by Blossom Point, Md.; Millstone, Mass.; the Range Measurements Laboratory, Patrick AFB, Fla. The tracking network is coordinated by the NRL Control Center (NRLCC), which has links (Fig. 7) to the GPS Master Control Station. Transfer orbit solutions were independently made by Bendix personnel at Blossom Point, Md.; RML, Patrick AFB; and Millstone Radar personnel using measurements from the launch tracking network. A merged orbit solution (9) was performed by the Naval Surface Weapons Center (NSWC) which was compared with the independent solutions using various data subsets. The AKM burn was performed at the sixth apogee which resulted in a near circular drift orbit.

The pre-launch drift orbit profile (Fig. 8) was chosen to allow the ascending node of NTS-2 to drift eastwards at a nominal value of 5 deg/day. The actual drift orbit (Fig. 9) had a larger drift rate than expected, resulting in NTS-2 reaching its pre-assigned position in the constellation of 28 ± 2 degrees West Longitude in 5 days. Three velocity increments (Fig. 9) ranging from 1 to 3 feet per second were used to increase the spacecraft period. The final orbit, excepting small microthrusts, was achieved 15 days after launch. Three axis gravity gradient stabilization and solar panel deployment was achieved within 18 days after launch.

The final drift orbit of NTS-2 in the GPS Phase I constellation is given by Figure 10. The locations of the five Navigation Demonstration Satellites (NDS) are possible positions; final satellite positions will be determined later. These six satellites will comprise the GPS Phase I Constellation.

NTS-2 follows a constant ground track orbit with an inclination of 63 degrees. Occasional orbital maneuvers of the spacecraft are performed, as necessary, to maintain the ascending node within the GPS specifications. Figure 11 presents a summary of four of the NTS-2 orbital parameters and the associated GPS specifications.

NTS-2 TRACKING NETWORK

The NTS-2 tracking network (Fig. 12) consists of U.S. stations located in Chesapeake Beach, Md. (CBD), Panama Canal Zone (PMA); overseas stations are located at the Royal Greenwich Observatory (RGO) in England and in Australia (AUS) at a Division of National Mapping site. United States stations are operated by Bendix Field Engineering, the overseas sites are operated by personnel from England and Australia, all under the direction of NRLCC. The NTS-2 measurements are used by these cooperating countries for time comparison with the U.S. Naval Observatory (USNO), independent orbit determination and polar motion studies. The network provides almost complete tracking coverage of NTS-2; Figures 13, 14, 15, and 16 depict the portions of the NTS-2 orbit when the spacecraft is above the horizon from PMA, RGO, AUS, and CBD, respectively. Figure 17 shows that only a small segment of the NTS-2 orbit is not observable from some station in the NTS network. Noteworthy is the coverage obtained from Panama (Fig. 13); NTS-2 is tracked for one complete revolution every day, thus allowing for immediate analysis of any cesium frequency adjustment performed by NRLCC. Each of these stations has at least three cesium standards whose offsets (independent of NTS-2) are related to the USNO Master Clock No. 1 by timing links as detailed in Figure 18.

PRECISE TIME AND FREQUENCY TRANSMISSIONS

Precise frequency signals for NTS-2 transmissions are obtained from one of the two spacecraft qualified (4) cesium frequency standards built by FTS. Each cesium standard may also be operated in a quartz oscillator mode which requires less power. The reduced power, quartz only mode was used for the first 15 days after NTS-2 launch. The cesium standard was locked following solar panel deployment

which allowed full power operation.

NTS-2 timing information is continuously transmitted in two modes, a side tone ranging system, called the Orbit Determination and Tracking System (ODATS); the other a Pseudo Random Noise Subsystem Assembly (PRNSA). Time difference measurements between the spacecraft clock and ground station clocks are made through special receivers (10, 11) which measure time difference by comparing a waveform similar to that transmitted by the spacecraft. These measurements are then used to determine the spacecraft orbit, clock difference (12), frequency difference and other parameters associated with GPS operation.

FREQUENCY DETERMINATION

GPS requirements for the NTS-2 mission called for cesium controlled frequency operation after full power was available, following solar panel deployment. The first FTS cesium standard to be used, designated as PRO-5, was locked up (Fig. 19) on the first attempt on Day 190, 1977,at 1418 UTC following a frequency tune to bring the PRO-5 quartz oscillator frequency within the VCXO tuning range of the cesium resonance frequency. Figure 19 presents the theoretical range minus the observed range (T-O) values (13) which are calculated from measurements collected at a one-minute interval from the Panama site. These (T-O) values yield a measure of the spacecraft clock offset with respect to the PMA clock. Knowledge of the station clock offset with respect to the USNO Master clock permits the spacecraft to be referenced to USNO. Figure 20 presents a plot of (T-O) values (13) from PMA over a six day span. The (T-O) slope gives the frequency offset of +442.5 $ppl0^{12}$ with respect to the PMA clock. Inclusion of the PMA frequency offset of +0.6 $ppl0^{12}$ produces an NTS measured value of +443.1 $ppl0^{12}$. Comparison of this value to the predicted value of the relativistic offset of +445.0 $ppl0^{12}$ gives a difference of -3.1 $ppl0^{12}$. On Day 215, 1977, the NTS-2 PRO-5 output signal was offset (Fig. 21) through the use of a frequency synthesizer (4). Closer frequency synchronization to the UTC rate is obtainable by use of cesium C-field tuning which provides a resolution of 1.3 $ppl0^{13}$. Before applying the C-field tune, the NTS-2 frequency offset was re-determined using the CBD station. Figure 22 presents a plot of UTC (USNO MC No. 1) - UTC (CBD), where CBD denotes the clock used for the CBD receiver. The slope of this line yields a frequency offset of 18.0 $ppl0^{13}$. Figure 23 presents a plot of (NTS-CBD); a frequency offset of 10.1 $ppl0^{13}$ was measured. Combining these results Figure 24 produced a frequency offset of

+7.9 ppl0^{13}. On Day 287, 1977 (14 Oct), a C-field tune of 6 bits was applied. Figure 25 presents a plot of the (T-O)'s after the C-field tune; a resultant frequency of -6.6 ppl0^{13} was measured. The net measured change was 14.5 ppl0^{13} which exceeded the expected value by 6.7 ppl0^{13}. Figure 26 presents the preliminary results of the C-field tune; the cause of the small differences are being investigated. A frequency history of NTS-2 since launch is presented by Figure 27, a split logarithmic scale is used so that positive and negative values of frequency offset with respect to UTC (USNO) may be included over a large range.

TIME TRANSFER

Preliminary time transfer results have also been obtained. Figure 28 depicts the technique and the links which are used to relate a time difference, measured with respect to NTS-2, back to UTC (USNO). The time transfer results are of interest to the PTTI community, but also significantly to the GPS community because four simultaneous time transfers measured between a user and four GPS satellites form the basis of a GPS navigation and time synchronization. Figure 29 presents NTS-1 time transfers results between the NASA station located at Cape Kennedy and USNO via the CBD ground station link to USNO. The results in Figure 30 present time transfer results using identical ground station equipment but with measurement obtained from the NTS-2 spacecraft; these results are obtained with a single channel 335- MHZ receiver (14) and are not corrected for ionospheric delay. The NASA laser network which will use these receivers is given by Figure 31.

INTERNATIONAL TIME TRANSFER EXPERIMENT

As a result of the encouraging time transfer results, an international time transfer experiment has been planned in 1978. Figure 32 lists the different participants from seven countries. Extensive use will be made of the single channel 335-MHZ receiver; ionospheric delay will be minimized by using measurements at the time of closest approach of NTS-2. It is anticipated that a worldwide time synchronization accuracy of 100 nsec or less will be achieved by this effort.

LASER ORBIT VERIFICATION PROGRAM

A laser program has been started for the purpose of verification of the GPS orbit accuracy. Initially, laser returns will be used to

verify one component of the orbit at the time of the observation; later as more laser stations track NTS-2, an independent orbit will be calculated. An important part of the laser program is to obtain near-simultaneous laser and time difference observations at co-located sites which will be used for precise clock analysis in addition to orbit determination. These and other objectives are summarized in Figure 33.

NTS-2 is equipped with a laser retroflector similar to NTS-1 which also had a retroflector. One element of the retroflector is designed for light emitted in the ultra violet region. Figures 34 and 35 show the retroflector elements for NTS-1 and NTS-2. In addition to the NASA network, the Smithsonian Astrophysical Observatory (SAO) has four stations capable of making laser observations on NTS-2; those stations in the SAO network are detailed in Figure 36. Additional laser observations may be obtained from stations (Fig. 37) located in France, Germany, Holland, and Australia. Figure 38 presents measurement resolutions from some of those stations with NTS tracking capability. Laser returns have already been obtained from the SAO Mt. Hopkins, Arizona, site. Figures 39 and 40 present the residuals referenced to the NTS-2 orbit. The measured biases of 56 and 17 nsec provide preliminary verification of the NTS orbit. The noise levels of 6 and 5 nsec are typical of the expected laser measurement noise level for this laser configuration; implementation of a more accurate laser pulse should improve these results.

A proposed laser precise orbit tracking network is shown by Figure 41. This proposed network includes possible laser tracking at the operational TRANET sites which are under the direction of the Defense Mapping Agency.

NTS-2 ACHIEVEMENTS

GPS objectives that have been achieved to date are:

(1) launch insertion into GPS constellation position

(2) demonstrated orbit stability and controllability

(3) first cesium frequency standard in space

(4) verification of relativity theory

Other GPS objectives that are being pursued are:

(1) satellite clock analysis

(2) error budget determination

(3) navigation with NDS satellite

(4) worldwide timing system synchronization

(5) refine coefficients of geopotential

(6) measure earth rotation rate

REFERENCES

1. Parkinson, Col. B.W., "NAVSTAR GLOBAL POSITIONING SYSTEM (GPS)," National Telecommunications Conference, Vol. iii, 1976.

2. Bartholomew, C.A., "Quartz Crystal Oscillator Development for TIMATION," NRL Report 7478, October 25, 1972.

3. McCaskill, T.B. and Buisson, J.A., "Quartz- and Rubidium-Oscillator Frequency-Stability Results," NRL Report 7932, December 12, 1975.

4. White, J., et al, "NTS-2 Cesium Beam Frequency Standard," Proceedings of the Eighth Annual PTTI, 1976.

5. Easton, R.L., "The Hydrogen Maser Program for NAVSTAR GPS," Proceedings of the Eighth Annual PTTI, 1976.

6. Easton, R.L., Lynch, D.W., Buisson, J.A., and McCaskill, T.B., "International Time Transfer Between the U.S. Naval Observatory and Royal Greenwich Observatory via the TIMATION II Satellite," NRL Report 7703, April 18, 1974.

7. McCaskill, T.B., Buisson, J.A., and Lynch, D.W., "Principles and Techniques of Satellite Navigation Using the TIMATION II Satellite," NRL Report 7252, June 17, 1971.

8. Buisson, J.A. and McCaskill, T.B., "TIMATION Navigation Satellite System Constellation Study," NRL Report 7389, June 27, 1972.

9. O'Toole, J.W., "Celest Computer Program for Computing Satellite Orbits," NSWC/DL TR-3565, October 1976.

10. Landis, G.P., Silverman, I., and Weaver, C.H., "A Navigation Technology Satellite Receiver," NRL Memorandum Report 3324.

11. Raymond, L., et al, "Navigation Technology Satellite (NTS) Low Cost Timing Receiver," Goddard Space Flight Center Report X-814-77-205, August 1977.

12. McCaskill, T.B., Buisson, J.A., and Buonaguro A., "A Sequential Range Navigation Algorithm for a Medium Altitude Navigation Satellite," Journal of the Institute of Navigation, Vol. 23, No. 2, Summer 1976.

13. Buisson, J.A., McCaskill, T.B., Smith H., Morgan, P., and Woodger, J., "Precise Worldwide Station Synchronization via the NAVSTAR GPS, Navigation Technology Satellite (NTS-1)," Proceedings of the Eighth Annual PTTI, 1976.

14. Raymond, L., et al, "Navigation Technology Satellite (NTS) Low Cost Timing Receiver Development," Proceedings of the Eighth Annual PTTI, 1976.

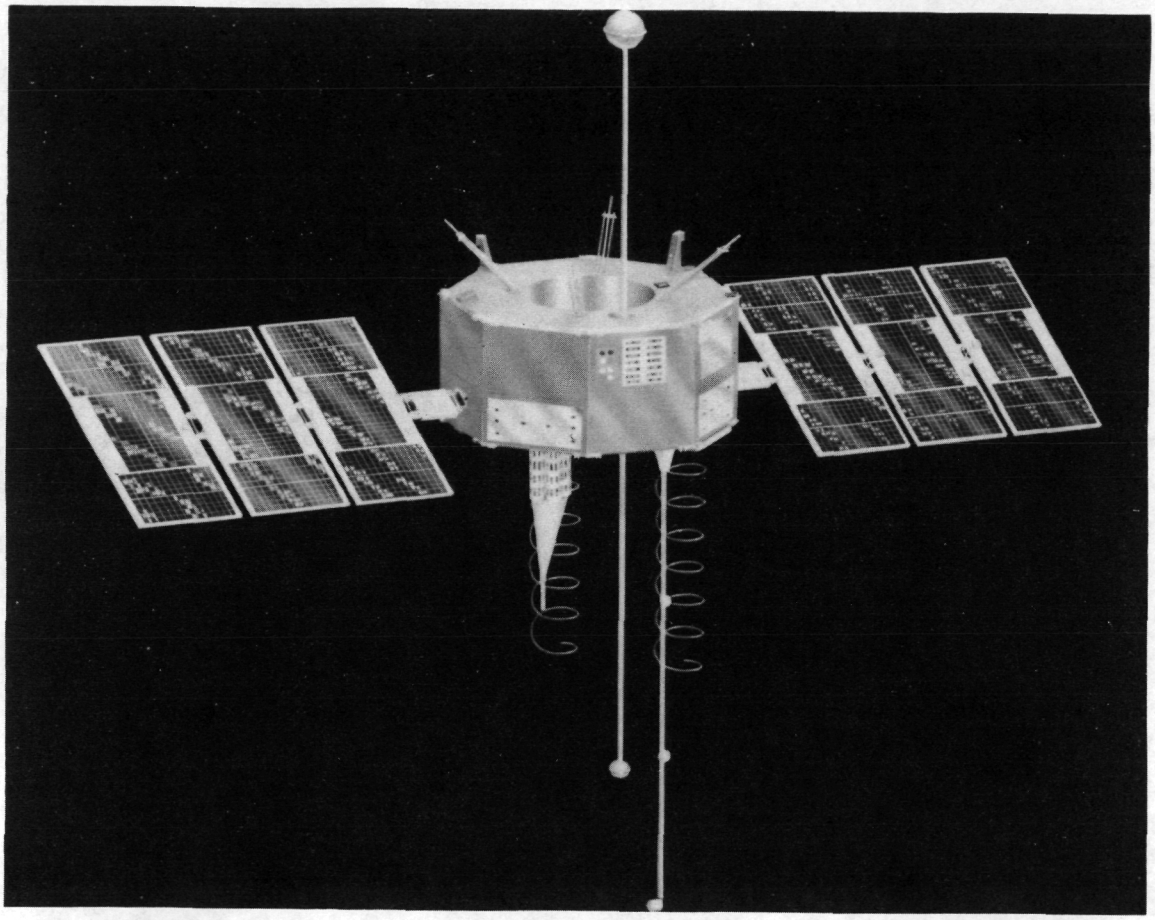


Fig. 1 - NTS-2

	T-1	T-11	T-111 NTS-1	NTS-2	NTS-3
Launch	5/31/67	8/30/69	7/14/74	6/23/77	1981
Alt. (n.mi.)	500	500	7400	10,900	10,900
Incl.	70°	70	125	63°	63°
Ecc.	.0008	.002	.007	.0004	.001
Wt. (lbs)	85	125	650	950	1080
Power (W)	6	18	100	445 BOL	475 BOL
Freq.	UHF	VHF/UHF	UHF/L Band	UHF/L, L_1, L_2	UHF/L, L_1, L_2
Osc.	Qtz	Qtz	Qtx/Rb	Qtz/C_s	Qtz/H_2
$\Delta f/f$(day) pp10^{13}	300	100	5-10	2	.1
Range Error ft/day	2400	240	40-80	16	.8

Fig. 2 - Technology satellites

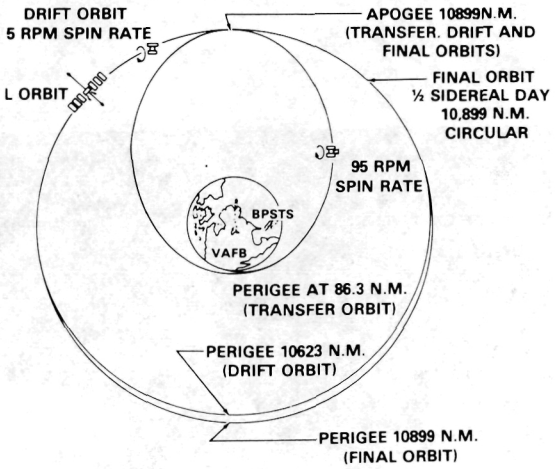


Fig. 3 - Mission sequence of NTS-2 events

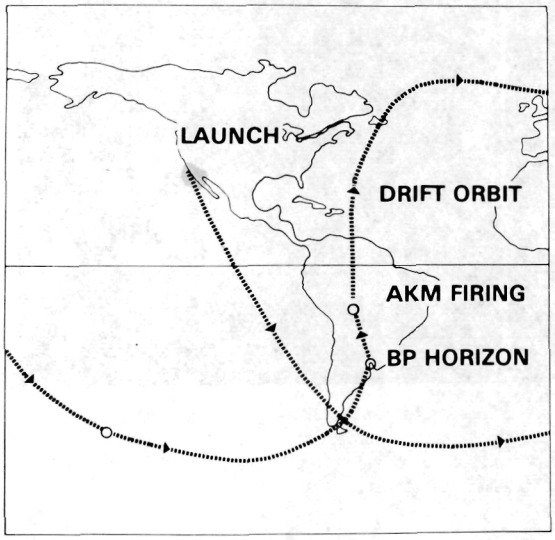


Fig. 4 - NTS-2 transfer orbit

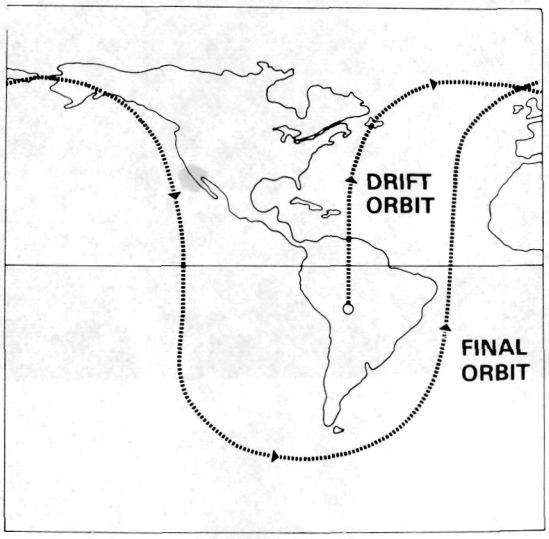


Fig. 5 - NTS-2 drift orbit

TASK: DETERMINE ORBIT TO 1SEC PERIOD

DATA TYPE	STATION LOCATION	ANTENNA APERTURE
1. AZ EL TRACK		
BLOSSOM POINT,	MD.	(20 FT)
SUGAR GROVE,	W.VA.	(150 FT)
RANGE MEASUREMENTS LAB,	FLA.	(48 FT) OPTICALLY
2. RANGE AND DOPPLER		
BLOSSOM POINT,	MD.	(20 FT)
SUGAR GROVE,	W.VA.	(150 FT)
CBD,	MD.	(4 FT)
PANAMA,	CZ.	(4 FT)
3. RADAR RANGE		
MILLSTONE,	MASS.	(85 FT)

Fig. 6 - NTS-2 launch tracking network

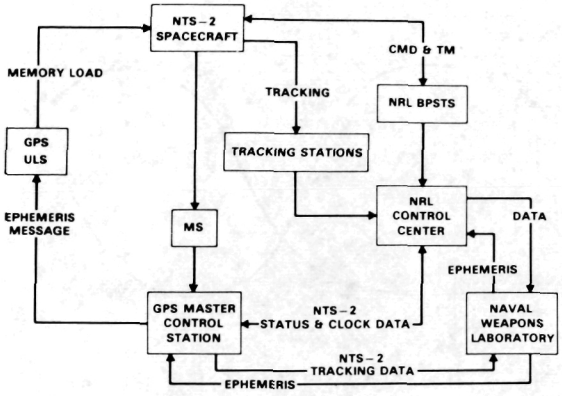


Fig. 7 - NTS-2 command and telemetry links

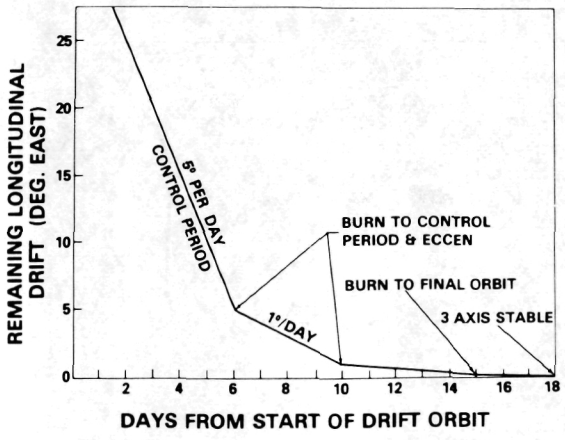


Fig. 8 - Pre-launch NTS-2 drift orbit profile

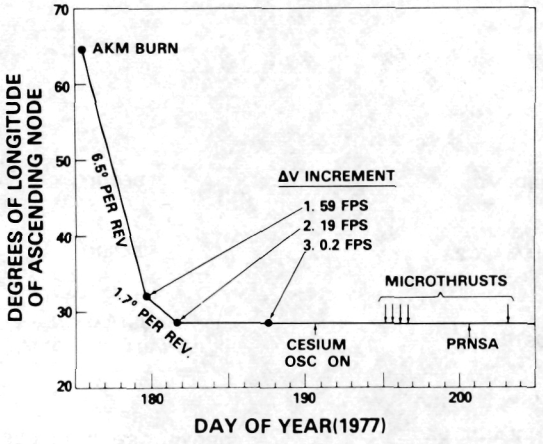


Fig. 9 - NTS-2 drift orbit adjustments

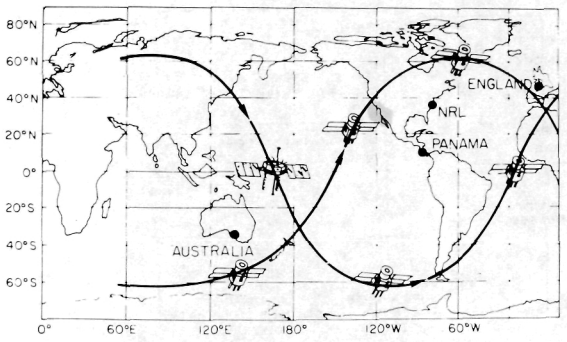


Fig. 10 - NAVSTAR GPS Phase I orbit traces

DAY (1977)	PERIOD (MIN.)	ECCENTRICITY	INCLINATION (DEG.)	LONGITUDE OF ASCENDING NODE (DEG. W)
177	704.9	.012	63.4	
	ADJUST			
180	714.5	.002	63.4	
	ADJUST			
184	717.94	.0003	63.3	28.48
	ADJUST			
192	718.04	.0004	63.3	
	ADJUST			
202	717.984	.0004	63.3	28.80
	ADJUST			
230	717.967	.0002	63.4	
273	717.956	.00032	63.43	28.35
295	717.946	.00034	63.44	28.10
		GPS SPECS		
	717.973	≤.003	63 ± .67	28 ± 2

Fig. 11 - NTS-2 orbital parameters

CBD, MD	BENDIX
PANAMA, C.Z.	BENDIX
AUSTRALIA	AUSTRALIAN (LUNAR LASER, DNM)
ENGLAND	BRITISH (ROYAL GREENWICH OBS.)

Fig. 12 - NTS-2 tracking network

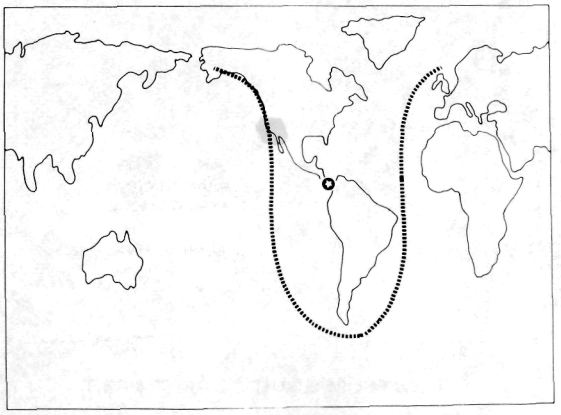


Fig. 13 - Panama NTS-2 coverage

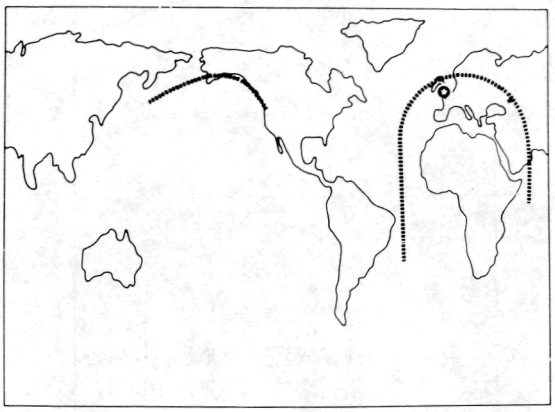


Fig. 14 - Royal Greenwich Observatory NTS-2 coverage

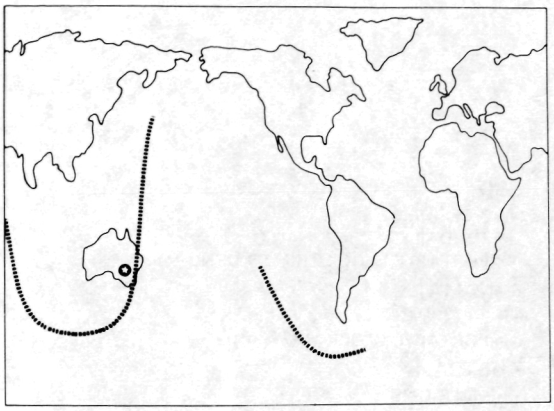


Fig. 15 - Australia NTS-2 coverage

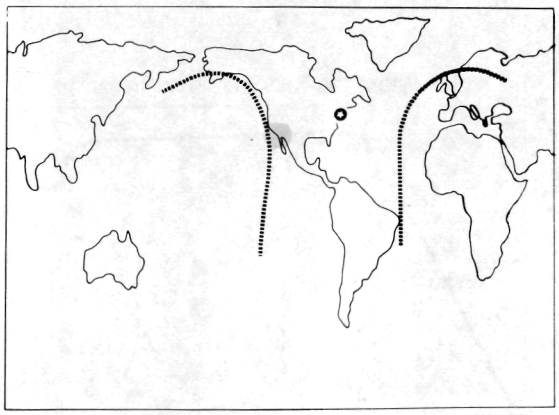


Fig. 16 - Chesapeake Bay Division NTS-2 coverage

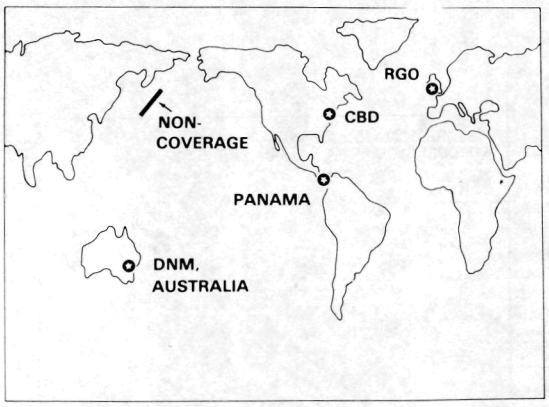


Fig. 17 - NTS-2 orbital non-coverage

CBD
- 3 CESIUMS
- TV (DAILY)
- PORTABLE CLOCK TRIP TO USNO (1X/Week)

PANAMA
- 3 CESIUMS
- PORTABLE CLOCK (1X/YEAR)

AUSTRALIA
- 5 CESIUMS
- PORTABLE CLOCK (2X/YEAR)

ENGLAND
- 3 CESIUMS
- LORAN C
- PORTABLE CLOCK (2X/YEAR)

Fig. 18 - NTS-2 ground timing links

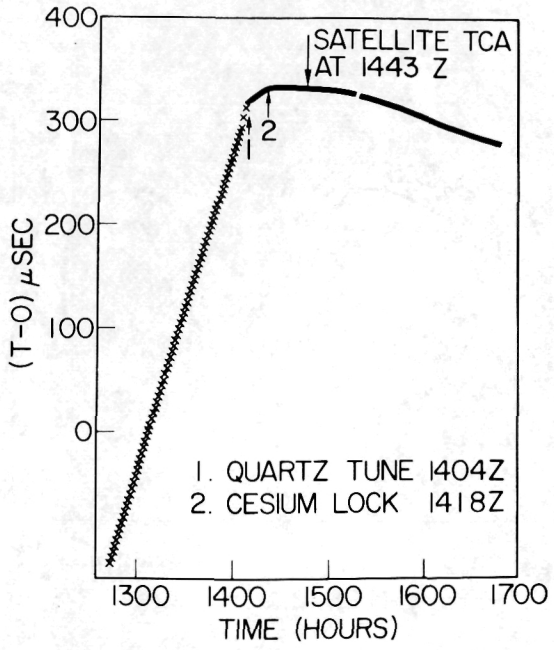


Fig. 19 - Cesium frequency standard lock up, 1977 day 190, 1418 UTC

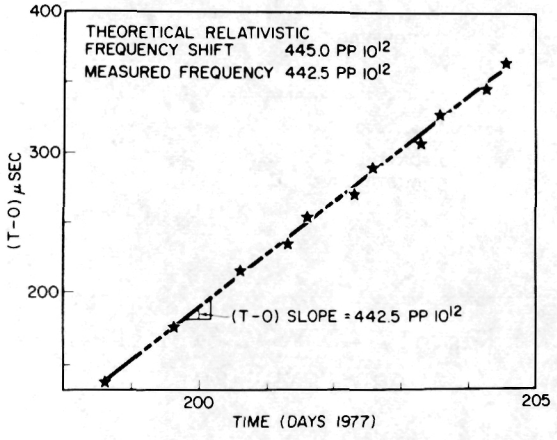


Fig. 20 - Cesium frequency via (T-O) slope

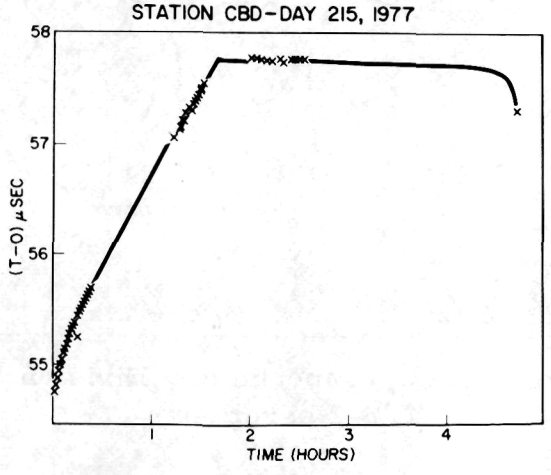


Fig. 21 - Effect of relativity correction

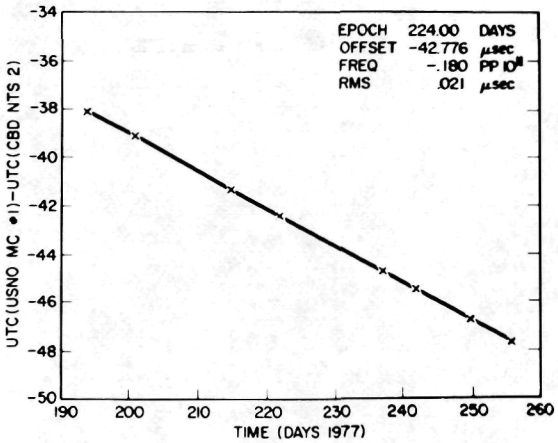


Fig. 22 - Frequency, USNO-CBD

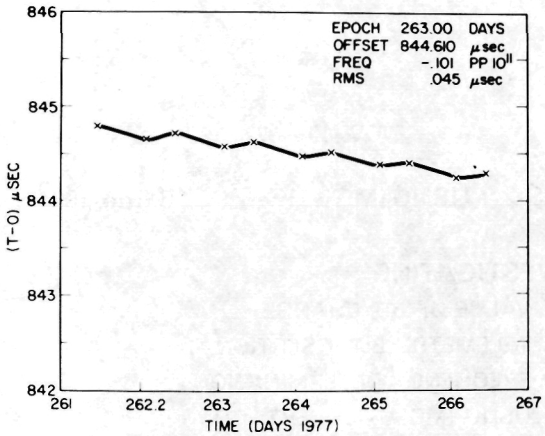


Fig. 23 - Frequency, NTS-CBD

CBD – USNO (MC#1) VIA PORTABLE CLOCK TRIPS	$1.80PP10^{12}$
CBD – NTS 2 VIA SATELLITE RANGE OBS.	$1.01PP10^{12}$
NTS 2 – USNO (MC#1)	$7.9PP10^{13}$
NTS 2 CESIUM OSCILLATOR C FIELD ADJUSTED 14 OCT 77	$7.8PP10^{13}$

Fig. 24 - NTS-2 cesium frequency

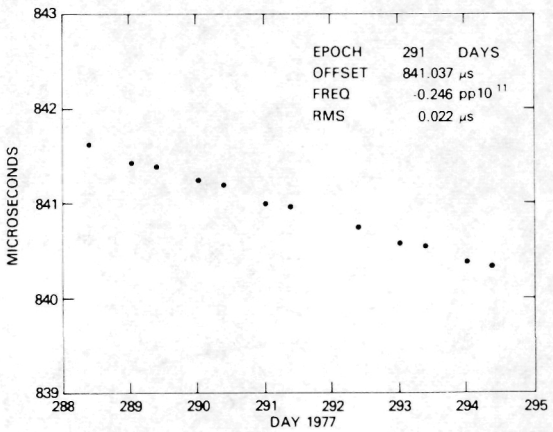


Fig. 25 - Frequency, NTS-CBD after C-field adjustment, 1977 day 287

NOV. 10, 1977

NTS-2 – USNO (MC #1) -6.6pp 10^{13}

INVESTIGATING

1. VALUE OF BIT CHANGE
2. TELEMETRY BIT INSERTION
3. FREQUENCY DETERMINATION
4. USNO (MC #1) UNCERTAINTY

Fig. 26 - Preliminary NTS-2 C-field adjust results

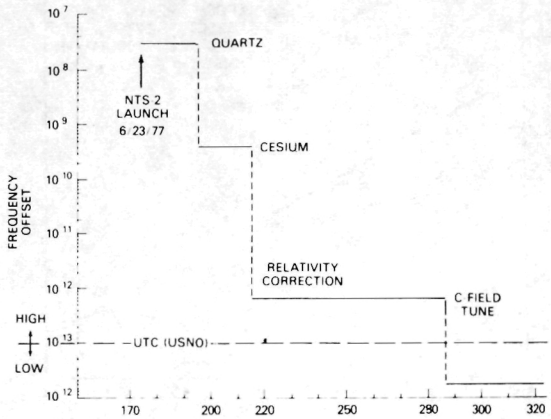


Fig. 27 - Frequency offset summary

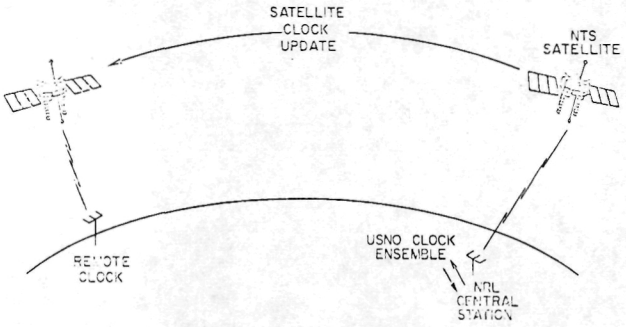


Fig. 28 - Time transfer, NAVSTAR GPS, navigation technology segment

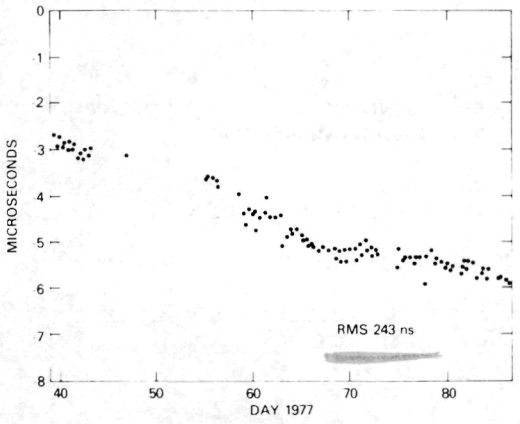


Fig. 29 - NTS-1 time transfer, NASA Cape Kennedy Station

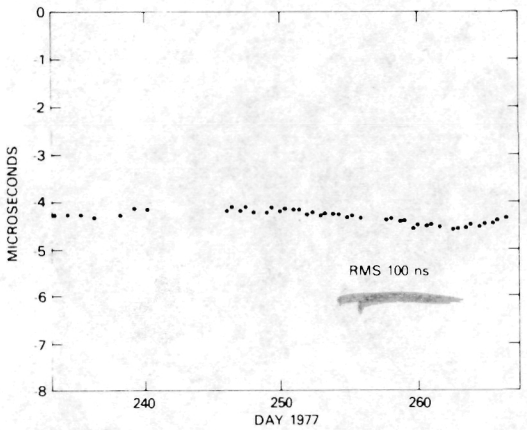


Fig. 30 - NTS-2 time transfer, NASA Cape Kennedy station

STALAS

GODDARD

RAMLAS

PATRICK AFB

MOBLAS

HAYSTACK
OWENS VALLEY
GOLDSTONE
5 ADDITIONAL

Fig. 31 - NASA laser network

ORGANIZATION	COUNTRY
NASA GODDARD SPACE FLIGHT CENTER	USA
U.S. NAVAL OBSERVATORY	USA
NAVAL RESEARCH LABORATORY	USA
NATIONAL BUREAU OF STANDARDS	USA
THE BUREAU OF INTERNATIONAL DE L'HEURE (BIH),	FRANCE
THE ROYAL GREENWICH OBSERVATORY (RGO),	ENGLAND
THE DIVISION OF NATIONAL MAPPING (DNM),	AUSTRALIA
THE NATIONAL RESEARCH COUNCIL (NRC),	CANADA
THE RADIO RESEARCH LABORATORIES (RRL),	JAPAN
THE NATIONAL RESEARCH LABORATORY OF METROLOGY (NRLM),	JAPAN
THE INSTITUT FÜR ANGEWANDTE GEODÄSIE,	GERMANY

Fig. 32 - International time comparison experiment

OBJECTIVES:

RESOLVE SCALE BIAS PROBLEM
LONG RANGE STATION POSITION STABILITY
LASER NET OBSERVATION
REFINE COEFFICIENTS OF GEOPOTENTIAL
PRECISE GPS ORBITS
HYDROGEN MASER EVALUATION

Fig. 33 - Laser orbit program objectives

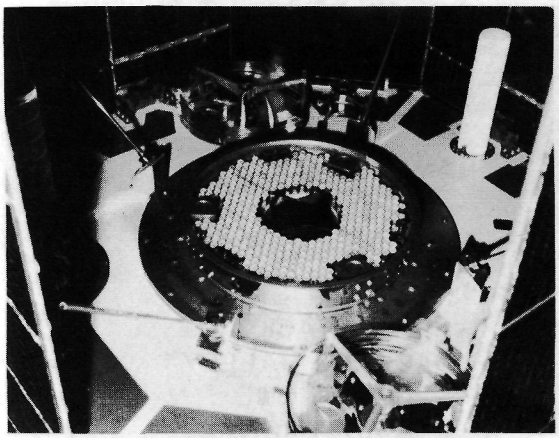


Fig. 34 - NTS-1 laser retroflector

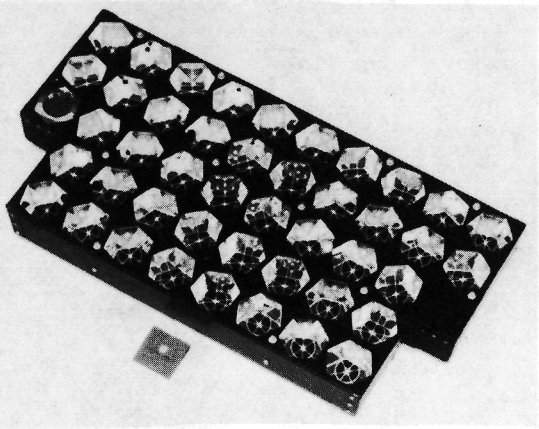


Fig. 35 - NTS-2 laser retroflector

- AREQUIPA, PERU
- NATAL, BRAZIL
  SAN FERNANDO, SPAIN
  ATHENS, GREECE
- ORRORAL VALLEY, AUSTRALIA
- MT. HOPKINS, ARIZONA
- NTS-2 CAPABILITY

Fig. 36 - SAO network

WETZELL, GERMANY
DELF, HOLLAND
TOKYO, JAPAN
GRASSE, FRANCE

Fig. 37 - Cooperating laser sites

DATA TYPE	STATIONS	MEASUREMENT RESOLUTION
TIME DIFFERENCE	NTS TRACKING NETWORK	48 CM
LASER	NASA, SAO, GERMANY, AUSTRALIA	15 CM
OPTICAL	PATRICK AFB	1 2 ARC SEC

Fig. 38 - Typical measurement resolution

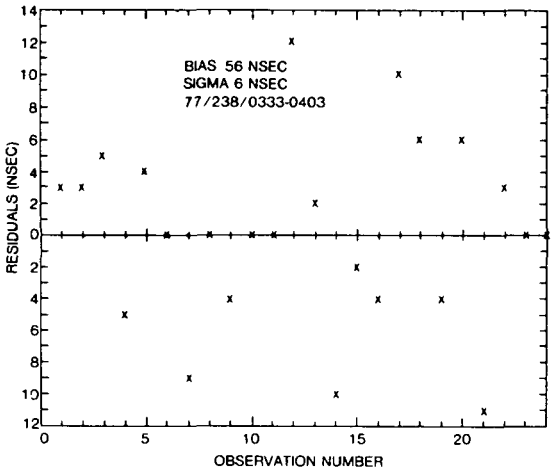


Fig. 39 - Laser residuals, Mt. Hopkins, 1977 day 238

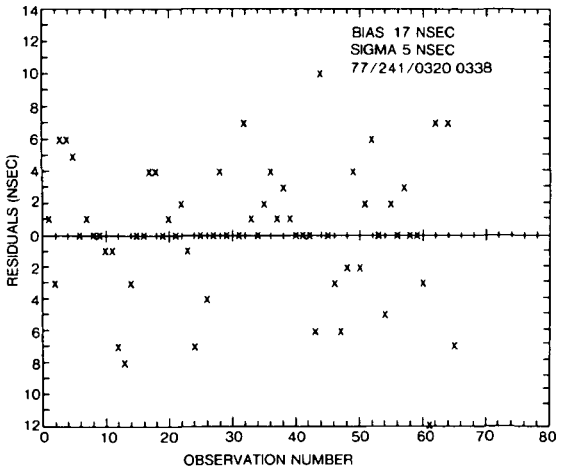


Fig. 40 - Laser returns, Mt. Hopkins, 1977 day 241

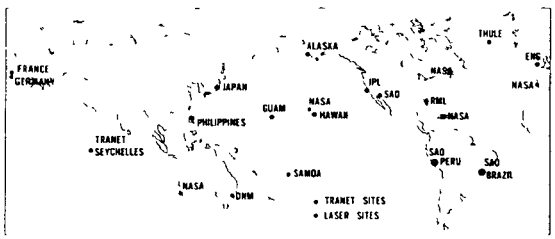


Fig. 41 - Proposed precise laser orbit tracking network

QUESTIONS AND ANSWERS

DR. VICTOR REINHARDT, NASA Goddard Space Flight Center:

When you load the C-field adjustment into the cesium, is there a possibility of glitching due to the serial-loading procedure that could have given you hysteresis?

MR. BUISSON:

I guess the possibility exists, but we don't think so. We were there when the load occurred, and it was a very clean load. There was no uncertainty in the bit change whatsoever. We got immediate acknowledgement of the numbers that were sent up.

DR. REINHARDT:

My question is not quite the same. Do you latch in the data after it is loaded, or is it loaded as it serially comes in so there could be a large C-field change during loading time?

MR. BUISSON:

It is a two-step process. It is an immediate load, which takes microseconds to do.

MR. LAUREN RUEGER, Johns Hopkins University Applied Physics Lab:

Would you be able to operate this in the timing mode when you are working with the GPS program? Or is that sort of a temporary thing? Or do you use them simultaneously?

MR. BUISSON:

This satellite will be operational. It is designed for a three-to-five year lifetime, and we would expect to be using it right up through NTS-3 launch in 1981.

MR. RUEGER:

No, I mean the side-tone ranging. Is that what you're receiving? You will be able to operate them simultaneously?

MR. BUISSON:

Yes, it is being operated simultaneously right now. It has been since we turned on around day 200 of this year.

DR. HELMUT HELLWIG, National Bureau of Standards:

Back to the C-field problem. We have done some measurements at the Bureau that indicate that in cesium, the magnetic shielding properties may be responsible for not producing the calculated values from the C-field adjust in the output frequency. In this case, I think the reason is that you have put the cesium standard in a totally different magnetic environment--actually a very low magnetic field without degaussing--and now any touching of the C-field will relax the magnetic stress in the shielding material.

MR. BUISSON:

That is correct. Bob Kern mentioned that yesterday.

DR. GERNOT M. R. WINKLER, U. S. Naval Observatory:

I completely agree because the same thing happens to portable clocks, for instance, when you make adjustments. Am I correct that during the tests of that satellite timing equipment, you did check the C-field adjustment but only for small steps? You did not go through such a large adjustment. Is that correct?

MR. BUISSON:

Well, a paper was presented by Joe White, I think, at the Frequency Control Symposium. And I think it was done. I know it was done at 100 to 200-bit changes. I don't know if it was done individually, one bit at a time. We did a 6-bit change, and possibly there is some uncertainty. The hysteresis is unknown on a single 1,2,3-bit change.

DR. ROBERT H. KERN, Frequency and Time Systems:

We have been speculating on what is taking place. It is my understanding that the cesium was launched, turned on, and no C-field adjustments were made. Is that true? The 6-bit change was the first time the C-field was touched?

We were indeed very fortunate, as it came up, to come within about 7 parts in 10^{13} of the USNO clock. What Dr. Winkler has suggested is the hysteresis effect which we have all come to know anytime you put a perturbation (mechanical, thermal, or magnetic) into the C-field of the cesium standard. I think the one thing that amazes me is the stability of the data over the first 50 days or so where we did not see any aging in the C-field. And yet, upon the impact of the 6-bit load, something dramatic certainly happened, whether the loading was correct or.... But the stability that we see over time is not characteristic of a thermal environment change. Jim (Buisson) showed us 30 degrees, I guess, change in the bird.

So it still remains to be determined what actually happened and further tests should bring it out nicely.

MR. WOLFGANG BAER, Ford Aerospace:

I notice you have very low eccentricity numbers. Do you plan to maintain that orbit as close to circular as possible and if so, do you require continual orbit adjustments?

MR. BUISSON:

We will maintain the period so that we have a constant ground track. And in doing that, whenever we do a period adjust, we have the capability of doing an eccentricity adjust also. Right now we are quite satisfied with 0003. The specs were something like 01 or 001. But whenever we do a period adjust to keep it on station, yes, we will hope to keep the eccentricity as circular, if not more circular.

MR. DAVE DOUGLAS, University of Rochester:

In one of the plots in which you showed microseconds versus time, I thought I saw a periodicity. What was that? The oscillation with time?

MR. BUISSON:

A lot of this is due to the uncertainty of the orbit determination at present. You are looking at one side of the orbit and then the other side of the orbit, and it could occur in the order of 0.5 microsecond or less. And I think that is what you are referring to on one of the long-term slides.

DR. HELLWIG:

Going back to the C-field problem. It is important to state again that these effects, like magnetic hysteresis and large external magnetic field changes, are common to all present atomic clocks and are generic; that is, it is a magnetic shielding problem. We see that even in our primary standards, so it should not be held against a particular standard.

DR. MULHOLLAND, University of Texas:

Commenting on the previous remark about the periodicity in the residuals, that in fact occurred on two slides in which you had plots of normal points--essentially one point for each pass: It looked as though the periodicity was about half a day which would have to be the orbit.

MR. BUISSON:

Yes, we agree. That is being actively pursued now by Naval Surface Weapons Center.

Page intentionally left blank

Page intentionally left blank

PRECISE TIME TRANSFER TO THE NASA SPACEFLIGHT TRACKING AND DATA NETWORK (STDN) VIA THE TRACKING AND DATA RELAY SATELLITE SYSTEM (TDRSS)

G. P. Gafke
Johns Hopkins University/Applied Physics Laboratory

J. W. McIntyre
Johns Hopkins University/Applied Physics Laboratory

S. C. Laios
NASA/Goddard Space Flight Center

S. C. Wardrip
NASA/Goddard Space Flight Center

ABSTRACT

Data communication via the Tracking and Data Relay Satellite (TDRS) is to become available to users in 1980. The ranging and data services provided by the Tracking and Data Relay Satellite System (TDRSS) are to be an integral part of NASA's post-1980 Spaceflight Tracking and Data Network (STDN). The synchronous orbit TDR satellites are to be positioned so as to provide near worldwide coverage, depending upon user satellite orbit or user earth location. An essential service that NASA will provide to its own tracking network (STDN) is precise time transfer using the TDR satellites. The network ground station's transmit/receive hardware will be essentially a non-flight version of the TDRSS user transponder.

The paper discusses the time transfer technique and the ground Time Transfer Unit (TTU) which contains a microprocessor for determining and averaging various time interval measurements. The TTU interfaces with the local ground station timing system and with the transponder that will be available at the NASA Network sites for TDRSS orbit determination.

Time transfer communication between the TDRSS ground station at White Sands and the STDN stations will be in a Multiple Access service standard mode of operation. This mode uses a combination of pseudorandom (PRN) codes and data modulation for ranging and telemetry. A selected code state indicator (e.g., the "all 1's" state) provides stable event markers.

To transfer time via the TDRSS, the time interval between a specific event marker and the master station clock's 1 PPS is measured. A similar interval is measured by the user as his transponder receives the PRN code and hence the event markers. The time interval measurements and other information are exchanged between master and user by forward and return telemetry. The master makes a second time interval measurement to allow estimation of the forward delay time.

The Time Transfer Unit includes a microprocessor and associated peripheral chips used for synchronizing and multiplexing the time transfer telemetry frame and for computing clock error. The time interval measurements required will be obtained from precision time interval counters. The error in the clock difference measurement is expected to be less than 40 nanoseconds and to be available once each second. The total elapsed time required to complete a time transfer should be less than five minutes.

1.0 SUMMARY OF THE TRACKING AND DATA RELAY SATELLITE SYSTEM (TDRSS)

1.1 General

The tracking and Data Relay Satellite System (TDRSS) is being developed for NASA by an industry team composed of Western Union Space Communications Inc. (WU), Harris Electronic Systems Division (HESD), and TRW Systems Group. The ranging and data services provided by TDRSS are to become an integral part of NASA's post-1980 Spaceflight Tracking and Data Network (STDN).

1.2 Coverage

Data communication accessibility will be nearly worldwide depending upon user satellite altitude and inclination. This coverage is to be provided by three synchronous orbit relay satellites, two of which (TDRS East and TDRS West) are spaced 130 apart in longitude. Considering remote ground stations as potential TDRSS users to receive precise time transfer, the zone of coverage would include East Longitude locations to the east coast of Africa and West Longitude locations to the west coast of Australia. This region of coverage at the earth's surface includes all currently anticipated STDN stations. A basic illustration of communication relay via TDRSS is shown in Figure 1.1.

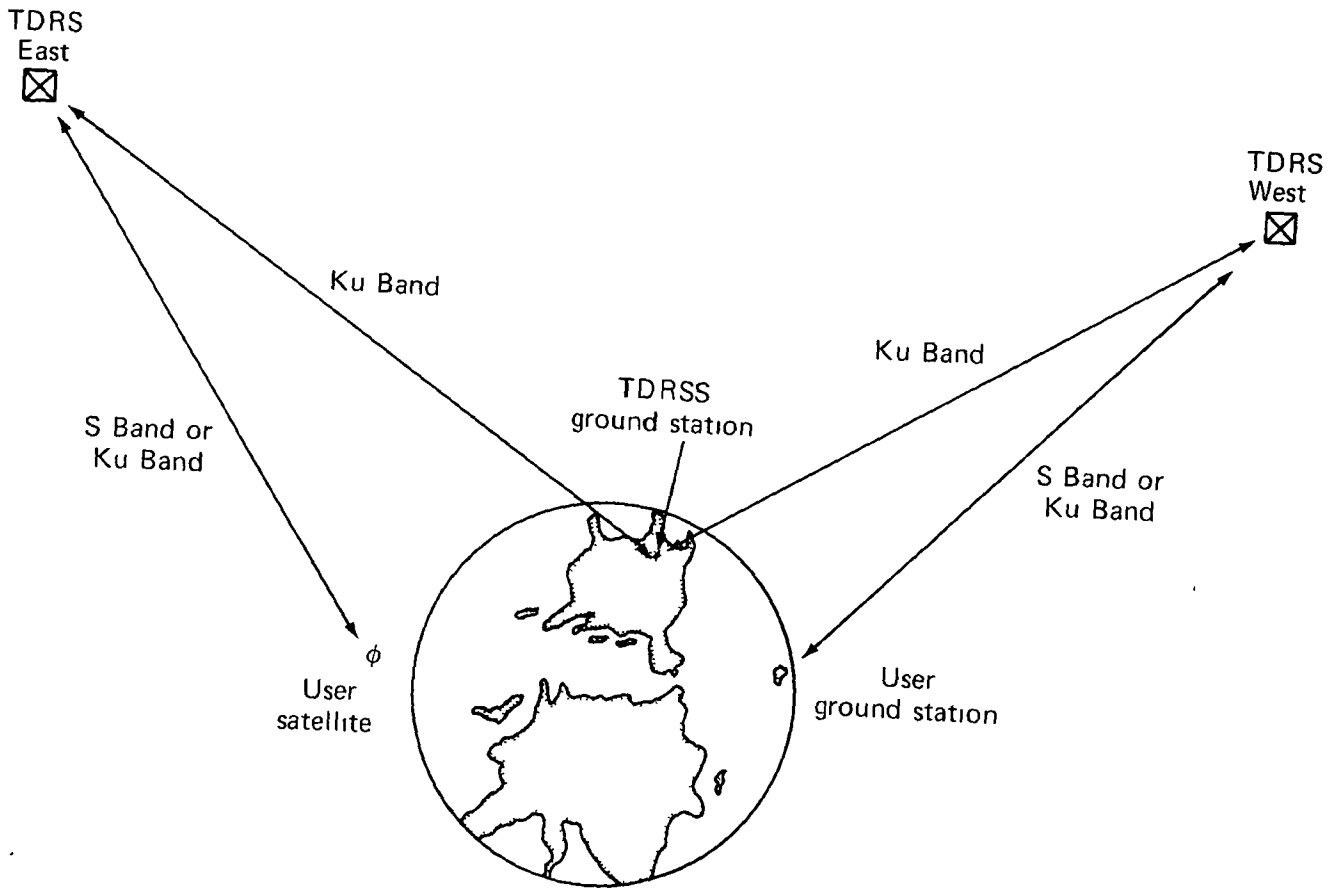


Fig. 1.1 Communication Relay via the Tracking Data Relay Satellite System

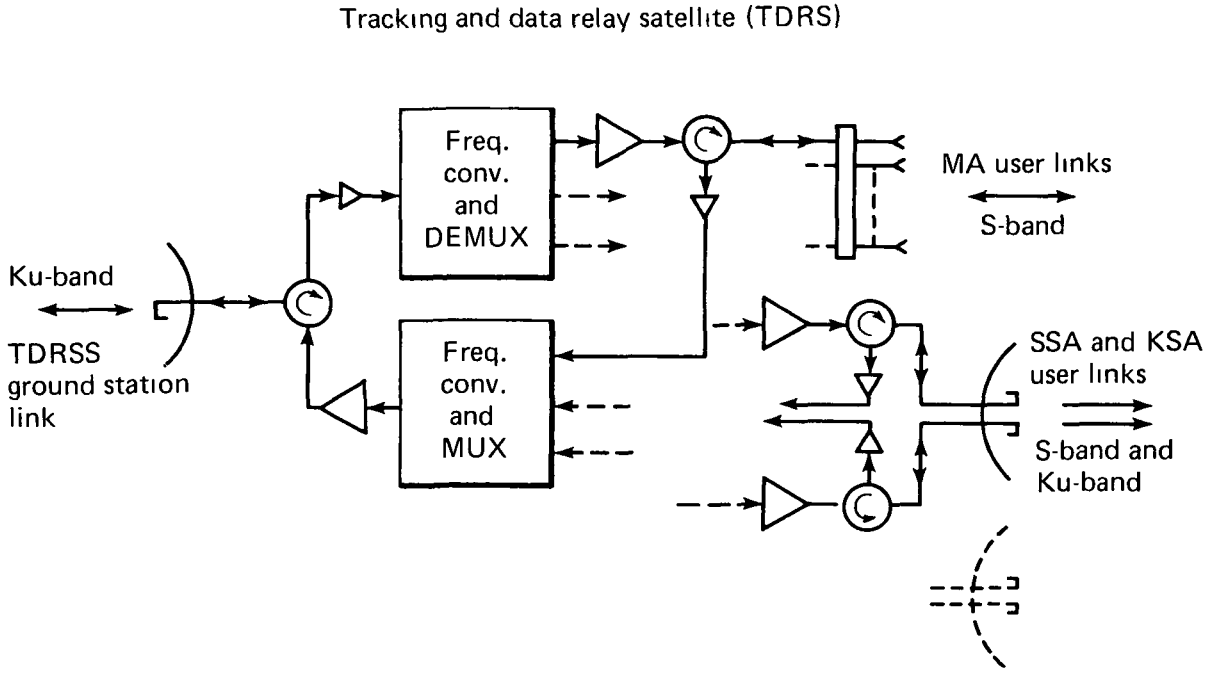


Fig. 1.2 Forward and Return Relay via the Tracking and Data Relay Satellite (TDRS)

1.3 TDRSS Services

Two basic types of service will be provided by TDRSS, Single Access and Multiple Access. For Single Access service, each TDR satellite has two steerable dual-feed antennas. The dual feeds provide for S-Band and Ku-Band communication (SSA and KSA) to and from users. For Multiple Access (MA) service, each TDR satellite has a planer S-Band array antenna capable of both forward and return beam forming. Forward link beam forming to a user is done at the TDR satellite and return link beam forming from a user is done at the TDRSS ground station. Each MA user, therefore, has the equivalent of a directed beam.

Forward and return relay between the TDRSS ground station and the TDR satellites is at Ku-Band. The required multiplexing, demultiplexing and frequency translations to and from the user are done at the TDR satellite. Figure 1.2 is a simplified block diagram of the signal flow through a TDR satellite.

1.4 TDRSS Signal Design

In order to best satisfy the combined requirements of limited radiation flux density, Single and Multiple Access ranging and data services, and individual beam forming for each Multiple Access user, a pseudorandom (PRN) code signal design was chosen for TDRSS.

The capability of simultaneous ranging and data communication is directly applicable to time transfer. Ranging is accomplished by synchronized forward and return link PRN codes in a "round trip" or "two way" ranging mode (TDRSS Mode 1). Forward and return telemetry data are modulated onto the respective codes allowing simultaneous two-way data transfer. The PRN code "epoch" signals or "state indicators" serve as event markers for time transfer. Signal margins are such that these markers will be quite stable and code acquisition times relatively short.

1.5 TDRSS Interface

The basic type of interface between users and TDRSS is a data interface, available with both Single and Multiple Access services. Baseband digital data and data clock are applied at the TDRSS ground station to a forward link data interface. Baseband digital data and data clock are returned from the user via a return link data interface. The forward and return PRN code "epochs" or "state indicators" will be utilized for time transfer to the NASA ground network stations (STDN).

A block diagram of the time transfer hardware and the interface with the TDRSS ground station at White Sands is shown in Figure 1.3.

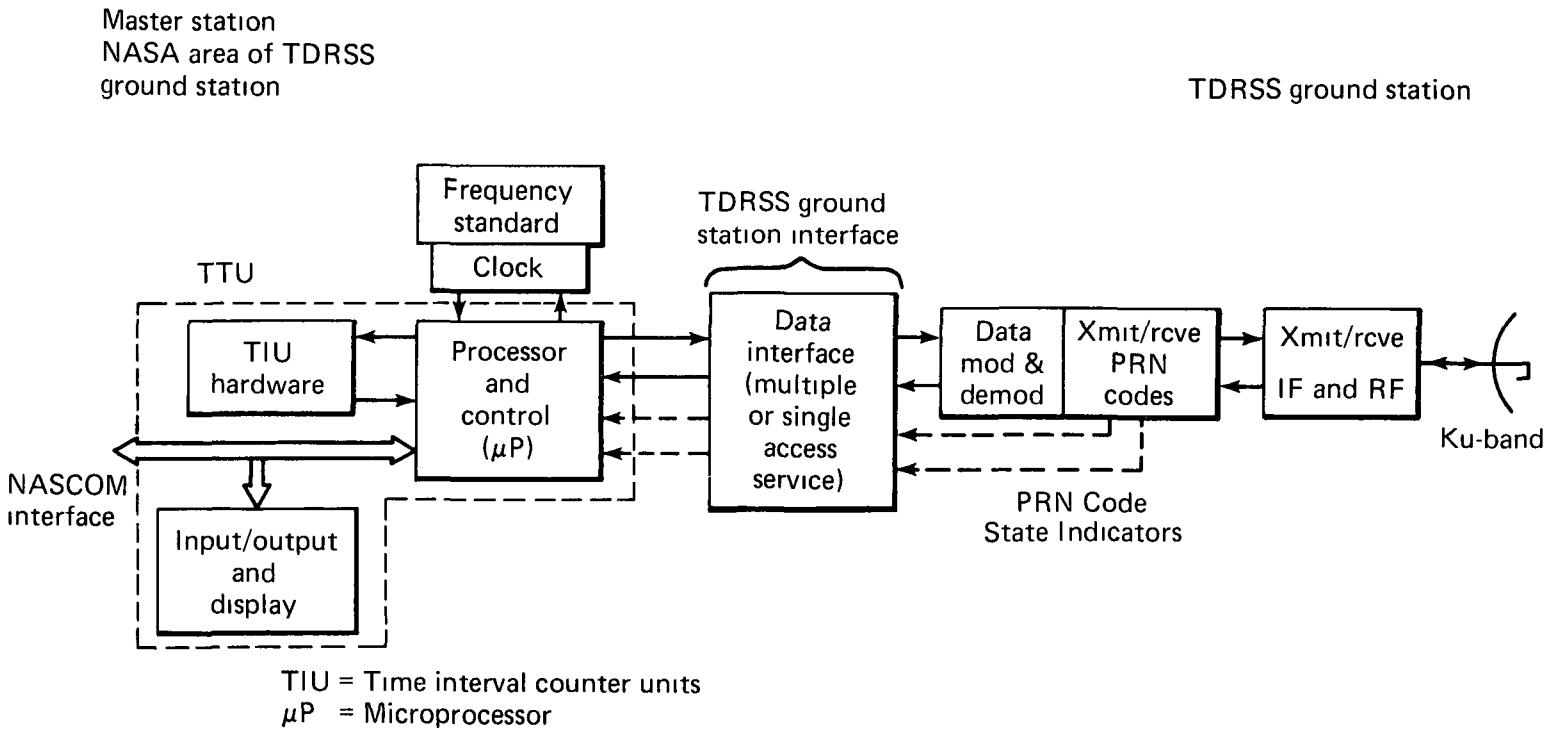


Fig. 1.3 Time Transfer Hardware and TDRSS Ground Station Interface

The basic time transfer unit (TTU) includes the microprocessor with associated peripheral hardware, the time interval counting units, and the frequency standard and clock.

A block diagram of the STDN station TTU and TDRSS interface hardware is shown in Figure 1.4. Essentially the same hardware is used here as issued at the TDRSS ground station except that the transmit/receive interface is with a TDRSS user transponder.

2.0 TDRSS TIME TRANSFER TECHNIQUE

For the purposes of this paper, the transfer of time is defined to mean the determination of the difference between the clock times of two physically separated stations. It is assumed that each station has a clock 1 PPS signal derived from and having the accuracy of its own time standard. This allows the time interval between clocks to be measured as the time interval between occurrences of the stations' respective 1 PPS signals. The objective of the technique described herein is to determine the time interval between those 1 PPS signals (i.e., the clock error, ϵ).

2.1 Clock Error Calculation

The technique described below can assume a Master/Slave relationship between the stations where in fact the master station would be the NASA terminal at the White Sands TDRSS ground station. The slave station would be one of the STDN tracking stations or other suitably equipped TDRSS user. The implementation could be such that essentially the same hardware but slightly different software (Section 3.0 discusses implementation) would make the two stations reciprocal, so that either station could act as the master. This would be advantageous if a given station was required to have the capabilities of either master or slave, as in a chain-type time transfer.

To determine the clock error, ϵ, the master must know when the slave's 1 PPS occurred relative to his own. This is achieved by having both master and user measure the time interval from their respective 1 PPS signals to a common reference. The common reference is an epoch or state indicator signal of the PRN code being relayed between master and slave, via the TDR satellite.

As this code is generated, the code vectors or state indicators (SI's) occur repeatedly, once for each full cycle of the code. To avoid ambiguity, one specific SI is selected or tagged so that both slave and master refer their measurement to the same SI. A timing diagram illustrating the intervals to be measured (Δ_2 and Δ_3) is given in Figure 2.1a. From the diagram, one can express the clock error as;

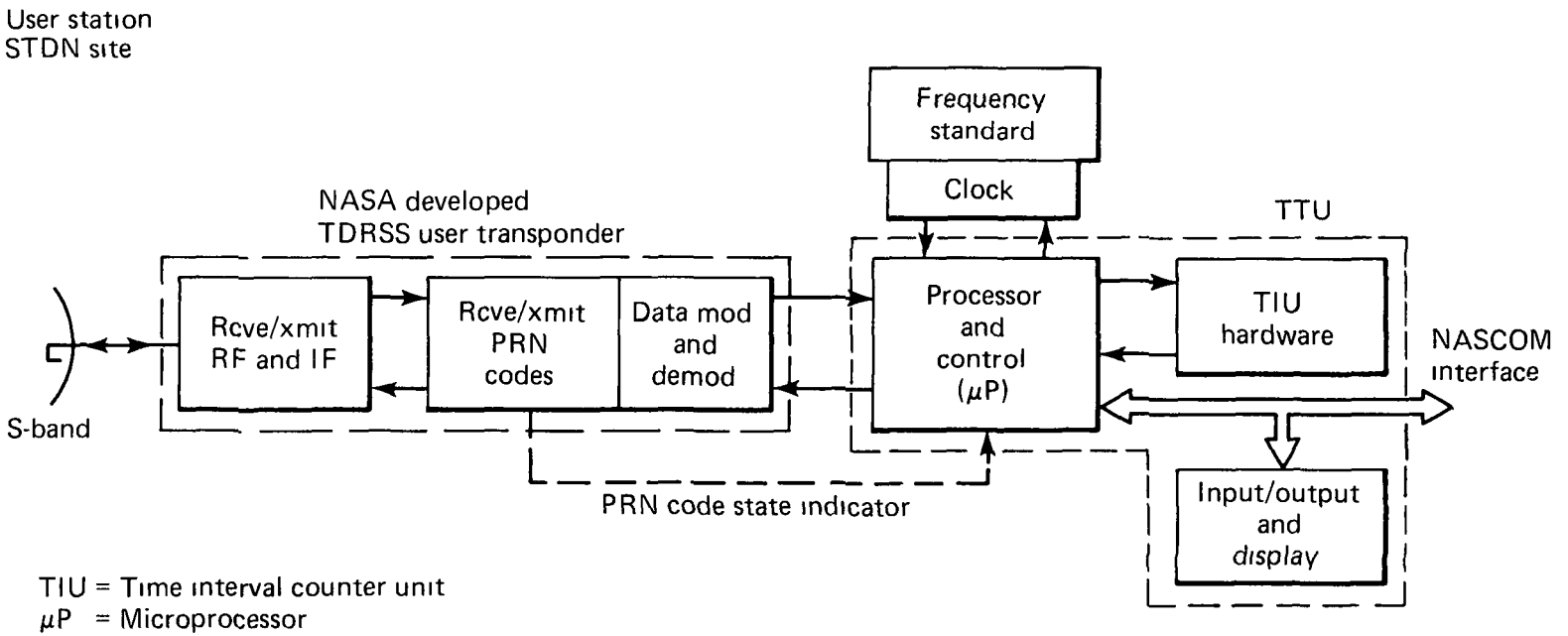
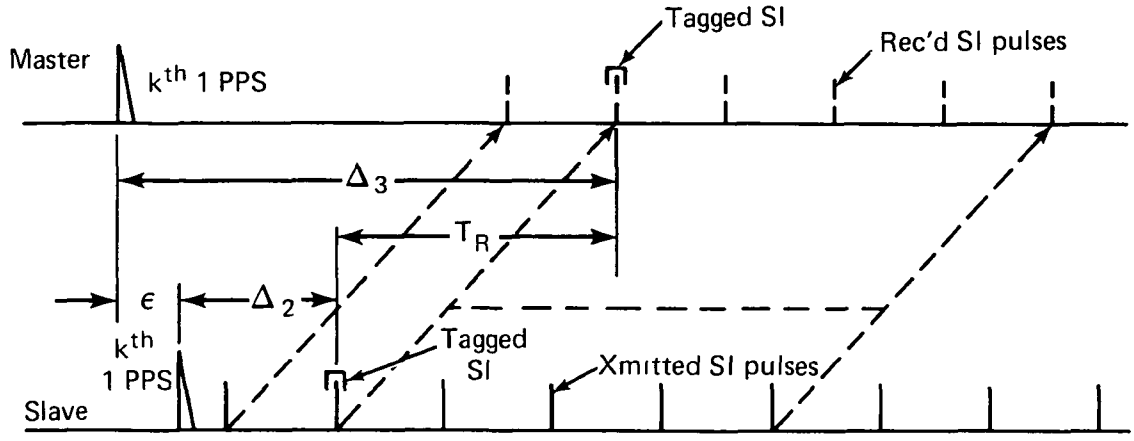
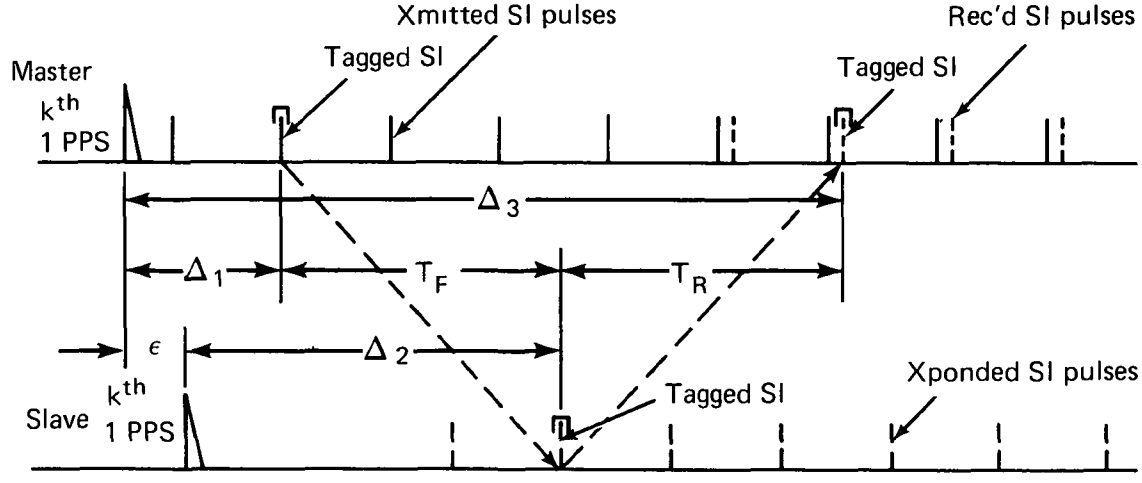


Fig. 1.4 Time Transfer Hardware and STDN User Interface



(a) One-way (Slave-to-master) Time Transfer SI Timing Diagram



(b) Two-way Time Transfer SI Timing Diagram

Fig. 2.1 Basic Time Transfer Signals and Time Intervals

$$\epsilon = \Delta_3 - \Delta_2 - T_R \qquad (2.1\text{-}1)$$

This represents a "one way" or "return only" method of time transfer in which Δ and Δ are the intervals measured by the slave and master, respectively, and T_R is the return link path delay from slave to master. (It is assumed that any hardware delays have been taken into account; this will be discussed in Section 4).

To actually calculate ϵ, the delay T_R must be determined. For a one-way link of user-to-master (TDRSS Mode 2 return link only), T_R would have to be calculated using ephemeris data on the TDR satellite, as well as the exact locations of slave and master.

A second method of determining T_R is to estimate it from measurements using a two-way link (TDRSS Mode 1). In this mode, the master originates the PRN code; the slave receives and retransmits the code, and makes his Δ_2 measurement which is also sent back during the next one-second measurement interval. The returning code enables the master to make not only an initial interval measurement (Δ_1), but also a second interval measurement (Δ_3). The measurements are made from his 1 PPS to the tagged SI as it is being transmitted (Δ_1) and received (Δ_3). Figure 2.1b illustrates the timing for this situation.

From Figure 2.1b one can see that the total path delay, T_F+T_R is;

$$T_F+T_R = \Delta_3 - \Delta_1 \quad .$$

where T_F is the forward link path delay from master to slave. Hence, the two measurements made by the master, Δ_1 and Δ_3, allow estimation of the path delay. If we now assume that the forward and return delays through the satellite hardware are equal and that the satellite is motionless relative to the earth, the return path delay, T_R, is equal to the forward path delay, T_F. Using this assumption and Eq. (2.1-2), Eq. (2.1-1) becomes;

$$\epsilon = \frac{\Delta_3-\Delta_1}{2} - (\Delta_2-\Delta_1) \quad . \qquad (2.1\text{-}3)$$

2.3 Summary

Several assumptions were made to obtain the simple result of Eq. (2.1-3), namely equal forward and return delays through satellite, master and user station hardware, and a "stationary" satellite. The influence of hardware delay and satellite motion in the clock error estimate are illustrated in Section 4.

Satellite motion can cause an error in the computed value of of about 25 nanoseconds over an interval of about 1 minute for a linear radial motion of 30 meters/sec. The time transfer system proposed herein is capable of estimating the first order (linear) motion of the

satellite using the time interval measurements. With a set of measurements being made once each second (corresponding to each 1 PPS), the previous two seconds of measurements will be sufficient to estimate linear motion. Section 4 contains a more complete description of satellite motion, hardware delay, and signal jitter contributions to time transfer error.

3.0 IMPLEMENTATION OF THE TDRSS TIME TRANSFER TECHNIQUES

Section 2 discussed the general technique used to effect a "time transfer" using the TDRSS. The details of implementation were ignored. These will now be discussed.

3.1 Data Link

A number of questions were left unanswered in Section 2, such as how the master obtains the measurements made at the slave station, and especially how one particular SI is "tagged" so that both stations recognize it. (This essential feature will be described in Section 3.2.2, paragraph 2.) Communication through the TDRSS data link and the format of this communication provide the answers. Modulated onto the PRN code is data in block form as shown in Table 3.1. This data, generated by the Time Transfer Terminal (TTU), is used to transfer such required information as:

a. The quantities necessary for clock error calculations including time interval measurements, time-of-day, and, in a "one-way" situation, range information perhaps in the form of position constants.

b. A status word used to communicate between master and user such things as data validity, loss of frame, end of transmission, and others.

c. Sync words which indicate the beginning of the telemetry frame and also generate a "range gate" to resolve the state indicator (SI) ambiguity by tagging a particular SI. This is discussed in more detail in a later subsection.

d. A sixteen-bit SUMCHK is used to provide transmission error detection since no allowance was made for word parity. The SUMCHK holds the complement of the modulo 2^{16} sum of the contents of the previous 27 bytes. In addition, the sync words, frame ID, and status word also help maintain frame integrity.

Sufficient information is included in the formats to allow either master or user to calculate the error between clocks.

Table 3.1

TDRSS Time Transfer
Telemetry Frame Format – k^{th} Interval

Byte No.	Master TLM Description	User TLM Description
1	Frame Sync	Frame Sync
2	Frame Sync	Frame Sync
3	Frame ID	Frame ID
4	STATUS WD	STATUS WD
5	STATION ID	STATION ID
6	TIME-OF-DAY, DAYS	TIME-OF-DAY, DAYS
7	TIME-OF-DAY, DAYS	TIME-OF-DAY, DAYS
8	TIME-OF-DAY, HRS	TIME-OF-DAY, HRS
9	TIME-OF-DAY, MINS	TIME-OF-DAY, MINS
10	TIME-OF-DAY, SECS	TIME-OF-DAY, SECS
11	Δ_1 (k-1)	Δ_2 (k-1)
12	Δ_1 (k-1)	Δ_2 (k-1)
13	Δ_1 (k-1)	Δ_2 (k-1)
14	Δ_1 (k-1)	Δ_2 (k-1)
15	Δ_1 (k-1)	Δ_2 (k-1)
16	Δ_3 (k-1)	ϵ (k-2)
17	Δ_3 (k-1)	ϵ (k-2)
18	Δ_3 (k-1)	ϵ (k-2)
19	Δ_3 (k-1)	ϵ (k-2)
20	Δ_3 (k-1)	ϵ (k-2)
21	Position Const ID	SPARE
22	Position Const	SPARE
23	Position Const.	SPARE
24	Position Const	SPARE
25	Position Const.	SPARE
26	SPARE	SPARE
27	SPARE	SPARE
28	SUMCHK (LSB)	SUMCHK (LSB)
29	SUMCHK (MSB)	SUMCHK (MSB)
30	ETX (End of Text)	ETX (End of Text)

The data frames include thirty eight-bit bytes (or words) for a total of 240 bits. At the proposed bit rate of 1200 BPS (a standard modem baud rate), the frame period is 200 msecs. The resulting byte period is 6.7 msecs, and the bit period is 0.83 msecs. It is suggested that all numeric data be in a packed BCD format (two decimal digits per byte). This allows the use of the data-independent values 10_{10}-15_{10} in 4-bit nibbles for conveying alphabetic information such as sync words, end-of-text (ETX), and frame and user ID.

3.2

The hardware used to generate, format, and control the transmission and reception of the data frame is shown in Fig. 3.1 for both master and slave. This hardware must also accept the necessary inputs and make all calculations required to determine clock error, as well as provide an interface to the ground network via NASCOM. For discussion purposes, this hardware is separated into three general areas:

1. TDRSS (ground station and user transponder) equipment.

2. Equipment which provides various required inputs to the processor.

3. The processor unit.

3.2.1

The TDRSS equipment is used to provide the communications link between master and slave. It also provides a common event marker reference (the PRN code SI pulses) and a means of relaying the data involved.

3.2.2

The second level hardware includes the items indicated below.

1. Time interval counters are required to measure the Δ_i's.

2. Logic gates and latches are required to provide timing synchronization for the interval counters via START/STOP pulses and synchronization of certain interrupts. These units also tag or gate the proper SI pulse using a Frame Sync detection signal. The tagged SI is in turn latched as a low level into the interval counter, thus stopping the Δ_1 count which had been started by the 1 PPS via the same latch. Hence, Δ_1 is a measure of the interval between the 1 PPS and the first SI pulse following the Frame Sync words. Since the data frame is now referenced to the PRN code (transmission is initiated by another SI pulse),

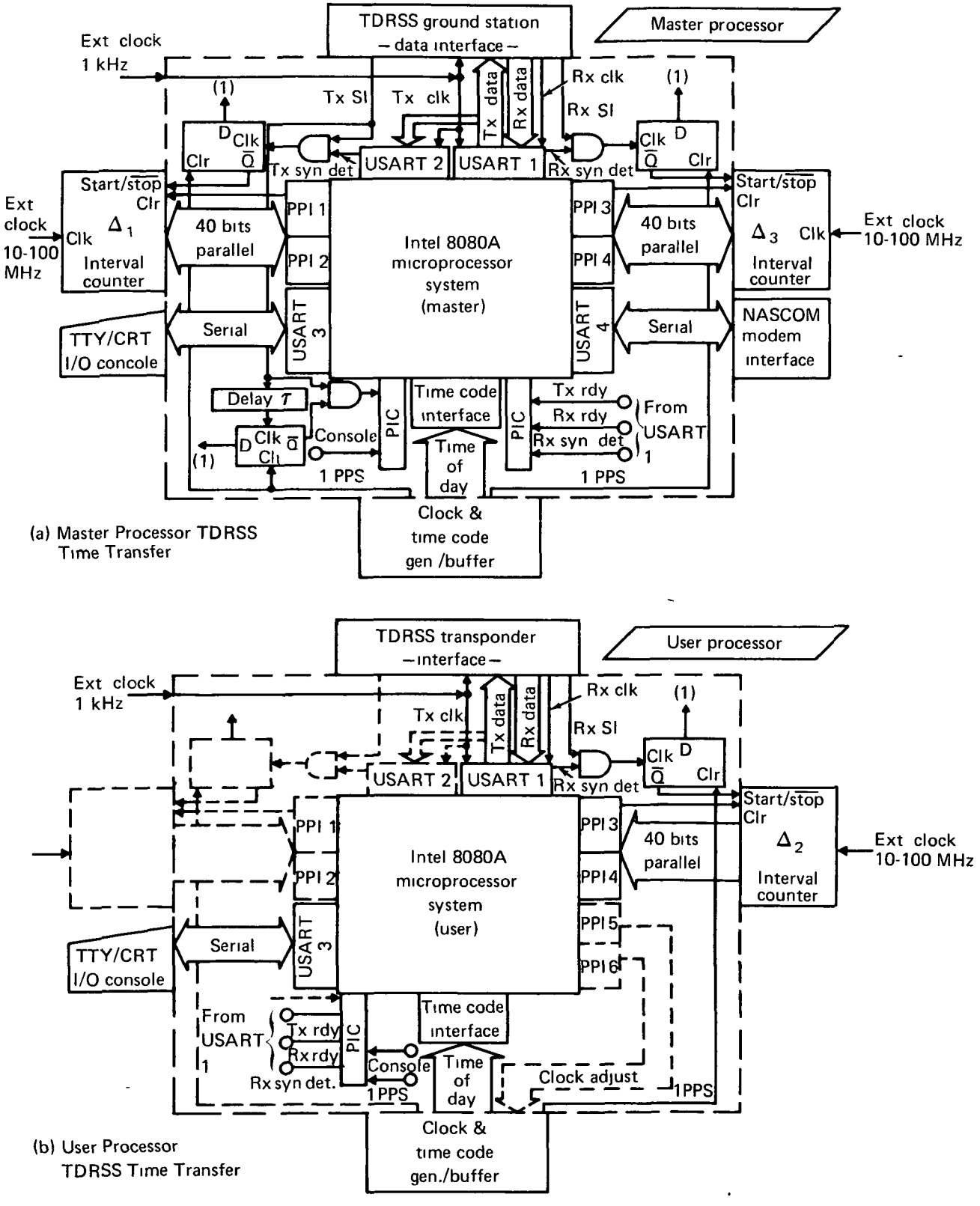


Fig. 3.1 Time Transfer Processor

the tagged SI pulse will always be the first one following the Frame Sync. (During reception of a "turned-around" code, the same sequence occurs, yielding the interval Δ_3.)

3. The frequency standard, station clock, and time code generator/buffer hardware provide the 1 PPS signals and allow all data frames to be time tagged (hours/minutes/seconds).

4. A NASCOM interface is required to allow communications between the master station and controlling locations (e.g., GSFC/NTTF).

5. An operator I/O console facility is required to allow interaction between operators and the time transfer system. This allows data values such as clock error to be displayed on demand as well as providing a means of entering commands into the system.

3.2.3

The processor system, consisting of a microprocessor and associated peripheral I/O chips, is the basis of the Time Transfer Unit (TTU) hardware and does all required computation and most of the control. In an application where a small amount of simple calculation and a large amount of control are required, a microprocessor is the natural solution. For the time transfer system, the Intel 8080 was initially selected. Other processors (e.g., Zilog's Z-80) have similar capabilities and could also be used. The 8080 was selected because not only does it have a sufficient instruction set, word size, and speed, but also because it is currently well supported by available software, peripheral chips, development hardware, and second-source vendors.

Associated with the microprocessors (μPs) are three types of peripheral interface chips (refer to Fig. 3.1). The USARTs are universal synchronous/asynchronous receiver/transmitters which are used to convert the parallel data of the μP into synchronous serial data for the TDRSS transmission link and the reverse for reception. The USARTs provide sync words at the start of each data frame during transmission, sync word searching during reception, parity checking if desired, half- or full-duplex operation, and a number of other functions. The USARTs also interface naturally with interactive terminal devices (e.g., teletype, CRT console, etc.).

The PPIs are parallel peripheral interfaces which allow direct transfer of parallel data into and out of the μP. Each PPI has the capability of transferring 24 parallel bits. So, for example, to transfer the 40-bit interval measurements, two PPIs are required, leaving 8 bits for control purposes.

Finally, the PIC is a priority interrupt controller which accept external interrupt signals and, in a specified priority, allows one of

them to interrupt the μP while holding any others that have occurred. The PIC directs the μP to the processing routine corresponding to the interrupt that was accepted. Hence, the time transfer program operates as an interrupt driven system, making more efficient use of the μP.

3.3 Processor Operation

Functional flowcharts of the master and user systems are given in Fig. 3.2. In general, both master and user processors receive, store, and format the various inputs (e.g., Δ_i's and GMT time) into a data frame. This information is stored in one or more of three tables or buffers. One buffer contains the telemetry to be sent (TX BUFF), another stores the telemetry being received (RX BUFF), and the third retains a history of pertinent data (OLD DATA BUFF). During the kth interval TX BUFF and RX BUFF contain data measured during the (k-1)th interval as well as a running account of the calculated clock error, ϵ, which can be averaged. As part of each interval's calculation phase, the OLD DATA BUFF is updated from the RX BUFF and TX BUFF, and the TX BUFF is updated with new time interval measurements, time-of-day, and a status word.

Each processor will have a simple resident monitor program which allows communication with the I/O console, possibly with NASCOM, aids in debugging, and allows software modifications. Commands to initiate and terminate time transfer could be made by an operator from the console, via the monitor, to the time-transfer program. These commands could also come via NASCOM or be initiated automatically if one so desired. For example, a code lock indication from the TDRSS interface could initiate transfer, and, after a pre-set time (e.g., 30 seconds), the program itself could terminate transfer. There are many possibilities, some of which will prove to be more operationally acceptable than others.

Once initiated, the time transfer program is directed by a series of interrupts which are monitored by the processor's programmable interrupt controller (PIC). Flags can be set to convey certain information required by the program once the data exchange is completed (about 760 msecs into the one-second interval).

The processor is responsible for other activities as well. As the serial data are received by the USART (universal synchronous/asynchronous receiver/transmitter), data validity is checked in various ways. As valid data is accepted and stored, calculations needed to determine clock error are made and checks for End-of-Transmission (EOT) are made.

Finally, following EOT, the processor has the option of performing various kinds of analyses that may be desired and the

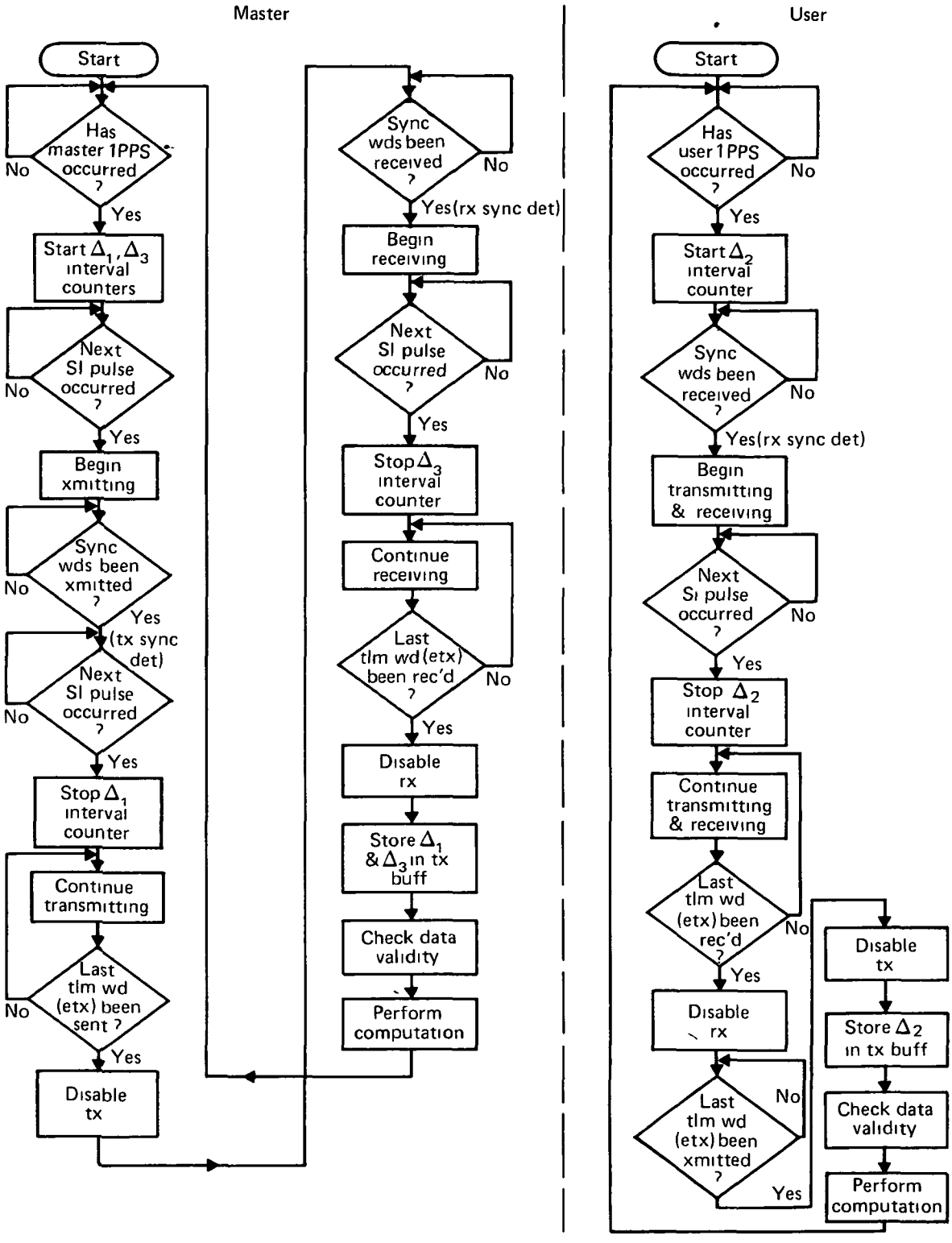


Fig. 3.2 Time Transfer Algorithm — Data Flow Control

capability of displaying requested results on the console or other devices. From there, program control returns to the monitor to await operator commands (either locally via console or remotely via NASCOM).

4.0 TIME TRANSFER ACCURACY

4.1 The TDRSS Relay Path Model

The time interval measurements and clock error calculations which were discussed in Section 2 can be illustrated by the linear model of the TDR satellite relay path shown in Figure 4.1. This linear model assumes that TDR satellite motion results in a constant range rate relative to each station over the time period required for time transfer. The three basic factors which contribute to time transfer error can also be visualized from Figure 4.1. These factors are:

a. The variation in the transmission time or relay path due to both satellite motion and propagation effects. The variation due to TDR satellite motion is a potentially greater source of error if not accounted for than propagation effects.

b. Hardware delays at the TDRSS ground station, the STDN user station, and through the TDR satellite.

c. Variation or "jitter" in the PRN code state indicators (SI's) due to noise in the tracking loops.

The contributions of these factors to the estimate of overall time transfer error is tabulated in Table 4.1 of Section 4.3.

4.2 Calculations Based on the Linear Model

One form of the basic clock error calculation given in Section 2 is:

$$\hat{\epsilon} = \hat{T}_F - (\Delta_2 - \Delta_1) \quad . \tag{4.2-1}$$

Each of the terms of Eq. (4.2-1) is illustrated on Figure 4.1. The intervals Δ_1 and Δ_2 are measured between a clock one pulse per second (1 pps) and a PRN code state indicator (SI). The forward relay time, T_F, is to be estimated from measurements of the "round trip" relay time, $T_T=\Delta_3-\Delta_1$, based on the linear model. The estimate of the forward relay time is:

$$\hat{T}_F = \frac{1}{2}\left[1 - \frac{(\gamma_1 + \gamma_2)}{2}\right] T_T + \frac{1}{2}\left(\tau_{FM} - \tau_{RM}\right) \tag{4.2-2}$$

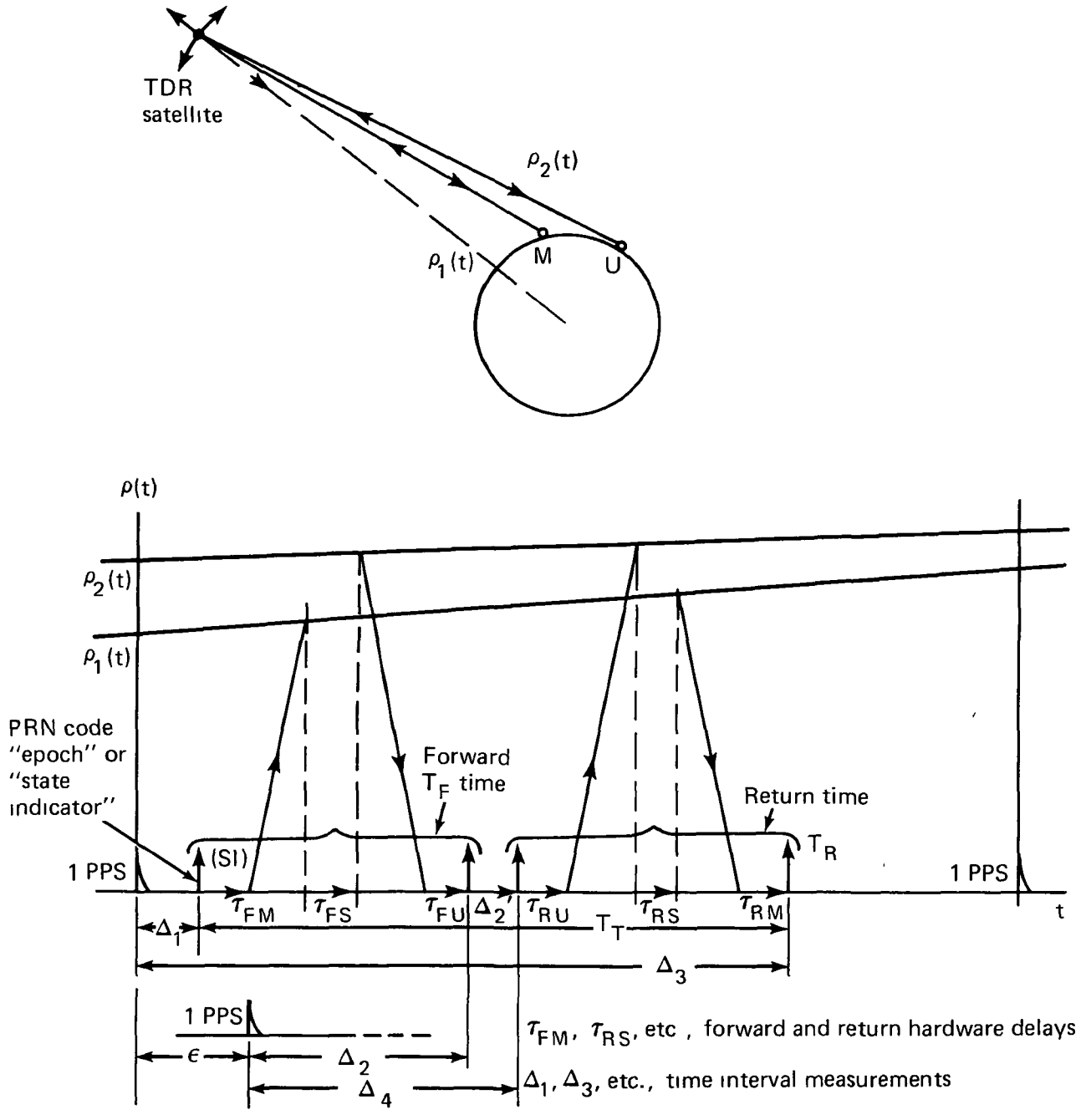


Fig. 4.1 Basic Linear Model of Time Transfer Relay Path

Table 4.1
Error Summary

- Column A assumes currently specified maximum delay variation ($\sim 3\sigma$) for the TDRSS ground station, TDRS Satellite and TDRSS user transponder
- Column B assumes currently specified "repeatability" of delay variation ($\sim 1\sigma$) for the TDRSS ground station, TDR satellite and TDRSS user transponder

	Source	Error (A)	Error (B)
1.	Time Interval Measurements and Calculations Based on Linear Model	6 nsec	6 nsec (no avg. or data smoothing)
2.	Differential Delay of STDN Station Hardware (TDRSS Transponder)	30 nsec	10 nsec
3.	Differential Delay at TDRSS Ground Station Hardware	20 nsec	7 nsec
4.	Differential Delay at TDR Satellite	30 nsec	10 nsec
5	Differential Propagation Effects	$\sim$ 1 nsec?	$\sim$ 1 nsec?
6.	Total RMS	47 nsec	17 nsec

$$+ \frac{1}{2}(\tau_{FS}-\tau_{RS}) + \frac{1}{2}(\tau_{FU}-\tau_{RU})$$

$$- \frac{\Delta_2'}{2}\left[1 + \frac{1}{2}(\gamma_1+\gamma_2)\right]$$

$$+ \frac{1}{4}(\gamma_1+\gamma_2)\left[(\tau_{FM}+\tau_{RM}) - (\tau_{FU}+\tau_{RU})\right]$$

$$- \frac{1}{4}(\gamma_1-\gamma_2)(\tau_{FS}+\tau_{RS})$$

where $\gamma_1=\dot{\rho}_1/v_p$ and $\gamma_2=\dot{\rho}_2/v_p$ are the range rate parameters relative to the two stations, e.g., Master and User stations. The velocity of propagation, $v_p=c/n$, with $n\sim1$ and $c=2.998\times10^8$ meters/sec. A large value of $\gamma_1+\gamma_2$ for a synchronous satellite orbit is $\gamma\sim10^{-7}$. As stated in Section 2, this can contribute about a 25 nanosecond bias error over approximately a one minute interval.

Eq. (4.2-2) was derived directly from Figure 4.1 by equating time intervals. Higher order terms in γ, e.g., γ^2, γ^3, etc., are neglected.

The interval Δ_2' at the user, may be a fixed and known PRN code epoch offset, a variable offset requiring measurement, or $\Delta_2'=0$, implying a "coherent retransmission" of the code received by the user. The delay terms, τ_{FM}, τ_{RM}, etc., refer to the forward and return link delays at the Master, User and TDR satellite.

The rate parameter, $\gamma_1+\gamma_2$, can be estimated from the time interval measurements as:

$$\widehat{\gamma_1+\gamma_2} = \frac{T_T(t_2)-T_T(t_1)}{t_2-t_1} = \frac{(\Delta_3-\Delta_1)_{k+1} - (\Delta_3-\Delta_1)_k}{1+(\Delta_{1_{k+1}}-\Delta_{1_k})} \quad (4.2\text{-}3)$$

(A more elaborate "data filter" could be employed to continually update the estimate of both T_T and $\gamma_1+\gamma_2$, using all the time interval measurements obtained over a period of time.)

Eq. (4.2-2) shows that the hardware delays depicted in Figure 4.1 appear as a differential delay effect, e.g., $\frac{1}{2}(\tau_{FM}-\tau_{RM})$. These differential delays will have to be independently measured or "calibrated out". Accurate ranging via TDRSS also requires knowledge of these delays. Delay measurements for the channels in service will be made as part of normal TDRSS operating procedure. The terms which indicate total hardware delay show either a difference in total delay or are significantly reduced by a differential range rate parameter.

Propagation path delay will also occur as a differential delay between the forward and return paths. Since the forward and return

propagation paths are through the same regions of space and the forward and return transmissions occur within a very short time span, the differential delay should be quite small. This should be the case even though the forward and return Ku-band and S-band frequencies are different.

4.3 Time Transfer Accuracy

The linear model discussed in the preceding sections allows the factors which contribute to time transfer error to be categorized. The time interval measurements Δ_1, Δ_2, and Δ_3 which are used in the estimation of forward time, $\hat{T}_F$, the range rate parameters $\gamma_1+\gamma_2$, and the clock error calculation are all subject to noise or "jitter" in the PRN code tracking loops. At the signal margins available for time transfer this tracking jitter would be quite small and averaging (or data filtering based on the linear model) can reduce this contribution even further. The linear model itself should be quite accurate over relatively short intervals, e.g., 10 minutes or so. The time required for forward and return link signal acquisition, data accumulation, and clock error calculation will be about 5 minutes.

Unknown or uncalibrated hardware delay appears to be the largest potential source of time transfer error. Specification data on ground station, satellite and user transponder hardware delay contributions to TDRSS ranging accuracy can be used to estimate time transfer accuracy. These specifications were used to compile Table 4.1 which summarizes the anticipated accuracy of time transfer via TDRSS. Analysis and test data on PRN code tracking stability is used to estimate the effect of jitter. The error summary of Table 4.1 is for "two-way" or "round trip" estimation of forward delay to the user (TDRSS Mode 1).

5.0 SUMMARY OF OPERATIONAL CONSIDERATIONS

If two standard frequencies differ by a few parts in 10^{12} from their nominal frequency of 5 MHz the corresponding clock rate divergence would be about 150 nanoseconds per day or about one microsecond per week. Once a week then, could be a reasonable rate at which to check STDN station clock error. Also, "intensive" test periods of several weeks could be used to establish a "predicted" clock behavior with each stations' clock error being measured twice a day, for example.

5.1 TDRS System Loading

As stated in Section 4.3 the total time transfer interval is expected to be about 5 minutes. This includes forward and return link PRN code and carrier acquisition, data acquisition, and one to two minutes of clock error calculation with sample values occurring at a rate

of one per second. The 5 minute interval does not include service configuration time. For example, the time to verify that an assigned Multiple Access (MA) channel is available and operating properly is not included.

If it is assumed that each STDN station's clock error is being checked "regularly", 30 to 40 minutes per week might be required. This would not appear to be a serious operational burden. It was noted in Sections 2.0 and 4.0 that the role of Master and User stations could be interchanged so that the error of the TDRSS ground station clock could also be checked as a routine procedure.

5.2 Forward Beam Sharing

Since the Multiple Access (MA) service is to have 20 return channels per TDR satellite (potential total of 3x20=60 channels) but only one forward channel per TDR satellite (a total of 3) it will be the forward link accessibility that places whatever limitations might arise on time transfer via TDRSS Mode 1 operation. This mode is the two-way "coherent ranging" mode which permits estimation of the forward propagation time by the "round trip" measurements discussed in Section 4.2. Since the MA forward antenna beam is relatively broad, i.e., about 10°, the possibility of several time transfer users sharing the same forward beam exists and will be considered as an operational possibility. Sharing a forward beam would permit clock error estimates to be made for several STDN stations in rapid succession. This approach would require additional time transfer signal multiplexing in the processor/controller.

5.3 "One-Way" Time Transfer Accuracy

The basic technique and hardware discussed in Sections 2 and 3 and the model described in Section 4.1 permit clock error calculation either by forward-link-only transmission from the TDRSS ground station to the STDN user station or by return-link-only (TDRSS Mode 2) from the STDN user station to the TDRSS ground station. The fundamental difference is that for these "one-way" transmissions, the estimate of forward propagation time $\hat{T}_F$ (or $\hat{T}_R$) required for the clock error calculation must be obtained from TDR satellite ephemeris data rather than a "round trip" delay measurement. Hardware and propagation delays affect the error calculation directly, not as a delay difference as in the "two-way" transmission case. The accuracy available with return-link-only or forward-link-only transmission should be in the order of 600 nanoseconds depending upon the validity of TDR satellite orbit predictions for the time period over which the clock error is being estimated. As noted in Section 1.5, one purpose of the TDRS user transponder at the STDN stations is for the support of TDR satellite orbit determination by "bilateration ranging". This support will contribute to the accuracy of time transfer to a STDN

station when the transponder is used for that purpose in a "one-way" transmission mode.

QUESTIONS AND ANSWERS

DR. GART WESTERHOUT, U. S. Naval Observatory:

Five speakers described satellite time transfer systems, all of them different but all of them doing the same thing. Is there a movement afoot to eventually standardize some of this?

MR. McINTYRE:

I'm not aware of any such efforts. The TDRS system is really to be part of the NASA Tracking and Data Network in the 1980's, and it is satisfying NASA purposes in supporting space missions of all varieties--the space shuttle, for example. It turns out that the particular signal design and implementations we have discussed here are very suitable to transferring time to the ground stations of that network. There is no attempt to duplicate or not duplicate what someone else is doing. It is here--we will use it.

MR. ROGER EASTON, Naval Research Laboratory:

Let me answer a little differently. Paper 11 had 100 microseconds as far as accuracy. Paper 12 was 25 microseconds, and paper 14 was about 100 nanoseconds. So there is quite a difference in the accuracy of several of the systems.

Page intentionally left blank

Page intentionally left blank

A PRECISION MICROWAVE FREQUENCY AND TIME DISTRIBUTION SYSTEM*

John W. MacConnell
Richard L. Sydnor
Jerrold T. Hinshaw

ABSTRACT

This paper describes a precision microwave frequency and time distribution system capable of distributing frequencies with stabilities of several parts in 10^{15}, and time to the 10 ns level.

A method for distributing a hydrogen maser frequency standard between sites separated by 20 km is required by the Jet Propulsion Laboratory for the Deep Space Network. A distribution system offers several advantages over individual standards at each site. To verify the performance of a hydrogen maser, a minimum of two masers is required at each location, which becomes expensive when multiple sites are involved. A frequency distribution system allows several masers to be maintained at a central standards laboratory, where calibration, maintenance and data logging are more efficient. Since the frequency distribution system is substantially lower in cost than a hydrogen maser, significant cost savings can be realized if such a system is utilized. Using a frequency distribution system rather than individual standards also eliminates frequency offsets between sites, since one standard is effectively present at all the sites.

*This paper presents the results of one phase of research carried out at the Jet Propulsion Laboratory, California Institute of Technology, under Contract No. NAS 7-100, sponsored by the National Aeronautics and Space Administration.

INTRODUCTION

Distribution of stable frequencies over one-way radio links longer than a few hundred meters is not possible without degradation of the source stability. For example, a 50 km path has a stability of about 10^{-10} (reference = NRL RPT 7140). This limits the stability of the source after distribution to 10^{-10}, unless some type of compensation for the path can be provided. One method of compensation is to use a two-way link that allows measurement of and compensation for the path between the source (Master) station and the remote (Slave) station.

In order to distribute time, the path delay between stations must be estimated, and the time code advanced by that delay prior to transmission to the remote site. Such a process can be realized by techniques similar to those being employed in the frequency distribution system.

BASIC SYSTEM CONCEPT

The basic concept of the frequency distribution system is shown in Fig. 1. A frequency $\omega/\underline{\omega\tau}$ is transmitted from the maser site to the remote site. After encountering a delay of τ, the phase of the received signal is $\omega/\underline{0}$, the reference frequency to be distributed, at the reference phase angle. This signal is then returned to the master station, where the phase is $\omega/\underline{-\omega\tau}$. By forcing the transmitted signal to lead the reference phase by the same amount that the received signal lags the reference phase, correction for perturbations in the path can be effected. This whole system is predicated on reciprocity of the path. If τ is different for the two directions, it will be impossible to obtain proper correction. Any equipment that is common to both transmit and receive functions (coax, waveguide, antennas, etc) will be considered part of the path and will be corrected. Any phase shifts that are not reciprocal will appear directly at the output of the remote site.

PRACTICAL CIRCUIT CONSIDERATIONS

The circuit in Fig. 1 shows conceptually the operation of a self-correcting frequency distribution system. There are, however, a host of problems with the design as shown. Probably the most obvious difficulty is that both stations are simultaneously transmitting and receiving the same frequency. There are two simple solutions to this problem: have each station (Master and Slave) transmit at a different frequency, or alternately transmit and receive at each station. Unfortunately neither of these solutions is a perfect solution. If widely differing frequencies are employed the dispersive effects of the medium cause the path to become non-reciprocal, violating one of the

basic premises of such a system. If the two transmitters operate at very nearly the same frequency (say .002% separation) broadband noise from the transmitter leaks into the receiver severely limiting the sensitivity. The second alternative is to transmit and receive at the same frequency but at different times. One major drawback with this system is keeping the transmitter leakage in the off state to an acceptable level. The required isolation is approximately 160 db for a 20 km path. (The isolation requirement increases as the path length increases). This amount of isolation is extremely difficult to obtain. A second difficulty is reflections off objects in the path. It is not unusual for the reflections to be 10 to 20 db stronger than the desired signal from the other station. This problem could be alleviated by employing a long pulse with a dead time to allow all reflections to die out. Such a system might be a viable solution (assuming the necessary isolation could be obtained), however it requires very narrow loop bandwidths. This requires a VCO at the slave station with medium-term stability not now available.

The solution settled upon is a combination of the two schemes mentioned above. The two transmitters are run at very nearly the same frequency (less than .002% separation) and the system is switched on and off. Any leakage or reflections of the transmitter, being at a different frequency than the received signal (100 KHz at 8 GHz) can be filtered out in the IF amplifiers. The problem of noise is eliminated since the transmitter and receiver are never operating at the same time.

The final difficulty with the configuration shown in Fig. 1 lies in the phase detectors. Such a circuit requires perfectly matched phase detectors. These detectors must remain matched over an entire cycle, since many cycles of phase go by in a typical system. The ideal solution here would be a system with a single phase detector that continuously operates at the zero point on the S-curve.

Fig. 2 shows a basic system that meets all of the criteria previously discussed. (It should be remembered that this is a basic circuit, and could not be implemented exactly as shown). Fig. 3 is the same diagram as Fig. 2 with all the phases and frequencies shown in general terms. Some mention should be made of the synthesizer marked "X M/N". This synthesizer multiplies the 5 MHz signal at its input by the ratio M/N (The ratio of slave to master station transmit frequencies) and shifts the frequency such that a 5 MHz input yields a 5 MHz output. This is a non-trivial synthesis. For example, in the first system constructed, the ratio M/N is 81001/81000. Since the input and output of the synthesizer are at the same frequency, and the multiplication is very nearly one (1.000012... in the system above) it might be interesting to consider the effects on performance if this synthesizer were to be deleted entirely. It is intuitively apparent that the correction in such a system will be in-exact, that is to say, there will be some

artifacts of the path present in the output. These residual contributions of the path will be reduced over the uncompensated amount by some constant factor. If the amount of correction could be made sufficiently large, the contribution of the path would be sufficiently small as to be masked by the stability of the standard being distributed. The derivation of a correction factor for such an "approximate" system is presented in Fig. 3. If K can be made large, very large correction factors can be obtained. K is defined (Fig. 3) to be $F_{master}/(F_{slave}-F_{Master})$ or the frequency of the master station divided by the difference in frequency between the master and slave stations. In the first JPL system K=8100/.1=81000, yielding a correction factor of 1.6×10^5. It was mentioned earlier that the intrinsic path stability is approximately 10^{-10}. By employing such an "approximate system" the path stability is improved to approximately 6×10^{-16} : which is sufficient for frequency standards presently available. If, in the future, it becomes necessary to improve system performance the synthesizer could be added without disturbing the rest of the system.

JPL FREQUENCY DISTRIBUTION SYSTEM

The first distribution systems being constructed at JPL are approximate systems. There were two reasons for this decision. The first was mentioned above: sufficient performance could be obtained with the approximate system. The second reason is that it is questionable if the hardware in the link itself could be made sufficiently stable to observe the added performance that would be predicted by employing the synthesizer.

Upon completion of the first system, two sets of lab tests were run. The test configurations are shown in Figs. 4a and 4b. Fig. 4a shows the method used to measure the stability of the system with no path contributions. This stability was found to be about 2.3×10^{-15}. This is really a very good stability when one considers the large amount of hardware present in such a system. Fig. 4b shows the setup used to measure the correction factor. We were able to resolve correction factors of 10^5 with the setup shown in Fig. 4b. With this setup we were not able to measure the correction factor of the link, which implies it is probably near its theoretical value.

The first link has been moved to Goldstone for preliminary testing with a real path. At this point, we have no actual performance data. The tests we have run seem to indicate the link is functioning: although its actual performance cannot be verified until the second link is installed. Fig. 4c shows the test that will be run once two distribution systems are available. With this setup a signal is distributed to the remote sight by the first link. A second link then distributes the output of the first link back to its origin. This

allows direct comparison of the input signal to itself after passing through two sets of distribution systems. Testing in this manner removes uncertanties that are present if one link and two H-masers are employed for testing.

CONCLUSION

Self correcting microwave links appear to be a viable solution to the problem of providing multiple widely separated locations with stable frequencies. Besides being lower in cost than individual high performance frequency standards, they provide essentially the same frequency at each station, eliminating the frequency offsets that are inevitably present when separate frequency sources are employed. One requirement for the same reference frequency at multiple sites is when differential VLBI techniques are to be used for precision angle measurement of spacecraft, e.g., with respect to the fixed stars.

In the future it is planned to distribute time by suitably modulating the transmitters with a time code and using similar path compensation techniques to those employed in the frequency distribution system. Once the clocks are in synchronization they should remain so, since the same frequency is available at each site.

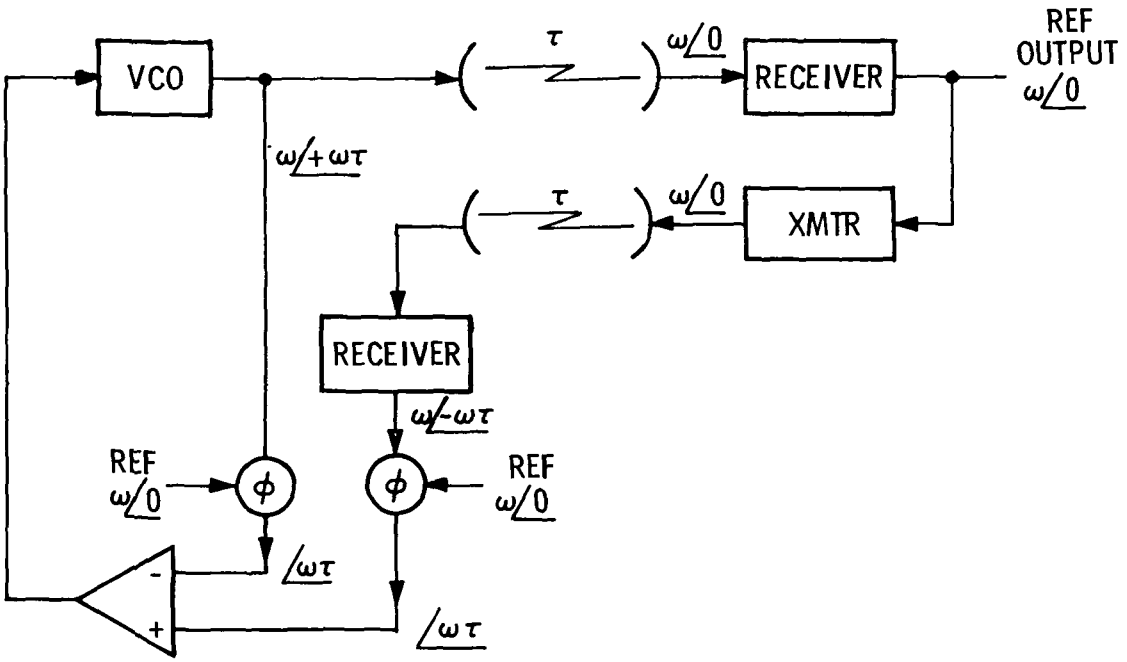

VCO
τ
ω/0
RECEIVER
REF
OUTPUT
ω/0
ω/+ωτ
τ
ω/0
XMTR
RECEIVER
ω/-ωτ
REF
ω/0
REF
ω/0
-
+
/ωτ
/ωτ

Fig. 1

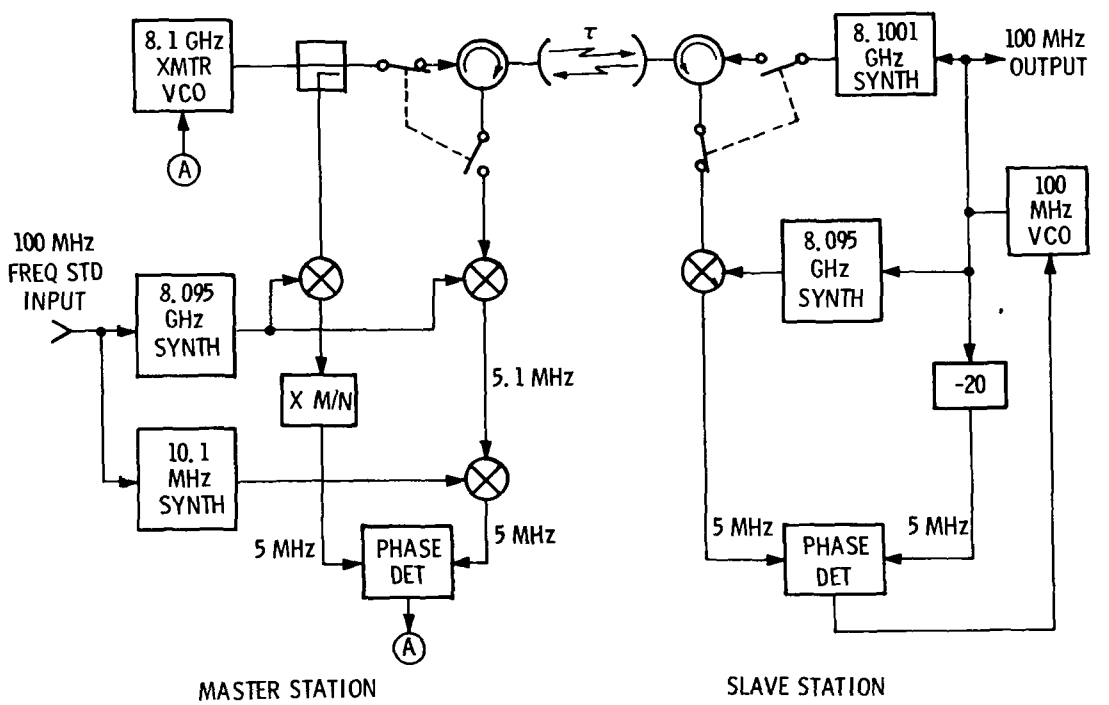
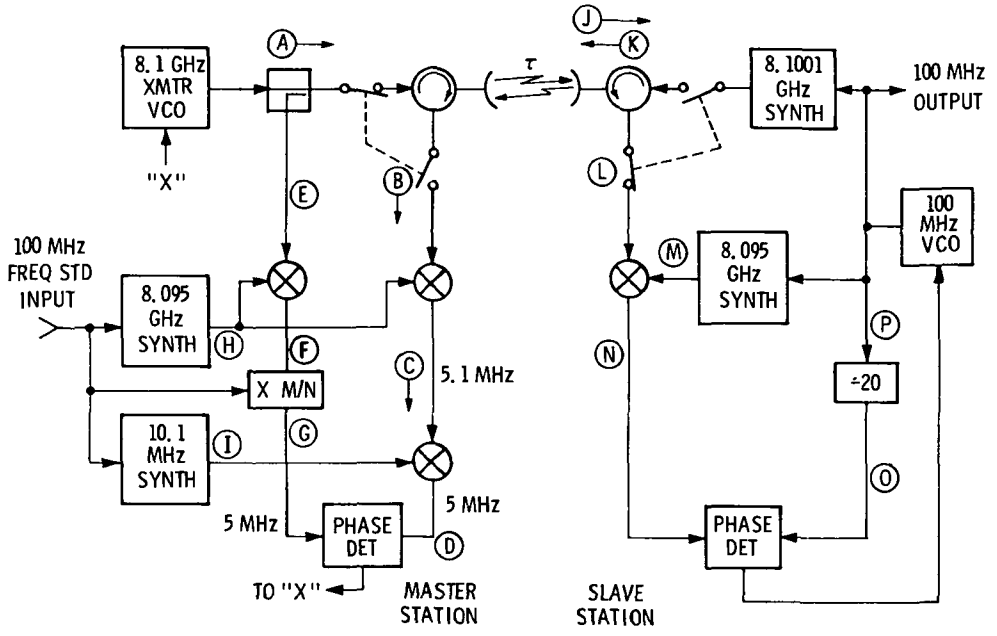

8.1 GHz
XMTR
VCO
A
τ
8.1001
GHz
SYNTH
100 MHz
OUTPUT
100 MHz
FREQ STD
INPUT
8.095
GHz
SYNTH
X M/N
5.1 MHz
10.1
MHz
SYNTH
5 MHz
PHASE
DET
5 MHz
A
MASTER STATION
100
MHz
VCO
8.095
GHz
SYNTH
-20
5 MHz
PHASE
DET
5 MHz
SLAVE STATION

Fig. 2



MASTER

(A) $K\omega_R \angle K\phi$

(B) $K\text{-}\angle(K+1)\omega_R\tau$

$= (K+1)\omega_R \angle (K+1)\phi - 2(K+1)\omega_R\tau$

(C) B - H

$= 51\omega_R \ (K+1)\phi - 2(K+1)\omega_R\tau$

(D) = I - C

$= 50\omega_R \angle 2(K+1)\omega_R\tau - (K+1)\phi$

(E) = A

(F) = A - H

$= 50\omega_R \angle K\phi$

(G) $= \frac{(K+1)}{K}$ (F) (FOR PHASE ONLY)

$= 50\omega_R \angle (K+1)\phi$

G = D (WHEN SYSTEM IS LOCKED)

$\therefore \phi = \omega_R\tau$

SLAVE

(J) $= A\text{-}\angle K\omega_R\tau = K\omega_R \angle K\phi - K\omega_R\tau$

(L) = J, (K) = (K + 1) P

(M) $= (K-50)\omega_R \angle \theta$

(N) = L - M

$= 50\omega_R \angle K\phi - K\omega_R\tau - (K-50)\theta$

(O) $= 50\omega_R \angle 50\omega\theta$

(P) $= 1000\omega_R \angle 1000\theta$

N = O (WHEN SYSTEM IS IN LOCK)

SOLVING FOR θ

$\theta = \phi - \omega_R\tau$

IN APPROXIMATE SYSTEM (X M/N IS DELETED)

F = D

SOLVING FOR ϕ

$$\phi = \frac{2(K+1)}{(2K+1)}\omega_R\tau$$

$$\text{ERROR} = \left| 1 - \frac{2(K+1)}{(2K+1)} \right| = \frac{1}{2K+1}$$

$$\text{CORRECTION FACTOR} = \frac{1}{\text{ERROR}}$$

$$\text{DEFINITION} \cdot \ K = \frac{F_{MASTER}}{F_{SLAVE} - F_{MASTER}}$$

Fig 3

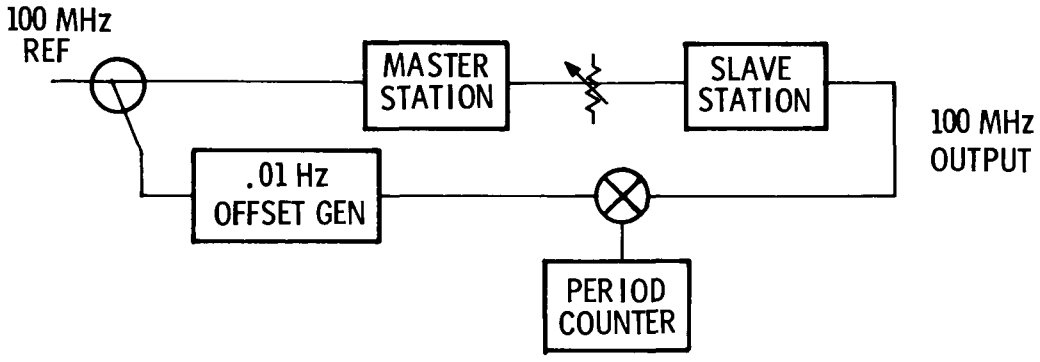


Fig. 4a

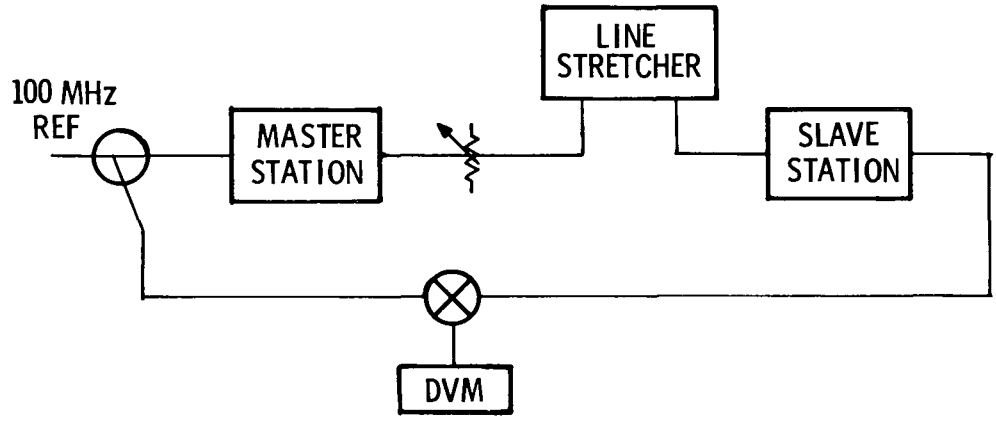


Fig. 4b

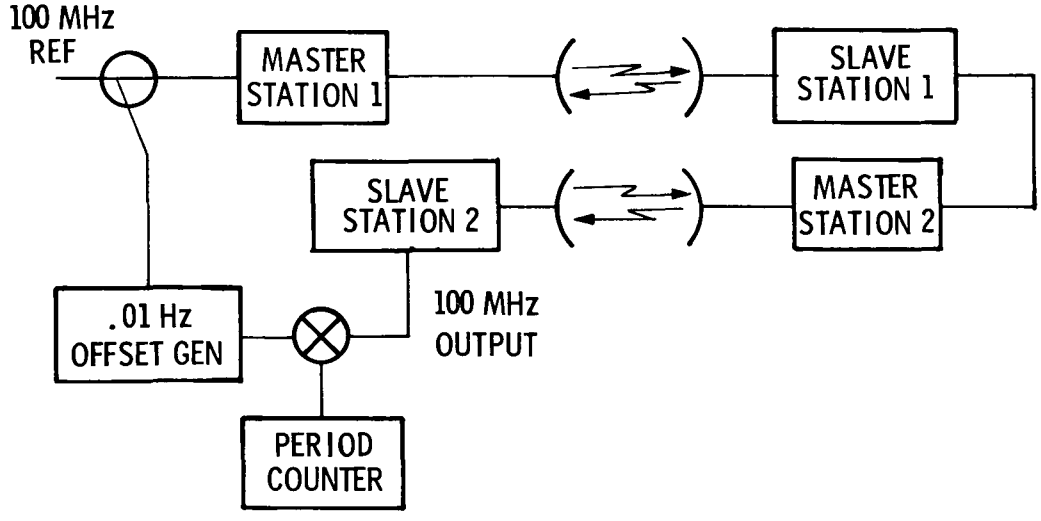


Fig. 4c

MR. DANE CURKENDALL, Jet Propulsion Laboratory:

How is it working?

MR. MACCONNELL:

Like I said, we haven't been able to measure it against the maser. We measured it looking at the return signal from the other station, and we could see the path on it and see it correcting. It looks like it is working okay. But until we actually do a round trip with a pair of stations or get a pair of masers, we can't be positive it works, although I really don't see any reason it shouldn't.

DR. VICTOR REINHARDT, NASA Goddard Space Flight Center:

You mentioned you got about 2.5 parts in 10^{15}. Over what averaging time was that?

MR. MACCONNELL:

One hundred seconds. I think we'll find it's going to be fairly white noise. I think that we will be able to improve upon that after we get a chance to work with it. This is really the first prototype system, and we have some ideas about what's causing that and may be able to improve it three or four times.

DR. REINHARDT:

Did you look at the phase stability at longer intervals for diurnal shifts?

MR. MACCONNELL:

We ran some phase measurements on the thing sitting in the lab with the air conditioning going up and down, and we could see maybe two or three degrees peak-to-peak phase drift at X-band. For a clock, I think this would be really a nice system because you could

take two clocks and sync them up -- two or three degrees at X-band doesn't correspond with very many nanoseconds offset between clocks.

DR. REINHARDT:

That one or two degrees at X-band is less than a picosecond, which is considerably less than a nanosecond.

MR. RONALD WEIMER, National Radio Astronomy Observatory:

You've mentioned transferring time, and I was just wondering if you have done anything like that?

MR. MACCONNELL:

At this point, we haven't built a system for controlling the time. However, we have some ideas about how we are going to do it. I think we can do it by controlling the on and off pulsing of the transmitters and receivers. The system will have a loop around it similar to the frequency control loop to take out the path delay. Also, because we have such good resolution of the X-band phase, we'll be using that somewhat too.

MR. WEIMER:

How do you currently control the turning on and turning off of these things?

MR. MACCONNELL:

We have a small frequency synthesizer that is just controlling the gates on the transmitter and receiver. We run at about 150 kHz for the on-off ratio. We have another synthesizer at the slave station. We have a system that has ten phase-lock loops, which are all auto acquire. Before it turns on the last transmitter, it lines up the phase of the synthesizer with the phase of the incoming burst of rf. When it gets lined up, it switches over and turns on its transmitter. Then it is running purely open loop at that point. Both synthesizers are locked to the same reference, so there is no problem there.

On the burst of rf: Actually, both transmitters transmit at the same time, but there is a delay before the burst of rf that it transmits gets to the second station. So we set it up so we have

an integer number of half cycles of the switching array in the path. The frequency that we chose to switch the transmitter and receivers on and off is a function of the path length. We decided to choose 150 kHz because we wanted a frequency higher than 100 kHz so sidebands due to the switching wouldn't lay on top of the other station.

Page intentionally left blank

Page intentionally left blank

PRECISE TIME TRANSFER UNIT (PTTU)

John J. Wilson and James E. Britt
US Naval Ocean Systems Center
San Diego, CA

Philip A. Mitchell
US Army Satellite Communications Station
Camp Roberts, CA

Herbert A. Parrish
US Army Communications Systems Agency
Ft Monmouth, NJ

Tony Willis
FAA Western Region
Los Angeles, CA

ABSTRACT

The Precise Time Transfer Unit (PTTU) was developed by the Naval Ocean Systems Center in support of an effort by the US Army Communications Command to demonstrate the feasibility of transferring PTTI from the Army Satellite Communications Station at Camp Roberts, California, to a remote location, via the existing Federal Aviation Administration Radar microwave link system The demonstration will be in two phases

Phase 1, a loop test, sending PTTI information from Camp Roberts to the Temblor Radar Microwave Link/Repeater where it is looped back and returned to Camp Roberts.

Phase 2, transfer of PTTI information from Camp Roberts to a user site

Time at stations having precise time standards is compared by this system. Each station transmits its time, and receives time sent by the other station. Received time is then compared with local time at each end, and given the two measurements, the difference between the two clocks is computed. The computation removes propagation time and assumes only that the propagation time is the same in both directions.

In order to implement this test two configurations of the basic equipment were developed. (1) A terminal configuration, which receives the incoming 3.2MHz timing signal, correlates a locally generated pseudo random sequence with the received signal to acquire the inherent microsecond timing, and decodes the one

second epoch information The received time is then compared with local time and the difference displayed on the equipment front panel. The terminal output encodes the local time on a 3 2MHz carrier for transmission. (2) A regenerator configuration, which receives the modulated 3.2MHz timing signal, correlates a locally generated pseudo random sequence with the received signal, and encodes the received one second epoch information on the locally generated pseudo random sequence This signal is then used to bi-phase modulate a 3.2MHz carrier for re-transmission on another microwave link

Phase 1 tests were conducted during October and November 1977. These tests demonstrated the feasibility of this technique with tenths of a microsecond accuracy. Concurrently it was proved that the PTTI signal did not interfere with existing FAA signal traffic.

I. INTRODUCTION

This paper presents some results of a test to demonstrate PTTI transfer over the Federal Aviation Administration Radar Microwave Link System. The phase I test was run 19–21 October 1977 with Army SATCOMSTA, FAA Western Region, and Naval Ocean Systems Center personnel participating. It successfully demonstrated the time transfer technique between Camp Roberts, California, and the FAA Temblor Radar Microwave Link/Repeater (RML/R) located approximately 65 miles to the southeast. The time transfer demonstration was repeated 1, 2 November 1977 by the original test participants, and witnessed by Army Communications Command and Naval Observatory representatives.

A number of requirements were placed upon time transfer equipments, as follows.

a. Provide entry and exit to the FAA System.

b. Do not degrade existing traffic on the microwave link

c. Maintain existing inter-system isolation when crossing between the FAA Systems.

To achieve this the Precise Time Transfer Unit (PTTU) was developed by NOSC[1]. Section II discusses, in brief, the design of the PTTU and the two configurations used in the Phase I test. Figure 1 is an illustration of this equipment.

---

[1]The NOSC design was based on a Satellite PTTI Modem design by J A Murray of NRL (ref 1) The name Precise Time Transfer Unit (PTTU) was chosen to avoid confusion with the existing CM-427 Time Transfer Unit.

Ref (1) J.A. Murray, "Mini Modem for PTTI Dissemination", Proceedings of the Third PTTI Conference, pp 103-110, 1971.

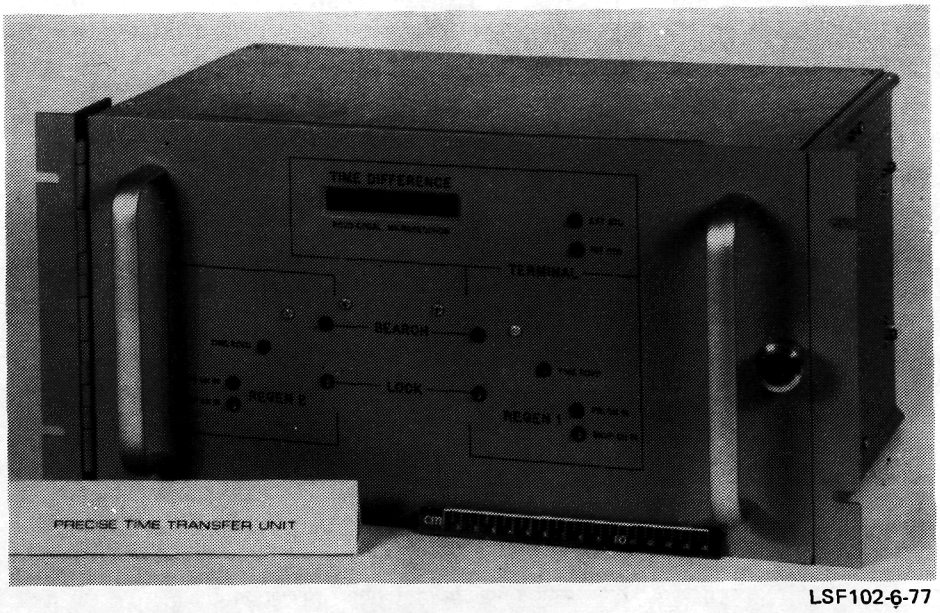


Figure 1. Photograph of PTTU

II. PTTU DESIGN

Time is transferred between stations with precise time standards. Each station sends its time and receives time sent from the other station. The received time is then compared with the local time standard. The measurable quantitites at each end are the time differences between received time and local time. The desired quantity is the difference between the two clocks, however the measurable quantity also contains the transmitter to receiver propagation time, which is in general not known[2]. If the propagation time is the same in both directions, the clock difference is half the difference between the measurable quantities at each end, i.e.,

$$C_2 - C_1 = \frac{M_1 - M_2}{2} \tag{1}$$

where C_1 = station 1 clock time

C_2 = station 2 clock time

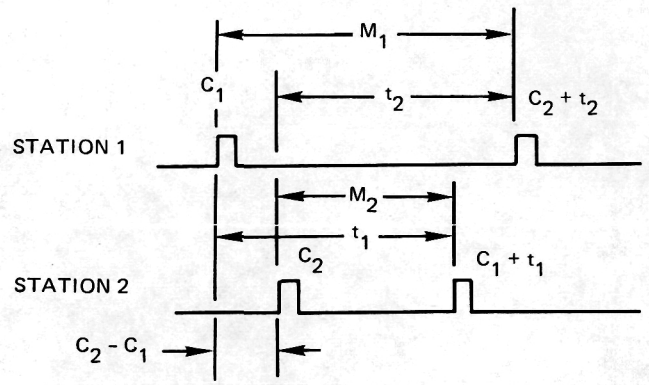
M_1 = measured difference between received time and local time at station 1

M_2 = measured difference between received time and local time at station 2

This is illustrated in figure 2.

---

[2]It is anticipated that propagation time will be calibrated in an operational system, making one-way time transfer possible. However this is not a necessary condition.



$$C_2 - C_1 = \frac{M_1 - M_2}{2}$$

$$M_1 = C_2 + t_2 - C_1$$

$$M_2 = C_1 + t_1 - C_2$$

where t_1 = propagation time from station 1 to station 2

t_2 = propagation time from station 2 to station 1

$$C_2 - C_1 = \frac{(C_2+t_2-C_1)-(C_1+t_1-C_2)}{2}$$

$$= \frac{2C_2-2C_1+t_2-t_1}{2}$$

$$= C_2 - C_1 \text{ if } t_2 = t_1$$

Figure 2. Difference between clocks located at different terminals

The time is sent by synchronizing a pseudo random sequence (prs) so that the "all ones" state coincides with the local clock each second. The prs is bi-phase modulated onto a 3.2MHz carrier for transmission. A maximal length prs of length $2^{13}-1=8,191$ states truncated to an even 8,000 state length is used. The sequence is clocked at 1MHz which establishes an integer relationship of 125 periods per second[3]. The 191 deleted states represent only 2.3% of the sequence length so the correlation properties of the prs are not appreciably degraded by this procedure.

The 8,000 state prs is used to bi-phase modulate the carrier to produce a spread spectrum signal. The timing information is not conveyed by a time domain pulse, but rather by the

---

[3]The original 8,191 state sequence does not have a real time cyclic integer relationship using standard, or easily derived, clock frequencies. For example: at a clock frequency of 1MHz an 8,191 state sequence, with a period of 8,191 microseconds, has 122.08521 . . . periods per second, thus precluding synchronizing the sequence with one pulse per second time ticks from a local clock.

correlation properties of the prs modulation. Correlation to the prs provides fractional microsecond timing, but with an ambiguity period of 8 milliseconds. The phase of every 125th prs is reversed to indicate the 1 second time tick.

Two different PTTU configurations were required for the test:

a. TERMINAL Configuration; to provide entry and exit to the microwave system.

b. REGENERATOR Configuration; to provide the link to cross over between independent microwave systems.

Figure 3 illustrates these configurations. The basic PTTU can be put into each configuration by plugging in the proper printed circuit cards.

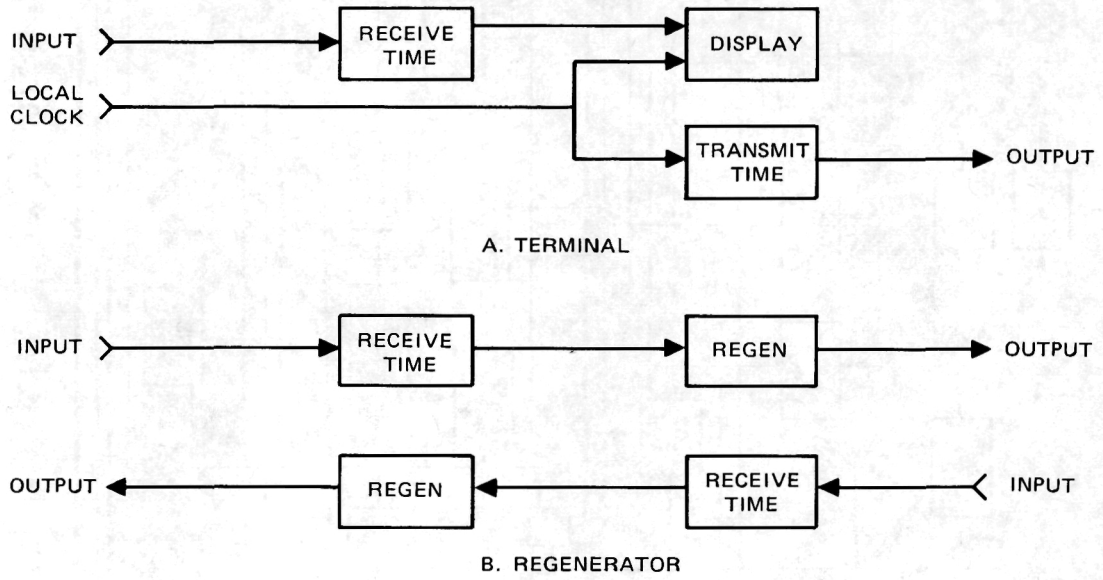


Figure 3. PTTU configurations

Figures 4 and 5 are block diagrams of the PTTU configurations. Much of the circuitry is common; the basic differences being in input and output circuitry. The two configurations accomplish the following:

Terminal Configuration. The terminal receives the incoming modulated 3.2MHz timing signal, correlates a locally generated pseudo random sequence with the received signal to acquire the inherent microsecond timing (8 millisecond ambiguity), and decodes the one second epoch information. The received time is then compared with local time and the difference displayed on the front panel. The terminal output encodes the local time on a 3.2MHz carrier for transmission.

Regenerator Configuration. The regenerator receives the modulated 3.2MHz timing signal, correlates a locally generated pseudo random sequence with the received signal, and encodes

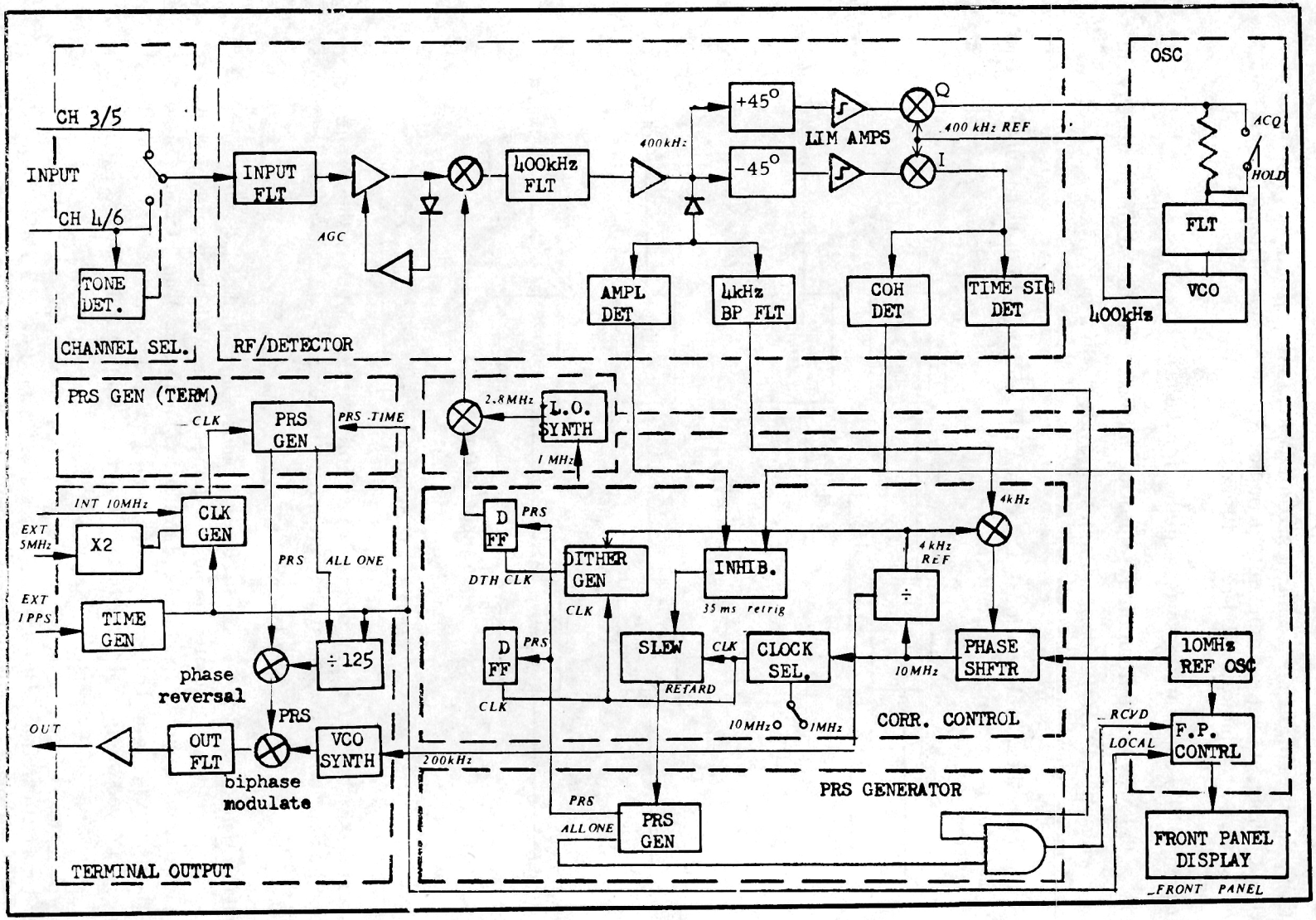


FIG 4 TERMINAL CONFIGURATION

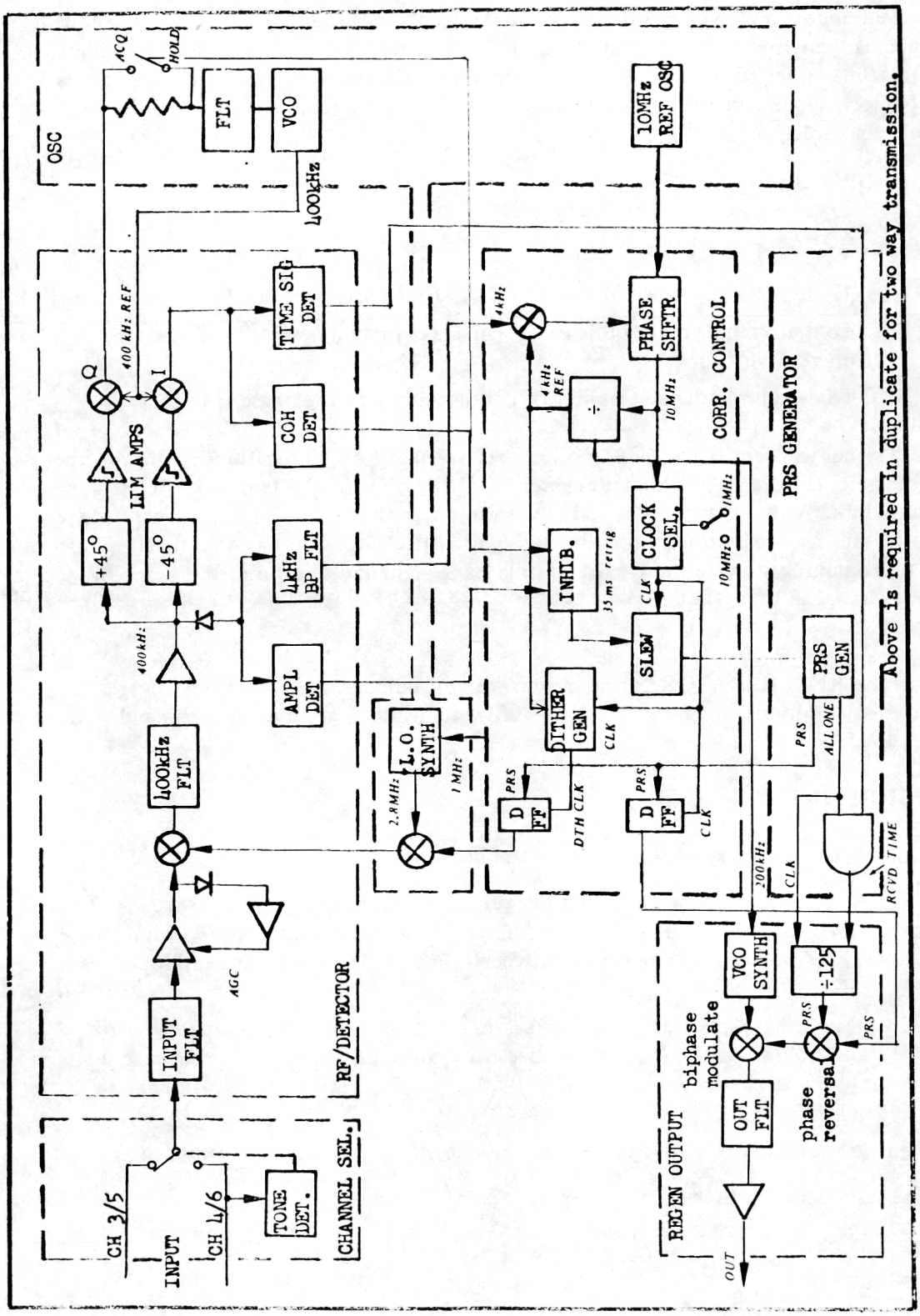


FIG 5 REGENERATOR CONFIGURATION

the received one second epoch information on the locally generated pseudo random sequence. This signal is then used to bi-phase modulate a 3.2MHz carrier for re-transmission on another microwave link. This configuration thus "regenerates" the received timing signal and passes it on. No local clock is required. There are two regenerator circuits; one to pass the PTTI signal in each direction.

III. TEST DESCRIPTION

The objectives of the phase I test were:

1. To demonstrate feasibility of this PTTI transfer technique.
2. To determine whether this PTTI signal is compatable with the FAA microwave system.
3. To determine the desirability of continuing on to the phase II tests.

The PTTI signal was sent from the Camp Roberts Satellite Communications Station to the Paso Robles Radar Microwave Link/Repeater (RML/R) by way of a two way 15GHz microwave radio link. At the Paso Robles RML/R it was entered into the FAA microwave system and sent to the Black Mountain Long Range Radar (LRR) site, where it was transferred from the FAA Oakland System to the FAA Los Angeles System and sent on to the Temblor RML/R. The time transfer demonstration was carried out between Camp Roberts and Temblor.

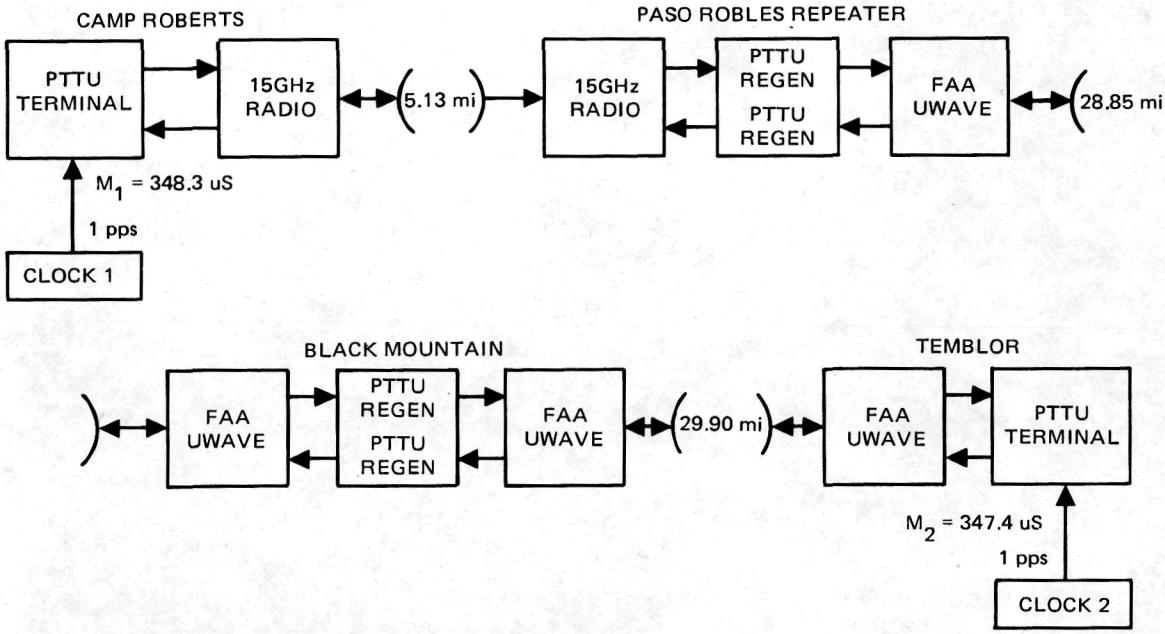
PTTUs in the REGENERATOR configuration were installed at the Paso Robles RML/R, and at the Black Mountain LRR. TERMINALS were installed at Camp Roberts and at the Temblor RML/R.

IV. TEST RESULTS

The following is a summary of the results of the Phase I test:

1. Feasibility of transferring PTTI over the FAA system using this spread spectrum technique was demonstrated. Fractional microsecond timing was successfully transferred between Camp Roberts and the Temblor RML/R, some 65 miles distant.
2. The spread spectrum PTTI signal was demonstrated to be compatible with the FAA system. No interference with normal FAA operations was noted by FAA test participants, or by FAA control centers in Los Angeles and Oakland.
3. Desirability of continuing on to the Phase II test was clearly established.

Figure 6 presents the test results in greater detail.



TIME TRANSFER:

M_1 (measurement at Camp Roberts) ..... 348.3 uS

M_2 (measurement at Temblor) ..... 347.4 uS

$C_2 - C_1$ (time transfer clock difference calculation) =

$$\frac{M_1 - M_2}{2} = \frac{348.3 - 347.4}{2} = \text{.....} \quad 0.45 \text{ uS}$$

(NOTE: Expected accuracy for this system ±0.2 uS)

$C_2 - C_1$ (clock difference measured between the two clocks before transporting CLOCK 2 to Temblor) ..... 0.42 uS

RECIPROCITY:

TIME DELAY ROBERTS TO TEMBLOR 347.4 + 0.4 (clock error) .... 347.8 uS

TIME DELAY TEMBLOR TO ROBERTS 348.3 - 0.4 (clock error) .... 347.9 uS

Figure 6. Tests between Camp Roberts and Temblor, time transfer

Page intentionally left blank

Page intentionally left blank

REAL TIME DISTRIBUTION VIA CONTROLLED TV TRANSMISSIONS

J. D. Lavanceau
U. S. Naval Observatory
Washington, D. C. 20390

L. F. Shepard
ILC Data Device Corporation
Bohemia, L. I., New York

ABSTRACT

Since first introduced as an experiment at the Third Annual PTTI Conference in Washington, DC (1971), this system has become operational at the television stations, WTTG (Channel 5), Washington, DC and KTTV (Channel 11), Los Angeles, CA. It permits independent and continuous transfers, without change in the broadcast format, with accuracies in the nanosecond region, as referenced to the U. S. Naval Observatory master clock.

This paper describes the present system with details of the equipment used in the control of transmissions and decoding, and shows the results of transfers made between some timing centers.

SUMMARY

A technique to distribute absolute time and frequency via controlled television transmissions was developed at the U. S. Naval Observatory (USNO) and successfully demonstrated in 1971 by an experiment performed between the Metromedia TV Station WTTG and the U. S. Naval Observatory (reference (1)).

This system is now operational from the TV stations WTTG (Channel 5) in Washington, DC, and KTTV (Channel 11) in Los Angeles, CA. It is used routinely by some laboratories around those areas to set their clocks to the U. S. Naval Observatory master clock (USNO MC) with accuracies and precision in the nanosecond region.

This paper describes the present system in detail, shows the results of transfers made routinely between some local

timing facilities, and the USNO MC and describes some of its capabilities, limitations and applications.

INTRODUCTION

The technique consists of keeping TV transmissions synchronized to a reference clock within limits of the FCC broadcast specifications. These time coordinated transmissions are then used to set local clocks, or to measure their time and frequency differences with the USNO MC.

REVIEW OF NTSC TV FUNDAMENTALS

For those of you who are not familiar with the current NTSC color television standards, we would like to review them as they apply to precision time transfer.

In the USA, commercial TV broadcasts are generated at a rate of 30 pictures or frames per second. Each frame is composed of 525 lines and it takes about 33 milliseconds to transmit or to reproduce them. To minimize picture flicker, each frame has been divided into two groups of horizontal lines. Those groups, called odd and even fields, are transmitted so as to interlace each other. The process is called interlaced scanning. In this mode of operation the end of one field is separated from the start of the other by one half (1/2) a horizontal line (31.75 μs). The first nine lines of both fields contain equalizing and vertical pulses used to control the position and motion of the lines. The horizontal line 10 of the odd field was selected as a time marker because it is an easy line to identify.

At the transmitter, all of the recurrent waveforms and frequencies used in the modulation envelope are derived, or may be derived, from a single frequency. For example, let us start with 5 MHz. To derive the color subcarrier (SC):

$$SC = 5 \times \frac{63}{88} = 3.5795454...\text{MHz} \rightarrow 279.36 \text{ ns.}$$

In case of the horizontal scan rate (H):

$$H = \frac{2SC}{455} = 5 \times 10^6 \times \frac{63}{88} \times \frac{2}{455} = 15734.266 \text{ Hz} \rightarrow 63.55...\mu\text{s}$$

For the vertical (frame) rate (V):

$$V = \frac{H}{525} = 5 \times 10^6 \times \frac{63}{88} \times \frac{2}{455} \times \frac{1}{525} = 29.97...\text{Hz} \rightarrow 33.366...\text{ms}.$$

Since all pulse signals are derived from the subcarrier frequency, we can establish and maintain the pulses properly positioned in the time domain by phase shifting the subcarrier continuously until the desired pulse position is obtained. If we now consider the time period occupied by 30,000 frames:

$$33.36667 \times 10^{-3} \times 30{,}000 = 1001 \text{ seconds},$$

exactly. Thus, having caused an event which is periodic at the television vertical rate to coincide with a 1 pps pulse from the USNO MC, another coincidence must occur exactly 1001 seconds later.

By establishing an arbitrary time of coincidence, it is possible to calculate the dates (times) at which subsequent coincidences will occur between the one pulse per second time marks from the USNO MC and the emitted TV line 10 odd field pulse. These times of coincidence have been computed by assuming an initial coincidence at zero hours UT 1 January 1958. They are published by the USNO as TV TOC tables, Time Service Announcement Series 8.

These tables have the same format as those presently used for Loran-C. Table 1 gives the first TV TOC for each day in hours, minutes, and seconds. Table 2 gives all relative TOC's in a day. By adding the relative TOC's to the first TOC of any day, one obtains all absolute TOC's for that day. Table 3 gives the time differences for every second of the time interval between the TOC's.

For precise time application, the line 10 pulse must be precisely defined. We have defined this event as follows:

> "The Timing Mark shall be the 50% point on the leading edge of the first H synchronizing pulse following, by 1/2 line (31.78 μs), the last post-equalizing pulse in the vertical interval or, the H synchronizing pulse at the start of line 10 in fields 1 and 3 of the NTSC format in accordance with EIA RS 170A as emitted."

This Timing Mark is shown on Figure 1.

At this time we would like to call attention to the standard TV timing diagrams which appear in many publications including the FCC rules (Fig. 2&3). These timing diagrams invariably show the start of the odd fields and the start of the even field at the same T = 0 datum. The start of the field is defined as the leading edge of the first preequalizing pulse in the vertical interval (line 1). After the vertical interval which has a duration of 9 lines, the line 10 pulse appears. In the case of the fields 1 and 3, this pulse occurs 1/2 line or 31.75 µs after the start of the last post equalizing pulse; while in fields 2 and 4, the line 10 pulse occurs a full line (63.6 µs) after the last post equalizing pulse. Since the pulses start at the same datum (vertical rate), one could erroneously draw the conclusion that the horizontal pulses in alternate fields are not in phase. To accurately show the sequence of events in the extended horizontal time domain, the vertical interval should be displayed to the left in the case of fields 2 and 4. This would show that ALL pulse leading edges, even those of the equalizing pulses and the broad vertical serrations are synchronous and in phase at a period of 63.55 µs. During the vertical interval, extra pulses are inserted but synchronism is maintained by inserting these extra pulses at intervals of precisely twice the horizontal line rate.

By using circuitry which responds to all sync pulses and ignoring those occurring at a 1/2 line period, the extra pulses in the vertical interval, we obtain a uniform pulse train with a period of 63.55 µs (15734 Hz). Every 525 lines we obtain a pulse which coincides with the line 10 odd field pulse. This pulse train is processed by a phase locked tracking filter with a 500 ms loop time constant. A single pulse coincident with line 10 fields 1 and 3 is gated out of the system as the timing pulse.

For sync timing, a dedicated high stability NTSC sync generator is included in the transmitter control system. Additional signals are also available from the line 10 receiver for various display and calibration purposes.

REVIEW OF PAST WORK

The original system concept was evaluated on an experimental basis at station WTTG in Washington, DC, starting in July 1971. This system involved stabilizing the time base of the station sync generators to a cesium reference oscillator and adjusting the phase of the emitted pulse

in the time domain (Figure 4). By monitoring the time of arrival of the line 10 pulses at the USNO, and correcting for propagation delays and equipment delays, error information was used to manually adjust the phase of the transmitted pulses in order to maintain correct emission time.

The frequency adjustments required at the transmitter were subsequently greatly reduced by the development of a controller, presently known as the TV time synchronizer, which compared emitted pulses with reference pulses generated internal to the system and issued phase-shift commands to the station sync generators in order to maintain on-time emission. Several safety devices were necessary to assure that the TV station would remain within FCC specifications and to inform users if the emission was controlled and on time.

Introduction of the servo loop at the transmitter did stablize the emission time of the transmitter and absolute times of emission were held to within a few hundred nanoseconds. Analysis of data taken before the installation of the servo loop showed considerably less scatter (phase instability) over short term observations with the absolute error removed. These observations prompted a study into the interaction of the TV station equipment, the receiving equipment, and the servo control system, with the object of attaining the short term (1 second) stability of the open loop system with the accuracy of the closed loop.

The study resulted in the following conclusions:

1. The period of the H pulses sampled at the vert. rate varied from frame to frame in excess of 150 ns.

2. The start and width of pulses were controlled by R-C mono-stable multivibrator. Only the start of blanking which preceeds sync by about 1.5 μs was controlled by the reference oscillator.

3. The sync separator in the consumer type TV receiver used to monitor the transmitter and feed back to the servo was deliberately made slow to improve noise immunity and also introduced about 100 ns additional jitter.

4. With the loop open, the short term stability of the sub-carrier phase was excellent (in the picosecond region).

5. Differential phase and gain in the receiver had to be improved and stabilized if pulse fidelity was to be maintained.

6. Differential phase and gain, as well as power supply regulation in the transmitter, influenced pulse stability, especially during changes in APL (average picture level). (Did we say that what happened between the pulses didn't concern us?)

The approach taken to system upgrading consisted of reducing jitter by speeding up the receiver sync separator, improving waveform fidelity, and reduction of sync generator jitter. If these measures would reduce jitter to below about 120 ns, the stable subcarrier (1/2 period 140 ns) could be used to clock control the timing pulses, thus removing the residual jitter.

A prototype receiver system was constructed, aligned for optimum phase and gain uniformity, and a very high speed comparator used for sync separation. In addition, the transmitter was equipped with a digital sync generator for the experiment. The result, as predicted, reduced jitter to the 100 ns range; low enough to warrant using the regenerated subcarrier to synchronize the timing pulse.

To evaluate this technique, the first zero crossing of the regenerated subcarrier following the 50% point on the leading edge of the line 10 (odd) pulse was selected as the timing point. The results of this experiment were encouraging. During some segments of program material, standard deviations well below ±1 ns were obtained consistently, while at other times, and during black and white programming, standard deviations increased to ±100-200 ns. The reason for the change during black and white transmission was, clearly, the loss of burst during monochrome transmissions. This condition was expected. The color transmission inconsistencies were traced to random phase relationship of H sync to subcarrier from one program segment to another. Since the film chains, tape machines, and studio cameras were phase matched at the studio switching point (within limits), the problem was isolated to the source material. No requirement existed in the specifications for consistence of phase between subcarrier and sync.

Discussions with TV network engineering officials confirmed our findings, but lent a note of encouragement. This aspect of the specification, while it was an expedient in the early days of color operations, was causing problems now since, without Subcarrier Horizontal phase Coherence (SCH), differentiation between fields one and three, as well as between fields two and four of the field NTSC color format, could not be readily accomplished. This fact causes many problems in tape editing. Several proposals are under consideration by the broadcast committee of the EIA. At this writing, a new specification has been proposed which specifies subcarrier phase to sync but is limited to studio operations and not yet applied to transmitted signals. Until the total television system establishes "SCH" the use of subcarrier sync will have to wait.

The subcarrier phase and its consistency with chrominance information in the picture is of great importance since it directly and obviously affects the color fidelity of the received picture. To maintain this quality, minor phase perturbations are reduced by a color lock loop. H sync, since it is less critical and at a much lower frequency, does have residual jitter. This jitter (approx. 100 ns) has negligible effect on picture quality for the viewer.

CURRENT SYSTEM CONFIGURATION

A. The system has been set up at the transmitter as shown by Figure

1. A cesium beam oscillator supplies a 5 Mhz frequency, via a phase microstepper, to a TV time synchronizer.

2. The TV time synchronizer performs the following main functions:

a) Synthesizes the 3.58 Mhz color subcarrier frequency for the TV transmitter.

b) Generates a reference time scale composed of line 10 odd field pulses which are set "on time" to the USNO MC via the TOC table.

c) Automatically corrects the phase of the generated 3.58 Mhz color subcarrier frequency, when necessary, to maintain synchronization between the emitted TV transmission and the USNO MC.

3. A TV receiver and line 10 discriminator continuously monitor the emitted TV transmissions. Any change in the time of emission of these transmissions (line 10 odd) is detected in the TV time synchronizer by comparing the received (or emitted) line 10 pulses output of the discriminator against the generated "on time" line 10 pulses reference.

If this difference is other than zero, but no more than ±10 μs, the time of emission of the TV transmissions is adjusted automatically by the TV time synchronizer by advancing or retarding the phase of the generated 3.58 Mhz color subcarrier frequency, until synchronization is again secured.

If this time difference exceeds ±5 μs, a slow modulation of ±0.5 μs is impressed on the 3.58 Mhz generated color subcarrier, and thus on the emitted TV program, to warn the PTTI user of a temporary large error in the time of emission of the TV transmissions.

NOTE: Changes in the time of emission of the TV transmissions occur when TV programs are switched from film library to video tape recording, to live programs, etc. Most of these changes are usually small.

The phase microstepper permits precise adjustment of the cesium output frequency to the USNO MC and thus maintains the generated line 10 odd reference on time.

B. The basic receiving or monitoring system used at the USNO, or at any of the local clock locations, is shown in Figures 7 and 8.

The TV receiver is tuned to the synchronized TV transmissions (KTTV or WTTG). Line 10 pulses are generated from the discriminator and their time of arrival, referenced to a local clock, are measured on a time interval counter.

When the measurement is made or reduced at a TOC (USNO Time Service Bulletin Series No. 8), the time difference obtained represents the time difference between the local clock and the TV clock (emitted signal) plus the propagation and system delay - or:

[(local clock - TV line 10 received) + C].

The propagation and system delay (C) can be computed or measured.

Since the USNO publishes the daily absolute time corrections to be applied to the WTTG and KTTV transmissions (USNO MC - TV emitted, USNO Time Service Bulletin Series No. 4), Table 4, the actual time difference between the USNO MC and the local clock can be obtained as follows:

$$(\text{USNO MC} - \text{local clock}) = [(\text{USNO MC} - \text{TV emitted}) - (\text{local clock} - \text{TV received}) - C].$$

Sophisticated TV transmitting, receiving and decoding equipment has been developed, and is available commercially, to implement this system and to display the absolute time difference between a local clock and the TV transmissions.

SYSTEM SYNCHRONIZATION AND CAPABILITIES

The USNO monitors continuously the transmissions from WTTG and KTTV (Fig. 9&10) and maintains them synchronized with the USNO MC by changing, when necessary, the frequency output of the cesium oscillators installed at the TV transmitters. An arbitrary excursion limit of up to ±2.5 μs has been allowed in the TV transmissions before introducing a rate correction to the TV clock. This limit could be reduced, if desired.

Automatic time rate corrections as small as 0.86 nanosecond per day can be initiated from the phase microstepper. Figures 9 and 10 are plots of [USNO MC - WTTG] and of [USNO MC - KTTV]. They show how well this synchronization has been maintained in the last few months.

The daily time differences between the USNO MC and WTTG and KTTV are given as corrections on USNO Time Service Annoucements, Series 4 and 5, and by telephone announcements available by dialing (202) 254-4662 or AUTOVON 294-4662.

Various organizations and laboratories are presently utilizing this precise time distribution system to set or to compare the time of their own reference clock standard with that of the USNO MC. These TV time transfers are done routinely to real time accuracies of ±20 nanoseconds (ns) or better.

As an illustration, Figures 11 and 12 show how well two independent organizations, located approximately 25 km from WTTG measure the time difference between their reference clocks and the USNO MC.

Figure 11 shows the time relationship between the USNO MC and the USCG Washington Radio Station clock, located in Alexandria, VA, obtained by portable clock and by TV time measurement of WTTG transmissions. Neither statistical manipulation nor selection has been applied to the data used for this plot.

The measurements were obtained by utilizing a very simple system which consists of a TV receiver/line 10 discriminator and a time interval counter.

Figure 12 shows the time relationship between the USNO MC and the Applied Physics Laboratories (APL) clock, located in Laurel, MD, obtained by portable clock and by TV time measurements of WTTG transmissions with the slope removed.

The APL measurements were obtained by using an automatic TV monitor system.

The RMS deviation of these TV real time transfers, as verified by portable clock measurements, is within ±20 ns.

WTTG and KTTV transmissions are used routinely to distribute USNO MC time and frequency to locations as far away as Fort Detrick (MD) (60 km from WTTG), Dover, DE (130 km from WTTG), and Point Mugu, CA, approximately 95 km from KTTV.

Greater accuracies can be achieved by taking the TV measurements during periods when no phase corrections are made to the 3.58 MHz color subcarrier frequency at the TV transmitters (this can be ascertained easily by observing the stability of the received color subcarrier frequency or by looking at the received TV video), or by some statistical recognization or filtering of the data. Dr. Winkler of the USNO has recently experimented with an exponential weighted smoothing rejection technique to reduce the time differences between the USNO MC and WTTG transmissions measured at the USNO and found that a precision of 1 ns or better is obtainable from this TV system.

Tests on the receiving systems, performed by using RF generators of known stability, show that these receiving systems are capable of an absolute calibration accuracy of better than ±15 ns, and 1 sigma scatter consistently below 500 ps. The phase detector in the transmitter loop showed a dead band of ±2 ns and the digital phase shifter has a quantizing error of less than ±4 ns. The video processing in the TV plant inserts at least two slaved pulse generators before reaching the modulator, and finally, less than ideal regulation of the transmitter power supplies, especially during the vertical interval, cause changes in sync tip levels and leading edge slopes.

At the receiving site, antenna movement, transmission line propagation delay changes with temperature and humidity, and RF path propagation variations all contribute to limit system precision. All factors considered, this present line 10 time transfer system, as implemented, should be considered to have a precision capability of ±20 ns or better over path lengths of 100 μs or less and approaching ±50 ns at path lengths up to 350 μs. These figures are well confirmed by the time transfers reported above.

FUTURE PLANS AND APPLICATIONS

A problem encountered in installation of this system has been selection of a TV station which has mostly local program origination. Network affiliates were ruled out since they must operate off network feeds for a large percentage of the time. However, as reported and noted recently in the NBS Monthly Time and Frequency Bul. #238, some of the larger network outlets are installing Frame Synchronizers. These Frame Synchronizers destroy the usefulness of the station for relative time and frequency transfer using network observations. Simultaneous use of the same transmitters is unaffected, but they present an ideal situation for installation of the absolute time and frequency system discussed in this paper, since emission times may now be precisely controlled locally through the Frame Synchronizers.

The USNO presently has plans underway to implement this TV time distribution system in additional TV stations in the Washington/Baltimore Area in order to evaluate this technique as a means of providing an extremely accurate position/navigation system. Further applications in the fields of collision avoidance, geodesy

and real time computer operations will be possible at low cost. Rapid navigation on the Capital Beltway, as mentioned by the Scientific Director of the U. S. Naval Observatory, may also be made possible.

There are approximayely 800 TV transmitters operating in the U.S. at this time and they offer tremendous potential for the distribution of real time, synchronized, transmissions at relatively little cost.

ACKNOWLEDGEMENTS

We would like to express our appreciation to the people at WTTG, KTTV, Austron, and the USNO, to Mr. B. W. Shaw of the Applied Physics Laboratory, Mr. Putyson of USCG, and Mr. McConnell of Jet Propulsion Laboratory for their cooperation and assistance, with special recognition to Messrs. Harmon, Swarthout, and Barriclaw of WTTG and Mr. Saltzman of KTTV for their "hands-on" experience and help and to Dr. Winkler of the USNO for his continuing guidance and encouragement.

REFERENCES

1. Lavanceau, J. D., and Carroll, D., "Real Time Synchronization via Passive Television Transmissions", Third Annual DoD Precise Time and Time Interval Strategic Planning Meeting, 16-18 November 1971, held at Naval Research Laboratory, Washington, DC.

TABLE 1
FIRST TOC FOR EACH DAY

TIMES OF COINCIDENCE (NULL) EPHEMERIS

TELEVISION LINE 10 CCD SYNC

33,366 MICROSECONDS/PERIOD

DATE 1977	TIME H	M	S	DATE 1977	TIME H	M	S	DATE 1977	TIME H	M	S
OCT 1	0	6	15	NOV 1	0	10	51	DEC 1	0	4	0
2	0	1	1	2	0	5	37	2	0	15	27
3	0	12	28	3	0	0	23	3	0	10	13
4	0	7	14	4	0	11	50	4	0	4	59
5	0	2	0	5	0	6	36	5	0	16	26
6	0	13	27	6	0	1	22	6	0	11	12
7	0	8	13	7	0	12	49	7	0	5	58
8	0	2	59	8	0	7	35	8	0	0	44
9	0	14	26	9	0	2	21	9	0	12	11
10	0	9	12	10	0	13	48	10	0	6	57
11	0	3	58	11	0	8	34	11	0	1	43
12	0	15	25	12	0	3	20	12	0	13	10
13	0	10	11	13	0	14	47	13	0	7	56
14	0	4	57	14	0	9	33	14	0	2	42
15	0	16	24	15	0	4	19	15	0	14	9
16	0	11	10	16	0	15	46	16	0	8	55
17	0	5	56	17	0	10	32	17	0	3	41
18	0	0	42	18	0	5	18	18	0	15	8
19	0	12	9	19	0	0	4	19	0	9	54
20	0	6	55	20	0	11	31	20	0	4	40
21	0	1	41	21	0	6	17	21	0	16	7
22	0	13	8	22	0	1	3	22	0	10	53
23	0	7	54	23	0	12	30	23	0	5	39
24	0	2	40	24	0	7	16	24	0	0	25
25	0	14	7	25	0	2	2	25	0	11	52
26	0	8	53	26	0	13	29	26	0	6	38
27	0	3	39	27	0	8	15	27	0	1	24
28	0	15	6	28	0	3	1	28	0	12	51
29	0	9	52	29	0	14	28	29	0	7	37
30	0	4	38	30	0	9	14	30	0	2	23
31	0	16	5					31	0	13	50

NOTES

TABLE 2
INTERPOLATIONS FOR ALL TOC'S IN A DAY
TIMES OF COINCIDENCE (NULL) EPHEMERIS
TELEVISION LINE 10 ODD SYNC

33,366 MICROSECONDS/PERIOD

H	M	S
0	0	0
0	16	41
0	33	22
0	50	3
1	6	44
1	23	25
1	40	6
1	56	47
2	13	28
2	30	9
2	46	50
3	3	31
3	20	12
3	36	53
3	53	34
4	10	15
4	26	56
4	43	37
5	0	18
5	16	59
5	33	40
5	50	21
6	7	2
6	23	43
6	40	24
6	57	5
7	13	46
7	30	27
7	47	8
8	3	49
8	20	30
8	37	11
8	53	52
9	10	33
9	27	14
9	43	55
10	0	36
10	17	17
10	33	58
10	50	39
11	7	20
11	24	1
11	40	42
11	57	23
12	14	4
12	30	45
12	47	26
13	4	7
13	20	48
13	37	29
13	54	10
14	10	51
14	27	32
14	44	13
15	0	54
15	17	35
15	34	16
15	50	57
16	7	38
16	24	19
16	41	0
16	57	41
17	14	22
17	31	3
17	47	44
18	4	25
18	21	6
18	37	47
18	54	28
19	11	9
19	27	50
19	44	31
20	1	12
20	17	53
20	34	34
20	51	15
21	7	56
21	24	37
21	41	18
21	57	59
22	14	40
22	31	21
22	48	2
23	4	43
23	21	24
23	38	5
23	54	46

TABLE 3
INTERPOLATIONS FOR ALL SECONDS BETWEEN TOC'S

TELEVISION LINE 10 ODD SYNC
33,366 MICROSECONDS/PERIOD

M	S	(μS)	M	S	(μS)	M	S	(μS)	M	S	(μS)
0	1	1000.000	0	51	17633.333	1	41	900.000	2	31	17533.333
0	2	2000.000	0	52	18633.333	1	42	1900.000	2	32	18533.333
0	3	3000.000	0	53	19633.333	1	43	2900.000	2	33	19533.333
0	4	4000.000	0	54	20633.333	1	44	3900.000	2	34	20533.333
0	5	5000.000	0	55	21633.333	1	45	4900.000	2	35	21533.333
0	6	6000.000	0	56	22633.333	1	46	5900.000	2	36	22533.333
0	7	7000.000	0	57	23633.333	1	47	6900.000	2	37	23533.333
0	8	8000.000	0	58	24633.333	1	48	7900.000	2	38	24533.333
0	9	9000.000	0	59	25633.333	1	49	8900.000	2	39	25533.333
0	10	10000.000	1	0	26633.333	1	50	9900.000	2	40	26533.333
0	11	11000.000	1	1	27633.333	1	51	10900.000	2	41	27533.333
0	12	12000.000	1	2	28633.333	1	52	11900.000	2	42	28533.333
0	13	13000.000	1	3	29633.333	1	53	12900.000	2	43	29533.333
0	14	14000.000	1	4	30633.333	1	54	13900.000	2	44	30533.333
0	15	15000.000	1	5	31633.333	1	55	14900.000	2	45	31533.333
0	16	16000.000	1	6	32633.333	1	56	15900.000	2	46	32533.333
0	17	17000.000	1	7	266.667	1	57	16900.000	2	47	166.667
0	18	18000.000	1	8	1266.667	1	58	17900.000	2	48	1166.667
0	19	19000.000	1	9	2266.667	1	59	18900.000	2	49	2166.667
0	20	20000.000	1	10	3266.667	2	0	19900.000	2	50	3166.667
0	21	21000.000	1	11	4266.667	2	1	20900.000	2	51	4166.667
0	22	22000.000	1	12	5266.667	2	2	21900.000	2	52	5166.667
0	23	23000.000	1	13	6266.667	2	3	22900.000	2	53	6166.667
0	24	24000.000	1	14	7266.667	2	4	23900.000	2	54	7166.667
0	25	25000.000	1	15	8266.667	2	5	24900.000	2	55	8166.667
0	26	26000.000	1	16	9266.667	2	6	25900.000	2	56	9166.667
0	27	27000.000	1	17	10266.667	2	7	26900.000	2	57	10166.667
0	28	28000.000	1	18	11266.667	2	8	27900.000	2	58	11166.667
0	29	29000.000	1	19	12266.667	2	9	28900.000	2	59	12166.667
0	30	30000.000	1	20	13266.667	2	10	29900.000	3	0	13166.667
0	31	31000.000	1	21	14266.667	2	11	30900.000	3	1	14166.667
0	32	32000.000	1	22	15266.667	2	12	31900.000	3	2	15166.667
0	33	33000.000	1	23	16266.667	2	13	32900.000	3	3	16166.667
0	34	633.333	1	24	17266.667	2	14	533.333	3	4	17166.667
0	35	1633.333	1	25	18266.667	2	15	1533.333	3	5	18166.667
0	36	2633.333	1	26	19266.667	2	16	2533.333	3	6	19166.667
0	37	3633.333	1	27	20266.667	2	17	3533.333	3	7	20166.667
0	38	4633.333	1	28	21266.667	2	18	4533.333	3	8	21166.667
0	39	5633.333	1	29	22266.667	2	19	5533.333	3	9	22166.667
0	40	6633.333	1	30	23266.667	2	20	6533.333	3	10	23166.667
0	41	7633.333	1	31	24266.667	2	21	7533.333	3	11	24166.667
0	42	8633.333	1	32	25266.667	2	22	8533.333	3	12	25166.667
0	43	9633.333	1	33	26266.667	2	23	9533.333	3	13	26166.667
0	44	10633.333	1	34	27266.667	2	24	10533.333	3	14	27166.667
0	45	11633.333	1	35	28266.667	2	25	11533.333	3	15	28166.667
0	46	12633.333	1	36	29266.667	2	26	12533.333	3	16	29166.667
0	47	13633.333	1	37	30266.667	2	27	13533.333	3	17	30166.667
0	48	14633.333	1	38	31266.667	2	28	14533.333	3	18	31166.667
0	49	15633.333	1	39	32266.667	2	29	15533.333	3	19	32166.667
0	50	16633.333	1	40	33266.667	2	30	16533.333	3	20	33166.667

NOTES

U. S. NAVAL OBSERVATORY
WASHINGTON, D.C. 20390

3 NOVEMBER 1977

DAILY PHASE VALUES AND TIME DIFFERENCES SERIES 4 NO. 561

THE TABLE GIVES: UTC(USNO MC) - TRANSMITTING STATION UNIT = ONE MICROSECOND

	WASH. DC WTTG EMITTED	L.A. CA KTTV EMITTED	NATIONAL TELEVISION NETWORKS NBC 1925 UT	NBC 1931 UT	CBS 1926 UT	CBS 1932 UT	ABC 1927 UT	ABC 1933 UT
OCT. 27	-2.17	0.2	21,530.9	14,509.7	12,120.6	5,098.0	9,194.1	2,171.6
28	-2.21	0.2	4,451.4	30,795.6	11,708.0	4,675.4	25,485.8	18,463.4
29	-2.25	-	20,753.0	13,730.7	13,711.0	6,691.3	431.7	26,776.0
30+	-2.29	-	188.2	26,532.5	10,347.3	13,696.9	32,499.4	25,315.4
31+	-2.36	0.2	16,465.6	9,443.1	7,075.2	42.6	4,135.9	30,480.0
NOV. 1+	-2.39	0.3	32,756.0	25,733.5	6,643.5	16,336.1	20,428.6	13,406.1
2+	-2.42	0.4	15,681.7	8,659.2	6,286.4	15,913.4	3,353.9	29,698.0

+ VALUES FOR THESE DAYS WERE OBTAINED DURING THE 2000 UT HOUR FOR NBC, CBS, AND ABC.

REFERENCES: (A) TIME SERVICE INFORMATION LETTER OF 15 AUGUST 1973
(B) TIME SERVICE ANNOUNCEMENT, SERIES 9, NO. 125 (LORAN-C)
(C) DAILY PHASE VALUES AND TIME DIFFERENCES, SERIES 4, NO. 195 (TV)

NOTES:

(1) PROPAGATION DISTURBANCES WERE OBSERVED NEAR THE FOLLOWING TIMES:
28 OCT. 1900/4
29 OCT. 1240/4, 1645/4, 2005/3
30 OCT. 1505/4.

(2) NAVY STATION OFF-AIR TIME:
NWC 31 OCT. 0250 TO 0301 UT

Table 4. USNO Series No. 4

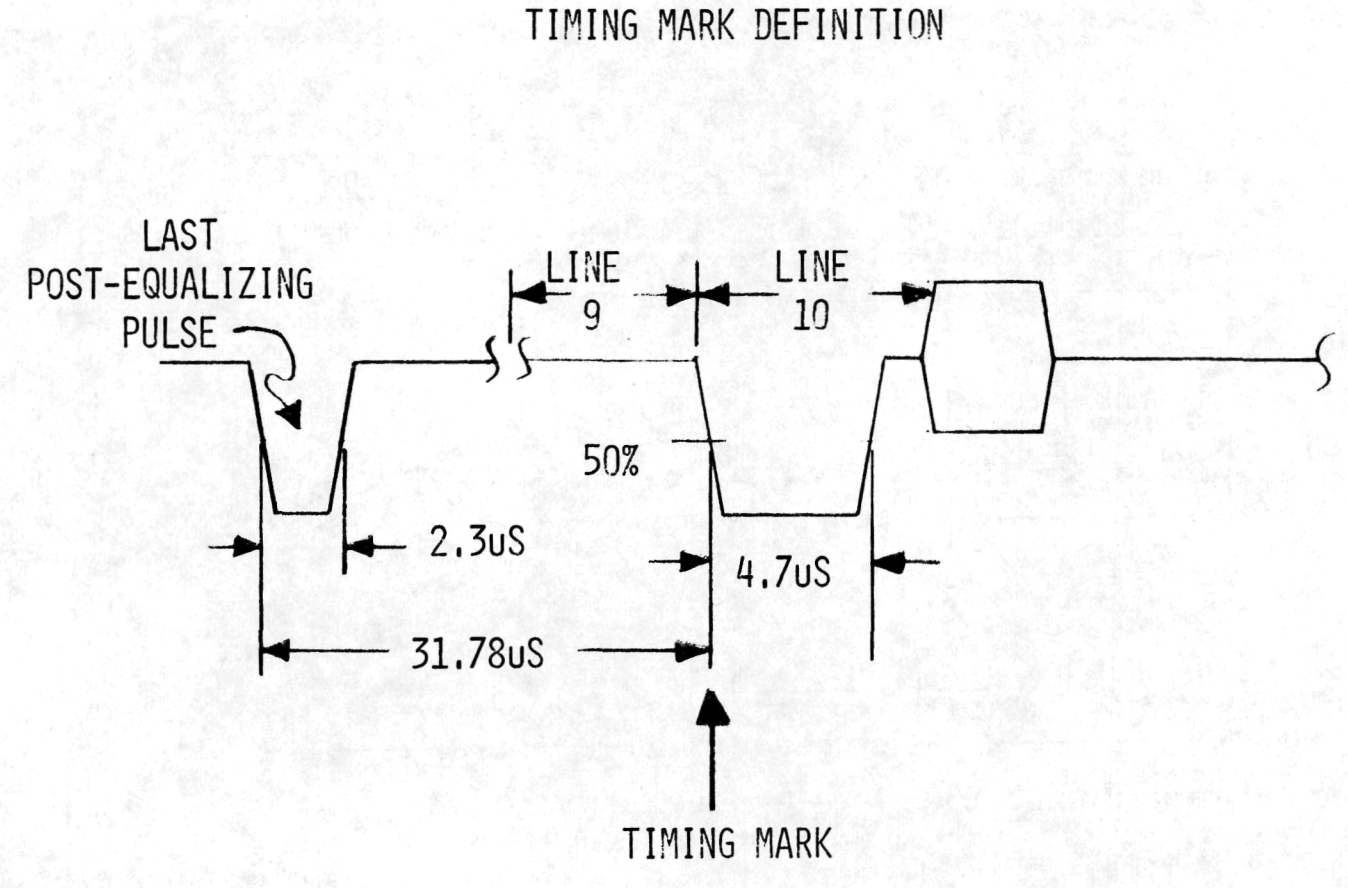


Fig. 1. Timing Mark Definition

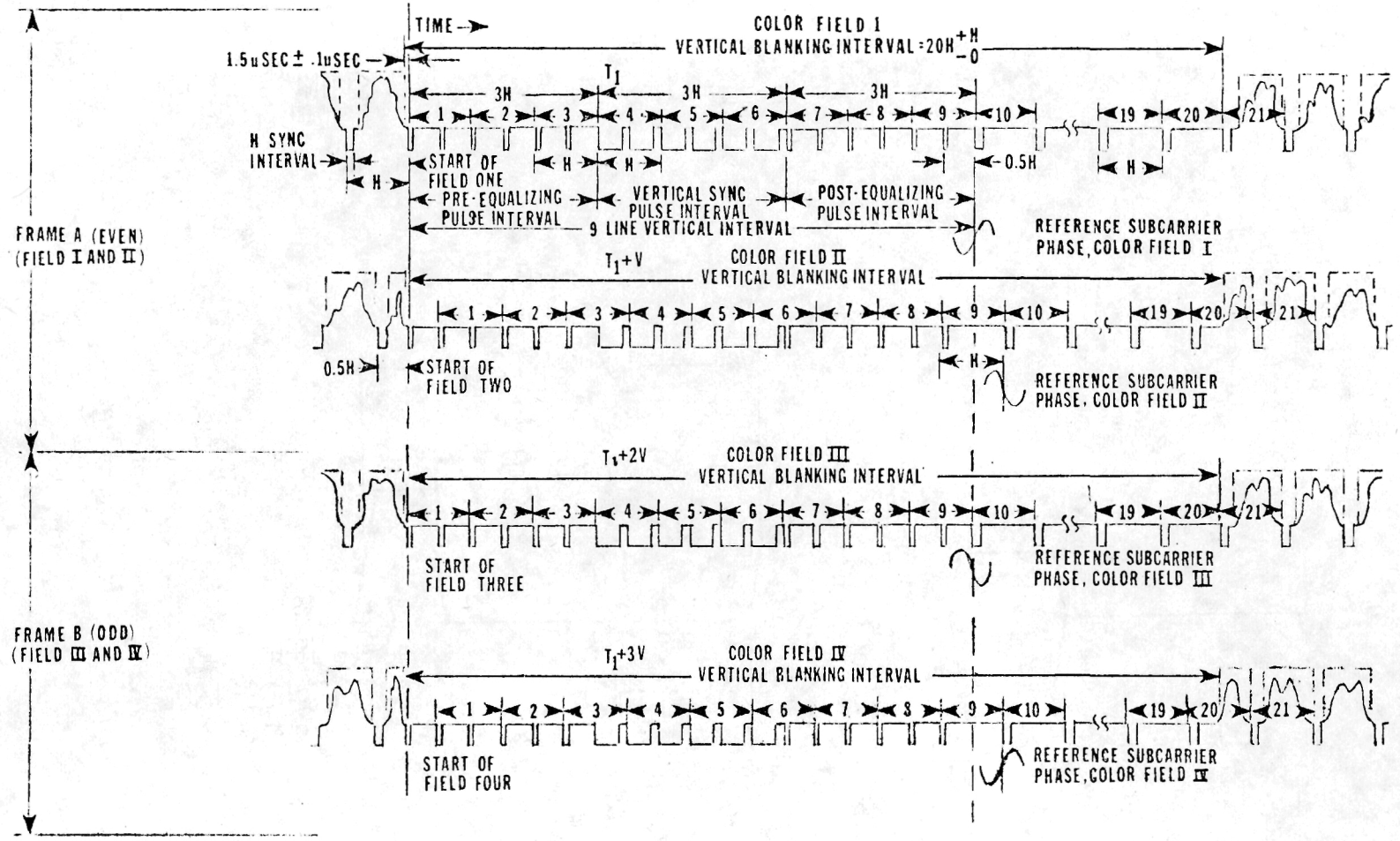


Fig. 2. Standard TV Diagrams

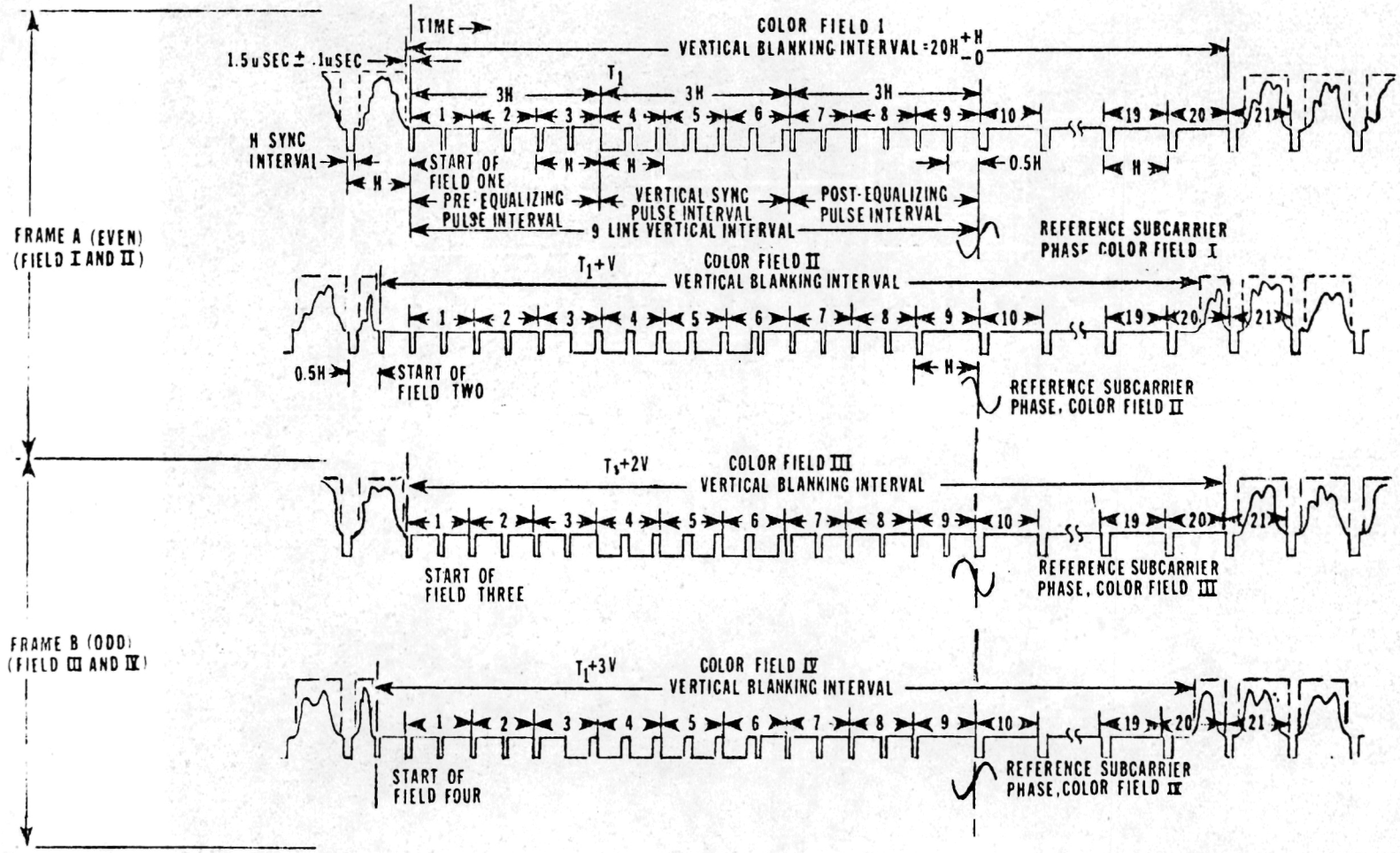


Fig. 3. Standard TV Diagrams with Fields 2 & 4 Displaced

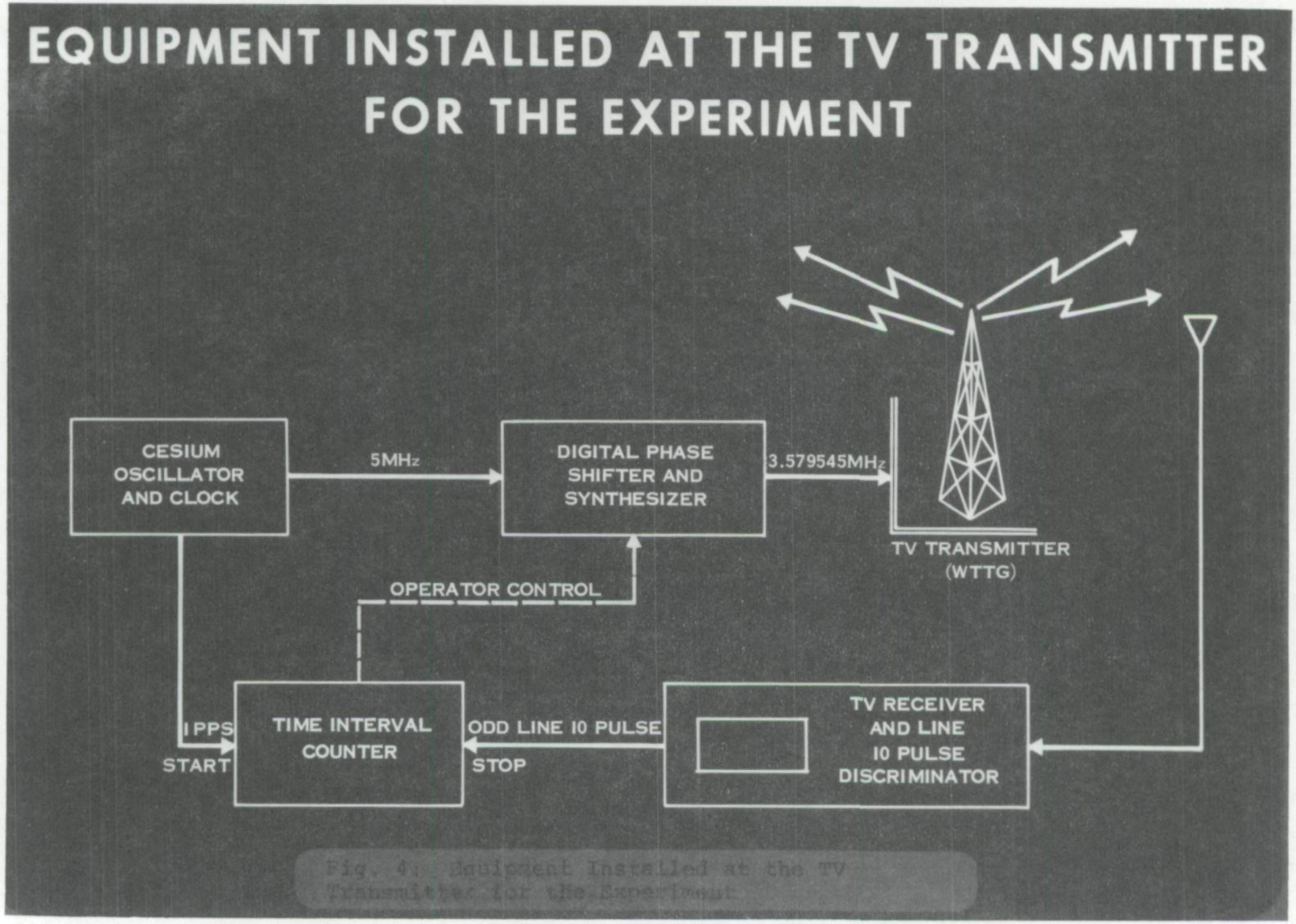


Fig. 4: Equipment Installed at the TV Transmitter for the Experiment

TYP. TRANSMITTER INSTALLATION

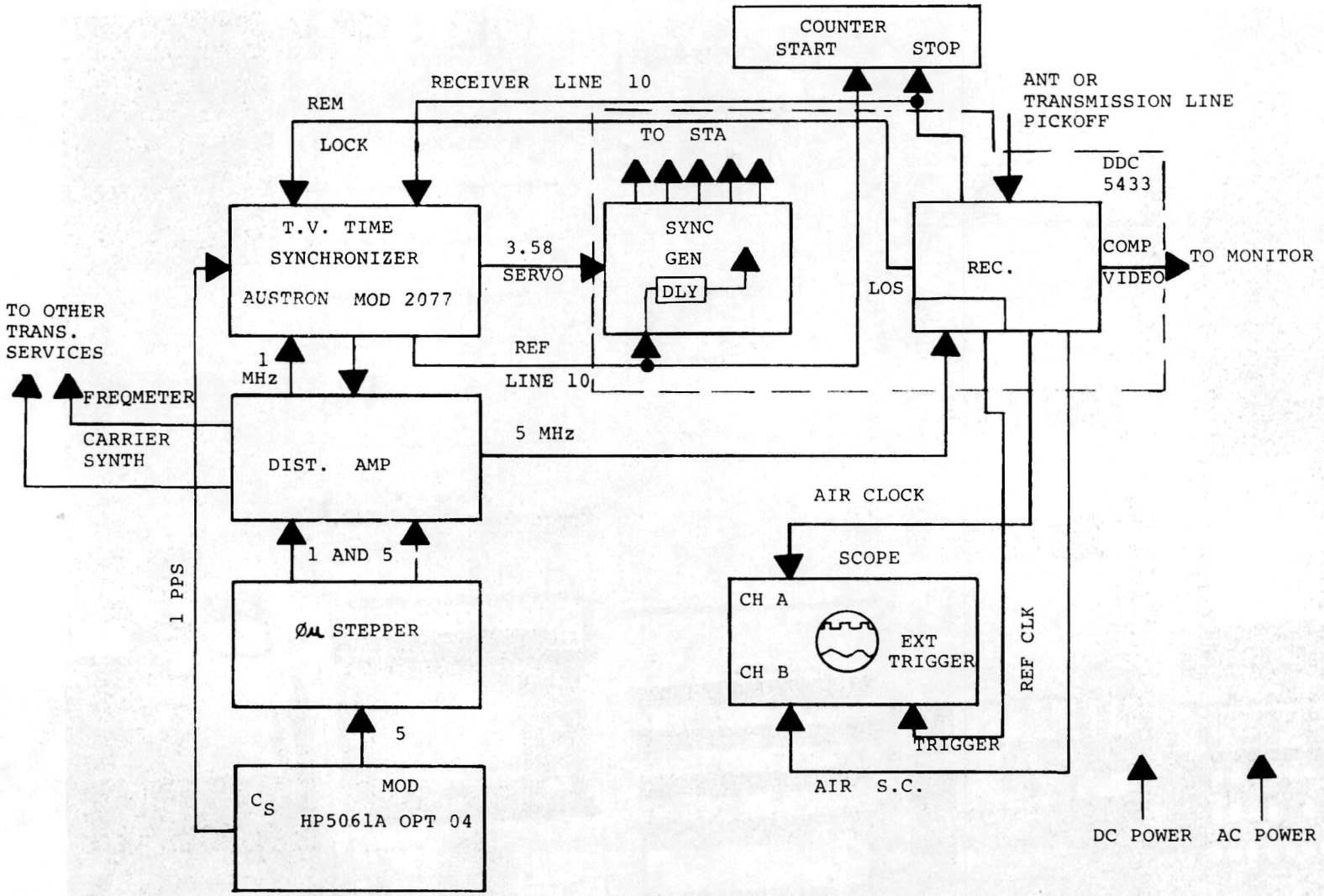
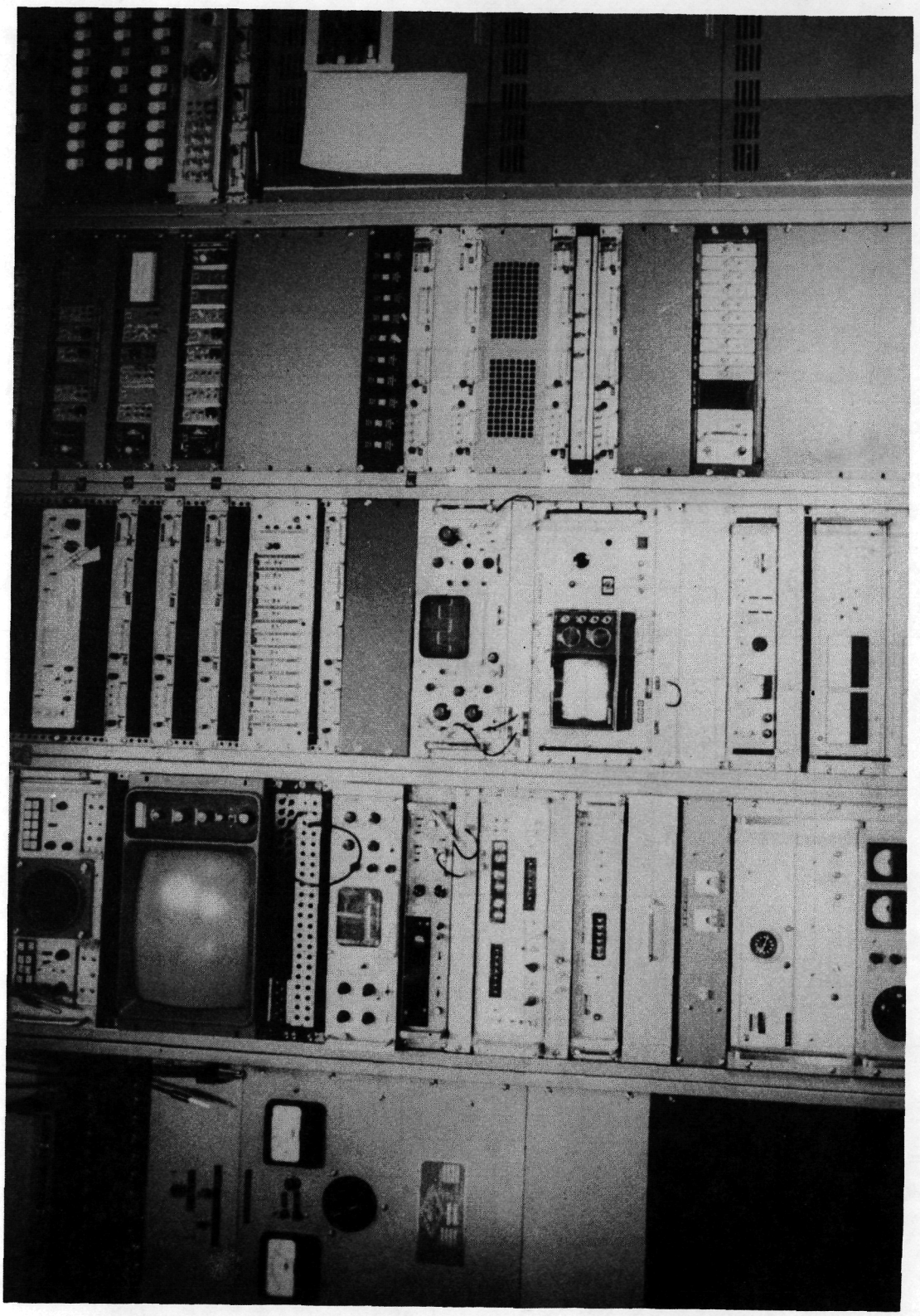


Fig. 5. Transmitter Control System



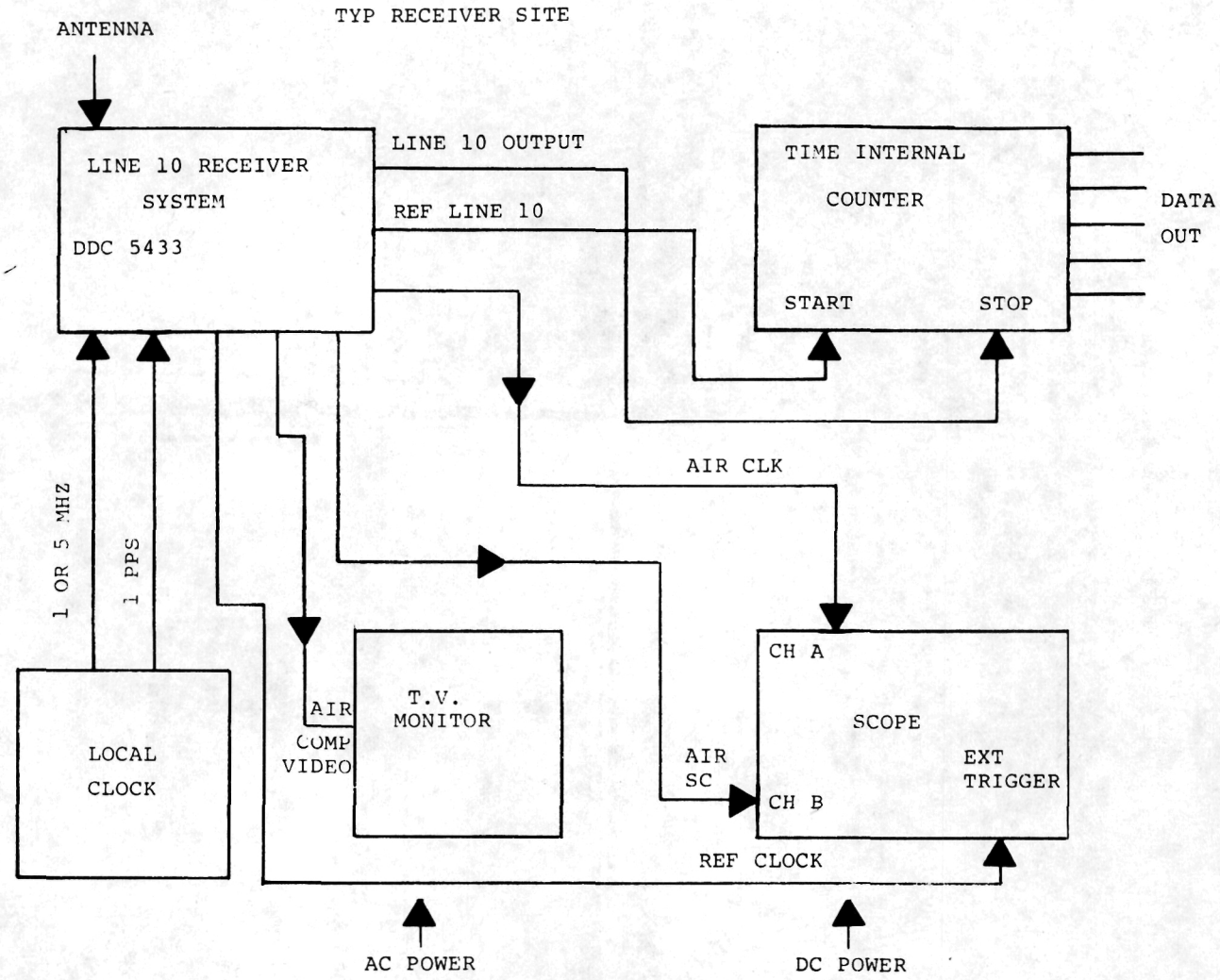
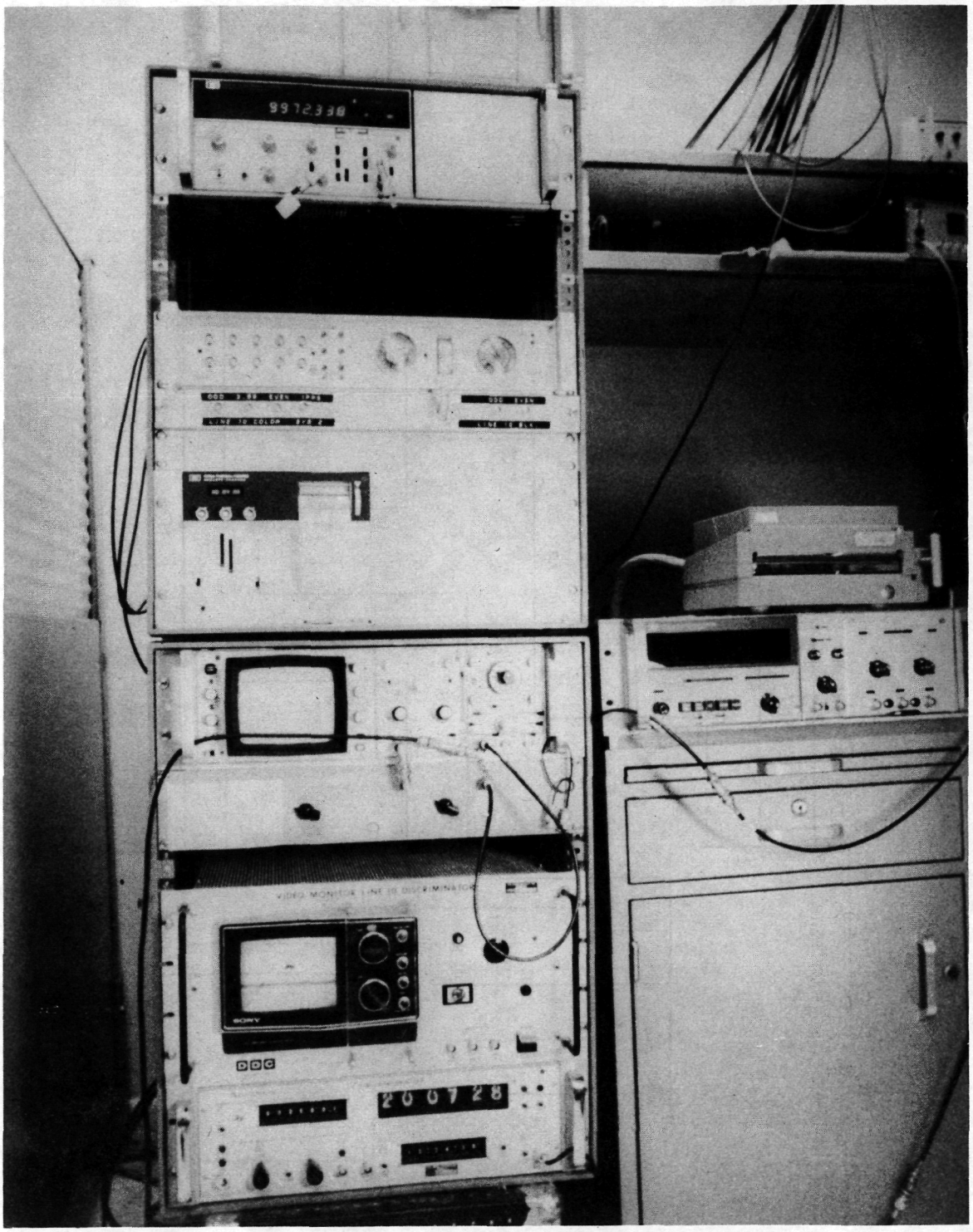


Fig. 7. Receiving Decoding System


SONY
DDC

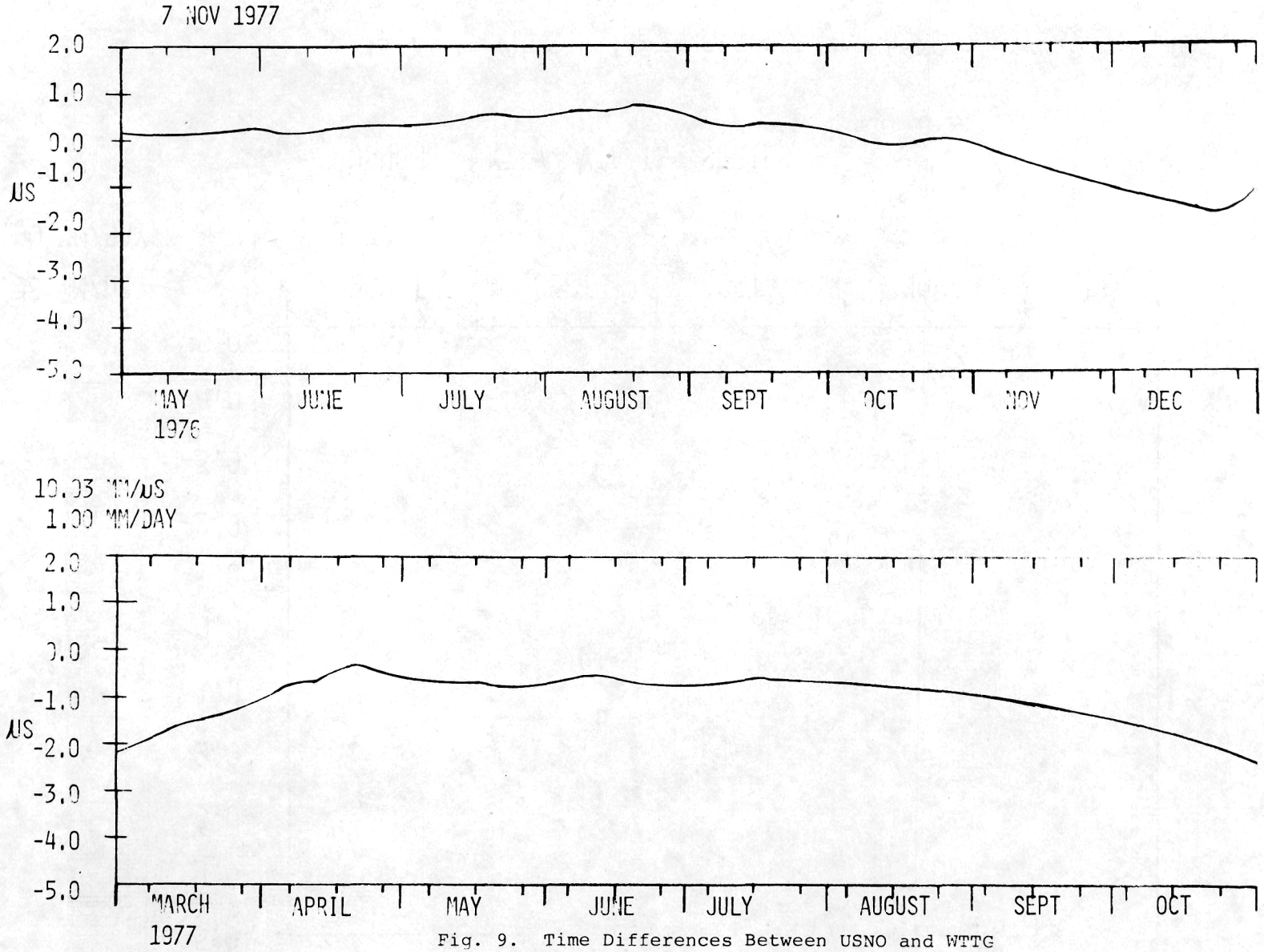


Fig. 9. Time Differences Between USNO and WTTG

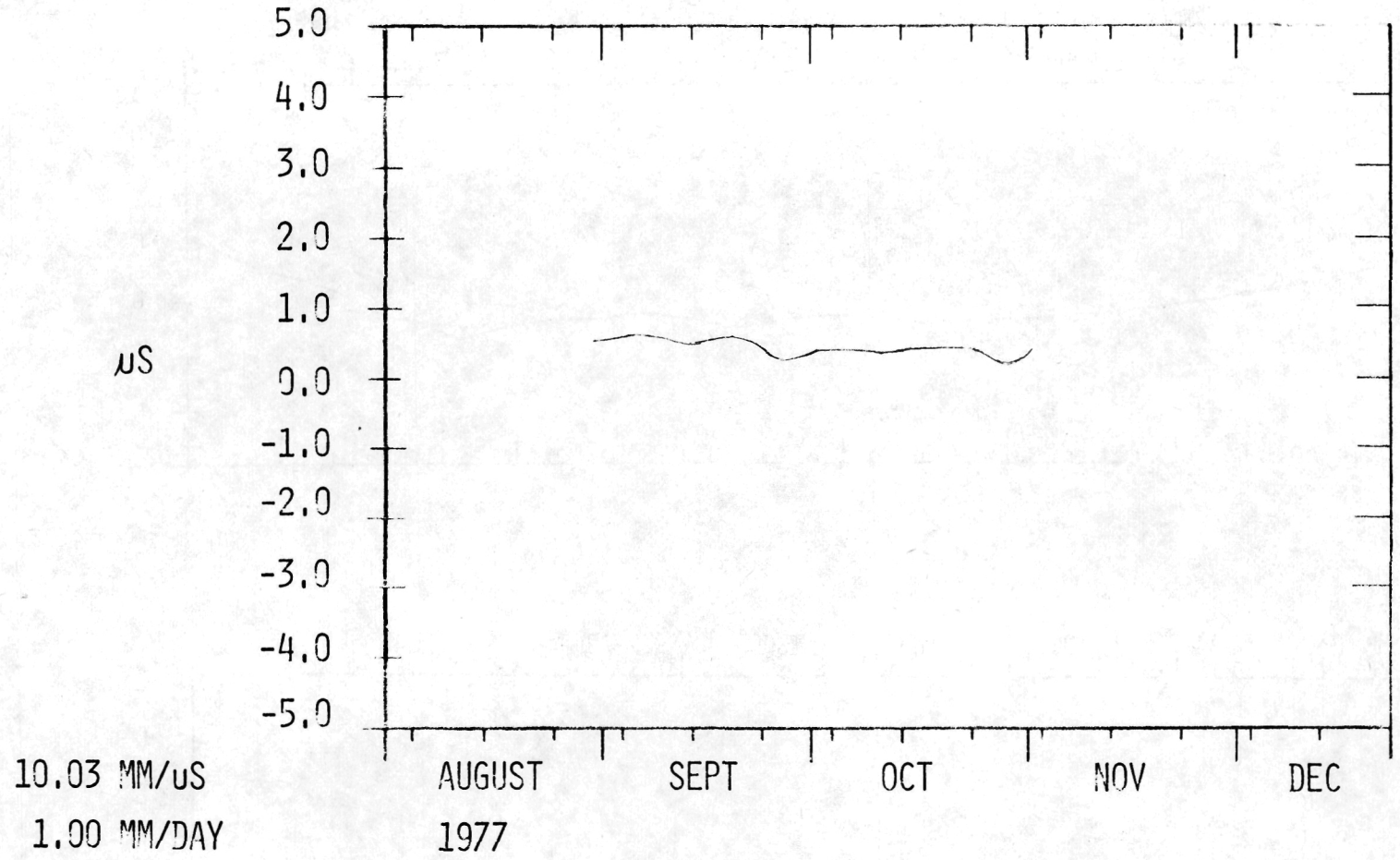


Fig. 10. Time Differences Between USNO and KTTV

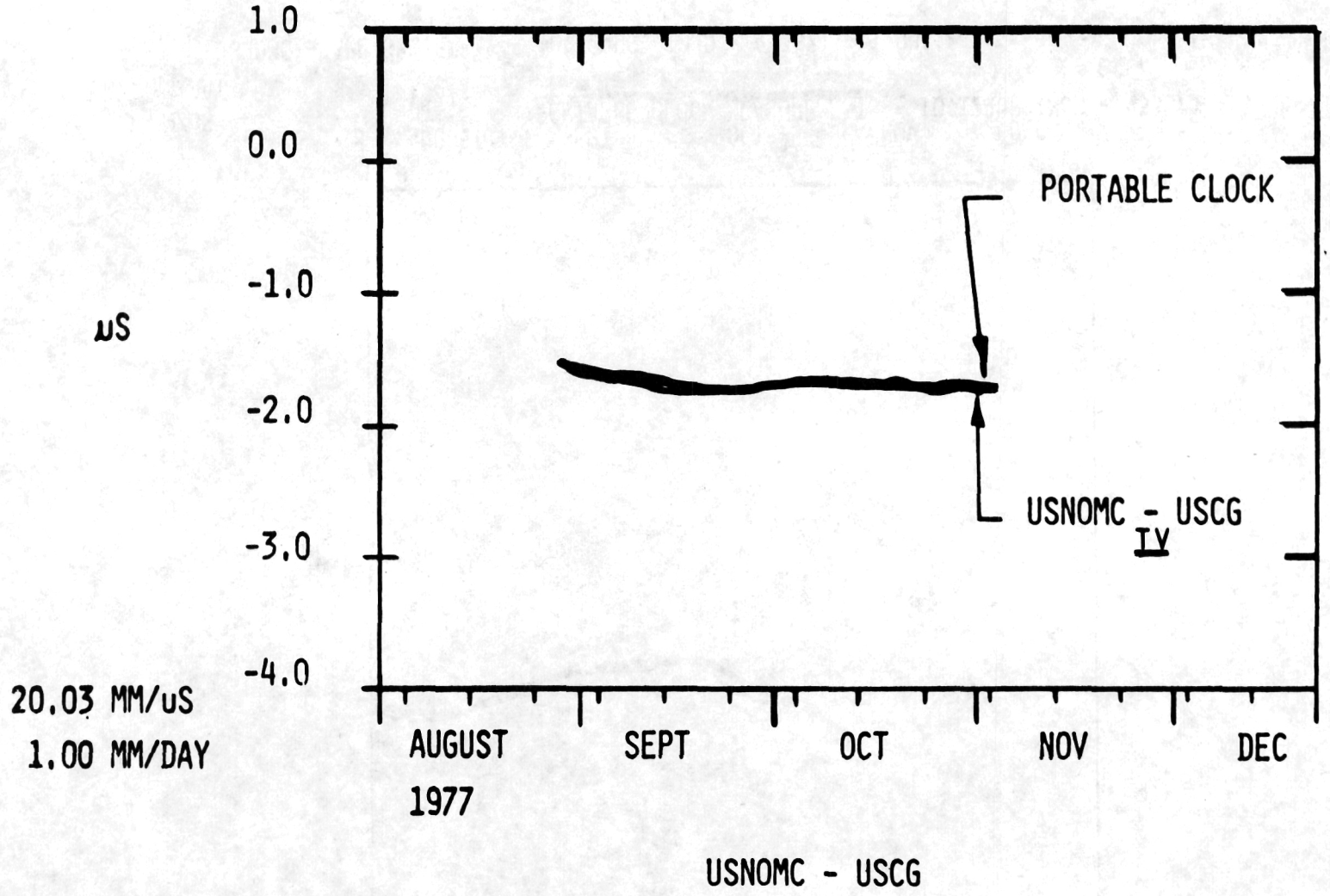
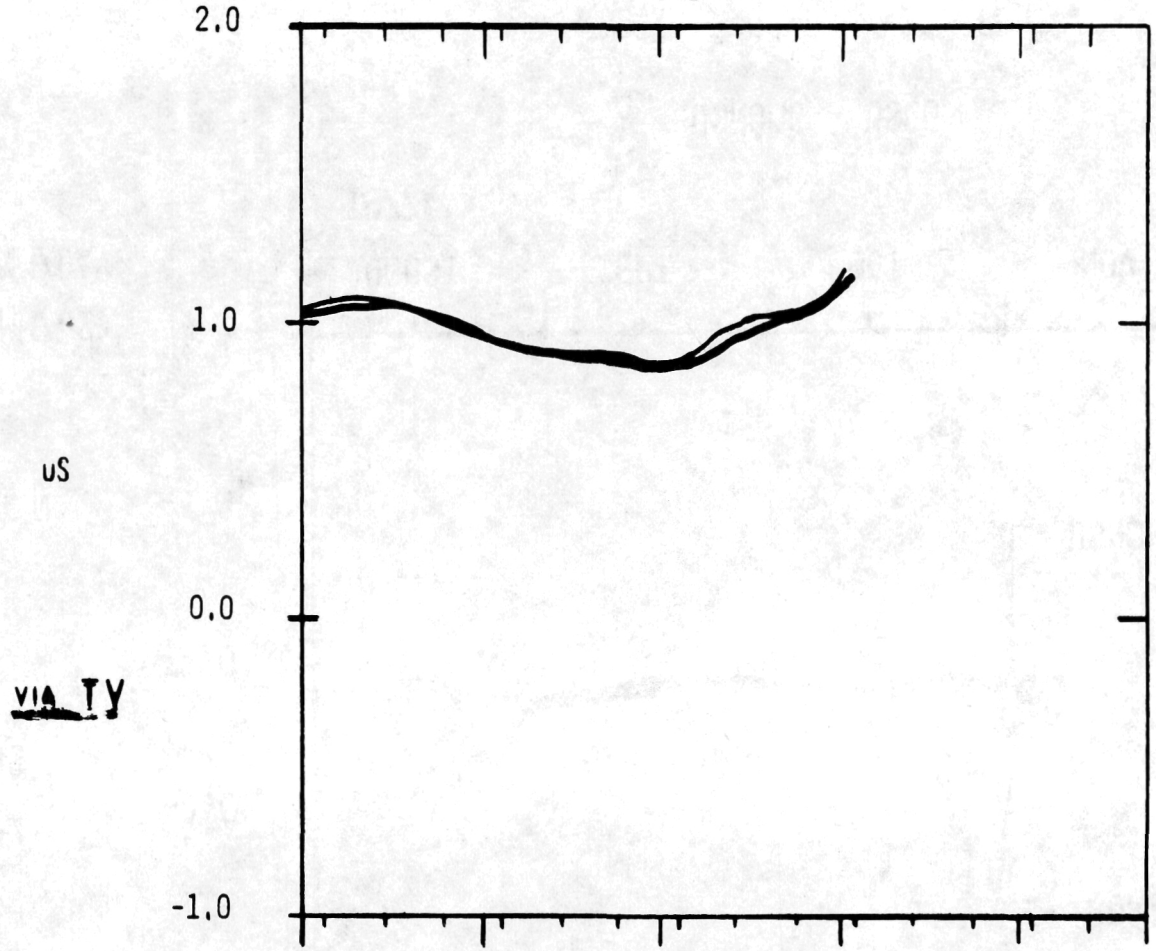


Fig. 11. Time Differences Between the USNO MC and USCG

Fig. 12. Time Differences Between the USNO MC and APL With Slope Removed



NEW POSSIBILITIES FOR TIME AND STANDARD FREQUENCY DISSEMINATION OVER TV NETWORKS

Bogosav Ž. Kovačević, Faculty of Electronic Engineering,
University of Niš, Niš, Yugoslavia

ABSTRACT

This paper describes the principles of a new Time and TV Synchro System developed and currently in experimental use at the TV Studio Belgrade in Yugoslavia. This Time and TV Synchro System secures the time of coincidence every second by definition for all programs originating within the TV studio Belgrade. The incorporation of the digital TV frame synchronizer in the video path enables its application with the same quality of dissemination of time and standard frequency signals, regardless of the place from which the particular program originates. The system can also be applied in connection with TV broadcasting over geostationary TV satellites.

INTRODUCTION

Recent research in many countries has resulted in a number on conclusions which indicate new possibilities for using the existing TV networks for dissemination of time and standard frequency signals. The advantage of such a system in many applications is obvious, and it involves a relatively small investment of the capital for the adaptation of the existing TV network. The ordinary TV receiver can easily be adapted for the purpose of a user at a small cost. Such an adapted TV receiver is very inexpensive compared to many time and standard frequency facilities it offers to its user in the actual exploitation.

Practical realization of the system for time and standard frequency dissemination over the TV networks necessitates the consideration and solution of many technical programs, such as:

1. Determination and maintenance of the time signals at the TV transmitting point in relation to the time scale (UTC);

2. The precise knowledge of the propagation time from the transmitter to the receiver and the maintenance of that propagation time to a fixed (constant) value as closely as possible;

3. Problems associated with a given particular TV system (NTSC, PAL, SECAM, etc.);

4. Problems associated with the instantaneous TV picture formation mode within the given TV system (live transmission from a camera, VTR program, film presentation program, other TV network program, etc.).

The purpose of this paper is to describe in principle a new Time and TV Synchro System developed and currently in experimental use at the TV studio Belgrade in Yugoslavia. This Time and TV Synchro System secures the Time of Coincidence every second in the transmission of the second pulses.

TIME AND TV SYNCHRO SYSTEM

The TV studio Belgrade, Yugoslavia began over four years ago the experimental transmission of time and standard frequency signals by using the so-called active TV system (Kovacevic 1973 and 1974, Kovacevic et al. 1976; also cf. Howe 1972). In this system, second pulses, standard frequency and the coded time of day are injected into the 19th and the 332nd line of the video signal, v. Figure 1. On the other hand, the time signals, standard frequency and the TV sync pulses are all derived from the cesium clock which itself is located within the TV studio premises.

At this point we define and understand by the complete or full synchronization for the purposes of this system such a technical realization of synchronization, in which the second pulses appear every second at precisely the same point or place of a single selected line of the TV picture. Since the second pulses must appear at the same place of the selected line in accordance with the requirement of the full synchronization, that means that the time information must be injected only once within a single complete frame. This obviously necessitates that the vertical interval TV sync pulses be referred and adjusted in accordance with the second pulses from the same standard clock. This can easily be realized in the case of all European TV systems, since one second, the period of the second pulses, is an even integral multiple of the field period of 20 ms. On the other hand, in the case of the US TV system, the nominal field period is 16 and 2/3 ms, which is not contained in one second as an even integer. For the TV systems with 60 Hz as the fundamental frequency, the Time of Coincidence is 16 min. and 41 sec. (CCIR 7/26E 1973, Davis 1975), or thereabouts

depending on the actual field frequency in use. In that respect, it should be mentioned that if there is no synchronism between the TV frame frequencies and the time signals, the upper limit of ambiguity of the time information transmission is 40 ms for the 50 Hz TV systems (Europe), or 33 and 1/3 ms for the 60 Hz TV systems in the USA and elsewhere, as the consequence of the waiting for the selected line into which time information is injected. Possibilities of various TV systems for time and standard frequency dissemination are shown in Table 1.

COLOR STANDARD	Passive		Active		Nominal field frequency
	Subcarrier frequency f_{sc}	Field frequency f_{ℓ}	Second pulses	1 MHz Burst	
NTSC	yes	yes	no	yes	60 Hz
PAL	yes	yes	yes	yes	50 Hz
SEKAM	no	yes	yes	yes	50 Hz

TABLE 1

With reference to Figure 2, which shows in principle the Time and TV Synchro System realized at the TV studio Belgrade, the time of coincidence is realized every second in the case of the PAL 50 Hz TV system in use at the TV Belgrade. It is clear from Figure 2 that the synchronization between the clock and the Master TV Sync Generator is required not only with respect to the frequency, but also with respect to the phase. Figure 2, which shows in principle the realized Time and TV Synchro System at the TV studio Belgrade, is self-explanatory to a large extent. Note that the coincidence circuit resets the selected line number 19, whenever the synchronization has been interrupted for any reason, provided of course that the circuitry remains operable.

Figure 3 shows how the described Time and TV Synchro System was incorporated within the normal TV circuit (video path), with some obvious simplifications of the principle circuit diagram as shown in Figure 2.

Figure 4 shows the adapted TV receiver with all the standard signals at the disposal of the user at the receiving point, which are: 1 pps UTC (YU) with minute and hour markers, 1 MHz, the subcarrier of 4.43 MHz, the line frequency of 15,625 Hz, the field frequency of 50 Hz, and the frame frequency of 25 Hz. An ordinary commercially manufactured TV receiver has been adapted. The 13 digits, which appear on the TV screen as shown in Figure 4, are obtained through the appropriate blanking of the video signal. The accuracy code digit, which is encoded in the time of day pulse train (v. Figure 1), indicates the location of the source of the actual video signal, since the realized accuracy, i.e., precision, of the time and standard frequency transmission depends on that location. The difference between the UTC and the local time (clock) (UTC - LOCAL TIME in Figure 4) is displayed on the screen as the last six digits. The difference is given in the appropriate units which can be chosen by the operator in microseconds or tens of nanoseconds.

PRACTICAL TV BROADCASTS AND TIME OF COINCIDENCE

As already stated, the synchronization between the time signals and the TV picture is achieved by the Master Sync Generator (v. Figure 2 and 3), and forms as such a part of the entire developed system. The time of coincidence is fully assured in this system whenever the TV program originates within the system itself by definition. During the exploitation of the developed system at the TV studio Belgrade it was noticed, which was theoretically anticipated, that the time of coincidence is subject to random fluctuations in the case of the VTR programs. Also by definition the Time of Coincidence cannot be achieved when an external program is being aired. The external program is normally not locked on the same Master Sync generator, and there is also some random fluctuation of the propagation time of that external program from a distant studio. Thus, the accuracy is not the same all the time, and it depends on the program itself and the means used for its realization. The best quality is assured and is achieved practically when a local live fully electronic video signal is transmitted (live camera within the system). For instance, during local VTR broadcasting, the random fluctuation (jitter) of the sync pulses and the standard frequency of 1 MHz, including the second pulses, is normally 3 to 10 times greater compared to similar fluctuation during the live fully electronic camera programs.

Considering the fact that over 80% of the TV programs are often obtained from VTR's and other networks, as is the case for the TV studio Belgrade and most TV stations all over the world, then there remains only 10 to 15% of broadcast time for telecine films and live camera programs which offer the optimal conditions for time and standard frequency dissemination. This practically means that there

are only two to three intervals longer than 1,000 seconds for the optimal time and standard frequency dissemination, which may not be sufficient for the practical purposes of the users.

This disadvantage can be successfully overcome by utilizing a digital TV frame store synchronizer in the video path and its incorporation in the Time and TV Synchrosystem as previously outlined (Kano et al. 1974 and Butler 1974). Figure 5 shows the simplified block diagram of the frame synchronizer. The basic characteristics of this scheme is that it can store in the digital form one entire TV frame. The digital recording-writing is accomplished by the application of the parameters of the original composite sync pulses. The readout is accomplished by the application of the Master Sync Generator (MSG). Thus, since the MSG itself is locked within the Time and TV Synchro System, the Time of Coincidence is realized every second with the accompanying optimal time and standard frequency dissemination for the entire duration of such a program, regardless of the place from which that original video signal is transmitted. Figure 6 shows how the frame synchronizer is incorporated in the TV video path. It should also be mentioned that this system normally introduces a significant improvement of the quality in the video signal processing.

During the last three days of the 1976 Montreal Olympic Games, the receiving and converting service for the European TV viewers was secured only through the Yugoslav TV facilities. The above described system was used during that 1976 Montreal Olympic Games coverage for Europe, but the digital memory from the Standard Converter (525/60-NTSC into 625/50-PAL) was read by using the appropriate signals from the Master Synchro Generator of the Time and TV Synchro System as shown earlier in Figure 2. To the best of this author's knowledge, this system has been used for the first time in this instance for the TV coverage of a program over a wider geographic area. Detailed measurements during that transmission have clearly proved that the quality of the time and standard frequency dissemination through the TV network to the receiving point is the same as the quality which is normally achieved during the live camera programs, although the program originated about 7,000 km (geographic distance) from the Yugoslav Ground TV Station to Satellite TV facility. Of course, the time and standard frequency signals were injected at the TV studio Belgrade during all that coverage for Eurovision.

TV SATELLITES AND TIME AND TV SYNCHRO SYSTEM

According to the planned distribution of TV satellites for Europe, each European country has already been allocated at least one geostationary TV satellite, which will cover only the territory of that country (Geneva 1977, World Administrative Radio Conference for the Satellite Broadcasting). The above described Time and TV Synchro System can be

applied to TV transmission over TV broadcasting satellites. The formation and injection of the time and standard frequency signals can be performed either at the TV studio, or at the TV ground transmitting facility.

The variations of the propagation time between the Earth and the geostationary satellite are considerable and of the order of miliseconds. These variations are the consequences of well-known causes and they are relatively slow during the 24 hour period (Spilker 1977). These variations can cause degradation of the quality of time and standard frequency dissemination during TV satellite broadcasting, as compared to the quality obtainable with the ground TV system. However, these variations can be in principle corrected within the described Time and TV Synchro System, and the Time of Coincidence can be achieved every second for the entire duration of such a program. This correction consists of delaying or advancing the second pulses with reference to the average propagation time, so that the received second pulses at the TV receiving ground point (v. Figure 8) coincide with the UTC (YU), while the formation of the TV sync pulses are coordinated with and referred to the advanced second pulses. Note that the second pulses are all the time advanced for the total propagation time during such a transmission, which is evident from Figure 8. The correction of these variations can be improved over a given wide geographic area by averaging delay times measured at a number of the fixed ground receiving points which are connected to the center via fixed ground facilities.

The Yugoslav TV system has no geostationary TV satellite of its own at the moment, and for that reason some limited experiments have been performed by utilizing the Yugoslav ground facilities and the INTELSAT-IVA telecommunications satellite. The results of those measurements and analytical comparison with the theoretically introduced corrections have proved that it is possible to realize the time and standard frequency dissemination TV system covering the entire territory of Yugoslavia, whose second pulses will never deviate from any receiving point for more than 20 microseconds.

CONCLUSIONS

On the basis of the extensive experimental data, the following conclusions have been obtained by this author:

1. It is possible to realize complete synchronization between the TV picture and the second pulses for those TV systems for which the field frequency is 50 Hz. This practically means that the second pulses appear at precisely the same place of a selected line of the TV picture. Therefore, the Time of Coincidence for such a system is every second, by definition.

2. The utilization of the digital frame synchronizer in the video signal processing offers the possibility to achieve the Time of Coincidence every second for every program in the case of all 50 Hz TV systems with the same quality of dissemination of the time and standard frequency signals within the wide area TV system.

3. The described Time and TV Synchro System also offers the possibility for the correction of the propagation time variations encountered during the TV broadcasting over the geostationary TV satellite with the accompanying Time of Coincidence every second, and without any interference with the video signals.

REFERENCES

Howe, D. 1972 *"Nationwide precise time and frequency distribution utilizing an active code within network television Broadcasts", IEEE Trans. Instr. Meas., IM-21, 1972*

Kano, K. et al. 1974 *"Television Frame Synchronizer", Reprinted by SMPTE "Digital Video", pp. 74-79, New York, 1977*

Kovačević, B. 1973 *"The first experimental results of time and frequency dissemination via TV network" - JUKEM - Proc. 1973, XXV/13 Belgrade (in Serbocroat).*

1974 *"Time and its Measurements" Academy of Art and Science, 1974, Vol. 23, Belgrade (in French)*

1976 *"TV System and Time Synchronization" IBC-London 1976*

Palii, N. 1972 *"Experimental High Precision System for Transmitting Time Units and Frequency Over Television Channels", Izmeritel'naya Teknika, No. 1, pp. 34 - 37, 1972.*

Spilker, J. 1977 *"Digital Communications by Satellite", Prentice-Hall, 1977.*

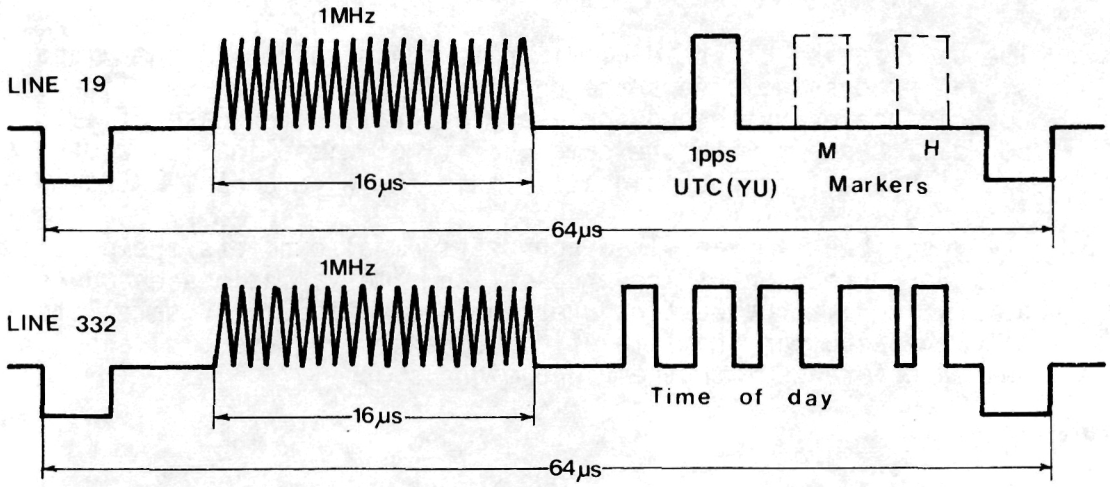


Fig. 1

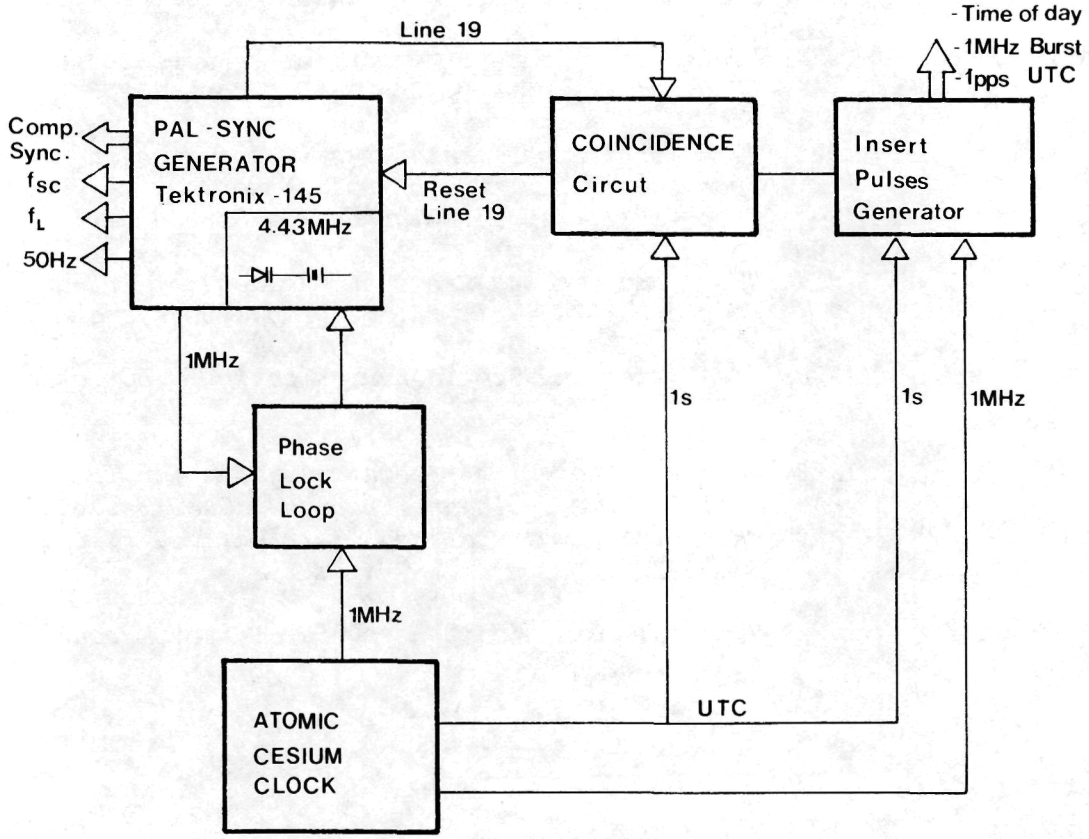


Fig. 2 - TIME and TV Synchro System

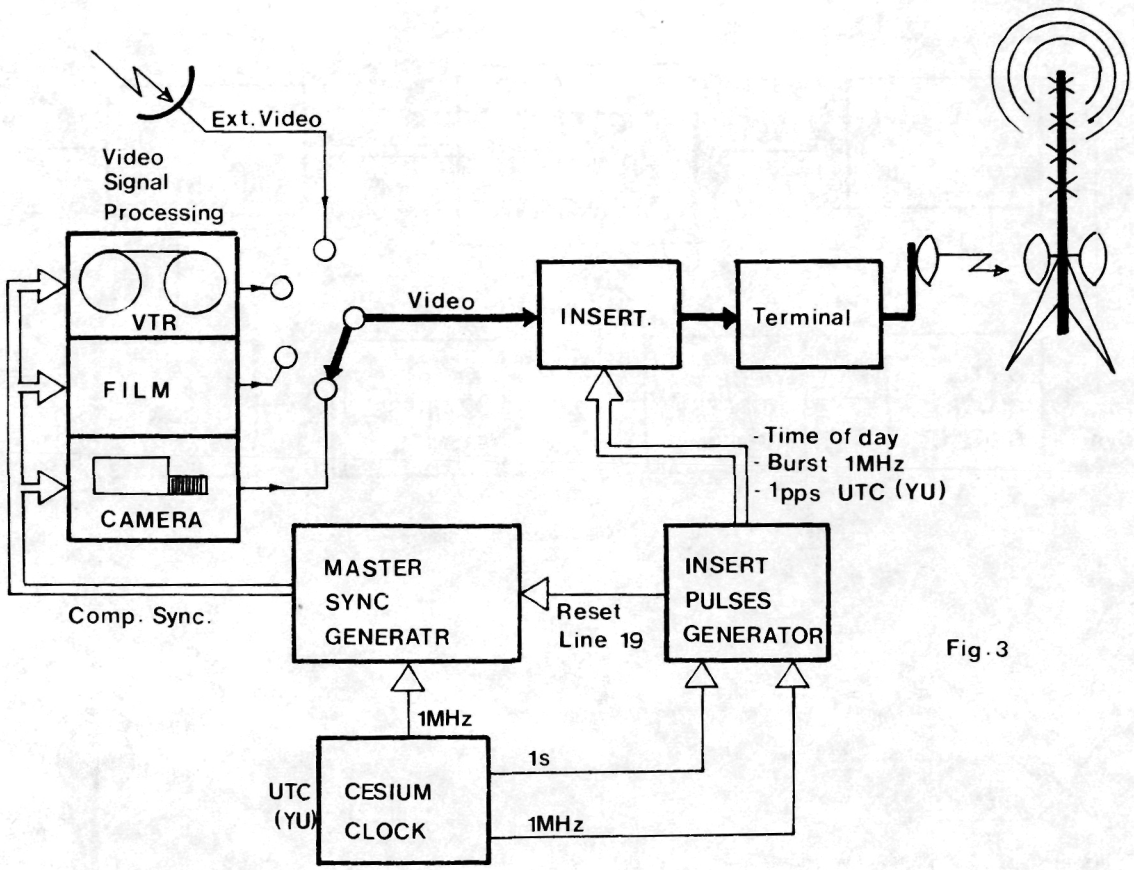

Ext. Video
Video
Signal
Processing
VTR
FILM
CAMERA
Video
INSERT.
Terminal
- Time of day
- Burst 1MHz
- 1pps UTC (YU)
MASTER
SYNC
GENERATR
Comp. Sync.
Reset
Line 19
INSERT
PULSES
GENERATOR
1MHz
UTC
(YU)
CESIUM
CLOCK
1s
1MHz

Fig. 3

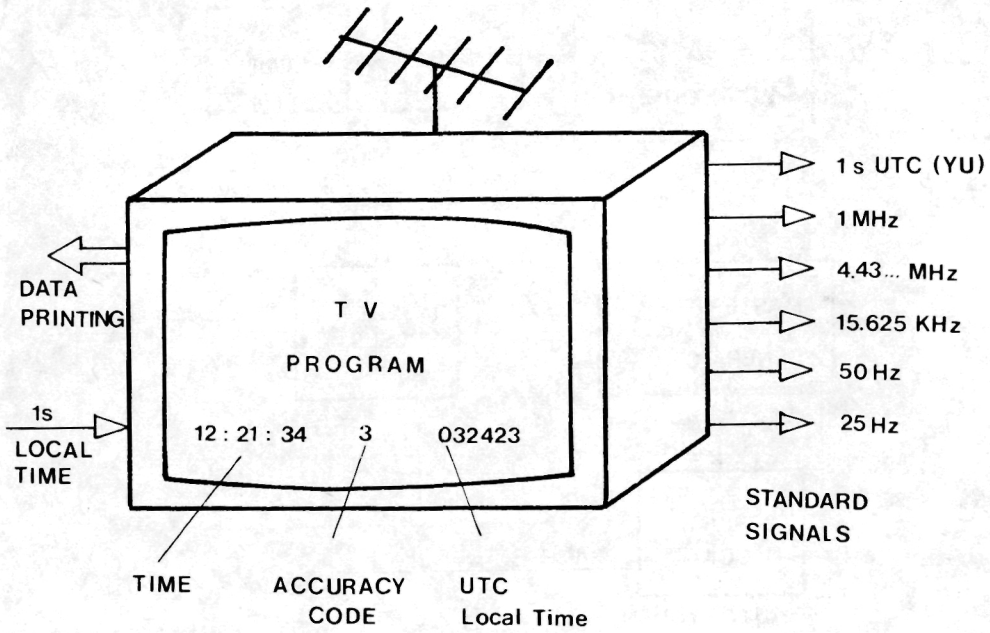

DATA
PRINTING
1s
LOCAL
TIME
T V
PROGRAM
12 : 21 : 34
3
032423
TIME
ACCURACY
CODE
UTC
Local Time
1 s UTC (YU)
1 MHz
4.43... MHz
15.625 KHz
50 Hz
25 Hz
STANDARD
SIGNALS

Fig. 4

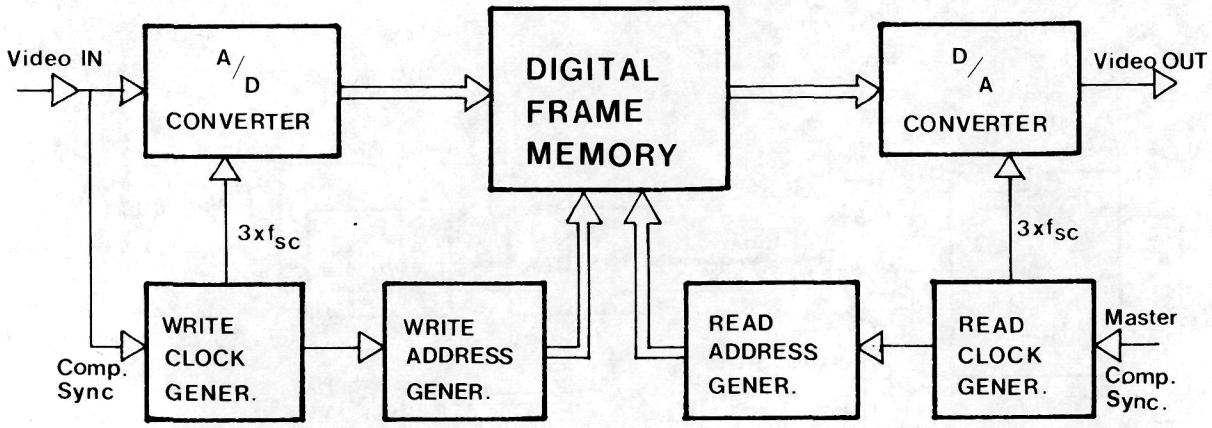


Fig. 5 - Frame Store Synchronizer

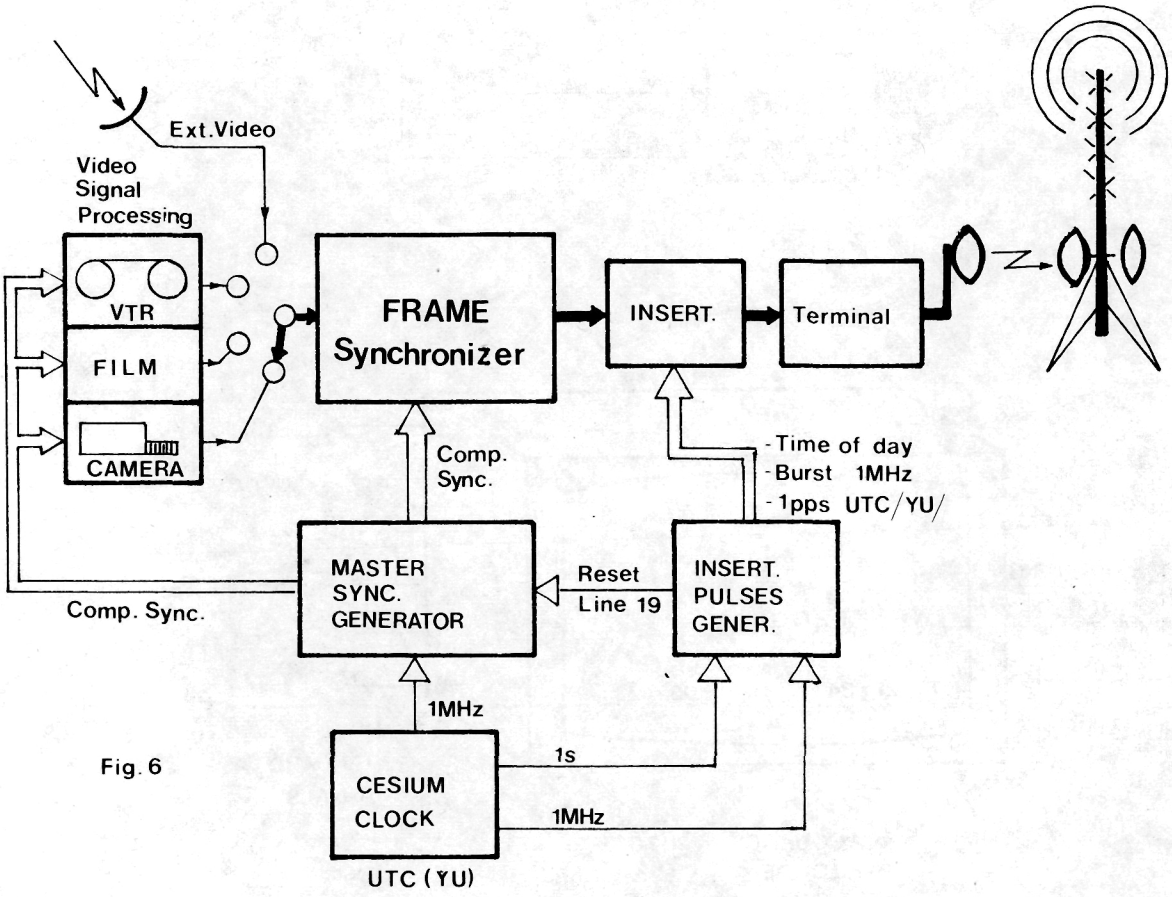


Fig. 6

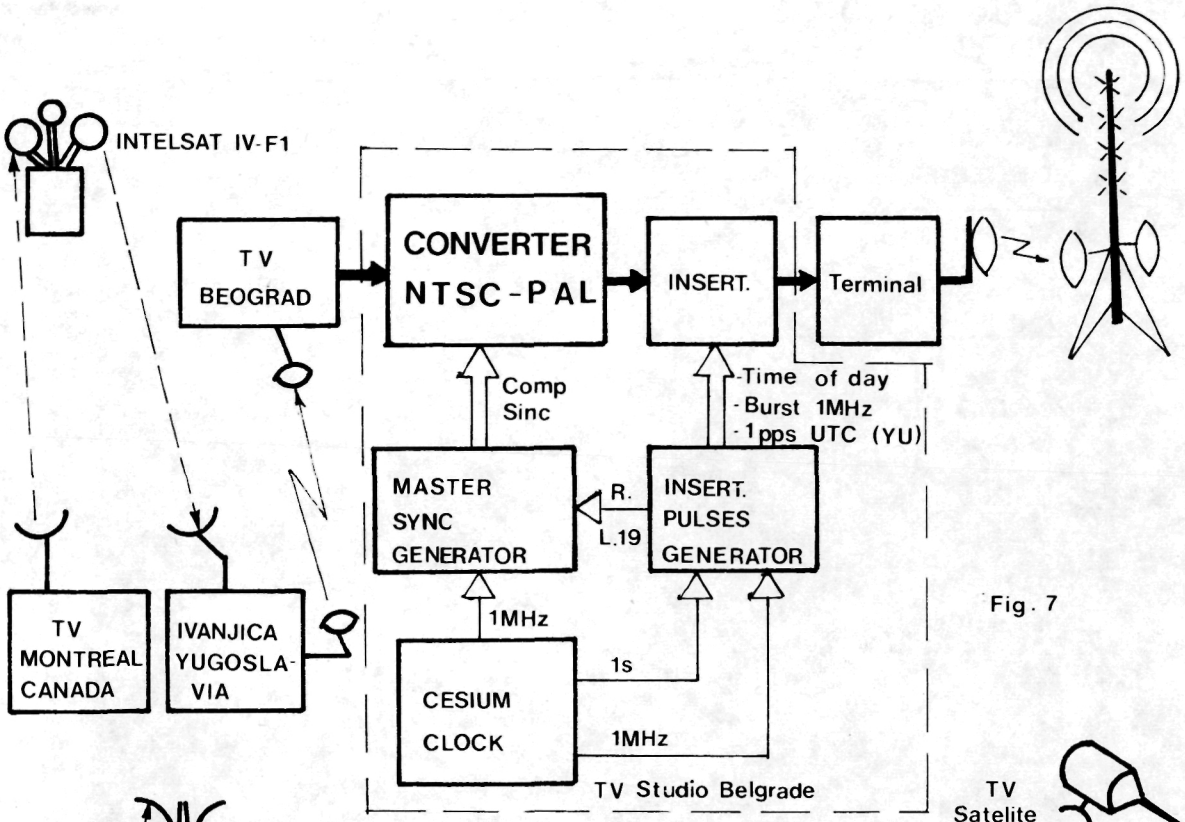


Fig. 7

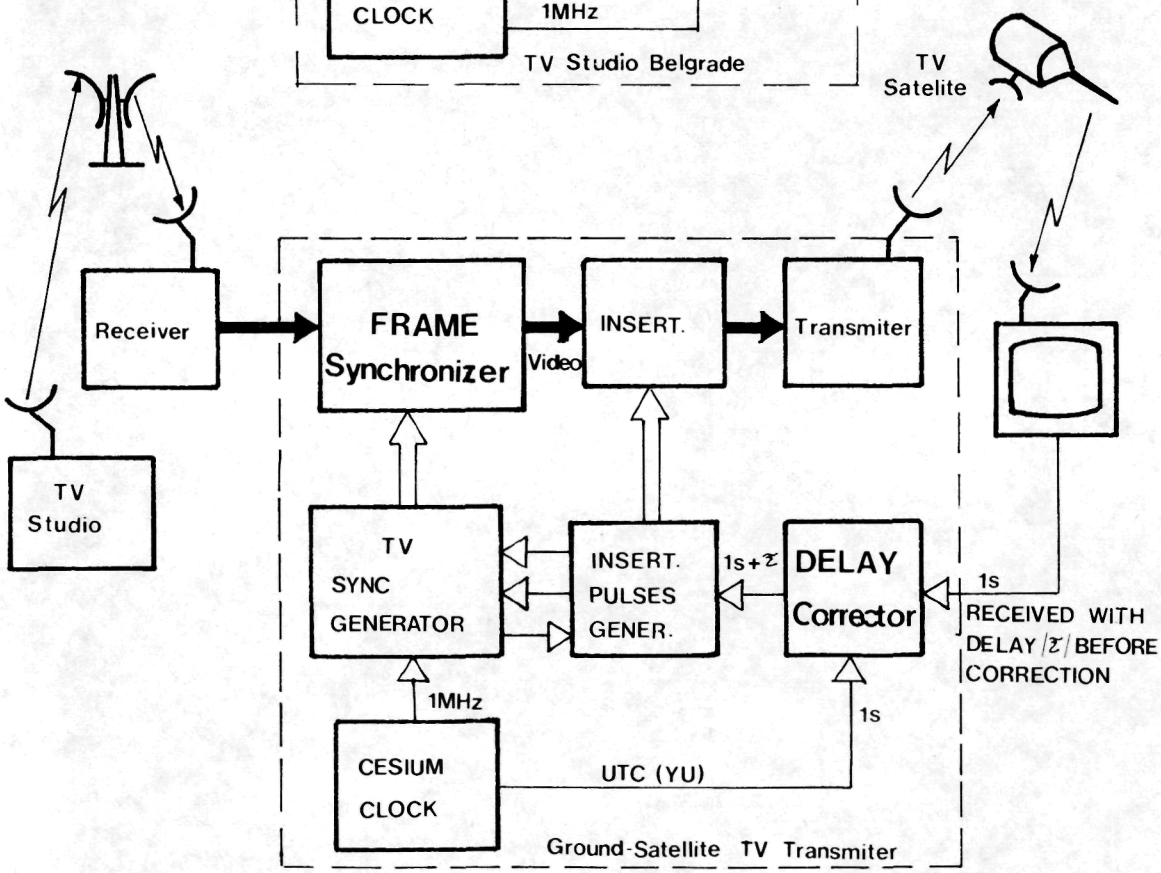


Fig. 8 - TIME DISSEMINATION VIA TV SATELLITE

Page intentionally left blank

Page intentionally left blank

INTERNATIONAL TIME AND FREQUENCY COMPARISON FOR LONG TERM VIA VLF AND LORAN-C

Yoshiyuki Yasuda, Haruo Okazawa, Kohsuke Akatsuka
and Toyoshi Matsuura

Frequency Standard Division
Radio Research Laboratories
Ministry of Posts and Telecommunication
Koganei, Tokyo, Japan

ABSTRACT

The results are given of the time and frequency comparison for about eight years between Radio Research Laboratories(RRL), Tokyo and the U. S. Naval Observatory(USNO), Washington, D. C. via the VLF transmission, NLK, on 18.6 kHz from Jim Creek, Washington and Loran-C transmission from Iwo-Jima.
The phase of the received signal from Jim Creek for daytime path showed a seasonal variation, and was the most stable in summer. The values of stability of frequency comparison, $\sigma_y(\tau)$, between RRL and USNO in summer were $\simeq 1 \times 10^{-11}$ and $\simeq 6 \times 10^{-13}$ for the averaging times of one day and one month, respectively. The long-term stability of the time comparison in summer was about 2 μs (1σ) for recent six years.
On the other hand, long-term stability of time comparison via Loran-C was as good as 0.3 μs for recent four years because of the improvement in the Loran-C monitoring system of the U. S. Coast Guard and USNO including the time transfer by satellites.

Reception of VLF transmission from NPG/NLK[1] commenced in 1964 at RRL and that of Loran-C from IWO-Jima in around 1965. The locations of transmitters of NLK and Loran-C and receving sites are shown in Fig. 1.

In the case of NLK, daily values of phase of the received signals at RRL[2] and USNO[3] for the daytime paths ($\sim$ 7700 km and $\sim$ 3700 km, respectively) are used, and they are shown by (a) UTC (RRL)-NLK and (b) UTC (USNO)-NLK in Fig. 2. Seasonal variations are found in (b) as

well as (a), the amplitude of the former is much larger than the latter. After removing the long-term drifts in (a) and (b), $\sigma_y(\tau)$ for UTC (RRL)-NLK and UTC (USNO)-NLK were calculated for winter as well as summer and plotted in Fig. 3 (a) and Fig. 3 (b). The difference of the phase values between (b) and (a) in Fig. 2 gives the relative time difference between USNO and RRL, and corresponding values of $\sigma_y(\tau)$ are plotted in Fig. 3 (c). The values for summer are as follows:

$$\sigma_y(1\ \text{day}) \simeq 1 \times 10^{-11}, \quad \sigma_y(10\ \text{days}) \simeq 1 \times 10^{-12},$$

and

$$\sigma_y(1\ \text{month}) \simeq 6 \times 10^{-13}$$

The values of the time difference between USNO and RRL, via Loran-C, are plotted at intervals of ten days associated with the values via portable clock of USNO. Relative variations are very small. Fig. 4 shows the variations of mean values for 90 days, centered on the summer solstice, of UTC (USNO)-UTC (RRL) via NLK (Fig. 2) relative to the corresponding mean values of that via Loran-C. Scatter of the values as a whole is as large as 10 μs in one sigma, but it is only 2 μs for the period 1972 to 1977 because an old homemade receiver was replaced in 1972 by a new commercial one (TRACOR 599-J). No significant correlation is found from Figs. 2 and 4 between the phase and the sunspot number in the long term.

Fig. 5 shows the relation between the amplitude of yearly variation of time difference and the sunspot number, but it is not evident whether the correlation exists or not, because the number of data is too small.

As to the Loran-C, the data analysis was made of the published values of time of emission from Iwo-Jima by RRL[2] and USNO [3] after 1969. Since the greater part of the propagation path from Iwo-Jima to Tokyo consists of sea water, day-to-day phase variations of the received signal at RRL have been 0.1 μs or so. Stability of the time difference between RRL and USNO via Loran-C, with respect to the time difference via the portable clock is shown in Fig. 6. The stability has been very good — about 0.3 μs (1σ) — because of the improvement in the Loran-C monitoring system of the U.S. Coast Guard and USNO including the time transfer by satellites.

Besides, the phase stability of several types of Loran-C receivers has been investigated in Japan by the Radio Research Laboratories and the Tokyo Astronomical Observatory. The analysis of four years of signal reception data from these two laboratories produced a standard deviation of less than 0.3 μs and indicated that the yearly mean could vary by as much as ± 0.3 μs, corresponding to a rate of about 1×10^{-14} for a year. The magnitude of the receiver delay instability is therefore not of great significance even in frequency comparisons among recent primary atomic standards [4].

References:

(1) Yoshio Azuma, Results of the phase measurement of VLF radio waves received from NPG/NLK, Journal of the Radio Research Laboratories, Vol. 13, No. 65, pp. 13-23, January 1966.

(2) Standard Frequency and time Service Bulletin, Radio Research Laboratories, Koganei, Tokyo, JAPAN.

(3) Daily Phase Values and Time Differences Series 4, U. S. Naval Observatory, Washington, D. C.

(4) CCIR Report 363-3 (Rev. 76).

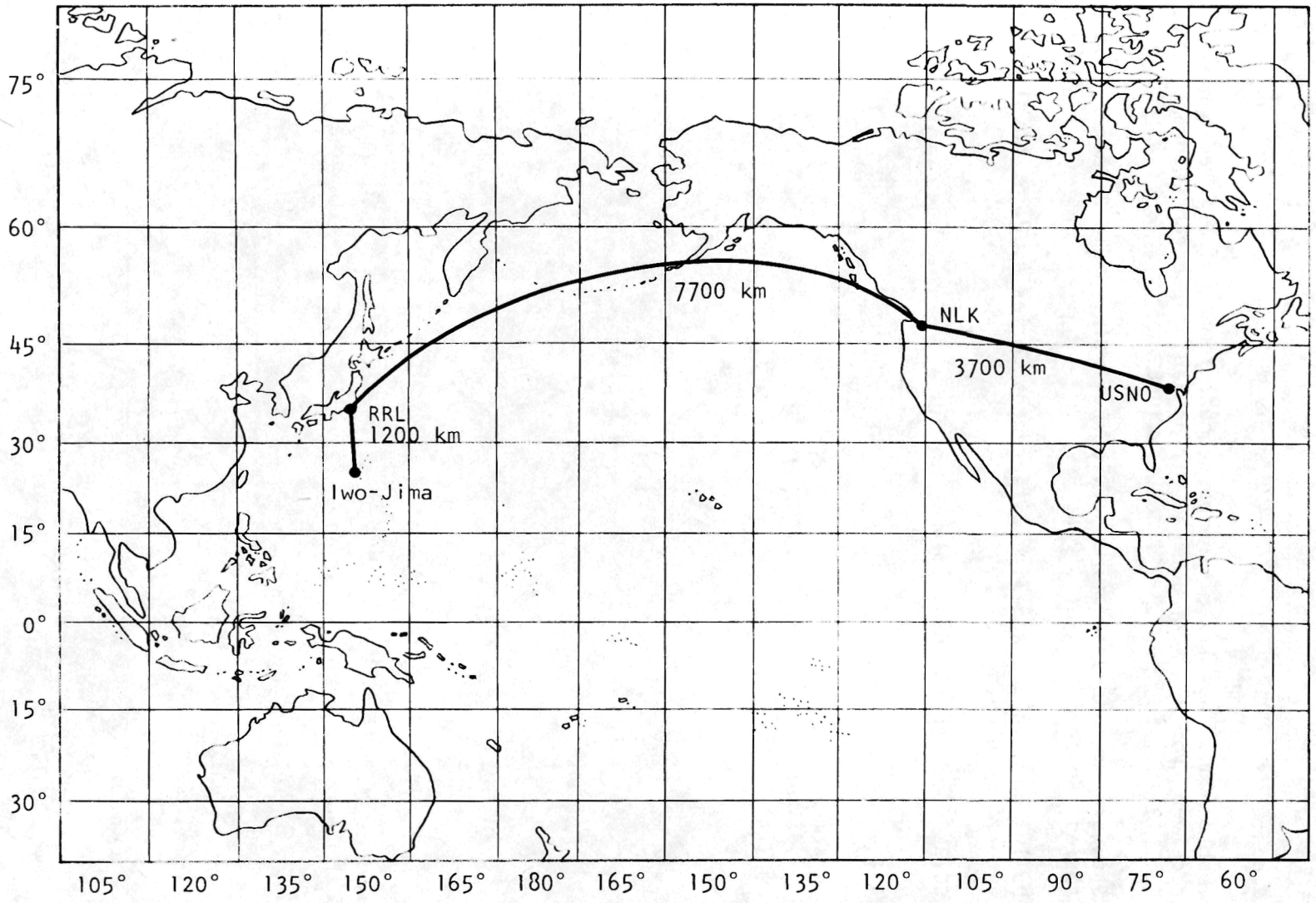


Fig. 1 Locations of transmitters of NLK and Lorna-C and receiving sites.

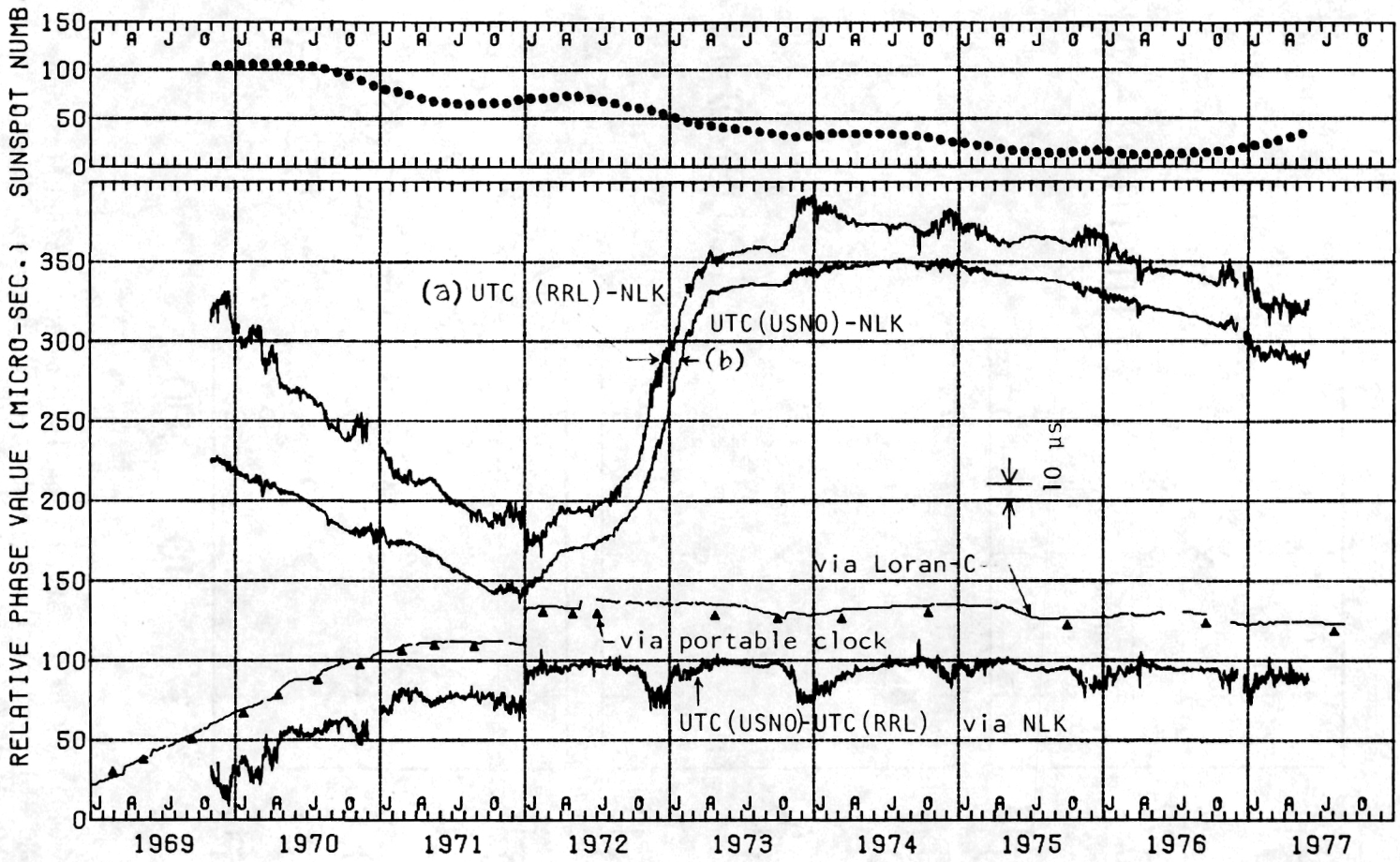


Fig. 2 Time comparisons between RRL and USNO via NLK, Loran-C and Portable clock.

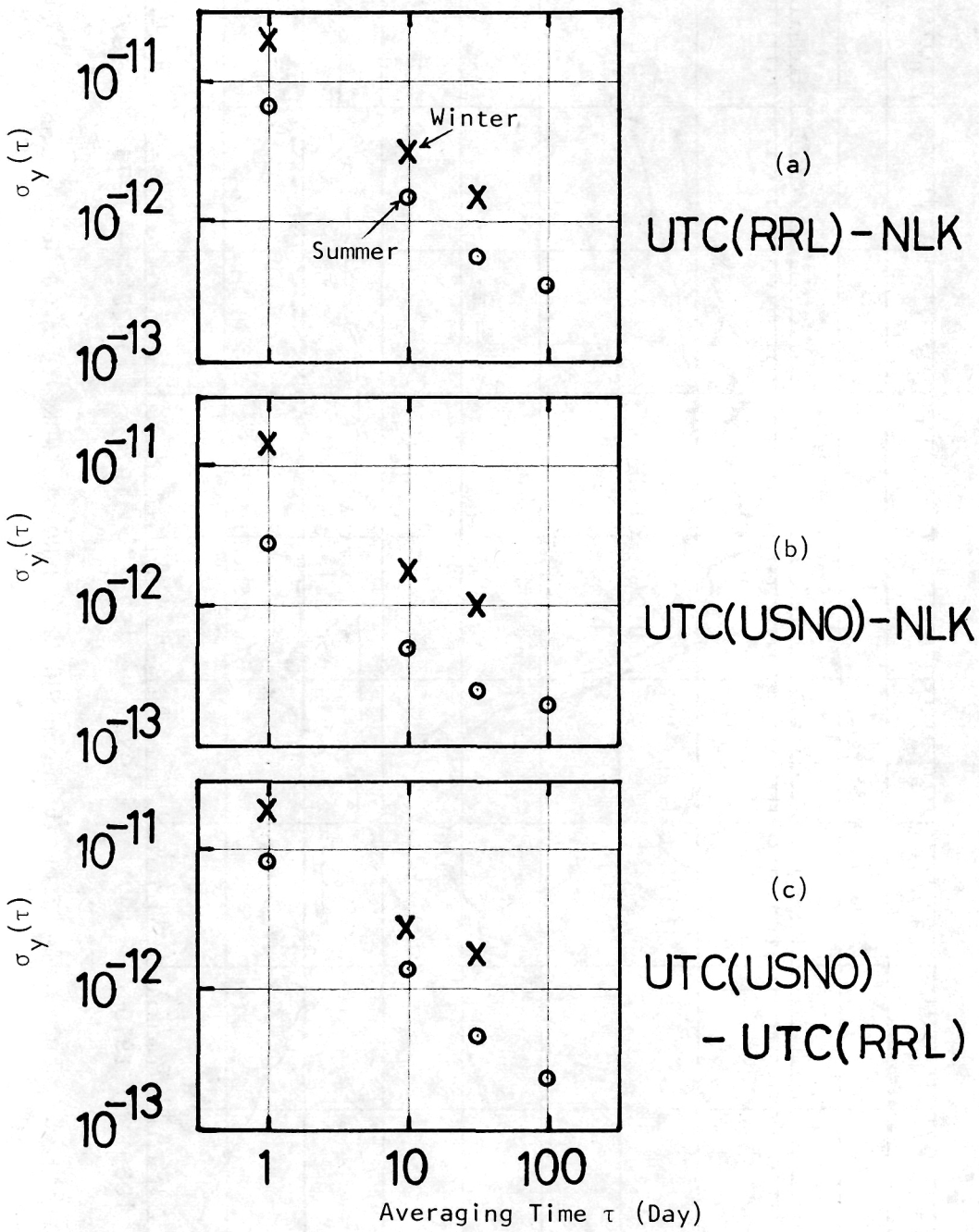


Fig. 3 Stabilities of received signals from NLK at RRL (a) and USNO (b), and of the time difference between RRL and USNO via NLK (c).

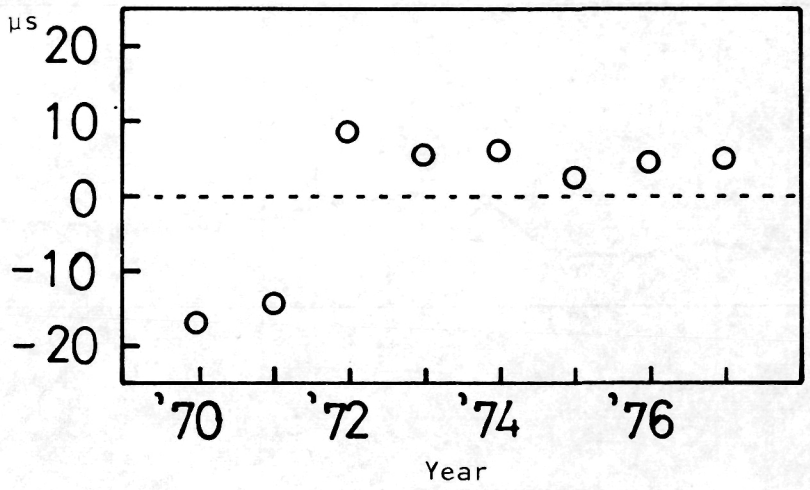


Fig. 4 Long-term stability of the time comparison via NLK relative to that via Loran-C.

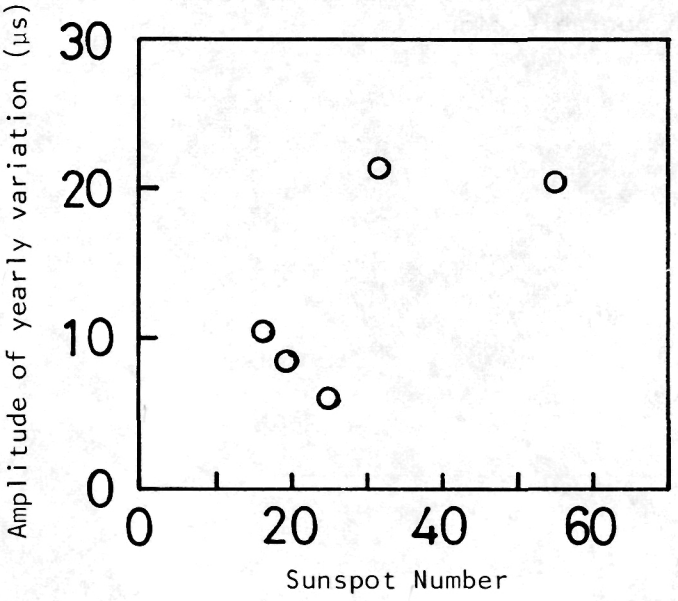


Fig. 5 Correlation between the amplitude of yearly variation of time difference and sunspot number.

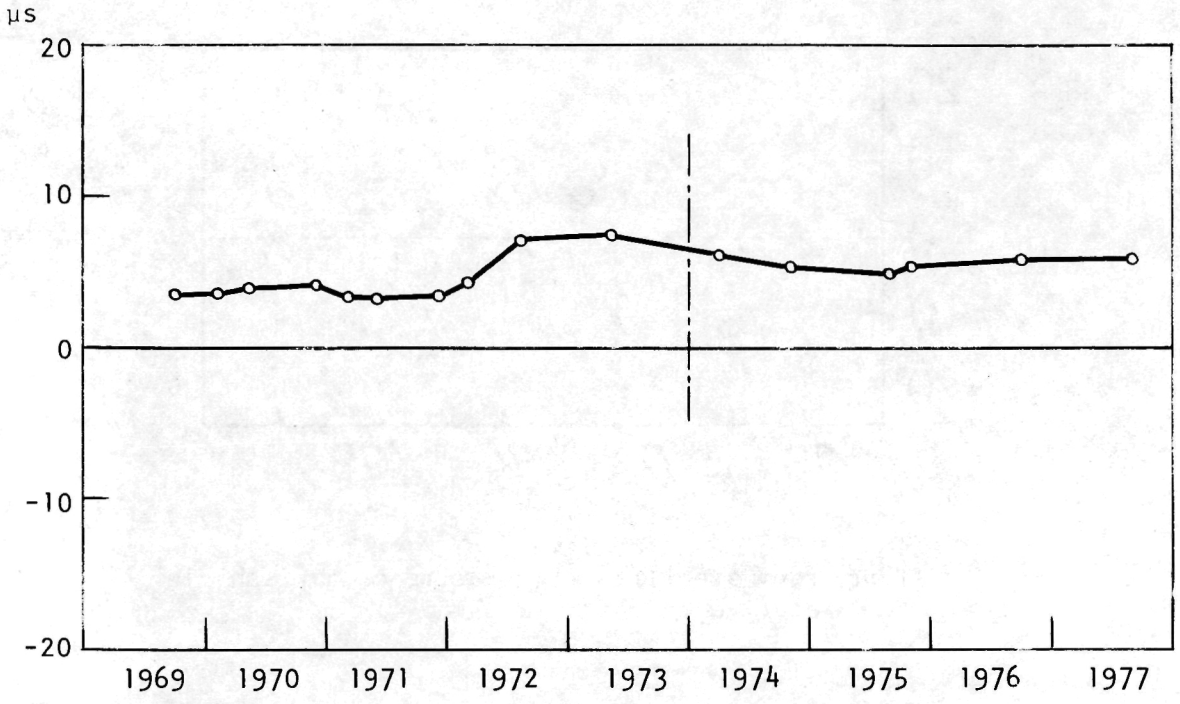


Fig. 6 Long-term stability of the time comparison via Loran-C relative to that via the portable clock.

DIURNAL VARIATIONS IN LORAN-C GROUNDWAVE PROPAGATION

Walter N. Dean, Magnavox Government and Industrial Electronics Company,
Fort Wayne, Indiana

ABSTRACT

Measurements have been made of the time of arrival of Loran-C groundwave signals propagated over a 1000 km land path in which diurnal variations of several hundred nanoseconds are observed. These variations are well correlated with air temperature along the path, but show a negative correlation with refractive index. Correlation with simultaneous measurements at other locations confirms it to be a propagation rather than equipment-related phenomenon. A relationship with the "dry" component of the refractivity is established, and an empirical algorithm is developed using surface weather data which reduces variations by a factor of 2.5.

INTRODUCTION

Temporal variations in the apparent propagation velocity of Loran-C signals have been observed for over 20 years (Ref. 1-8). Many of these variations have a diurnal as well as a seasonal character. Early measurements involved measuring the difference in the time of arrival of two signals, making it difficult to identify the source of the apparent variations. Recent data, however, represents single paths, using cesium standards at the receivers.

Using two AN/BRN-5 Loran-C receivers for a U. S. Coast Guard field test program, recordings of time-of-arrival (TOA) data from the U. S. East Coast Loran-C chain, relative to a local cesium standard, were obtained in the spring of 1977. Most of the data analyzed concerns the TOA of the Master signal from Carolina Beach, N.C., propagated over an approximately 1000 km path to Fort Wayne, Ind. Records from the National Weather Service (NWS) were obtained from the National Climatic Center in Asheville, N.C., in an effort to identify phenomena which could explain observed TOA variations.

INSTRUMENTATION

The instrumentation used, called the Precision Loran Data Collection System (PLDCS) by the Coast Guard, consists of a prototype model AN/BRN-5 borrowed from the Navy, an HP 2808 computer, an HP 5061 Cesium Standard,



Fig. 1 - PLDCS Configuration

and a TI ASR 733 keyboard-printer and cassette recorder. Figure 1 shows how these equipments were mounted. The antenna consisted of a 1.3 meter whip with a ground plane and an untuned transformer matching twin-conductor leadin.

The PLDCS is programmed to record a variety of signal and receiver status parameters at periodic intervals. These include signal TOA for three stations, two time differences, signal amplitudes, signal-to-noise ratios, and pulse envelope measurements. Most of the data collected were at 15 minute intervals.

After being recorded on cassettes, the data were transferred to an in-house disk system, and selected data plotted for easier analysis.

Selected TOA data from the U.S. Naval Observatory (USNO) Washington, D.C. and Newark AF Station, Ohio, were read visually from strip chart recordings and plotted manually for comparison with local data.

Weather data for selected locations obtained from the NWS were used in a BASIC program to calculate the index of refraction. Both surface and upper air (radiosonde) data were processed.

DATA COLLECTED

Most of the data analyzed consists of TOA measurements of the Loran-C master station at Carolina Beach, N.C. (see Figure 2). The 1000 km path to Fort Wayne is a mixed one of high and low conductivities. TOA measurements were made over periods of several days taken in February, March and April 1977.

OBSERVATIONS

Variations in TOA of several hundred nanoseconds were observed which tended to have a diurnal character. Explanations for these effects have been put forward, including:

1. Temperature effects in the receiver
2. Temperature effects at the transmitter
3. Skywaves
4. Index of Refraction

The BRN-5 receiver contains an automatic calibration system which measures and compensates for changes in phase shift through the receiver, to an accuracy of one nanosecond. Additionally, a recording of room temperature showed no correlation with TOA variations. Receivers at different locations showed similar variations. It is concluded that the receiver is not the culprit.

Changes in antenna characteristics could cause changes in the phase of the transmitted signal. However, a servo control loop at each transmitter

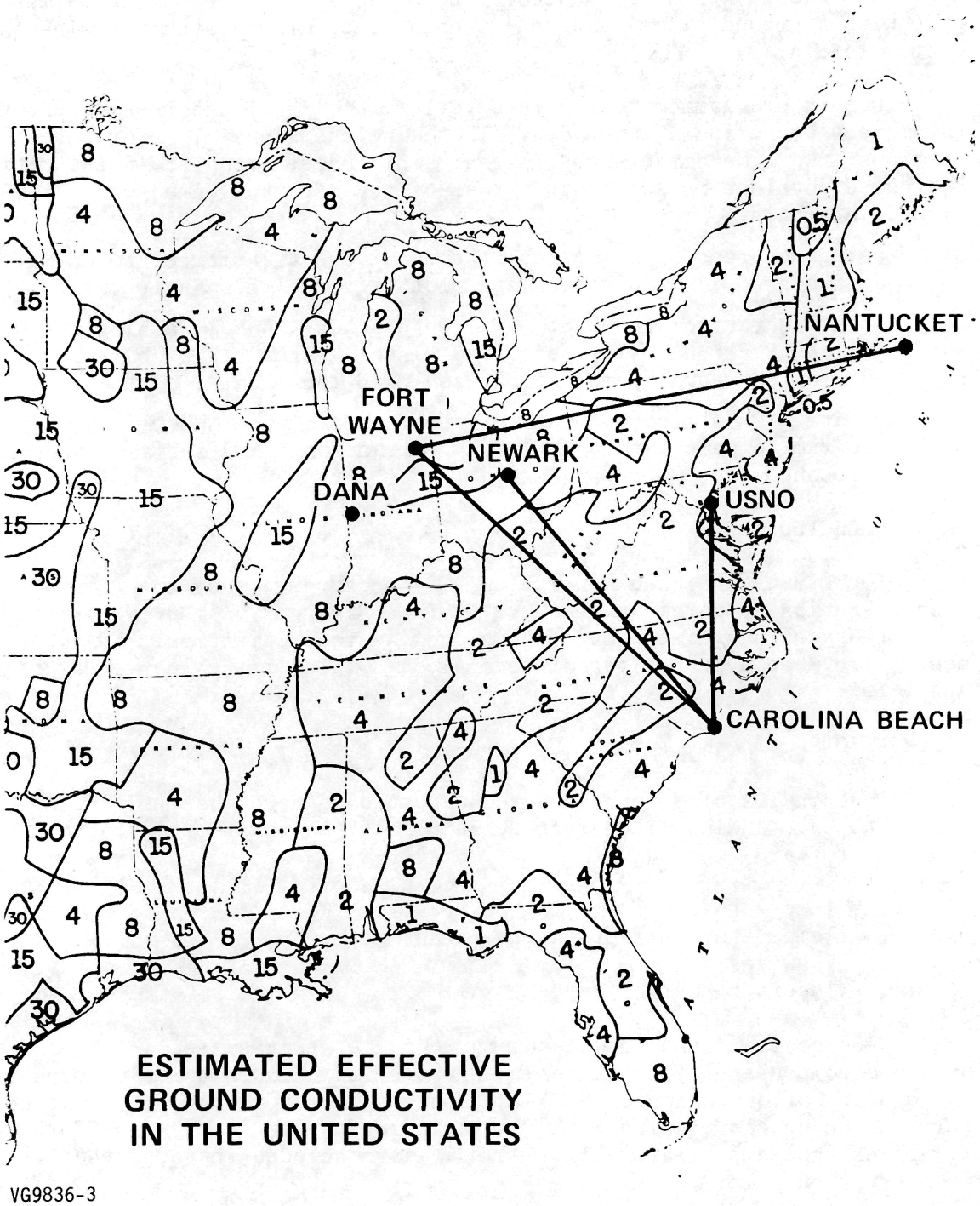


Fig. 2 - Measurement Area

continuously compares the phase of the transmitted signal with a local reference and adjusts the transmitter drive to maintain constant phase output. Also, if the variations were due to the transmitter, all receivers would see the same variation. Data from the USNO showed this not to be so. The transmitter is exonerated.

Skywaves have been suspected as the cause of the phase shift, but the tests proved this not to be so. The rationale is as follows.

Figure 3 shows the envelope of a Loran pulse, on a logarithmic amplitude scale, out of the BRN-5 receiver. Assuming an unheard-of worst case of a skywave delayed only 22 microseconds gives the dashed curve in Figure 3. Now, if a receiver is sampling at 45 μs, the skywave will be -20 dB, and a phase fluctuation of 317 ns could be encountered. If, simultaneously, a receiver is sampling at 30 μs, the skywave will be -60 dB, and fluctuations will be 3 ns.

Figure 4 shows the results of testing this hypothesis. The only apparent difference between the performance of the two receivers is the increased random fluctuations resulting from the 12 dB poorer signal-to-noise ratio of the receiver sampling at 30 μs. It follows that no skywaves are affecting the measurements at 45 μs.

To further test the hypothesis that the propagation velocity is varying, TOA data were obtained from two other locations, the U.S. Naval Observatory (USNO), Washington, D.C. and the Air Force Newark Air Station, Ohio. Figure 5 shows the Newark data compared with the Fort Wayne data. Figure 6 shows the measurements taken on two receivers at USNO compared to the Fort Wayne data. The degree of correlation is readily apparent. Also notable is the fact that the path to the USNO is approximately one-half the length of the path to Fort Wayne.

INDEX OF REFRACTION

The natural phenomenon that experiences relatively rapid temporal changes and can affect radio wave propagation is the index of refraction. Doherty and Johler (5) correlate propagation variations with variations in N-dry, and associate the phenomenon with changes in the α factor. Other observers (6, 9) have variously referred to lapse rate, or α factor, without numerical confirmation. These hypotheses are examined in more detail.

Travel time of the groundwave Loran pulse is given by the expression

$$\tau = \frac{dn}{c} + t_c \qquad (1)$$

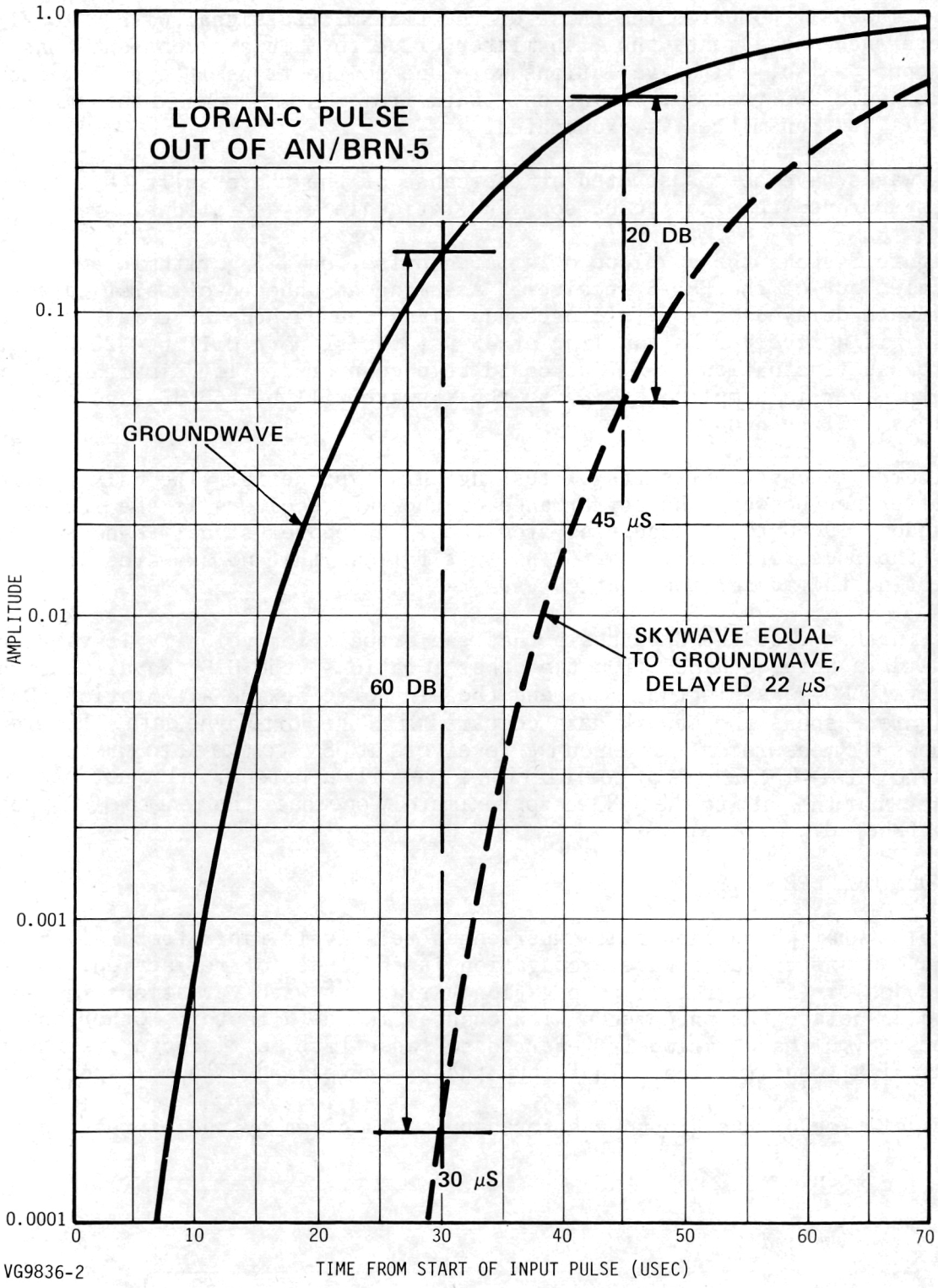


Fig. 3 - Loran Pulse Envelope

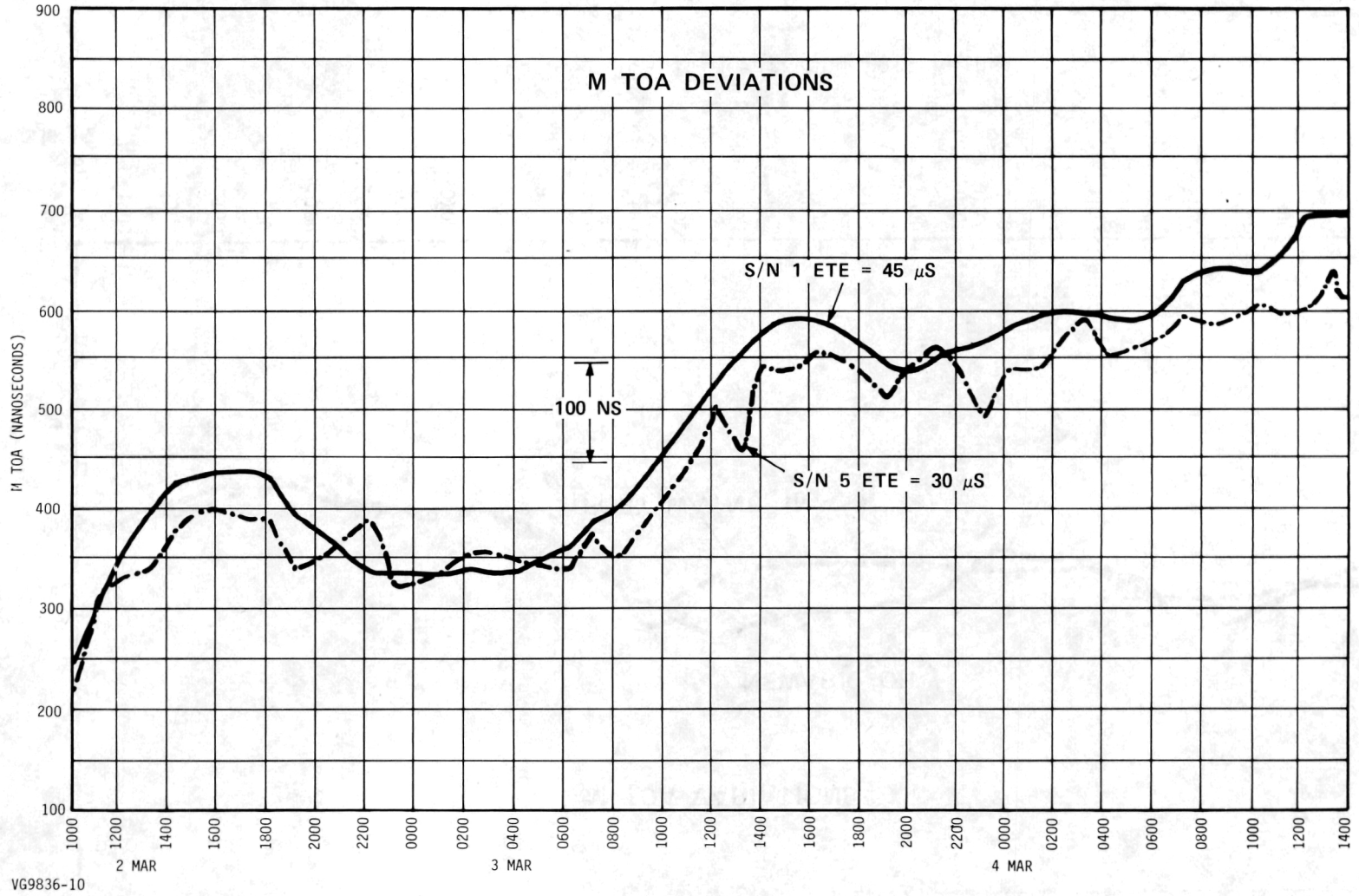


Fig. 4 - TOA Measured by Two References

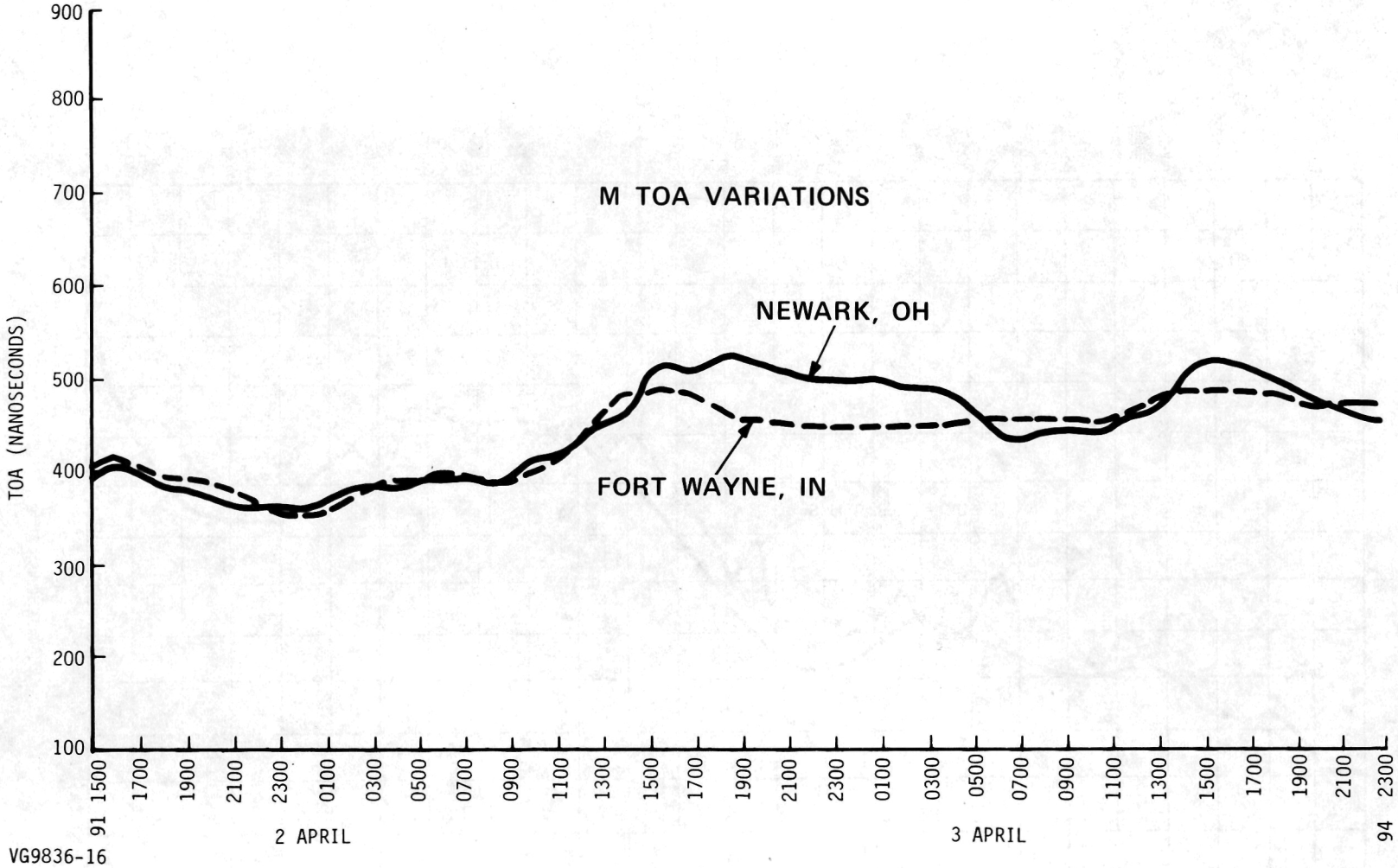


Fig. 5 - MTOA at Newark and Fort Wayne

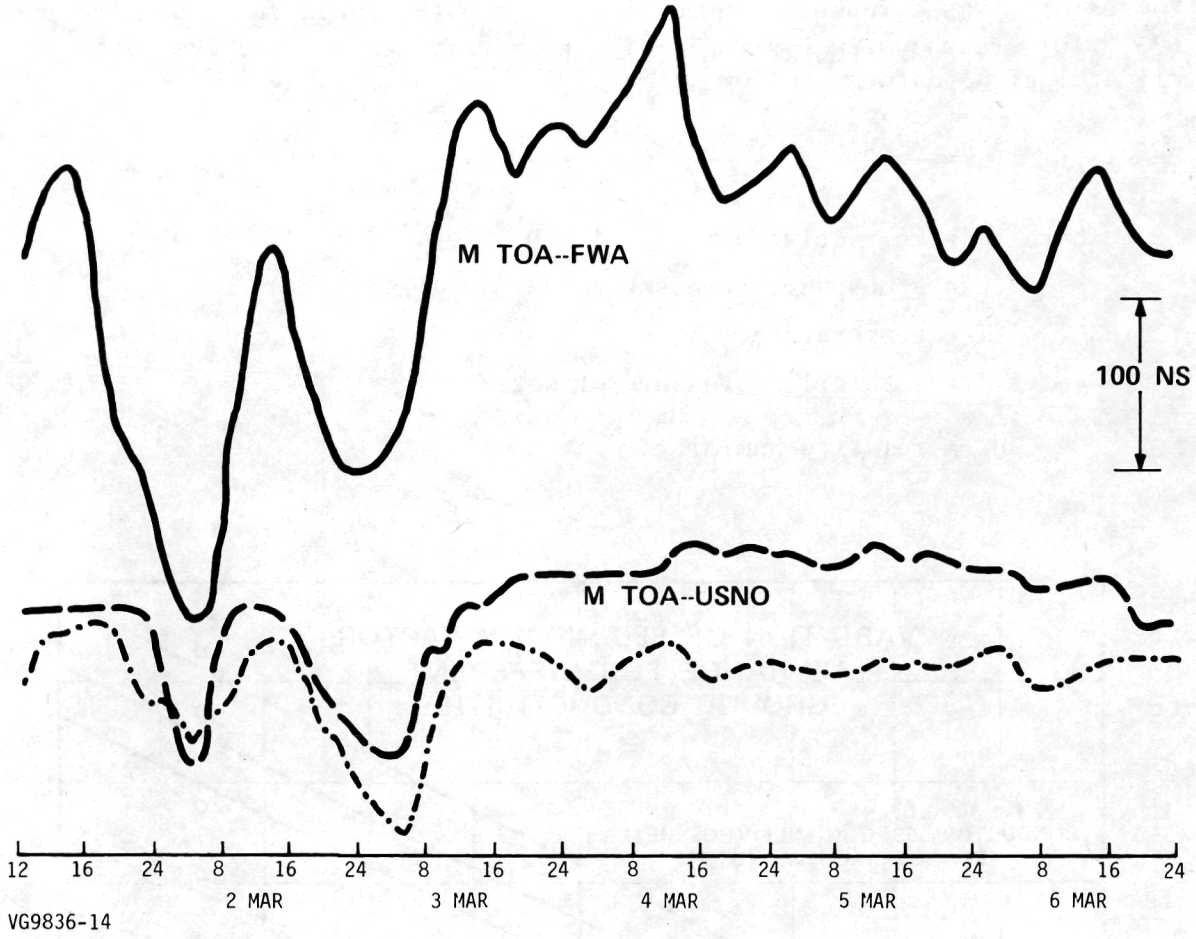


Fig. 6 - MTOA at NOBS and Fort Wayne

where τ = travel time in microseconds

d = distance in kilometers

c = velocity of light in kilometers per microsecond

n = index of refraction

t_c = secondary phase factor

Values of t_c as a function of earth conductivity, taken from NBS Circular 573, (10) are shown in Figure 7. Index of refraction is derived from climatological data as follows:

$$N = \frac{77.6\ P}{T} + \frac{3.76 \times 10^5\ e_s\ RH}{T^2} \qquad (2)$$

where N = refractivity = $(n - 1)\ 10^6$

P = atmospheric pressure

T = temperature, ^oK

e_s = saturation pressure of water

RH = relative humidity

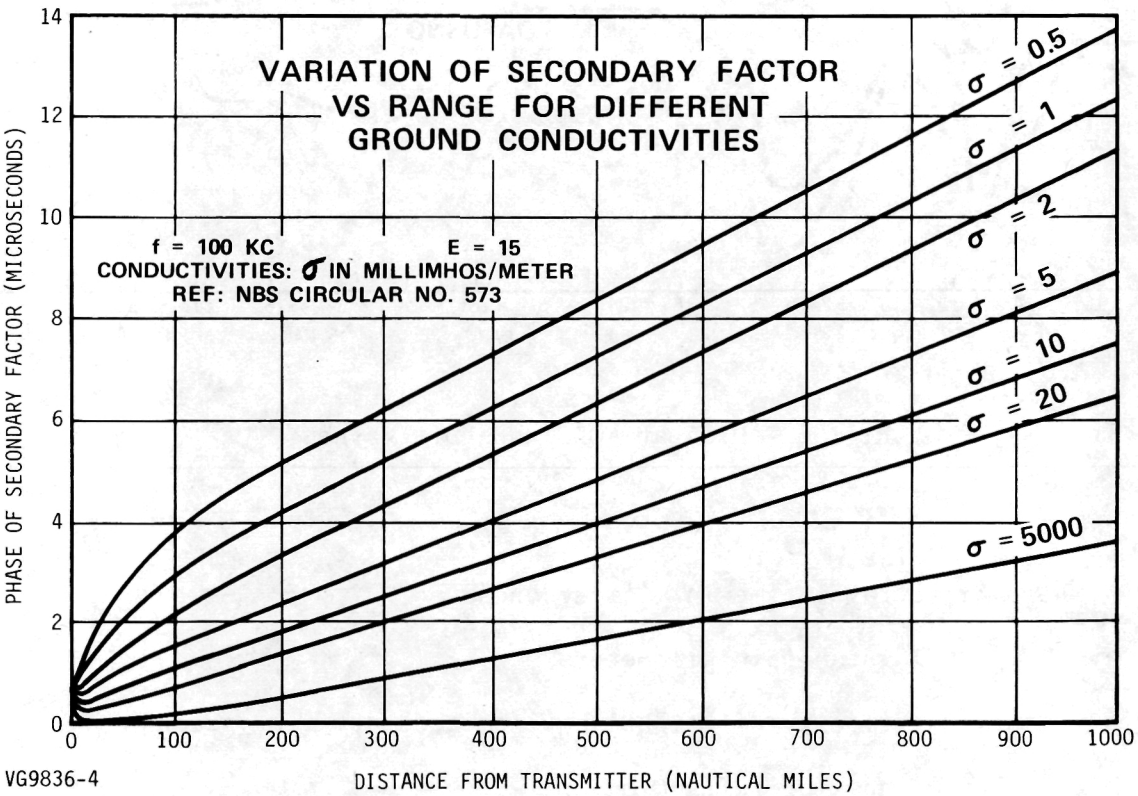


Fig. 7 - Variation of Secondary Factor vs Range for Different Ground Conductivities

The first term, sometimes called the "dry" term, represents 90 - 95% of the refractivity, while the second, the "wet" term represents the remainder. To test the correlation between N and the observed variation, consider the period 0800 - 1800 on 2 March 1977. The value of N along the path of propagation decreased 20 N units. According to equation 1, the propagation velocity should go up by 20 x 10^{-6}, and the propagation time from Carolina Beach to Fort Wayne should decrease 67 nanoseconds. Instead it increased 220 nanoseconds.

The explanation for this discrepancy is found in NBS 573, which indicates that the secondary factor t_c is also a function of the lapse rate of the refractivity.

Figure 10 of NBS 573 shows the variation of t_c with lapse rate in ΔN units per kilometer, for various distances over good earth (σ = 5 millimhos/meter). This shows that, as the lapse rate increases, t_c decreases. Re-plotting the data we find a linear relationship between the rate at which the change in lapse rate causes a decrease in t_c, and the distance. This is shown in Figure 8. On the assumption, to be discussed later, that the lapse rate is directly related to the surface value of N, a second curve is shown in Figure 8 representing the net phase delay correction taking into account the effect of refractivity on wave velocity.

Lapse rate of the refractivity can be calculated from data collected by radiosonde by NWS. Unfortunately, these measurements are made, because of the cost, only at relatively few selected places and times.

Examples of refractivity lapse rates calculated from data taken twice daily at Dayton, Ohio are shown in Figure 9. It had been hoped that some relationship between refractivity at the surface and the lapse rate would be observed, but none is obvious. A plot of the lapse rate of temperature, Figure 10, shows another erratic pattern.

The dry term of the refractivity, however, is something else. Figure 11 shows the lapse rate of N-dry for the same period as Figures 9 and 10. The value of N-dry at one kilometer above the ground is approximately equal to 250, independent of the value at the ground. Data at other stations and times confirm this. This means that an estimate of the lapse rate of N-dry for the first kilometer of height can be obtained from the value of N-dry at the surface by the simple relationship

$$\frac{\Delta N}{km} = \text{N-dry} - 250 \qquad (3)$$

Having found a convenient way to find the lapse rate of N-dry, it is relevant to test the hypothesis that it is this change in lapse rate of N-dry which causes the variation in propagation time. Variations in propagation time from Carolina Beach to Fort Wayne (MTOA) during the period 1 -

6 March 1977 are shown in Figure 12 along with variations in air temperature at a point near the propagation path, Roanoke, Va. A high degree of correlation is apparent. This correlation between propagation time and temperature has been observed many times over the past 20 years.

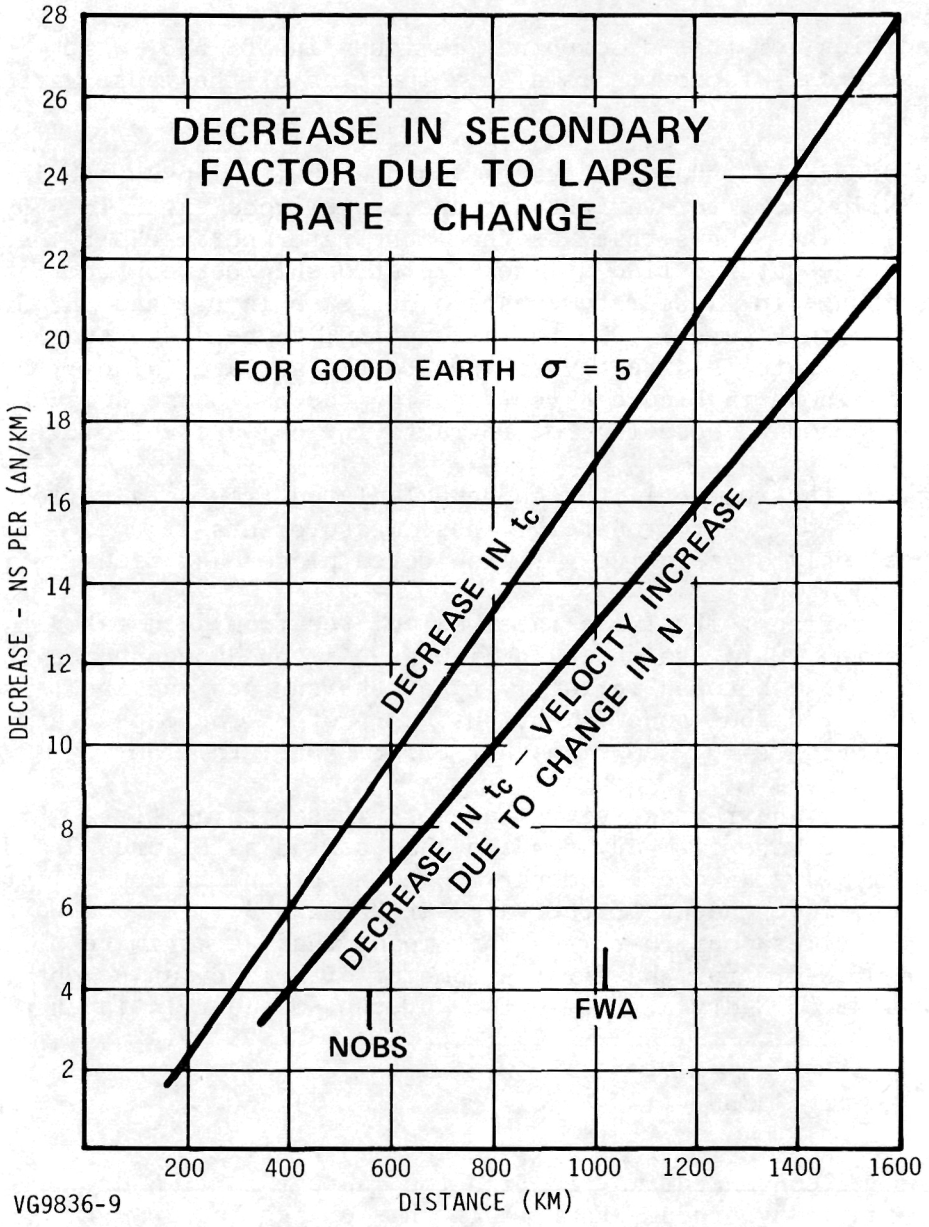


Fig. 8 - Decrease in Secondary Factor due to Lapse Rate Change

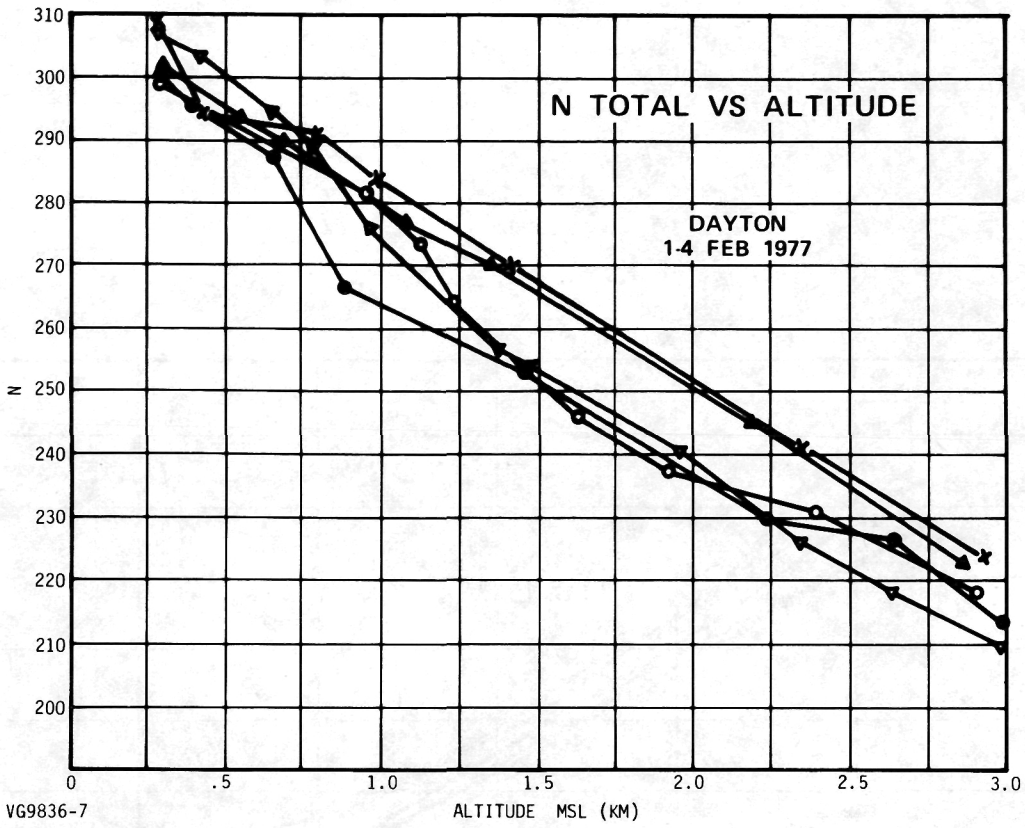


Fig. 9 - Lapse Rate of N at Dayton

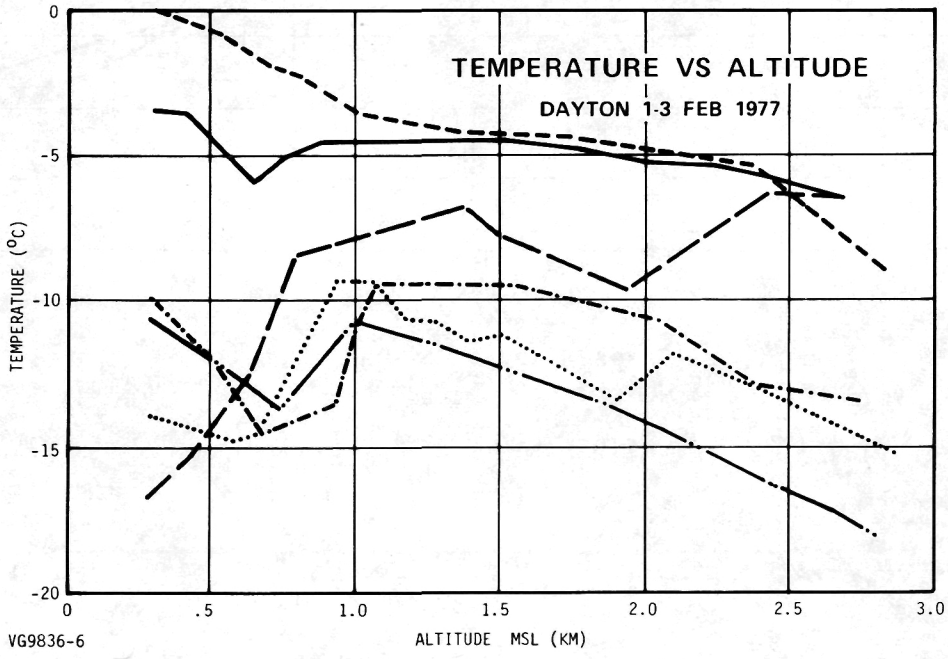


Fig. 10 - Lapse Rate of Temperature at Dayton

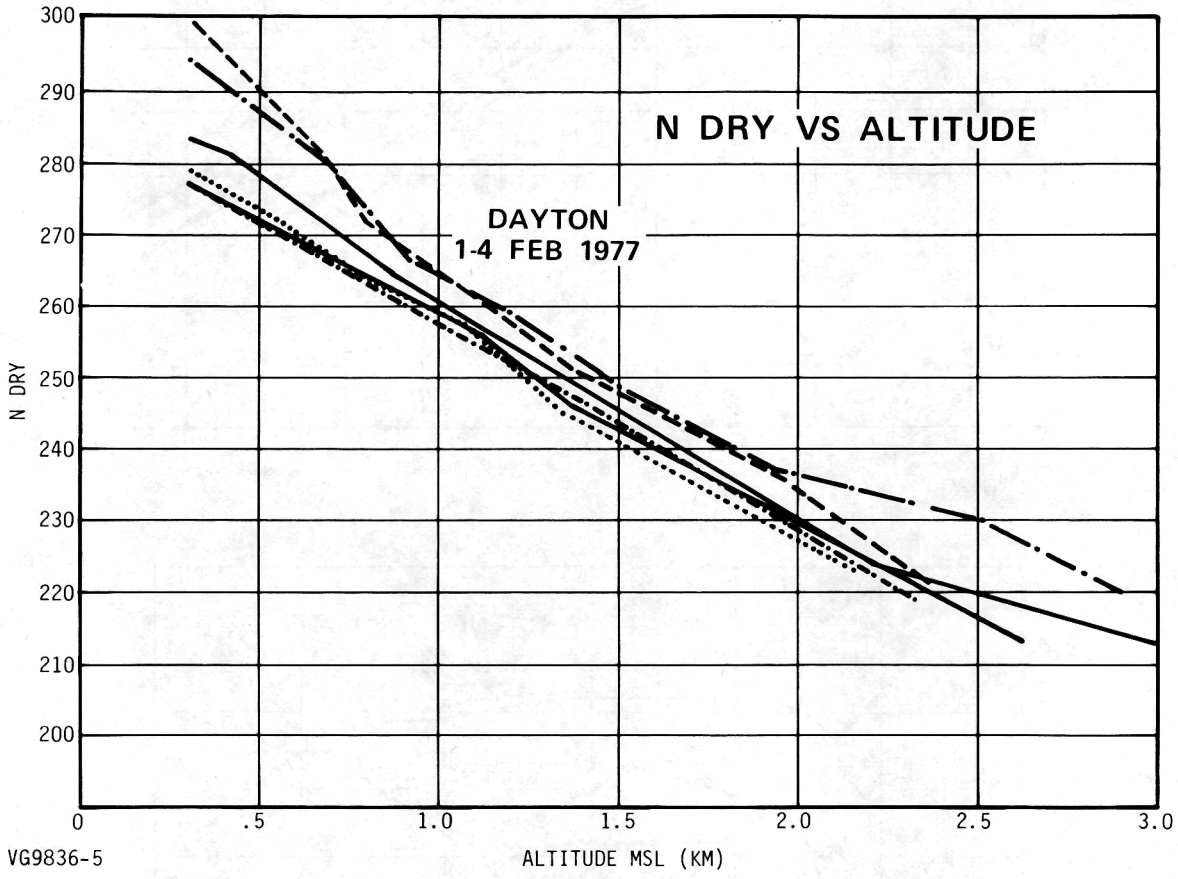


Fig. 11 - Lapse Rate of N-Dry at Dayton

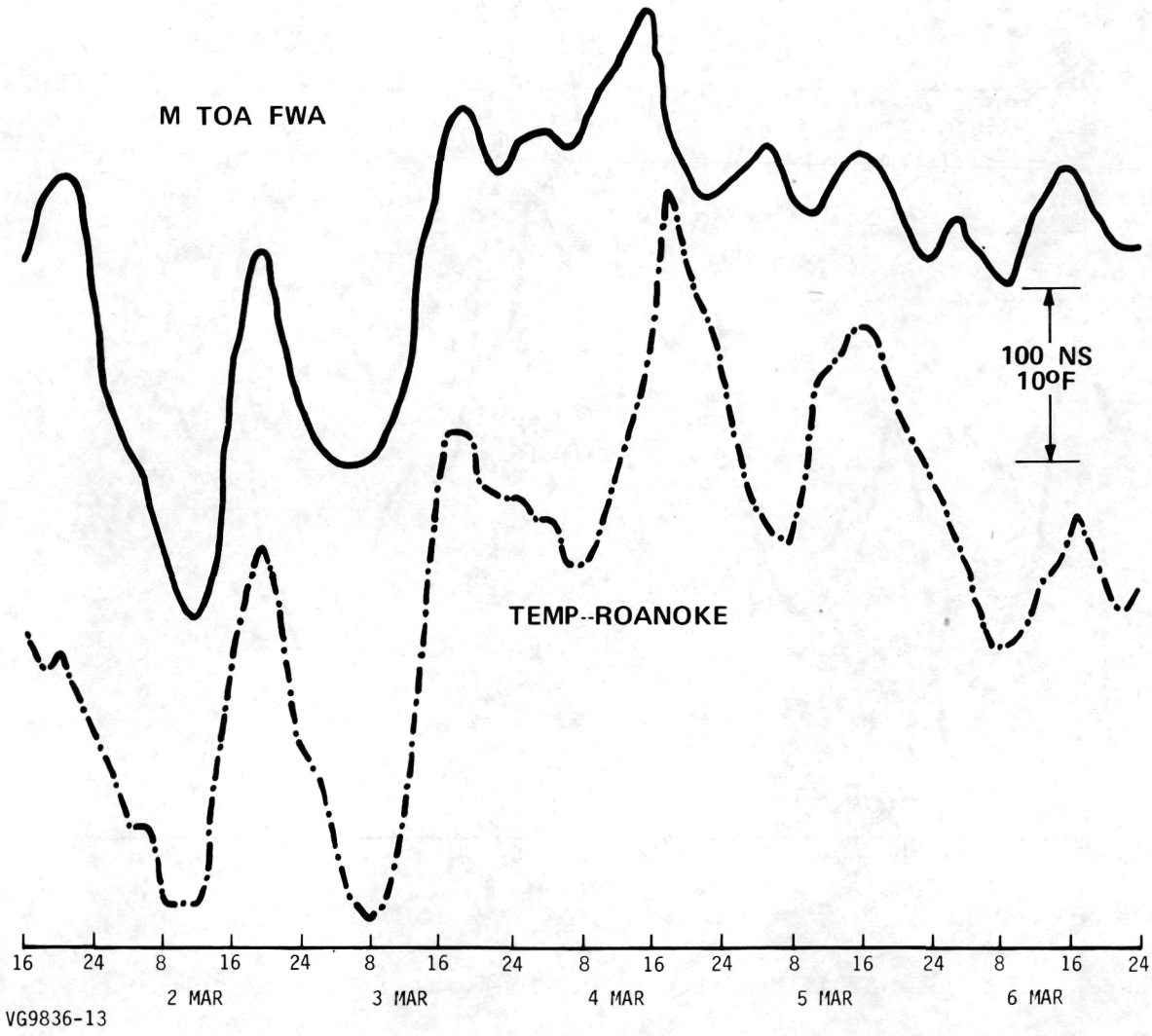


Fig. 12 - MTOA at Fort Wayne and Roanoke Temperature

Figure 13 shows the same variation in arrival time and the variation of refractivity (N-total) at Roanoke. It is obvious that the correlation of N-total is not nearly as good as that of temperature. Figure 14 shows the same MTOA data with N-dry at Roanoke. The high degree of (negative) correlation is obvious.

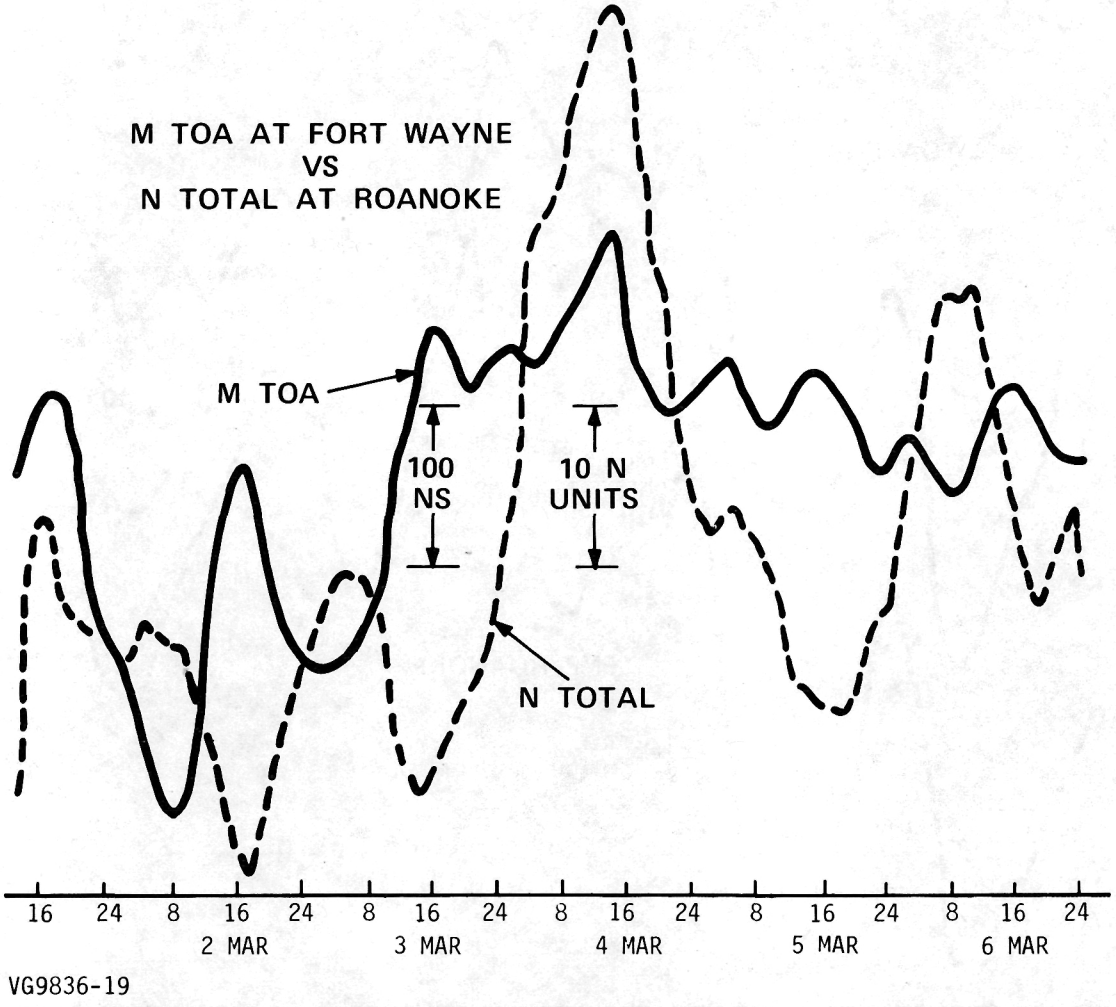


Fig. 13 - MTOA at Fort Wayne and N-Total at Roanoke

To further test the hypothesis that the changes in propagation time are correlated with N-dry, the curve of Figure 8 was combined with the approximation for lapse rate to give the following relationship for propagation time correlation.

$$\Delta t = (.015d - 2)\ (Ndry - 250) \text{ nanoseconds} \qquad (4)$$

where d is the path length in kilometers

$$Ndry = \frac{77.6\ P}{T} \quad \text{(from Equation 2)}$$

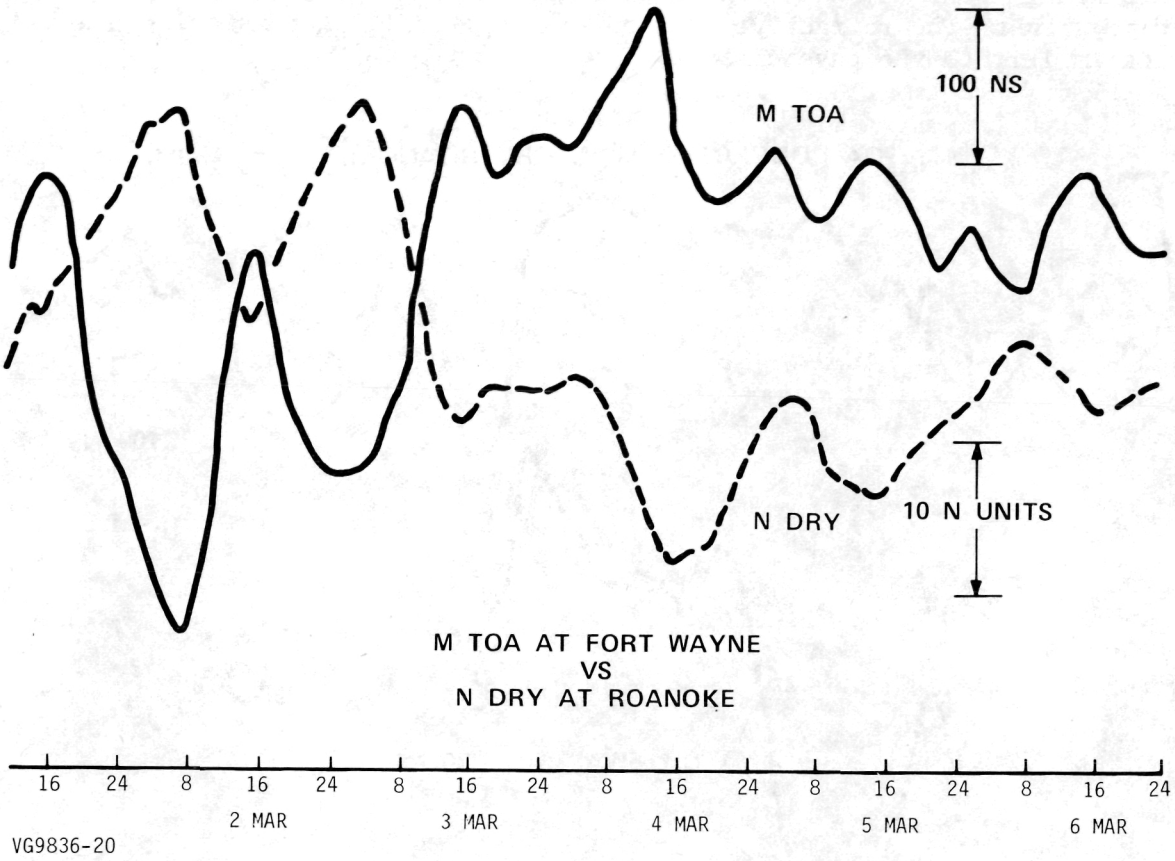


Fig. 14 - MTOA at Fort Wayne and N-Dry at Roanoke

Figure 15 shows the MTOA data of 1 - 6 March corrected by the above formula, using pressure and temperature data from Roanoke. The RMS fluctuation is decreased by a factor of 2.

Huntington, W. Va. is located closer to the center of the Carolina Beach - Fort Wayne path than Roanoke. Using data from that station produces results shown in Figure 16. The RMS fluctuations after correction are reduced to 30% of the original.

CONCLUSIONS

It has been shown that observed variations in time of arrival of Loran-C signals which tend to have a diurnal character are caused by changes in effective propagation velocity and not by hardware or by skywave interference. Further, the correlation with the "dry" term of the refractivity along the path has been established. A relationship of the dry term at the surface to the lapse rate, and therefore to changes in second phase factor, has been shown. A numerical expression capable of reducing fluctuations over a 1000 km path by a factor of 2.5, using surface weather

data along the path, has been demonstrated. The rationale for use of the "dry" term of the refractivity is purely empirical. A physical explanation is left to the physicists.

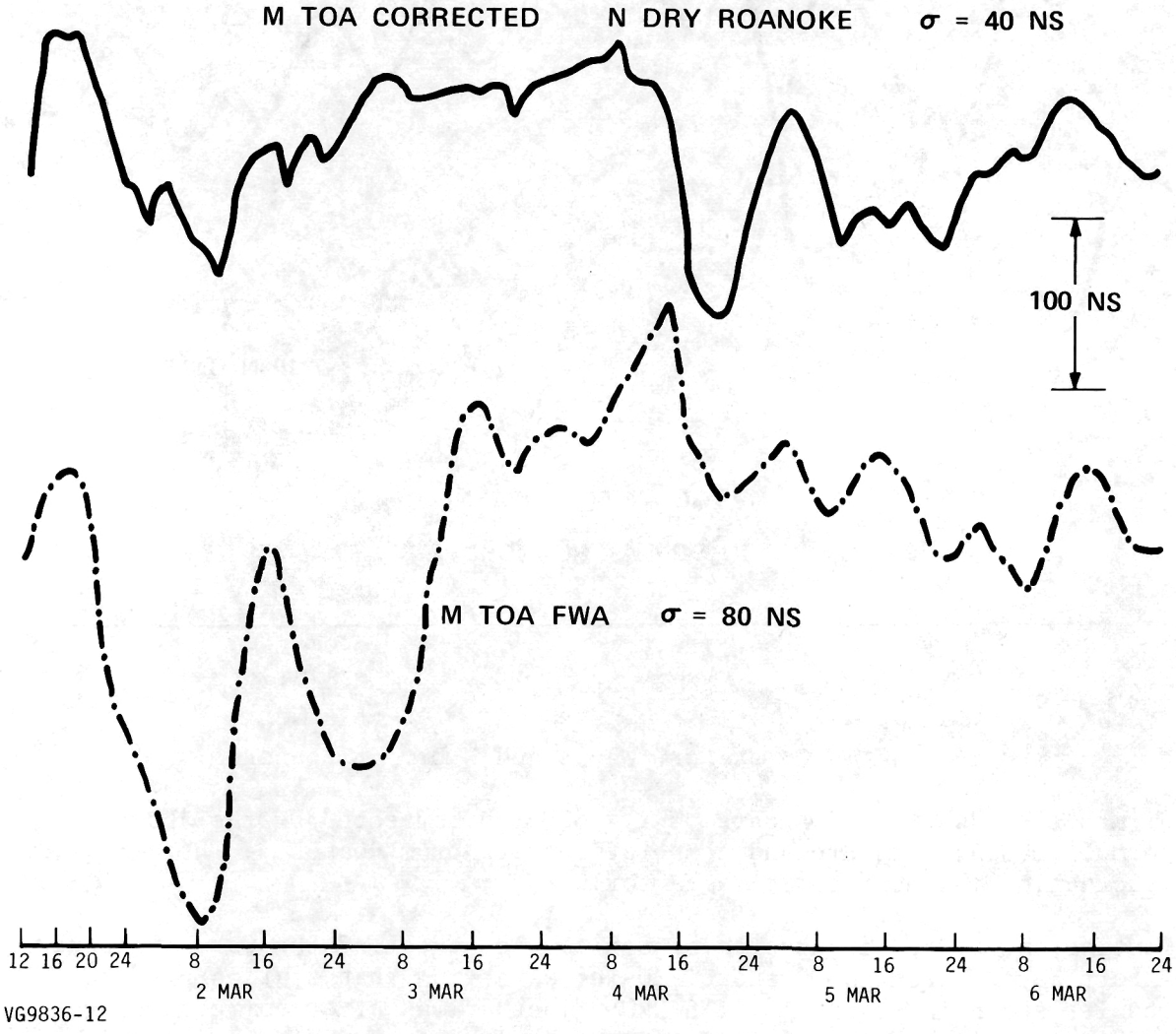


Fig. 15 - Correcting MTOA using Roanoke Weather

ACKNOWLEDGEMENT

The data collection and anlaysis were supported, in part, by U.S. Coast Guard R&D Contract DOT-CG-79042-A.

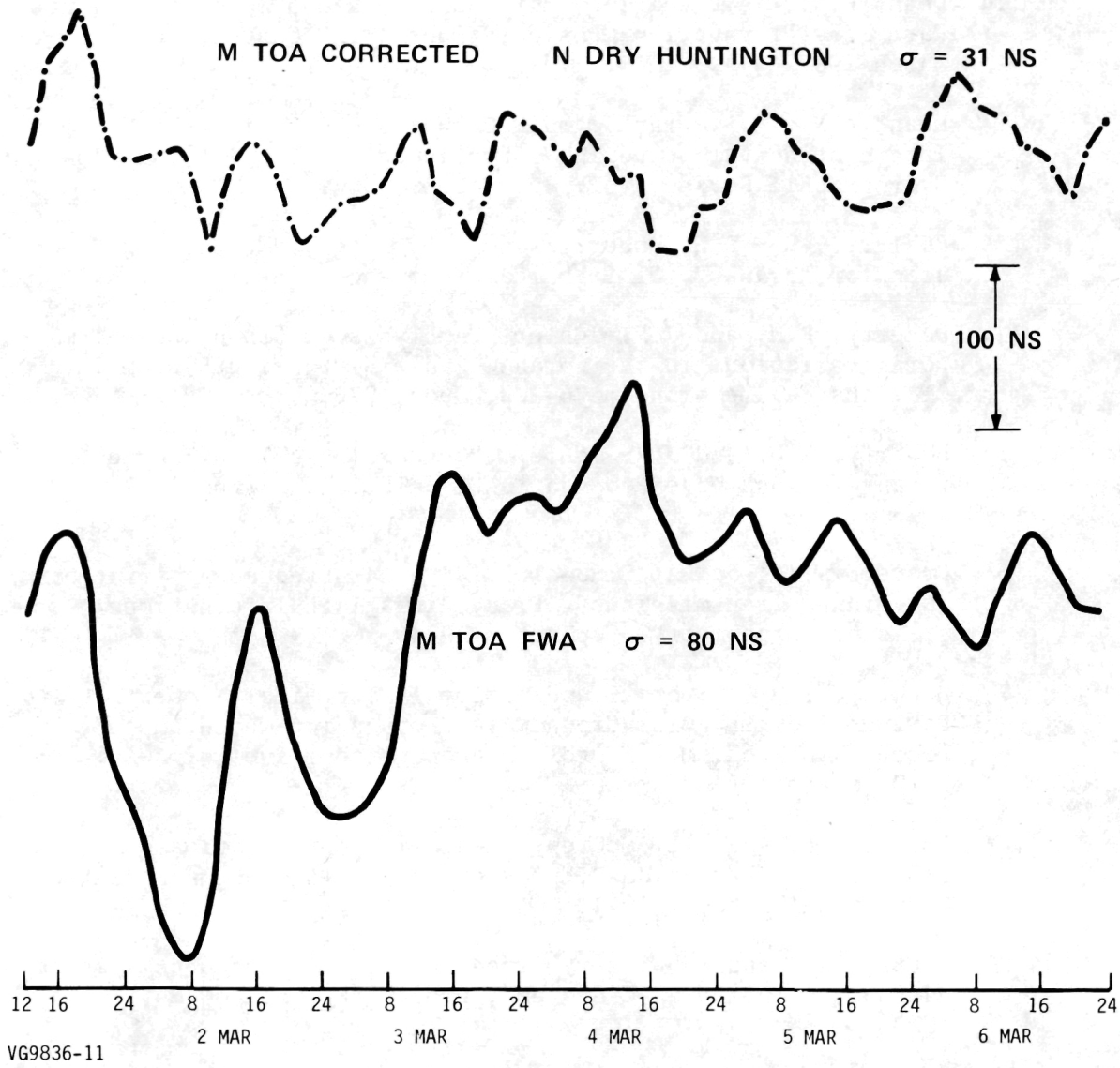


Fig. 16 - Correcting MTOA using Huntington Weather

REFERENCES

(1) Dean, W.N., "A Precision Multi-Purpose Radio Navigation System - Part II - Propagation Considerations", IRE Convention Record, March 1957.

(2) Dean, W.N., R.L. Frank, and P.C. Watts, "Use of Loran-C for Intercontinental Surveying", Supplement to the International Hydrographic Review, Vol. 3, October 1962.

(3) Johler, J.R., R.H. Doherty, and L.B. Burch, "Nanosecond Precision for Loran-C", OT Technical Memorandum 76-216, March 1976.

(4) Doherty, R.H. and J.R. Johler, "Analysis of Ground Wave Temporal Variations in the Loran-C Radio Navigation System", OT Technical Memorandum 76-222, June 1976.

(5) Doherty, R.H. and J.R. Johler, "Meteorological Influences on Loran-C Ground Wave Propagation", JATP Vol. 37, pp 1117-1124, 1975.

(6) Proverbia, E. and A. Simoncini, "Diurnal Frequency Variations In Loran-C Transmissions", Proceedings IXth International Congress of Chronometry, September 1974.

(7) Doherty, R.H., "Spatial and Temporal Electrical Properties Derived from LF Pulse Groundwave Propagation Measurement", Proc. XXth Tech. Meeting of EM Propagation Panel of AGARD-NATO, March 1974.

(8) Frank, R.L. and D.L. McGrew, "Real Time Compensation of Loran-C/D Temporal Variations", presented at Wild Goose Association Convention, October 1974.

(9) Potts, C.E. and B. Wieder, "Precise Time and Frequency Dissemination via the Loran-C System", Proc. IEEE Vol. 60 No. 5, May 1972.

(10) Johler, J.R., W.J. Keller, and L.C. Walters, "Phase of the Low Radiofrequency Ground Wave", NBS Circular 573, June 1956.

MR. WAYNE H. CANNON, York University:

Please clarify one point. You just used the metrological data at the same site as your LORAN receiver is located? Is that correct?

MR. DEAN:

No, that is wrong. The data I used consisted of data at a couple of different points along the path between the two. And actually that last curve used the data at Huntington, West Virginia, which is approximately the midpoint between Carolina Beach and Fort Wayne.

MR. CANNON:

So, you are attempting some kind of metrological average along the path?

MR. DEAN:

That is correct, and we did some work on taking the average temperature along the path. That seemed to be a little better correlated than any individual point. The only problem was that all of this was being done by hand, and the labor became so great that we didn't do very many.

MR. CANNON:

I saw the ground conductivity classifications there on the map. Did you do anything with that data at all?

MR. DEAN:

No, because the data that I got out of NBS-573 was just for a $\sigma 5$. I just made the simplifying assumption that the average conductivity was about 5 and let it go at that. I am sure that we could go back into Johler's formulas. He may have written up some new ones since then and that could be worked out. But I just haven't done it.

Page intentionally left blank

Page intentionally left blank

NANOSECOND TIME TRANSFER VIA SHUTTLE LASER RANGING EXPERIMENT

Victor S. Reinhardt, Don A. Premo,
Michael W. Fitzmaurice, S. Clark Wardrip
NASA/Goddard Space Flight Center
Greenbelt, Maryland
and Peter O. Cervenka,
Phoenix Corp., McLean Virginia

ABSTRACT

A method is described to use a proposed shuttle laser ranging experiment to transfer time with nanosecond precision. All that need be added to the original experiment are low cost ground stations and an atomic clock on the shuttle. It is shown that global time transfer can be accomplished with 1 ns precision and transfer up to distances of 2000 km can be accomplished with better than 100 ps precision.

INTRODUCTION

The Shuttle Geodynamic Ranging System (SGRS) as presently conceived will employ laser ranging technology to achieve a one shot measurement precision of 10 centimeters standard deviation.[1,2] The instrument will contain a narrow pulse neodymium-YAG frequency-doubled laser and an accurate pointing system to direct the 1/2 milliradian laser beam from Shuttle to each of a large number of reflective targets placed strategically throughout an area of interest on the surface of the earth. The instrument's primary function is precise measurement of baselines and relative heights between these targets where a typical maximum baseline distance is five hundred kilometers. The applications are varied but mainly rely on the ability of the system to perform its task with centimeter precision. For instance, measurement of baseline changes can yield information about tectonic plate motion and strain accumulation across faults. Similarly, intertarget vertical motion can be interpreted as dilatancy (thought to be a precursor to earthquakes) or as subsidence due possibly to fluid extraction from or influx into subsurface regions. Figure 1 pictures SGRS in operation over the San Andreas fault in California.

SGRS does not measure baselines directly. Rather, it measures the range between itself and each retroreflector target by measuring the

time it takes laser pulses to traverse the distance between the spacecraft and the target and back. To measure baselines, a ranging sequence is used which minimizes the effects of spacecraft motion. Baselines are computed from the sequence of range measurements and the equations of motion of the spacecraft. Error analysis indicates that a ranging system having an accuracy of 10 centimeters for single measurements and operating in this mode can indeed yield centimeter precision with respect to intertarget measurements, assuming that several thousand range observations are obtained per target.

To see how the SGRS can be used for time transfer, one must look closely at the range system since the laser pulse is the only signal which is common to both the SGRS and the ground. Figure 2 shows a block diagram of the ranging subsystem as it is planned. The subsystem will use a frequency-doubled neodymium-YAG Laser with a pulse width of about 12 ns which is fired at about a 10 pps rate. Observe that both the transmitted and reflected pulses will be measured through the same channel to avoid range biases. The real-time correlator and peak detector will operate in a fashion similar to a constant fraction discriminator to find the center of the pulse independent of returning pulse amplitude. This discriminator will have a dynamic range greater than 100:1 to compensate for atmospheric scintillation and other effects. Notice that an event clock will replace the usual "time of measurement" and "range time interval" units. This event clock will record the epoch of transmitted and reflected laser pulses with an accuracy of better than 40 picoseconds. Thus, the range time interval to a target is the difference in epoch of the two pulses and the time of measurement is the average epoch of the two pulses. The time of measurement, which is also an estimate of the time of arrival of the laser pulse at the target, is sufficiently accurate for ranging purposes. When corrected for range rate effects, this time is also sufficiently accurate for time transfer purposes.

A range precision of 10 centimeters implies a range timing precision of 667 picoseconds and, if independence is assumed, a single pulse timing precision of 471 picoseconds. This number includes all effects of consequence within a time period comparable to the range time interval; i.e., up to 7 milliseconds. Because of the common channel, it is possible to compute the time of arrival of the laser pulses at the ground target with respect to the SGRS clock from a knowledge of the two event times and the range rate. The errors expected are those related to pulse timing and to non-common channel effects. Therefore, if the pulse timing precision on the ground is assumed to be the same as that of the SGRS, a total one shot timing precision at the ground target of 577 picoseconds should be expected.

Laser Time Transfer

To use SGRS for time transfer all one need add is a ground station capable of recording the epoch of laser pulses as they are reflected from the station. Such a station is depicted in Figure 3. The way these stations would be used to transfer time is shown in Figure 4. As the shuttle flies over two or more remote clock sites equipped with ground stations, it would range to them. Concurrently each ground station would record the epoch of laser pulses as they hit the station relative to its remote clock. The data on board the shuttle would allow the computation of the epoch of arrival of laser pulses on the ground relative to the on board frequency standard. By comparing all the data after the fact, one obtains a synchronization between each remote clock and the shuttle's on-board frequency standard. Therefore, one transfers time between two ground sites by using the shuttle frequency standard as a transfer standard.

For long range time transfers, one is limited by the transfer error of the on-board frequency standard. It can be shown that the transfer error of the on-board standard for times long compared with the pulse transit time is approximately the two-sample Allan Variance for the transfer time. Figure 5 uses this to show the transfer error of several atomic frequency standards. Notice there are several standards which will maintain 1 ns for about 10^4 seconds, a little under three orbits. This time is sufficient to cover most pairs of sites. This will be discussed in further detail later in the paper.

For short range time transfer up to 2000 Km, one can use the moveable mirror on SGRS to sequentially hit several ground stations and thus eliminate the transfer error of the on-board frequency standard. This would allow one to average many measurements to reduce the one shot measurement error. How much this can be done is determined by the limits imposed by systematic errors or slowly varying time delays effecting the measurement. Past results with ground-based laser measurements and analysis of atmospheric effects indicate that the shuttle system will contribute less than 100 ps error.[1] The effects of the ground receiver on ultimate accuracy are discussed in the next section.

Laser Time Transfer Receiver

A block diagram of the Laser time transfer ground station is shown in Figure 5. The ground station has four basic elements: a retroreflector receiver, a constant fraction discriminator, an event clock, and a data logger. The retroreflector-receiver would consist of a cube corner array to reflect the laser pulses and a photomultiplier tube or a photodiode to detect the arrival of laser pulses

For the detector, relatively inexpensive photomultiplier tubes are available[3] with transit times of 10 to 30 ns, rise times of 1 to 3 ns, and for the pulse amplitudes of concern here, Jitter[4] of less than 100 ps. Errors caused by delay changes due to temperature or other variations occur principally through changes in power supply voltage. With a total power supply stability of 0.1%, variations in transit time are less than 20 ps. Any direct effects on the photomultiplier itself can be eliminated by shielding and temperature control of the tube, though this will probably not be necessary.

The constant fraction discriminator is necessary to compensate for received pulse amplitude variations caused by angular effects and scintillation. The discriminator would be set to trigger typically on the half amplitude point to minimize amplitude to time conversion effects. Constant fraction discriminators are available with a time walk of less than 120 ps over a 100:1 change in pulse amplitude.[5] This is more than sufficient to compensate for pulse amplitude variations to be seen by the time transfer receiver. Temperature coeficients are such to keep total time stability better than 120 ps. In any case, since constant fraction discriminators with sufficient accuracy can be built into a photomultiplier tube house, if necessary, one can remove temperature effects with a temperature controlled shroud around the photomultiplier assembly.

The event clock will run off 5 MHz and 1 pps supplied by the local clock. Interpolators which measure intervals of 100 ns to 500 ns in length to a resolution of 100 ps to 500 ps are available as standard CAMAC modules. This means that an event clock with only a 100 ns to 500 ns resolution would have to be constructed which could easily be accomplished with standard TTL logic. Of course care would have to be exercised in relating the 1 pps input to the interpolation measurement. This can be accomplished without too much difficulty provided the 1 pps input has a relatively fast rise time. If this is a problem, a scheme similar to that on the shuttle in which a laser diode at the receiver input is triggered by the 1 pps input can be used to record the epoch of the ground clock. Just as in the shuttle system, this would cancel most systematic delay effects in the time transfer ground station.

Since the pulses to be measured will occur only at a 10 pps rate for 30 seconds or so, the data logger need not be complicated. At these speeds a simple parallel printer can handle the data. Alternatively a calculator can be used to collect the data and store it on a tape cassette.

Shuttle Time Transfer Feasibility Study

For time transfer to be feasible via the shuttle laser ranging system

not only must the laser system be capable of time transfer, but the shuttle orbit must also allow time transfers between reasonable site locations. To determine whether the shuttle orbit would allow such reasonable time transfers, a study of shuttle passes over selected sites during a 12 day orbit was made. The sites are listed in Figure 7. The sites were selected for use in a validation experiment; they either had VLBI capability or had clocks available with nanosecond per day stabilities.

For this study, a twelve day 50° inclination orbit was used. A pass was defined as having at least a 20° inclination in the range vector between the shuttle and the site. For this study, the sites were given code numbers as listed in Figure 7. After a list of passes were compiled and time-ordered, the list was searched for pairs of passes at selected sites within time intervals from 60 seconds to 10^5 seconds. The results of these passes are shown in Figures 8 through 15. These charts contain the results of a computer search in which the computer went sequentially down the master list to define the first site of a pair and then counted the number of times the second site appeared within the specified period after the time of the first site pass. The results were summed as the computer went down the list sequentially for the first site. This method of counting yields very large numbers for long time intervals, but can be useful in combining weather data where multiple occurences of a second site increase the probability of obtaining a clear shot. In any case, the relative sizes of the numbers can be used in site selection. On each of the charts the first column and first row are the code numbers of the sites. Notice that pass pairs for the same site are included twice.

One can qualitatively understand the data by looking at Figure 17 which shows a one day shuttle orbit superimposed over the sites. Of course the extreme latitude of Onsala makes it a poor candidate for a site as verified by the data. However, because the 20° inclination allows the shuttle to hit anything within $\pm$1000 Km of the orbit position, even Onsala has passes during the twelve day period. Since the orbit is non-repeating over the earth, any two sites within $\pm$50° latitude will be connected. The data shows that within 10^4 seconds most of the sites are connected and within 3×10^4 seconds all of the sites are connected. For short time intervals sites close together were of course connected. As can be verified by the data, sites along orbit paths are favorable for short term transfers even when separated by large distances. An especially favorable site is Westford since it sits on many orbit paths in common with other sites.

References

[1]T.E. McGunigal, et. al. "Satellite Laser Ranging Work at the Goddard Space Flight Center", NASA Doc. #X-723-75-172 (July, 1975).

[2]F. O. Vonbun, et. al "Spaceborne Earth Applications Ranging System (SPEAR)", Journal of Spacecraft and Rockets, Vol 14, No. 8, pp 492-495 (August, 1977).

[3]The data quoted is based on an RCA Model 4836 Photomultiplier Tube.

[4]Jitter measurements courtesy of Jim Abshire, Goddard Space Flight Center (Private Communication).

[5]Ortec Model 270/271 Constant Fraction Discriminator.

Figures

1. Shuttle Geodynamic Ranging System

2. SGRS Ranging Subsystem

3. Laser Time Transfer Receiver

4. Shuttle Laser Time Transfer

5. On Board Clock Transfer Error

6. Time Transfer Ground Station

7. Laser Time Transfer Feasibility Study Locations

8. Number of pass pairs within 6.0 E+01 seconds

9. Number of pass pairs within 1.2 E+02 seconds

10. Number of pass pairs within 3.0 E+02 seconds

11. Number of pass pairs within 1.0E+03 seconds

12. Number of pass pairs within 3.0E+03 seconds

13. Number of pass pairs within 1.0E+04 seconds

14. Number of pass pairs within 3.0E+04 seconds

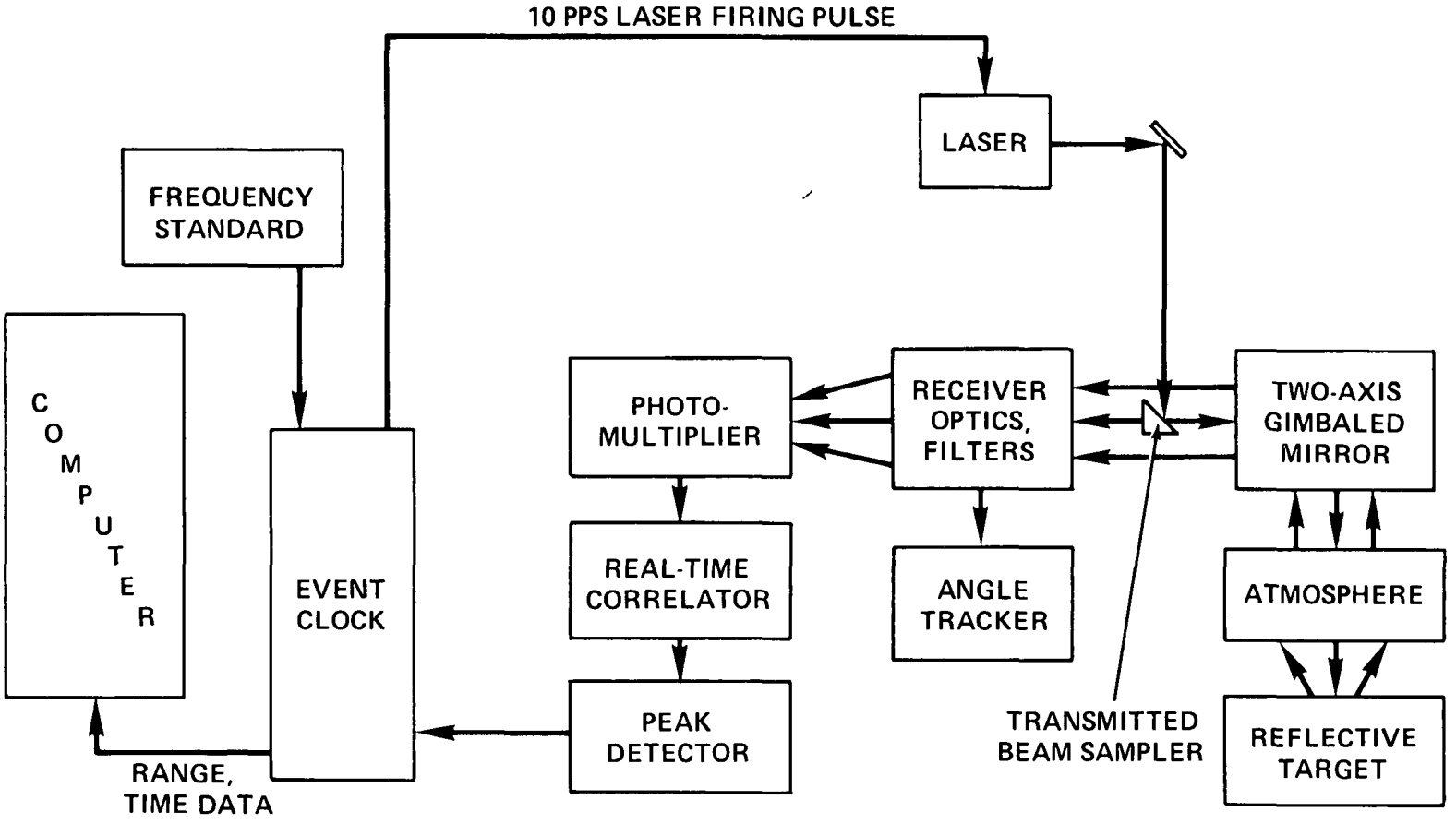
15. Number of pass pairs within 1.0E+05 seconds

16. Typical Shuttle One Day Orbit


RETROREFLECTOR TARGET -
SPACEBORNE LASER RANGING
SAN ANDREAS FAULT

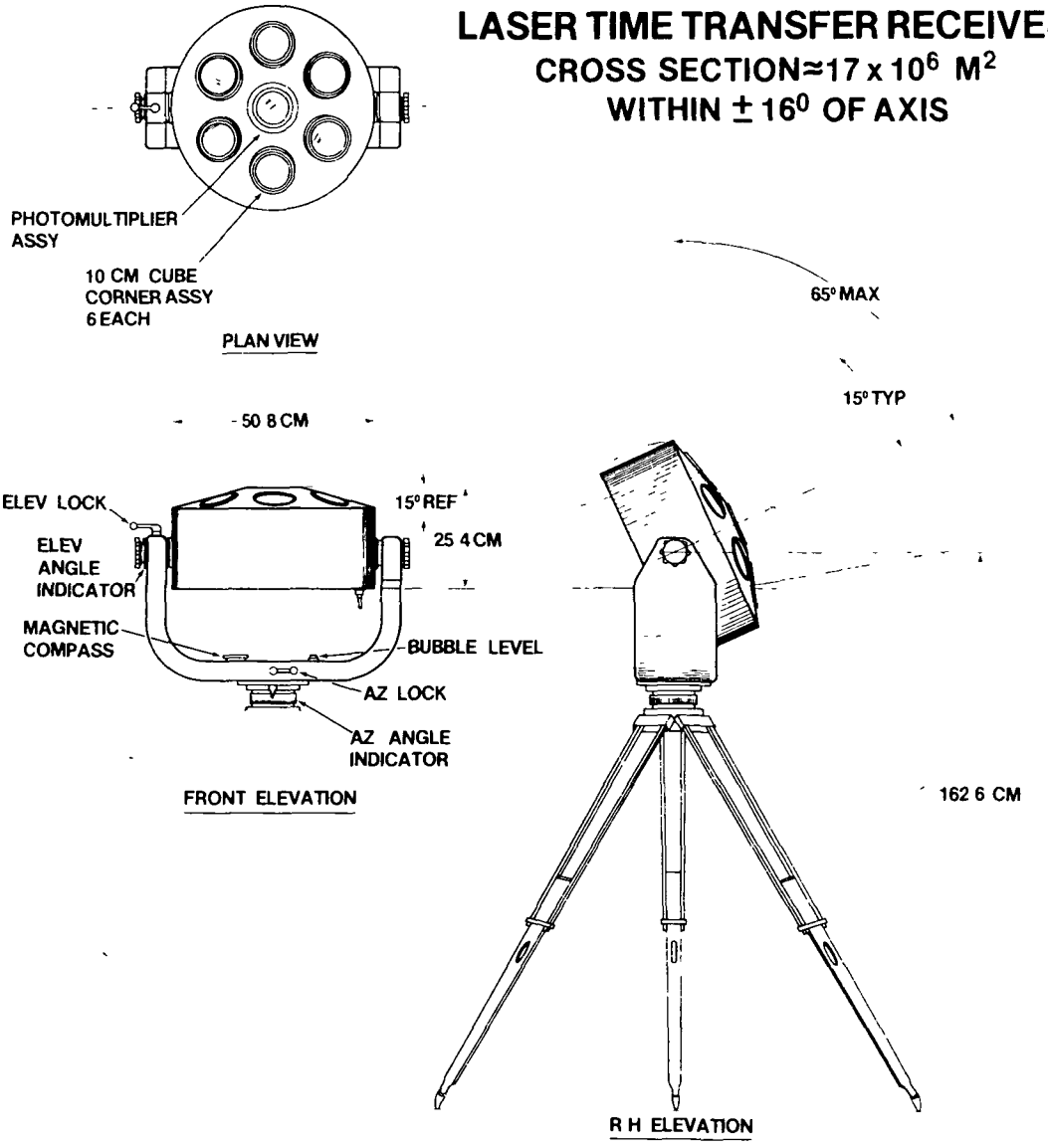
SPACEBORNE LASER RANGING SYSTEM

RANGING SUBSYSTEM

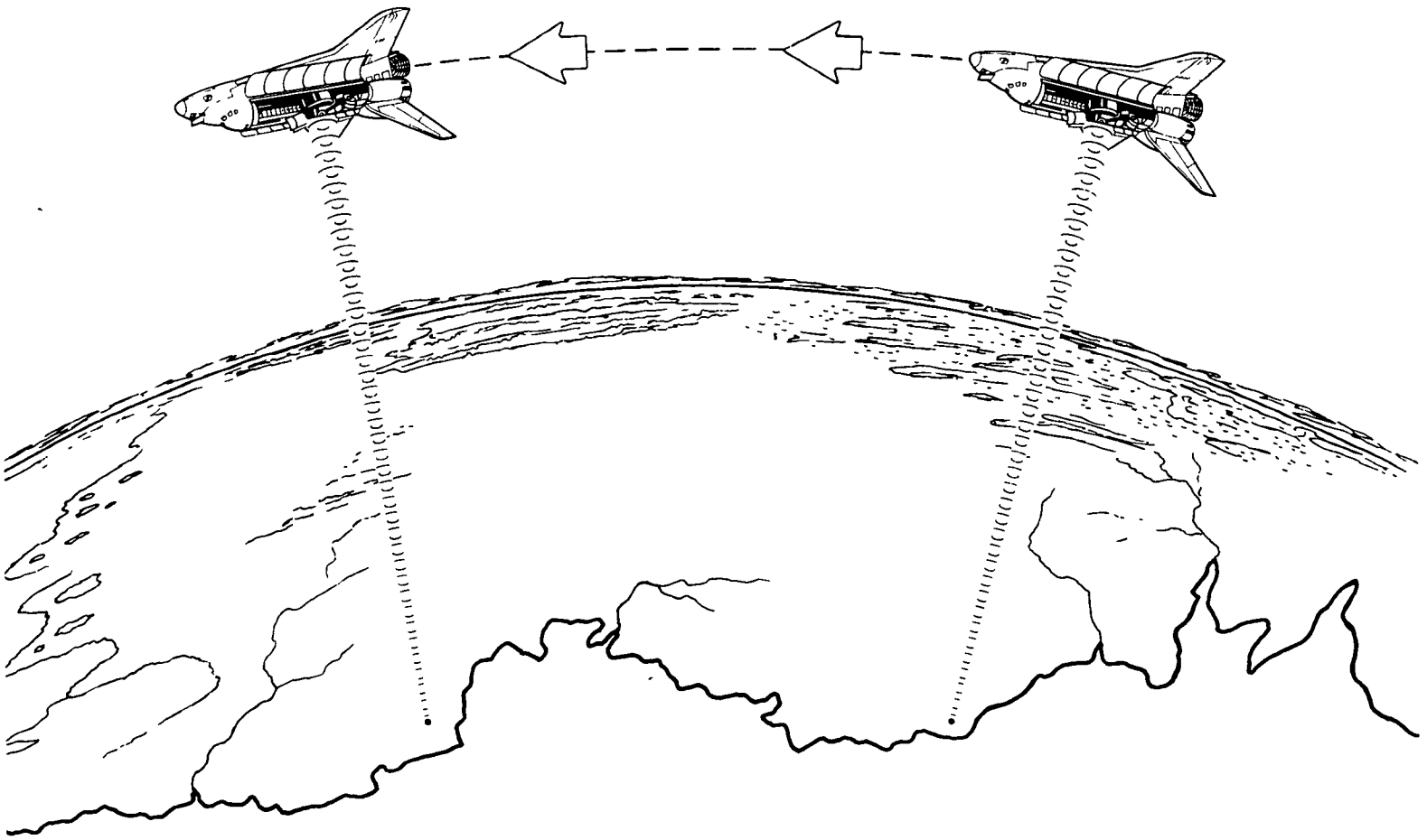


LASER TIME TRANSFER RECEIVER

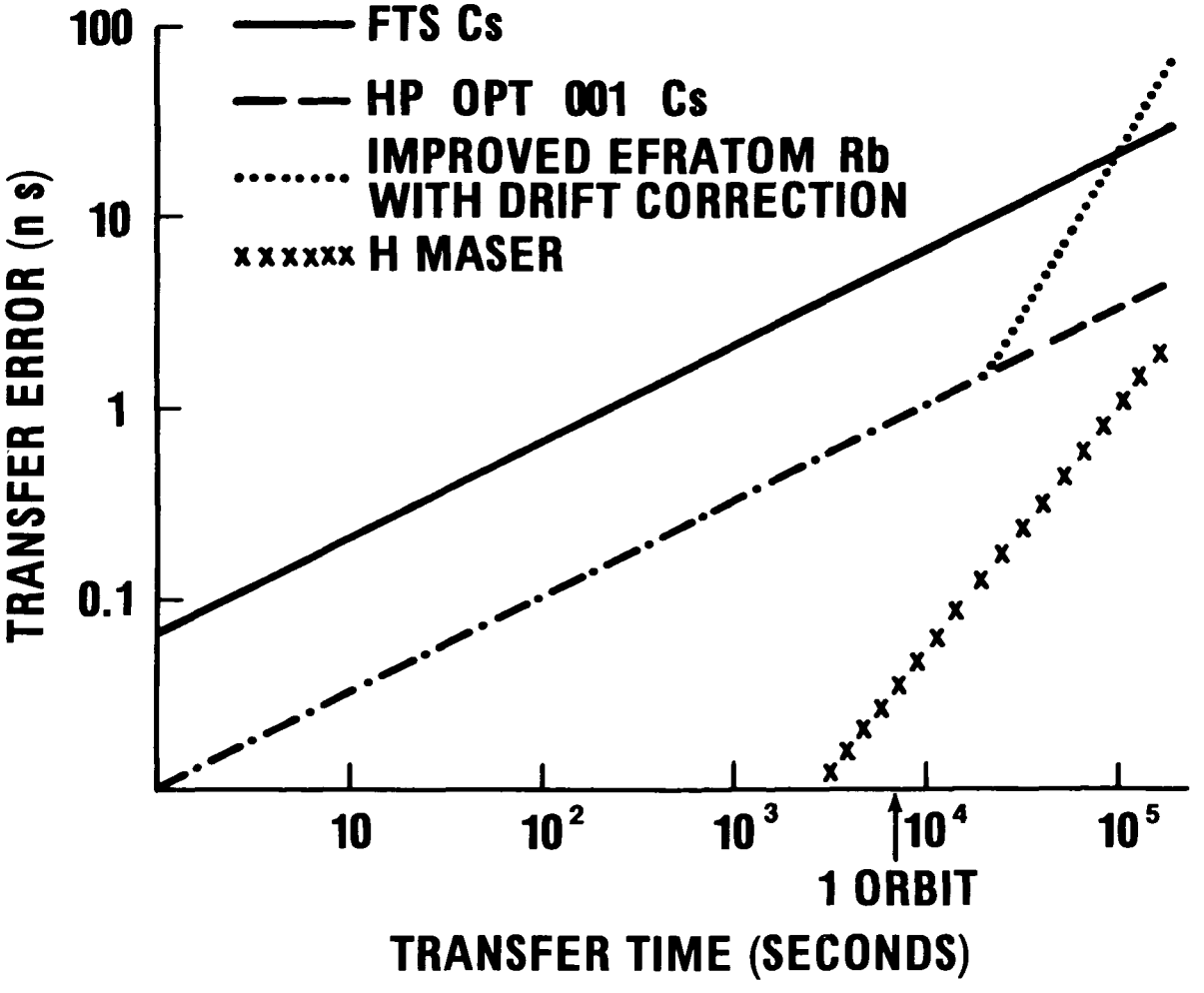
CROSS SECTION≈17 x 10^6 M^2
WITHIN ± 16^0 OF AXIS



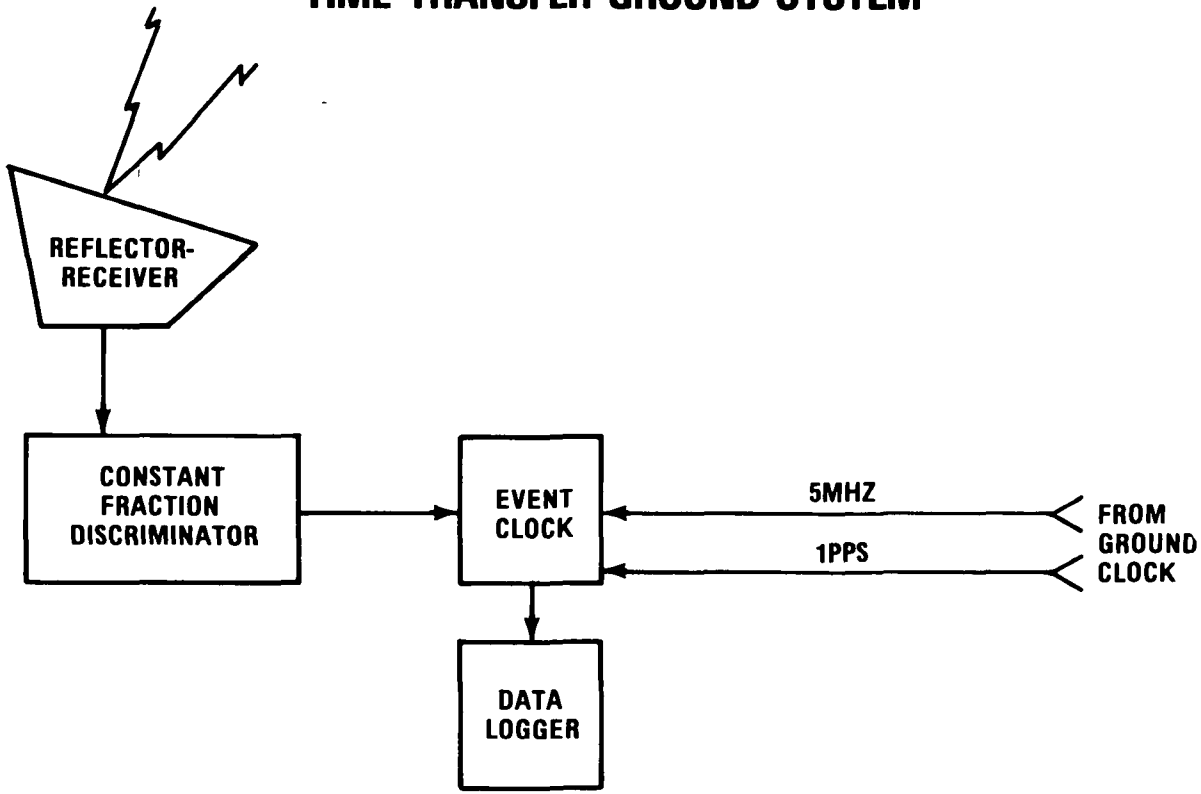
SHUTTLE LASER TIME TRANSFER



ON BOARD CLOCK TRANSFER ERROR



TIME TRANSFER GROUND SYSTEM



LASER TIME TRANSFER
FEASIBILITY STUDY LOCATIONS

NAME	LOCATION	LONGITUDE	LATITUDE	LOC. NO.
GREENBANK	WEST VIRGINIA	W79 50.2	N38 26 17	1
RGO	ENGLAND	W0 20.3	N50 52 18	2
MADRID	SPAIN	W3 41.3	N40 24 30.0	3
OTTAWA	ONTARIO	W75 53.6	N45 23 13	4
PARKES	AUSTRALIA	E148 15.7	S33 00 0.04	5
RIVERSIDE	MARYLAND	W77 14.0	N38 22 26.1	6
TOKYO	JAPAN	E139 32.4	N35 40 18.2	7
WESTFORD	MASSACHUSETTS	W71 29.5	N42 37 2.4	8
OWENS VALLEY	CALIFORNIA	W118 17.6	N37 13 53.8	9
BOCHUM	GERMANY	E7 11.5	N51 25 43	10
BOULDER	COLORADO	W105 7.4	N40 5 28	11
FORT DAVIS	TEXAS	W103 57	N30 38 00	12
GOLDSTONE	CALIFORNIA	W116 50.9	N35 23 34.2	13
ONSALA	SWEDEN	E11 55.2	N57 23 36.1	14
LAKE TRAVERSE	ONTARIO	W78 4.4	N45 57 19.4	15
PARIS	FRANCE	E2 20.2	N48 50 11	16
USNO	WASHINGTON, D.C.	W77 3.9	N38 55 14.0	17
GREENBELT	MARYLAND	W76 49.6	N39 1 11.48	18

NUMBER OF PASS PAIRS WITHIN 6.0E+01 SECONDS

	1	2	3	4	5	6	7	8	9	10	11	12	13	14	15	16	17	18
1	0	0	0	21	0	33	0	10	0	0	0	0	0	0	24	0	34	33
2	0	0	9	0	0	0	0	0	0	33	0	0	0	0	0	38	0	0
3	0	9	0	0	0	0	0	0	0	4	0	0	0	0	0	10	0	0
4	21	0	0	0	0	26	0	51	0	0	0	0	0	0	51	0	29	29
5	0	0	0	0	0	0	0	0	0	0	0	0	0	0	0	0	0	0
6	33	0	0	26	0	0	0	18	0	0	0	0	0	0	19	0	37	36
7	0	0	0	0	0	0	0	0	0	0	0	0	0	0	0	0	0	0
8	10	0	0	51	0	18	0	0	0	0	0	0	0	0	29	0	20	22
9	0	0	0	0	0	0	0	0	0	0	4	2	31	0	0	0	0	0
10	0	33	4	0	0	0	0	0	0	0	0	0	0	13	0	40	0	0
11	0	0	0	0	0	0	0	0	4	0	0	6	7	0	0	0	0	0
12	0	0	0	0	0	0	0	0	2	0	6	0	0	0	0	0	0	0
13	0	0	0	0	0	0	0	0	31	0	7	0	0	0	0	0	0	0
14	0	0	0	0	0	0	0	0	0	13	0	0	0	0	0	0	0	0
15	24	0	0	51	0	19	0	29	0	0	0	0	0	0	0	0	21	21
16	0	38	10	0	0	0	0	0	0	40	0	0	0	0	0	0	0	0
17	34	0	0	29	0	37	0	20	0	0	0	0	0	0	21	0	0	38
18	33	0	0	29	0	36	0	22	0	0	0	0	0	0	21	0	38	0

NUMBER OF PASS PAIRS WITHIN 1.2E+02 SECONDS

	1	2	3	4	5	6	7	8	9	10	11	12	13	14	15	16	17	18
1	0	0	0	26	0	33	0	27	0	0	0	0	0	0	24	0	34	33
2	0	0	17	0	0	0	0	0	0	34	0	0	0	12	0	38	0	0
3	0	17	0	0	0	0	0	0	0	4	0	0	0	0	0	19	0	0
4	26	0	0	0	0	27	0	53	0	0	0	0	0	0	51	0	29	29
5	0	0	0	0	0	0	0	0	0	0	0	0	0	0	0	0	0	0
6	33	0	0	27	0	0	0	31	0	0	0	0	0	0	25	0	37	36
7	0	0	0	0	0	0	0	0	0	0	0	0	0	0	0	0	0	0
8	27	0	0	53	0	31	0	0	0	0	0	0	0	0	51	0	33	33
9	0	0	0	0	0	0	0	0	0	0	16	3	31	0	0	0	0	0
10	0	34	4	0	0	0	0	0	0	0	0	0	0	13	0	40	0	0
11	0	0	0	0	0	0	0	0	16	0	0	16	10	0	0	0	0	0
12	0	0	0	0	0	0	0	0	3	0	16	0	5	0	0	0	0	0
13	0	0	0	0	0	0	0	0	31	0	10	5	0	0	0	0	0	0
14	0	12	0	0	0	0	0	0	0	13	0	0	0	0	0	13	0	0
15	24	0	0	51	0	25	0	51	0	0	0	0	0	0	0	0	27	27
16	0	38	19	0	0	0	0	0	0	40	0	0	0	13	0	0	0	0
17	34	0	0	29	0	37	0	33	0	0	0	0	0	0	27	0	0	38
18	33	0	0	29	0	36	0	33	0	0	0	0	0	0	27	0	38	0

NUMBER OF PASS PAIRS WITHIN 3.0E+02 SECONDS

	1	2	3	4	5	6	7	8	9	10	11	12	13	14	15	16	17	18
1	0	0	0	26	0	33	0	28	0	0	11	3	0	0	24	0	34	33
2	0	0	19	0	0	0	0	0	0	34	0	0	0	12	0	38	0	0
3	0	19	0	0	0	0	0	0	0	19	0	0	0	4	0	25	0	0
4	26	0	0	0	0	27	0	53	0	0	2	0	0	0	51	0	29	29
5	0	0	0	0	0	0	0	0	0	0	0	0	0	0	0	0	0	0
6	33	0	0	27	0	0	0	31	0	0	8	1	0	0	25	0	37	36
7	0	0	0	0	0	0	0	0	0	0	0	0	0	0	0	0	0	0
8	28	0	0	53	0	31	0	0	0	0	0	0	0	0	51	0	33	33
9	0	0	0	0	0	0	0	0	0	0	25	17	31	0	0	0	0	0
10	0	34	19	0	0	0	0	0	0	0	0	0	0	13	0	40	0	0
11	11	0	0	2	0	8	0	0	25	0	0	16	24	0	13	0	9	8
12	3	0	0	0	0	1	0	0	17	0	16	0	17	0	0	0	0	0
13	0	0	0	0	0	0	0	0	31	0	24	17	0	0	0	0	0	0
14	0	12	4	0	0	0	0	0	0	13	0	0	0	0	0	13	0	0
15	24	0	0	51	0	25	0	51	0	0	13	0	0	0	0	0	27	27
16	0	38	25	0	0	0	0	0	0	40	0	0	0	13	0	0	0	0
17	34	0	0	29	0	37	0	33	0	0	9	0	0	0	27	0	0	38
18	33	0	0	29	0	36	0	33	0	0	8	0	0	0	27	0	38	0

NUMBER OF PASS PAIRS WITHIN 1.0E+03 SECONDS

	1	2	3	4	5	6	7	8	9	10	11	12	13	14	15	16	17	18
1	0	10	15	26	0	33	0	28	0	6	11	10	1	0	24	12	34	33
2	10	0	19	8	0	12	0	12	0	34	0	0	0	12	6	38	12	12
3	15	19	0	20	0	14	0	20	0	19	0	0	0	4	18	25	15	15
4	26	8	20	0	0	27	0	53	18	4	21	14	17	0	51	10	29	29
5	0	0	0	0	0	0	0	0	0	0	0	0	0	0	0	0	0	0
6	33	12	14	27	0	0	0	31	0	8	9	9	0	0	25	14	37	36
7	0	0	0	0	0	0	0	0	0	0	0	0	0	0	0	0	0	0
8	28	12	20	53	0	31	0	0	18	8	21	14	17	0	51	14	33	33
9	0	0	0	18	0	0	0	18	0	0	25	17	31	0	18	0	0	0
10	6	34	19	4	0	8	0	8	0	0	0	0	0	13	2	40	8	8
11	11	0	0	21	0	9	0	21	25	0	0	16	24	0	21	0	10	9
12	10	0	0	14	0	9	0	14	17	0	16	0	17	0	14	0	10	10
13	1	0	0	17	0	0	0	17	31	0	24	17	0	0	17	0	1	1
14	0	12	4	0	0	0	0	0	0	13	0	0	0	0	0	13	0	0
15	24	6	18	51	0	25	0	51	18	2	21	14	17	0	0	8	27	27
16	12	38	25	10	0	14	0	14	0	40	0	0	0	13	8	0	14	14
17	34	12	15	29	0	37	0	33	0	8	10	10	1	0	27	14	0	38
18	33	12	15	29	0	36	0	33	0	8	9	10	1	0	27	14	38	0

NUMBER OF PASS PAIRS WITHIN 3.0E+03 SECONDS

	1	2	3	4	5	6	7	8	9	10	11	12	13	14	15	16	17	18
1	0	10	15	26	3	33	0	28	0	6	11	10	1	0	24	12	34	33
2	10	0	19	8	11	12	0	12	0	35	0	3	0	12	6	39	12	12
3	15	19	0	20	16	14	0	20	4	19	8	14	6	4	18	25	15	15
4	26	8	20	0	15	27	0	53	18	4	21	14	17	0	51	10	29	29
5	3	11	16	15	0	5	0	15	4	14	2	0	1	3	15	14	6	6
6	33	12	14	27	5	0	0	31	0	8	9	9	0	0	25	14	37	36
7	0	0	0	0	0	0	0	0	13	0	4	9	14	0	0	0	0	0
8	28	12	20	53	15	31	0	0	18	8	21	14	17	0	51	14	33	33
9	0	0	4	18	4	0	13	18	0	0	25	17	31	0	18	0	0	0
10	6	35	19	4	14	8	0	8	0	0	0	0	0	13	2	40	8	8
11	11	0	8	21	2	9	4	21	25	0	0	16	24	0	21	0	10	9
12	10	3	14	14	0	9	9	14	17	0	16	0	17	0	14	5	10	10
13	1	0	6	17	1	0	14	17	31	0	24	17	0	0	17	0	1	1
14	0	12	4	0	3	0	0	0	0	13	0	0	0	0	0	13	0	0
15	24	6	18	51	15	25	0	51	18	2	21	14	17	0	0	8	27	27
16	12	39	25	10	14	14	0	14	0	40	0	5	0	13	8	0	14	14
17	34	12	15	29	6	37	0	33	0	8	10	10	1	0	27	14	0	38
18	33	12	15	29	6	36	0	33	0	8	9	10	1	0	27	14	38	0

NUMBER OF PASS PAIRS WITHIN 1.0E+04 SECONDS

	1	2	3	4	5	6	7	8	9	10	11	12	13	14	15	16	17	18
1	11	27	28	64	31	57	19	70	24	23	45	28	22	2	60	29	60	58
2	27	27	57	28	39	30	0	36	4	89	8	17	6	33	24	99	31	31
3	28	57	15	48	41	28	16	52	20	57	28	24	23	17	44	67	30	30
4	64	28	48	41	58	67	9	139	56	20	73	37	51	0	131	32	73	72
5	31	39	41	58	5	34	0	62	24	44	30	14	21	15	56	48	36	36
6	57	30	28	67	34	13	18	75	24	26	45	28	21	4	63	34	65	63
7	19	0	16	9	0	18	8	9	22	0	19	18	22	0	0	0	18	16
8	70	36	52	139	62	75	9	45	56	28	73	41	51	4	135	42	81	80
9	24	4	20	56	24	24	22	56	11	0	54	37	51	0	56	6	26	25
10	23	89	57	20	44	26	0	28	0	28	4	11	2	38	16	102	27	27
11	45	8	28	73	30	45	19	73	54	4	16	41	52	0	71	10	48	46
12	28	17	24	37	14	28	18	41	37	11	41	3	37	0	35	19	29	28
13	22	6	23	51	21	21	22	51	51	2	52	37	9	0	51	8	24	23
14	2	33	17	0	15	4	0	4	0	38	0	0	0	1	0	38	4	4
15	60	24	44	131	56	63	0	135	56	16	71	35	51	0	39	28	69	68
16	29	99	67	32	48	34	0	42	6	102	10	19	8	38	28	34	35	35
17	60	31	30	73	36	65	18	81	26	27	48	29	24	4	69	35	15	67
18	58	31	30	72	36	63	16	80	25	27	46	28	23	4	68	35	67	14

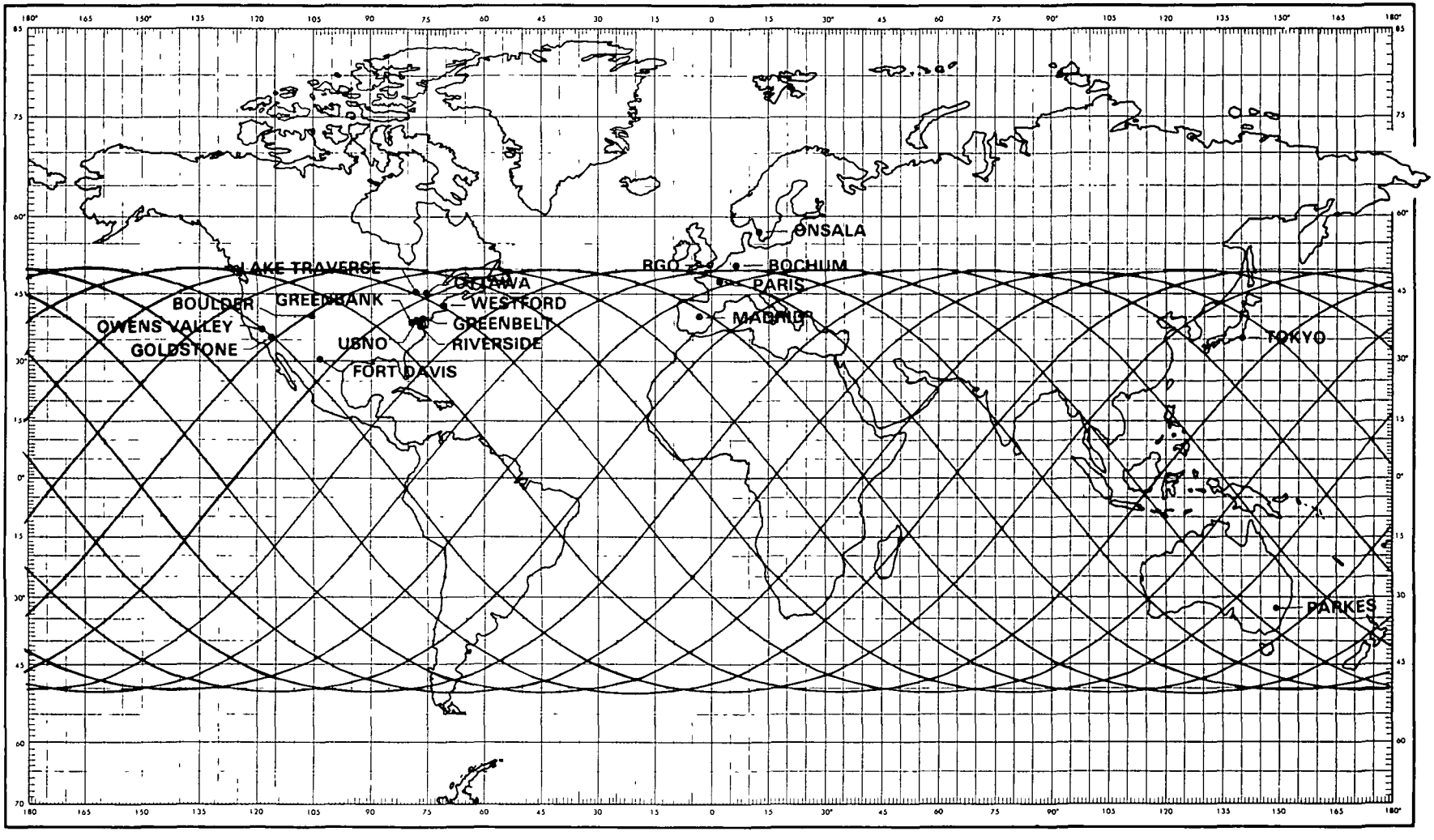
NUMBER OF PASS PAIRS WITHIN 3.0E+04 SECONDS

	1	2	3	4	5	6	7	8	9	10	11	12	13	14	15	16	17	18
1	36	88	85	153	65	110	47	167	88	86	110	71	82	25	147	102	115	111
2	88	46	126	158	90	96	51	170	66	128	85	52	59	42	152	150	101	100
3	85	126	45	146	81	90	47	158	77	132	96	63	73	42	138	150	96	95
4	153	158	146	92	109	161	67	253	145	157	171	115	136	51	227	182	171	167
5	65	90	81	109	22	69	38	118	66	88	74	50	62	31	103	103	72	71
6	110	96	90	161	69	41	49	176	96	91	116	74	86	28	155	111	123	119
7	47	51	47	67	38	49	30	73	66	52	65	50	63	17	65	60	51	48
8	167	170	158	253	118	176	73	108	151	169	179	119	140	56	243	196	186	181
9	88	66	77	145	66	96	66	151	38	59	119	79	103	19	143	77	101	99
10	86	128	132	157	88	91	52	169	59	48	79	47	57	43	149	154	98	97
11	110	85	96	171	74	116	65	179	119	79	46	89	111	21	166	101	122	119
12	71	52	63	115	50	74	50	119	79	47	89	18	74	15	113	61	79	77
13	82	59	73	136	62	86	63	140	103	57	111	74	32	18	134	71	92	90
14	25	42	42	51	31	28	17	56	19	43	21	15	18	1	49	49	30	30
15	147	152	138	227	103	155	65	243	143	149	166	113	134	49	84	174	165	161
16	102	150	150	182	103	111	60	196	77	154	101	61	71	49	174	66	118	117
17	115	101	96	171	72	123	51	186	101	98	122	79	92	30	165	118	45	125
18	111	100	95	167	71	119	48	181	99	97	119	77	90	30	161	117	125	42

NUMBER OF PASS PAIRS WITHIN 1.0E+05 SECONDS

	1	2	3	4	5	6	7	8	9	10	11	12	13	14	15	16	17	18
1	106	275	272	381	213	256	205	408	248	272	281	189	235	92	368	314	268	260
2	275	157	320	408	236	290	219	445	249	357	283	205	239	121	388	408	302	295
3	272	320	132	415	234	289	220	451	246	328	275	196	235	108	395	373	303	297
4	381	408	415	278	315	401	287	648	376	406	431	279	355	130	586	476	421	411
5	213	236	234	315	69	224	157	338	186	235	217	148	176	74	301	275	234	228
6	256	290	289	401	224	117	218	428	261	287	294	197	245	94	385	335	282	274
7	205	219	220	287	157	218	90	311	206	223	223	157	193	75	278	257	225	218
8	408	445	451	648	338	428	311	317	400	442	455	300	377	142	623	518	449	438
9	248	249	246	376	186	261	206	400	106	252	280	191	238	76	362	295	275	268
10	272	357	328	406	235	287	223	442	252	161	282	207	241	123	386	412	300	294
11	281	283	275	431	217	294	223	455	280	282	136	213	266	89	416	330	309	301
12	189	205	196	279	148	197	157	300	191	207	213	60	183	70	268	239	207	201
13	235	239	235	355	176	245	193	377	238	241	266	183	97	75	342	282	259	252
14	92	121	108	130	74	94	75	142	76	123	89	70	75	14	124	139	99	97
15	368	388	395	586	301	385	278	623	362	386	416	268	342	124	257	453	405	395
16	314	408	373	476	275	335	257	518	295	412	330	239	282	139	453	213	350	343
17	268	302	303	421	234	282	225	449	275	300	309	207	259	99	405	350	128	287
18	260	295	297	411	228	274	218	438	268	294	301	201	252	97	395	343	287	121

TYPICAL SHUTTLE ONE DAY ORBIT



QUESTIONS AND ANSWERS

DR. DERRAL MULHOLLAND, University of Texas:

Don't you have to know not only the orbit of the spacecraft to 15 centimeters, but also the position of the ground station with respect to the geocenter to 15 centimeters and the position of the clock with respect to the CG of the spacecraft to 15 centimeters?

DR. REINHARDT:

No. Let me explain that a little better. This is two-way transfer. Because the shuttle itself is ranging, you have the time that the pulse leaves the spacecraft to the time the pulse arrives. You can compute the time that it arrives on the graph. You don't have to know the location at all. The orbit is only a high-order fraction. The first order, the time that the pulse hits the ground, is just the average of the transmit-to-receive time. There is a very small correction due to the motion of the spacecraft--about 25 nanoseconds. It is so small, in fact, that all path considerations just drop out in terms of accuracy. Does that answer your question?

DR. MULHOLLAND:

It answers it, but it doesn't convince me.

DR. REINHARDT:

It is just a two-way time frame. It is the same as if you had two stations on the ground using a satellite and beaming back and forth over the same path. Don Premo, maybe you can help me.

MR. DON PREMO, NASA Goddard Space Flight Center:

Yes. The reason why we don't have to concern ourselves with the orbit calculations or position of the instrument running through to the center of gravity is that we have measured the path itself. Since we measured that, we don't need to make any calculations of the path. We measured the time it takes for the pulse to travel down to the receiver and to return.

Some Recent Progress in Microwave Frequency and Time Standards at the National Bureau of Standards

D. W. Allan, R. J. Besson*, G. Busca**, R. M. Garvey,
H. Hellwig, D. A. Howe, S. Jarvis, A. Risley
S. R. Stein, F. L. Walls, D. J. Wineland

Frequency and Time Standards Section
National Bureau of Standards
Boulder, Colorado 80302

ABSTRACT

Research and advanced development at the National Bureau of Standards (NBS) in the area of microwave frequency and time standards is discussed. New insights into the causes of flicker noise and long-term instability of cesium standards are discussed. A new cesium beam tube configuration is described with a potential accuracy of $\sim 10^{-14}$. Results and design of a passive hydrogen maser system are given showing stabilities of better than 10^{-14}. Causes for frequency instabilities in rubidium gas cell standards and on line-asymmetries are described. New quartz crystal standards and special purpose atomic standards for field use appear possible. Excellent short-term stability can be realized by superconducting cavity and quartz crystal oscillators.

INTRODUCTION

It is the intent of this paper to summarize and review efforts at the National Bureau of Standards (NBS) in the area of advanced development and improvement of microwave frequency and time standards. These efforts are aimed at fundamental improvements of accuracy, short- and long-term stability, environmental insensitivity, and practical utility for both laboratory and field applications. They are motivated by scientific and engineering opportunities uncovered within and outside of NBS as well as by the needs for improved primary frequency and time references and the demands of modern navigation and communication systems.

Progress in the area of traditional atomic standards is being made, opening up new capabilities for cesium beam, hydrogen maser, and rubidium gas cell standards. Coupling new electronic servo principles with one of the best known quantum electronic resonances, the inversion transition in ammonia, has demonstrated the feasibility of atomic standards of modest performance but of small size and a high degree of ruggedness. Advances in quartz crystal standards and

* Ecole Nationale Supérieure de Chronométrie et de Micromécanique de Besançon, Cedex, FRANCE

** Laval University, Québec, CANADA.

superconducting cavity oscillators are opening up new performance levels in short-term stability. In addition, long-term stabilities in novel crystal standards may soon rival those of some atomic standards, and atomic standards may improve because of better slave (crystal) oscillators.

Cesium Beam Standards

One of the fundamental limitations to the accuracy of cesium beam frequency standards is the Ramsey cavity phase shift (1st order Doppler shift). The performance of commercially available cesium standards as well as laboratory standards is significantly affected by this effect. A novel approach to remove this limitation has been conceived at NBS [1] and is now being investigated experimentally.

Rather than attempt to adjust to zero the relative electrical phase of the two cavity arms, two separate cavities with slightly different microwave frequencies are employed. In this way, the relative cavity phase continually changes, producing a signal envelope free from the effects of cavity phase shift. For cesium beams with broad velocity distributions, little loss in signal linewidth is incurred.

Not only may the accuracy of the standard be improved but the stability may also be increased by the reduction of effects (as cavity phase shift) which couple device parameter changes (as velocity distribution) to frequency changes.

It is important not only to investigate fundamental improvements but also to study limitations of the existing concepts. Of particular practical importance in clock applications is an understanding (and cure!) of those parameters which adversely affect the long-term stability of cesium beam clocks [2,3]. Changes of frequency have been correlated with changes in velocity distributions, changes in microwave power, changes in voltages at the cesium beam detector, changes in polarity of the C-field current, and changes in temperature.

A novel way of controlling the microwave power is being developed which should reduce the sensitivity to temperature variations. Figure 1 illustrates for a high performance commercial tube the microwave power dependence of the amplitude of the signal at the detector, of the most probable transition velocity, and of the Ramsey pattern side-lobe peak frequency. Figure 2 more graphically indicates the sensitivity of the side-lobe peak frequency with microwave power. A 1% duty cycle sampling of the side-lobe frequency with respect to the Ramsey center peak would allow one to control the power to about 0.01 dB. Such a servo may reduce, to first order, effects on frequency caused by changes in the Ramsey pattern; e.g., velocity distribution, microwave power, velocity selection at the detector, etc.

Hydrogen Maser Standards

Theoretical and experimental work at NBS is aimed at developing a clock with substantially less long-term time dispersion than the best present clocks. This has been accomplished by developing new electronic servo concepts and applying them to a passively operating hydrogen maser [4,5].

Using this new technique the microwave cavity is locked with great precision to a probe signal which is in turn accurately locked to the hydrogen resonance

line. There is no need for a second reference maser as previously required. This new ability to accurately control the cavity frequency permits one to correct for environmental perturbations to the cavity and also to greatly simplify the mechanical, thermal, and electrical designs.

Since the passive maser does not oscillate, one is even able to reduce the hydrogen density, thereby reducing spin exchange frequency pulling and the size of the vacuum pumps, and to increase reliability. Moreover, the traditional bulky microwave cavity (~30 cm dia) and separate internal quartz bulb can be replaced by a small (15 cm dia) dielectrically loaded cavity with an integral storage bulb.

The results obtained with the first prototype passive hydrogen maser frequency standard are shown in figure 3. Once calibrated, the low drift of less than 6×10^{-16}/day and the excellent long-term stability of this new standard yield an unsurpassed potential memory of the SI second.

Upgraded and reliable electronics are now being completed which should allow us shortly to begin operating a passive maser in the NBS time scale and also in the International Atomic Time scale. Progress is also being made on two small dielectrically loaded cavity units.

Rubidium Gas Cell Standards

Frequency measurements versus microwave power ($P_{\mu\lambda}$) and lamp temperature (T_L) of a passive Rb^{87} frequency standard have been made. This is the first report of the frequency sensitivity as a function of $P_{\mu\lambda}$. The basis for the sensitivity to $P_{\mu\lambda}$ and T_L has been shown to be the spatial inhomogeneities related to high buffer gas density. The type of Rb gas cell studied was an NBS-purchased, commercially available, integrated cell. It must be realized that the data reported herein are for a single unit, and that the coefficients stated below may change markedly for different settings of the microwave power, of the Rb excitation lamp temperature, and of the temperature of the gas cell. In fact, turnover points were found which, of course, greatly reduce the frequency sensitivity to changes in that particular parameter. The following coefficients only give a general value for nominal operating conditions: for microwave power, $\sim5\times10^{-11}$/db; for lamp temperature, $\sim7\times10^{-11}$/C°; and for gas cell temperature, $\sim4\times10^{-10}$/C°.

The overall results of this work gave some very interesting insights into the causes of frequency instabilities in rubidium gas cell standards. Most importantly, a possible method of avoiding some of the key problems was suggested by this work and will be investigated [6].

Ammonia Frequency Standard

The feasibility of a special purpose frequency standard based on microwave absorption in ammonia gas has been investigated [7]. Such a device could potentially fill a need in certain communications and navigation applications for an oscillator which has medium stability, and greater accuracy ($\sim10^{-9}$) than that provided by crystal oscillators, but a cost significantly smaller than that of

more sophisticated atomic frequency standards. A device was constructed* using a stripline oscillator at ~0.5 GHz whose multiplied output was frequency locked to the absorption of the 3-3 line in $N^{15}H_3$(~22.8 GHz). An output between 5 and 10 MHz was provided by direct division from the primary oscillator. Observed stability was 2×10^{-10} from 10 to 6000 s, and reproducibility (accuracy) is estimated to be $\pm\ 2\times10^{-9}$. The unique features of this device include: 1) realization of a high performance stripline oscillator; 2) use of digital servo techniques; 3) unique oscillator cavity servo; 4) pressure shift compensation scheme; 5) and the potential for high acceleration insensitivity.

Quartz Crystal Standards

Quartz crystal controlled oscillators, because of their small size and weight, low power consumption, and commercially unexcelled, short-term stability, have been used as the basic frequency reference in literally millions of systems. Their main limitations have been the sensitivity of the quartz resonator to shock and vibration, temperature variation, changes in driving amplitude, and long-term aging.

Recent advances in quartz resonator design promise to greatly reduce all of these effects, although perhaps not simultaneously. Of particular importance are the new SC, TCC and electrodeless crystals [8,9,10,11]. Several laboratories, including NBS, are developing new electronic circuits which will more fully exploit these new advancements in resonators. Acceleration sensitivities of less than 1×10^{-10}/g, 10 second frequency stabilities $\sigma_y(10s) < 1\times10^{-13}$ and aging rates of less than 10^{-12}/day now appear feasible. Frequency retrace after turn-off/turn-on are also much improved.

If one were to optimally lock a quartz crystal controlled oscillator with excellent short-term stability ($S_\phi(f) \simeq -180$ dB, 1 kHz $\lesssim f \lesssim$ 100 kHz) to a resonator or oscillator with the above expected performance, the resulting standard would be more stable than most present atomic standards for a very large range of sample times, τ. The main limitation would be in the absolute accuracy.

The use of such a hybrid quartz controlled oscillator as the reference oscillator of atomic standards would greatly improve the combined, overall performance including the vibration sensitivity. For example, such an oscillator locked to a commercial cesium device would yield a stability of better than a few $\times10^{-13}$ for all measurement times longer than ≃.02s. Therefore, we expect quartz crystal controlled oscillators based on these new resonators, possibly in combination with presently available oscillators, to play an important role in the following areas: frequency metrology, oscillators for field use, reference oscillators for atomic standards, and spectrally pure sources for high order multiplication applications, plus low temperature.

Superconducting Cavity Oscillator

Another nonatomic device with very interesting properties is the superconducting oscillator. The frequency determining element is a superconducting microwave

*This research was supported by the Advanced Research Project Agency of the Department of Defense and was monitored by ARPA under Contract #3140.

resonator. At 10 GHz, superconducting niobium cavities can be fabricated with Q-factors up to 10^{11}. In addition, these resonators have much smaller nonlinearities than quartz resonators and can be operated with very large internal stored energy. Since the white frequency noise of an oscillator is inversely proportional to both the stored energy and the Q, and the additive white phase noise is inversely proportional to the power delivered to the load, such an oscillator should have excellent spectral purity. Using reasonable parameters, the theoretical noise limit has been predicted to be [12]

$$S_\phi(f) = 10^{-20} f^{-2} \text{ Hz} + 2\text{x}10^{-18} \text{ Hz}^{-1} .$$

Since the resonators are mechanically and electrically very stable and the linewidth is very narrow, superconducting oscillators achieve state-of-the-art medium-term stability. For averaging times between 10s and 1000s, the demonstrated stability is $\sigma_y = 6\text{x}10^{-16}$ for one type of oscillator which used the cavity as a passive frequency discriminator [13].

The high frequency and potential spectral purity of superconducting oscillators make them very desirable for use in frequency multiplication. One of the goals of NBS is to synthesize frequencies from the infrared to the visible with the full accuracy and stability of the primary cesium standard. If suitable nonlinear elements were available, then it would be theoretically possible to multiply the signal from a superconducting oscillator all the way to the visible without loss of the carrier. Other fields can also utilize the high frequency and stability of superconducting oscillators. For example, millimeter wave VLBI and deep space tracking could both utilize the increased coherence time (low flicker noise floor) of superconducting cavity stabilized oscillators.

Conclusion

We believe that our work, as part of other advanced activities in the United States and many other countries of the world, adds credibility to the following predictions: commercial cesium standards with accuracies approaching 10^{-13} may become widely available while laboratory devices may reach 10^{-14}. Long-term stabilities over days and weeks of cesium and hydrogen standards in reasonably protected environments may reach reliably 10^{-15} resulting in time dispersions of less than 10 ns in 10 days. Rubidium and quartz crystal standards may become available with significantly reduced frequency drift; i.e., much less than 10^{-13} per day for rubidium and less than 10^{-12} per day for crystal standards. Clocks and frequency standards for special applications under severe operational or environmental constraints could be developed. Such devices could be based on new quartz resonator types of configurations, and/or on quantum electronic resonances such as rubidium or ammonia.

Devices could be built based on a systems integration of two or more concepts featuring exceptional stability over a large range of averaging times. Examples are a crystal oscillator servoed to a crystal resonator (projected performance: 10^{-13} for $0.1\text{s} \leq \tau \leq 10^5\text{s}$) or a superconducting cavity oscillator servoed to a passive hydrogen maser (projected performance: 10^{-15} for $1\text{s} \leq \tau \leq 10^6\text{s}$).

Finally, it must be realized that the above only touches those possibilities which appear realizable with devices based in the rf and microwave region. In numerous laboratories and organizations, including NBS, research and advanced development are carried out on novel standards and metrology in the far infrared,

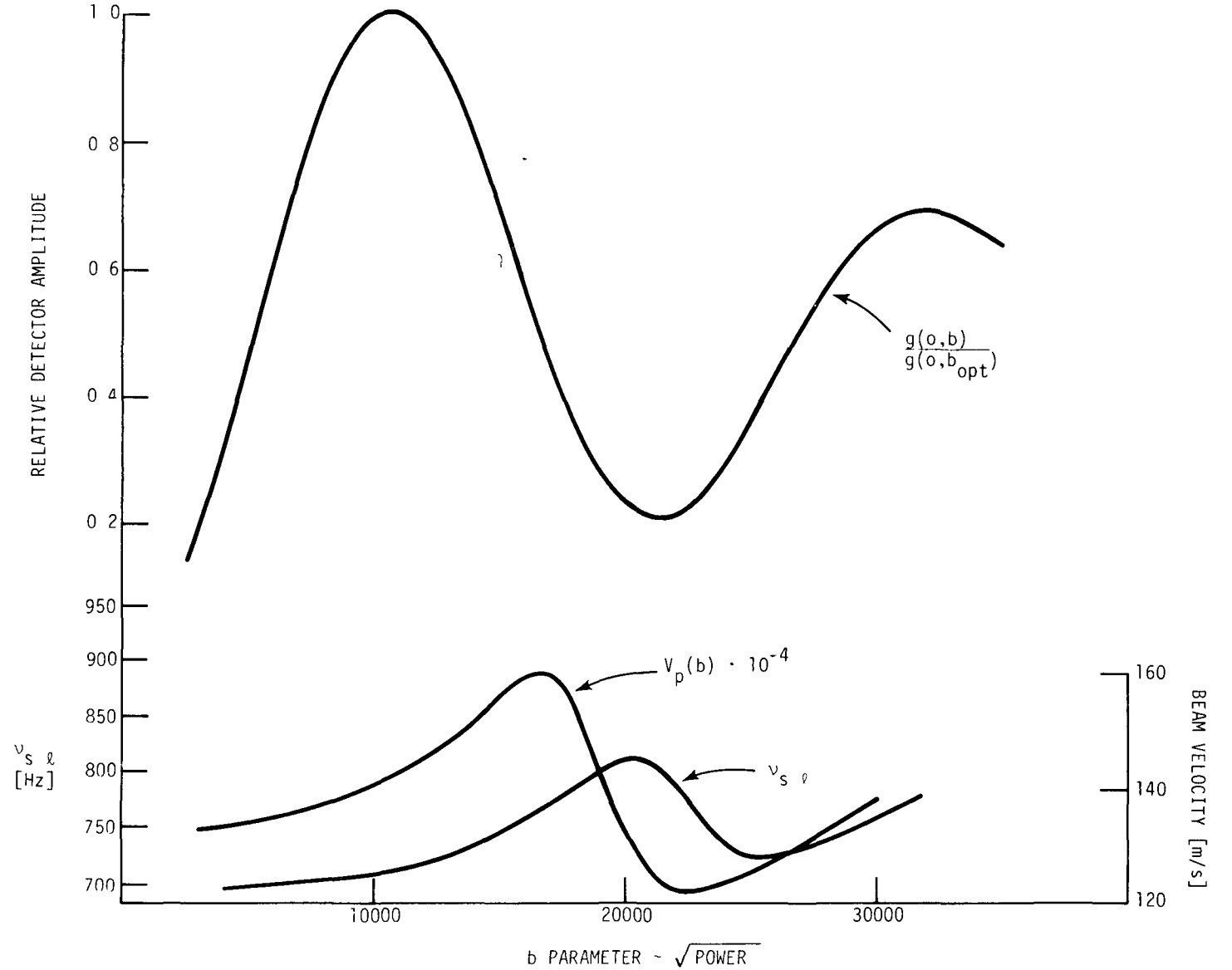


Fig. 1-The dependence of the amplitude of the detected signal ($g(o,b)/g(0,b_{opt})$), of a most probable transition velocity ($V_p(b)\cdot 10^{-4}$), and of the frequency displacement of the first side peak or side lobe with respect to the center peak ($\nu_{s.l.}$) as a function of the b parameter (a parameter proportional to the microwave power) in a high performance commercial cesium standard.

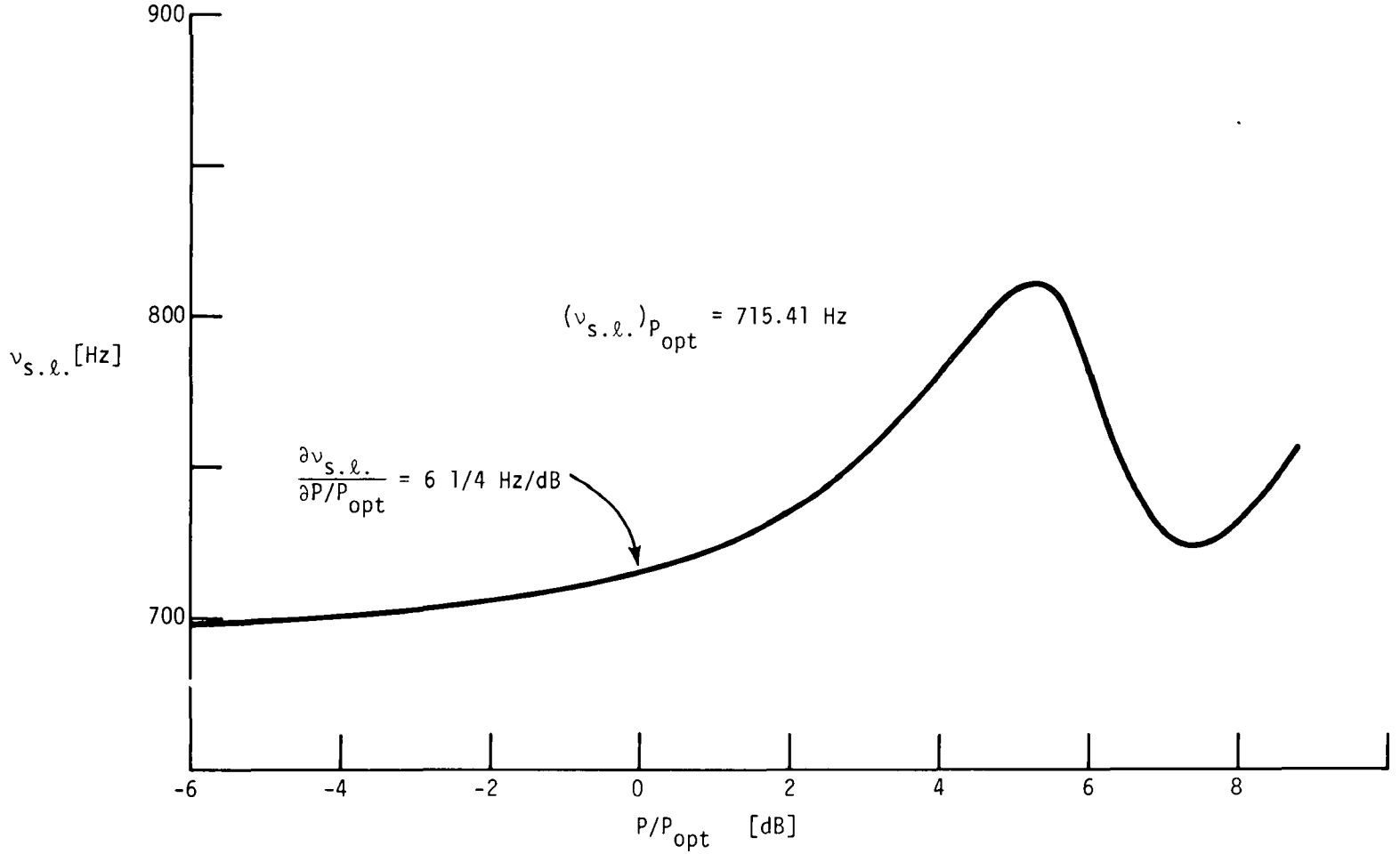


Fig. 2-The dependence of the Ramsey pattern side lobe frequency offset from the center peak as a function of microwave power for a high-performance commercial cesium standard. Optimum power (P_{opt}) is the power setting for maximum signal at the cesium detector.

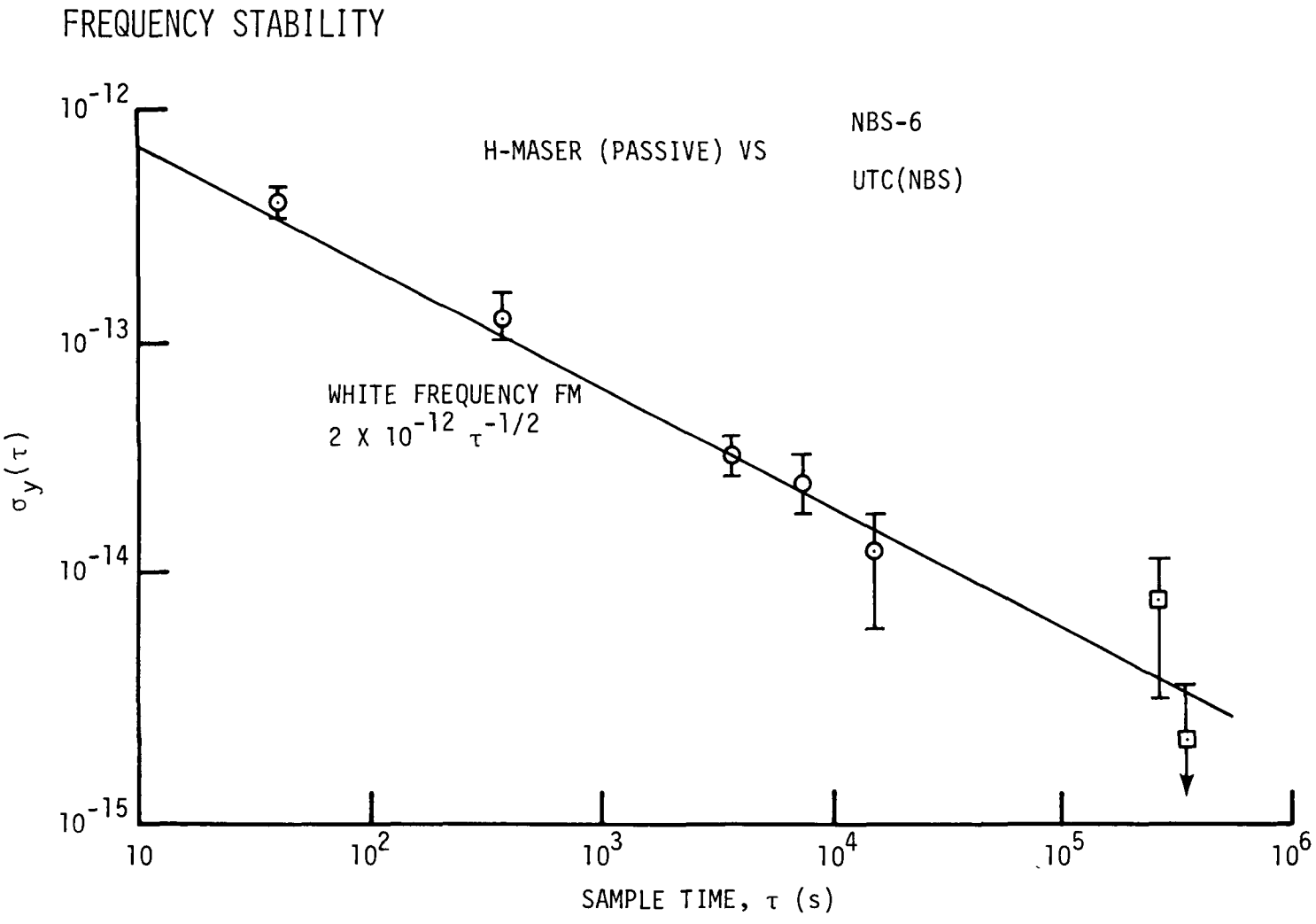


Fig. 3-Frequency stability measurements of an NBS prototype passive hydrogen maser frequency standard--showing no apparent flicker floor at well below 10^{-14}.

QUESTIONS AND ANSWERS

DR. JACQUES VANIER, Laval University:

You mentioned accuracy for rubidium, and you mentioned at the same time a breakthrough to get this accuracy. Could you elaborate on this?

MR. ALLAN:

No. I would rather let the investigators have their chance. They have to do their thing before it can be talked about.

MR. ANDREW CHI, NASA Goddard Space Flight Center:

I notice that the data that you give in the last slide is a mix between projected and present-day performance. In the projected data, for instance, the cesium stability for 10 days is approximately 1 part in 10^{15}. Can you state at what time you can anticipate that performance?

MR. ALLAN:

On NBS-4, we have already seen 7 parts in 10^{15} flicker floor at sample times approaching 10 days. For commercial standards, I would project that we would see consistent stabilities below 1 part in 10^{14} in the next three or four years.

MR. CHI:

Was this measured by two cesium standards or just one?

MR. ALLAN:

It depends. There are several ways you can do it, of course. If you have a very good standard, you can use just one standard as the reference. Let me mention specifically that the measurements on the passive hydrogen maser were extremely difficult--it took a whole ensemble just to measure that one device. Our net assessment was that the passive hydrogen was as good as our whole clock ensemble--maybe better.

DR. ROBERT VESSOT, Smithsonian Astrophysical Observatory:

I think the acceleration question is probably the key to how you treated the temperature coefficient, because it is a question of engineering. I remember vividly when we were testing the Probe, we had to estimate the effect of gravity. So we turned it upside down and measured the two g effect. And it was a good deal less than a part in 10^{11} per g, and we did that just by making sure that the end plates and the cavity were about the same weight so they sagged by the same amount.

I should think the same sort of tricks could be done with cesium. And in the case of quartz, it is obvious that the device is in fact a mechanical thing and therefore subject directly to stress of gravitational loading, and the same with the superconducting cavity. So, I think you are right in saying you have to take it with a grain of salt.

DR. REINHARDT, NASA Goddard Space Flight Center:

The fact that some of the standards use phase lock loops and some use frequency lock loops greatly changes their sensitivity to crystal effects used in the VCO. I don't think in the hydrogen you can say that there is an actual frequency offset due to crystal effects--A phase shift, yes, but not a frequency offset.

MR. ALLAN:

In the oscillator?

DR. REINHARDT:

Yes, due to the crystal oscillator being stressed.

MR. ALLAN:

Right. Of course, even in the passive hydrogen, if you have a tight locked loop, you only see the output frequency move by one over the loop gain times the natural frequency change of the quartz oscillator. So it probably could be much less than the coefficient shown in the slide also--in other words, not limited by the quartz but by the atomic resonance.

ANALYSIS OF DEGRADED HYDROGEN DISSOCIATOR ENVELOPES BY AES*

Victor H. Ritz, Victor M. Bermudez, and Vincent J. Folen
Naval Research Laboratory
Washington, DC 20375

ABSTRACT

The performance of hydrogen dissociators used in atomic clocks is known to degrade after prolonged operation, requiring large increases in rf power to maintain a constant output of atomic hydrogen. Auger electron spectroscopy (AES) has been used to characterize the inner surfaces of Pyrex dissociator envelopes obtained from NASA Goddard Space Flight Center and Smithsonian Institution Astrophysical Observatory hydrogen masers. Prolonged operation of the dissociators leads to buildup of a dark film incorporating large quantities of carbon in its amorphous and carbide forms and smaller amounts of nitrogen. Possible mechanisms by which the film could interfere with the operation of the dissociator are given which involve its electrical conductivity and its role as a catalyst in the recombination of atomic hydrogen.

INTRODUCTION

A hydrogen maser will be used as a very accurate and stable frequency standard in a Navigation Technology Satellite (NTS-3) for the NAVSTAR Global Positioning System (GPS). The atomic hydrogen for the maser will be supplied by a dissociator of the type shown schematically in Fig. 1. The device operates by maintaining a rf glow discharge of $\approx$100 MHz in low pressure hydrogen gas admitted to the glass dissociator envelope. A gradual degradation in performance of such dissociators has been observed which apparently results from changes in the glass envelope after several months of operation. This degradation requires large increases in rf power to maintain a resonable output of hydrogen atoms from the dissociator and limits its useful lifetime in satellite applications. The degradation is apparently connected with the concomitant darkening of the glass which is observed to occur as a light to dark brown film builds up on the inner surfaces of the dissociator. A photograph of a used dissociator envelope obtained from a Smith-

*Sponsored by The Naval Electronic Systems Command.

sonian Institution Astrophysical Observatory hydrogen maser is shown in Fig. 2. The arrow points to a dark brown discolored area. We have characterized such films by using Auger electron spectroscopy (AES) with in-depth sputter ion profiling. This paper will describe our recent measurements and summarize those obtained earlier [1].

EXPERIMENTAL TECHNIQUES AND RESULTS

Auger electron spectroscopy is a method of surface chemical analysis which is accomplished by energy analysis of the electrons ejected from a sample while it is bombarded with an electron beam [2]. The general arrangement of the apparatus (Physical Electronics Industries) is shown in Fig. 3. Samples are placed on a carrousel target holder and bombarded with monoenergetic electrons (3-5 kV) from either of the electron guns. The sample emits "Auger electrons" whose energies are characteristic of the atoms from which they were ejected. The Auger electrons are detected by the electron multiplier in the single pass cylindrical mirror analyzer and, after electronic processing, an Augér spectrum is displayed on an X-Y recorder. Since the Auger electrons which are detected come from the top few layers (i.e., depths of 10-20 Angstroms), AES is primarily a surface analytical technique. Information about the composition of the sample at greater depths can be obtained by ion-milling the surface with Argon ions from the sputter ion gun also shown in Fig. 3.

Our AES measurements were made with a Physical Electronics Industries cylindrical mirror analyzer (Model 10-155) operated at 5 kV in the derivative mode. The sample holder was oriented so the beam from the coaxial electron gun struck the dissociator glass at grazing incidence to minimize charging effects. The ultrahigh vacuum system was pumped down to $\approx 5 \times 10^{-10}$ Torr without bakeout before being backfilled with Ar for profiling with a PHI model 04-161 sputter-ion gun operated at 2 kV. An approximate calibration of the sputter-etch rate was obtained by profiling Ti films of known thickness deposited on glass substrates.

A typical AES spectrum for dissociator glass is shown in Fig. 4. The derivative of the number of electrons detected in each Auger peak by the analyzer is plotted as a function of the Auger electron energy. The various peaks have been labeled according to their corresponding elements. A quantitative chemical analysis may then be obtained from these raw peak heights by applying appropriate corrections. The elemental sensitivity factors of Palmberg et al. [3] obtained with the electron beam at 3 kV were scaled to 5 kV using correction factors measured in our apparatus for each element and SiO_2 . The raw Auger peak heights were processed with these sensitivity factors and summed over all the elements in the sample to obtain the atomic fraction of each element. The dissociator glass was Pyrex with a nominal composition (mol%) of 81% SiO_2, 13% B_2O_3, 4% Na_2O, and 2% Al_2O_3. Na was

rather difficult to detect reproducibly because of its high mobility during AES at room temperature [4], and a constant atomic fraction equal to 0.023 was assumed for it in summing the AES peaks.

In a dissociator of the NASA-Goddard configuration shown in Fig. 1, the rf power is introduced capacitively, and the glass surface immediately beneath the electrodes remains clear while the surrounding walls are darkened. Presumably, the sputtering action of the glow discharge near the electrodes continuously cleans the surface. Samples were cut from adjacent clear and slightly darkened areas of a degraded NASA-Goddard dissocator (sample 1) and subjected to AES analysis. The results are shown in Fig. 5. Both the atomic fraction and depth scales should be considered to be approximate. The upper half of the left side of Fig. 5 shows the main constituents of the clear portion of sample 1. O, Si, B, and Al are present in large concentrations which approach the nominal composition of Pryex (shown on the right-hand ordinate) after the contaminated surface layer has been sputter-etched away. A large amount of C is present on the surface which is removed fairly rapidly as the etching progresses. The lower half of Fig. 5 shows the elements present in smaller concentrations. The analysis of the slightly darkened portion of sample 1 is given on the right side of Fig. 5. It is distinguished by a very high C concentration on the surface which persists throughout the depth analyzed. N is also a prominent contaminant but at lower concentrations.

Samples of clear and darkened glass were also taken from another NASA-Goddard dissociator (sample 2). In this case, the darkened glass had a thick dark brown opaque film on it. AES was performed on the opaque film on the inner surface of the dissociator and also on the outer surface of an adjacent clear area as a check on the composition of a surface which had never been exposed to the glow discharge. Results for most elements parallel those for sample 1, and are shown in Fig. 6. Again, the primary difference was the presence of C and, to much lesser extent, N in the darkened glass.

In principle, the shape and position of the Auger peaks (e.g., Fig. 4) should yield some information about the chemical bonding in these films which are probably a mixture of amorphous C, SiO_2, SiC and Si_3N_4. The chemical bonding shifts which have been seen by other workers [5] [6] for the Si LMM and KLL peaks are shown schematically in Fig. 7. The Si_3N_4 LMM peak at 82 eV, is a shoulder of the main peak at 87eV, and moves to 80 eV when the Si_3N_4 is grown in the presence of oxygen [5]. Unfortunately, the close spacing of these shifts and the fact that several of these compounds were present simultaneously made it impossible for us to resolve them. Erratic charging of the sample to 5-10 Volts during analysis also contributed to the problem. More definitive results were obtained for C. Close inspection of the Auger spectra for the darkened portion of sample 1 revealed that the C peak changed from that characteristic of amorphous C[7] the "carbide type"

oberved by Grant and Haas [6]. Details of our Auger spectra for the amorphous and graphitic forms of C are shown in Fig. 8 along with the "carbide type" peak. We were thus able to distinguish between the amorphous and carbide forms of C as the films were sputter etched.

The atomic fractions of C in the clear and darkened portions of NASA-Goddard samples 1 and 2 are plotted in Fig. 9. The carbide peaks are designated by solid triangles. Figure 9 suggests that the surfaces of the dissociator fall into several categories. The clear outside surface of sample 2 incorporates very little C and no detectable N. This surface is easily cleaned of C by sputter etching and behaves in a way similar to that of a clean smooth microscope slide. The lightly darkened portion of sample 1 has a thin amorphous C layer on the surface and a persistent high concentration of carbide underneath it. A smaller concentration of N is also present. The clear portion of sample 1 under the electrodes has a layer of amorphous C and N which can be etched off fairly rapidly. The very thick opaque film analyzed in the darkened portion of sample 2 has amorphous C as its principal impurity along with smaller amounts of N. It does not etch off as easily, and has substantial amounts of C remaining at depths where the clear portions are quite clean.

AES was also performed on the dissociator from a Smithsonian Institution Astrophysical Observatory hydrogen maser which was operated continuously for 3 years at Maryland Point. This dissociator presented a variety of opaque discolorations which might be described as being milky, light brown, and dark brown. A milky portion of the inside of the dissociator was analyzed and compared to a portion of the outside. The most outstanding feature of the analysis was a heavy coating of amorphous C on the inside. The results are shown in Fig. 10 and generally parallel those of Fig. 9. Note that the film has been sputter-etched to a much greater depth and appears to be 1000-2000 Angstroms thick.

In addition to AES, some optical studies were made of the dissociator films. Optical spectra were obtained in the so-called "window" region of the glass substrate in the wavelength range between 300 nm and 4μ. Optical studies of NASA-Goddard dissociator sample 1 in the visible are shown in Fig. 11. The darkened glass in characterized by a structureless absorption edge monotonically rising from a low value in the near infrared to a high value in the ultraviolet. The results in the visible are similar to the broad background observed by Mattern et al. [8] in the course of H^+ - implantation experiments on fused silica and attributed to beam-assisted formation of a carbon film from organic contaminants. The assignment of the darkening to a carbon deposit is also supported by the proton irradiation work of Greer and Hapke [9], who point out that this absorption may be partly due to radiation-induced color center formation in the glass. However, the dominant effect would seem to be C-film buildup.

Optical measurements in the infrared are shown in Fig. 12 for portions of NASA-Goddard dissociator sample 1. The difference in transmission between the clear (1) and dark brown (2) samples indicates the presence of a weak band at $\approx 3240\ cm^{-1}$; i.e. 3.1μ. This band disappeared when the dark brown sample was scraped to remove the film (3) and was therefore intrinsic to the film. The band is too low in energy to be assigned to the O-H stretching vibration in isolated Si-OH or C-OH groups (3600 - 3750cm^{-1}) [10] and is lower in energy than the band observed in H^+-implanted fused silica (3680cm^{-1}) [8]. It is, however, higher in energy than the C-H stretching vibration in alkanes or alkenes (2800 - 3100cm^{-1}) and the Si-H mode in silanes (2150 - 2250cm^{-1}) [10]. The band falls within the range expected for hydrogen-bonded O-H groups but is too sharp in comparison with the broad, asymmetric band which results from internal O-H groups in the glass (3600cm^{-1}). Si_3N_4 films formed by decomposition of gaseous mixtures of SiH_4 and NH_3 show a band at about 3340cm^{-1}, assigned to the impurity N-H stretching vibration [11]. Since the dissociator film contains a high concentration of N, this is a possible explanation for the infrared data. Furthermore, the 3240cm^{-1} band lies within the range of C-H stretching frequencies in alkynes (monosubstituted acetylenes, 3200 -3350cm^{-1}) [10], in which the bonding orbitals on the carbon are in s-p hybridization. If this latter interpretation is correct, it indicates the presence of highly unsaturated carbon - carbon bonds in the film, which may be an important contribution to its photoconductivity.

DISCUSSION

Our experimental results indicate that the darkening of the glass dissociator envelope is caused by the formation of a composite film incorporating large quantities of C in its amorphous and carbide forms and smaller amounts of N. There are two general mechanisms by which formation of the film can interfere with the operation of the hydrogen dissociator: The electrical conductivity of the film can be high enough to exclude a fraction of the rf field, or the film can catalyze the recombination of hydrogen atoms.

The room temperature dc conductivity of various appropriate materials is given in Table I. It is seen that the dc conductivity of graphite ($\approx 7 \times 10^2$ ohm^{-1}-cm^{-1}) is much less than that of Cu ($\approx 6 \times 10^5$). Measurements on amorphous C films [12] have shown even lower conductivity (≈ 10 ohm^{-1}-cm^{-1}), as have Si_3N_4 (2×10^{-6} ohm^{-1}-cm^{-1}) and amorphous SiC (10^{-2} to 10^{-4} ohm^{-1}-cm^{-1}). However, higher values ($\approx 3 \times 10^3$) have been observed for SiC doped with ≈ 0.005 atomic fraction of N [13]. Using the latter value, one may calculate the classical skin depth to be $\approx 100\ \mu$ at 100 MHz, and a rather thick film would be required to attentuate the rf input to the dissociator. One might also note that a large impurity photoconductivity has been observed in SiC [14], although no similiar data are available for impure carbon. Thus it is

possible that the conductivity of the composite film on the dissociator walls is higher than indicated in Table I under actual operating conditions when illuminated by the hydrogen glow discharge. In general, however, it would appear that very thick films would be required to effectively exclude the rf field.

Either direct or catalyzed reaction of the atomic hydrogen at the film would result in decreased output from the dissociator as the film is deposited. The principal reaction product of direct reaction of atomic hydrogen with carbon is known to be CH_4 and its rate of reaction with molecular H_2 is negligibly small below 1000°C [15]. However, King and Wise [16] have found that the direct reaction is a minor process in the carbon-atomic hydrogen system below 200°C and accounts for no more than 0.5% of the hydrogen atom removal. At higher temperature, the direct reaction increases but is still much smaller than catalytic recombination of the hydrogen atoms at the carbon film. It should be pointed out that the low pressures under which the dissociators operate ensure that recombination at the walls is much larger than in the volume of the gas itself.

There is a great variation in literature values of the heterogeneous recombination coefficient γ, defined as the fraction of atoms striking the surface that recombine. The discrepancies among values for the same material result from differences in thermal and chemical history and in surface roughness and contamination. A summary of values which have been obtained by various workers is given in Table II. Values for γ_5 at room temperature of $\approx 580 \times 10^{-5}$ for Pyrex and of $\approx 1000 \times 10^{-5}$ for an evaporated C film have been obtained by Wise and coworkers [16][17]. More recently, values of $\approx (5\text{-}50) \times 10^{-5}$ have been measured for clean Pyrex and fused silica, while studies of pyrographite and electrode graphite have yielded values from 5000-10,000 $\times 10^{-5}$ [18]. Thus, a contaminating C film can be expected to increase the efficiency of recombination via atom-wall collision by at least a factor of 2 and perhaps by as much as a factor of 10-100.

Some possible sources of the C which builds up on the hydrogen dissociator walls are the residue left by inadequate initial cleaning of the glass, pump oil, CO, CO_2 or CH_4 outgassed from the walls and O-rings and the breakdown of epoxy cement into its constituents. Steps to minimize the influence of these sources would seem to be a sensible precaution in any hydrogen dissociator to be used for long periods of time.

ACKNOWLEDGEMENTS

The authors thank H. Peters and R. Vessot for providing samples of used dissociator chambers from NASA-Goddard Space Flight Center and Smithsonian Institution Astrophysical Observatory hydrogen masers, respectively. D.L. Griscom provided the drawing used as Figure 1.

REFERENCES

[1] V.H. Ritz, V.M. Bermudez, and V.J. Folen, J. Appl. Phys., 48, 2096 (1977).

[2] For a review see C.C. Chang, in Characterization of Solid Surfaces, (Plenum Press, New York, 1974), Ed. by P. Kane and G. Larrabee, pps. 509-561.

[3] P.W. Palmberg, G.E. Riach, R.E. Weber, and N.C. MacDonald, Handbook of Auger Electron Spectroscopy (Physical Electronics Industries, Edina, Minn., 1972).

[4] C.G. Pantano, D.B. Dove, and G.Y. Onoda, J. Non-Cryst. Solids 19, 41 (1975).

[5] P.H. Holloway, Surface Sci. 54, 506 (1976).

[6] J.T. Grant and T.W. Haas, Phys. Lett. 33A, 386 (1970).

[7] R. Ducros, G. Piquard, B. Weber, and A. Cassuto, Surface Sci. 54, 513 (1976).

[8] P.L. Mattern, G.J. Thomas, and W. Bauer, J. Vac. Sci. Technol. 13, 430 (1975).

[9] R.T. Greer and B.W. Hapke, J. Geophys. Res. 72, 3131 (1967).

[10] L.J. Bellamy, "Advances in Infrared Group Frequencies" (Methuen, London, 1968).

[11] Yu. I. Prokhorov, V.A. Sologub and B.A. Sukhodaev, Zh. Prikl. Spektr. 19, 520 (1973) - Engl. Transl.: J. Appl. Spectr. 19, 1211 (1973).

[12] M. Morgan, Thin Solid Films 7, 313 (1971).

[13] G.A. Slack and R.I. Scace, J. Chem. Phys. 42, 805 (1965).

[14] G. Jungk, K. Thiessen, and F. Witt, Phys. Status Solidi 3, 735 (1963).

[15] R.K. Gould, J. Chem. Phys. 63, 1825 (1975); B. McCarroll and D.W. McKee, Carbon 9, 301 (1971); Y. Sanada and N. Berkowitz, Fuel 48, 375 (1969).

[16] A.B. King and H. Wise, J. Phys. Chem. 67, 1163 (1963).

[17] B.J. Wood and H. Wise, J. Phys. Chem. 66, 1049 (1962).

[18] V.A. Lavrenko et al, Sov. Powder Metall. and Metal Ceram. 4(64), 320 (1968).

TABLE I

D.C. CONDUCTIVITY OF
VARIOUS MATERIALS

Material	σ in ohm^{-1} cm^{-1}
Copper[a]	6×10^5
Graphite[a]	7×10^2
Amorphous Carbon Film[b]	10
Silicon Nitride[c]	2×10^{-6}
Amorphous SiC Film[d]	10^{-2} to 10^{-4}
SiC with 0.5% Nitrogen[e]	3×10^3

a "Handbook of Chemistry and Physics — 54th Ed." (C R C Press, Cleveland, 1973), p F-155

b M Morgan, Thin Solid Films 7, 313 (1971)

c A V Gritsenko et al., Microelectronics 5, 170 (1976)

d G V Bunton, J Phys D 3, 232 (1970)

e G A Slack and R I Scace, J Chem Phys. 42, 805 (1965)

TABLE II

RECOMBINATION COEFFICIENTS FOR ATOMIC HYDROGEN

Material	γ
Vycor[a]	7×10^{-5}
Pyrex[b]	60×10^{-5}
Pyrex[c]	70×10^{-5}
Pyrex[d]	580×10^{-5}
Carbon Film[e]	$1{,}000 \times 10^{-5}$
Pyrographite[f]	$\approx 6{,}800 \times 10^{-5}$
Electrode Graphite[f]	$10{,}000 \times 10^{-5}$
Silicon Carbide[g]	$2{,}400 \times 10^{-5}$

a A Mandl and A Salop, J Appl Phys 44, 4776 (1973)

b M Coulon et al , J Chim Phys 70, 1493 (1973)

c G A Melin and R J Madix, Trans Faraday Soc 67, 2711 (1971)

d B J Wood and H Wise, J Phys Chem 66, 1049 (1962)

e A B King and H Wise, J Phys Chem 67, 1163 (1963)

f V A Lavrenko et al , Sov Powder Metall and Metal Ceram 4(64), 320 (1968)

g V A Lavrenko et al., Dopov Akad Nauk Ukr RSR, Ser B, 30(3), 262 (1968)

LIST OF FIGURES

Fig. 1 Schematic of hydrogen dissociator for production of atomic hydrogen.
Fig. 2 Discolored area of used Smithsonian Astrophysical Observatory dissociator.
Fig. 3 Apparatus for Auger electron spectroscopy.
Fig. 4 Typical AES spectrum for dissociator glass.
Fig. 5 AES elemental analysis as a function of material removed for the clear and darkened portions of sample 1 (NASA-Goddard).
Fig. 6 AES elemental analysis as a function of material removed for the clear (outside) and darkened portions of sample 2 (NASA-Goddard).
Fig. 7 Chemical bonding shifts expected for Si Auger peaks in various compounds.
Fig. 8 Auger peaks for graphite (amorphous) and "carbide type" C.
Fig. 9 Atomic fraction of C as a function of material removed for the clear and darkened portions of NASA-Goddard samples 1 and 2. The solid triangles indicate a "carbide-like" peak. The clear portion of sample 2 was analyzed on the outside for comparison.
Fig. 10 Atomic fraction of C as a function of material removed from the inside (milky) and outside portions of a S.A.O. dissociator.
Fig. 11 Optical absorption of the clear and darkened portions of NASA-Goddard dissociator sample 1.
Fig. 12 Percent transmission of clear (1), dark brown (2) and scraped dark brown (3) portions of NASA-Goddard dissociator sample 1.

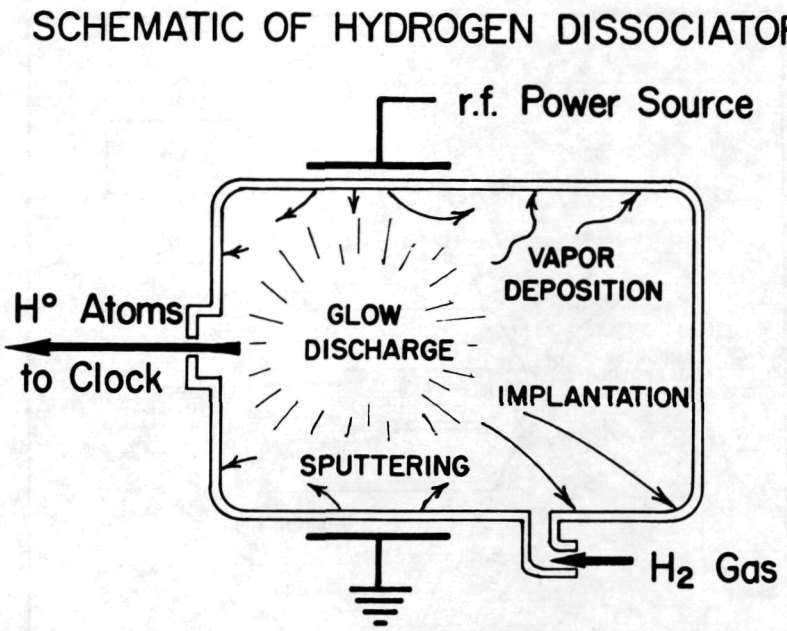


Fig. 1 Dissociator for production of atomic hydrogen.

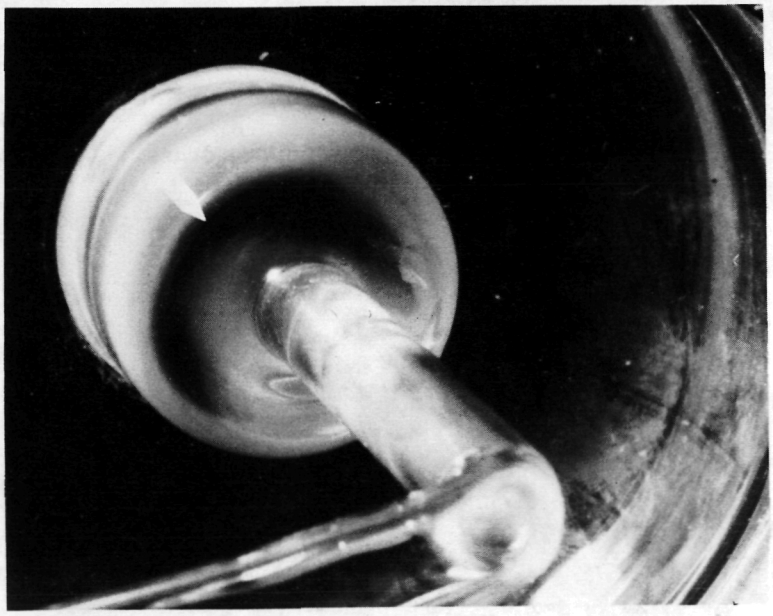


Fig. 2 Discolored portion of S.A.O. dissociator.

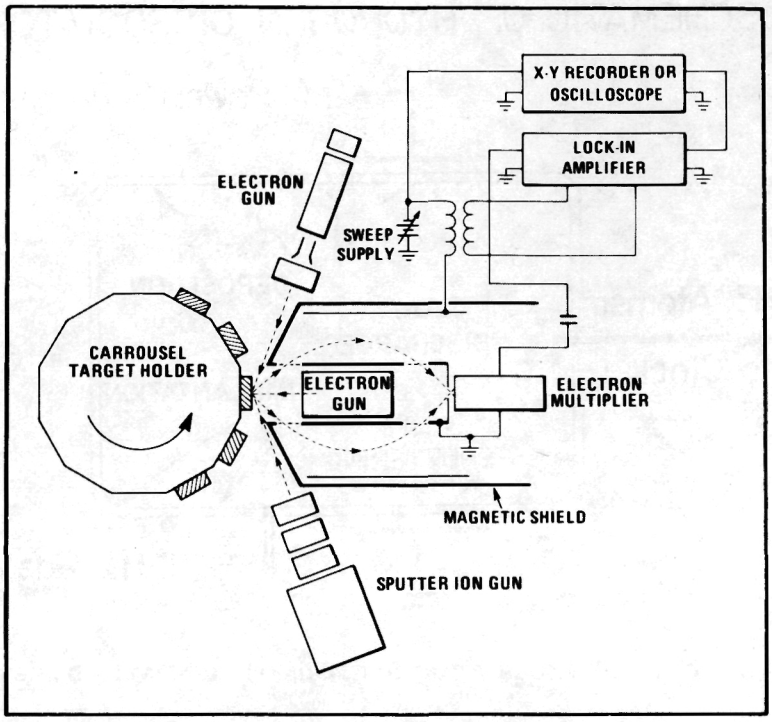


Fig. 3 Apparatus for Auger Electron Spectroscopy.

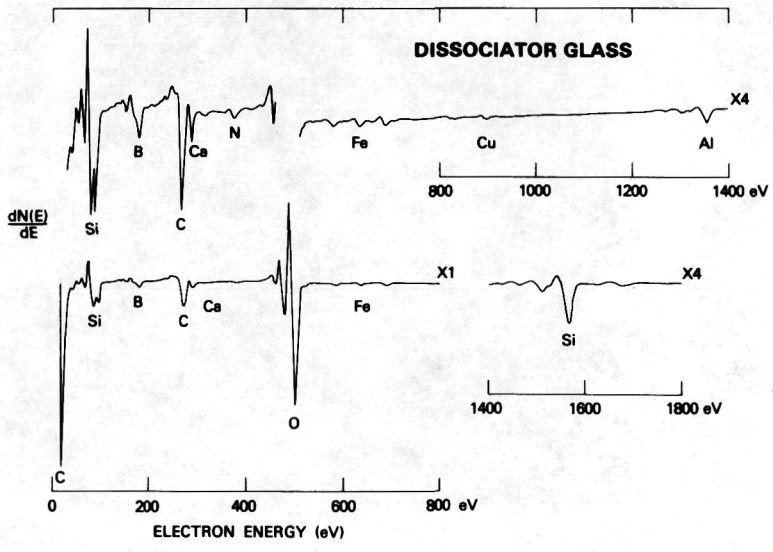


Fig. 4 Typical AES spectrum of dissociator glass.

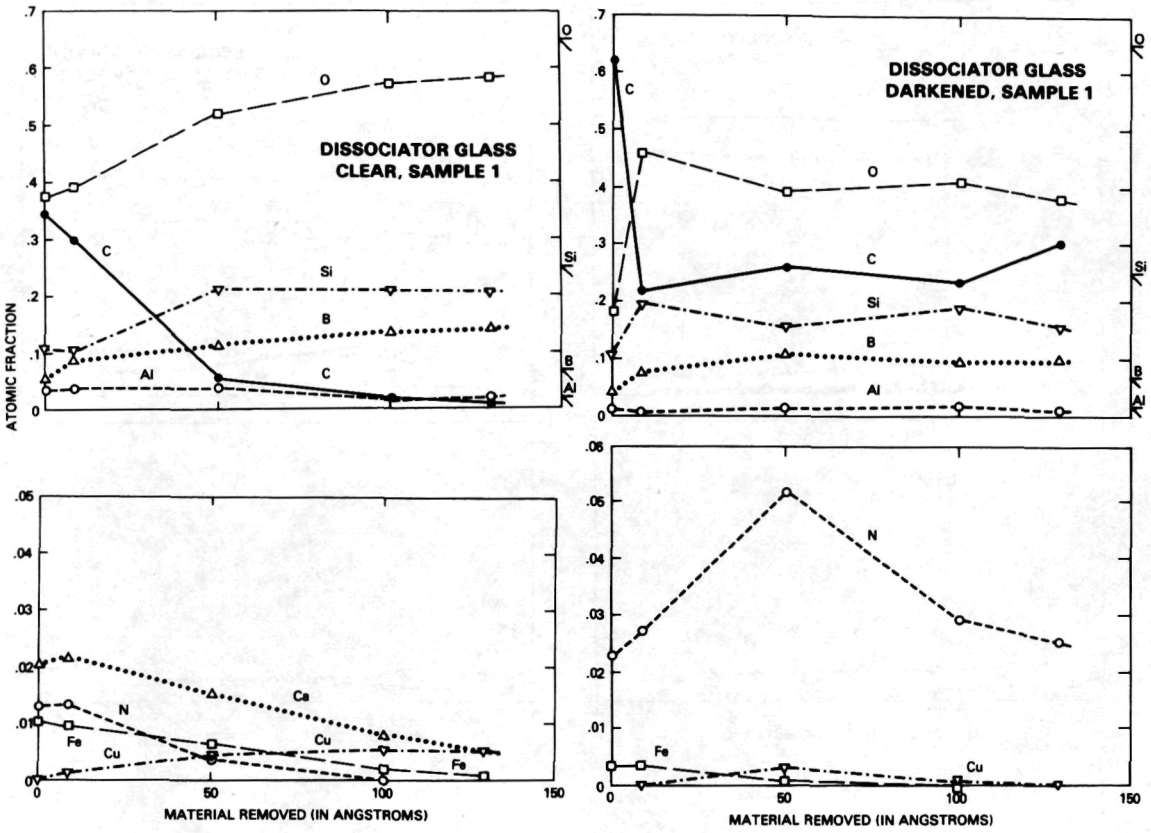


Fig. 5 AES elemental analysis as a function of material removed for the clear and darkened portions of sample 1 (NASA-Goddard).

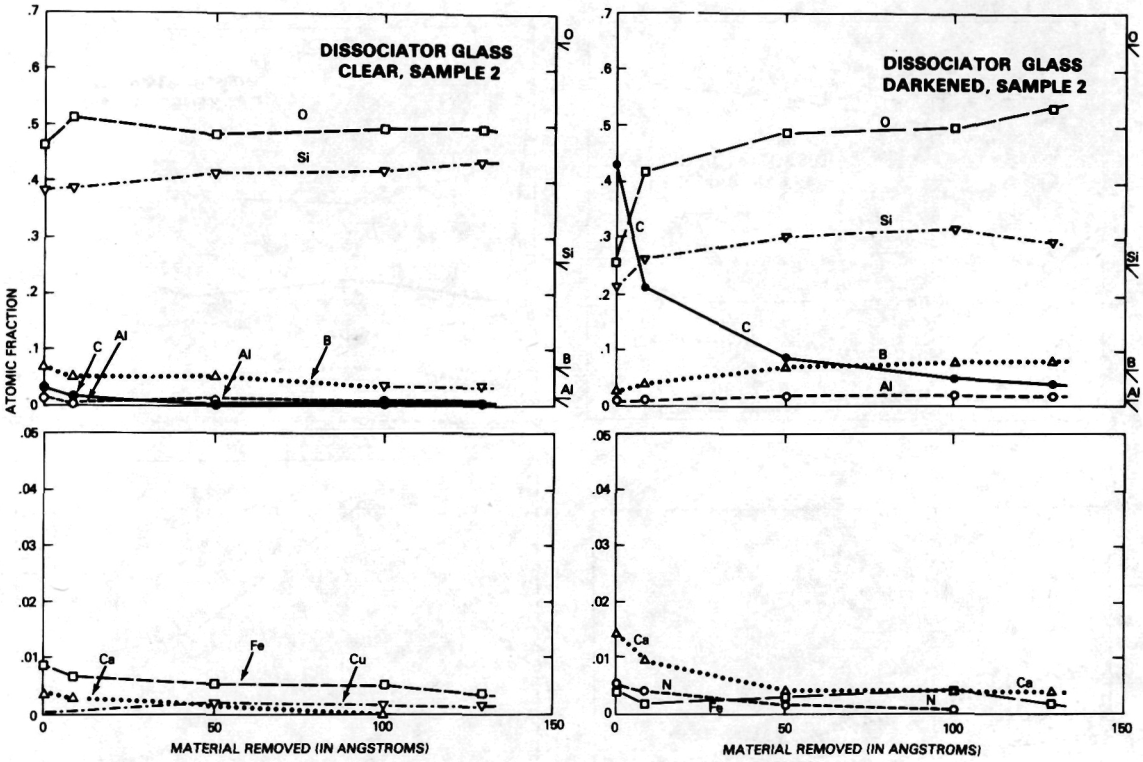


Fig. 6 AES elemental analysis as a function of material removed for the clear (outside) and darkened portions of sample 2 (NASA-Goddard).

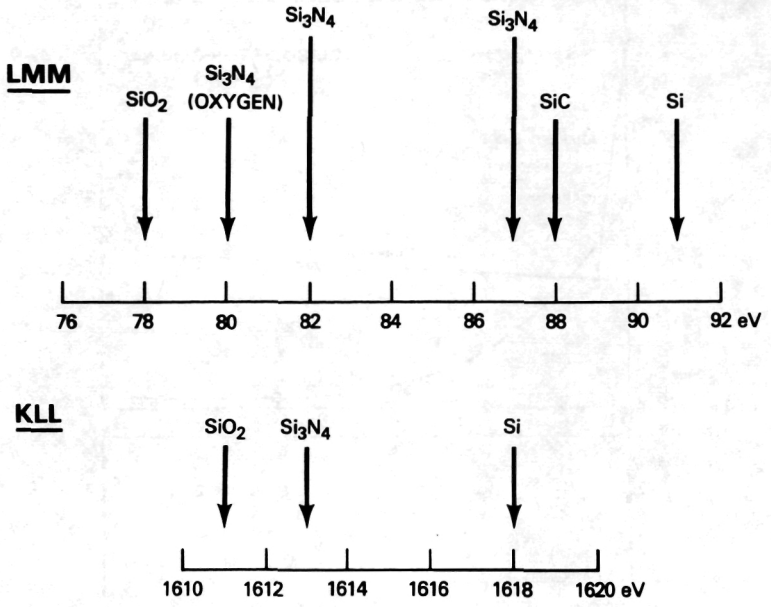


Fig. 7 Chemical bonding shifts for Si.

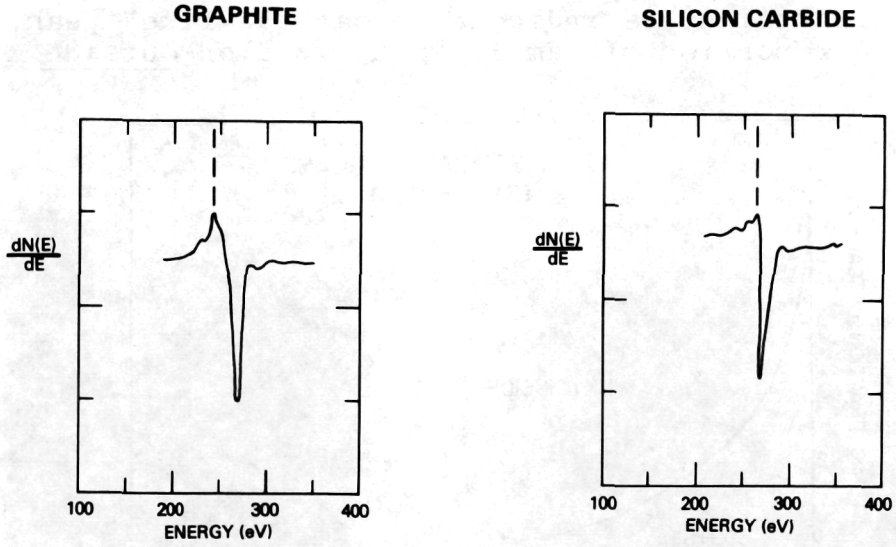


Fig. 8 C Auger peaks in graphite and silicon carbide.

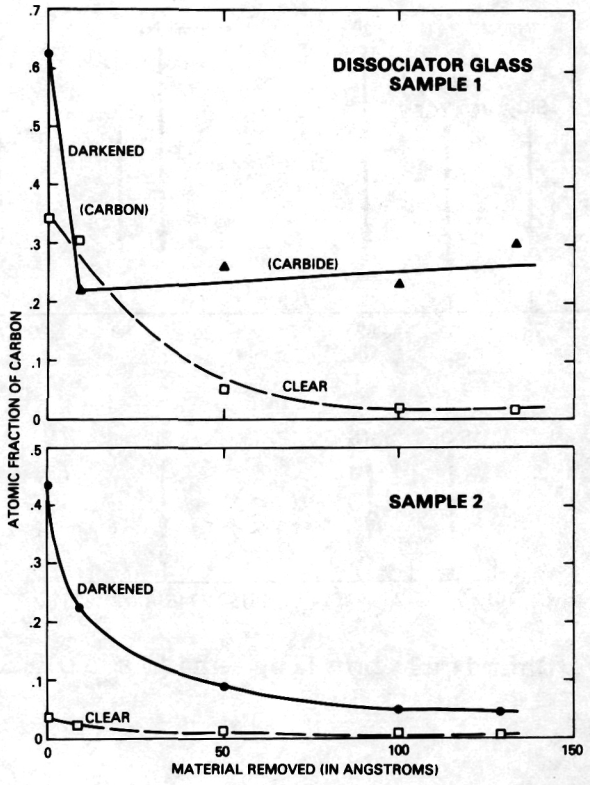


Fig. 9 C content vs depth for NASA-Goddard samples 1 and 2. Solid triangles indicate a "carbide-like" peak. Clear portion of sample 2 analyzed on outside.

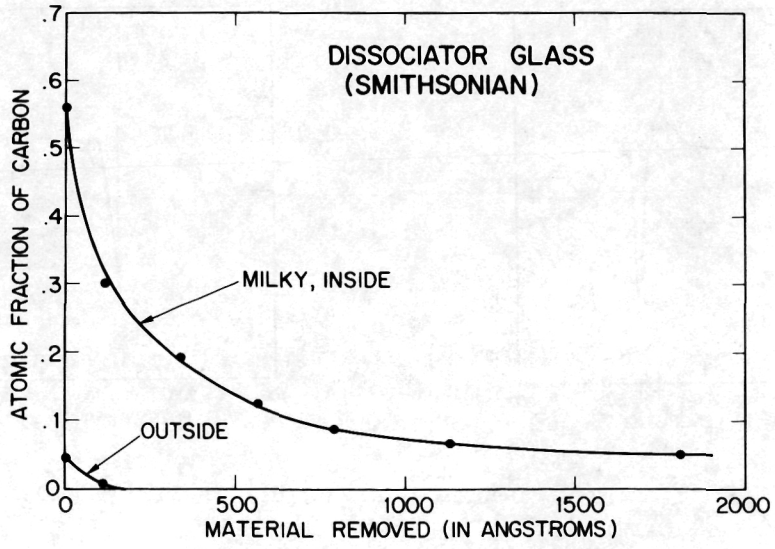


Fig. 10 C content vs depth for a S.A.O. dissociator.

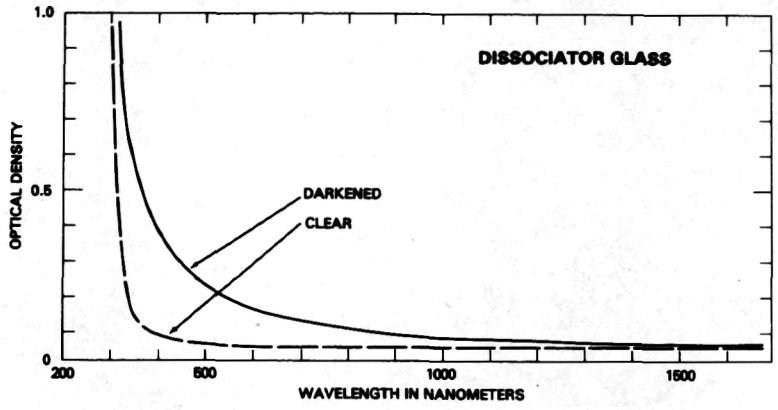


Fig. 11 Optical absorption of the clear and darkened portions of NASA-Goddard dissociator sample 1.

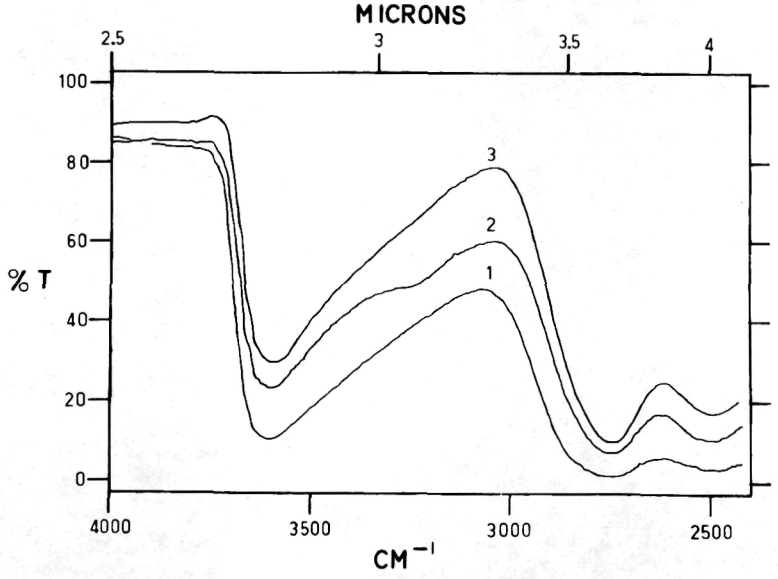


Fig. 12 Percent transmission of clear (1), dark brown (2) and scraped dark brown (3) portions of NASA-Goddard dissociator sample 1.

Page intentionally left blank

Page intentionally left blank

AN INVESTIGATION OF POLYMER COATINGS USED IN HYDROGEN MASER STORAGE BULBS

N. H. Turner
Chemistry Division
Naval Research Laboratory
Washington, D. C. 20375

ABSTRACT

X-ray photoelectron spectroscopy has been used to investigate the surface composition (top 50 Å) of some fluorinated polymers that either have been, or could be, used to coat the storage bulbs in hydrogen masers. The results indicate inadequacies of some of the coatings, and the long term effect of exposure to hydrogen atoms. Recently developed fluorinated polymers have been investigated also as possible coating materials.

INTRODUCTION

With hydrogen masers under consideration as a timing standard in the NAVSTAR Global Positioning System, this paper will report the results of a study of some of the fluorinated polymer surfaces that have been used in hydrogen maser storage bulbs. The possibility of the use of some fluorinated polymers recently developed at the Naval Research Laboratory (NRL) has been considered also. The surface of the hydrogen maser storage bulbs may play an important role in both the short term and long term stability of the maser. For example, it has been reported that the lowest surface hydrogen atom recombination coefficient observed (by about two orders of magnitude) is that in which the surface has been coated with Teflon (1); this effect could be somewhat larger, but precision of the reported results was poor. This comparison was made with a wide number of surface treatments (2). Hydrogen atom recombination would take away hydrogen atoms that could be involved in the maser action. Thus, the surface of the hydrogen maser storage bulb could contribute to the poorly understood temperature effect on frequency changes that have been noted with hydrogen masers.

Over the past several years many new techniques for the investigation of surfaces have become widely available. One of these recent methods is X-ray Photoelectron Spectroscopy (XPS), and it has been used to investigate the surfaces of a large number of materials including polymers. A thorough review of XPS with an emphasis upon fluorocarbon polymers has been made by Clark and Feast (3), but a few highlights will be given here. A low intensity X-ray source (usually about 1253 or 1486 eV)

impinges upon the material of interest. Both orbital and valence electrons are ejected, and the kinetic energy of these electrons is measured. The binding energies of the various levels of an element can be determined from the following equation:

$$E_{BE} = h\upsilon - E_{KE} - \phi_{SP} \quad (1)$$

E_{BE} is the binding energy of the level of interest, $h\upsilon$ is the photon energy, E_{KE} is the kinetic energy of the ejected electron, and ϕ_{SP} is the work function of the spectrometer. XPS spectra can be observed for all of the elements except hydrogen and helium, and each element has a unique spectrum. The mean escape depth for X-ray induced photoelectrons is about 20 Å, but with carbonaceous material the mean escape depth may be greater. Changes in the atomic environment can be followed by the observation of shifts in the binding energy. For example, the shift in the binding energy for the C 1s line is about 7 eV between polytetrafluoroethylene (PTFE, compound I) and polyethylene (3).

$$\{CF_2 - CF_2\}_n$$

I

EXPERIMENTAL

Materials

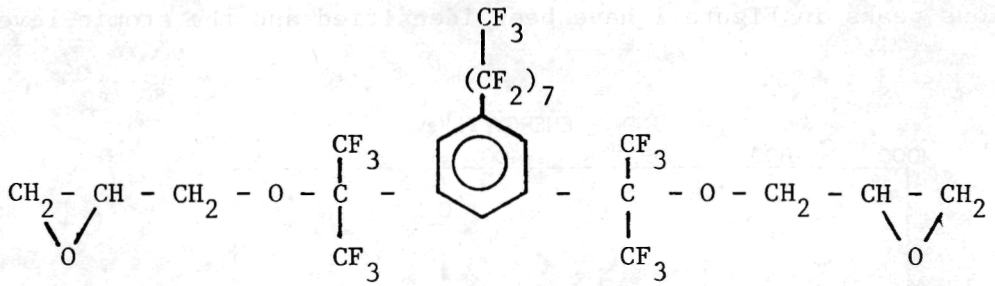
Three different types of fluorinated polymer samples have been investigated. All of the samples were put onto 2 by 1 cm stages. The first set of samples was a FEP Teflon coating of various configurations on gold-coated Al and quartz stages, and was prepared under the direction of Dr. R. Vessot of the Smithsonian Astronomical Observatory (SAO), Cambridge, Mass. The coatings covered either part or all of the underlying substrate and were thought to be on the order of a few thousand Å. Au was selected as one substrate so that the $4f_{7/2}$ photoelectron line could be used as a standard, and quartz was chosen to simulate a substrate used in a maser. The coatings were made from an FEP-120 dispersion, an aqueous dispersion of FEP Teflon containing a volatile wetting agent; FEP Teflon is a mixture of polytetrafluoroethylene (PTFE) and polyhexafluoropropylene (HFP), Compound II.

$$\{CF_2 - \underset{\displaystyle CF_3}{\underset{|}{CF}}\}_n$$

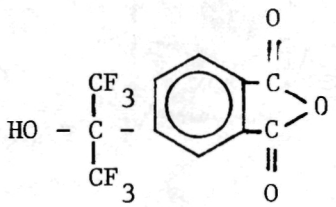
II

The second set of samples was from a film of FEP Teflon that came from

the storage bulb of a used maser from SAO. This thick film had been removed from the maser bulb by an overnight soaking with a few cc of water. After receipt at NRL, the sample was manipulated with cleaned tweezers and placed on fresh, clean aluminum foil; plastic gloves were used also in the handling of the film. When the sample was unfolded, two distinct regions of the film were observed; one region was clear and the other, much smaller in area, had a brown color. The third set of samples was a fluorinated diglycidyl ether, compound III, and the coupling agent compound IV, a fluorinated anhydride, which form a very high molecular weight cross-linked polymer. Fluorinated amines have been employed as coupling agents also.



III



IV

Some of the specimens of this set contained about 50%, by weight, PTFE. These fluorinated polymers have the ability to "wet" PTFE, whereas most polymers do not have this property.

EXPERIMENTAL PROCEDURES

Spectra were obtained with a Physical Electronics XPS/AES electron spectrometer operating in the 10^{-6} Pa region. The X-ray source was MgKα radiation (1253.6 eV) at 10 KV and 30 or 40 ma and a pass energy of either 100 or 25 V was used for all spectra. The area of analysis is a few mm^2. Elemental ratios were determined from the model developed by Carter, Schweitzer, and Carlson (4), as given in equation (2).

$$\frac{n_1}{n_2} = \frac{N_1 \sigma_2 \lambda_2 S_2}{N_2 \sigma_1 \lambda_1 S_1} \qquad (2)$$

N is the area under the curve of the photoelectron peak, σ is the photoelectron cross section (5), λ is the mean escape depth of the photoelectron (4), and S is the spectrometer response, as a function of energy (6). More detailed consideration of this model for the determination of elemental ratios in polymers will be given elsewhere (7).

RESULTS AND DISCUSSION

A. Thin FEP Film from SAO

In Figure 1 is shown the XPS spectrum of a thin film made from FEP-120 dispersion on a quartz substrate. From known binding energies (8), the various peaks in Figure 1 have been identified and the atomic levels

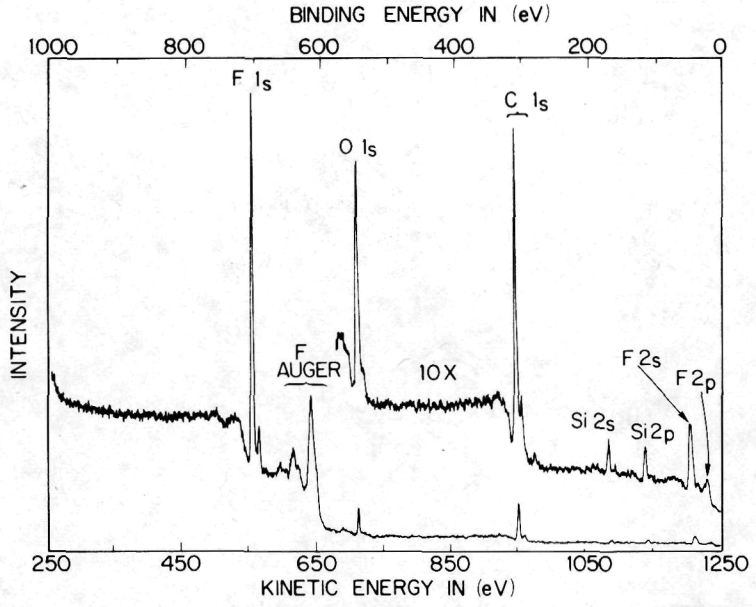


Figure 1: XPS spectrum of a quartz stage coated with FEP 120 Teflon dispersion. Elemental peaks are identified on the figure.

indicated. The identification of the X-ray-induced F Auger peaks was made on the basis of the observed kinetic energy. In addition to the expected C and F XPS peaks, both Si and O XPS lines were observed. Thus, it appears that the coating is either in the form of "islands," or that portions of the coating are so thin (perhaps 10-20 A at the most) that the underlying quartz substrate can be observed. If the peaks ascribed to O and Si are not considered, the spectrum in Figure 1 is very similar to that reported by Clark and Feast (3) for PTFE.

From a detailed analysis of the small peaks due to the Mg $K\alpha_{3,4}$ radiation (9) it was concluded that the minor peak on the high kinetic energy side of the main C1s peak, was due, in part, to some hydrocarbon present in the coating, possibly the residue of the wetting agent in the FEP-120 dispersion.

Table 1 gives the elemental ratios determined for the quartz sample covered by the FEP-120 coating as determined by the use of equation 2.

Table 1

Elemental and Group Ratios of FEP-120 Teflon-Coated Quartz, as Determined by XPS

Ratio	Experimental	Theoretical
C(1s)/F(1s)	0.47 ± 0.04	0.5
C(1s)/F(2s)	0.46 ± 0.02	0.5
Si(2s)/O(1s)	0.6 ± 0.1	0.5
CF_2/SiO_2 (First location on sample)	9.0 ± 0.6	
CF_2/SiO_2 (Second location on sample)	15 ± 2	

The observed Si/O and C/F (C ascribed to C-F bonds) ratios agree well with the theoretical ratios. These results are gratifying considering the approximations made and some of the small signals observed. For the analysis of the C/F ratio, the contribution by the different C-F bonds in HFP to the C 1s signal has been neglected (9). The results show that little, if any, O is present, except that from the quartz. On a completely polymer coated gold-covered Al stage, only a very faint O signal was observed. Thus, it appears that the coating or surface contamination contributes very little O to the surface region.

After these encouraging results were obtained from the Si/O and C/F ratio measurements, an attempt was made to find the amount of the fluorocarbon coating relative to the quartz substrate. For this purpose the number of apparent CF_2 groups vs. the number of SiO_2 groups is of interest. The C/Si, F/O, C/O, and F/Si ratios were determined with the proper consideration to stoichiometry, and the results are given also in Table 1. Unfortunately, these ratios do not help answer the question of whether there are blank spots in the coating or just some very thin sections.

B. Thick FEP Film From SAO

In Figure 2 (clear portion) and Figure 3 (brown portion) the XPS spectra of the film obtained from a used hydrogen maser are shown. The

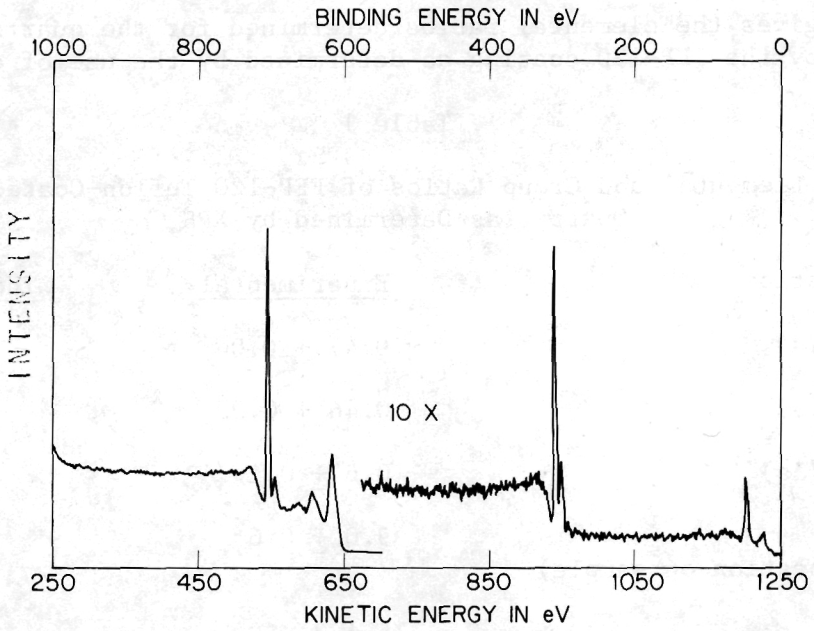


Figure 2: XPS spectrum of the clear portion of the FEP Teflon from a used hydrogen maser.

spectra were from the side of the film that was believed to be exposed to hydrogen atoms (this tentative suggestion was prompted by the shape of the film). All of the films appeared to be continuous, since peaks from the substrate beneath the films were not detected, and the C/F ratio (C ascribed to C bonded to F) was close to the expected ratio (0.5) for FEP Teflon. By the same type of analysis mentioned previously it was concluded that the clear part of the film indicated a small hydrocarbon contribution to the C 1s signal, while on the other side of the film there appeared to be little, if any, hydrocarbon type C present. Oxygen was not detected on either side of the clear portion of the film.

The spectrum in Figure 3 (brown film) has marked differences from the spectrum of the clear portion of the film. The spectra from both sides of the brown colored film were similar. The C signal due to non-fluorine bonded C was about one third of that due to F bonded C, while the O present had about one sixth the intensity of the non-fluorine bonded C. These results definitely show that there are differences

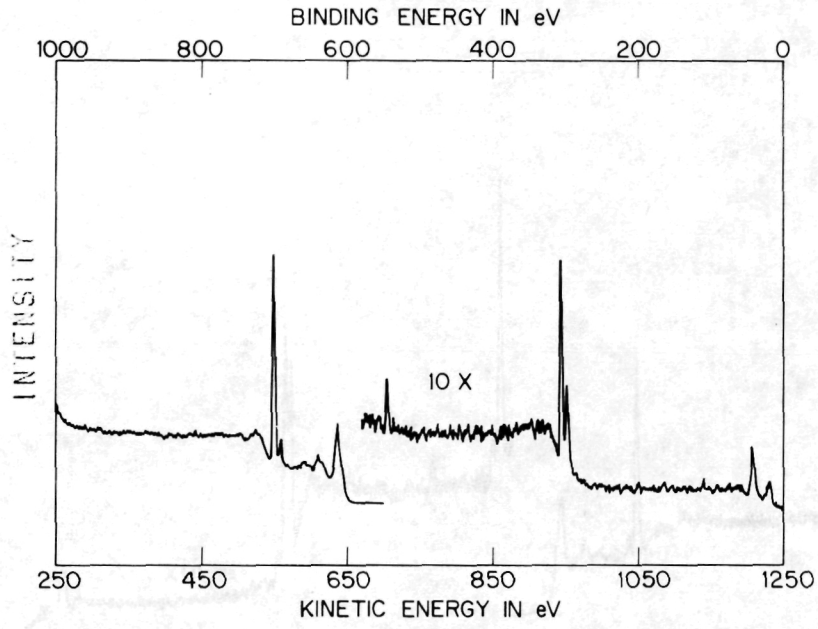


Figure 3: XPS spectrum of the brown portion of the FEP Teflon from a used hydrogen maser.

between the clear and the brown portions of the film. It seems reasonable to suggest that the brown portion of the film was exposed directly to the hydrogen atom source, and that the changes extended throughout the extent of the film. Due to the prior handling and treatment of the film the absolute results of these analyses cannot be given with certainty; however, the differences between the clear and brown portions of the film do appear to be real.

C. NRL Developed Fluorocarbon Polymers

In Figure 4 (spectrum B) the XPS spectrum of the epoxy polymer mixture derived from compounds III and IV is shown. Detailed consideration of these spectra will be given elsewhere (7) but a few comments will be made. The surface composition, as determined by XPS, appeared to be close to that of the expected bulk composition. The two peaks in the C region are expected also. Spectrum A in Figure 4 is the spectrum of the polymerized mixture of compounds III and IV containing 50 percent by weight of powdered PTFE. As can be seen, the difference between the spectra in Figure 4 is minimal. In a polymer system similar to that in spectrum A of Figure 4, Hunston, Griffith, and Bowers (10) found that the frictional behavior closely resembled that of pure PTFE. As a

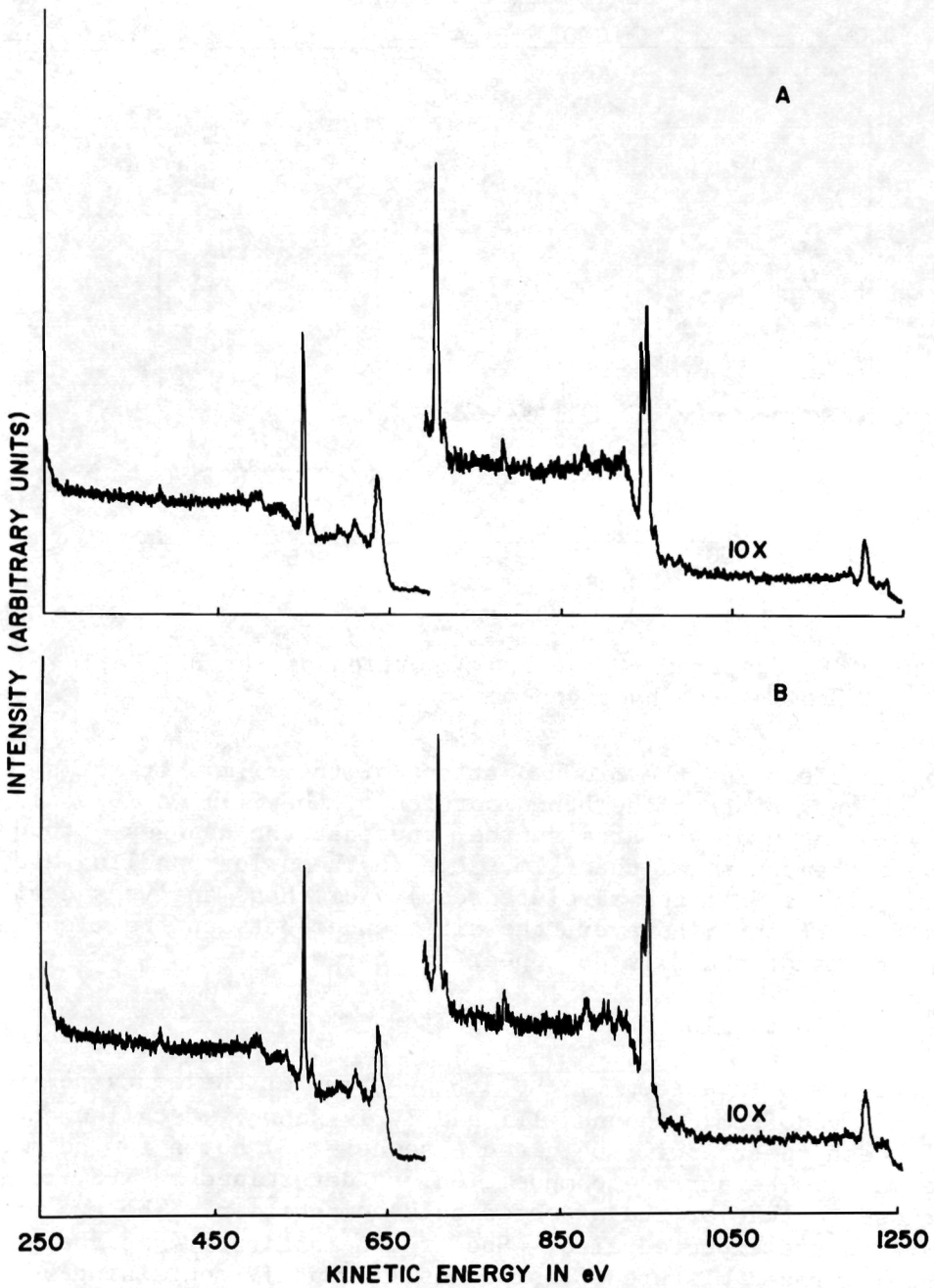


Figure 4: Spectrum A. XPS spectrum of compounds III and IV with 50 percent by weight powdered PTFE. Spectrum B. XPS spectrum of compounds III and IV.

result of a simple scraping of the polymer mixture used in Figure 4 (spectrum A), the XPS spectrum of the resultant film that was observed is shown in Figure 5. As can be seen this spectrum is vastly different

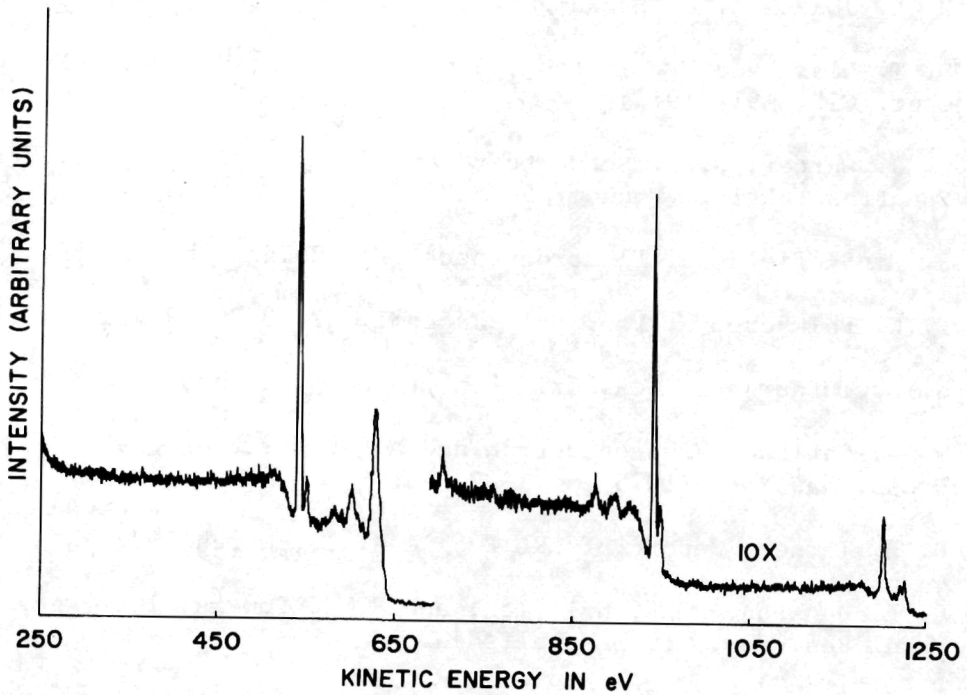


Figure 5: XPS spectrum after scraping of the mixture used in spectrum A, Figure 4.

from the spectra in Figure 4. The O and the non-fluorine bonded C peaks have been reduced quite markedly. The C (bonded to F) to F ratio is close to that expected for PTFE. These results suggest that it is possible to form a film similar to PTFE from mixtures of PTFE and compounds III and IV. (Compounds similar in chemical structure to III and IV probably could also be used equally as well). Thus, it appears that PTFE films could be produced in configurations that would be difficult to fabricate from commercially available films or dispersions.

CONCLUSIONS

XPS can be used to examine the fluorocarbon polymer coatings used in hydrogen masers both before and after use in a maser. Films that appear to be similar to PTFE can be made from powdered PTFE combined with compounds such as III and IV.

REFERENCES

1. J. E. Bennett and D. R. Blackmore, J. Chem. Phys., 53, 4400 (1970).

2. W. E. Jones, S. D. MacKnight, and L. Teng, Chem. Rev., 73, 407 (1973).

3. D. T. Clark and W. J. Feast, J. Macromol. Sci. - Revs. Macromol. Chem., C12, 191 (1975).

4. W. J. Carter, G. K. Schweitzer, and T. A. Carlson, J. Electron Spectrosc. Relat. Phenom., 5, 827 (1974).

5. J. H. Scofield, J. Electron Spectrosc. Relat. Phenom., 8, 129 (1976).

6. P. W. Palmberg, J. Vac. Sci. Technol., 12, 379 (1975).

7. N. H. Turner and J. R. Griffith, to be published.

8. T. A. Carlson, "Photoelectron and Auger Spectroscopy", Plenum Press, New York, 1975, pp. 337-343.

9. N. H. Turner, Report of NRL Progress, 15, March 1977.

10. D. L. Hunston, J. R. Griffith, and R. C. Bowers, Ind. Eng. Chem., Prod. Res. Dev., to be published.

AN INVESTIGATION OF THE SHIELDING PROPERTIES OF MOLY PERMALLOY® SHIELDS DESIGNED FOR USE WITH A HYDROGEN MASER

S. A. Wolf and John E. Cox
Material Sciences Division
Naval Research Laboratory
Washington, D. C. 20375

Introduction

Hydrogen masers are being considered for use as the frequency standard in the next generation of navigational satellites (NAVSTAR GPS). For these masers to achieve the required frequency stability (1 part in 10^{14}), the magnetic field environment in which the maser operates must be accurately known and stable to 1 nT for ambiant magnetic field changes of 100,000 nT. (The earth's magnetic field is approximately 50,000 nT). The usual procedure is to surround the hydrogen maser by one or more concentric magnetic shields. The objective of this study is to verify the shielding characteristics of the magnetic shield system (Fig. 1) that has been designed for use with the VLG-11 ground based hydrogen maser.

Measurements were made in the 11.3 meter diameter Braunbek coil system at the Spacecraft Magnetic Field Site, Goddard Space Flight Center, Greenbelt, Md. (See Fig. 2). This coil system actively compensates for changes in the Earth's magnetic field and is capable of nulling the earth's field to better than 1 nT over a 1.3 m diameter

sphere. In addition, this system has the capability of applying a field, known to an accuracy of 1 nT over this volume, with a magnitude as large as 60,000 nT.

Both the transverse and axial shielding factors of a single layer shield and a four layer nested shield were determined using a fluxgate magnetometer with 0.1 nT resolution and a Superconducting QUantum Interference Device (SQUID) magnetometer with 0.001 nT resolution. Attenuation was studied as a function of external magnetic field, position within the shield, zero field magnetic moment (perm), and thermal cycling.

Single Shield Results

A single layer shield of Moly Permalloy[R*] of the type shown in Fig. 1 was placed at the center of the coil facility. Data were taken primarily with a three axis fluxgate magnetometer, however a limited number of measurements were also taken with a flip coil SQUID magnetometer.

Measurements were made of the internal field and the differential shielding factor (the change in external field divided by the change in internal field) as a function of: applied field, axial distance from the center of the shield, and "zero" field magnetic moment (perm) of the shield.

These measurements basically fell into three categories

characterized by the magnitude of the applied field:

(a) Low magnetic fields (50 to 500 nT): Here the changes in the internal field in a given direction for a given change in the external field in the same direction was constant, reproducible, and reversible, i.e., the "zero" field readings which were taken after each application and removal of the external field were reproduced to within 1 nT. These results were independent of the perm that the shield had before initiating the measurements. Figure 3 displays the transverse and axial shielding factors as a function of axial distance from the center of the shield. The shielding factor at the center of the shield varied from 33 in both transverse directions to 20 in the axial direction.

(b) Intermediate magnetic fields (500 to 30,000 nT): These data are characterized by internal fields and shielding factors which are dependent on the recent magnetic history of the shield and the initial perm. In this field region, the perm of the shield is dependent on the magnetic history. Figure 4 illustrates a typical hysteresis loop where the perm in the axial direction was initially small[1]. In this range of magnetic fields, the shielding factor always exceeded the low-field shielding factor.

(c) High magnetic fields (30,000 to 55,000 nT or a field comparable to the Earth's magnetic field): In this

range, the magnitude of the applied field is sufficiently large that the perm and previous magnetic history are not important. In this field range, an absolute shielding factor was determined rather than the differential one. Results for the two orientations are included in Figure 3. For a maximum applied field of 55,000 nT, the internal field never exceeded 1000 nT at the center and 3400 nT at axial distance of 200 mm from the center of the shield.

Aside from the determination of the details of the shielding characteristics of this shield, another significant result is that the perm of the sample shield was unaffected (to the 1 nT level) by uniform fields of up to 500 nT. Thus in any shield design where the perm must remain stable to this level, an upper limit on the fields that a similarly fabricated shield can be exposed to and have the perm remain unchanged has been established.

Four Layer Nested Shield Set Results

These measurements were made on a set of four shields acquired from Allegheny Ludlum Corp. and built to SAO specifications. The outermost shield of this set is essentially of the same design as the single shield discussed above. To preserve the high permeability of these shields they were "nested" using carved balsa wood spacers and foam rubber between successive layers. The spacing of the shields was in conformance with specifictions supplied by

SAO. These spacers and foam seperators were fashioned so that the four layer set could be placed on its side or inverted without changing the relative orientations of the shields.

Prior to each of the measurements, the shields were depermed using a combination of techniques[2]. The shields were placed at the center of the 11.3 m coils and the ambient field was nulled to approximately one nT. Before the initial deperm, the internal field was at most 67 nT. A pair of 3.05 m diameter coils spaced 2.24m apart were placed on opposite sides of the shields. (See Fig. 5) A 60 Hz current in the coils was raised to 100 amps (corresponding to a field at the shields of 3×10^6 nT) and lowered in 10 seconds. The shield was then rotated 90° about the vertical axis and the current was again brought to 100 Amps and decreased at the same rate. As a result of this phase of the deperm sequence, the internal field was now typically approximately 5 nT. A cable was then run axially through the shield forming a single loop, and a 250 amp 60 Hz current was passed through the cable. The current was then reduced from 250A to 30 A in 2 minutes time, then increased to 60 A and reduced to zero again in 2 minutes. The remnant internal field was consistently below 0.1 nT.

Axial measurements were made with both a fluxgate and a SQUID magnetotmeter, with the shields depermed prior to

either measurement. Data were obtained by increasing the applied field in incremental steps from 0 to 60,000 nT parallel to the Z axis (up direction), then incrementally decreased to zero and then again increased incrementally to 60,000 nT directed antiparallel to the Z axis (down direction) and thence back to zero.

The fluxgate magnetometer was suspended at the center of the shield with its sensing axis along the Z axis. The SQUID magnetometer had a sensing coil which could be rotated 360° in the horizontal plane and 270° in the vertical plane, permitting arbitrary field directions to be evaluated. Transverse measurements with the fluxgate magnetometer were inconclusive due to a lack of sensitivity, the SQUID magnetometer performed with satisfactory precision. Results for the axial fields are shown in Fig. 6 and the transverse measurements are shown in Fig. 7. In Fig. 6, we see that for a total field change of 120,000 nT (+60,000 to -60,000 nT) the total internal field change was approximately 2nT, resulting in a shielding factor of 6×10^{4}. The residual moment or perm after traversing this one cycle changed by 0.25 nT. The transverse shielding factor was determined to be 3.75×10^{5} and the change in perm was 0.05 nT.

Shielding factors as a function of axial distance from the center of the shield were determined in the following fashion. Axial fields of $\pm$ 60,000 nT were applied to the

shields and the internal fields at the center of the shield were determined. The fields were monitored by the stationary magnetometers as the shields were raised by discrete amounts. (Fig. 8). The shields were then inverted and the measurements were repeated. In this manner any asymmetry introduced by the magnetometer probe itself is removed from the final results. Note the large asymmetry in the internal fields towards the welded end as compared to the press fit end. This could be due to the fact that there are larger access holes at the press fit end than at the welded end, the incomplete ferromagnetic circuit due to a lack of continuity of the shields, the stress of assembly at the press fit end, or any combination of these factors.

Thermal Shock Test

The shields were placed in a thermostatically controlled oven and maintained at 65C for two hours and allowed to cool to 25C in 40 minutes. The magnetic shielding measurements detailed above were repeated. No difference was detected from the earlier results.

Discussion of Results

These results reflect significantly on the performance of a hydrogen maser since the effect of a magnetic field is to change the frequency of the maser according to the following equation[3]

$$\Delta\nu/\nu = 3.9\text{x}10^{-16}H\Delta H$$

where υ is the frequency and H is the field in nT required to provide the quantization direction. For state-of-the-art masers, H is in the range 10 to 50 nT. Thus an axial Δ H of 2 nT as measured at the center of the shield would produce a frequency shift of from 0.7 part in 10^{14} for a field of 10 nT and one of 3.5 parts in 10^{14} for a field of 50 nT. The large measured anisotropy in the shielding factor indicates that this estimate of frequency stability is optimistic, since the maser cavity takes up a significant portion of the inner shield volume and therefore the effective shielding factor will undoubtedly be less than the value at the center. The lack of any measurable effect of the mild thermal shock was not unexpected but is encouraging since no degradation of the shielding was observed.

Conclusions

The present configuration of four shields designed for use with ground based masers provides only marginally adequate field attenuation for ambient excursions of 60,000 nT. This is based on the stability requirement of one part in 10^{14}. If space applications require shielding of 60,000 nT ambient fields, some modifications in the shield design appear necessary in order to assure the required performance.

Acknowledgements: The authors wish to thank William Brown, Charles Harris, Ralph Ricucci and William Pruett of the Spacecraft Magnetic Field Site, NASA, for their hospitality and assistance.

References

1. 3.05 m diameter deperming coils were used in one transverse direction only. The result was to reduce the "zero" field moment of the shield in the two perpendicular directions. The perpendicular transverse direction had a very small perm (<3nT) after running the 60 Hz field in the deperming coils to 3×10^6 nT and slowly reducing it.

2. Private Communications, Charles Harris of NASA-Goddard and Robert Vessot of SAO.

3. D. Kleppner, H. M. Goldenberg and N. F. Ramsey, Phys. Rev. 126, 603(1962).

*R Allegheny Ludlum Corp.

FIGURE CAPTIONS

1. Four shield nested array.

2. Artists conception of NASA-Goddard Spacecraft Magnetic Test Facility.

3. Transverse and axial shielding factors as a function of axial distance from the center of the shield for a single Moly Permalloy® shield. For the upper two curves, the shielding factor was calculated by dividing the applied field by the internal field. For the lower two curves, the shielding factor was calculated by dividing the applied field by the change in the internal field parallel to the applied field. The filled circles are the SQUID data.

4. The internal axial field as a function of the external axial field 150 mm from the center of the single shield. The data were taken as follows: the field was increased from "zero" with the axial perm small until 55,000 nT was reached (the maximum field that could be uniformly applied). The field was then decreased to zero and then increased to 55,000 nT in the opposite direction. The field was decreased to zero again and reversed and increased to 55,000 nT in the original direction. The field was decreased to zero again and reversed and increased to 55,000 nT. This cycle is shown by the solid curve. The field was then decreased to zero and increased to 55,000 nT in the same direction as it had just been before. This last cycle is illustrated by the dashed curve. Notice that the internal field at 55,000 nT always reproduces.

5. (a) Deperming coils used to reduce the internal field to approximately 5 nT.

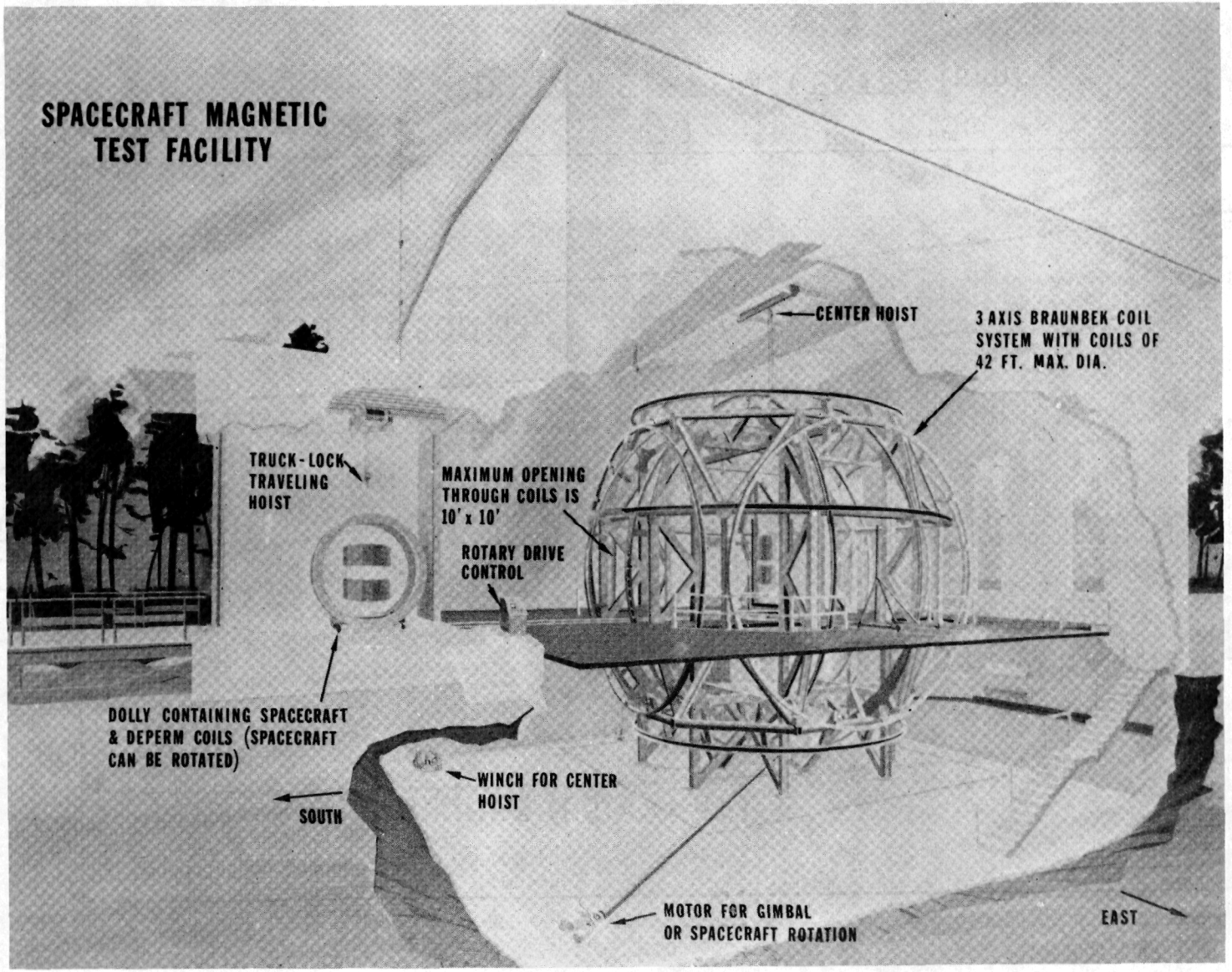
   (b) The 250 amp cable used to reduce the remmant internal field to 0.1 nT is visible as it is passed axially through the shields in the box.

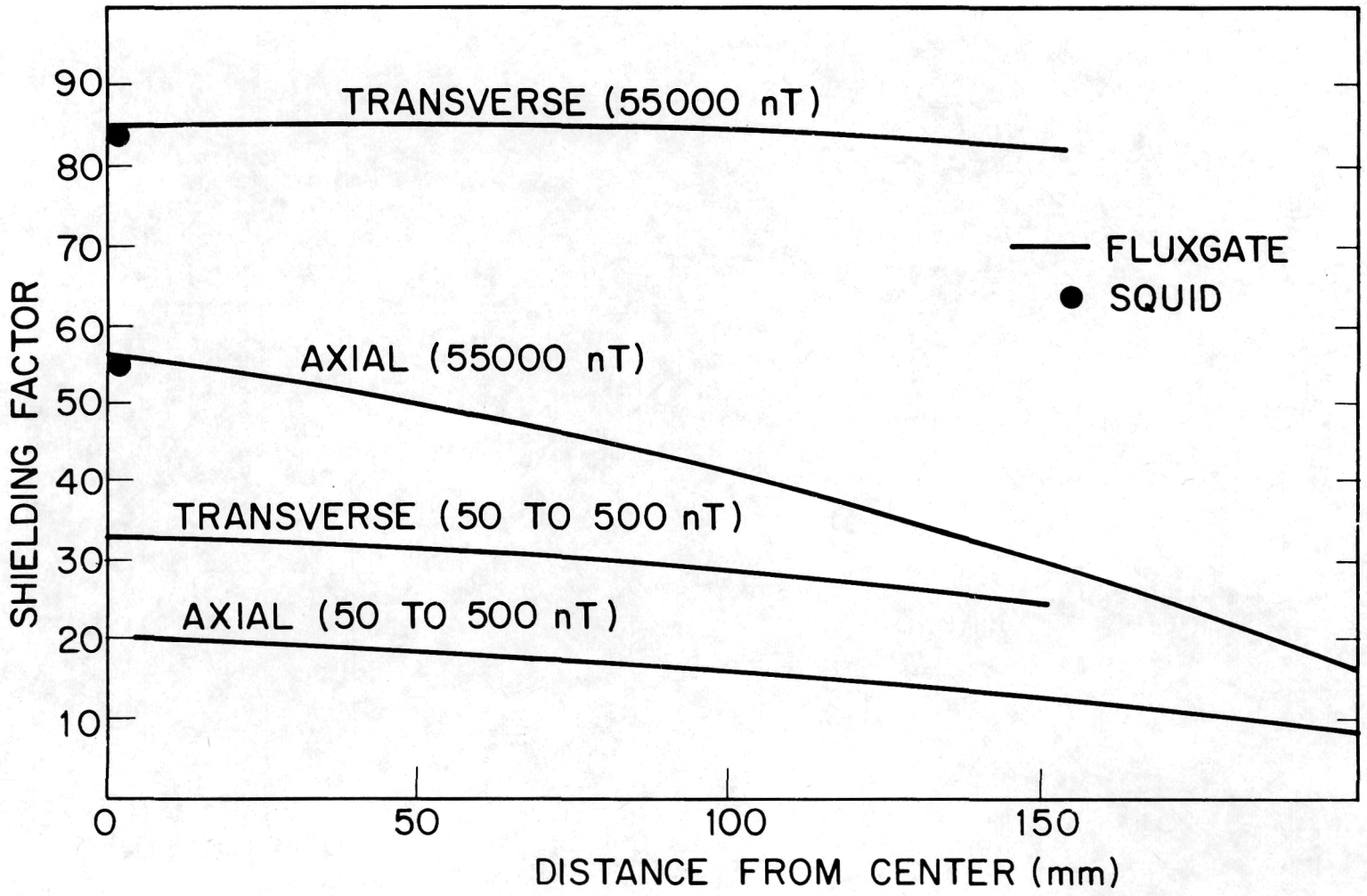
6. Internal fields of a 4 layer nested Moly Permalloy® shield set as a function of applied axial fields.

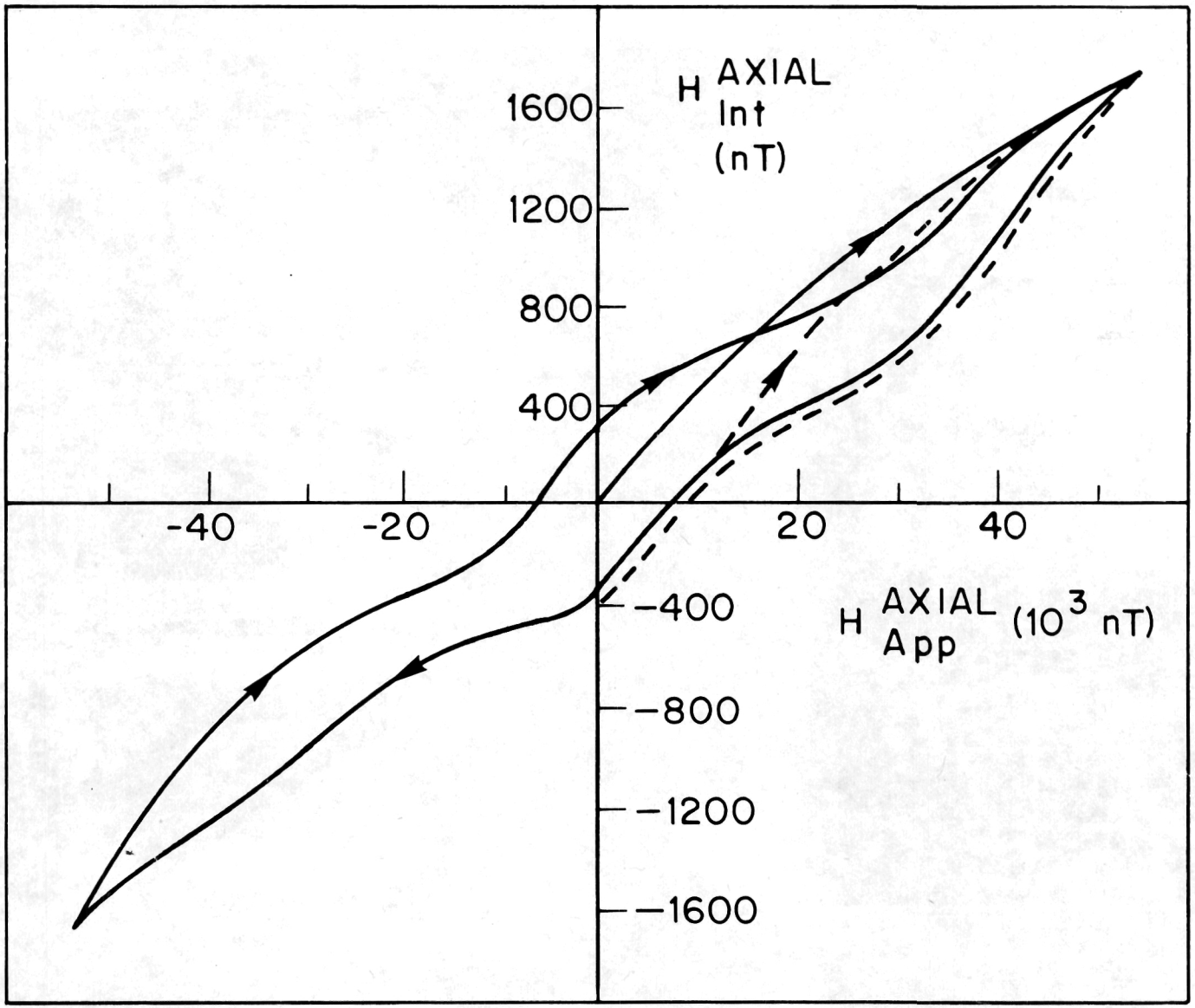
7. Internal fields of a 4 layer nested Moly Permalloy® shield set as a function of applied transverse field.

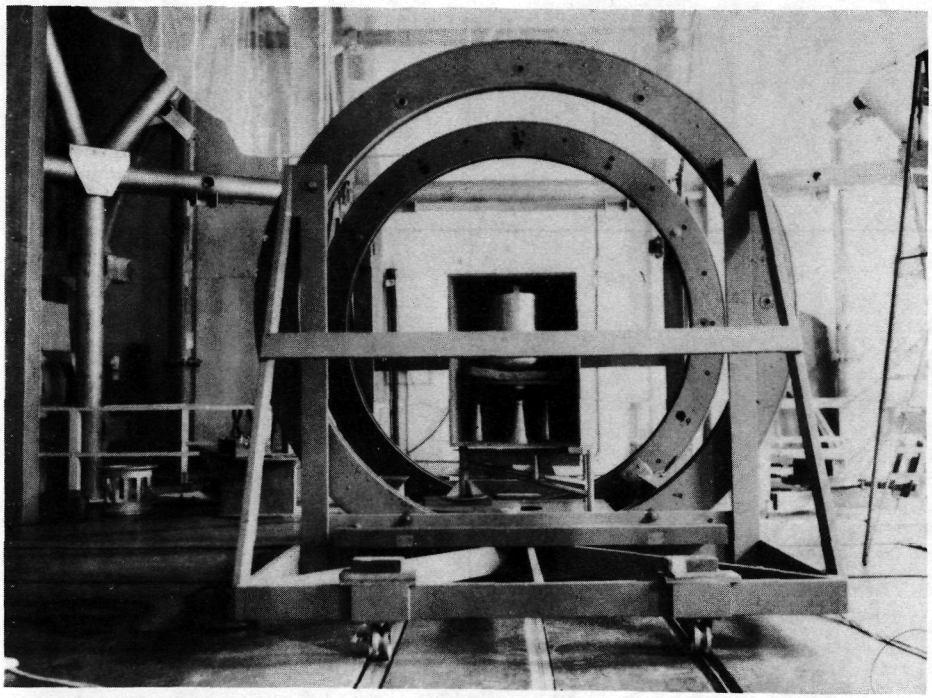
8. Shielding factors as a function of axial distance from

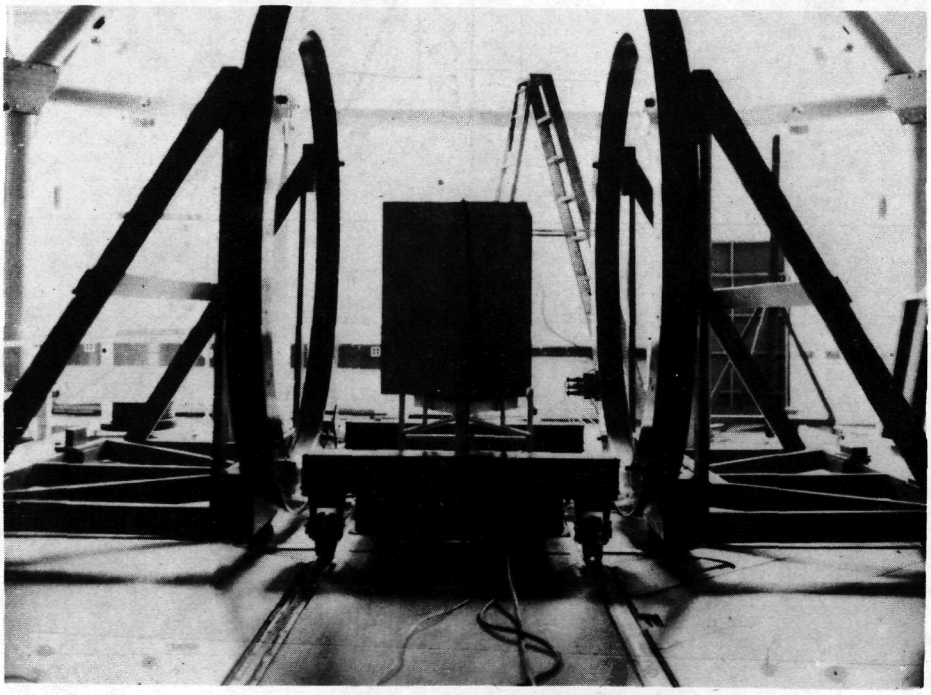
the center of the shield for applied axial field. Shielding at the welded end is much more effective than at the press fit end.

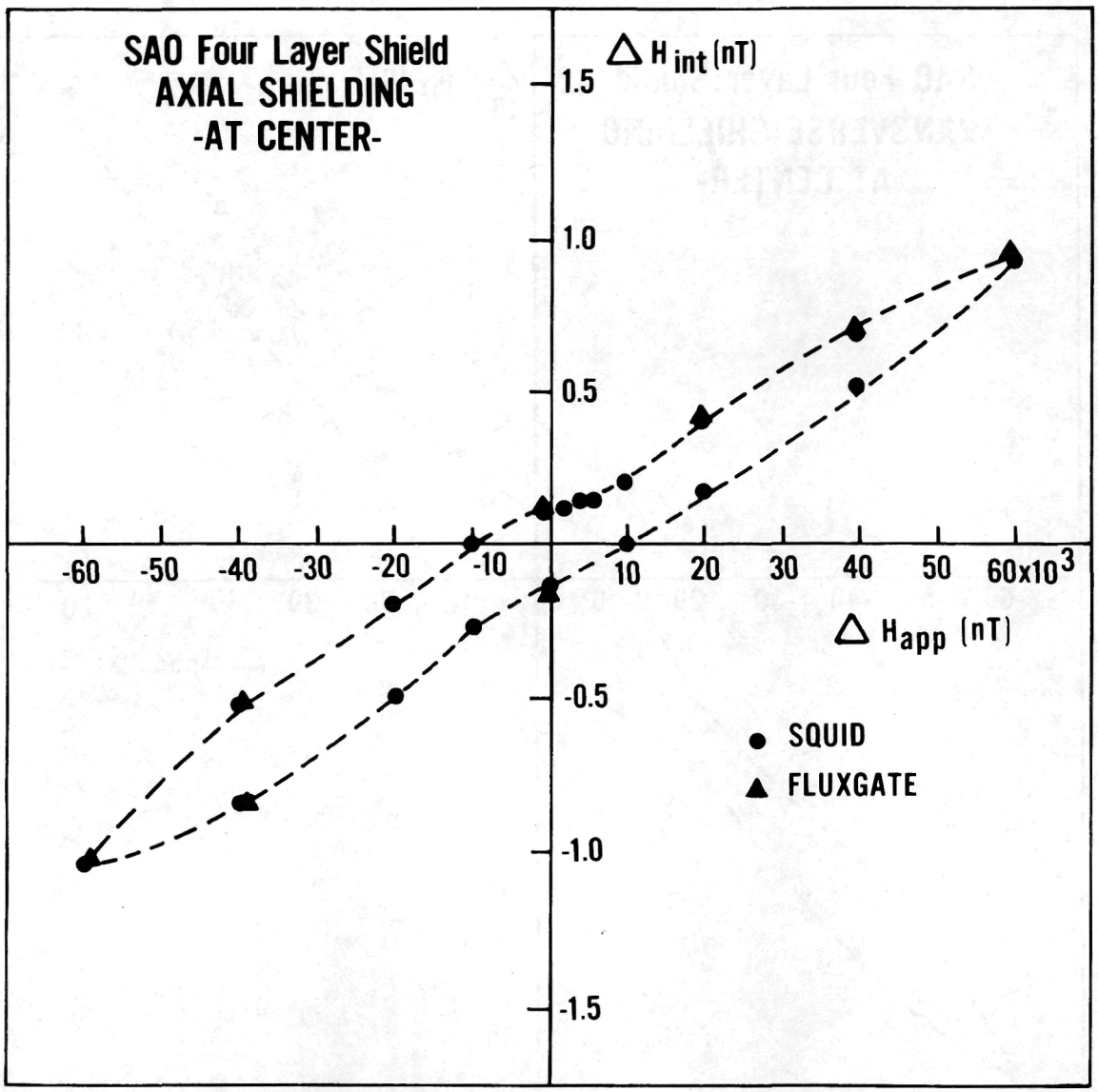

SPACECRAFT MAGNETIC
TEST FACILITY
CENTER HOIST
3 AXIS BRAUNBEK COIL
SYSTEM WITH COILS OF
42 FT. MAX. DIA.
TRUCK-LOCK
TRAVELING
HOIST
MAXIMUM OPENING
THROUGH COILS IS
10' x 10'
ROTARY DRIVE
CONTROL
DOLLY CONTAINING SPACECRAFT
& DEPERM COILS (SPACECRAFT
CAN BE ROTATED)
WINCH FOR CENTER
HOIST
SOUTH
MOTOR FOR GIMBAL
OR SPACECRAFT ROTATION
EAST

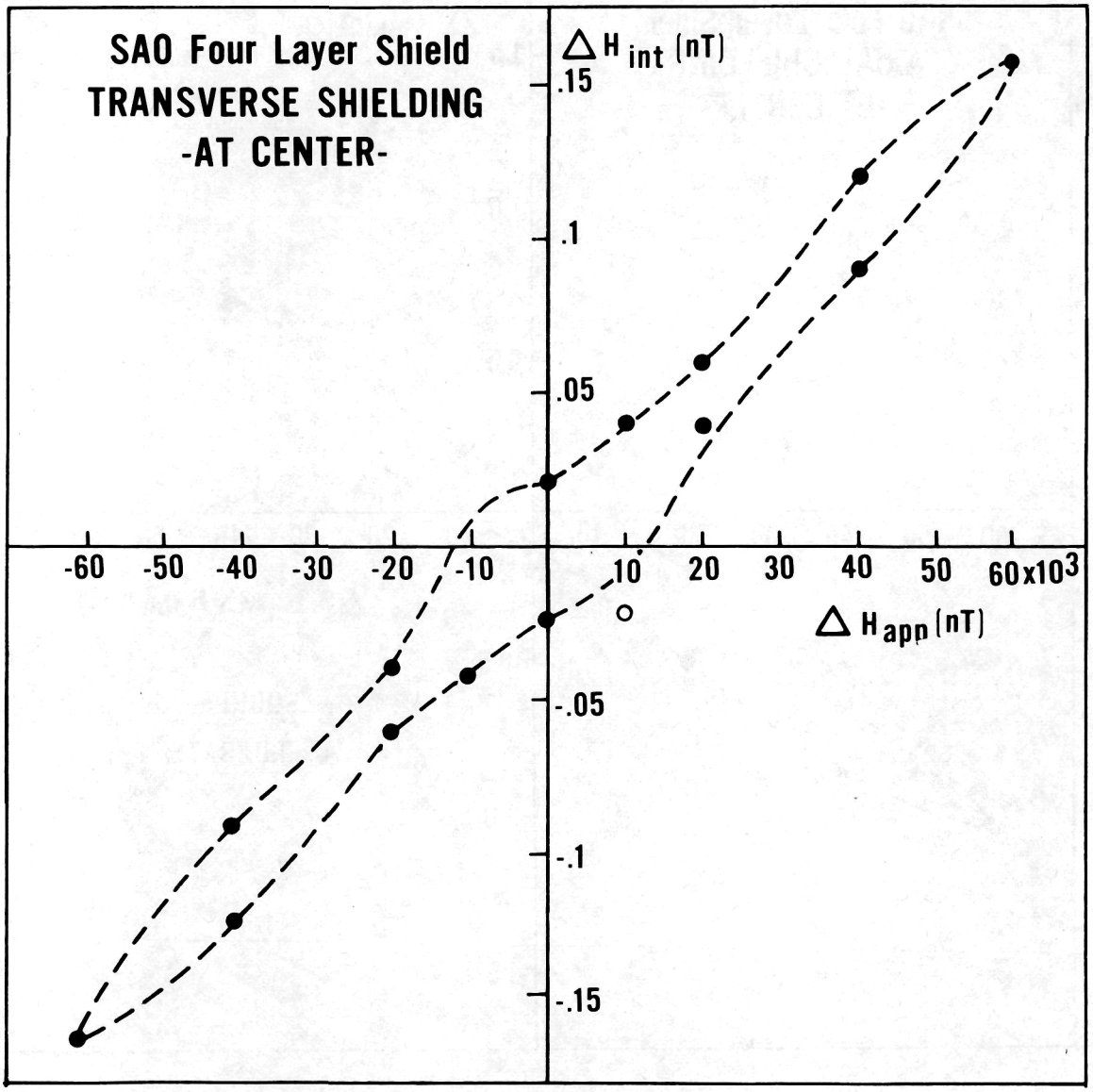

TRANSVERSE (55000 nT)
AXIAL (55000 nT)
TRANSVERSE (50 TO 500 nT)
AXIAL (50 TO 500 nT)
FLUXGATE
SQUID
SHIELDING FACTOR
90
80
70
60
50
40
30
20
10
0
50
100
150
DISTANCE FROM CENTER (mm)

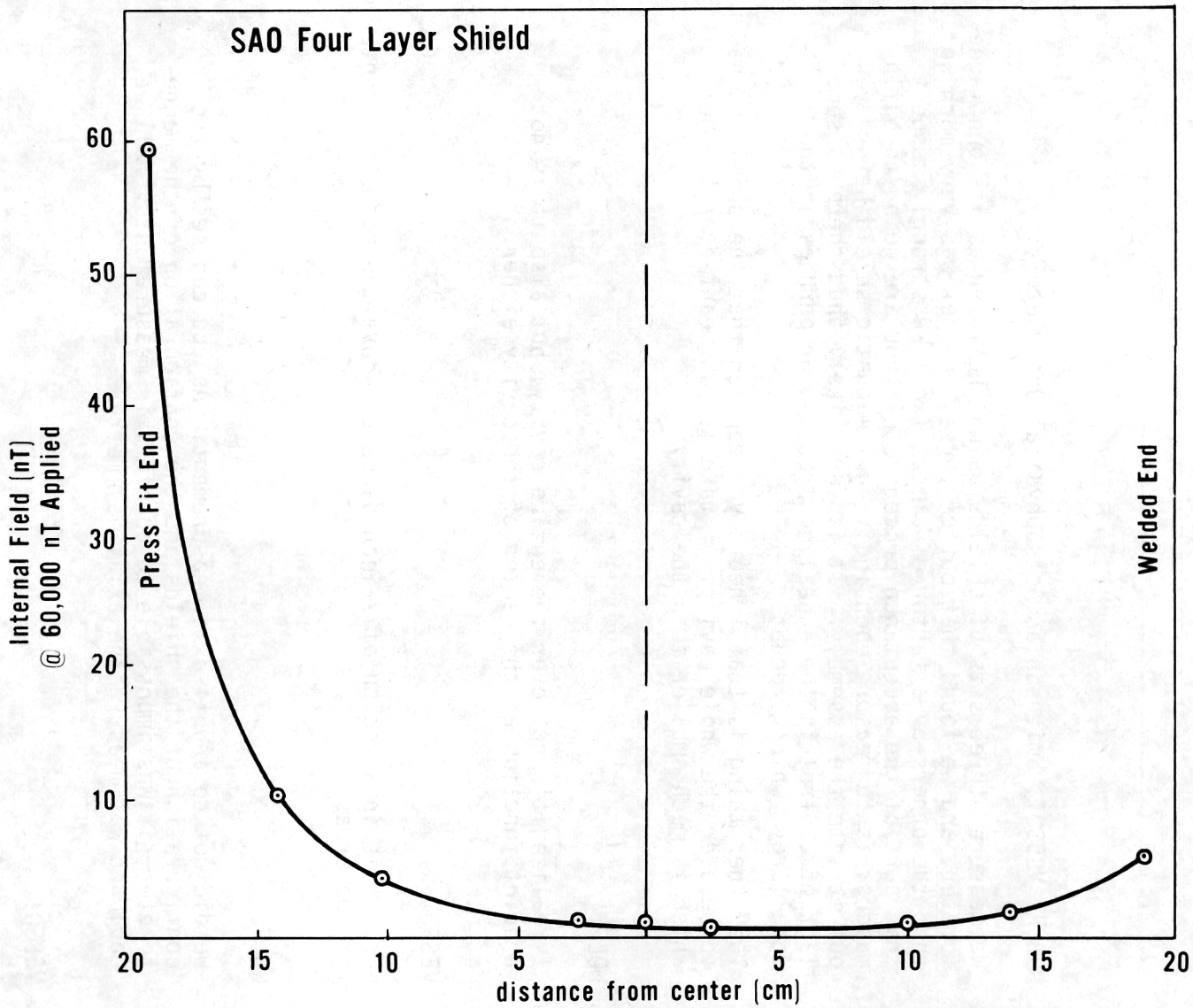

H AXIAL
Int
(nT)
1600
1200
800
400
-40
-20
20
40
-400
-800
-1200
-1600
H AXIAL
App
(10^3 nT)






SAO Four Layer Shield
AXIAL SHIELDING
-AT CENTER-
Δ H int (nT)
1.5
1.0
0.5
-0.5
-1.0
-1.5
-60
-50
-40
-30
-20
-10
10
20
30
40
50
60x10^3
Δ Happ (nT)
SQUID
FLUXGATE


SAO Four Layer Shield
TRANSVERSE SHIELDING
-AT CENTER-
Δ H int (nT)
.15
.1
.05
-.05
-.1
-.15
-60
-50
-40
-30
-20
-10
10
20
30
40
50
60x10³
Δ H app (nT)


SAO Four Layer Shield
Internal Field (nT)
@ 60,000 nT Applied
60
50
40
30
20
10
Press Fit End
Welded End
20
15
10
5
5
10
15
20
distance from center (cm)

DR. ROBERT VESSOT, Smithsonian Astrophysical Observatory:

We measured three sets of shields using the maser as its own magnetometer, and we found that out of three, one set was very much worse than the others by a factor of almost two. We strongly suspect that part of the acceptance procedure, if you are going to build masers, is to measure each individual magnetic shield before you put it into the assembly. It is very likely that there is some lack of control in the annealing process, or perhaps in the metallurgy, which I doubt.

The other thing is that I heard you mention that the shielding had to be over the whole cavity. I take it you meant over the bulb, which is much smaller than the cavity.

MR. WOLF:

I realize it's not over the entire cavity, but also it is not a point function at the center of the cavity either.

DR. VESSOT:

No, it is in a region of 7-inch diameter above the geometric center of the array.

MR. WOLF:

We did not do an off-axis measurement. As you can see by the configuration of the shields and the configuration of the magnetometer, it was impossible to do off-axis measurements. All we could do was measure the axial asymmetry.

DR. VESSOT:

I agree with you. More work is certainly needed on magnetic shields if you are expecting 60,000 nanotesla variations.

MR. WOLF:

About the quality of shields: Are you saying that we should measure each individual layer of the four-layer system as opposed to the four nested layers as they are?

DR. VESSOT:

Yes.

Page intentionally left blank

Page intentionally left blank

A Spaceborne Hydrogen Maser Design*

A.E. Popa, H.T.M. Wang, W.B. Bridges†, J.E. Etter, and D. Schnelker
Hughes Research Laboratories
Malibu, California

F.E. Goodwin, C. Lew, and M. Dials
Hughes Space and Communications Group
El Segundo, California

ABSTRACT

This paper presents the design for a space-qualifiable hydrogen maser optimized to fit into the Naval Research Laboratory's NTS-3 spacecraft. The design is derived from our experience with an advanced development model (ADM) developed for and delivered to the Naval Research Laboratory (NRL). The NTS-3 satellite is a technology satellite built as part of the Navy support for the NAVSTAR/Global Positioning System

INTRODUCTION

The excellent performance and superior stability of the atomic hydrogen maser are well known. However, the sizes and weights of typical masers designed for ground-based applications are not suitable for spaceborne applications. In past maser designs a long hydrogen-beam drift space was considered essential for effective state selection, and large sputter ion pumps were employed to maintain the high vacuum necessary for maser operation. For spaceborne applications the maser must be smaller and lighter than past designs and operate with a minimum of operator intervention.

Spacecraft Constraints

The spaceborne maser must interface with the NTS-3 spacecraft, which will be built by the Naval Research Laboratory (NRL) for launch in 1981. The spacecraft constraints shown in Figure 1, include a 15 in. (38 cm) maximum allowable diameter and a maximum length of 30 in. (78 cm). The maser must weigh less than 100 lb and consume less than 100 W from the spacecraft power bus. The operational temperature range will be 20°C ± 10°C and an operating life greater than 5 yr is required.

---

*This work has been supported by the Naval Research Laboratory under Contract N00014-75-C-1149.

†Present address: California Institute of Technology, Pasadena, CA 91125.

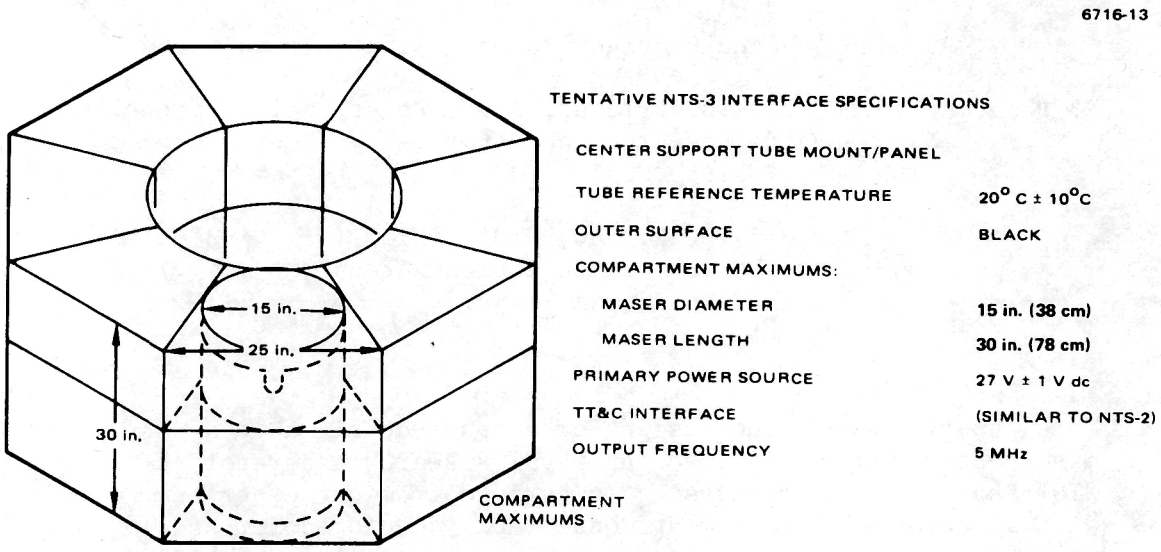


Figure 1. Tentative NTS-3/hydrogen maser interface layout.

System Description

A block diagram of our advanced development model maser (ADM) is shown in Figure 2 and a photograph of the physics unit is shown in Figure 3. We anticipate the spaceborne design will be quite similar to the ADM units. The spaceborne design is shown in cross section in Figure 4 and a detailed description of each subsystem follows.

Hydrogen Flow

A space-qualified high-pressure hydrogen storage and control subsystem has been selected for the space maser to ensure reliability and to minimize development costs. A 10-yr supply of hydrogen gas is stored at 1500 psi in a small lightweight pressure vessel and the subsystem is activated, on command, by a high-pressure solenoid valve. A strain gauge sensor measures the tank pressure for telemetering, and a space-qualified mechanical pressure regulator reduces the hydrogen pressure entering the palladium valve assembly to 10 psi. The hydrogen pressure between the palladium valve and the mechanical regulator is also measured and telemetered.

The palladium valve assembly shown in Figure 5 is used to reduce and regulate the hydrogen pressure in the dissociator to 50 mTorr ±1%. Incorporated into the palladium valve assembly are a temperature-stabilized thermistor bridge to measure dissociator pressure, and two redundant palladium valves which diffuse hydrogen when heated by an electric current from the hydrogen flow control servo. The dissociator pressure is telemetered and one of the parallel palladium valves

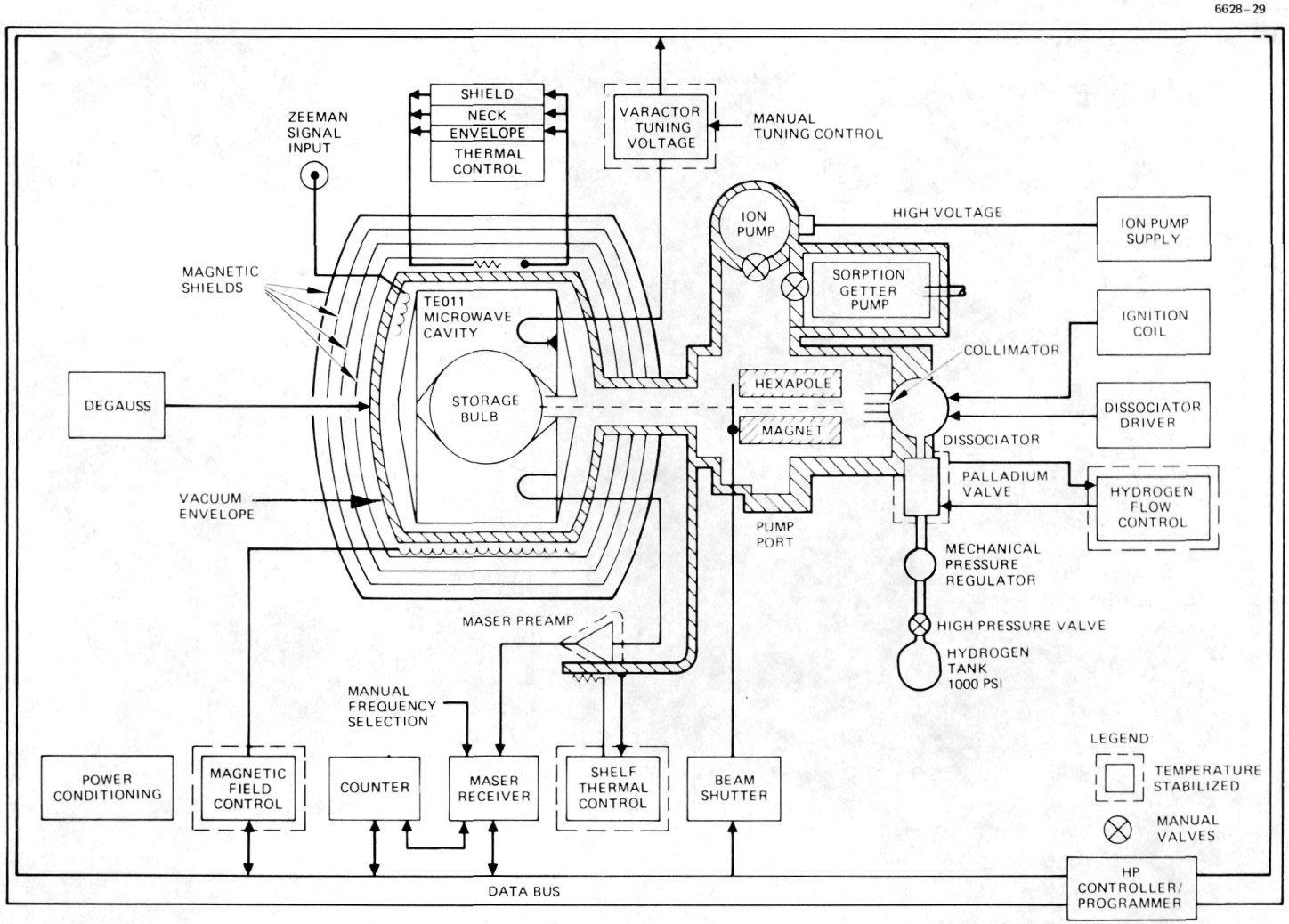


Figure 2. HYMNS III physics unit and electronics unit interface.

M12403-4

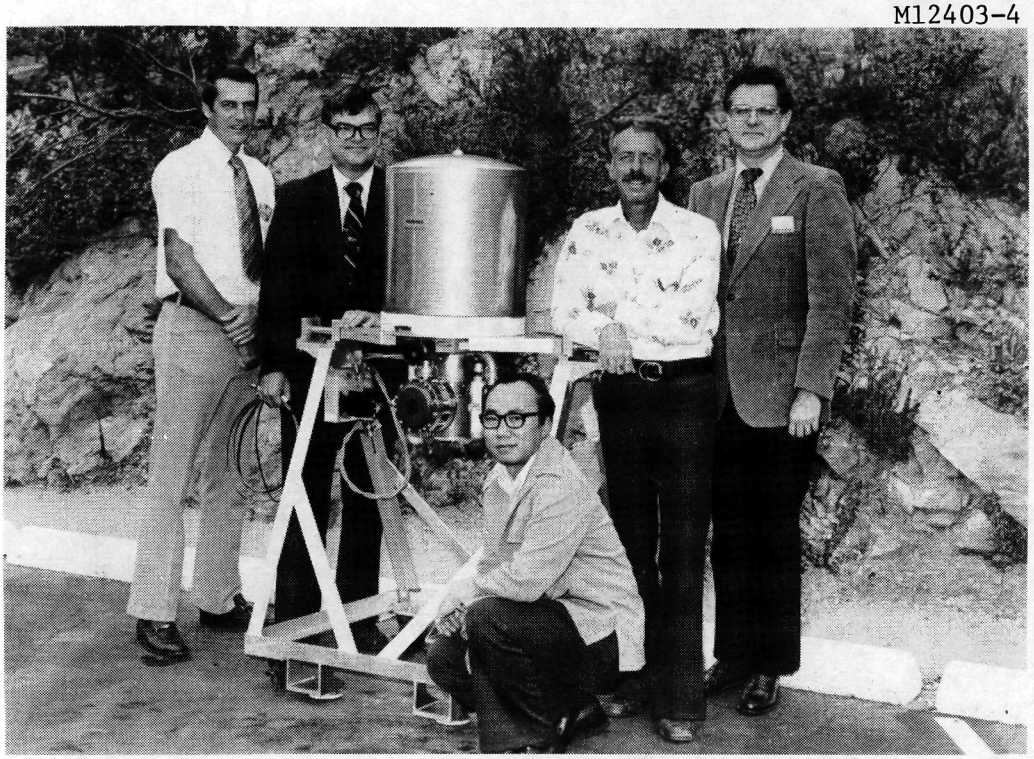


Figure 3. HYMNS III advanced development model physics unit.

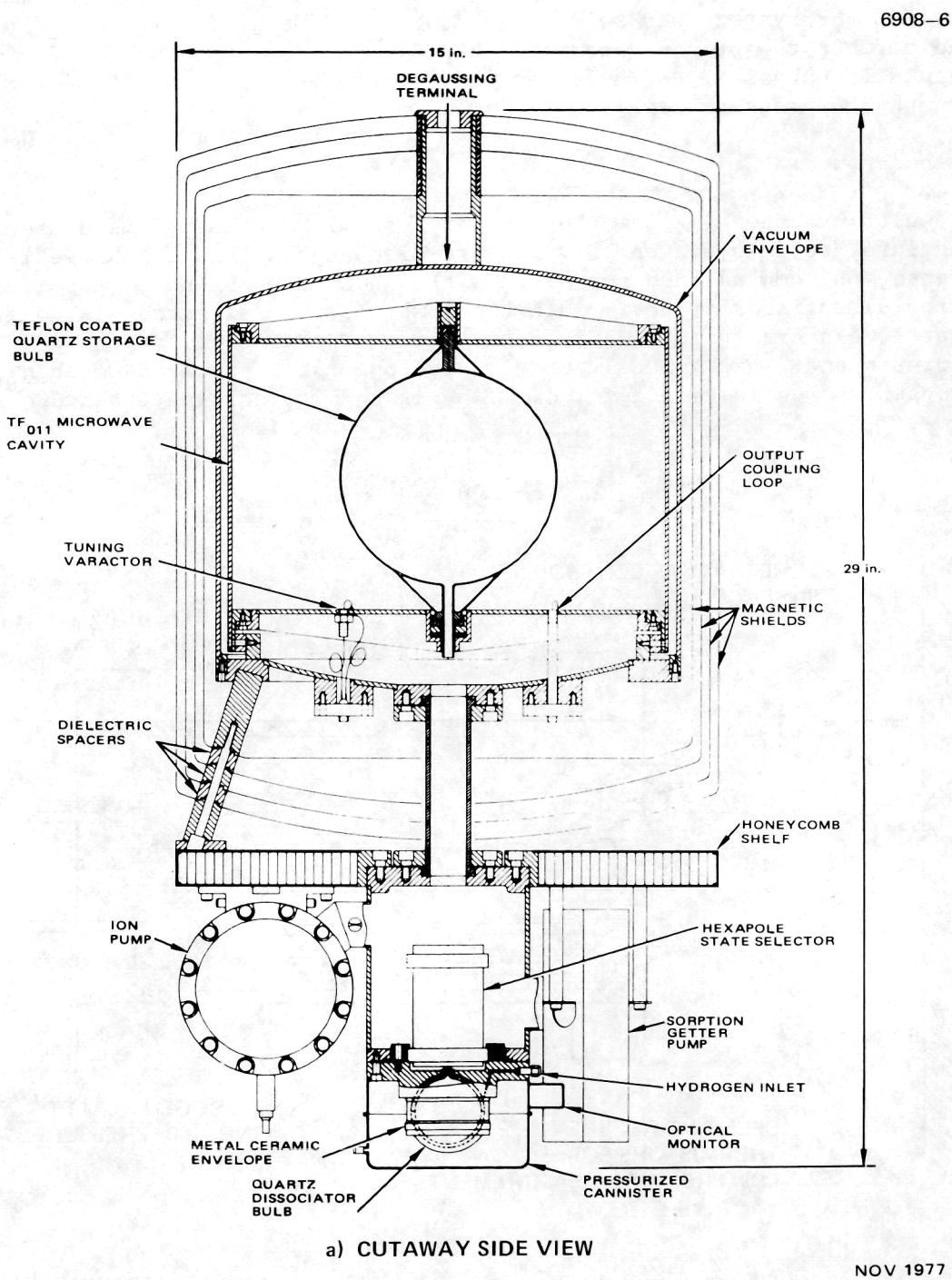


Figure 4. Engineering development model layout.

operates the system when selected by command. Metal tubing is to be used between the pressure tank and the dissociator input port. For diagnostic purposes, the hydrogen flow control servo can be programmed through 256 pressure levels.

Dissociaton

Molecular hydrogen (H_2) at the regulated 50 mTorr pressure is dissociated into atomic hydrogen (H) in an rf discharge. This discharge is ignited, on command, and sustained with 5 W of 150 MHz power supplied by the dissociator driver. Both the absorbed and reflected dissociator power levels are measured and telemetered. The dissociator shown in Figures 6 and 7 has a metal-ceramic envelope for thermal and mechanical strength and encloses a 2-in. diam. pyrex bulb to confine the hydrogen atoms.

6014–19

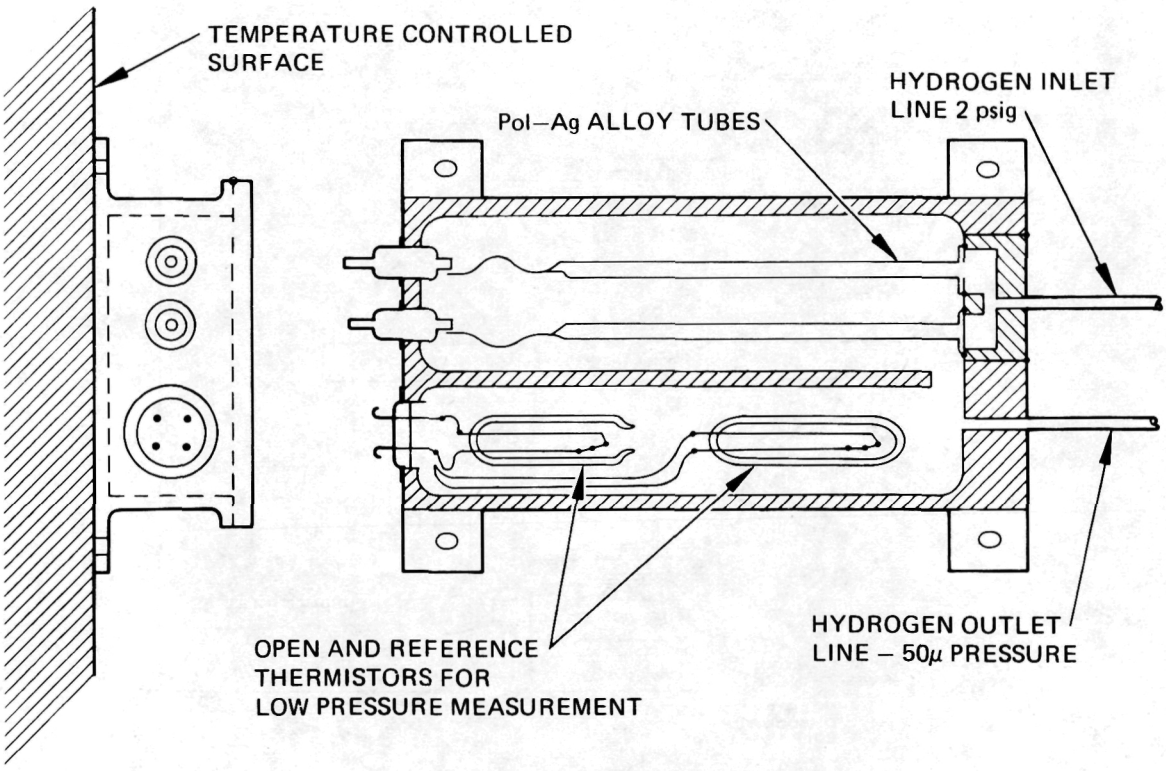


Figure 5. Integrated Pd-Ag regulator and thermistor pressure sensor. Electrical connections are made through vacuum tight ceramic feedthrough terminals.

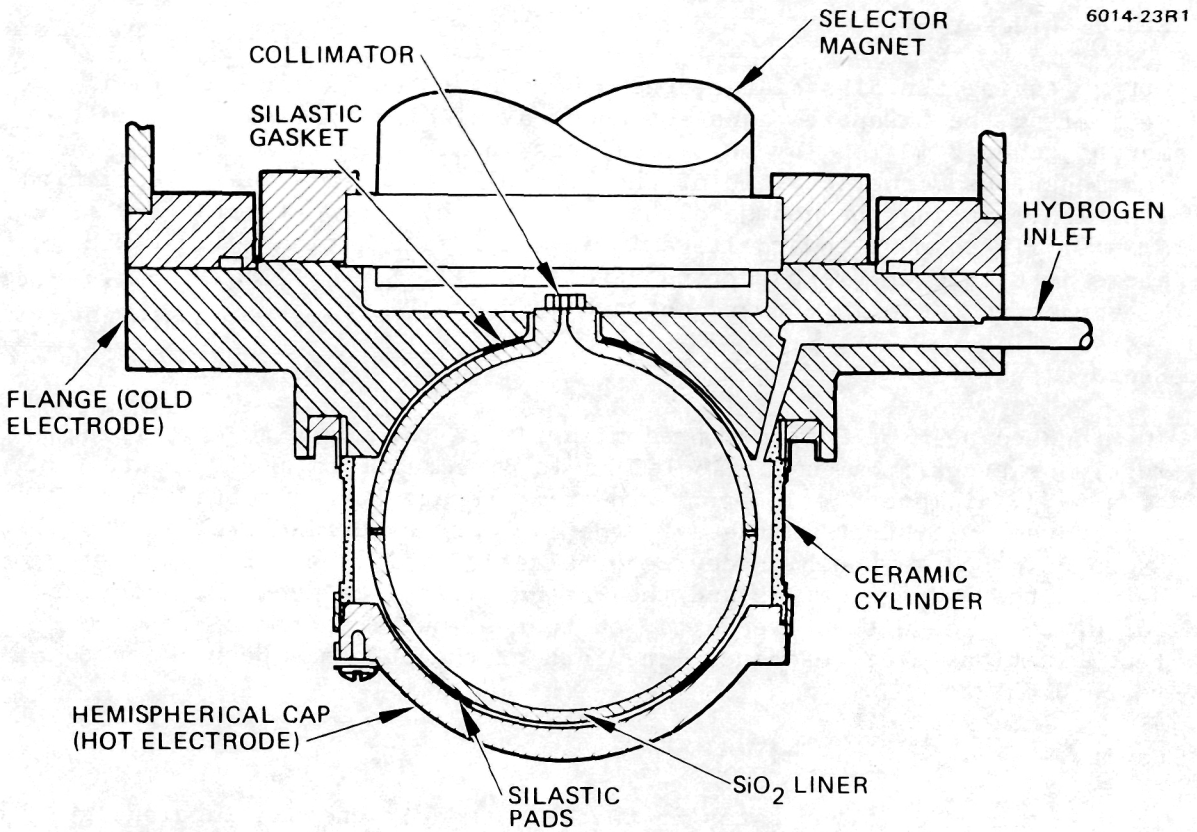


Figure 6. Proposed hydrogen dissociator design utilizing a metal-ceramic vacuum envelope with a spherical SiO_2 liner.

M12026

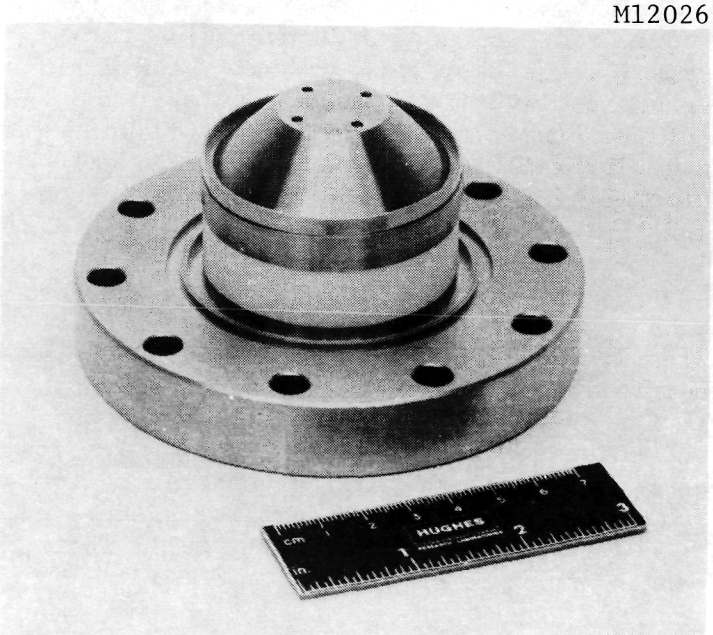


Figure 7.
Laboratory prototype of hydrogen dissociator.

State Selector

After leaving the dissociator, the atomic hydrogen is directed in a beam along the hexapole magnet by an array of close-packed glass collimating tubes 2 mm long by 50 micrometers in diameter. The strongly inhomogeneous magnetic field of the hexapole magnet provides a selection function, causing the atoms in the upper two hyperfine levels ($F = 1$, $M_F = 0, +1$) to move toward its axis in a focusing action while the H atoms in the lower two hyperfine levels ($F = 1$, $M_F = -1$, and $F = 0$, $M_F = 0$) move radially outward and are defocused.

Storage Bulb

The focused beam of H atoms (predominantly in the upper two hyperfine levels) emerges from the hexapole and is directed into the aperture tube of a 6-in. diameter Teflon-coated quartz storage bulb situated in a microwave cavity that is tuned to the 1420 MHz hyperfine frequency of hydrogen. Due to the high degree of elasticity in the collisions between the hydrogen atoms and the Teflon walls, the atoms are confined for up to 1 sec without deexcitation to the lower hyperfine states or recombination. The resonance linewidth of the bulb has been measured to be 0.65 Hz.

Cavity

The microwave cavity operates in the TE_{011} mode. One distinguishing feature of the cavity design shown in Figure 8 is the use of a squashed geometry with a diameter to length ratio of 1.6. The overall height is 3.5 in. less than typical designs which use ratios equal or greater than 1.0.

A solenoid with second-order correction produces a dc magnetic field that defines a quantization axis for the sublevels so that the $F = 1$, $M_F = 0$ states are coupled to the microwave field in the cavity. When the stimulated-emission gain of the atomic transition is sufficient to overcome the storage bulb and cavity wall losses, the system can self-oscillate. (For diagnostic purposes, the magnetic field control is commandable in 256 field increments between 10 μG and 30 mG.)

Cavity Thermal Control

For structural and thermal integrity, a lightweight cavity with a Q in excess of 70,000 is fabricated from beryllium or quartz and frequency stabilized within 1 Hz by both the envelope thermal-control servo and the cavity-tuning control. The envelope thermal-control servo with its associated thermistor and heaters maintains the cavity temperature to within a few millidegrees of 40°C; the loop error signal is telemetered. Figure 9 shows interchangeable quartz and beryllium cavity walls that are now being studied for strength and stability.

M12030

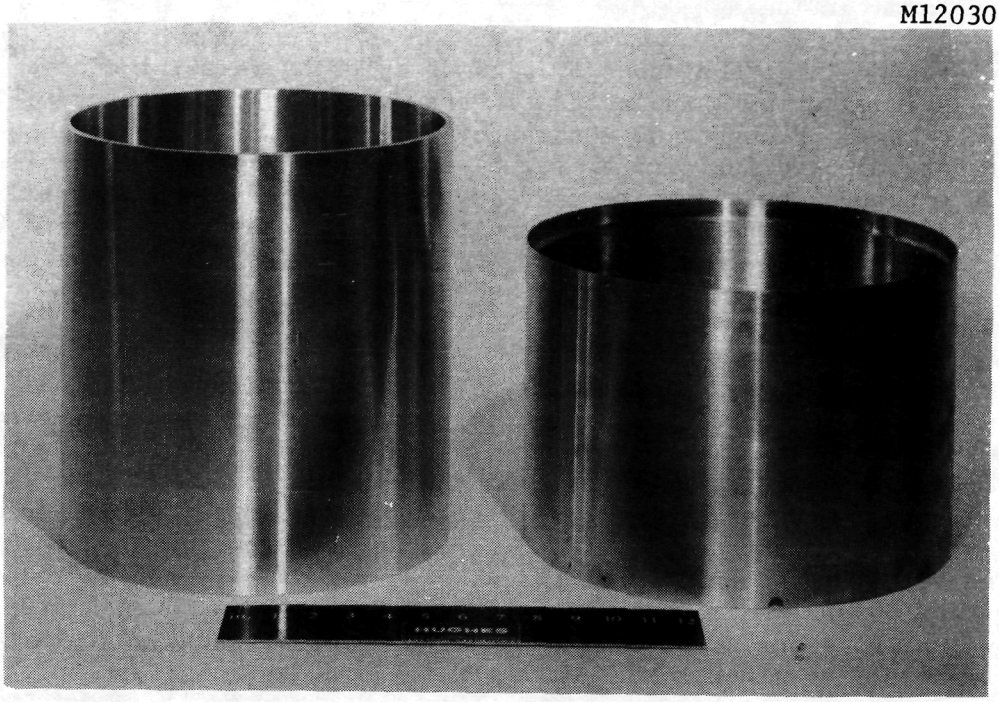


Figure 8. D/L = 1.6 short cavity alongside a D/L = 1 right cylindrical cavity normally used in laboratory masers.

M12290

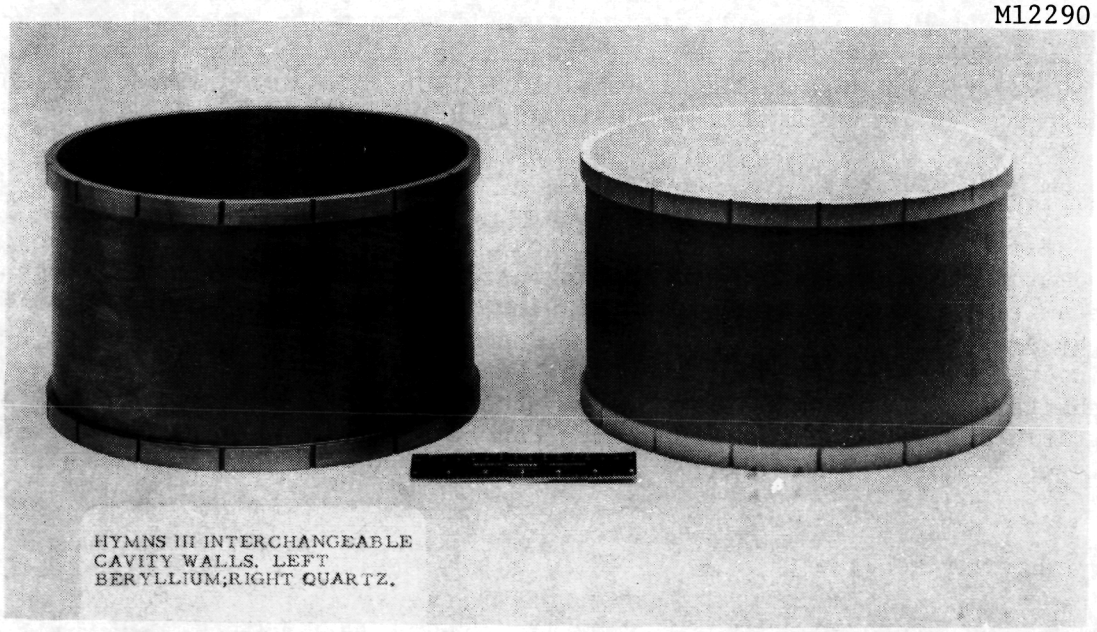


Figure 9. Interchangeable beryllium (left) and quartz cavities for HYMNS III testbed maser.

Cavity Varactor Tuning

Cavity tuning is accomplished by biasing a tuning varactor made of nonmagnetic materials and located in the cavity. The varactor will tune the maser through a 50 kHz range. The varactor tuning is controlled by onboard logic or by ground command. Commandable dc offsets in the control loop allow the clock system to be compensated for long-term drift of the thermal sensor and possible mechanical detuning of the cavity during launch.

Receiver Subsystem

The 1,420,405,751.xxxx Hz maser signal is amplified by space-qualified, low-noise, temperature-stabilized microwave amplifier and down-converted in a series of low noise mixers to 5751.xxx Hz. The phase of another 5751.xxx Hz signal, synthesized from the receiver's 5 MHz VCXO, is compared to the downconverted maser signal, and a phase error signal with a loop bandwidth of 0.1 to 10 Hz is derived to lock the frequency of the VCXO to the atomic transition. The receiver synthesizer developed for the ADM is programmable over a 2 Hz range, with each step equivalent to about 1 part in 10^{14} of the maser frequency. This control enables the clock to be corrected for gravitational red shift and other systematic errors in the GPS.

Zeeman Generator

For diagnostic purposes a Zeeman generator and beam shutter have been incorporated into the ADM maser design to detect long-term maser frequency pulling by magnetic inhomogeneities and cavity tuning errors. If required, a degaussing circuit can be activated on command to remove magnetic anomalies in the magnetic shield assembly.

Beam Modulation

A beam shutter with a small mechanical iris is located in the hydrogen beam near the hexapole magnet, and on command can reduce the hydrogen beam flux by 50%. If the maser cavity frequency is tuned precisely to the spin-exchange-tuned frequency, the maser frequency should then be independent of the intensity of the hydrogen beam flux (i.e., beam-shutter position). Using the beam shutter, long-term frequency-pulling statistics by beam-flux modulation can be accumulated by comparing the maser frequency with another onboard clock or by clock comparison on the ground.

Vacuum Maintenance

The spent hydrogen atoms emerging from the storage bulb are selectively pumped by an ambient-temperature sorption getter pump. A small ion pump is also used to pump hydrogen and other contaminant gases while

serving simultaneously as a high-vacuum gauge. We have conducted extensive life testing of the getter material and find it should be sufficient to pump the hydrogen supply of the maser when combined with a small ion pump to scavange impurities. The ion-pump voltage and current will be telemetered. A space-qualified, squib-actuated vacuum vent valve may be incorporated into the maser and on command vent the maser to space to provide additional life after the ion pump and getter pump are exhausted. The data in Figure 10 indicate venting is feasible within the first year in orbit. If successful, the vent to space would allow a significant reduction in the pump weight of future masers and promises greatly increased operational life for the hydrogen maser clock system in space.

CONCLUSIONS

Through a systematic analysis and design program encompassing all phases of hydrogen maser technology, we have designed and tested a compact hydrogen maser compatible with the constraints imposed by the NTS series spacecraft. Without sacrificing performance or operational life, a significant reduction in size was accomplished by analytical and experimental optimization of the hydrogen beam optics and microwave interaction assembly. As in our traveling-wave tube devices, the maser has been built in modular form to facilitate component interchange and standardization. During the course of the technology program we have also developed multiple vendor and in-house sources to supply critical components including quartz cavities, magnetic shields, quartz storage bulbs, and nonmagnetic varactors to assure an orderly progression into the space hardware phase of the program.

Acknowledgment

The authors would like to acknowledge Renyold Johnson, Joseph Schmid, Hubert Erpenbach, and Dion Rettberg for their aid in the design, fabrication, and testing of the testbed masers.

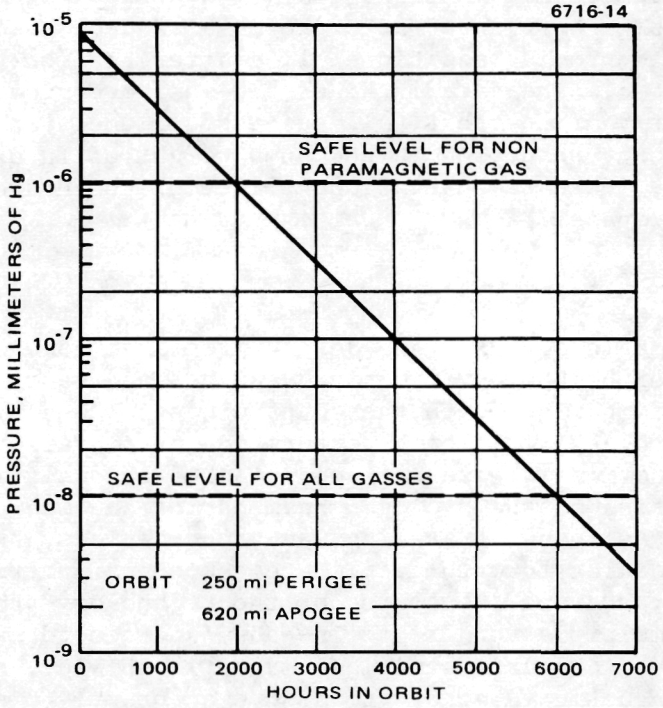


Figure 10. OGO spacecraft outgassing history.

OPERATIONAL CHARACTERISTICS OF A PROTOTYPE SPACEBORNE HYDROGEN MASER*

H.T.M. Wang, A.E. Popa, W.B. Bridges†, and D. Schnelker
Hughes Research Laboratories
Malibu, California 90265

ABSTRACT

The operational characteristics are described of an advanced development model of a spaceborne hydrogen maser developed for the Naval Research Laboratory for possible use in their NTS-3 spacecraft. The NTS-3 is a technology satellite built as part of the Navy's support for the NAVSTAR/Global Positioning System. Size reduction is shown to not necessarly degrade maser performance.

INTRODUCTION

This paper describes our experiences in developing and operating an advanced development model (ADM) hydrogen maser testbed for the Naval Research Laboratory (NRL). The design of a space-qualifiable version based on these experiences has been described in a companion paper and will not be repeated here.

The advanced development model maser, shown in Figure 1 and termed "HYMNS III" (Hydrogen Maser for Navigational Satellites, IIIrd version) was delivered to the NRL in October 1977 and was immediately operational. Prior to delivery, some weeks of operating experience were obtained at Hughes Research Laboratories on the completed maser, and prior to this, considerable operating experience was obtained with an earlier version, HYMNS II, and a demountable testbed, HYMNS I. Separate tests were also made on various subsystems as well. For convenience and ease of reference, the operational characteristics of HYMNS III are described under the headings of its major subsystems.

Vacuum System and Pumps

For this prototype spaceborne maser, no particular attempt was made to fabricate a completely sealed, all-metallic system. Several viton O-rings as well as an indium wire seal and copper gaskets were employed.

---

*Supported by Naval Research Laboratory under Contract N00014-75-C-1149.

†Present address: California Institute of Technology, Pasadena, CA 91125.

M12043-9



Figure 1. HYMNS III advanced development model testbed maser.

Typical residual pressure in the maser was about 3×10^{-7} Torr. A Varian Hi-Q ion pump with a rated speed of 30 liter/sec for hydrogen and weighing about 20 lb was selected early in the program for its compactness and relatively small stray magnetic field. With an operational hydrogen through-put of about 0.05 μ-liter/sec, the pump dissipates only about 7 W of electrical power, thus eliminating the need for cooling water. With a claimed 8000 Torr-liter hydrogen capacity, the Hi-Q pump would have an estimated life of 7.6 yr. Unfortunately, the pump requires a 7.5 kV operating voltage which is considered undesirable for use in space. Laboratory life tests at only slightly accelerated hydrogen flow rates also indicated that premature pump failure is likely to occur due to short circuits caused by detached flakes of hydrogen-saturated cathode material. As a result, alternative vacuum pumps were considered; active-metal chemical getter pumps were evaluated in several life tests and were found to be satisfactory for both the ADM and the proposed spaceborne design. As a result of these tests, a SAES getter cartridge pump was added to the HYMNS III maser. After an initial activation at high temperature, this zirconium-aluminum alloy cartridge pumps hydrogen at room temperature with no power consumption. Its specified end-of-life capacity of about 20,000 Torr-liter has been confirmed by accelerated life tests giving it an estimated life of about 12.7 yr. under normal maser operation without an ion pump. The singular disadvantage of the sorption pump is that at room temperature its pumping speed for gases other than hydrogen is very small. Thus a small supplementary ion pump will be required to scavenge impurities. For this reason the Varian Hi-Q pump was retained on HYMNS III. Even if the efficiency of the beam optical system were to remain at the level demonstrated in HYMNS III, we can confidently project a total pump subsystem weighing no more than 20 lb and consuming less than 3 W for a spaceborne maser with a five-year design life.

Magnetic Field and Shielding

HYMNS III employs four layers of Mu-80 cylindrical magnetic shields with domed end caps. During the development process we evaluated shields fabricated from three different materials (molypermalloys, hypernom and Mu-80) from three different suppliers. As far as can be judged from the maser performance, we have no reason to prefer one over the others. The response to degaussing is also very similar for the three materials.

To generate the small quantization field required to operate HYMNS III, a solenoid with a second-order correction is employed. Since the current through the correction coil is a constant fraction of that in the main coil, no separate optimization was required. The homogeneity of the magnetic field averaged over the maser storage bulb is such that strong maser oscillation was obtained at applied magnetic fields as low as 50 μG. In fact, steady maser oscillation was observed at applied

fields as low as 20 μG, at which point residual fields from the shields and stray fields from the ac heaters of the temperature control system introduce significant perturbations.

Thermal Control System

Temperature-control resistive heater windings in HYMNS III employ alternating currents. Since perfect bifilar windings are difficult to obtain, perturbations to the maser oscillation frequency caused by magnetic field fluctuations arising from direct-current heater current variations are substantially reduced by using ac. This makes a significant contribution to the excellent operational characteristics of the maser at very low applied magnetic fields. Four separate heaters and control circuits are employed. Glass bead thermistors with nominal resistance of 50 kΩ at 25°C are used as sensors.

Atomic Hydrogen Source and Beam Optics

Atomic hydrogen is obtained by rf discharge in a 2-in. diam pyrex bulb. Delays in material delivery prevented the incorporation of a novel metal-ceramic dissociator in the delivered HYMNS III maser. However, a prototype metal-ceramic dissociator had been bench-tested separately and was found to be at least as efficient in hydrogen atom production. The metal-ceramic structure provides significantly improved mechanical strength and eliminates any possibility of breakage in the feed lines supplying hydrogen. Dissociator pressure regulation is obtained by a thermally regulated palladium-silver alloy valve in the form of a thin-wall tubing which formed part of the electrical circuit. Typical power consumption to heat this valve was about 0.5 W with a control constant of about 30 sec. The rf power supply utilized a linear power amplifier driven by a crystal-controlled oscillator at about 150 MHz. For normal maser operation, a sustaining rf power of about 3 to 5 W is sufficient. It is necessary to momentarily raise the rf level to about 10 W to ignite the discharge. The low sustaining drive level is desirable to extend the life of the dissociator. Moreover, higher rf levels do not give correspondingly higher atom production, as proved by actual measurement using thermal wire-bridge detectors and optical photometers in a separate test-stand evaluation of dissociator performance.

A hexapole magnet (FTS model HM-2) is used for state selection. Since the spacing between the hexapole magnet and the storage bulb aperture is only 8 in., a beam stop is necessary to block the unselected atoms travling along the axis of the magnet. However, the efficiency of the system is such that under normal operation conditions, a total hydrogen throughput of less than 0.05 micron-liter/sec is sufficient.

For spin-exchange tuning, the flux is modulated by an electrically operated beam shutter with a beam attenuation of about 50% rather than by changing the flow or rf drive to the dissociator bulb. Since the

shutter operates independently of the dissociator, the response is essentially instantaneous. More important, the dissociator operating parameters remain constant, and the chances for irreversible damage to the dissociator by pressure or drive modulation are greatly reduced.

Microwave Cavity

The TE_{011} microwave cavity is fabricated from a precision-machined satin-fused silica cylinder with aluminum end plates. The inside dimensions are 12 in. diam by 7.4 in. long, giving a length reduction of about 3.5 in. compared to the right cylindrical cavity. It is equipped with a linear varactor tuning loop and a single 50 Ω output coupling line. A high-conductivity silver coating gives the cavity a measured loaded Q of 65,000 with a coupling coefficient of 0.21. This is about 98% of the theoretical maximum. The resonant frequency of the cavity when loaded with the 6-in. maser storage bulb has a measured temperature coefficient of 1.3 kHz/°C.

To prevent the long-term drift in the cavity resonant frequency from limiting the maser stability performance, an electronic cavity frequency monitoring and control system was designed. The system operated by coherently detecting switched test signals at frequencies symmetrically situated with respect to the spin-exchange-tuned cavity frequency, and offset from it by about half the cavity resonant width. The error voltage thus derived is used to bias the varactor tuning loop. A prototype tuning system was tested on the HYMNS II maser, however, the use of a single-line cavity coupling system resulted in poor signal-to-noise ratio and the system has not been implemented on HYMNS III. In the future, by using a two-port cavity coupling system, we expect significant improvement in signal-to-noise, and the system should prove to be a valuable diagnostic tool in addition to the electronically stabilizing the cavity resonant frequency.

Maser Storage Bulb

The storage bulb is a 6-in. diam blown fused quartz sphere. It is coated with FEP-120 teflon by standard techniques. Although the spherical bulb geometry was selected for ease of fabrication, the filling factor in the D/L = 1.6 microwave cavity is very nearly the same as the optimal value of 0.37 for an ellipsoidal bulb. The geometrical storage time is designed to be 1.25 sec. Although no systematic measurement and analysis of linewidth contributions have been made yet, the full maser transition linewidth under normal operating conditions was measured as 0.75 Hz, corresponding to a line Q of 1.9×10^9. This value compares very favorably with those for full-size laboratory masers.

Maser Receiver

The triple-conversion maser receiver provides standard outputs at 5 and 10 MHz, phase-locked to the maser. It is equipped with a synthsizer at 5751.xxxx Hz and is adjustable in steps of 1 part in 10^{14} of the maser frequency. For tuning and diagnostic purposes, the receiver can be operated open-loop with an external 5 MHz reference signal. Down-converted 5.75 kHz maser signal as well as low-frequency beat notes are available for measurements by a counter.

Spin-Exchange Tuning and Stability Measurement

The automated operating features of HYMNS III represent a significant advance in maser design. The procedures generally encountered in maser operations can be carried out simply by depressing appropriate control buttons. An operator with detailed knowledge of maser theory is not required to carry out what used to be a long, tedious and intricate spin-exchange tuning process. In fact, when the spin-exchange tuning program is executed, the process continues automatically until specified precision is achieved, or it can be terminated at any time desired. As mentioned earlier, since a beam shutter is employed for flux modulation, long waiting periods for the dissociator to stabilize are unnecessary, and a significant savings in tune-up time is obtained.

The system controller is a Hewlett-Packard Model 9825A programmable calculator. Programs for functions such as initial setup, spin-exchange tuning, stability measurement, adjustments of applied magnetic field, varactor bias and receiver synthesizer, etc. are stored in the calculator memory and are instantly accessible. As an illustration, a typical spin-exchange tuning run is shown in Figure 2. When the program is called, interactive messages are displayed. After the desired precision expressed by the varactor bias tolerance, the low-high flux pulling, and the number of periods averaged and counter readings to produce a frequency sample are specified, the program runs automatically. The data were taken with a VLG-10 maser as an external reference, and the tuning process was completed in less than 35 min. The specified 5×10^{-3} V varactor bias tolerance corresponds to a possible tuning error of 2 parts in 10^{13}.

Preliminary stability data taken by NRL which compares the testbed with a VLG-10 are shown in Figure 3. These data, taken with the exploratory development model receiver can be improved by a factor of 3 when the maser is used with our HYMNS II laboratory breadboard receiver. We plan to continue refinement of the receiver electronics as we proceed in our technology studies.

```
START SPIN EXCH TUNING

AUTO TUNING

Period Avged
1e5
Readings/Set
5
Pull Tol
1.4e-5
VARB Tol
5e-3

VARB:     5.18292

LoBm
        5751.655968
        5751.655866
        5751.655833
        5751.655598
        5751.655925
AvF:    5751.655838
+/-        Ø.ØØØ144

HiBm
        5751.653649
        5751.653583
        5751.653553
        5751.653676
        5751.653653
AvF:    5751.653623
+/-        Ø.ØØØØ52

LoBm
        5751.655866
        5751.655896
        5751.656Ø31
        5751.655791Ø
        5751.655833
AvF:    5751.655883
+/-        Ø.ØØØØ92

Full+     -Ø.ØØ2238
+/-        Ø.ØØØ1ØØ

VAR        5.6826Ø
```

```
END SPIN EXCH TUNING

VARB:      5.43789

LoBm
          5751.672737
          5751.672539
          5751.672Ø7
          5751.673Ø91
          5751.672638
AvF:      5751.672683
+/-          Ø.ØØØ259

HiBm
          5751.672463
          5751.672929
          5751.672Ø6
          5751.672741
          5751.672Ø8
AvF:      5751.672649
+/-          Ø.ØØØ19Ø

LoBm
          5751.672774
          5751.672Ø5
          5751.672Ø9
          5751.672Ø6
          5751.672638
AvF:      5751.672Ø6
+/-          Ø.ØØØ11Ø

Pull=        Ø.ØØØØØ5
+/-          Ø.ØØØ236

SETVB        5.437327
+/-          Ø.Ø26795

Wd Av        5.438Ø5
+/-          Ø.ØØ474

Cov SETd at VB =
             5.438Ø5
```

Figure 2. Frequency comparison of the Hughes testbed maser and the SAO VLG-10 maser using the XDM receiver in the Spin Exchange Tuning mode. Only the final 10 digits are shown.

CONCLUSIONS

The operational characteristics of HYMNS III along with extensive life-test data obtained during our technology program lead us to the conclusion that a reduced size, long-lived spaceborne maser can be space qualified using existing technology. We also conclude that the maser can be made compatible with the size, weight, and power constraints of the NTS-3 spacecraft without any sacrifice in the superior stability performance exhibited by laboratory devices.

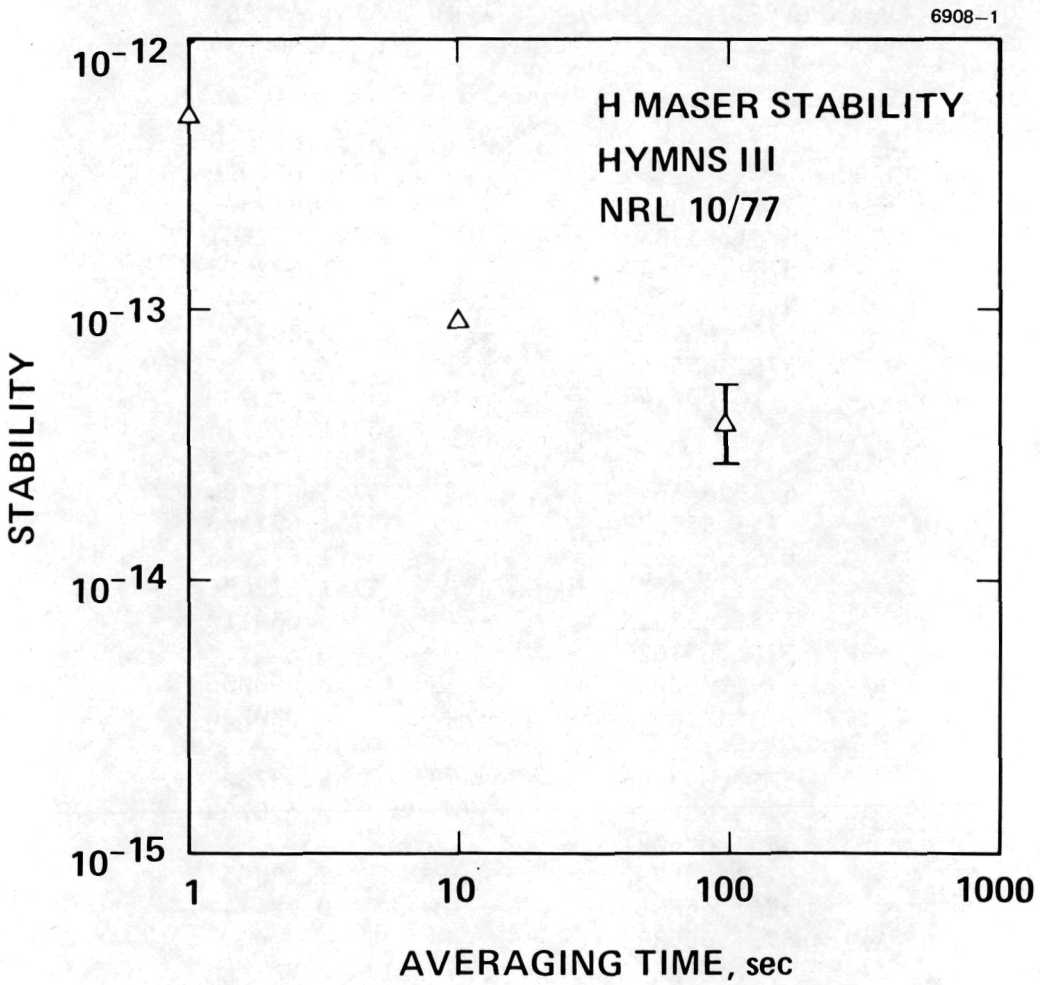


Figure 3. Preliminary stability data.

QUESTIONS AND ANSWERS

MR. WOLFGANG BAER, Ford Aerospace:

What is the final weight that you expect on the NTS-3 satellite? Where do you expect weight and size to go on the hydrogen maser designs?

MR. WANG:

I guess the weight and size, as given in the previous talk, depends on the spacecraft. Tentatively we are shooting for 100 pounds and consuming less than 100 watts with a 15-inch diameter and less than 30-inches long. But that is very tentative. Roger Easton or some people from NRL will be able to define those parameters better for you.

MR. BAER:

Do you have any feeling for where you might go in terms of weight and size in the maser development?

MR. WANG:

I feel that we can probably reduce the length and diameter by another inch or two on this active maser, but probably not much more. The weight, of course, depends on the polymer you finally select as well as the magnetic shield. Those are the heaviest components.

DR. ROBERT VESSOT, Smithsonian Astrophysical Observatory:

To give a little perspective on this, the one we flew weighed 88 pounds. It was 19-inches in diameter and about 24 inches tall. With a TE 111 cavity, allowing the same spacing between 4 layers of magnetic shields, you could make a maser fasten in a 12-inch diameter tube and be on the order of, I think, 20 inches in length. The cavity is a valid concept because it does oscillate and it will work.

In relation to the cartridge, we found that we could run the cartridge well over a year and it didn't saturate and it was a marvelous getter. But we just needed a very, very small ion pump to take care of the stuff that wasn't hydrogen, as I think you have also seen. But the function of the ion pump was also to take apart molecules that contained hydrogen as a dissociator.

I really think the future of hydrogen pumping for the maser is in the cartridge. I feel that we are contributing noise to our system by having a glow discharge. Even if it is in the milliamps, that is just not a wholesome thing to have, plus the fact we have these monstrous magnets in the vac ions, the weight, the shield, and all the rest of it. I really feel that the way to go is in the cartridge.

MR. WOLF:

I agree.

THE NEW STATE TIME AND FREQUENCY STANDARD OF THE USER AND THE DEVELOPMENT OF THE SYSTEM OF STANDARD FREQUENCY AND TIME SIGNAL EMISSION

V. G. Il'In
N. A. Tel'puchovskyi

V. V. Sazhin
USSR Gosstandart
9 Leninsky Av.
Moscow 147049, USSR

ABSTRACT

The new state time and frequency standard of the USSR includes the primary cesium beam frequency standard with a transition distance of 75 cm. Frequency reproducibility from switching to switching is $\leq \pm 5 \cdot 10^{-13}$. This standard is used as a base one for producing the units of frequency and time intervals in the SI system. The hydrogen masers with reproducibility not less than $\pm 1 \cdot 10^{-13}$ are the standby clocks providing a clock on the units of frequency intervals. The state time and frequency standard is preserved by hydrogen masers and cesium atomic beam standards. The comparison between the state standard of the USSR and the BIH standards in 1975-1977 showed that frequency and time units producing by the above standards coinsided better than $1 \cdot 10^{-13}$ with almost constant difference of $5 \cdot 10^{-14}$. The secondary time and frequency standard at the Siberian branch of VNIIFTRI (All-Union Research Institute for Physics and Radio Engineering Measurements) has close metrological parameters with somewhat different standard structure.

For comparison of the USSR state standard with the secondary standards of the USSR and standards of the foreign countries we use portable atomic clock, lines of meteor communication, radiostation transmission in the LF- and VLF- range as well as by means of meteor lines.

Time scale and standard frequency transmission from the standards to the users is effected by means of meteor radiolines (accuracy is not worse than 100 ns), television channels (accuracy from 0.5 μs to 1-2 μs), navigation radiostations of LF- range, carrier frequencies of VLF- radio stations as well as by means of radio stations in LF- and HF- range. In the above channels there are shown the achieved results and also the trends of further development of the transmission system.

(Paper not Presented)

Page intentionally left blank

Page intentionally left blank

STEERING OF A TIME SCALE

Michel Granveaud. Bureau International de l'Heure.
Paris - France
Jacques Azoubib. Bureau International des Poids et Mesures
Sèvres - France

ABSTRACT

The atomic time scales can present some large time and frequency errors. The primary cesium standards which are the references allow to correct them. These devices can be used as frequency standards running from time to time or as clocks ; and two approaches to the steering problem appear possible.

The starting point of this study is an independent atomic time scale S computed by the laboratory 1 ; independent means that the scale has no intentional relationship with the time scale of another laboratory m and/or with a reference time and frequency standard . It is computed using only the data coming from a set of atomic clocks running freely and this computation is managed to get a time scale with a long term good stability. Models of such time scales have been developed [1, 2] . Figure 1 shows a purely random simulated time scale over 120 years the stability of which has the following expression :

$$\sigma(\tau) = (324\ \tau^{-2} + 0.25 + 4 \times 10^{-4}\ \tau)^{\frac{1}{2}}$$

where $\sigma(\tau)$ is the square root of the pair variance of the time scale frequency and is expressed in 10^{-13}, the parameter τ being expressed in days. It appears that the time differences between this time scale and the ideal one can be pretty large after a couple of years. Figure 2 gives the mean frequency of the time scale during a ten years interval and shows an apparent frequency decrease of about 0.6×10^{-13} per year.

The only way to avoid so large time and frequency errors is to correct the time scale S using information coming from some references. Several authors have derived filters in order to obtain the best estimate of the frequency of a time scale from series of measurements of this frequency by the primary standards [1, 3, 4]. An empirical use of the results of the filter developed in [4] has been proposed by the Bureau

International de l'Heure (BIH) as an accuracy - stability algorithm for the International Atomic Time scale (TAI). It was shown from simulations that the accuracy could be ensured and the stability of the original time scale S could be maintained or improved [5]. However it is realized that estimation of the frequency and steering of the time scale are different problems, at least theoretically. We have tried to develop a steering filter. The figure 3 shows the general problem : the primary cesium standards are used to compute a correction useful for the present date t ; this one is applied to the original time scale S which has a good stability. It is desired that the corrected time scale S' be accurate and stable at any present date t. Finding a linear predictor filter which allows the corrected time scale S' to be accurate and stable is the problem. Solutions can be developed after some hypothesis are adopted and the choice of assumptions leads to a specific approach of the problem.

The table 1 details two approaches. The first one is the method presently used by the BIH. It is based on the estimation filter [4] and the steering process [5] ; it will be referred as approach 1. It corresponds quite well to the use of the primary standards as frequency generators and research devices ; the standards and/or the calibration measurements can be modified from one test to the other to obtain better results than before. The approach 2 corresponds to the use of the primary standards as clocks ; the standards are considered as metrological devices which must run a long time (several months) without changes.

Several points are common in both studies : the time scale model, the independence of the involved primary standards and the stability criterion. Important differences appear in the calibration models. In approach 1, the calibrations can take place at any time and have any duration, but they are supposed to be affected by white noise and constant error. For the second approach, there is no theoretical restriction concerning the calibrations noise but the calibrations have to be considered as regularly distributed every 60 days in succession without gap. The involved frequencies in this case are mean frequencies over 60 days which is considered as the unit of time interval. If several standards are involved in the computation, they are assumed independent of each other in both cases ; but, in the first approach, they are members of ensembles the statistical properties of which are known. An accuracy filter was derived for the approach 1 and was detailed in [4] . Pratical steering filters were proposed in [5] in this case.

APPROACH 1	APPROACH 2
TIME SCALE MODEL	
purely random time scale with white PM plus flicker FM plus random walk FM	idem
sampling period : 10 d	sampling period : 60 d
CALIBRATION MODEL	
the calibrations occur randomly and their duration is variable.	the calibrations occur periodically every 60 d and last 60 d.
the errors of the calibrations belong to a white noise.	
if several standards are involved, they are independent.	if several standards are involved, they are independent
each standard belongs to an ensemble the statistical properties of which are known.	
CORRECTED FREQUENCY	
It depends on the steering process see [5] .	the original frequency minus a weighted linear combination of the corrections from each standard.
ACCURACY CRITERION	
the weighted linear combination of all the calibration results near to the time scale frequency (in mean square) see [4] .	the corrected frequency near to the best estimate of the frequency of the standards (in mean square).
STABILITY CRITERION	
Pair variance of the corrected frequency has to be minimum .	idem

TABLE 1. Main characteristics of two steering approaches carried out by the Bureau International de l'Heure (BIH).

More details are given now for the approach 2. The corrected frequency is computed at the present date t (which means t times the sampling period 60 days). The data used to compute the correction are the mean frequency differences $Y^i - R^i$ at the date i between the time scale S and one primary standard, where i goes from 0 to $t - \alpha$; α represents the delay of the available data. If they are used in real time , $\alpha = 0$. These data enter a linear filter the impulse response is G ; the output of the filter is the convolution

$$C = (Y - R) \otimes G$$

or more explicitly, at any present time t :

$$C^t = \sum_{i=0}^{t-\alpha} g^i \, (Y^i - R^i)$$

When several independent primary standards are involved, the total correction is a weighted linear combination of the individual corrections as C^t ; the weight of a standard depends on its qualities. Let us come back to the simpler case of only one standard. The corrected frequency at the date t is :

$$y^t = Y^t - C^t$$

The scale S', represented by the time process y^t , is said accurate if

$$E \left[(y^t - R^t)^2 \right] \text{ is minimum}$$

where E designates an ensemble average . The quantity $y^t - R^t$ can be written :

$$y^t - R^t = Y^t - R^t - \sum_{i=0}^{t-\alpha} g^i \, (Y^i - R^i)$$

The functional diagram of the figure 4 represents this relation. It appears that the filter G which is looked for and satisfies the accuracy criterion is a pure prediction filter.

Let us see the stability criterion : the best stability of the corrected scale S' is obtained if the pair variance of y^t is minimum. The computation of the pair variance introduces the parameter τ (time interval between two successive data) and it will be possible to obtain the best stability for some specified value of τ . The expression of y^t is

$$y^t = Y^t - \sum_{i=0}^{t-\alpha} g^i \, (Y^i - R^i)$$

and is represented by the functional diagram of the figure 5. The role of the filter K in the chain is simply to convert the usual Wiener criterion (minimization of the variance of the error) into the new criterion : minimization of the pair variance of the error. The steering filter G which satisfies the stability criterion is a predicting filter which allows the signal Y^t to be extracted from the imput $Y^i - R^i$.

Solutions of both separate problems, i. e. filters G , are found using the Z transform domain [6] which is deduced from the Laplace one by

$$Z = e^{\theta p}$$

where θ is the sampling period (here 60 days). The solutions depend on the noise of the calibrations and this one of the time scale. The table 2 presents, as an example, the steering filters which are obtained when the time scale noise is either a flicker FM or a random walk FM and the calibration noise is white FM. The last hypothesis corresponds to the approach 1 and so the same exponential accuracy filter as in [4] is obtained. The stability filter depends on the parameter τ .

The second approach allows to obtain filters which ensure either accuracy or stability (for a specified value of τ) whatever is the calibration noise . A realistic steering filter will be a compromise between an accuracy filter and a stability filter. Furthermore it will depend on the noise of the primary standards and also on some practical limitations of the involved calibrations due to a possible drift of the time scale S, an improvement of the primary standards and/or of the calibration measurements.

REFERENCES

[1] ALLAN, D.W., HELLWIG, H., GLAZE, D.J. : Metrologia 11, 133 (1975)

[2] GUINOT, B., GRANVEAUD, M. : IEEE Trans. Instr. and Meas. IM. 21, 396 (1972)

[3] YOSHIMURA, K. : NBS Technical Note 626 (1972)

[4] AZOUBIB, J. , GRANVEAUD, M. GUINOT, B. : Metrologia 13, 87 (1977)

[5] CCDS, Rapport au Comité International des Poids et Mesures, 8th Session (1977). to be published

[6] LEFEVRE, P. : Optimalisation statistique des systèmes dynamiques, Dunod, 1965

TIME SCALE NOISE	FLICKER FM	RANDOM WALK FM
ACCURACY	● last calibration	● last calibration
steering filter	○ exponential type	○ exponential
STABILITY steering filter	● Weighted past values depends on τ	● weighted past values depends on τ
	○ idem	○ idem

Table 2. Steering filters obtained when using the second approach. The symbol ● refers to non delayed data and ○ to delayed data. The calibrations are affected by a white noise FM.

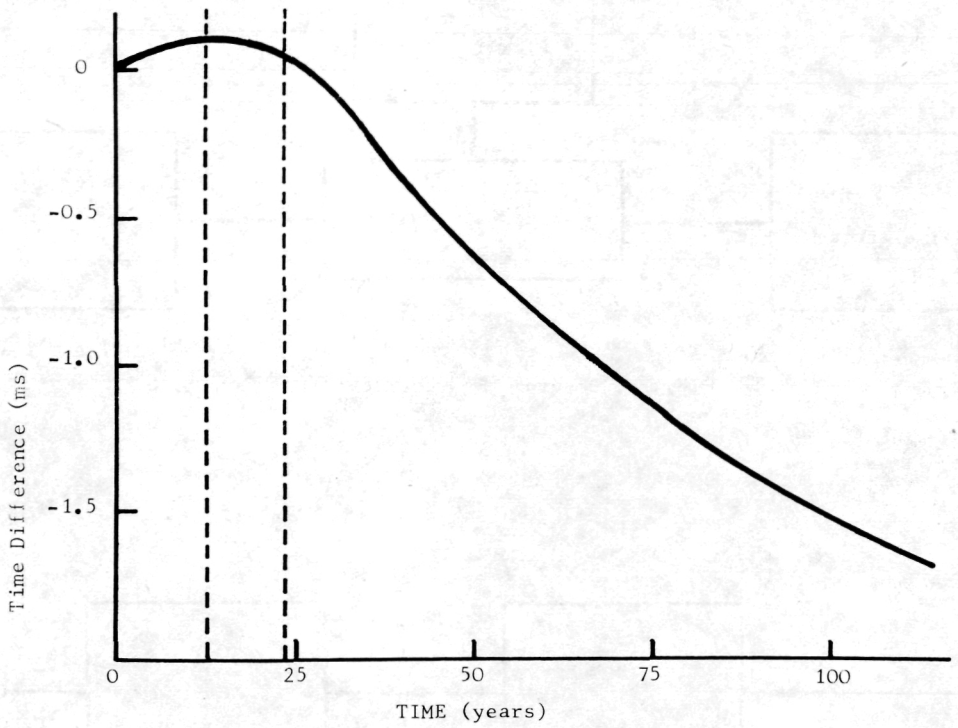


Fig. 1. Time difference between a simulated random time scale and the ideal one as a function of time.

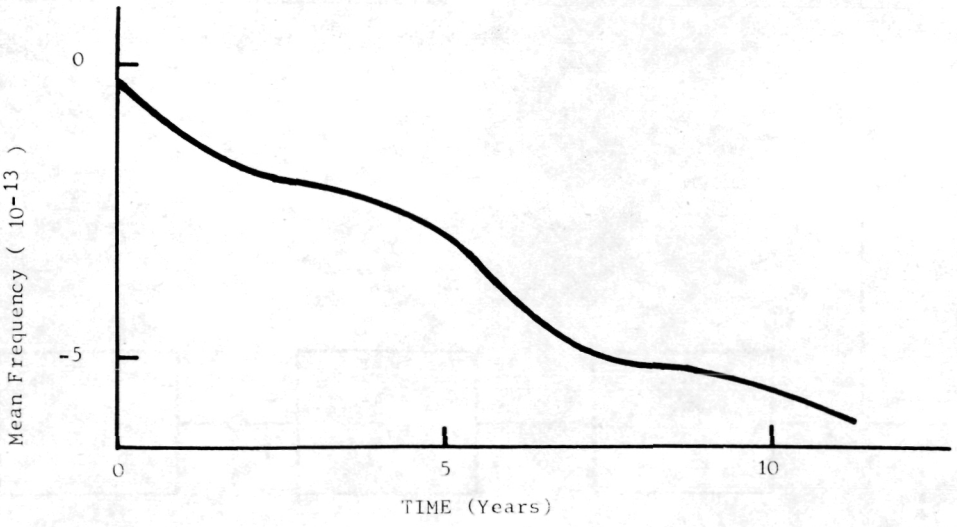


Fig. 2. Mean frequency of the figure 1 time scale during a 10 years interval.

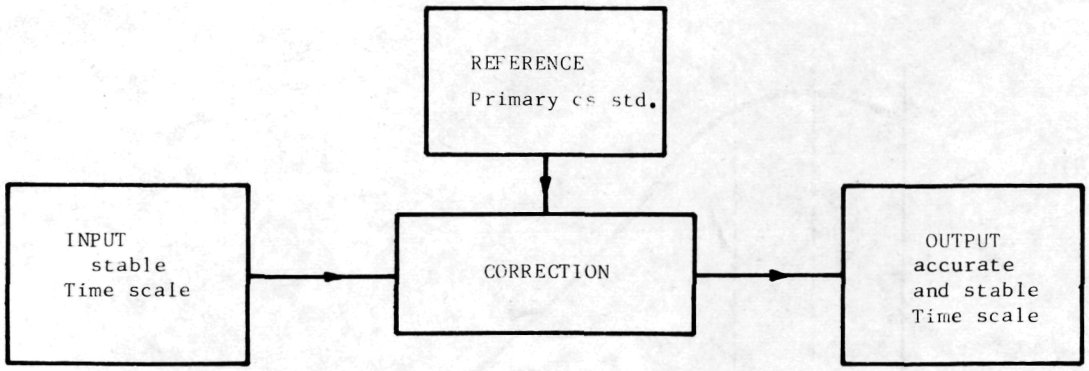


Fig. 3 . Diagram of a corrected time scale.

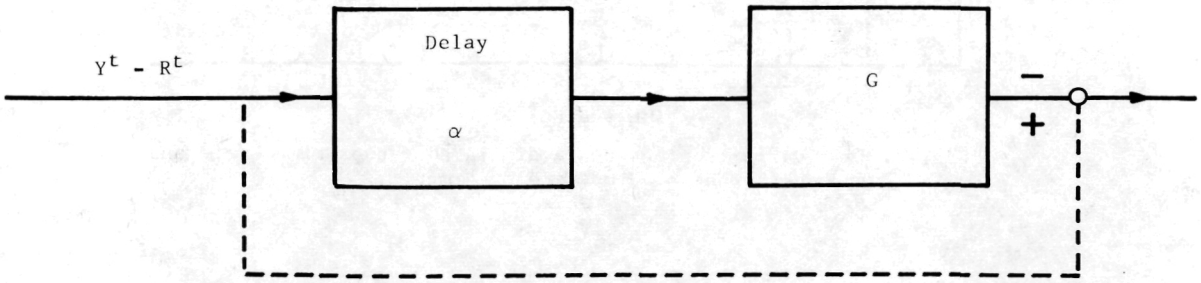


Fig. 4. Functional diagram of the accuracy filter.

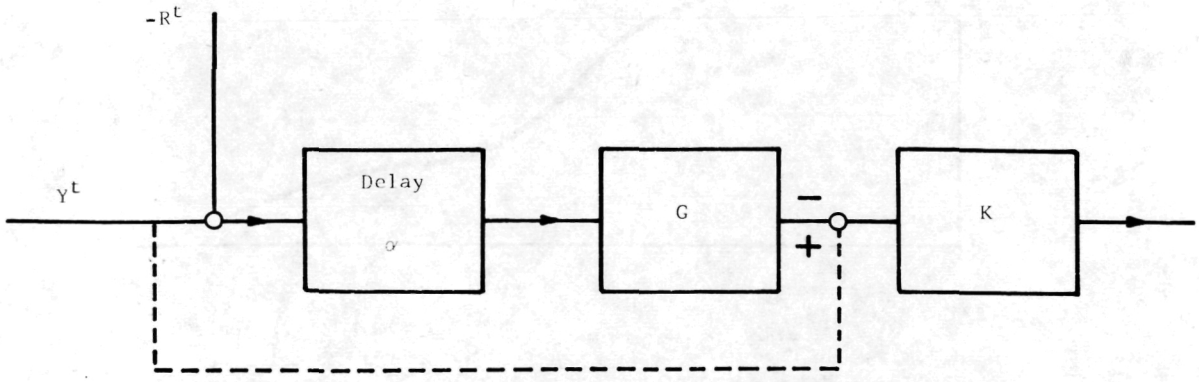


Fig. 5. Functional diagram of the stability filter.

QUESTIONS AND ANSWERS

DR. GERNOT M. R. WINKLER, U. S. Naval Observatory:

To what degree would your results change if you drastically change the assumed models by assuming a very large and overwhelming contribution from just phase noise?

DR. GRANDVEAUD:

It depends on whether you are speaking from a theoretical point of view or from the practical point of view. From a practical point of view, it seemed that choosing an exponential figure and doing some quite good manipulations produced satisfying results. But from the theoretical point of view, I think it is quite different and more complicated.

Page intentionally left blank

Page intentionally left blank

DEVELOPMENT OF AN ATOMIC RUBIDIUM VAPOUR FREQUENCY STANDARD AT NPL OF INDIA USING INDIGENOUS SOURCES

V. R. Singh, G. M. Saxena & B. S. Mathur
Time & Frequency Section
National Physical Laboratory, New Delhi - 110012.
India

ABSTRACT

The National Physical Laboratory (NPL) of India is responsible for disseminating, maintaining and developing standards of time and frequency. One of the major activities of the Time and Frequency Section of NPL is the development of atomic standards, presently a rubidium vapour frequency standard (RVFS) using indigenous sources available in the country. The standard mentioned above, will not, of course, be a novel contribution of the field of Time and Frequency Standards, but will be first of its kind of India. In this paper, design, development and fabrication of a rubidium vapour frequency standard is described with necessary modifications and adaptations made in the conventional design. The availability of the indigenously developed atomic standards will prove to be very useful in space, meteorological and other research and development work going on in the country.

This project has been undertaken in collaboration with the Indian Institute of Technology, Kanpur (India).

INTRODUCTION

As the custodian of physical standards in our country, National Physical Laboratory (NPL) of India took up the time and frequency standardization project in 1956 on the recommendation of the Indian National Committee for the International Radio and Scientific Union (URSI). Standard time and frequency signals from this station were first transmitted on February 4, 1959 under the code identification ATA, and since then it has been of continuous service to its users. During this period of seventeen years, ATA transmission has gone through several phases of development, more specially so during the last few years. The large gap in the International Time service between Turino (Italy) in the west, Tokyo (Japan) in the east and Irkutsk (USSR) in the north gives considerable importance to this station.

The NPL has various Time and Frequency activities and an overall view of such activities is mentioned in this paper along with the description of indigenous development of an atomic rubidium vapour frequency standards (RVFS). The work on RVFS is being done in collaboration with Indian Institute of Technology (IIT), Kanpur. The design, development and fabrication of the RVFS and its electronics along with the necessary modifications and adaptations made in the conventional design is discussed. The availability of such indigenous atomic standards will prove to be very useful in space, meteorological and other research and development work going on in the country.

AN OVERALL VIEW OF THE TIME AND FREQUENCY ACTIVITIES AT NPL

Figure 1 describes in a nut-shell the time and frequency set-up at NPL. This set up is in two establishments, one at the main building of NPL at Hillside Road which has generation and monitoring facilities, and the other at ATA, Greater Kailash which has generation and dissemination facilities. The two are at about 13 Kms crowfly distance (1).

Time Comparison:

Regular intercomparisons are made between the generation facilities of NPL and ATA via high frequency (HF) transmissions, portable standard and a direct line. Other techniques of time and frequency comparison like television pulse synchronization method (4); FM link which is being set up in collaboration with the Research Department of All

India Radio; and Microwave link (in collaboration with Microwave Section of NPL) are also being developed between the two stations. Some of these techniques of time synchronization and frequency comparison will later be extended to other user organizations as well.

Broadcasting:

The standard time and frequency broadcast (3) from ATA transmitting station is now at three carrier frequencies 5 MHz, 10 MHz and 15 MHz and the peak envelope power of each transmission is 8 kw. There has been a three fold increase in transmission hours from 4 hours/day to 12 hours/day and these will soon be made round the clock. The carrier frequencies and the electronically generated timing pulses are now directly from the atomic cesium standard and can claim the same order of accuracy. The new, completely electronic, time processor is ready to be installed at ATA (4). The details of ATA transmissions are given in Table 1. These broadcasts are being done in collaboration with Overseas Communications Service of Ministry of Communications, Government of India.

Updating of Electronics:

Another significant change during the last few years which was long due is the switch over at ATA from tube electronics to integrated circuit electronics, thus achieving not only reliability and ease of operation and maintenance, but also eliminating cumbersome 240 volts battery system needed for continuous uninterrupted operation of ATA time units. The ATA time system is now based only on two 12 volt batteries.

Generation:

The generation facilities at NPL main building consist of a variety of crystal oscillators which include Hewlett-Packard quartz frequency standards model 105B and Essen Ring quartz oscillators. The measured aging rates of these standards is found to be better than 1×10^{-10}/day. At present, we are limited by having only one atomic cesium standard which is kept at ATA. An additional atomic cesium standard and a rubidium standard will, however, soon be added to the list of standard time and frequency generating devices at NPL and ATA.

Monitoring:

So far, monitoring at NPL was done only at HF and the stations tracked are, besides ATA itself, JJY (Japan); RKW and RWM (USSR); WWV and WWVH (USA); etc. The reception of WWV and WWVH is not very regular and depends very much on weather conditions. A considerable accuracy has been achieved in the last few years in monitoring these stations and an epoch time to within a millisecond is easily realized. This improvement was possible due to the use of time interval counters and externally triggered dual trace or dual beam oscilloscopes. There is always an effort to track as many standard time and frequency broadcasts as possible and keep a log of all these stations.

Recently, intensive studies have been initiated at NPL on LF/VLF monitoring with the help of a Tracor LF/VLF receiver model 599k. VLF stations tracked so far are GBR (England) and NWC (Australia). The local frequency standards at NPL were calibrated against GBR and NWC and accuracy of better than 1×10^{-9} was achieved. As a typical example, the HP 105B oscillator as received had an accuracy of 5.43×10^{-9} (a drift of 88 μ sec. over an observation period of 4 1/2 hours). After setting against GBR an accuracy of 5.16×10^{-10} (a drift of 13 μ sec. over an observation period of 7 hours) was achieved. Since then, a continuous check is being kept on the calibration of these standards against GBR and NWC. Different antenna designs are being studied and tried for good LF/VLF reception. With a good antenna, it should be possible to track a number of LF/VLF stations around the globe.

Portable Clock:

As a part of time synchronization program, a portable clock is being developed at NPL to calibrate clocks which are far away from NPL and cannot be either physically brought or otherwise linked to NPL for calibration. A HP quartz frequency standard model 105B will be used as the frequency source of the portable clock.

Interface Logic Unit:

A time link between the atomic cesium clock at ATA and the All India Radio (AIR) 'Time-Pips' has already been established and now the 'Sixth-Pips' of AIR time signal is derived from the atomic cesium clock. A correction for the propagation time delay, of course, has to be made to get

very precise times (3, 5). This work is only a part of the project on achieving a 'time-Coordination' between different time keeping and time using organizations within the country.

Atomic Clock:

The development of atomic clocks using indigenous sources in India has already been started at NPL of India. The work on an indigenous development of a rubidium vapour frequency standard (in collaboration with IIT, Kanpur) is at quite an advanced stage and a laboratory model of rubidium vapour frequency standard is expected to be ready very soon. The development work is described in the next section.

DEVELOPMENT OF RVFS OPTICAL ASSEMBLY

The development of RVFS optical assembly is discussed in the following.

Figure 2 depicts the assembly of various parts and components of the RVFS optical unit on a test bench. This test bench is used for testing various components: rubidium lamp, absorption cell and photo-detector inside RVFS optical unit. The test-bench uses Zeeman pumping principle where the magnetic field and radio frequency field applied to absorption cell are tuned to the proper resonance line.

Detailed discussion of the fabrication of the system is for the hyperfine optical pumping microwave RVFS system.

Principle:

Operation of the rubidium standard is based on a hyperfine transition in rubidium 87 (Rb^{87}) gas. The rubidium vapour and an inert buffer gas (to reduce doppler broadening among other purposes) are contained in a cell illuminated by a beam of filtered light (Figure 2). A photodetector monitors changes, near resonance, in the amount of light absorbed as a function of applied microwave frequencies. The microwave signal is derived by multiplication of the quartz oscillator frequency. A servo-loop is used to connect the detector output and oscillator so that the oscillator is locked to the center of the resonance line.

By an optical pumping technique (15-19), an excess population is built up in one of the Rb^{87} ground-state hyperfine levels within the resonance cell. Population of the F = 2 level is increased at the expense of the F = 1 level. Rb^{87} atoms are optically excited into upper energy states from which they decay quickly into both the F = 2 and the F = 1 levels. Components linking the F = 2 level to the upper energy states are removed by filtering the excitation light. Since the light excites atoms out of the F = 1 level only, while they decay into both, an excess population builds up on the F = 2 level. Because fewer atoms are in the state where they can absorb the light, the optical absorption coefficient is reduced.

Application of microwave energy, corresponding to that which separates the two ground state hyperfine levels F = 2 and F = 1, induces transitions from the F = 2 to F = 1, level so that more light is absorbed. In a typical system arrangement, photodetector output reaches a minimum when the microwave frequency corresponds to the Rb^{87} hyperfine transition frequency of 6.834 GHz.

Resonance frequency is influenced by the buffer gas pressure and to a lesser degree by other effects. For this reason, a RVFS standard must be calibrated against a reference standard, e.g. cesium standard. Once the cell is adjusted sealed, the frequency remains highly stable.

RVFS OPTICAL ASSEMBLY

Optical Unit:

The RB-frequency standard optical unit consists of magnetically shielded region with a Rb^{87} lamp with oscillator, Rb^{85} vapour filter cell and a microwave cavity with Rb^{87} vapour absorption cell placed inside it (Figure 3).

The magnetic shield consists of one outer netic and three inner co-netic cylinders. The co-netic cylinders are used as inner shield because of its high attenuation characteristics. Outer netic cylinder has only medium attenuation, but does not saturate as easily as co-netic. Listing from the inner cylinder to the outer, the diameters are 12, 15, 17 and 20 cms respectively and their respective lengths are 33, 35, 37 and 42 cms. The space between the shielding cylinders is filled with the glass wool. This measure avoids conductive cooling and vibration. The ends of the

shielding cylinders are covered with caps of the same shielding material. The only openings in the outer magnetic shield are those for the wires of the necessary supply and control voltages and a small hole to provide access to the tuning shaft of the microwave cavity.

Rb^{87} Lamp:

This lamp consists of bulb blown from a Pyrex tubing to a diameter of 1 cm with the wall thickness of 0.1 mm (Figure 4). The bulb is filled with Rb metal and noble gas at 5 torr. The use of the noble gas lowers the striking potential for the lamp. The lamp is excited by a 100 MHz oscillator. The circuit is very simple and stable.

Filter Cell:

Filter cell is a cylinderical bulb filled with Rb^{85} and argon buffer gas at 50 torr. Addition of the buffer gas to the filter cell broadens and shifts the Rb^{85} absorption lines resulting in an improved filtering effect (Figure 5). When Rb^{87} resonance radiation is passed through the Rb^{85} filter cell, the undesired light component 'a' is absorbed by the component A in the filter cell while the component 'b' which is the desired pumping light is transmitted by the filter cell unobstructed and this pumps atoms mostly out of the F = 1 state of RB^{87} (Figure 6).

Microwave Cavity:

This is a brass cylinder with the outer diameter of 6.5 cm and a total tunable length 9.5 cm. The inside walls of the cavity are highly silver coated. On one side of the cavity there is a perforated tuning plunger which could be operated manually with the help of a shaft for tuning the cavity. The cavity is operated in TE 011 mode (Figure 7). The end plate on the other side has two holes. Through the central hole, light from the Rb^{87} absorption cell falls on the silicon photodiode which monitors the light intensity. The output of the silicon photodiode contains the required frequency correction in terms of the phase and the amplitude of 137 Hz modulation and is one input to the amplifier assembly of the electronic circuitry. The other hole in the end plate is used for providing the microwave input at the frequency 6.834 GHz through an Iris or a loop. Inside the cavity rests a RB^{87} absorption cell containing Rb metal with nitrogen buffer gas at 10 torr. The heater winding on the outer walls of the cavity maintains Rb^{87} vapour absorp-

tion cell at the desired temperature. The cavity along with the Rb^{87} absorption cell is placed inside a solenoid which provides the statis magnetic field along the cavity axis. The Q of the cavity has been measured and found to be above 15,000.

Power Supplies:

To run the lamp oscillator, a stabilized regulated power supply is provided. The lamp is run at 200 volts and 40 mA. The temperature of the Rb^{87} vapour absorption cell and Rb^{85} vapour filter cell is maintained through the heaters, powered by stabilized 12 volt, 4 amp. batteries. The temperature is stabilized with the help of a temperature sensor.

RB-lamp, Filtercell and Microwave cavity have been joined together in an orderly form with the help of fiber rings and two brass rods passing through these rings (Figure 8). These rings are tightly fixed inside a solenoid which is covered by magnetic shielding cylinders. The outermost layer of the shield and the panel and semicircular strips on which the unit rests, are of aluminium. The panel is provided with the binding posts for the various connections and wiring. This measure safeguards the unit against acceleration and vibration.

DEVELOPMENT OF ELECTRONICS FOR RVFS

Design and fabrication of electronics for RVFS was carried out as said above at the Advanced Center for Electronics System of the Indian Institute of Technology, Kanpur (7-9). The functional block diagram of the RVFS, as discussed above, is given in Figure 9. RVFS electronics can be functionally discussed into the following separate sub-headings.

Voltage Controlled Crystal Oscillator (VCXO):

The short-term stability specification for RVFS is the same as the short-term stability required of the VCXO. The HP-105A, 5 MHz quartz oscillator selected to function as VCXO in the RVFS has a stability of 1×10^{-11} over one-second averaging period and hence meets the RVFS short-term stability specification. The electronic frequency tuning range of this model is 4×10^{-8} for an input control voltage of -5 to +5 V. Coarse screw driver adjustment up to a range of 1×10^{-6} is provided on the front panel. The

harmonic distortion and the non-harmonic content are quite low. The unit is temperature controlled and features an aging rate better than 5 X 10^{-10} over 24 hours. It can give 1 V r.m.s. into 50 ohms at 5 MHz.

Temperature and Magnetic Field Control:

The RVFS is required to have a very effective magnetic and electrostatic shielding for the absorption cell to be kept in a high Q microwave cavity. The ultimate long-term and short-term stabilities of the RVFS are dependent upon the good optical assembly.

Frequency Multiplication and Synthesis:

The frequency multiplication and synthesis scheme is shown in Figure 10, which is used to generate the microwave frequency to match the Rb^{87} resonance frequency around 6.83468 . . . . GHz. The 1368 harmonic of the 5 MHz VCXO output is mixed with the output of the 5.314 . . . . MHz programmable frequency synthesizer in a harmonic generator-cum-mixer and the resulting side band viz 6834.68 . . . . MHz is selected by having the microwave cavity in the optical unit resonating at this frequency.

The tuning range and discrete step resolution specification for RVFS dictates the resolution and range to be realized from the programmable frequency synthesizer. A tuning range of 5000 X 10^{-10} and a resolution of 3 X 10^{-10} correspond to around 4 KHz and 2 Hz change respectively, at 6.83468 . . . . GHz. This is achieved (8) by designing the programmable frequency synthesizer tunable over 4 KHz is approximately 2 Hz discrete steps around 5.316 . . . . MHz (See Figure 11).

The Rb^{87} resonance line used as the frequency reference is extremely sharp and has a 3 dB bandwidth of about 25 Hz with the peak around 6.83468 . . . . GHz. The 137 Hz phase modulation of the exciting microwave signal around 6.834 . . . . GHz used to scan the peak of the atomic resonance is designed to have an extremely small modulation index resulting in a peak deviation of about 100 Hz at the excitation frequency. The phase modulated multiplier chain (9) for RVFS is given in Figure 12.

The HP VCXO used has an electronic tuning range of 4 X 10^{-8} for an input voltage range of -5V to +5V. This corresponds to 0.2 Hz in 5 MHz and when multiplied to the Rb^{87} response region results in 274 Hz. The feature of sensing the approach of this electronic tuning limit of the VCXO is provided in the Logic section of the RVFS system monitoring circuitry to be described in a later section. When the cumulative VCXO drift approaches this limit in the RVFS system operation, manual screw driver adjustment of the VCXO frequency is to be made until the error voltage delivered to VCXO is close to zero volt.

The 5 MHz tuned buffer amplifiers in Figure 10, act as distribution amplifiers distributing the VCXO output to the various RVFS subsystems. The 5 MHz output serving as the RVFS output is rectified and given to a panel meter to enable checking the RVFS output amplitude.

Synchronous Error Detection and Control:

Figure 13 shows the synchronous error detection and control scheme. The 137 Hz, harmonics and the noise appearing at the output of the photodiode in the optical assembly is amplified by a low noise A.C. preamplifier, passed through 274 Hz notch filter and a 137 Hz tuned amplifier and then given to the four quadrant analog multiplier used as a phase detector for synchronous phase detector for synchronous phase detection. The 137 Hz phase modulating signal is the reference for this phase detector. The 137 Hz is generated from a stable 274 Hz RC square wave oscillator by dividing it by 2 using a flip-flop and then filtering out the harmonic from the resulting 137 Hz fundamental thereby insuring that the 137 Hz second harmonic is about 70 dB down the fundamental. The filtered 137 Hz is sent to the 137 Hz phase modulator in the 5 MHz frequency multiplier chain through a continuous phase shifter to enable phase adjustments of the 137 Hz phase modulating signal. The phase shifter is capable of providing -180° to $+180^{o}$ phase shift. The phase detector output is amplified, passed through a precision loop error integrator and then delivered to the VCXO frequency control input for frequency adjustment consistent with the 137 Hz error signal amplitude and phase.

The preamplifier gain is continuously variable from 20 to 5000 in two steps. The overall gain of the 137 Hz error signal channel until it is fed to the phase detector is variable from around 10^2 to about 750 X 10^3 in two steps. The bandwidth of the 137 Hz tuned amplifier is about 6 Hz. The analog multiplier, the following amplifier and the 274 Hz square wave oscillator functions are derived from a single linear MSI chip. The analog multiplier has a variable gain and output zero adjust feature and the unit has excellent immunity against temperature variations. The loop error integrator employes an IC with excellent drift characteristics. A D.C. drift of about 10 mV at the output of the loop integrator results in a VCXO frequency drift of about 4 X 10^{-11}. The loop integrator time constant is normally one minute but provision is made to change it to one second. When the integrator is set to 1 minute time constant, the output should not drift more than 10 mV when the feedback path is initially shorted and the output voltage adjusted to zero, the short removed, and the output voltage is observed after a minute. The integrator designed and built meets this specification. The outputs of the D.C. preamplifier, 137 Hz tuned amplifier and the filtered 137 Hz reference frequency are sent to the RVFS Logic subsystem.

RVFS System Operation Monitor:

The RVFS system operation monitors the signal levels of importance at various stages in the standard and operates two front panel lights which indicate the status of the system (see Figure 13).

The monitor essentially consists of two logic gates, controlling the status of two lights on the front panel, whose output states are determined by the detected 274 Hz signal level from the optical assembly, the synchronously detected 137 Hz error signal level, the VCXO control voltage level and the 4.816 . . . . MHz frequency synthesizer lock indicating signal level. The voltage comparators, before the logic gates inputs, trip when the above signals exceed the preset levels at the comparators inputs. The preset levels correspond to those levels appearing at the normal operation of the system. The comparators have a small hysteresis. the VCXO input is monitored to provide indication on the panel if the VCXO electronic tuning limit is approached.

From the scheme, it is seen that the combined status of the two front panel lights provides indication of the proper functioning of the system and subsystem operation. When the standard is functioning normally, only the light indicating correct operation of the RVFS is 'ON'. To bring the malfunctioning of the standard even for a very small time to the notice of the operator of the standard, this correct operation indication light remains 'OFF' until it is manually reset when once put 'OFF' as a result of a small interruption on its continuous operation.

Regulated DC Power Supplies:

The RVFS derives its power from five well regulated DC power supplies operating on 230 V, 50 Hz mains. These DC power supplies deliver +28V, +15V, -15V, +5V and -5V and have sufficient output current ratings with adjustable current limit feature.

CONCLUSION

An overall view of Time and Frequency activities at NPL of India is given in a nutshell. The design, development and fabrication of rubidium vapour frequency standard along with its electronics, is described using indigenous sources in India. The development work of RVFS is quite at an advanced stage and the model will be ready soon. The skill and experience gained through the development work of RVFS will help taking up of making better frequency standards like cesium, hydrogen, etc.

The availability of the indigenous atomic standards will save a lot of foreign exchange and will help the ongoing research projects in the country and also in taking up new projects depending upon such available facilities.

ACKNOWLEDGEMENTS:

All the members of the Time and Frequency Section of NPL are thankfully acknowledged for their time-to-time help in the work. We are also grateful to the Advanced Center of Electronic Systems, Indian Institute of Technology, Kanpur, for allowing us to include the electronic system developed there, in this paper. Dr. A. R. Verma, Director, NPL is thankfully acknowledged for his kind encouragement in the work.

Mr. Hukam Singh is thanked for his patient typing.

REFERENCES:

1. Mathur, B. S., "Time and Frequency Activities at NPL", Proc. National Seminar on Time and Frequency, New Delhi (India), Nov. 18-20, 1976, pp. 77-86.

2. Ramanamurty, Y. V. and Nakra, D. R., "Omega Monitoring at NPL", see ref. 1, pp. 333-342.

3. Luthra, S. C., Sood, P. C. and Mathur, B. S., "Time and Frequency Broadcast From NPL", ibid ref. 1, pp. 87-95.

4. Banerjee, P., "Recent Development of ATA Time Signal Processing and Monitoring", ibid ref. 1, pp. 100-107.

5. Prabhakaran, S., "A Solid State Interface Logic Unit for Use with NPL Cesium Atomic Standard for Synchronization of Time Signal Pips Broadcast by All India Radio", ibid ref. 1, pp. 110-113.

6. Saxena, G. M. and Mathur, B. S., "Development of Rubidium Optical Assembly at NPL, New Delhi", ibid ref. 1, pp. 469-474.

7. Raju, Bh. A. R. B., et.al., "Design and Fabrication of Electronics for a Rubidium Vapour Frequency Standard", ibid ref. 1, pp. 475-486.

8. Raju, Bh. A. R. B., "A Programmable Frequency Synthesizer for Rubidium Vapour Frequency Standards", ibid ref. 1, pp. 496-506.

9. Trivedi, N. R. and Trivedi, D. K., "Phase Modulated Stable Multiplier Chain for Atomic Frequency Standards", ibid ref. 1, pp. 487-495.

10. Parshad, R. and Singh, V. R., "Observations on the Mechanical Strain in quartz crystals under Electric Field using Strain Gauge Instrumentation and Their Application for Determining the Goodness of Raw Quartz Crystals", Proc. 26th Annual Symp. on Frequency Control, Atlantic City, N. J. (USA), June 6-8, 1972, pp. 104-105.

11. Singh, V. R. and Mathur, B. S., "Development of Further Co-ordinated Facilities at NPL for Accurate Testing and Calibration of Time and Frequency in India", Proc. 17th Indian Standards Convention, Jaipur (India), Nov. 27 - Dec. 3, 1977, (Vol. S-6), pp. B(8) 1-4.

12. Singh, V. R. and Mathur, B. S., "Development of a Semiconductor Agnetic Field Measuring Device for a Rubidium Frequency Standard", paper presented at IETE Symposium on Electronic Devices held at Calcutta (India), Oct. 9-10, 1977.

13. Singh, V. R. and Mathur, B. S., "Problems in RVFS Design and Suggested Improvements", Prec. 21st IETE Technical Convention, New Delhi (India), Dec. 10-11, 1977.

14. Singh, V. R. and Mathur, B. S., "Optimization of the Output of a Rubidium Lamp Used for Frequency Standards", Proc. International Symposium on Instrumentation, Calcutta (India), Jan. 14-17, 1978 (in press).

15. "Fundamentals of Time and Frequency Standards", Application Note 52-1, (Hewlett-Packard, USA), Oct. 1974, pp. 2.4 to 2.5.

16. Gerard, V. B., "Atomic Frequency Standards Using Optical Pumping of Rb^{87} and Cs^{133} in Gas Cells", Brit. J. Appl. Physics, Aug., 1962.

17. Packard, M. E. and Swartz, B. E., "The Optically Pumped RVFS", IRE Trans. on Instrumentation Vol. 1-11, Dec. 1972, pp. 215-223.

18. Tannoudji, C. and Kastler, A., "Optical Pumping", Progress in Optics, Vol. V (1966), pp. 1.8.1.

19. Hellwig, H. W., "Atomic Frequency Standards", Proc. IEEE, 63 (No. 2), Feb. 1975, pp. 212-229.

TABLE 1

TIME & FREQUENCY SIGNAL DATA OF ATA

Call Sign	:	ATA
Location of the Station	:	Greater Mailash, Delhi N 28° 33' 36" E 77° 18' 48"
Type of Service	:	Experimental
Primary Standard	:	Commercial Atomic Cesium Standard. (HP Model 5061A with option 004)
Other Standards	:	"Essen Ring" type quartz crystals, Commercial quartz standards. (HP Model 105B).
Antenna	:	Horizontal Folded Dipole.
Carrier Power	:	8 KW (Peak Envelope Power).
Carrier Frequency	:	5 MHz, 10 MHz and 15 MHz.
Modulation Frequency	:	1 pps and 1000 Hz.
Time Broadcast	:	11 Hours Per Day on Monday to Saturday. (9:00 - 20:00 IST or: 3:30 - 14:30 GMT). 4 Hours Per Day on Second Saturday of the Month and Sundays. (10:00 - 14:00 IST or 4:30 - 8:30 GMT).
Time Scale Adopted	:	UTC
Accuracy of Time Interval	:	$\pm$ 1 X 10^{-10}
Accuracy of Frequency	:	$\pm$ 1 X 10^{-10}

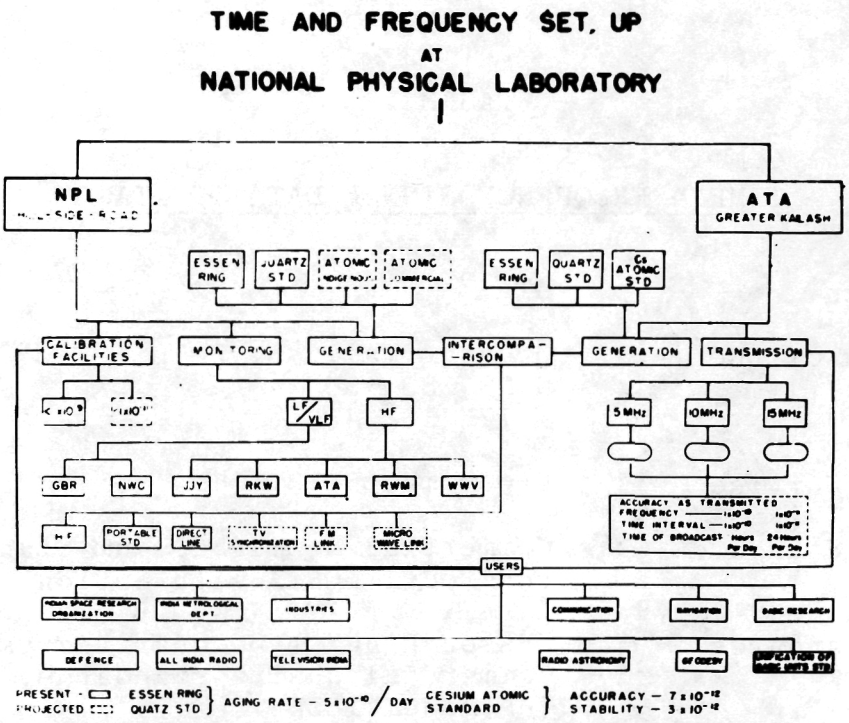


FIGURE 1: Time and Frequency Set Up at NPL of India

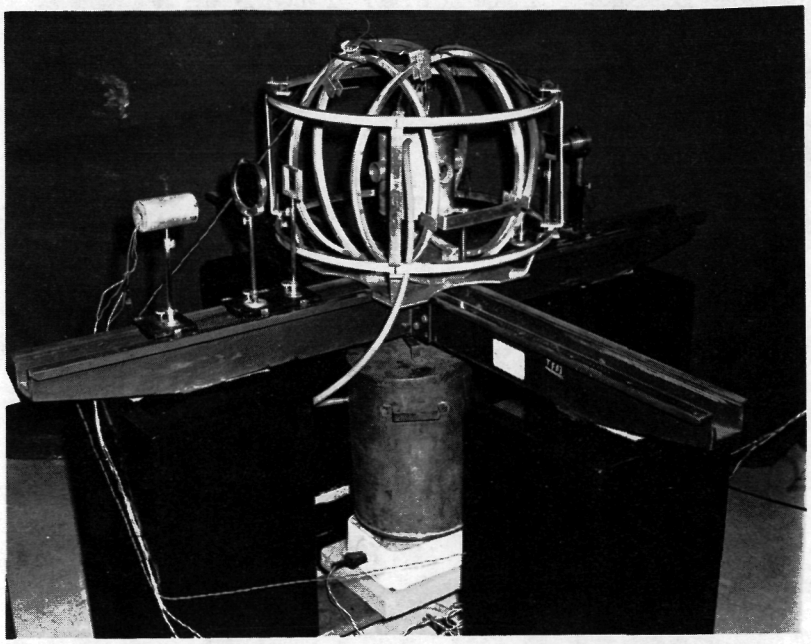


FIGURE 2: Photograph of RVFS Optical Pumping Experimental Set Up

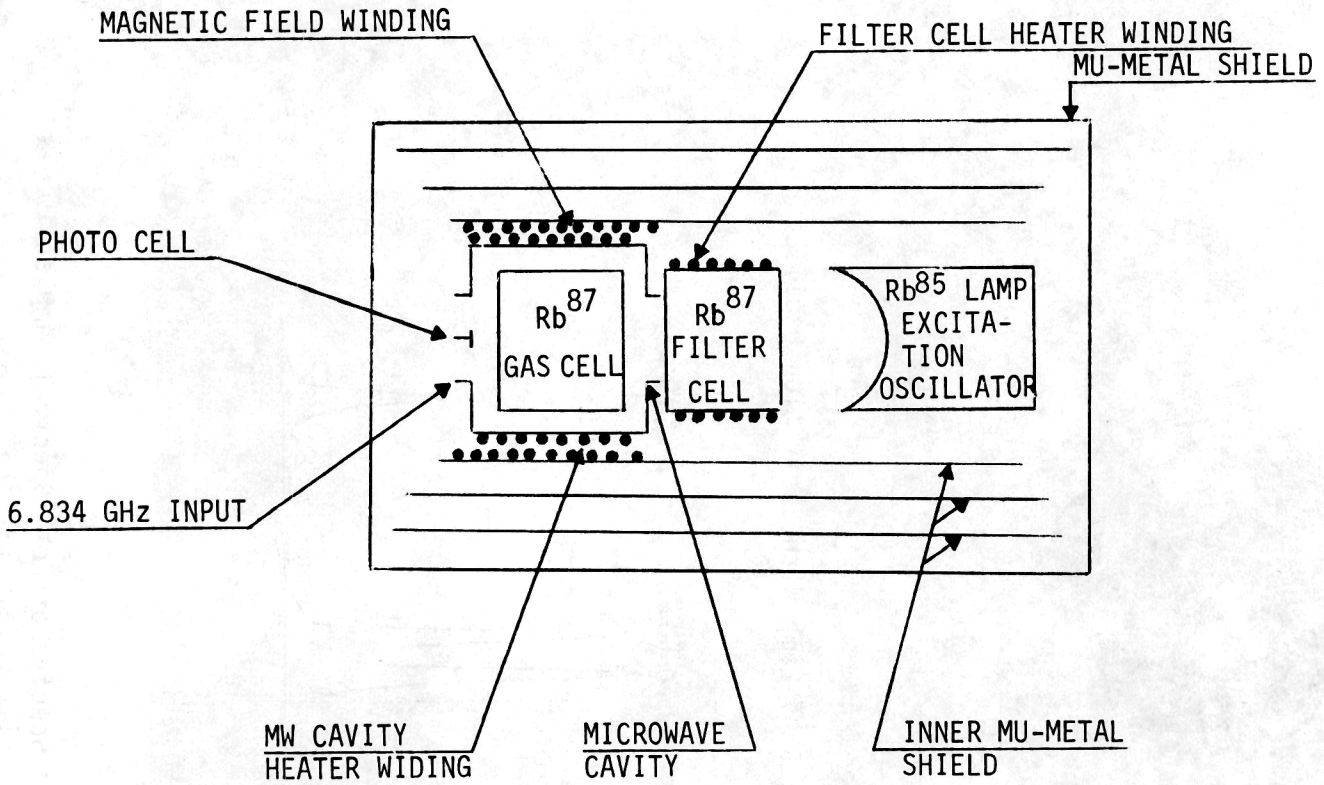


FIGURE 3: Block Diagram of the RVFS Optical Unit

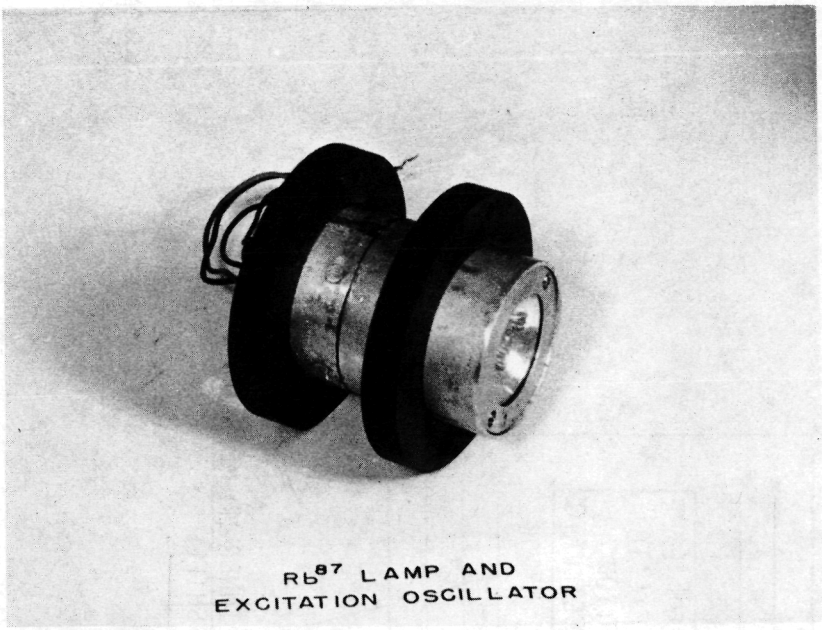


FIGURE 4: Rb^{87} Lamp With Excitation Oscillator

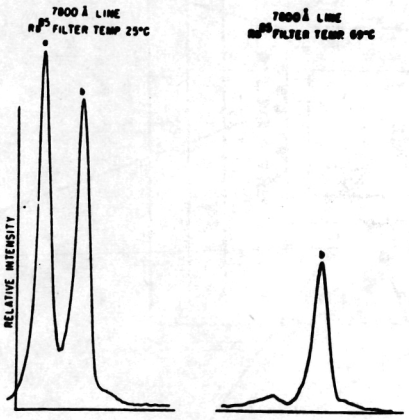


FIGURE 5: Spectra of Rb^{87} Spectral Lamp at Two Rb^{85} Filter Cell Temperatures

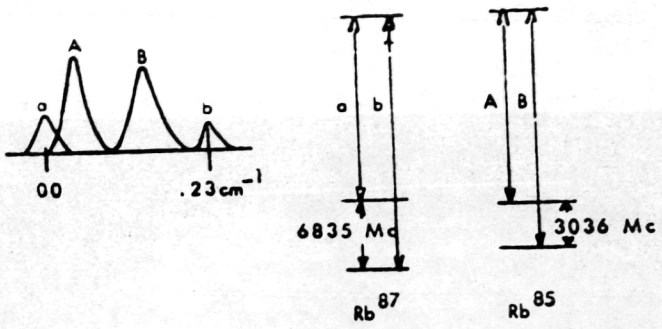


FIGURE 6: Simplified Energy Level Diagram for Rb^{87} and Rb^{85}

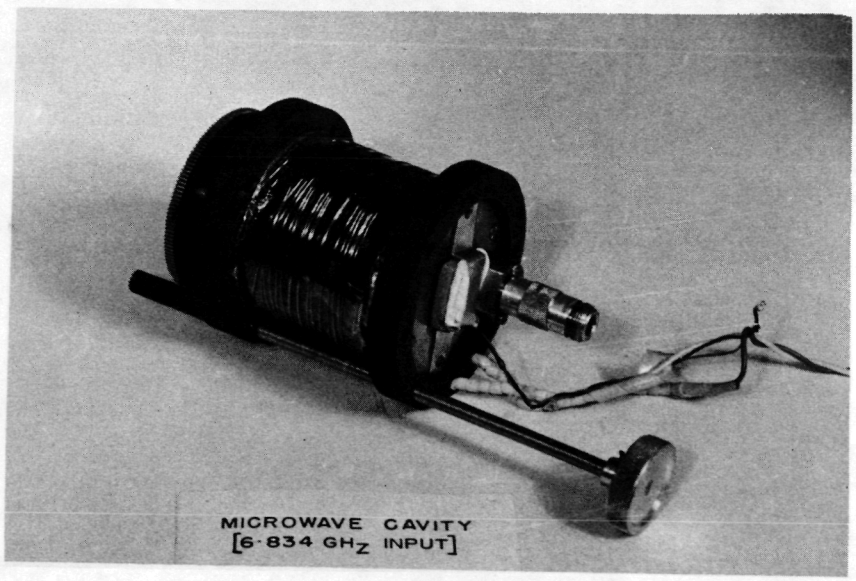


FIGURE 7: Microwave Cavity

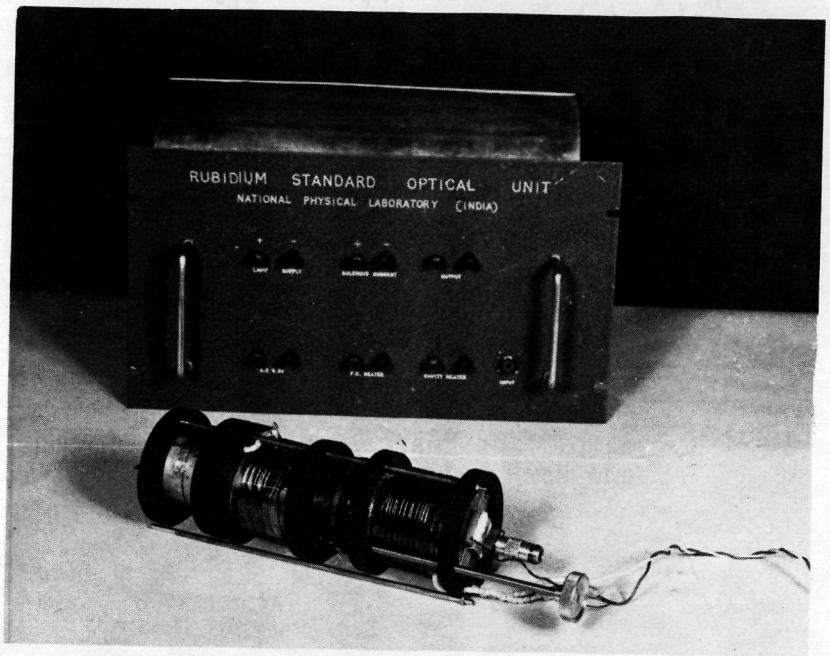


FIGURE 8: Photograph of the RVFS Optical Unit

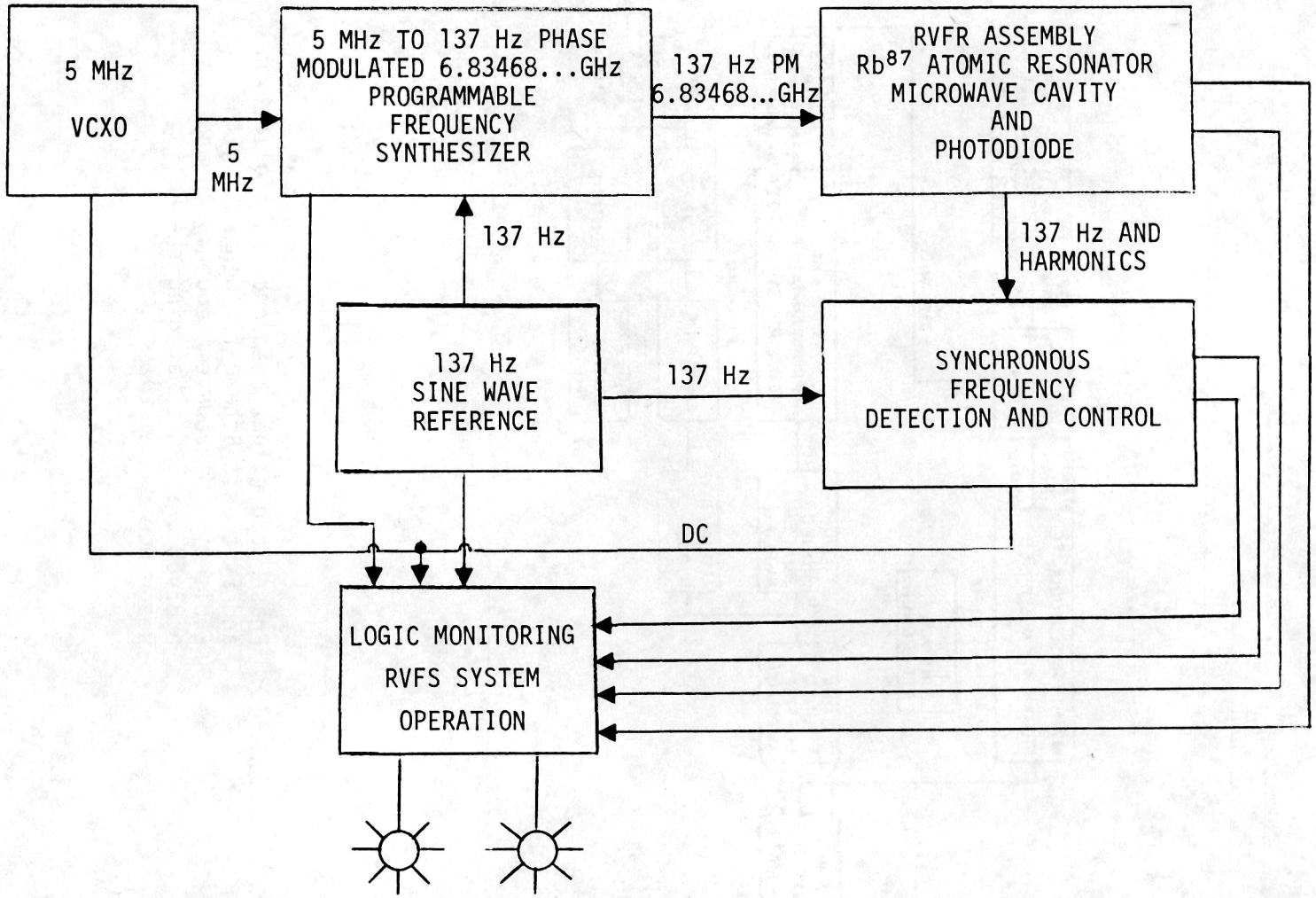


FIGURE 9: RVFS Functional Block Schematic Diagram

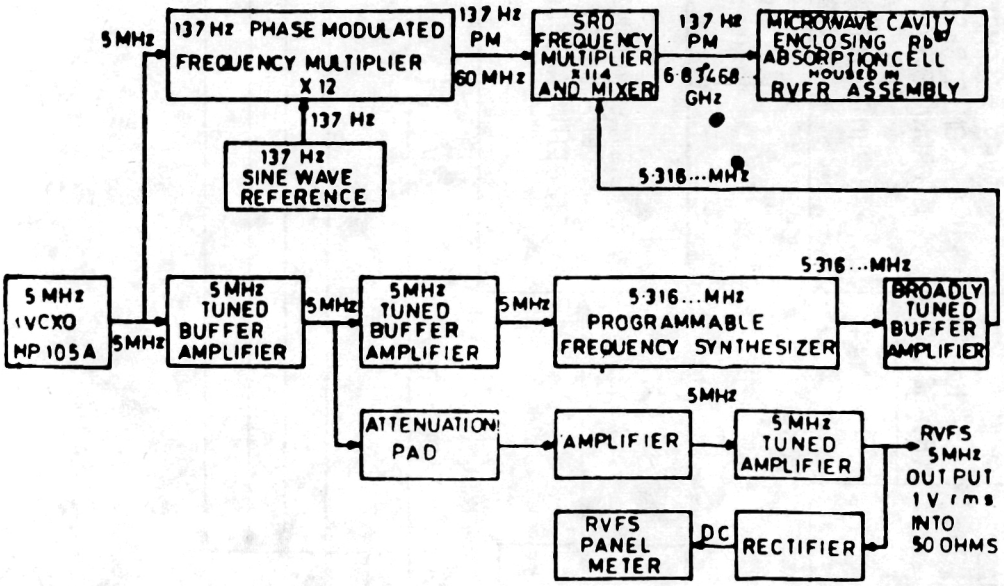


FIGURE 10: Phase Modulation, Frequency Multiplication and Synthesis Scheme for Generating the Excitation Microwave Frequency Around 6.83468 . . . GHz Matching the Rb^{87} Resonance

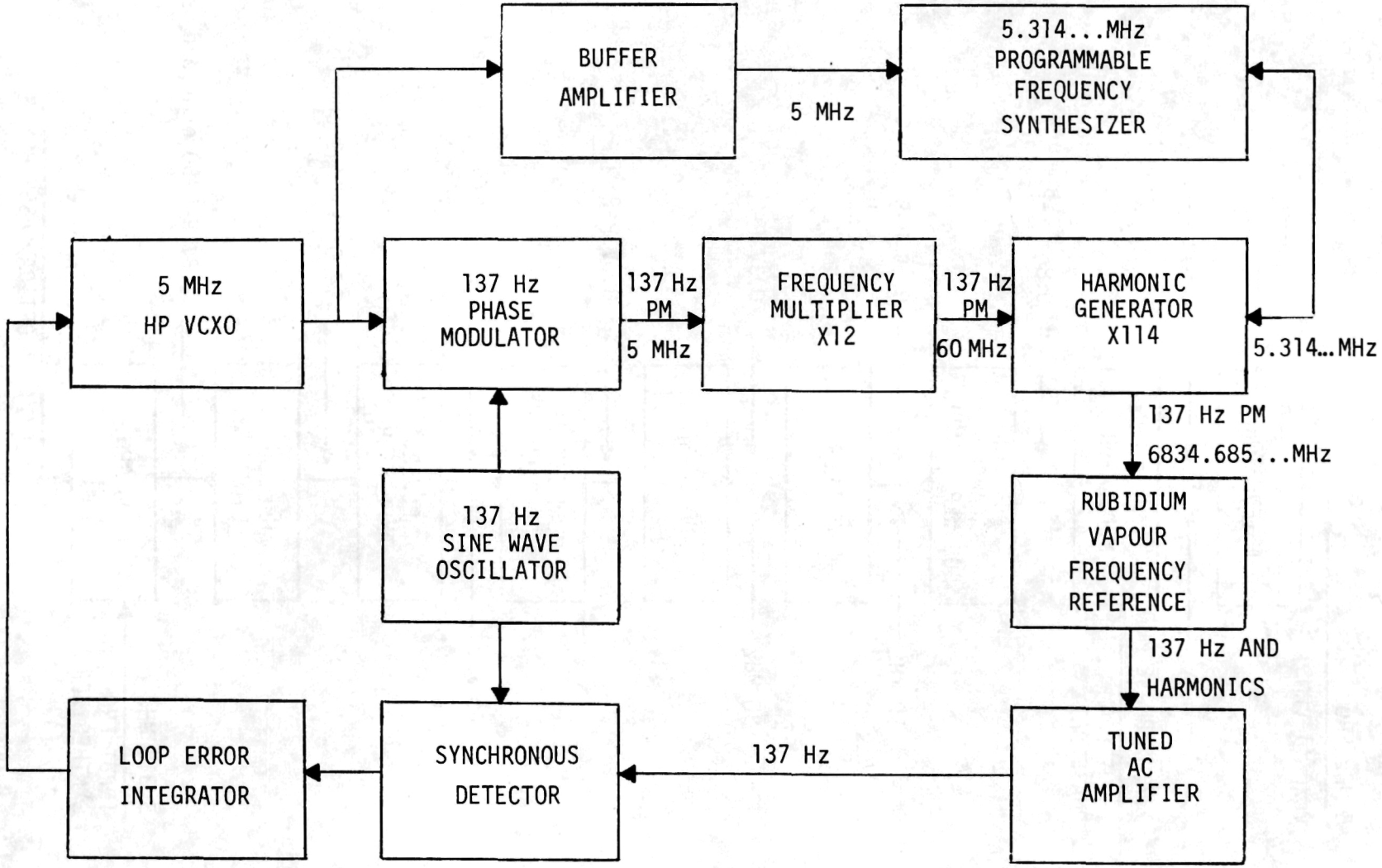


FIGURE 11: Block Schematic of the RVFS With the 5.314 . . . MHz Programmable Frequency Synthesizer

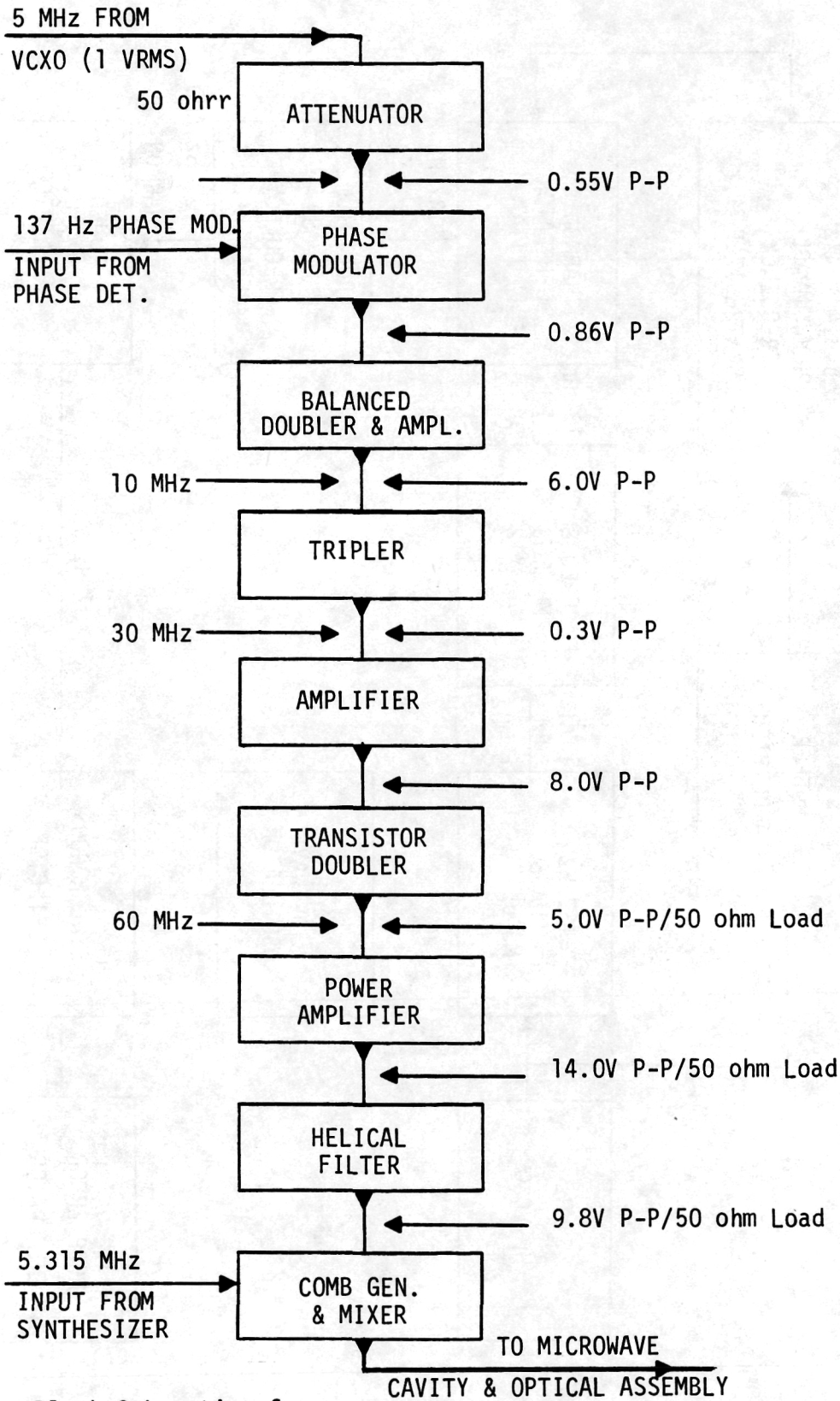


FIGURE 12: Block Schematic of the Phase Modulated Multiplier Chain

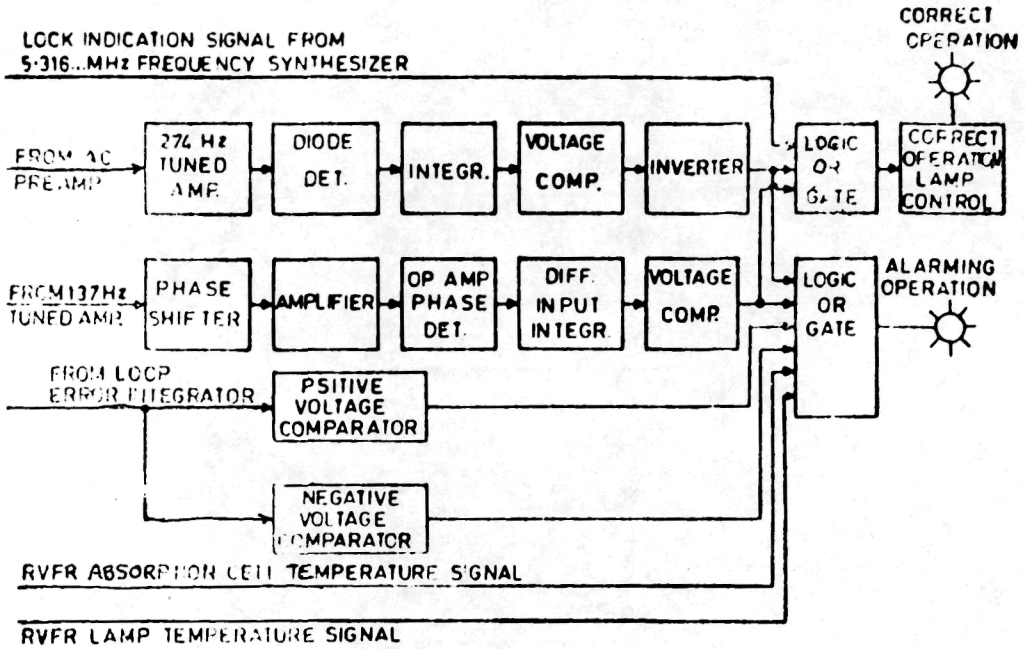


FIGURE 13: RVFS System Operation Monitor

Page intentionally left blank

Page intentionally left blank

PHASE NOISE CHARACTERISTICS OF FREQUENCY SOURCES

A. L. Lance, W. D. Seal, F. G. Mendoza, and N. W. Hudson
TRW Defense and Space Systems, Redondo Beach, California, 90278

ABSTRACT

In order to predict the requirements and specifications for a broad category of systems in today's technology, one must take into account the effects which oscillator instabilities produce in those systems.

The purpose of this presentation is to illustrate data plots of phase noise characteristics of various commercial frequency sources, a laser amplifier, Surface Acoustic Wave (SAW) oscillators, and Gunn oscillators. The phase noise characteristics are plotted in the frequency domain as the Normalized Phase Noise Sideband Power Spectral Density in dBc/Hz, which is called Script $\mathcal{L}(f)$. Two automated measurement systems are described with particular emphasis on practical experience in the measurements and assessed limitations and characteristics of each system.

Measurement data is shown for measurements close to the carrier.

INTRODUCTION

Phase Noise is the term most widely used to describe the characteristic randomness of frequency. Practical oscillators demonstrate noise which appears to be a combination of causally generated signals and random, non-deterministic noises. The random noises include thermal noise, shot noise, noises of undetermined origin (such as flicker noise), and integrals of those noises. The end result is time dependent phase and amplitude fluctuations.

Measurements are performed in the frequency domain using a spectrum analyzer which provides a frequency window following the phase or frequency detector. One system measures the combined phase noise characteristics of two sources. The two source signals are applied in quadrature to a phase sensitive detector (double balanced mixer) and the voltage fluctuations analog to the phase fluctuations are measured at the detector output. One measurement system is designed to measure the phase noise characteristics of a single oscillator. The single-

oscillator measurement system is designed using the delay line as an FM discriminator. Voltage fluctuations analog to frequency fluctuations are measured at the detector output.

The calibration and measurement steps are controlled by a calculator program. The calibration sequence requires several manual operations. The software program controls frequency selection, bandwidth settings, settling time, amplitude ranging, measurements, calculations, graphics, and data plotting.

A quasi-continuous plot of phase noise is obtained by performing measurements at Fourier frequencies separated by the IF bandwidth of the spectrum analyzer used during the measurement. Plots of other defined parameters can be obtained and plotted as desired. Data plots will be used to show the effects of phase lock loops, inadequate isolation of two sources when using the two-oscillator technique, and the limiting frequency range of measurements performed using the delay line as an FM discriminator.

In this presentation the Greek letter nu (ν) represents frequency for carrier-related measures. Modulation-related frequencies are designated (f). If the carrier is considered as dc, the frequencies measured, with respect to the carrier, are referred to as baseband, offset from the carrier, modulation, noise, or Fourier frequencies.

General Theory and Definitions

A representation of fluctuations in the frequency domain is a graph called spectral density. Spectral density is the distribution of variance versus frequency.

The spectral density $S_y(f)$ of the instantaneous fractional frequency fluctuations y(t) is defined as a measure of frequency stability [1].

$S_y(f)$ is the one-sided spectral density of fractional frequency fluctuations on a "per hertz" basis; the dimensionality is Hz^{-1}.

$$S_y(f) = S_{\delta\nu}(f)/\nu_o^2 \qquad [Hz^{-1}] \qquad (1)$$

$S_{\delta\nu}(f)$, in Hz^2/Hz, is the one-sided spectral density of frequency fluctuations $\delta\nu$. It is calculated as $(\delta\nu_{rms}^2/(\text{Bandwidth used in the measurement of } \delta\nu_{rms})$.

The spectral density of phase fluctuations is a frequency domain measure of phase fluctuations defined as follows:

$S_{\delta\phi}(f)$, in rad^2/Hz, is the one-sided spectral distribution of the phase fluctuations on a "per hertz" basis. It is calculated as

$$S_{\delta\phi}(f) = \frac{(\delta\phi_{rms})^2}{\text{Bandwidth used to meas. } \delta\phi_{rms}} \qquad [rad^2/Hz] \quad (2)$$

The phase and fractional frequency fluctuation spectral densities are related by:

$$S_{\delta\phi}(f) = (\nu_o^2/f^2)\, S_y(f) \qquad [rad^2/Hz] \quad (3)$$

A useful measure of frequency stability relates the sideband power associated with phase fluctuations to the carrier power level. The defined measurand is called Script $\mathcal{L}(f)$. $\mathcal{L}(f)$ is defined as the ratio of the power in one sideband, referred to the input carrier frequency, on a per hertz of bandwidth spectral density basis, to the total signal power, at Fourier frequency f from the carrier, per one device[2]. It is a normalized frequency domain measure of phase fluctuation sideband power.

$$\mathcal{L}(f) \equiv \frac{\text{Power Density (one phase modulation sideband)}}{\text{Carrier Power}} \; [Hz^{-1}] \qquad (4)$$

For the condition that the phase fluctuations occuring at rates f and faster are small compared to one radian, a good approximation is [2]

$$S_{\delta\phi}(f)\Big|_{\text{one device}} = (2\ rad^2)\ \mathcal{L}(f) \qquad [rad^2/Hz] \quad (5)$$

If the small angle condition is not met, Bessel function algebra must be used to relate $S_{\delta\phi}(f)$ to $\mathcal{L}(f)$.

Script $\mathcal{L}(f)$ often is expressed in decibels relative to the carrier per hertz (dBc/Hz) which is calculated as

$$\mathcal{L}(f) = 10 \log \left[\frac{S_{\delta\phi}(f)\big|_{\text{one unit}}}{2\ rad^2} \right] \qquad [dBc/Hz] \quad (6)$$

Basic Two-Oscillator Technique

A block diagram of the measurement system employing two oscillators is shown in Figure 1. NBS has performed phase noise measurements using this basic type system since 1967.

The double balanced mixer acts as a phase-sensitive detector so that when two signals are identical in frequency and nominally are in phase quadrature, the mixer output is a small fluctuating voltage δv, centered on approximately zero volts. This small fluctuating voltage represents the phase modulation PM sideband components of the signal.

If the two oscillator signals applied to the mixer of Figure 1 are slightly out of zero beat, a slow sinusoidal voltage with a peak-to-peak voltage of V_{ptp} can be measured at the mixer output. Under the conditions for which Equation (5) is valid, the relationship between mean-square fluctuations of phase $\delta\phi$ and voltage δv interpreted in a spectral density fashion has been shown to be [1]

$$S_{\delta\phi}(f) = S_{\delta v}(f)/2(V_{rms})^2 \qquad [rad^2/Hz] \quad (7)$$

Here, $S_{\delta v}$, in volts squared per hertz, is the spectral density of the voltage fluctuations at the mixer output. Since the spectrum analyzer measures rms voltage in a bandwidth B, the analyzer reading is in units of volts per $\sqrt{\text{Bandwidth}}$. Therefore,

$$S_{\delta v}(f) = [\delta v_{rms}/\sqrt{B}]^2 = \frac{(\delta v_{rms})^2}{B} \qquad [V^2/Hz] \quad (8)$$

where B is the noise power bandwidth used in the measurement.

If it is assumed that the reference oscillator did not contribute any phase noise, the voltage fluctuations $(\delta v)_{rms}$ represents the oscillator under test and the spectral density of the phase fluctuations in terms of the voltage measurements performed with the spectrum analyzer is

$$S_{\delta\phi}(f) = \frac{1}{2}\frac{(\delta v_{rms})^2}{B(V_{rms})^2} \qquad [rad^2/Hz] \quad (9)$$

The measurement system of Figure 1 yields the output noise from both oscillators. If the reference and test oscillators are the same type, a useful approximation is to assume that the measured noise power is twice that which is associated with one noisy oscillator. This

approximation is in error by no more than 3 dB for the noiser oscillator even if one oscillator is the major source of noise. The equation for the spectral density of measured phase fluctuations is

$$S_{\delta\phi}(f)\Big|_{\#1} + S_{\delta\phi}(f)\Big|_{\#2} = \frac{S_{\delta V}(f)\Big|_{\text{two devices}}}{2(V_{rms})^2}$$

$$\doteq 2\, S_{\delta\phi}(f)\Big|_{\text{one device}} \qquad [\text{rad}^2/\text{Hz}] \quad (10)$$

A determination of the noise of each oscillator can be made if one has three oscillators that can be measured in all pair combinations.

Automated Phase Noise Measurement System

The TRW Metrology Automated Phase Noise Measurement System is program controlled by the Hewlett-Packard 9830 Programmable Calculator. Each step of the calibration and measurement sequence is included in the program. The system is used to obtain a direct plot of Script $\mathscr{L}(f)$. The direct measurement of $\mathscr{L}(f)$ is represented by the following equation.

$$\mathscr{L}(f) \text{ in decibels relative to } 1\ \text{Hz}^{-1} = \frac{(\text{Noise Power Level})}{(\text{Carrier Power Level})} \text{ in dB}$$

$$-6\ \text{dB} + 2.5\ \text{dB} - 10\log(B) - 3\ \text{dB} \qquad [\text{dBc/Hz}] \quad (11)$$

The noise power is measured relative to the carrier power level and the remaining terms of the equation represent corrections that must be applied due to the type measurement and the characteristics of the measurement equipment as follows.

- The basic measurement of noise sidebands with the signals in phase quadrature requires the -6 dB correction due to the linear addition of the two phase sidebands at the mixer output [3,4].
- The non-linearity of the spectrum analyzer logarithmic IF amplifier results in compression of the noise peaks which, when average detected, require the +2.5 dB correction for the HP 3571A Tracking Spectrum Analyzer.
- The bandwidth correction is required because the spectrum analyzer measurements of random noise are a function of the particular bandwidth used in the measurement.

- The -3 dB correction is required since this is a measurement of $\mathcal{L}(f)$ using two oscillators, assuming that the oscillators are of a similar type and that the noise contribution is the same for each oscillator. If one oscillator is sufficiently superior to the other, this correction is not used.

The Calibration and Measurement Sequence

1. Automated Measurement of the noise power bandwidth of each IF bandwidth setting on the Tracking Spectrum Analyzer.

2. Obtain a carrier power reference level (referenced to the output of the mixer).

   a) The precision IF step attenuator is set to a high value to prevent overloading the spectrum analyzer.

   b) Normally, we drive the mixer with a 10 to 13 dBm signal from the reference then increase the signal arm input to obtain operation at a 50 ohm output impedance of the mixer (in the range of 1-3 milliwatts). If minimum noise floor is required, then approximately equal power is applied to the inputs of the mixer as required to obtain the 50 ohm output impedance of the mixer in our 50 ohm system. Special techniques are required to obtain the correct impedance when lower impedance is involved.

   c) If the frequency of one of the oscillators can be adjusted, adjust its frequency for an IF output frequency in the range of 10 to 20 kHz.

   d) The resulting IF power level is measured by the spectrum analyzer and the measured value is corrected for the attenuator setting. The correction is necessary since this attenuator will be set to its zero dB indication during the measurements of noise power.

3. Adjust for quadrature of the two signals applied to the mixer. After the carrier power reference has been established, the oscillator under test and the reference oscillator are tuned to the same frequency and the original reference levels that were used during calibration are re-established. The quadrature adjustment depends upon the type of system used. Three possibilities are illustrated in Figure 1.

   a) If the oscillators are very stable, have high resolution tuning, and are not phase-locked, the frequency of one oscillator is adjusted for zero dc voltage output of the mixer as indicated by the sensitive oscilloscope.

b) If the common reference frequency is used, as illustrated in Figure 1, then it is necessary to include a phase shifter in the line between one of the oscillators and the mixer (preferably between the attenuator and mixer). The phase shifter is adjusted to obtain zero dc output of the mixer.

c) If one oscillator is phase-locked using a phase-lock loop, as shown dotted-in on Figure 1, the frequency of the unit under test is adjusted for zero dc output of the mixer as indicated on the oscilloscope.

NOTE: Throughout the measurement process one should check and maintain phase quadrature.

4. Noise power is measured at the selected Fourier frequencies, the calculations are performed, and the data is plotted (or stored) using calculator and program control (fully automated).

5. Measure and plot the system noise floor characteristics if desired.

A plot of the noise floor characteristics is obtained by repeating the measurements with the unit under test disconnected and and the input to the mixer terminated in a matched load.

With the previous indicated offset power level at the mixer input, it is not necessary to change the power level into the mixer. However, if equal power levels are used, then the mixer input level from the reference must be increased to return the mixer output impedance to 50 ohms when the signal is disconnected for a measurement of the noise floor.

Basics of the TRW Metrology Automated System

1. The HP 3330B Synthesizer serves as the local oscillator for the HP 3571A Tracking Spectrum Analyzer. The calculator program controls the switching of the synthesizer to the desired Fourier frequencies.

2. The Fourier frequency increments are chosen to be equal to the selected IF noise bandwidth in order to obtain a continuous spectrum plot.

3. The minimum delay time for a measurement is determined by the IF filter build-up in the spectrum analyzer. The range is from 2.5 seconds for the 3 Hz bandwidth, decreasing to 70 milliseconds for the 10 kHz bandwidth setting.

4. Video smoothing is used in order to obtain a better approximation of the mean. The program can be designed so that a large number of measurements can be taken for better estimation of the mean value. From statistical theory the confidence in an average is improved by the square root of the number of samples.

5. The IF bandwidth settings for the Fourier (offset) frequency range selections are as follows:

IF Bandwidth (Hz)	Fourier Frequency	IF Bandwidth (kHz)	Fourier Frequency (kHz)
3	10 - 400 Hz	1	40 - 100
10	400 Hz - 1 kHz	3	100 - 400
30	1 - 4 kHz	10	400 - 1300
100	4 - 10 kHz		
200	10 - 40 kHz		

Program running time is 27 minutes when using 100 measurements at each Fourier measurement frequency out to 200 Hz.

6. The 60 Hz line frequency interference appears smaller than the actual amplitude if the noise corrections are applied as set forth in the noise measurement program. The corrections for the log amplifier and detection, bandwidth, and equal oscillator contribution should be removed for a plot of discrete frequencies.

7. Amplitude auto-ranging is used in the program to select the most sensitive range that does not result in overload conditions.

The low-pass filter prevents local oscillator leakage power from overloading the spectrum analyzer when baseband measurements are performed at the Fourier (offset) frequencies of interest. Leakage signals will interfere with autoranging and the dynamic range of the spectrum analyzer.

The low-noise, high-gain preamplifier provides additional system sensitivity by amplifying the noise signals to be measured.

Figure 2a illustrates phase-lock characteristics. The generator employs indirect synthesis, whereby, the output frequency is phase-locked to a reference oscillator. Line harmonics were plotted with noise corrections and, therefore, have higher amplitudes than shown.

Figure 2b illustrates a roll-off characteristic near the carrier. This is the effective loop bandwidth of the phase-locking between two similar oscillators which were not adequately isolated from each other. Radio station interference is observed since the measurements were not performed in a screen room.

Figure 3a is a plot of the phase noise of the Hewlett-Packard 5061A Cesium Beam Standard, with the "super tube". Figure 3b is the 5061A with the original tube. The Austron 5 MHz Oscillator (see Fig. 4a) was used as the reference when performing these measurements.

Figure 3c measurements of the Hewlett-Packard 8672A Microwave Synthesizer were performed at 18 GHz. Measurements were performed using two similar units.

Figure 3d is included to illustrate the effects of a phase-lock loop. Two Hewlett-Packard 8640B Signal Generators were measured using a phase-lock loop as illustrated in Figure 1.

Therefore, the oscillator phase noise characteristics are measured only beyond the phase lock-loop.

Figure 4a shows a comparison of measurements performed using the automated Hewlett-Packard 3045 System and the Rockland 512 Fourier Analyzer. The Fourier analyzer measurements were performed from one hertz to 100 kHz.

Figure 4b shows the phase noise characteristics of the Oscilloquartz High Stability Quartz Oscillator.

Figure 4c shows the phase noise characteristics of a frequency stabilized laser amplifier. One phase noise plot was obtained with the laser amplifier on and one plot was obtained when the amplifier was turned off. Two noise floor plots were obtained. One represents the noise floor of the complete system including the laser detector. One noise floor plot was obtained without the laser detector signal.

PHASE NOISE MEASUREMENTS USING DELAY LINE FM DISCRIMINATORS

Frequency fluctuations are measured directly using FM discriminator techniques [5,6,7,8]. One of the important advantages of this type system is that the phase noise characteristics of a single oscillator can be measured without the requirement of a similar or better source as a reference.

The delay line yields a phase shift by the time the signal arrives at the balanced mixer. The phase shift depends upon the instantaneous frequency of the signal. The presence of frequency modulation (FM) on a signal gives rise to differential phase modulation (PM) at the output of the differential delay and its associated (non-delay) reference line. This is the property which allows the delay line to be used as an FM discriminator. In general, the conversion factors are a function of the delay (τ_d) and the Fourier frequency (f), but not the carrier frequency.

The phase variation at the output of the two-channel system represents the same phase variation as if it consists of a noiseless reference signal and another noisy signal which has an equivalent noise at the output of [5]

$$\delta v = a[\text{Cos } 2\pi f(t - \tau_d) - \text{Cos } 2\pi ft] \qquad (12)$$

where, in general, (a) is a function of f. The plot of the spectral density of frequency fluctuations is, therefore, periodic in $2\pi f$ and this will be noted in the data plots as a limitation of the range of valid measurement at Fourier frequencies determined by the time delay of the delay line.

The maximum sensitivity of the transmission line discriminator depends upon the attenuation value of the delay line at the carrier frequency [5,7]. Analysis of the basic delay line system indicates that the length of the delay line is chosen so that the total attenuation is one neper (8.686 dB). This optimum value represented the point where the increase in delay was cancelled due to the increase in attenuation of the delay line, i.e., the basic system was power limited [4,6,7]. In our system this limitation does not occur, since we can maintain the mixer input at the desired operating level and provided that there is adequate source output power. The power input to the delay line can be increased to offset the delay line loss.

Figure 6. illustrates the relative sensitivity (noise floor) of phase noise measurement systems. The delay line system sensitivity differs from the two-oscillator system by $(2\pi f\tau_d)^2$ [5]. The power levels at the mixer were the same for each of these plots.

Discriminator Calibrations

The measurement system is shown in Figure 5. The calculator program performs the same functions as outlined for the measurement system of Figure 1. The automated program is used to measure the IF noise power bandwidths of the spectrum analyzer.

The oscillator under test is connected and the signal levels are established for 50 ohm mixer output impedance, as discussed, for the two oscillator technique. The phase shifter is adjusted to obtain phase quadrature of the input to the mixer (i.e., zero volts dc at the mixer output).

In this system Attenuator No. 4 is used to avoid overloading the spectrum analyzer during calibration. Calibration usually requires replacing the oscillator under test with a signal generator or oscillator that can be frequency modulated.

The power output and operating frequency of the generator must be set to the same precise frequency and amplitude values as the oscillator under test.

The source is modulated to produce a known modulation index (m) and the spectrum anlayzer displays a power reading corresponding to the selected modulation frequency. This power reading is corrected for the dB setting of Attenuator No. 4 and the resulting P(dBm) is used to calculate the discriminator calibration factor.

We use a modulation frequency of 20 kHz and adjust the modulation until the carrier is reduced to the first Bessel null of the carrier as indicated on a spectrum analyzer connected to Coupler No. 1.

The calibration factor is defined as:

$$CF = \Delta\nu_{rms}/V_{rms} \qquad [Hz/V] \qquad (13)$$

Where $\Delta\nu_{rms}$ is the rms frequency deviation of the carrier due to the intentional modulation and V_{rms} is the spectrum analyzer voltage measurement of the modulation sideband.

$$\Delta\nu_{rms} = \Delta\nu_{peak}/\sqrt{2} = m(fm)/\sqrt{2} \qquad [Hz] \qquad (14)$$

The calibration factor of the discriminator is calculated as:

$$CF = m\,(f_m)/\sqrt{2}\,V_{rms} \qquad [Hz/V] \qquad (14)$$

The discriminator calibration factor can now be calculated, since this power in dBm can be converted to the corresponding rms voltage using the following equation.

$$V_{rms} = \sqrt{\frac{10^{P(dBm)/10}}{1000} \times R} \qquad [V] \qquad (15)$$

where R is 50 ohms in this system.

The discriminator calibration factor is calculated as,

$$CF = m \cdot f_m/\sqrt{2}\, V_{rms} = 2.405 \cdot f_m/\sqrt{2}\, V_{rms} \qquad [Hz/V] \qquad (16)$$

since 2.405 is the modulation index (m) for the first Bessel carrier null as used in this technique. The modulation frequency is f_m.

Measurement and Data Plotting

After replacing the modulatable source with the unit under test, Attenuator No. 4 is set to zero dB indication and measurements and data plotting are completely automated.

Each Fourier frequency noise power reading P_n (dBm) is converted to the corresponding rms voltage designated as δv_{1rms}.

$$\delta v_{1rms} = \sqrt{\frac{10^{(P_n(dBm) + 2.5)/10}}{1000} \times R} \qquad [V] \qquad (17)$$

the rms frequency fluctuations are calculated as,

$$\delta\nu_{rms} = \delta\nu_{1rms} \times CF \qquad [Hz] \qquad (18)$$

The spectral density of frequency fluctuations is calculated as,

$$S_{\delta\nu}(f) = (\delta\nu_{rms})^2/B \qquad [Hz^2/Hz] \qquad (19)$$

where B is the measured IF noise power bandwidth of the spectrum analyzer.

The spectral density of phase fluctuations is calculated as,

$$S_{\delta\phi}(f) = S_{\delta\nu}(f)/f^2 \qquad [\text{rad}^2/\text{Hz}] \quad (21)$$

The normalized phase noise sideband power spectral density is calculated as,

$$\mathcal{L}(f) = \frac{S_{\delta\phi}(f)}{2\ \text{rad}^2} \qquad [\text{Hz}^{-1}] \quad (22)$$

Script $\mathcal{L}(f)$, expressed in decibels relative to 1 Hz^{-1}, is plotted in real time in our program.

Noise Floor Measurements

The system noise floor can be plotted by setting Attenuator No. 3 to maximum and repeating the automated measurements. We increase the LO power to obtain essentially the same mixer output impedance which exists when both signals are applied. In systems which require different impedance levels, it is necessary that the total input power (Signal and LO) be adjusted to produce the required mixer output impedance. This will require a method of measuring the mixer output impedance and re-estabilishing the particular value when measuring the noise floor.

Noise floor corrections can be performed as previously set forth.

Figure 7a illustrates measurements performed on a fundamental oscillator at 600 MHz multiplied up to 2.4 GHz. Two different delay lines were used. Note that the first null in the periodic plot, beyond the calibrated area, occurs at 2 MHz for the phase noise plot of the 600 MHz fundamental. Therefore, the line has approximately 500 nanoseconds delay. The null on the plot for the 2.4 GHz output is at 4 MHz and thus indicates that this delay line was shorter (approximately 250 ns) than the one used for the 600 MHz measurements.

Figure 7b is a plot of a cavity stabilized Gunn oscillator with an internal crystal oscillator reference. The phase noise plot shows the improvement in characteristics obtained using this phase-locking technique.

Figure 7c shows measurements from within one hertz of the carrier to 25 kHz as measured using the Hewlett-Packard 5420 Digital Signal Analyzer. The measurements agree closely with the continuous plot that was obtained using the automated Hewlett-Packard 3045 System.

Figure 7d is a plot of the AM and PM noise of a Gunn oscillator. The measurements were performed using the single oscillator delay line system described in the paper. The two Gunn oscillators were offset in frequency (37 - 36.2) = 800 MHz and the measurements were, therefore, performed at 800 MHz. This illustrates that the technique can be extended through the millimeter bands.

Measurement Uncertainty

There are many sources of uncertainties associated with phase noise measurement systems and the techniques used in the measurement process. Minimum uncertainty requires precise calibration of the measurement equipment and proper application of that equipment in the measurement process. Analysis of our specific system follows.

		Unc.(±dB)
1.	Power Level Measurements - (Relative to the unit under test when an additional source is used for calibration of the phase/frequency discriminator).	0.05
2.	Hewlett-Packard 3571 Spectrum Analyzer Attenuator - (Reduced from manufacturer's specifications by special calibration).	Range - 0.03 to 0.12 Linearity - 0.01 to 0.25
3.	Hewlett-Packard 355D Step Attenuator - Used in the calibration of the system.	0.06
4.	Mismatch Uncertainty - (associated with setting CW reference level).	0.15
5.	Uncertainty in ±2.5 dB Log/Det Amp. Correction - (This estimation is based on the ability to verify, with traceability, the calibration of the ±2.5 dB stated correction).	0.20
6.	IF Noise Power Bandwidth - (Based on measurements of actual noise power bandwidth).	0.20
7.	Relative IF Bandwidth Gain - (Relative gain between the different IF bandwidths in 3571A).	0.05
8.	Analyzer Frequency Response, 10 Hz to 13 MHz, Referenced to 250 kHz - (Impractical to calibrate out).	0.25
9.	Phase Discriminator Response - (Two-oscillator technique).	0.20
	Frequency Discriminator Response - (Single-oscillator technique).	0.30
10.	Random Error Due to Randomness of Noise - (Can be reduced to this value by averaging).	0.50

11. Setting Modulation Index of the Calibration Source When Calibrating the FM Delay Line Discriminator.	0.10
12. Noise Floor Contribution - (Can be essentially calculated out).	0.2

The uncertainty that can result when performing measurements using the two-oscillator technique has been discussed and must be taken into account in the overall error analysis.

The following calculations are for minimum and maximum uncertainties in measurement of relative measurements. The data represents these considerations, (1) linear summation of all uncertainties, (2) root-sum-square (RSS) of the errors that are small and independent, plus the linear summation of the mismatch uncertainty and the random errors, and (3) RSS of all uncertainties.

	UNCERTAINTY (±dB)			
	Two-Oscillator Technique		Single-Oscillator Technique	
	Min.	Max.	Min.	Max.
Linear Summation	2.01	2.33	2.11	2.43
RRSS (Systematic) + Mismatch + Random	1.14	1.21	1.17	1.26
RSS - All Uncertainties	.72	.77	.75	.80

ACKNOWLEDGEMENTS

We thank Marlyn Hed, Manager of TRW Metrology, for his support and interest in this work. We appreciate the evaluations, suggestions, and review of our work by, Dale Dryer of TRW, Dr. William Lindsey of the University of Southern California, Dr. J. Robert Ashley of the University of Colorado, Colorado Springs, and Gustaf J. Rast of the U.S. Army Missile Command.

We are very grateful to Dr. Donald Halford of NBS, in Boulder, Colorado for his interest, consultations, and valuable suggestions during the development of the system, review of the final paper, and for suggesting the technique for measuring phase noise of millimeter sources.

We thank Bob Perdriau, Webber McKinney, and Joe Oliverio, of Hewlett-Packard Company, Santa Clara, for the special instructions on the HP 5420 Digital Signal Analyzer.

REFERENCES

1. Barnes, J. A., Chi, A. R., Cutler, L. S., et al., "Characterization of Frequency Stability", NBS Technical Note 394, October 1970.

2. Shoaf, John H., Halford, D., and Risley, A. S., "Frequency Stability Specifications and Measurement", NBS Technical Note 632, January 1973.

3. Hewlett-Packard Application Note 207, "Understanding and Measuring Phase Noise in the Frequency Domain", October 1976.

4. Halford, Donald, Shoaf, John H., and Risley, A. S., "Frequency Domain Specification and Measurement of Signal Stability", Proc. Annual Symposium on Frequency Control, at Cherry Hill, New Jersey, 1973.

5. NBS Notebook, F 10, Pages 19-38, Dr. Donald Halford's notes on "The Delay Line Discriminator", April 1975.

6. Tykulsky, Alexander, "Spectral Measurements of Oscillators", Proc. IEEE, Vol. 54, No. 2, February 1966.

7. Ashley, J. R., Barley, T. A., and Rast, G. J., "The Measurement of Noise in Microwave Transmitters", IEEE Transactions on Microwave Theory and Techniques, Special Issue on Low Noise Technology, April 1977.

8. Lance, A. L., Seal, Wendell D., Mendoza, Frank G., and Hudson, N.W. "Automated Phase Noise Measurements", The Microwave Journal, June 1977.

9. Lance, A. L., Seal, W. D., Mendoza, F. G., and Hudson, N. W., "Automating Phase Noise Measurements in the Frequency Domain", Proceedings of the 31st Annual Frequency Control Symposium, June 1977.

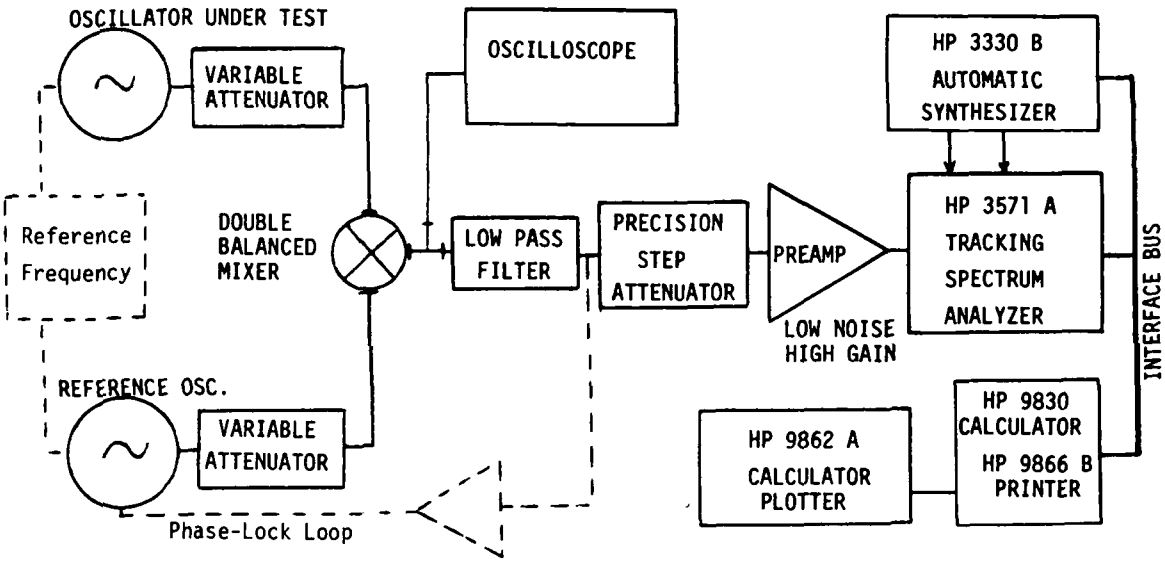
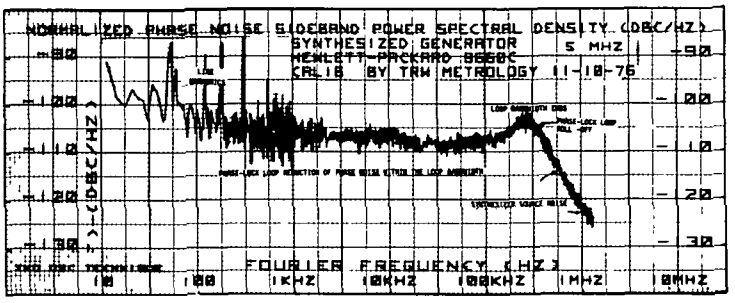
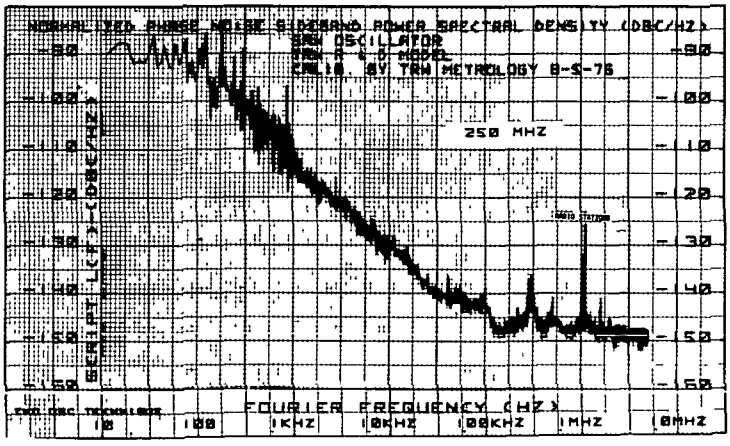


FIGURE 1. PHASE NOISE MEASUREMENT SYSTEM USING THE TWO - OSCILLATOR TECHNIQUE.



(a)



(b)

Figure 2. Phase noise plots. (a) Hewlett-Packard 8660C Synthesized Generator. (b) Surface Acoustic Wave Oscillator.

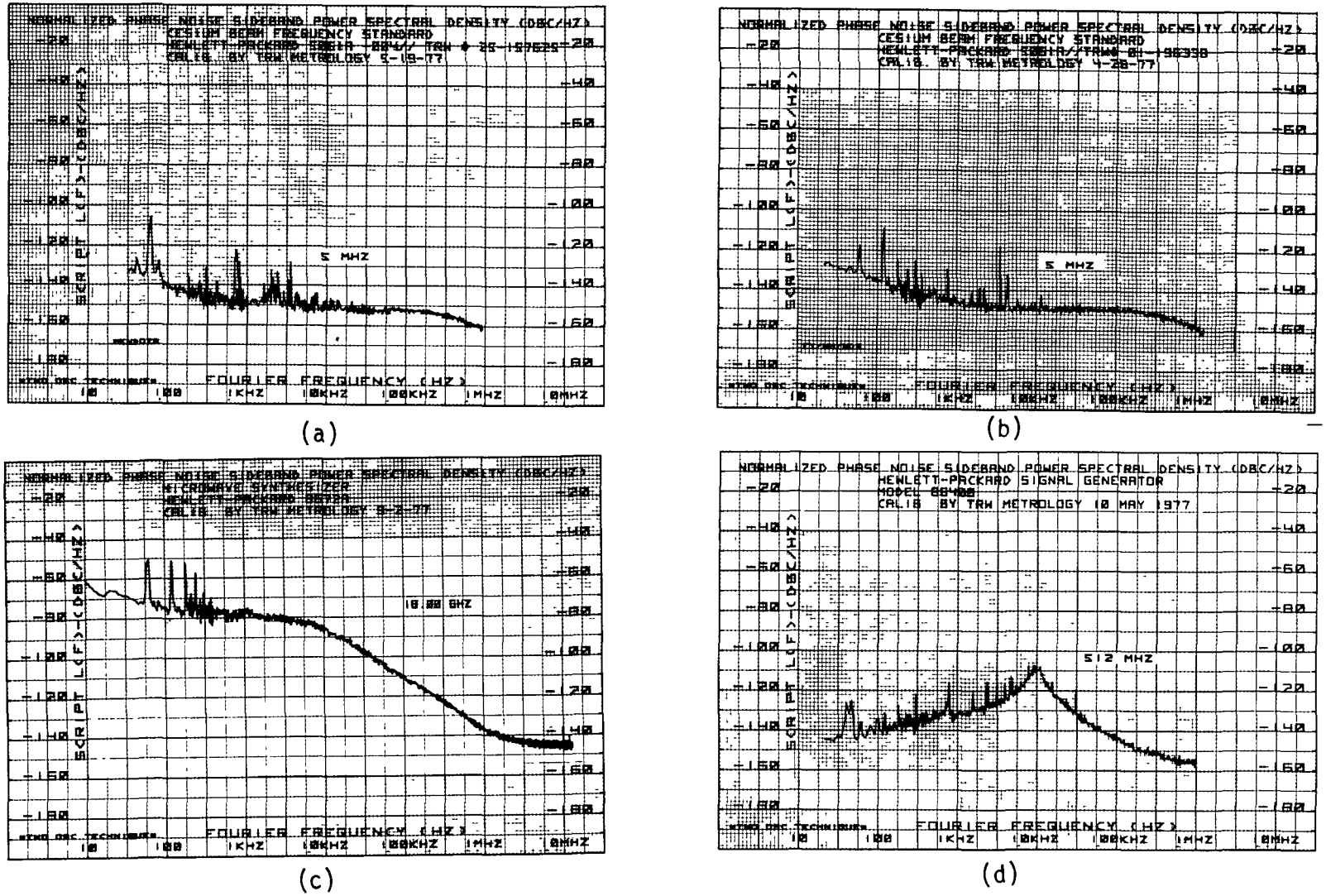
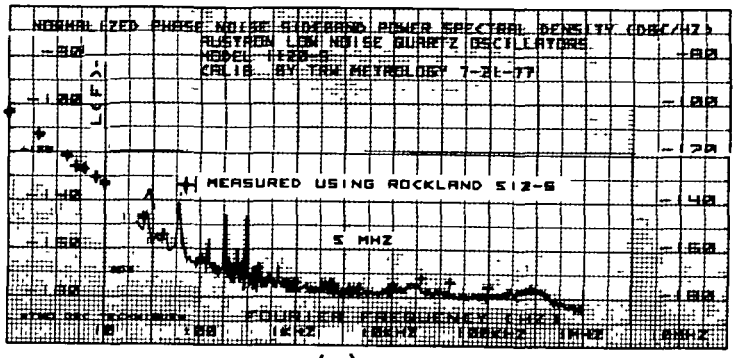
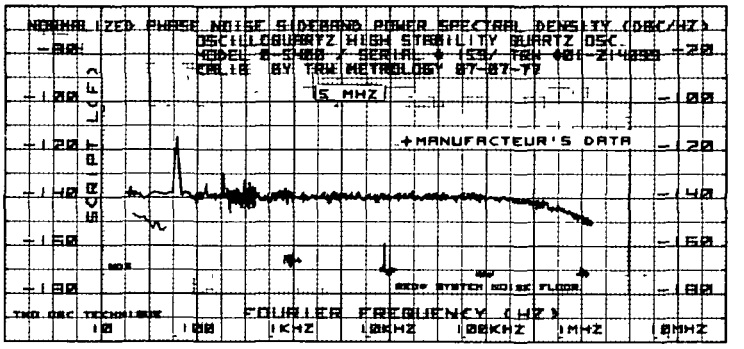


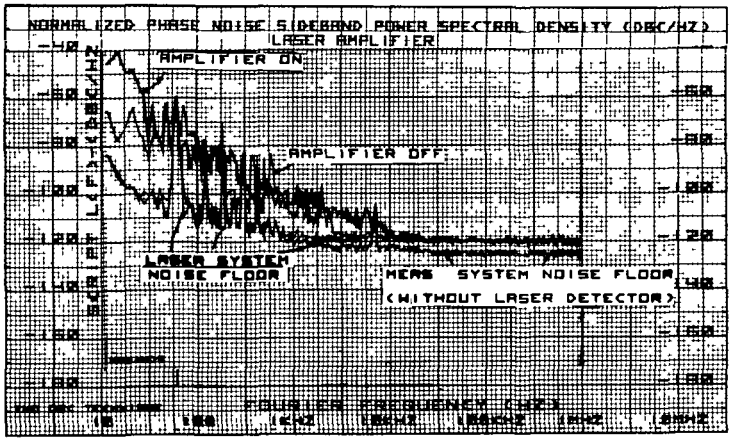
FIGURE 3. Phase noise plots. (a) HP 5061A Cesium Beam Frequency Standard with "Super Tube". (b) HP 5061A (original tube). (c) HP 8672A Synthesizer. (d) HP 8640B Generator.



(a)



(b)



(c)

FIGURE 4. Phase noise plots using the Two-Oscillator technique. (a) Measurements within one hertz of the carrier using the Rockland 512 FFT Analyzer. (b) The Oscilloquartz 3200 High Stability Quartz Oscillator. (c) Laser Amplifier phase noise characteristics.

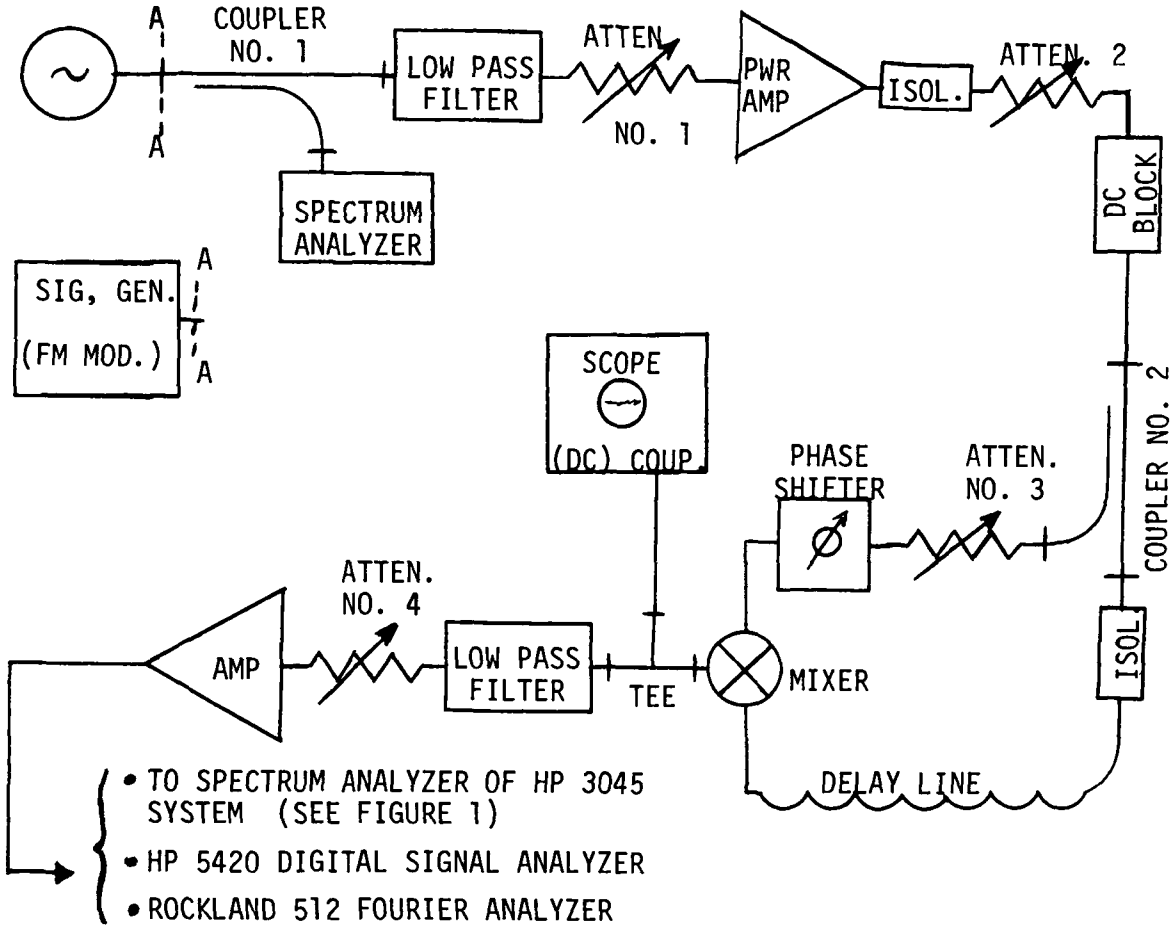


FIGURE 5. SINGLE-OSCILLATOR PHASE NOISE MEASUREMENT SYSTEM USING A DELAY LINE AS AN FM DISCRIMINATOR.

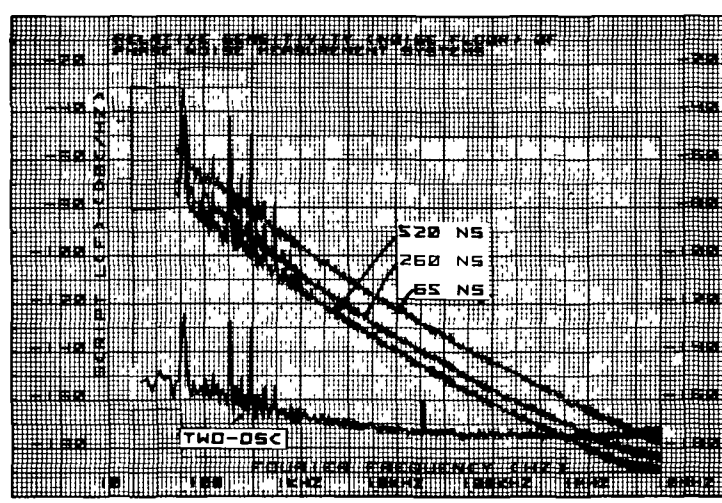
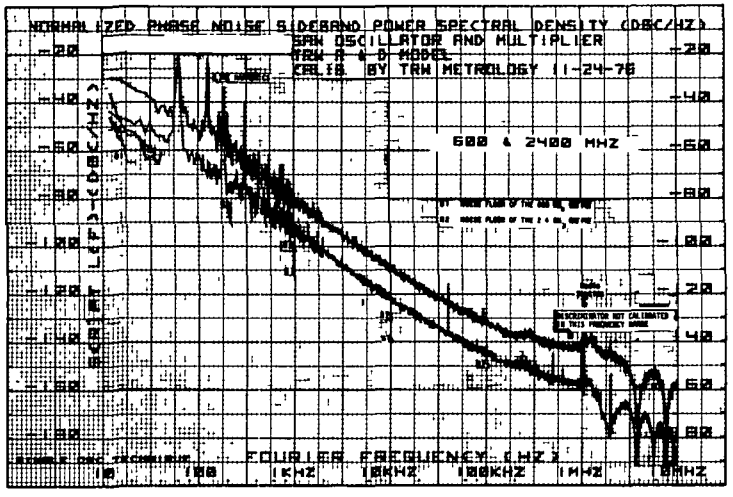
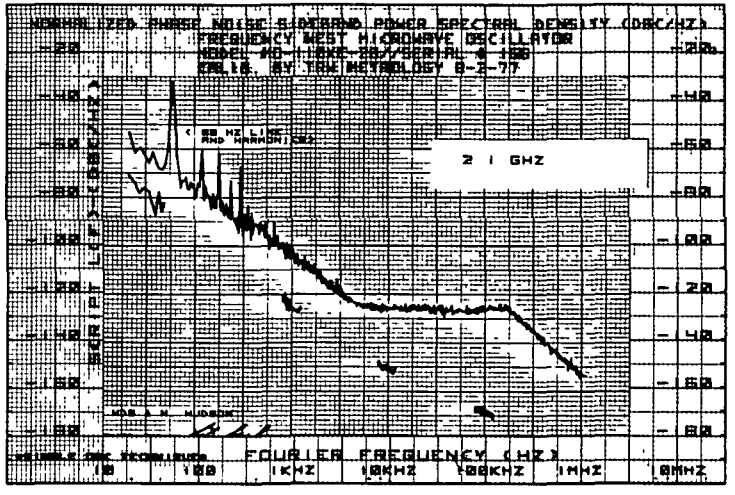


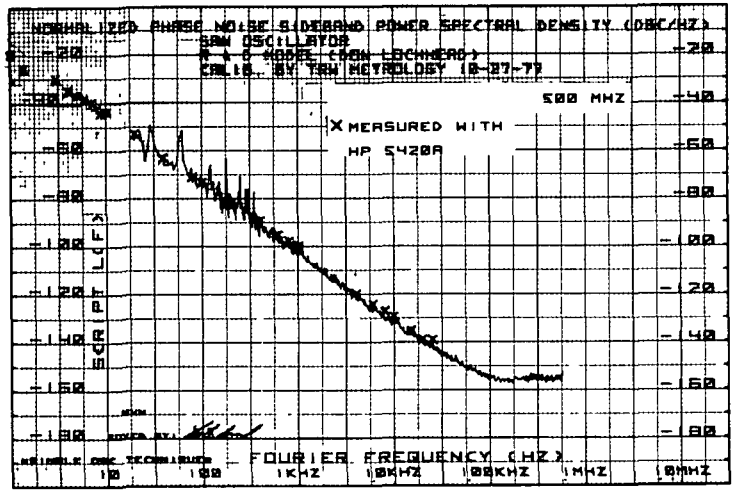
FIGURE 6. Relative sensitivity (noise floor) of phase noise measurement systems.



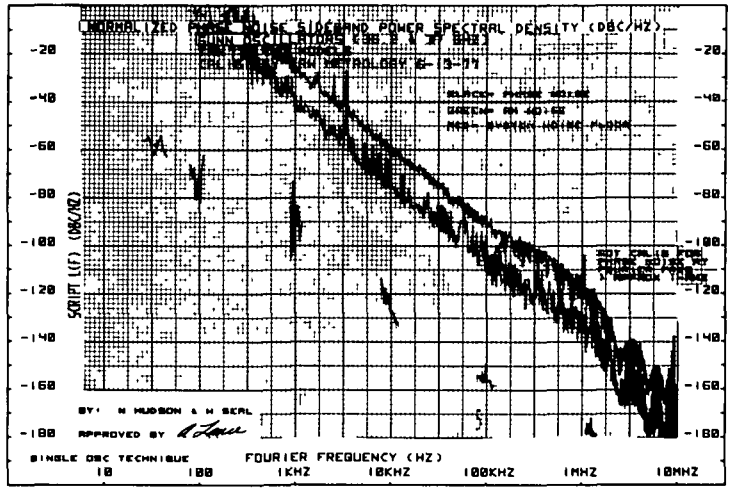
(a)



(b)



(c)



(d)

Figure 7. Phase noise characteristics obtained using the single-oscillator measurement technique.

Page intentionally left blank

Page intentionally left blank

INCREASED RESOLUTION FOR BEAT-PERIOD BASED FREQUENCY STABILITY MEASUREMENTS

By Eric L. Blomberg
Lincoln Laboratory
Massachusetts Institute of Technology
Cambridge, Massachusetts 02139

Much of the work of the founders of this meeting has dealt with the characterization of frequency sources by time domain measurements. Typically the sources are offset to provide a low frequency beat signal, statistics of whose period are collected. While the transformation of these time domain statistics is available to the user in manageable form, the actual beat measurement technique has some unexamined limitations. Let us look at the relation of errors in this measurement to their frequency stability interpretation.

The Relation of Beat Frequency and Timing Errors to Measurement Noise Floor

We wish to express the difference between two consecutive frequency measurements in several forms. First we have:

$$\Delta f = f_1 - f_2,$$

since $f = \frac{1}{t}$:

$$\Delta f = \frac{1}{t_1} - \frac{1}{t_2}$$

if $t = t_1$

and $t_2 = t_1 + \Delta t$ with Δt small

then $\Delta f = \frac{1}{t^2}\,\Delta t$

so $$\frac{\Delta f}{f} = \frac{1}{f} \cdot \frac{1}{t^2}\,\Delta t$$

Where t is the period measurement and Δt is the random error in this measurement. We must remember that our measurements are actually averages over the measurement interval; each quantity must be seen as a time average. Hence t represents the nominal beat period, and Δt represents the timing deviation normalized to a single period.

If the beat and averaging periods are both one second, the distinction is hard to see. If we choose a ten-period average of the one second beat period, and further assume that only system timing errors cause the deviations, then the difference is clear. If our timing error for one measurement is one microsecond, then the normalized error over the ten periods is only .1 microseconds, over 100 periods .01 microseconds. For a fixed beat period, the effect of timing errors goes down proportionately to the number of periods averaged.

Suppose that the beat period is changed to ten seconds and the same timing error applies. In this case the Δt term is not decreased, since only one period is averaged. The increased period, however, has a quadratic effect. The $\frac{\Delta f}{f}$ for the first case is:

$$\frac{\Delta f}{f} = \frac{10^{-6} \div 10 \text{ periods}}{(1 \text{ second})^2} = 10^{-7} \cdot \frac{1}{f}$$

for the second:

$$\frac{\Delta f}{f} = \frac{10^{-6} \div 1 \text{ period}}{(10 \text{ seconds})^2} = 10^{-8} \cdot \frac{1}{f}$$

or in general:

$$\frac{\Delta f}{f} = \frac{\Delta t/N}{\tau^2} \cdot \frac{1}{f}$$

Where τ is the beat period

N is the number of contiguous periods measured

Δt is the uncertainty of each measurement

Hence we find different noise floors for different beat periods and the same averaging time. (Measurement interval)

This would lead us to conclude that a longer beat period would yield better results. Unfortunately, for a sine wave beat signal, increasing the beat period proportionately decreases the slew rate which, in turn, proportionately increases timing error for the standard counter configuration. Hence this is a no win game, unless we desensitize our period measurement to slew rate.

The timing errors fall into two categories: those of much higher frequency than the 1 Hz signals of interest, and those of somewhat lower

frequency. The first corresponds to high frequency noise which can be seen simply as thermal noise at the input of the period measuring counter. The effect of this noise is well known and its effect on low slew rate measurements is often specified in commercial counters. Suppose we have generated a 1 Hz beat signal 10 volts in amplitude. Its slew rate at the zero crossings is about 30 volts/ sec. Hence a voltage excursion of 30 microvolts corresponds to an error in the period measurement of 1 microsecond. One commercial counter cites an uncertainty of 100 μs for such an input. If two 10 MHz sources are being compared, this implies a noise floor of 10^{-12} for the frequency stability measurement (10 periods measured).

The second source of error corresponds to longer term changes in the operating point of the measurement system. A good example is a time varying input offset voltage of a zero crossing detector or Schmitt trigger. This offset may come from the counter input stage, a preceding amplifier or even the balanced mixer. It is often affected by long term changes in the environment of the measurement system. The change in this offset corresponds to a change in trigger point which, as seen in Fig. 1, represents an over or under estimation of the period. If we could somehow track a feature of the waveform's geometry, such as the peak, rather than a level, we could acquire immunity to such long term drifts.

Proposed Circuit

The integrating A/D convertor framework provides three features to achieve this end. It establishes zero-crossings by integration, can cancel DC drifts over intervals longer than one-half the beat period and eliminates the dead-time associated with traditional counter regimes.

Consider the circuit of Fig. 2 with a 1 Hz sine wave input of 10 volts peak to peak. Suppose that the integrator is shorted initially and allowed to operate when the signal level first reaches -.6 volts. When the integrator output returns to zero, it is returned to the shorted condition. If the input is an ideal noiseless sine wave, then the integrator output waveform is symmetric about its peak value, which is analogous to the input's symmetry about its zero crossing. The best estimate of the zero crossing time is a period following the -.6 volt trigger time and equal to one-half the duration of the integrating interval. Clearly there is nothing sacred about the -.6 volt level. It merely provides an arbitrary starting point for the symmetric interval. If the input is corrupted by noise, any components with zero-mean and period less than the integrating interval will tend to be rejected. These are precisely the higher frequency components which cause the gate to flap when a conventional zero crossing detector confronts a low slew rate signal. Notice that this technique always estimates the true zero crossing of the input. If there is a residual DC offset to the input, then the trigger point will be skewed relative to the true mean value of

the input wave shape. Nonetheless this solves one of the difficulties of timing the slow rise time signal, even though it exhibits the same vulnerability to time varying offset as conventional means.

It is possible to perform this operation on both rising and falling edges of the input. Taking the midpoint of these two zero crossing estimates has the effect of rejecting DC offset altogether. It might be viewed as a best estimate of the peak of the sine wave input. Whether it actually corresponds to the peak or not is not significant. What this process does in fact accomplish is to establish the timing of a fixed point on the geometry of the waveform, so that our period measurement is actually a measurement of repetition of geometry rather than of some absolute level. While a varying DC offset certainly affects the zero crossings, it would not affect the timing between two consecutive peaks. This technique is vulnerable to changes in offset level which occur between the two integration intervals, but is able to reject such changes outside them. If we are measuring single periods, this method will reject a linear drift occurring over half the cycle. If we are measuring the length of a ten period sequence, it will reject level changes occurring over 9-1/2 of those periods. Since systematic drifts are most likely to occur over long measurement intervals, we find that this technique is extremely effective in removing them. This is not the case with a simple period counter technique, which counts clock pulses over the ten periods and suffers a trigger error equal to the total DC level change times the slew rate of the input.

We have actually formed a bandpass filter for the 1 Hz signal. Since the 10 volt peak-to-peak signal will slew from -.6 volts to +.6 in about 40 milliseconds, we have a high frequency cutoff of 25 Hz. (Actually a $\frac{\sin x}{x}$ response -3 dB at 12 Hz with a first null at 25 Hz.) This is sufficiently higher than the preceding amplifier's bandwidth that the system noise bandwidth is substantially unaffected. The low frequency response rolls off at 6 dB/octave below one half the beat frequency.

Notice that the information content of the 1 Hz signal is not affected. Its information is an FM modulation. Changes in frequency over 1000 second intervals are present as .001 Hz sidebands of the 1 Hz carrier, not as direct .001 Hz signals. Hence we have prevented systematic offsets from irreversibly mixing with the long-term frequency effects we seek to measure.

Construction Details

It was most desirable to implement a synchronous system to preserve resolution and also to minimize the ill effects of attempting to derive logic triggers from slow analog signals. This is, after all, the fundamental problem for which the proposed processor promises solace. The entire operation is that of a four-state machine, whose states may be

identified from the labels given the corresponding wave forms in Fig. 3. Before describing the sequencer in detail, I would first like to explain the overall means of obtaining a period measurement.

Consistent with my goal of a zero "dead time" system and my goals of simplicity and low cost, an interpolation technique is used. A counter with a 1 kHz clock (my "coarse" register) is used in precisely the traditional way to measure the period between -.6 volt initial trigger points (the point which initiates the entire double integration cycle). Its slow clock rate permits it to be strobed and reset on the fly, so that no period goes unmeasured. This counter is possessed of all the flaws previously described. Another register, the "fine," is controlled by the integrator, and contains, after both integration cycles are done, the timing from the somewhat arbitrary, but nonetheless synchronous, -.6 volt point to the midpoint of the positive half cycle of the wave. As mentioned earlier, this point is referred to the geometry of the waveform and is DC level independent. The best estimate for a given period is found by adjusting the coarse timing by the interpolations before and after it.

$$T = t_{c_n} + t_{f_n} - t_{f_{n-1}}$$

Where t_{c_n} is the contents of the coarse register (its measurement of the nth period) and t_{f_n} is the interpolation time for the end of the coarsely determined n^{th} period to the next cycle's midpoint. Since the output of the system is alternating readouts of t_f and t_c, it is a small matter to arrive at a running readout of actual periods. Let us now consider the operation of the integrator.

State A of Fig. 3 is the primordial state, the pre-interpolation mode. The coarse counter is making its measurement and the integrator is held in an auto-zero mode. This has an advantage over simply shorting the integrator in that it nulls out the integrator's offset voltage as well. Since the integrator never works for more than one-half second after an auto-zero, we can expect that long-term systematic changes in the integrator itself are well below the total system noise floor.

State B is the estimation of the positive zero crossing time. It is entered when the input first exceeds -.6 volt, synchronously with the 1 kHz coarse clock. This prevents a gross 1 millisecond quantization error. At this moment the contents of the coarse counter are strobed into the output latches and the coarse counter is reset to zero, long before its next 1 kHz clock edge. Thus the entry point of State B has an uncertainty range of ± 1 millisecond. At a 30 volt per second slope of the input, this is only a voltage band of ± 30 millivolts about -.6. The absolute time is unimportant as all residues are absorbed into the

interpolation measurement. When the integrator output is driven back to zero, the symmetric interval about the true zero crossing is over. This event is determined by a comparator which senses integrator output. Notice that the comparator is not included in the auto-zero loop. Its trigger point is actually biased .1 volts below zero. This prevents the oscillation which usually accompanies attempted linear operation of a comparator. This also provides a well defined comparator output. It will always be low during auto-zero and during positive integrator output. Thus it goes high only after the integrator has in fact crossed zero at the end of B. Since the integrator is slewing approximately as fast as the input here, there is a delay of 5 milliseconds until the comparator trigger point is reached. The comparator has a window of about 2 millivolts around its nominal trigger point within which noise will cause multiple transitions. Since the 5 millisecond delay is uniform from measurement to measurement and is only affected by changes in the slope of the input, and since the noise at the integrator output is quite small, we lose nothing to take the first comparator transition as the integrator output zero crossing. The net delay is subtracted out in the period determination algorithm and is uniform from period to period.

Thus the comparator causes the system to enter State C, which is almost identical to A. The integrator is auto-zeroed, and the coarse counter is still running, but the duration of State C is being timed in the fine counter.

State D is the exact analogue of State B, only it functions on the falling slope edge of the input. It is triggered by the input signal reaching +.6 volts (with no synchronization required this time). This state defines a time interval symmetric about the zero crossing and passes to State A when this is done, with the same convention on the comparator as State B.

To construct an interpolation interval from the durations of States B, C, and D is a simple matter. Suppose we assign the entry into State B as our time origin. This is also the timing edge of the coarse register, so it is the logical place to begin an interpolation. Clearly the time to the best estimate of the zero crossing (rising edge) is half the duration of State B. Similarly, the time to the best estimate of the zero crossing of the falling edge is the sum of the durations of B and C and half of D. Simple algebra yields a time to the midpoint of the zero crossings and shows that a counter clocked with relative rates of 3:2:1 during B, C, and D respectively will yield this same interval. (See Appendix 1). Specifically, rates of 15, 10, and 5 MHz will allow interpolation to 100 nanoseconds. CMOS clocking rates limited me to one quarter of this resolution. (See Fig. 4)

Thus we see how the interpolation is actually generated for the 1 Hz signal with a measurement of 1 second. Multiple period measurements

required adding a period counter to the trigger of State B. This way an interpolation will be performed initially and on the final period of the number selected, and not for intervening periods.

Preliminary Results

Time permitted only a crude evaluation of this technique, but the outcome shows the technique to be worth investigating further. A 1 Hz test signal was derived from a 5 MHz quartz oscillator locked to a hydrogen maser. It was shaped to approximately sine form with 10 volt peak-to-peak amplitude and some white noise added. Three cases were investigated, the traditional counter, the counter preceded by a high gain limiter, and the circuit of this paper. Only single period measurements were taken. The results are expressed as a fractional frequency referred to 10 MHz and are the root of an Allen variance for 100 trials, and may be compared to results of Allan [1] and Reinhardt [2].

Case 1: $\frac{\Delta f}{f} = 1.4 \times 10^{-11}$

A slew rate of 30 volts/sec applied to an HP 5327B close to the predicted error

Case 2: $\frac{\Delta f}{f} = 3.5 \times 10^{-12}$

The HP 5327B preceded by a gain of 1000 limiter, effectively increasing slew rates to 30,000 volts/sec

Case 3: $\frac{\Delta f}{f} = 6.0 \times 10^{-13}$

Although the proposed circuit clearly does have a lower noise floor, it is hard to say by how much. These results represent a noise floor approximately 5 times higher than Allan and 50 times higher than Reinhardt. Three factors come to mind. We may be nearing the noise level of the test signal itself. Here some further measurements would be useful. Secondly, the clocking rate used in this model yields a minimum relative quantization error of 2×10^{-13}. Thirdly, good low noise circuit techniques, as exemplified in both Allan and Reinhardt, may provide lower noise floors. Nonetheless, the 10^{-12} level is quite respectable for a low cost alternative to a dedicated frequency counter.

Response to Systematic Error

This is a fairly coarse test also, introducing about a 1 volt offset for two out of every ten periods of the 1 Hz 10 volt peak-to-peak input. Care was taken to make the transitions far from zero crossings so as to avoid changing trigger conditions. For a signal with a 20 volt per second slew rate we would expect a 50 millisecond timing error based purely on the zero crossing detector technique. Only the high gain limiter alternative was measured, as it would yield the same data as for the counter alone, but with less noise. Actual values of 42 milliseconds were observed. They occurred symmetrically since the long-term average frequency did not change.

Figure 7 shows some results for a step change representing drift during the integration period. Note that the counter's "dead time" yields only half as much data. It gives three normal periods, followed by a period 42 milliseconds too long, followed by one 42 milliseconds too short, then back to three normal periods. Looking at the processor output, we see seven normal periods, one 20 milliseconds too long, one normal, and finally one 20 milliseconds too short.

Notice how the full error is present in the coarse register and half is compensated by changes in the interpolation register. These and other data show a factor of 25 suppression of DC offsets occurring outside the integration period. Actual performance may be considerably better with the much smaller perturbations one would expect in a practical system.

Note that in Fig. 7, due to the lowered clock rates, the period is determined by:

$$T = t_{c_n} + 2\ (t_{f_n} - t_{f_{n-1}})$$

Conclusion

Even in coarse testing, the circuit has achieved the goals of noise floor reduction, reduced sensitivity to systematic drifts, and no dead time. This level of performance was achieved by a prototype wherein little attention was paid to low-noise techniques. Standard CMOS and BiFET parts were used. No shielding or separation of analog and digital grounds were attempted. The output of the prototype was 7 decades of BCD information from three registers which could have easily been transmitted through the IEEE bus through an appropriate interface. All subsequent calculations and choices of averaging time could be left to the minicomputer or calculator controlling the bus. It is interesting to note that the net cost of this technique is considerably below the counter it outperformed.

Acknowledgement

This work was performed while the author was with the Hydrogen Maser Lab of the Smithsonian Astrophysical Observatory and also represents a portion of a Master's Thesis submitted to the Department of Electrical Engineering and Computer Science at M.I.T. (June 1977). The initial concept of using the A/D converter topology is due to Professor James Roberge of M.I.T.

References

[1] Allan, David W., "Report on NBS Dual Mixer Time Difference System". NBSIR 75-827.

[2] Reinhardt, Victor and Donahoe, Theresa, "A Simple Technique for High Resolution Time Domain Phase Noise Measurement". Proceedings of the 8th Annual PTTI Meeting. NASA, GSF.

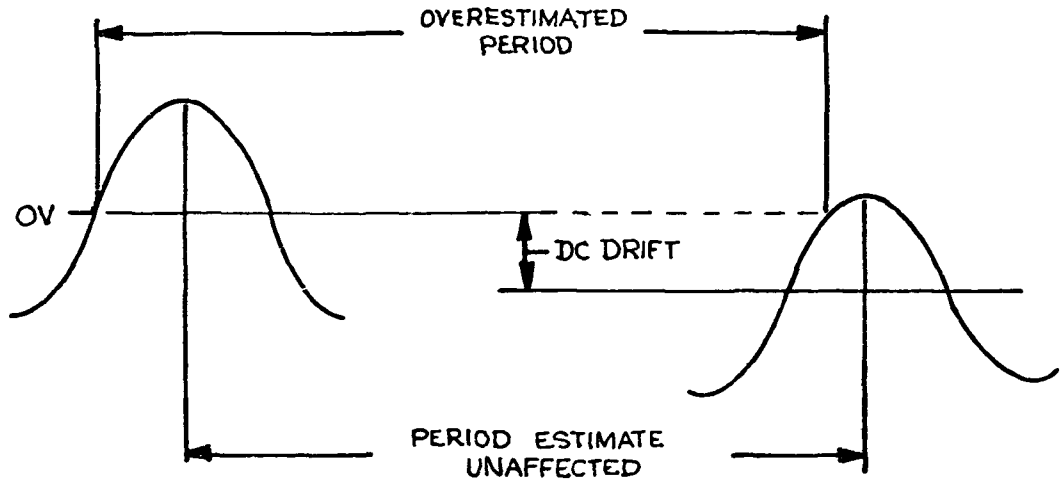


Figure 1. EFFECT OF DC OFFSET

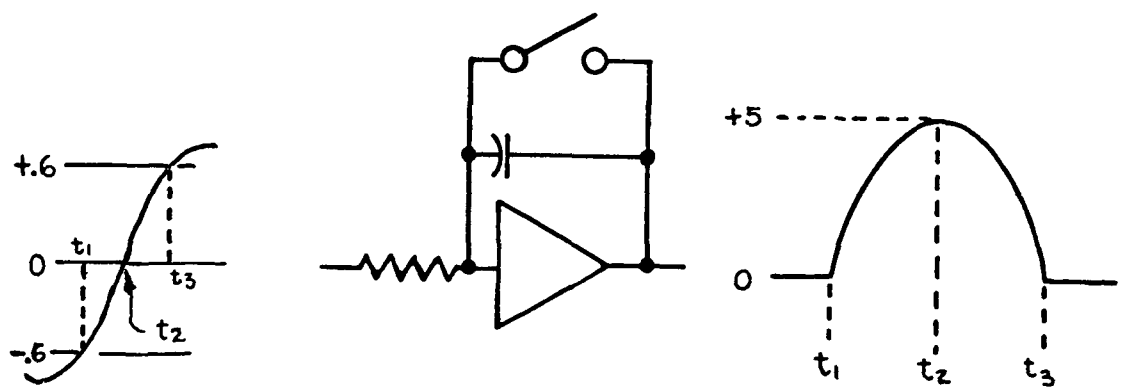


Figure 2. SWITCHED INTEGRATOR

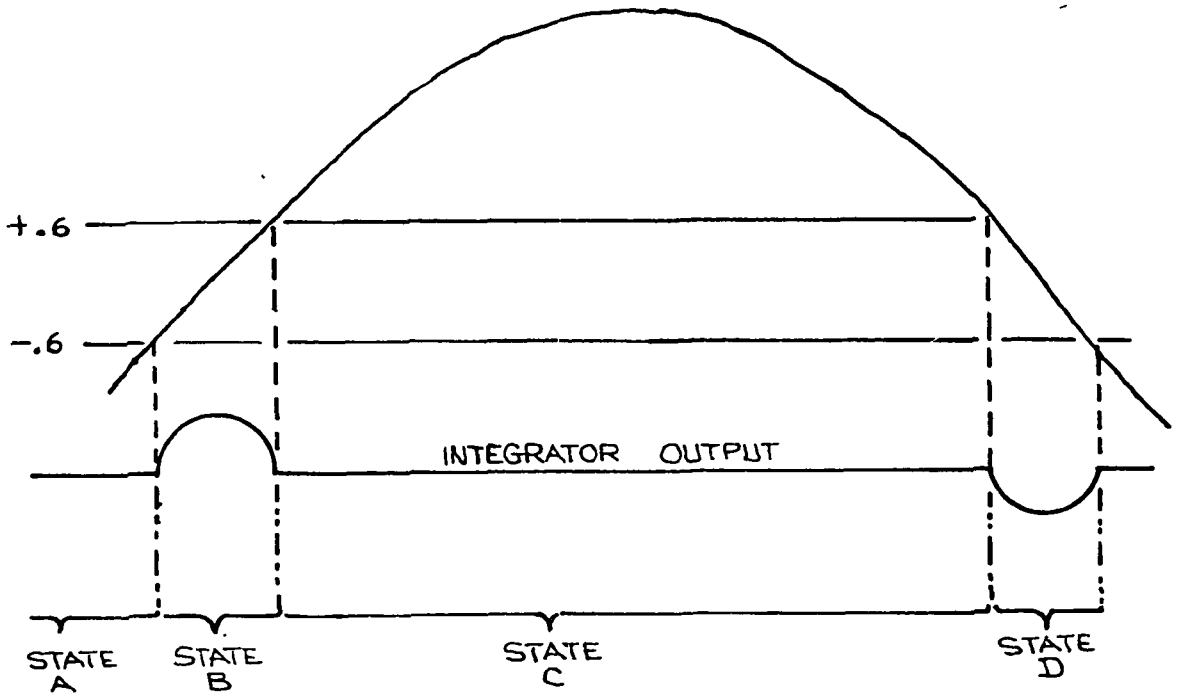


Figure 3. SYSTEM WAVEFORMS

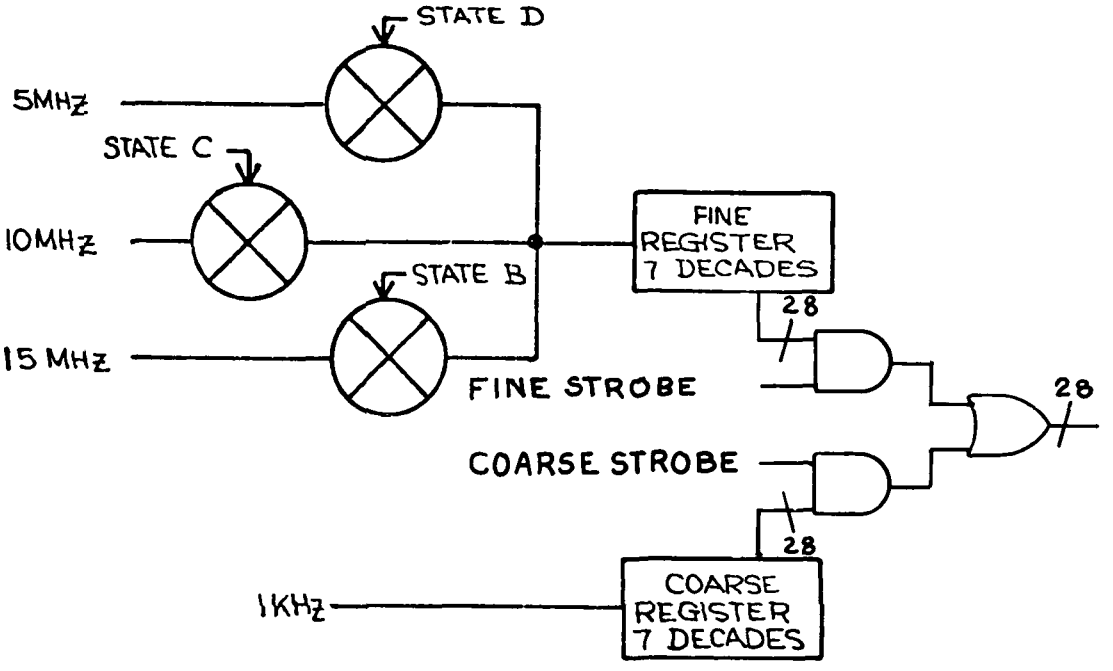


Figure 4. GATING SCHEME

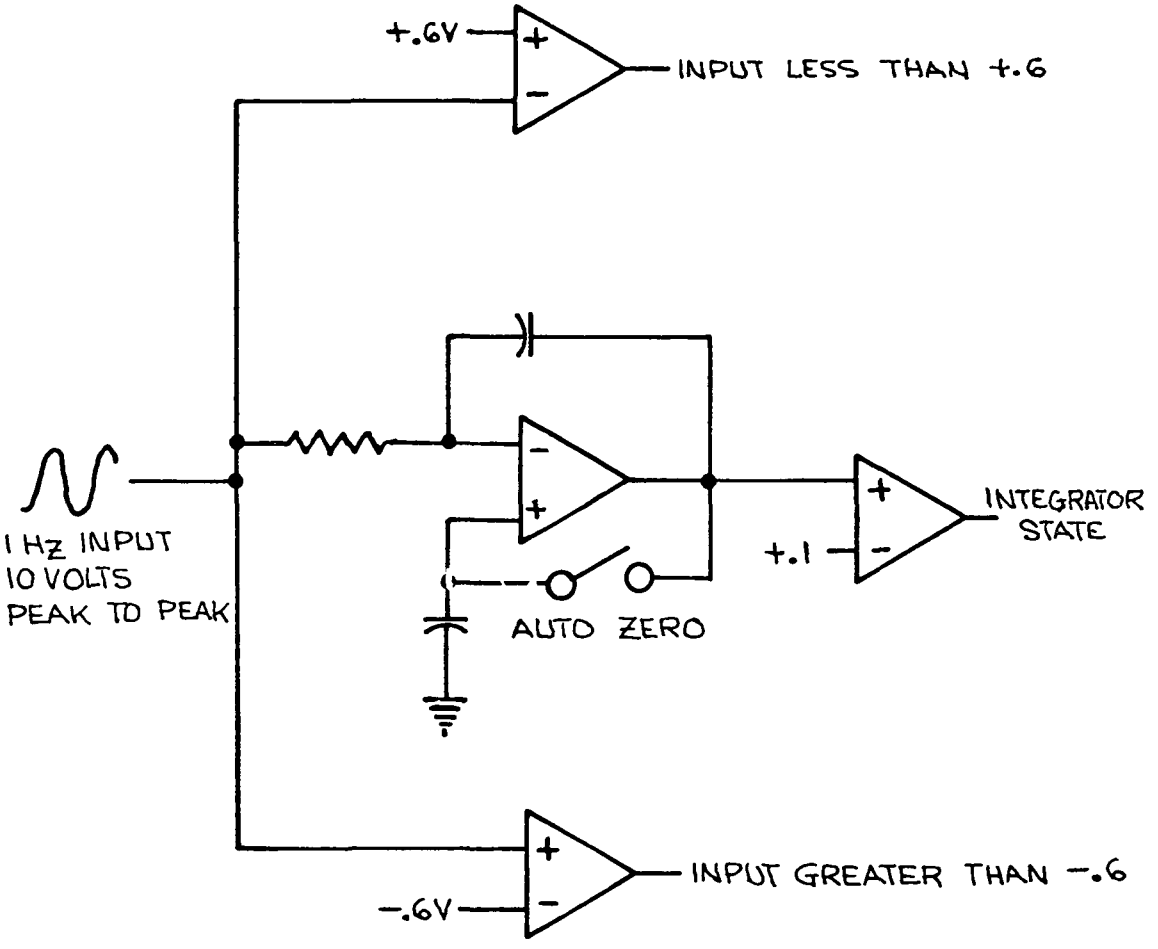


Figure 5. ANALOG SECTION

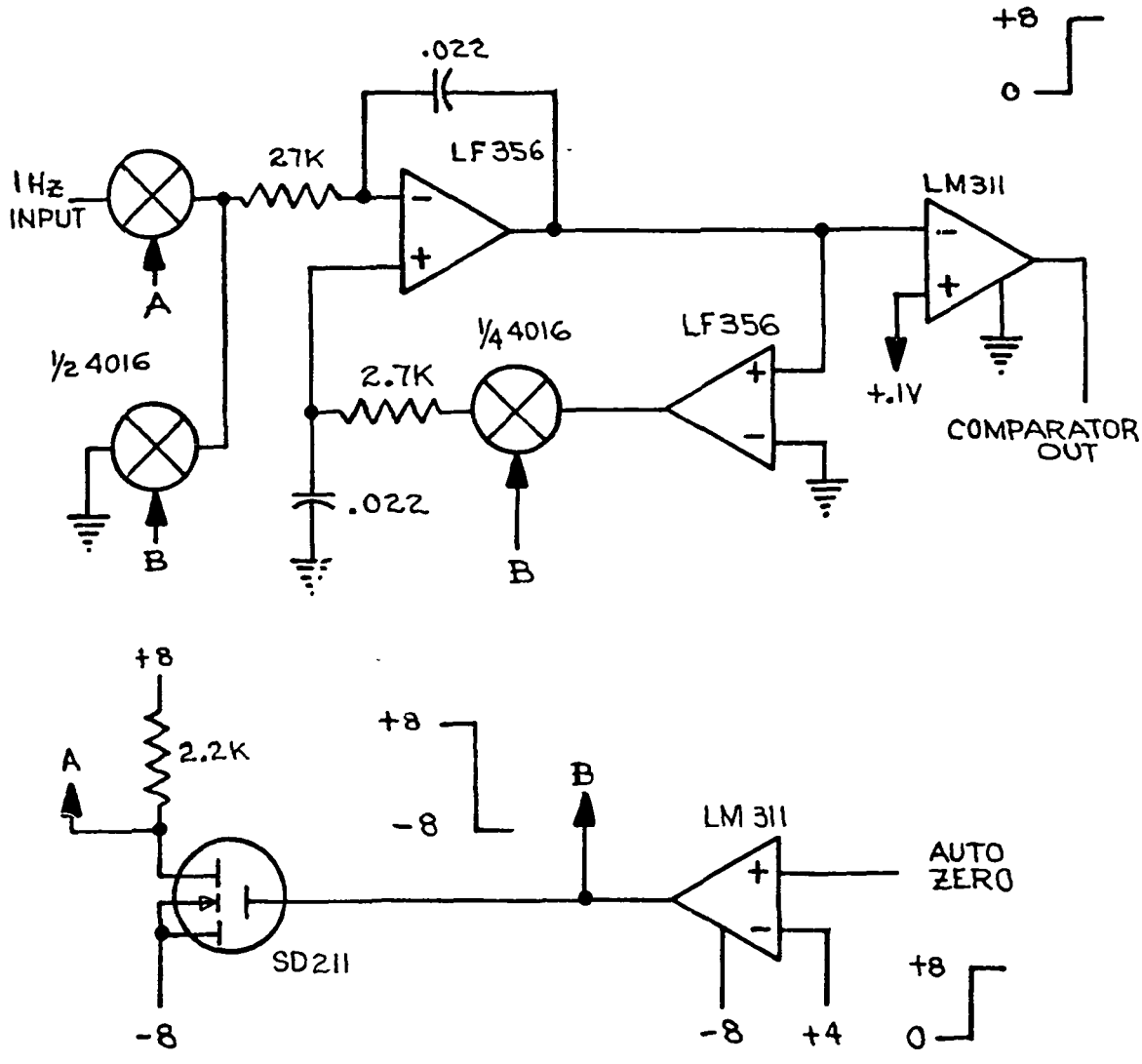


Figure 6. INTEGRATOR SCHEMATIC

COUNTER WITH LIMITER

DATA		Δt from 1.0 second in μs
9999903	T x 10^{-7} sec	-9.7
9578161		-42183.9
10422557		+42255.7
10000136		+13.6
9999904		-9.6
10000134		+13.4
9578080		-42192.0
10422487		42248.7
9999854		-14.6

PROPOSED CIRCUIT (with 1 volt drift during one period)

DATA		T	Δt (μs)
1724543	T_f in 2 x 10^{-7} sec	.9999978	-2.2
001000	T_c in 10^{-3} sec		
1724554		.9999998	-.2
001000			
1724555		.9792412	-20075.8
001040			
1828349		.9999816	-18.4
001000			
1828441		1.0208344	+20834.4
000960			
1724269		.9999426	-57.4
001000			
1724556			

Figure 7. EFFECT OF SYSTEMATIC OFFSETS

APPENDIX: Interpolation Interval

1) let t_o mark the entrance of State B

t_1 mark the entrance of State C

t_2 mark the entrance of State D

t_3 mark the end of State D

Note that the system is synchronized so t_o also marks an epoch of the coarse clock.

2) Since State B runs from t_o to t_1, its mid-point lies at

$$t_+ = 1/2\ (t_o + t_1)$$

This is the best estimate of the time of the positive zero crossing (referred to t_o).

3) Identically State D gives the best estimate of the negative zero crossing

$$t_- = 1/2\ (t_2 + t_3)$$

4) The "peak" is estimated by the mid-point of the two zero crossings

$$t_p = 1/2\ (t_+ + t_-)$$

$$t_p = 1/2\ [1/2\ (t_o + t_1) + 1/2\ (t_2 + t_3)]$$

$$= 1/4\ (t_o + t_1 + t_2 + t_3)$$

$$= 1/4\ (t_1 + t_2 + t_3)$$ Since we set t_o=0 as our reference point.

5) We have, however, measured the durations of B, C, and D and not their absolute timing.

Duration of State B = $t_B = t_1 - t_0 = t_1$

Duration of State C = $t_C = t_2 - t_1$

Duration of State D = $t_D = t_3 - t_2$

Substituting: $t_1 = t_B$

$t_2 = t_B + t_C$

$t_3 = t_B + t_C + t_D$

6) Substituting into the result of 4)

$$t_p = 1/4\ [t_B = (t_B + t_c) + (t_B + t_c + t_d)]$$

$$= 3/4\ t_B + 1/2\ t_C + 1/4\ t_D$$

hence the ease of computation by measuring the state durations with clock rates of 3:2:1.

QUESTIONS AND ANSWERS

DR. VICTOR REINHARDT, NASA Goddard Space Flight Center:

I think it is a very interesting approach, especially the summation of the positive and negative edge. We had some later data from our system--an equivalent dual-mixer system. In short term we did beat you, but we did notice diurnal variations equivalent to 20 picoseconds due to temperature effects. We traced it down to the mixer itself and not any of the components--the DC offsets in the mixer. So if Bob Vessot is going to give us a 10^{-17} oscillator, we certainly need approaches similar to yours to get out the drifts in the measurement system.

DR. BLOMBERG:

Thank you.

MR. HERMAN DAMS, National Research Council, Canada

You mentioned the problem of dead time in the dual balanced mixer system. In the system we built at NRC about three years ago, which was similar to Dave Allan's, we overcame that problem by simply having a counter with a dual front end so that you count continuously. You take your readout, of course, at the end of the one-second period from the front end counter, which at that time has stopped. The other one was still counting.

DR. BLOMBERG:

I mostly brought that up as a practical issue for systems that would be implemented with commercially available counters. I didn't mean to connect this with that effort.

Page intentionally left blank

Page intentionally left blank

TIME TRANSFER EXPERIMENTS FOR DCS DIGITAL NETWORK TIMING AND SYNCHRONIZATION

Peter Alexander
James W. Graham

CNR, Inc.
220 Reservoir Street
Needham, MA 02194

ABSTRACT

In the planned DCS digital network, the ability to coordinate clocks placed at geographically separated nodes will be of critical importance. Aside from the characteristics of the clocks themselves, medium and link equipment parameters play dominant roles in determining performance for the system. The emphasis in this paper is on troposcatter link parameters and their relationship to network clock synchronization. Following an analysis and discussion of the important physical effects in troposcatter propagation, a description is given of experiments and data acquired during a recent measurement program designed to establish a better understanding of the relevant troposcatter and line-of-sight medium and equipment effects.

INTRODUCTION

A digital transmission network can be visualized in its most elementary form as a collection of nodes interconnected by radio links or cascades of links. Bit streams originating from geographically-separated sources enter the node and typically require multiplexing for retransmission to a common destination node. While incoming data signals may be conveniently buffered to smooth out the path length variations, drift between originating node clocks, if unchecked, will eventually result in buffer depletion or overflow.

In the past few years, various methods of avoiding or minimizing these undesirable phenomena have been proposed, including independent highly stable atomic clocks [1], mutual frequency averaging [2], hierarchical master-slave [3] and self-organizing master-slave [4]. More recently, consideration has been given to the use of network facilities for systemwide transfer of a time reference [5], and theoretical models have been used to predict relationships between time transfer accuracy and link parameters. To satisfy normal communication requirements, relative time synchronization of the nodes is sufficient, i.e., the node clocks need not be phased identically as long as their mutual average frequency offsets are zero. On the other hand, transfer of a time reference throughout a network is equivalent to the requirement that node clocks be synchronized with zero phase offset. The utility of such a scheme will not be elaborated on here except to indicate that substantial link and subsystem resynchronization benefits accrue.

The DCS network involves a large number of links and nodes with various categories of transmission media, including line-of-sight microwave (LOS), troposcatter (TROPO), satellite, and cable. The variety of transmission equipment that is available now, or planned as part of the all-digital network, makes a complete and comprehensive evaluation of system performance difficult; therefore, the emphasis in the experimental work reported on here has been toward a separation of propagation and equipment effects. Furthermore, the scope of the effort was limited to measurement of TROPO and LOS links because of equipment and site availability. Of these two classes of transmission medium, troposcatter involves a greater degree of variability in its parameters, making its characterization and measurement substantially more difficult. Accordingly, a more complete treatment has been given in this paper on the subject of time transfer via TROPO links, as compared with the more widely understood LOS application.

TIME TRANSFER PARAMETERS

Before presenting the detailed experimental configuration and results, a brief review of the parameters controlling system time transfer is in order. Consider, in

particular, the transfer of time over a single link, as depicted in Fig. 1. In this example, a troposcatter propagation path is shown but, of course, other transmission media are of direct applicability.

The primary function of the link is the transfer of digital data between the nodes in both directions. At any node, incoming data is clocked into a buffer by clock signals derived from the receiver-demodulator bit tracking loop. This clock signal exhibits fluctuations and drift behavior as a result of transmit clock variations, medium variability, and tracking loop dynamics. In a synchronous network, the received data is later clocked out of the buffer by the node clock and multiplexed or switched with data from other terminated links for retransmission; the primary objective is to coordinate the collection of node clocks so that the buffers do not overflow or deplete. In addition, a timekeeping function for the node clock would involve the desire to meet the above objective with zero phase offset between the node clocks. Time is kept by the clocks at each end of the link in terms of a periodic sequence of time reference pulses (TRP's), which are synchronous with the high rate data clock. If ambiguity issues are ignored in this discussion, it can be simply stated that the time transfer objective is to align the two TRP transmissions. At node B, this is achieved by comparing the arrival time of a pulse transmitted from node A with the locally-generated pulse time, i.e., the node B clock pulse. Time transfer from A to B can then be implemented using this measurement, denoted τ_B, in one of two ways:

(1) Single-ended transfer, where τ_B is viewed as a combination of clock offset, average path/equipment delay, plus a zero mean fluctuating component. That is, if the average delay through the link is known a priori, sufficient averaging of τ_B should yield the clock offset and allow a correction to be made.

(2) Double-ended transfers, where a similar measurement, denoted τ_A, is carried out at node A, and the quantities τ_A and τ_B are exchanged by the two nodes. The difference parameter $\tau_A - \tau_B$, computed at either or both

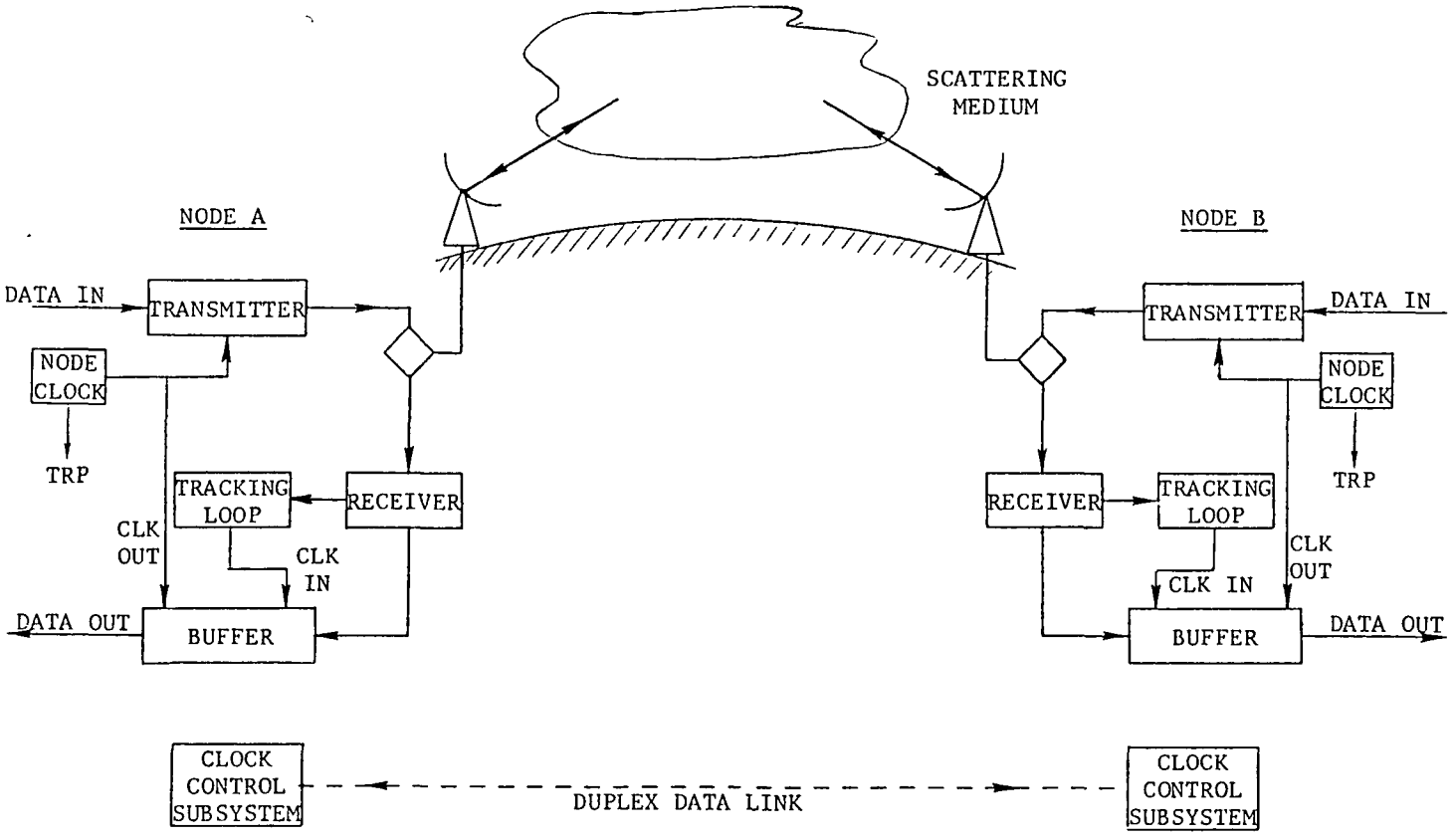


Figure 1 Block Diagram of a Digital Troposcatter Link

ends, is then proportional to the clock offset, provided the transmission time is identical in both directions. To the extent that this is true, $\tau_A - \tau_B$ may be used directly as a clock correction signal.

In both of these situations, the medium and equipment delay variations control the time transfer accuracy. For single-ended systems, variability around a long-term mean, in terms of both magnitude and spectral width, is the essential ingredient. However, the concept of a true known average will be suspect in most operational systems, and the magnitude of residual biases must also be estimated. Double-ended transfer methods depend for their success on similar parameters expressed instead in terms of bidirectional path delay differences; namely, the time structure and magnitude of the difference, along with residual biases which are not accounted for a-priori.

One-way and bidirectional delay parameters have been investigated for TROPO and LOS links at the RADC test facilities during the last year, with measurements carried out over a range of conditions encompassing seasonal, temperature, operating frequency, bit rate, signal level, and diversity angle effects. The temporal behavior of various links has been studied with averaging times ranging from seconds up to 20 minutes, and data records often extending over 3- or 4-day periods.

In the next section, some of the more significant properties of troposcatter links are highlighted. Line-of-sight links need not be described because of their comparatively placid and better-understood properties.

TIME TRANSFER VIA THE TROPOSCATTER MEDIUM

General Troposcatter Link Characteristics

The usual assumptions invoked when deriving theoretical models for troposcatter paths include a linear inhomogeneous weak scattering medium, separating two antennas which are not within line of sight to one another (see Fig. 2). As a result of the weak scattering assumption, a single scattering

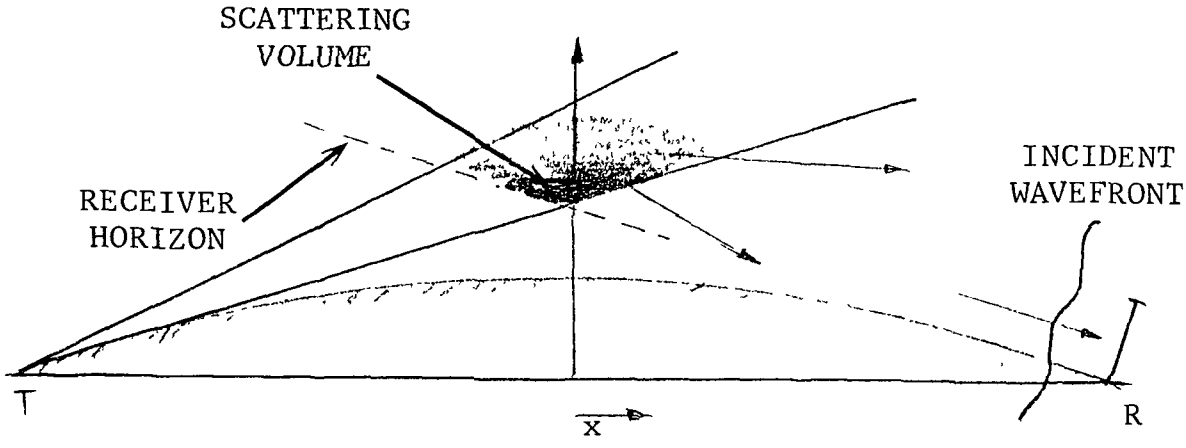


Figure 2 Troposcatter Path Geometry

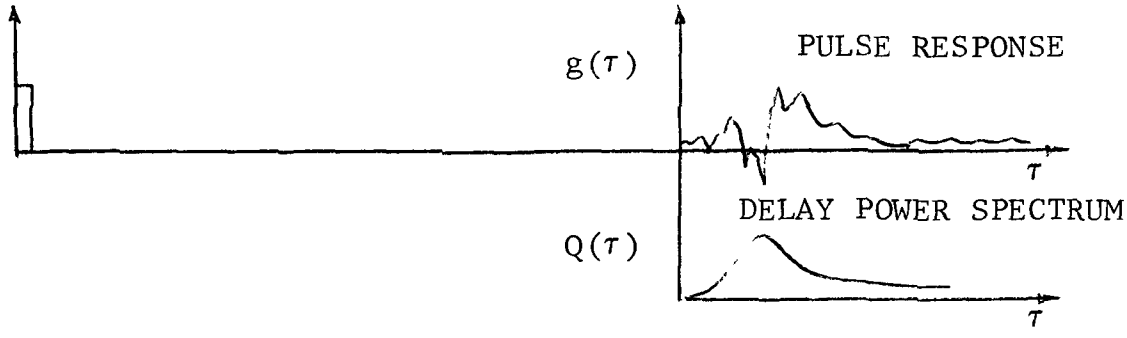


Figure 3 Troposcatter Link Response Characteristics

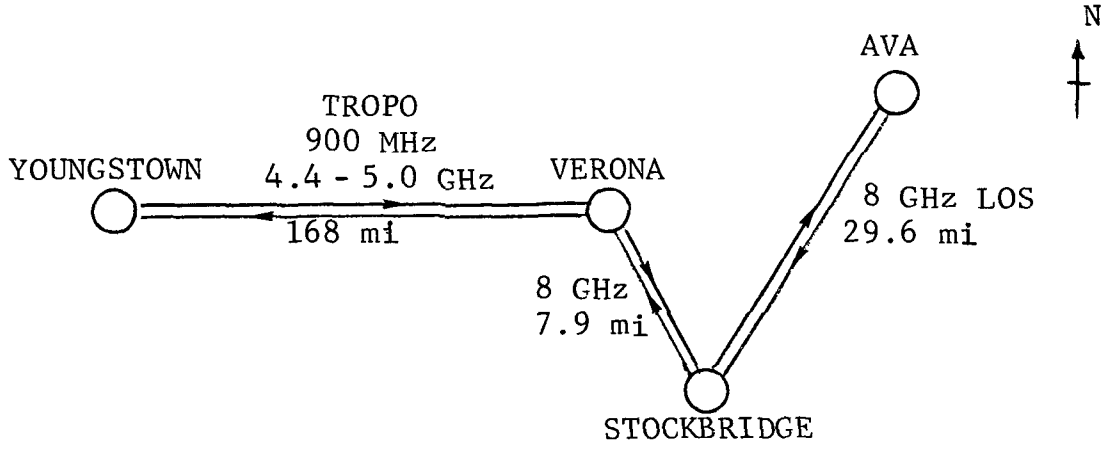


Figure 4 RADC Troposcatter/Line-of-Sight Test Configuration

model is normally used, with the refractivity inhomogeneities causing the scattering attributed to temperature, pressure, and water vapor variations in the atmosphere. The linearity assumptions allow the link to be characterized in terms of its (time-varying) pulse response $g(\tau)$ and, with some further very weak assumptions of the scattering mechanism, the process $g(\tau)$ can be described as a stationary Gaussian process with zero mean and second-order characteristic:

$$E\left\{|g(\tau)|^2\right\} \propto Q(\tau)$$

where E denotes statistical expectation, and Q is defined as the delay power spectrum [6]. The functions $g(\tau)$ and $Q(\tau)$, which are depicted in Fig. 3, typically extend over several hundred nanoseconds. A more complete statistical description of the received TROPO signal can be formulated, but is not required here.

It is convenient to introduce two different time scales associated with the quantities g and Q. Typically, the pulse response $g(\tau)$ varies rapidly over a period of seconds, depending on wind conditions, link geometry, and frequency of operation. A second time variation is, in effect, a deviation from the stationarity condition normally claimed. Large-scale meteorological influences, typically seasonal or diurnal in nature, give rise to changes in the shape of average characteristics such as $Q(\tau)$. A precise time-scale delineation of the two medium variation classes is not possible, but for measurement purposes the medium is usually considered to be stationary over nominal intervals of 20 minutes.

Time of Arrival Definitions

Even when the time-varying pulse response and its second-order statistic $Q(\tau)$ provide an adequate characterization of the troposcatter medium, there is clearly some difficulty in defining time of arrival for a hypothetical transmitted time reference pulse. An instantaneous arrival time parameter can be defined, for example, in terms of the response leading edge, energy centroid, energy median (early/late), or function maximum, and in sympathy with $g(\tau)$, the parameter will exhibit fluctuations of a short-term nature.

Furthermore, while two similar paths (e.g., forward and return) might have the same profile $Q(\tau)$, their instantaneous arrival time parameters could be quite different. Fortunately, in digital network applications one is normally relieved of the philosophical burden of defining transit time for multipath transmissions by the presence at every link termination of a bit synchronization tracking loop.

Bit synchronization circuits are provided in digital modems to accommodate the timing variations caused by the propagation medium and the timing clock at the transmitter. The function of the sync circuit is generally to smooth out short-term timing jitter present on the received signal so that only the long-term effects are tracked. For troposcatter channels, jitter occurs as a result of the multipath propagation as well as receiver noise. The techniques used vary widely but have the common feature of a continuous channel measurement, either explicitly with the transmission of separable pulses or an imbedded pseudo-noise probing sequence or, implicitly, by means of decision-directed adaptive equalization processing. The derived bit clock, therefore, responds to both short-term and long-term path length changes. An equivalent of the TRP situation is obtained when marked bits in the data stream, such as multiplexer frame patterns, are used as time-of-arrival events.

Virtually all troposcatter modem bit tracking loops have time constants which exceed a few seconds in order to smooth out short-term medium-induced timing fluctuations.

Reciprocity Considerations

One of the important fundamental parameters for a time transfer system is the differential transit time between the two nodes, since any residual difference directly corrupts the clock alignment procedure. One must suppress the immediate desire to invoke the reciprocity theorem, so that some of the more subtle reciprocity issues are at least examined. First consider the conditions under which reciprocity applies. The simplest form of Lorentz's reciprocity theorem [7] states that in a linear medium, a response of a system to a source is unchanged when the source and measurer

are interchanged. In the context of a troposcatter path, this can be applied to single antennas placed at nodes A and B. For a current pulse applied to the antenna terminals at A, the response at B, $g_B(\tau)$, will be identical to the response at A, $g_A(\tau)$, for a pulse originating at B. This will not necessarily be true, however, if the antennas are interchanged along with the source. Other factors of interest in a search for potential nonreciprocal effects can be listed as follows:

(1) Transmissions in opposite link directions will generally be on different (albeit close) carrier frequencies.

(2) Space diversity transmission configurations violate the assumptions necessary for application of the reciprocity theorem. Consider the use of a single current source at node A to generate two port outputs, $g_{B1}(\tau)$ and $g_{B2}(\tau)$, at node B. A composite signal, $g_B(\tau)$, is then formed in the diversity combiner. Transmission in the reverse direction (from B to A) normally uses only one of the B node antennas, with reception on two antennas at node A. Generally, there will not be correspondence between the two diversity combined responses $g_A(\tau)$ and $g_B(\tau)$ for the same current pulse transmission.

(3) Even with radios from the same family, differences in tuning and temperature will result in some path delay asymmetry. For example, if receivers are more sensitive to temperature than transmitters, complementary delay/temperature effects will not be exhibited for the two path directions.

With favorable geometry and recourse to some mild assumptions, it is often possible to demonstrate that the paths from A to B, and vice versa, will have the same delay power spectra $Q(\tau)$ if not the same instantaneous impulse response $g(\tau)$. In the experimental program to be described next, the emphasis was on long-term one-way link delay and bidirectional delay asymmetries.

EXPERIMENTAL RESULTS

Link Measurement Configuration

Figure 4 indicates the geographic layout of the sites used in the field test program. The LOS links were set up in a cascade with a loop back from the Ava site to give a total path length of approximately 75 miles. The Ava and Stockbridge sites were normally unattended. Troposcatter propagation experiments were carried out between Verona and Youngstown using frequencies in the vicinity of 1 GHz and 4 GHz.

The equipment set up for the troposcatter experiments is shown in block diagram form in Fig. 5. The atomic clocks shown were calibrated on a weekly basis by means of direct clock comparisons. A synchronized coded sequence transmission was initiated at each end using the 1-pps clock outputs as a trigger. By time-multiplexing the available equipment at each end, round-trip and one-way (Youngstown-Verona) transmissions were made on an 8-second cycle, with two seconds available for each combination. Time of arrival was established by means of centroid calculations of the measured delay power spectra (obtained with correlation techniques), and one-minute averages were printed out, followed by a cumulative 20-minute summary of signal level, fade rate, delay power spectrum, and arrival time at the end of the run.

Equipment Delay Characteristics

A thorough investigation of transit delay was carried out for each piece of equipment used in the experiments, including transmitters/receivers, waveguide runs, modulators/demodulators, and digital instrumentation.

To establish an understanding of the temperature stability of the more significant delay components, combinations of receivers and transmitters were cycled through a range of temperatures. An example of a delay-temperature characteristic is given in Fig. 6. The specified temperature is room temperature, and the three graphs show the delay for loops taken at the power amplifier output and

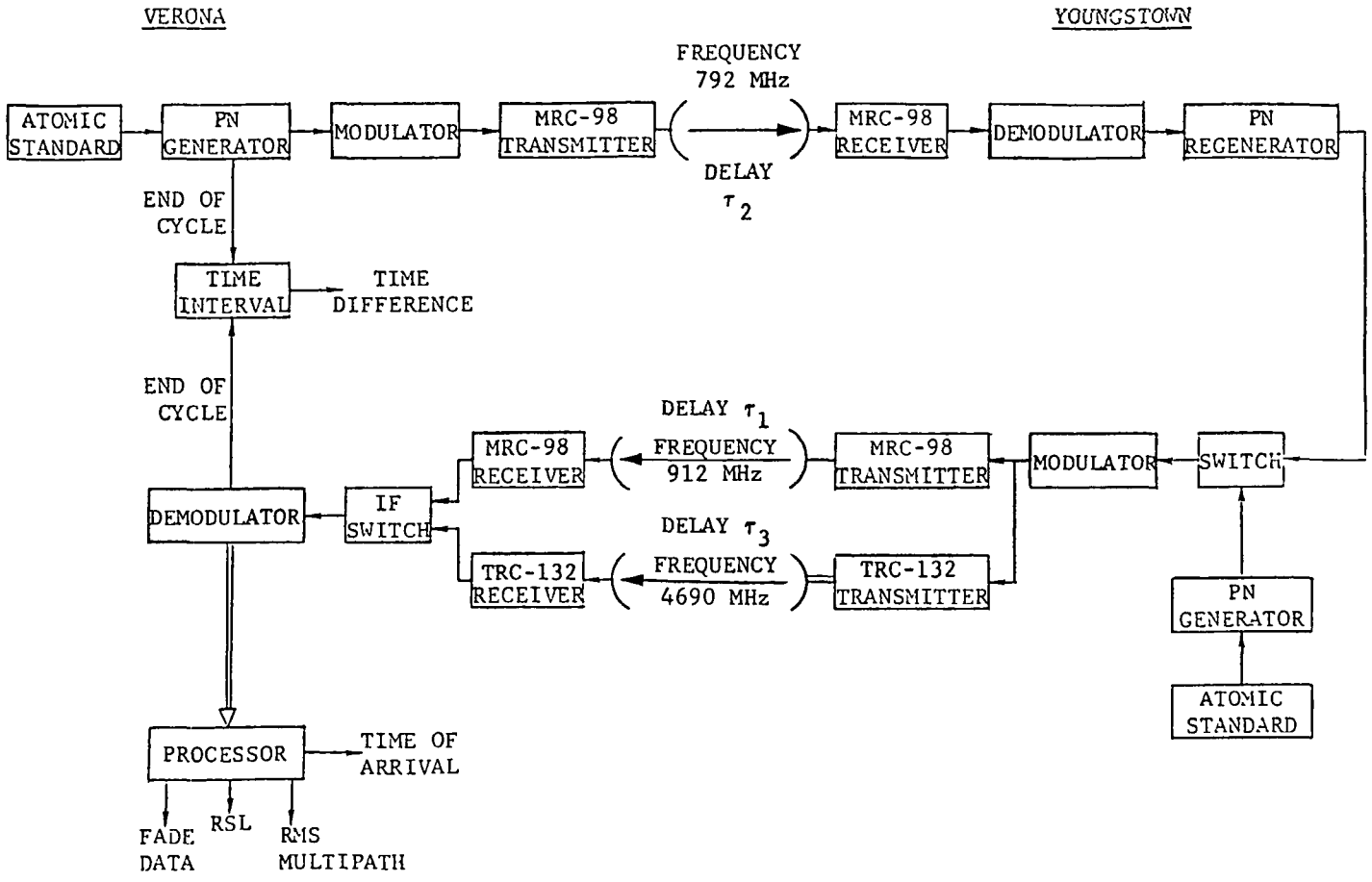


Figure 5 Differential and Absolute Delay Measurement Configuration

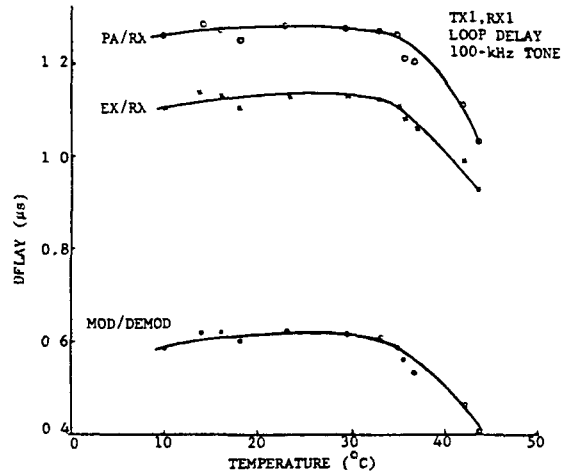


Figure 6 MRC-98 Radio Back-to-Back Delay

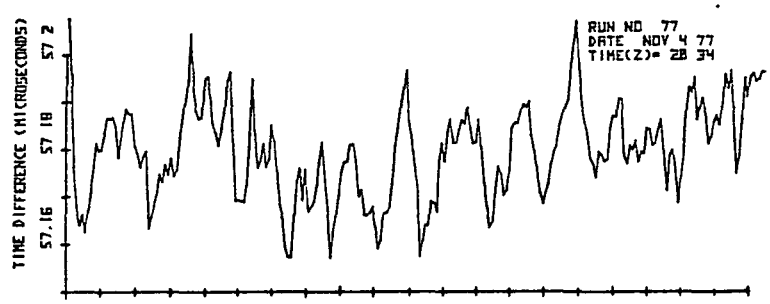


Figure 7 MDTS TROPO Modem Tracking Loop Jitter (3 Mb/s, 4 GHz)

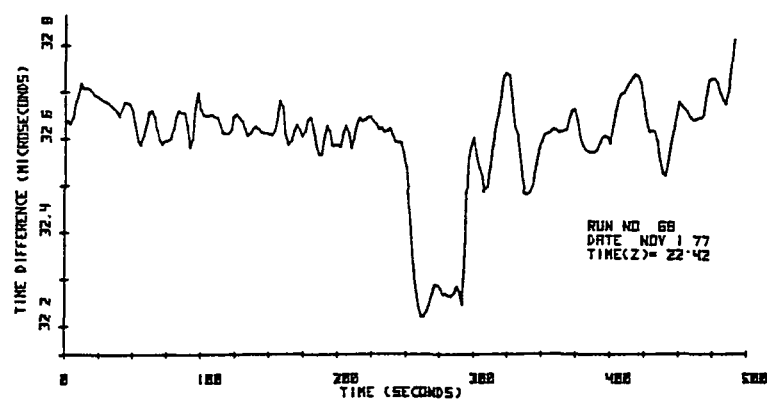


Figure 8 MDTS TROPO Modem Tracking Loop Jitter (6 Mb/s, 1 GHz)

exciter output across to the receiver, as well as the FM modulator and demodulator combination alone. These tests were carried out using 100-kHz, 200-kHz, and 500-kHz tone modulation. The results shown in Fig. 6 are for the 100-kHz case indicating the worst temperature sensitivity, most of which occurs in the modulator/demodulator units.

Digital TROPO Modem Jitter Characteristics

Two examples of the clock jitter measured at the output of digital MDTS troposcatter modems on the Verona-Youngstown link are shown in Figs. 7 and 8. Although these digital modems were only available for a brief period at the end of the experimental program, they are more representative of DCS network modems than most of the other equipment used, and are of interest for that reason. Both figures show the time jitter for a cascade of dual-diversity TROPO links equipped with MDTS modems. Figure 7 indicates performance with 3.088-Mb/s modems at 4 GHz, while Fig. 8 is for 6.276-Mb/s modems at 1 GHz. More severe fluctuations can be seen with the latter including a particularly deep excursion corresponding to a momentary loss of sync by the tracking loop.

Troposcatter Path Delay Data

We consider now the one-way and round-trip delay measurements taken with the time-multiplexed configuration illustrated in Fig. 5. The emphasis here is on longer averaging periods, typically 20 minutes, to eliminate the short-term fluctuations, such as those shown in Figs. 7 and 8. Furthermore, all of the equipment delay components have been edited out of the data so that pure path delay is obtained.

The results for a three-day data acquisition period are presented in Fig. 9. Each point plotted represents a 20-minute average of transmit time. A direct comparison between half the round-trip 792/912-MHz path delay and the one-way 912-MHz path delay is shown. Also indicated is the delay variation for one-way transmission on the C-band link. The significant feature in Fig. 9 is the close correspondence between one-way transit time and half round-trip

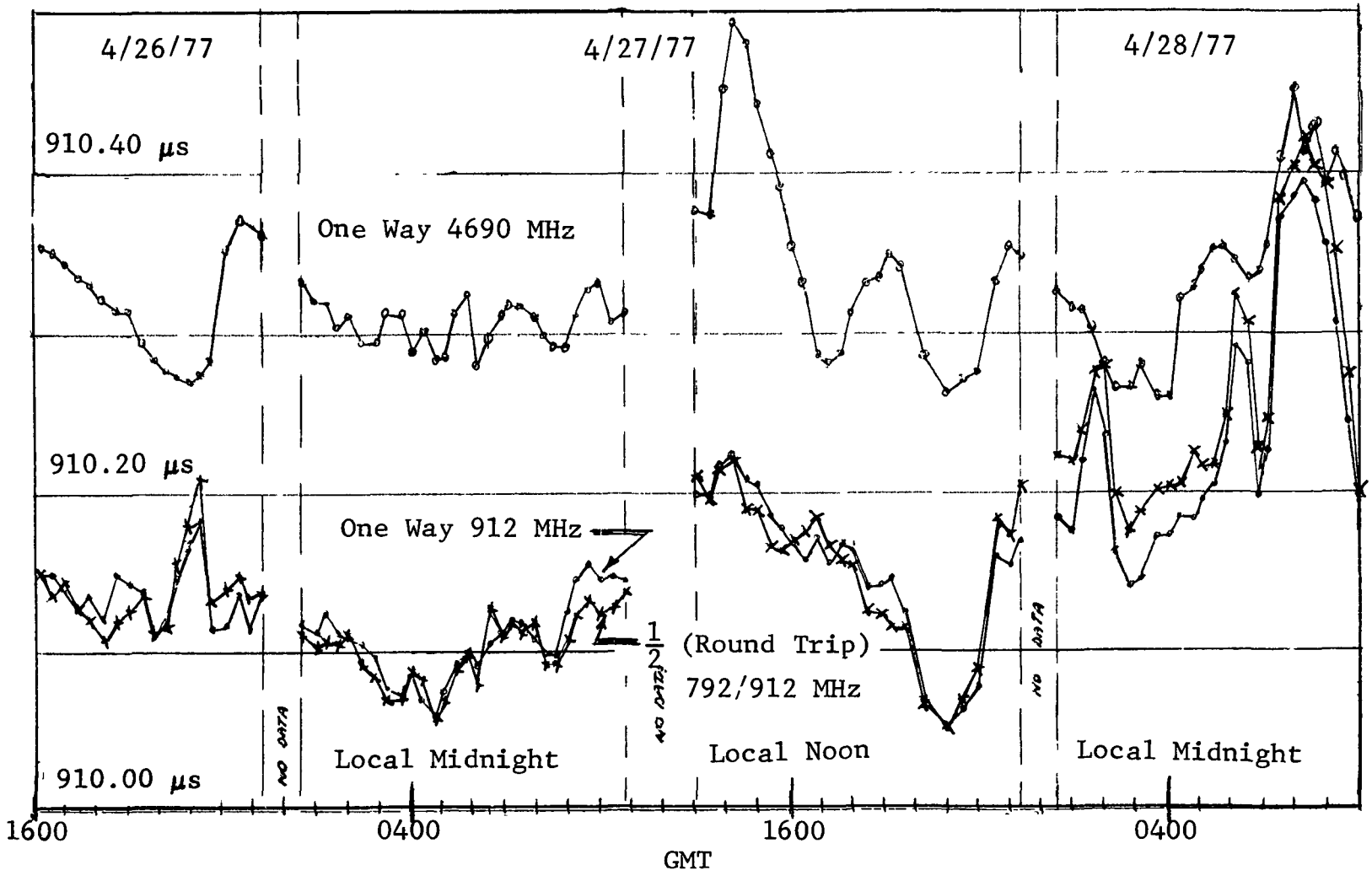


Figure 9 1- and 4-GHz TROPO Path Delay Variation

transit time for the low frequency transmissions. On the other hand, the one-way C-band data deviates from the corresponding 900-MHz data with the appearance of a bias on the order of 200 ns as well as a lack of correlation between fluctuations. Looking beyond the bidirectional asymmetry considerations, the time history of absolute delay variation is of interest from the point of view of single-ended time transfer system performance, where a fixed medium delay must be factored into the clock correction procedure, and path length variations contribute directly to clock errors. In addition, required capacity for the data buffers shown in Fig. 1 is weakly related to medium delay variation, but, as can be seen, the magnitude of the fluctuations amounts to a small number of bits at the highest anticipated bit rate.

Because of conflicting coordinate data originally available, the RADC sites were surveyed in July 1977 to re-establish geometric path lengths. Also, some refractive index data is available for correlation with the measured path delay. As a guide, the following delay budget indicates the relative importance of different effects, and provides some insight into the mechanisms inducing path delay fluctuations:

Great Circle Path Verona-Youngstown (1-GHz antennas)	272695 $\pm$ 3 meters
Uncorrected Transit Time (using speed of light in a vacuum)	909.612 μs
Correction for Refractivity with n = 320 N units	0.291 μs
Correction for Path Length corresponding to Delay Power Spectrum Average relative to the Great Circle Path	$\sim$ 0.150 μs
Total Path Delay	910.053 μs

Note that refractivity variations up to 20 N units are common at the test sites, resulting in corresponding delay

variations ranging as high as 20 ns. Similarly, refractive index gradients can cause the path length to vary by altering the propagation geometry. The quantitative aspects of this physical effect have yet to be explored.

Line-of-Sight Path Delay

By now it should be apparent that LOS links have relatively mild delay characteristics when compared with TROPO paths. Although several long data acquisition runs were carried out on the 75-mile LOS link cascade, measured transit time was generally confined to a $\pm$ 10-ns region about a nominal path. Figure 10 shows a portion of a 4-day run in which a quartz clock was set up to track a master cesium standard at the originating end of the links. The time constant selected in the clock control loop was 100 seconds. The plotted variable is the difference in time between the master and slave clocks. Path length variation on a time scale of less than 100 seconds should, therefore, be averaged out, while long-term path variations will be present.

CONCLUDING REMARKS

The results obtained in this experimental program, including those presented in this paper as being representative, must be used with some caution. It cannot be emphasized too strongly that the range of climatic conditions and equipment configurations involved was quite narrow. However, the results to date do offer quantitative data not previously available to the system designer, and suggest definite guidelines in the development of time transfer techniques to satisfy the DCS network requirements.

ACKNOWLEDGEMENT

The work reported on in this paper was supported by the Rome Air Development Center under Contract No. F30602-76-C-0347. The authors would like to acknowldge the assistance given by the RADC Project Engineer, W. Cote, and Site Supervising Engineers, W. Schneider and D. Mangold. Development and field testing of digital measurement and control instrumentation were carried out by D. Miller of CNR, Inc.

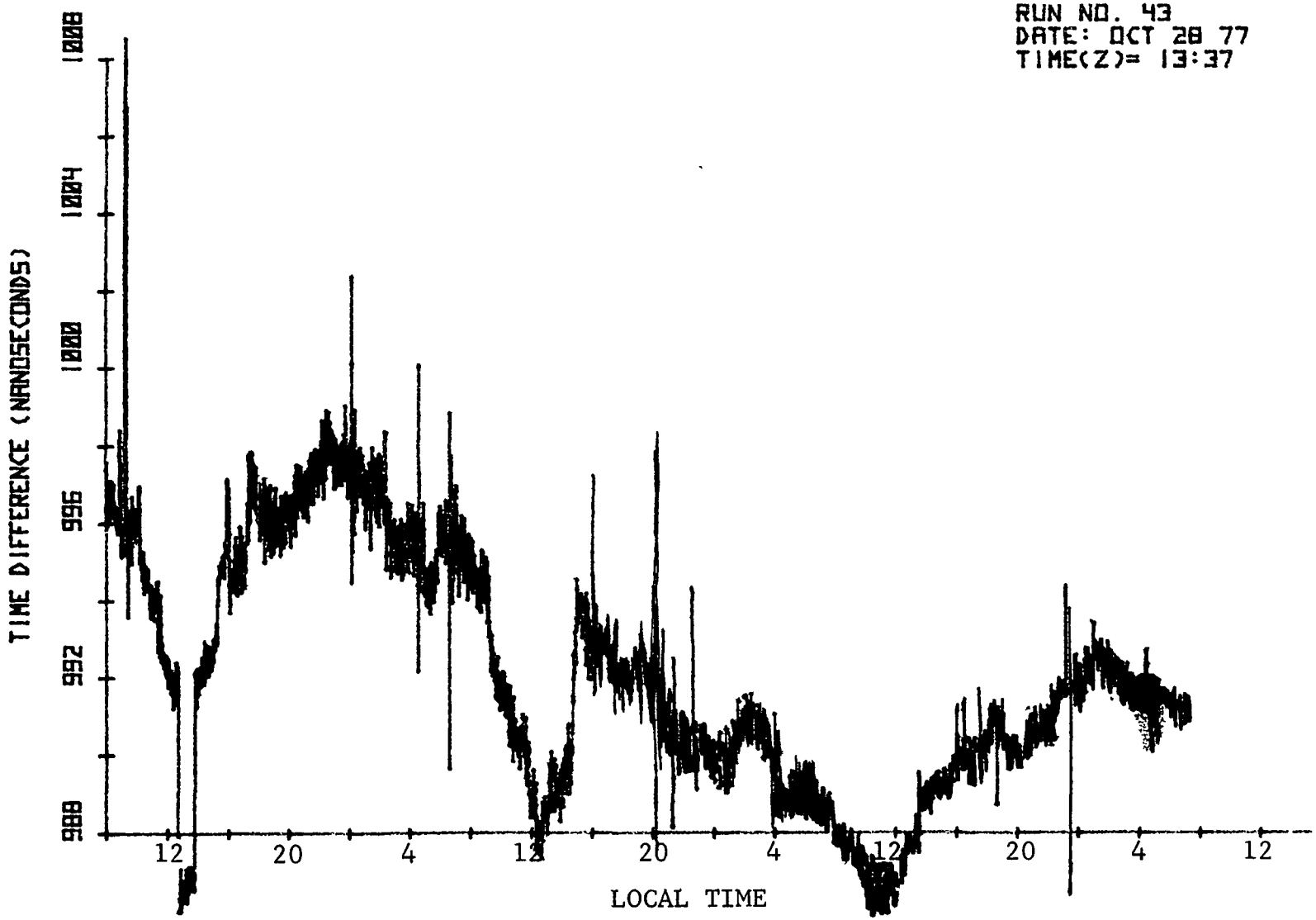


Figure 10 Path Delay Variations for 75-Mile Line-of-Sight Loop

REFERENCES

[1] V. I. Johannes and R. H. McCullough, "Multiplexing of Asynchronous Digital Signals Using Pulse Stuffing With Added Bit Signaling," IEEE Trans. on Comm. Tech., Vol. COM-14, No. 5, October 1966, pp. 562 - 568.

[2] M. W. Williard, "Analysis of a System of Mutually Synchronized Oscillators," IEEE Trans. on Comm. Tech., Vol. COM-18, No. 5, October 1970, pp. 467 - 483.

[3] B. R. Saltzberg and H. M. Zydney, "Network Synchronization," BSTJ, Vol. 54, No. 5, May 1975, pp. 879 - 892.

[4] J. G. Baart, et al., "Network Synchronization and Alarm Remoting in the Data Route," IEEE Trans. on Comm., November 1974, pp. 1873 - 1877.

[5] H. A. Stover, "Time Reference Concept for the Timing and Synchronization of the Digital DCS," DCASEF TC39-73, July 1973.

[6] P. A. Bello, "A Study of the Relationship Between Multipath Distortion and Wavenumber Spectrum of Refractive Index in Radio Links," Proc. IEEE, January 1971, pp. 47 - 75.

[7] R. F. Harrington, Time Harmonic Electromagnetic Fields, McGraw-Hill, New York, 1961, pp. 116 - 120.

QUESTIONS AND ANSWERS

MR. WALL, Jet Propulsion Laboratory:

Do high-flying aircraft have any appreciable effect?

DR. ALEXANDER:

Yes, they certainly do. When we were at the Tropo site, we were, of course, near an air base and the presence of aircraft can be observed by monitoring what is equivalent to that pulse response that I showed. However, we are averaging over 20 minutes in some of that data, and the occurrence of the aircraft is likely to be shortlived. We think it is an insignificant error in our measurements. But they are present, and they do have quite an effect on what you observe in the lab.

Page intentionally left blank

Page intentionally left blank

THE MECHANICS OF TRANSLATION OF FREQUENCY STABILITY MEASURES BETWEEN FREQUENCY AND TIME DOMAIN MEASUREMENTS

Andrew R. Chi
Goddard Space Flight Center
Greenbelt, MD

ABSTRACT

The mechanics of translation of the frequency stability measures from the frequency domain to the time domain and vice versa will be presented and discussed. The discussion will be based on the model proposed by Barnes, et al, of the Subcommittee on Frequency Stability of the Technical Committee on Frequency and Time of the IEEE's Group on Instrumentation and Measurement.

Examples based on published frequency stability data of various oscillators will be presented and examined.

1.0 INTRODUCTION

Theoretical models on frequency stability of oscillators have been developed and tested by various latoratories. Excellent reviews from different approaches and view points on the subject matter have also been published in the last two years. In addition, extensive references are given in these review papers.

This paper deals with the mechanics of translation of frequency stability measures from frequency domain to time domain and vice versa. The technique is to use discrete data points to approximate the characteristics of each noise source in the domain to which the data are translated. The difficulties encountered with this approach are often due to lack of complete data. In particular for flicker phase data hard decisions have to be made. The merit in using this technique is in the simplicity of translation and as such, it provides a quick handle for the users to examine the performance characteristics of oscillators of interest in terms of the requirements. If, however, accurate data on the performance characteristics of oscillators are needed, the simplest approach is still the direct approach by measuring the frequency stability in the domain of interest.

2.0 DISCUSSION OF THEORY

A theoretical model which is in wide use to describe the characteristics of frequency stability is the one recommended by the Subcommittee on Frequency Stability of the IEEE. This model is based on the assumptions that; (a) the instantaneous frequency fluctuations of the output signal of an oscillator is due to independent noise sources in the oscillator system; (b) as many as five noise sources may be needed to characterize the frequency instability observed in most oscillators; and (c) each independent noise source can be modeled by a power law. Since each noise source is independent of the other they may be combined by superposition.

2.1 FREQUENCY DOMAIN

In frequency domain measurement, the spectral density of a noise source in an oscillator that perturbs the frequency stability of the oscillator system can be considered as the average contribution of all individual perturbations of noise components each having a frequency, f, ranging from minus infinity to plus infinity. Thus the total noise power is the sum of the contributions of all of the noise components. In practical terms this frequency range is folded and covers only the range of frequencies from zero to positive infinity. The spectral density of a signal of only positive frequency components is called the one sided spectral density of frequency and is represented by $S_y(f)$ where f is the variable frequency component, also called Fourier frequency, and the subscript, y, is the fractional frequency change from the nominal frequency, ν_o of the oscillator. Thus the power law noise model may be written as

$$S_y(f) = h_\alpha f^\alpha \tag{1}$$

where h_α is a constant and is characteristic of an oscillator

α is the characteristic value of a noise source and takes the values of -2, -1, 0, 1 and 2.

Cutler and Searle have shown that

$$S_\phi(f) = 4\pi^2 \nu_o^2 S_y(f) \tag{2}$$

$$S_\phi(f) = (\nu_o^2/f^2) S_y(f) \tag{3}$$

$$S_x(f) = (1/4\pi^2 f^2) S_y(f) \tag{4}$$

where the subscripts denotes phase ϕ, $\dot{\phi} = d\phi/dt$ and $x = \phi/2\pi\nu_o$. X is phase measured in units of time and is often written as phase-time. Substituting equation (1) into equations (2), (3) and (4) one obtains the power law noise model for $\dot{\phi}$, ϕ and X.

$$S_{\dot{\phi}}(f) = 4\pi^2\nu_o^2 h_\alpha f^\alpha \equiv h_{\dot{\phi}} f^\alpha \tag{5}$$

$$S_\phi(f) = \nu_o^2 h_\alpha f^{\alpha-2} \equiv h_\phi f^\beta \tag{6}$$

$$S_x(f) = \frac{1}{4\pi^2} h_\alpha f^{\alpha-2} \equiv h_x f^\beta \tag{7}$$

where

$$h_{\dot{\phi}} = 4\pi^2\nu_o^2 h_\alpha \tag{8}$$

$$h_\phi = \nu_o^2 h_\alpha \tag{9}$$

$$h_x = \frac{1}{4\pi^2} h_\alpha \tag{10}$$

$$\beta = \alpha - 2 \tag{11}$$

Since the power law model is based on five independent noise sources and if they are all present in the oscillator, the one-sided spectral density becomes:

$$S_y(f) = h_{-2} f^{-2} + h_{-1} f^{-1} + h_0 f^0 + h_1 f^1 + h_2 f^2 \tag{12}$$

2.2 TIME DOMAIN

In the time domain measurement, frequency perturbations of a signal due to all frequency components of a noise source are measured collectively as a function of time and are averaged over a sampling time period. Thus the frequency stability characteristics are represented by variance or standard deviation of the measured frequency fluctutations based on statistical calculations. The expected value of the variance of fractional frequency fluctuations, y, from the nominal frequency of an oscillator is:

$$\langle \sigma_y^2(N,T,\tau) \rangle = \left\langle \frac{1}{N-1} \sum_{n=1}^{N} \left(\bar{y}_n - \frac{1}{N} \sum_{k=1}^{N} \bar{y}_k \right)^2 \right\rangle \tag{13}$$

where N is the number of data points
T is the time interval between the beginnings of adjacent measurements
τ is the sampling time within T
$\bar{y}$ is the average fractional frequency fluctuations over a sampling time
< > is a symbol denoting an infinite average

In statistical analysis, N is desired to be large approaching

infinity and the noise source is a random process. In real life N is finite and noise source is not always random. In addition, it may not even be stationary, thus corrections and approximations are needed in statistical analysis in order to match or to check the theory.

In the simplest case N = 2 and T = τ, Allan has shown that

$$\langle \sigma_y^2(2,\tau,\tau) \rangle \equiv \sigma_y^2(\tau) = \left\langle \tfrac{1}{2} (\bar{y}_{k+1} - \bar{y}_k)^2 \right\rangle \tag{14}$$

and Allan and Vessot have shown that

$$\langle \sigma_y^2(\tau) \rangle \sim |\tau|^{\mu} \tag{15}$$

This variance and its square root, the standard deviation, have been used to describe the frequency stability characteristics of oscillators in the time domain. The variance is known as the Allan variance.

2.3 CLOCK ERROR

Barnes has shown that to predict a clock reading error, X(t), one may define a time stability by a time variance:

$$\sigma_x^2(\tau) = \tau^2 \sigma_y^2(\tau) \tag{16}$$

3.0 TRANSLATION

The translation relationship between the frequency and time domain measures based on equations (12) and (13) was derived by Cutler and is given by

$$\langle \sigma_y^2(N,T,\tau) \rangle = h_\alpha C_\alpha \tau^{\mu} \tag{17}$$

where $\mu = -\alpha - 1$

$-3 < \alpha < 1$

and C_α is a transfer function given by

$$C_\alpha = \frac{N}{(N-1)\pi^{\alpha+1}} \int_0^\infty du\, u^\alpha \frac{\sin^2 u}{u^2} \left[1 - \frac{\sin^2 N r u}{N^2 \sin^2 r u} \right] \tag{18}$$

in equation (18) $u = \pi f \tau$

$r = T/\tau$ $(r=1$ if $T=\tau)$

In the case N = 2, r = 1

Allan variance becomes:

$$\langle \sigma_y^2(\tau) \rangle = h_{-2}\left(\frac{4\pi^2}{6}\right)\tau + h_{-1}(2\ln 2) + h_0\left(\frac{1}{2}\right)\frac{1}{\tau} + h_1\left[\frac{1.038 + 3\ln(2\pi f_h \tau)}{4\pi^2}\right]\frac{1}{\tau^2} + h_2\left(\frac{3f_h}{4\pi^2}\right)\frac{1}{\tau^2} \tag{19}$$

Where f_h is the high frequency cutoff of an idealized infinitely sharp cutoff low pass filter.

Equation (19) may be written also in the form of

$$\langle \sigma_y^2(\tau) \rangle = \sum_{\alpha=-2}^{2} h_\alpha C_\alpha \tau^\mu \tag{20}$$

so that

$$C_{-2} = \frac{4\pi^2}{6} \tag{21}$$

$$C_{-1} = 2\ln 2 \tag{22}$$

$$C_0 = \frac{1}{2} \tag{23}$$

$$C_1 = \frac{1.038 + 3\ln(2\pi f_h \tau)}{4\pi^2} \tag{24}$$

$$C_2 = \frac{3f_h}{4\pi^2} \tag{25}$$

Thus the six basic power law equations from Equations (5), (6), (7), (12), (16) and (20) may be collected together for convenience given below:

$$\left.\begin{aligned} S_y(f) &= h_{-2}f^{-2} + h_{-1}f^{-1} + h_0 + h_1 f + h_2 f^2 \equiv \Sigma h_\alpha f^\alpha \\ S_\phi(f) &= 4\pi^2 \nu_0^2 \Sigma h_\alpha f^\alpha \\ S_\phi(f) &= \nu_0^2\left(h_{-2}f^{-4} + h_{-1}f^{-3} + h_0 f^{-2} + h_1 f^{-1} + h_2\right) \equiv \nu_0^2 \Sigma h_\alpha f^\alpha \\ S_x(f) &= \frac{1}{4\pi^2}\Sigma h_\alpha f^3 \end{aligned}\right\} \tag{26A}$$

$$\left.\begin{aligned} \sigma_y^2(\tau) &= h_{-2}C_{-2}\tau + h_{-1}C_{-1} + h_0 C_0 \tau^{-1} + h_1 C_1 \tau^{-2} + h_2 C_2 \tau^{-2} \\ \sigma_x^2(\tau) &= h_{-2}C_{-2}\tau^3 + h_{-1}C_{-1}\tau^2 + h_0 C_0 \tau + h_1 C_1 + h_2 C_2 \end{aligned}\right\} \tag{26B}$$

Comparing term by term for each noise source between equations (26A) and 26B) one can derive the translation relationship. For example the first terms for the random walk of frequency noise are given by:

$$S_y(f) = h_{-2} f^{-2}$$

and

$$\sigma_y^2(\tau) = h_{-2}\left(\frac{4\pi^2}{6}\right)\tau$$

thus

$$S_y(f) = \frac{6}{4\pi^2}\left(\frac{1}{\tau}\sigma_y^2(\tau)\right)\frac{1}{f^2}$$

Figure 1 shows the log-log plots of frequency stability characteristics of oscillators in frequency and time domains based on the power law model of five noise sources. The equations to translate the frequency stability measured in the frequency domain to the time domain and vice versa are given in Table 1. The terms in the bracket are the measured quantitites. The subscript y for $S_y(f)$, $\sigma_y^2(\tau)$ and $\sigma_y(\tau)$ is often deleted in most texts without confusion if a subscript is always used for $\dot{\phi}$, ϕ and X. $\dot{\phi}$ is not listed in Table 1 because it is not used often; however, a general formula can be easily derived as shown in Table 1.

Since the theory in the frequency domain is modeled by a power law it is reasonable to assume the flicker phase noise is independent of the sampling time in the frequency domain. This assumption gives a starting point for the translation. If the flicker phase noise is translated from the frequency domain into the time domain the flicker phase noise becomes dependent on the sampling time. Flicker phase noise is generally lower in level than the white phase noise and becomes indistinguishable from the white phase noise in the time domain unless it is specially tested. The time dependence of the flicker phase noise in the time domain is therefore a major problem for translation of frequency stability from time domain to frequency domain.

4.0 EXAMPLES OF TRANSLATION FROM FREQUENCY DOMAIN TO TIME DOMAIN

4.1 DATA

Brandenberger et al published in 1971 an excellent set of

data of frequency stability measurement of a very high quality 5 MHz quartz crystal controlled oscillator. The spectral density of phase per oscillator measured in the frequency domain is shown in Figure 2 and is given for the frequency range between 0.1 and 10^4 Hz by:

$$S_\phi(f) = 1.58\times10^{-12} f^{-3} + 3.16\times10^{-13} f^{-1} + 3.98\times10^{-15} f^{0} \qquad (27)$$

The time domain measurements of the same oscillator are shown in Figure 3.

Using the coefficients of equation (27) one can plot the flicker frequency noise, flicker phase noise and white phase noise in Figure (2) by straight lines correspondingly proportional to f^{-3}, f^{-1} and f^{0} respectively. These data points are given in Table 2.

4.2 FLICKER FREQUENCY

The calculations for the translation of the flicker frequency, for an example, from frequency domain to time domain is given below:

$$\sigma^2(\tau) = \frac{C_1}{\nu_0^2}\left[f^3 S_\phi(f)\right]\tau^0$$

$$= \frac{21n2}{25\times10^{12}}\left[1^3 \times 1.58\times10^{-12}\right]$$

$$= 8.76\times10^{-26}$$

$$\sigma(\tau) = 2.96\times10^{-13}$$

If the calculated Allan variance is for one oscillator, the data plotted in Figure 3 are for both the test and reference oscillator. If this is true, a factor of 2 should be multiplied.
Thus

$$2\sigma^2(\tau) = 1.75\times10^{-25}$$

and

$$\sqrt{2}\,\sigma(\tau) = 4.18\times10^{-13}$$

4.3 FLICKER PHASE

Using Table 1 one obtains the translation equation to be

$$\sigma^2(\tau) = \frac{C_1}{\nu_0^2}\left[f S_\phi(f)\right]\tau^{-2}$$

$$= \frac{1}{4\pi^2\nu_0^2}\left[1.038 + 3\ln(2\pi f_h \tau)\right]\left[f S_\phi(f)\right]\tau^{-2}$$

for $f = 1$ Hz, $S_\phi(1) = 3.16 \times 10^{-13}$, $\nu_0 = 5$ MHz, and $f_h = 1$ kHz

$$\sigma^2(\tau) = \left(6.5516 + 3\ln f_h + 3\ln\tau\right)\left[\frac{S_\phi(1)}{4\pi^2\nu_0^2}\right]\tau^{-2}$$

$$= \left[8.7327 \times 10^{-29} + 4.6052 \times 10^{-28}\ln\tau\right]\tau^{-2}$$

The calculated $\sigma^2(\tau)$ and $\sigma(\tau)$ for flicker phase noise for three values of τ are given in Table 3.

4.4 WHITE PHASE

Again using Table 1 one obtains the translation equation to be

$$\sigma^2(\tau) = \frac{C_2}{\nu_0^2}\left[f^0 S_\phi(f)\right]\tau^{-2}$$

$$= \frac{3 f_h}{4\pi^2\nu_0^2}\left[f^0 S_\phi(f)\right]\tau^{-2}$$

for $S_\phi(f) = 3.98 \times 10^{-15}$, $\nu_0 = 5$ MHz, and $f_h = 1$ kHz

$$\sigma^2(\tau) = \frac{3 \times 10^3}{4\pi^2\nu_0^2}\left[3.98 \times 10^{-15}\right]\tau^{-2}$$

$$= 1.2098 \times 10^{-26}\,\tau^{-2}$$

$$\sigma(\tau) = 1.1 \times 10^{-13}\,\tau^{-1}$$

The calculated values of $\sigma^2(\tau)$ and $\sigma(\tau)$ for white phase noise are also given in Table 3.

4.4 COMPARISON OF RESULTS

For comparison purposes a summary of the time domain data for the crystal oscillator translated from the frequency domain is shown in Table 4 together with the measured time domain data taken from Figure 3. One can see the agreement is generally good except for the flicker frequency noise. The difference is 2.2 db which is within the measured accuracy. This difference could be explained if the data either in Figure 2 or in Figure 3 is plotted for both the test and reference oscillators instead of for only one oscillator.

One can see the dependence of the flicker phase noise on the sampling time. The error it can introduce in translation by a straight line approximation from the time domain to the frequency domain should be obvious. In the first place the "-1" slope data of the sigma-tau plot in the time domain is the sum of the white phase noise and flicker phase noise power. In the second the level of the flicker phase noise is lower than the level of the white phase noise and is also lower for shorter sampling time.

5.0 EXAMPLES OF TRANSLATION FROM TIME DOMAIN TO FREQUENCY DOMAIN.

Figures 4 and 5 show the frequency stability of a high performance cesium beam tube oscillator measured in time domain and frequency domain respectively. The straight lines are the translated or predicted values using the power law model for N = 2 and $T = \tau$. These data are based from publications by Babitch and Oliverio and private communications from M. Fischer.

Using the measured data points in Figure 4 one can translate the identified noise sources from the time domain to the frequency domain by using the relationship given in Table 1. The results are given in Table 5. The calculated spectral density of phase for the flicker phase noise from the time domain data are based on f_c = 50 KHz and ν_o = 5 MHz.

Sample calculation of translating the flicker phase noise from time domain to frequency domain are given below:

$$S_\phi(f) = \frac{\nu_o^2}{c_1}\left[\tau^2\sigma^2(\tau)\right] f^{-1}$$

$$c_1 = \frac{1}{4\pi^2}\left(1.038 + 3\ln(2\pi f_h \tau)\right)$$

$$= \frac{1}{4\pi^2}\left(39.011 + 3\ln\tau\right)$$

Thus $$S_\phi(f) = \frac{4\pi^2\nu_o^2}{39.011+3\ln\tau}\left[\tau^2\sigma^2(\tau)\right] f^{-1}$$

For $\tau = 10^{-1}$ sec.

$$S_\phi(f) = 3.0743\times10^{11}\left[\sigma^2(\tau)\right] f^{-1}$$

For $\tau = 10^{-2}$ sec.

$$S_\phi(f) = 3.9172\times10^{9}\left[\sigma^2(\tau)\right] f^{-1}$$

a. Use measured data points in Figure 4 for $\tau = 10^{-1}$ and $\tau = 10^{-2}$ seconds respectively

$$\sigma(10^{-1}) = 4.0\times10^{-12}$$

$$\sigma(10^{-2}) = 2.5\times10^{-11}$$

Thus for $\tau = 10^{-1}$ sec., $\sigma(10^{-1}) = 4.0\times10^{-12}$

$$S_\phi(f) = 4.919\times10^{-12} f^{-1}$$

$$10\log S_\phi(10) = -123.1 \text{ db}$$

$$10\log S_\phi(10^2) = -133.1 \text{ db}$$

For $\tau = 10^{-2}$ sec., $\sigma(10^{-2}) = 2.5 \times 10^{-11}$

$$S_\phi(f) = 2.448 \times 10^{-12} f^{-1}$$

$$10 \log S_\phi(10) = -126.1 \text{ db}$$

$$10 \log S_\phi(10^2) = -136.1 \text{ db}$$

b. Use the translated data (straight line) in Figure 4 also for $\tau = 10^{-1}$ and 10^{-2} seconds

$$\sigma(10^{-1}) = 5.6 \times 10^{-12}$$

$$\sigma(10^{-2}) = 5.0 \times 10^{-11}$$

Thus for $\tau = 10^{-1}$ sec., $\sigma(10^{-1}) = 5.6 \times 10^{-12}$

$$S_\phi(f) = 9.641 \times 10^{-12} f^{-1}$$

$$10 \log S_\phi(10) = -120.2 \text{ db}$$

$$10 \log S_\phi(10^2) = -130.2 \text{ db}$$

For $\tau = 10^{-2}$ Sec., $\sigma(10^{-2}) = 5.0 \times 10^{-11}$

$$S_\phi(f) = 9.793 \times 10^{-12} f^{-1}$$

$$10 \log S_\phi(10) = -120.1 \text{ db}$$

$$10 \log S_\phi(10^2) = -130.1 \text{ db}$$

It can be seen from Table 5 for the flicker phase noise the translated results from the time domain to the frequency domain show a better agreement when the actual measured data in the time domain are used. This is to be expected since the straight line data in (b) are translated from the frequency domain. Further, the results in (a) are better for lower values of tau.

6.0 DISCUSSION

Historically the frequency stability measurements as most

people have pointed out were made in a larger number of oscillators, in the time domain. This is because of the readily available electronic counters in the laboratories for making the period measurements. In addition, the sigma-tau plot of frequency stability in the time domain seems to be easier to communicate the concept of the characteristics of the noise model based on the power law. The difficulties are in the data analysis and in the identification of noise processes. For example, the flicker frequency noise in Figure 4 could be deleted if the dashed lines were used. In this case only one data point is discarded (i.e., t = 2 sec). Another question can be raised. "Is white phase noise present in Figure 4 in the time domain measurement?" The answer is "negative" based on the spectral density of phase measurement in the frequency domain in the frequency range measured. Obviously there is no answer to the question if only time domain data is available. Frequency stability measurements in the frequency domain are becoming more available as improved design and computer operated spectrum analyzers are becoming available in laboratories. Thus, the interest in the relating of the measured data in the two domains are continuously on the increase.

Figures 6 and 7 show the relative frequency stability of typical oscillators measured in the time domain and frequency domains respectively. These data are based on the results of Fischer and Vessot. It is to be noted that the apparent random walk of frequency (lines with +1/2 slope in Figure 6) is normally not shown in frequency stability of sigma versus tau plots. This is because the random walk of frequency noise is likely to be the net result of the noises in the electronic circuit of the frequency locked loop, the white phase of the quartz crystal oscillator, and the flicker phase of the cesium beam tube. The random walk of frequency behavior (less than the servo loop time constant) is therefore a characteristic of the system design of a manufacturer.

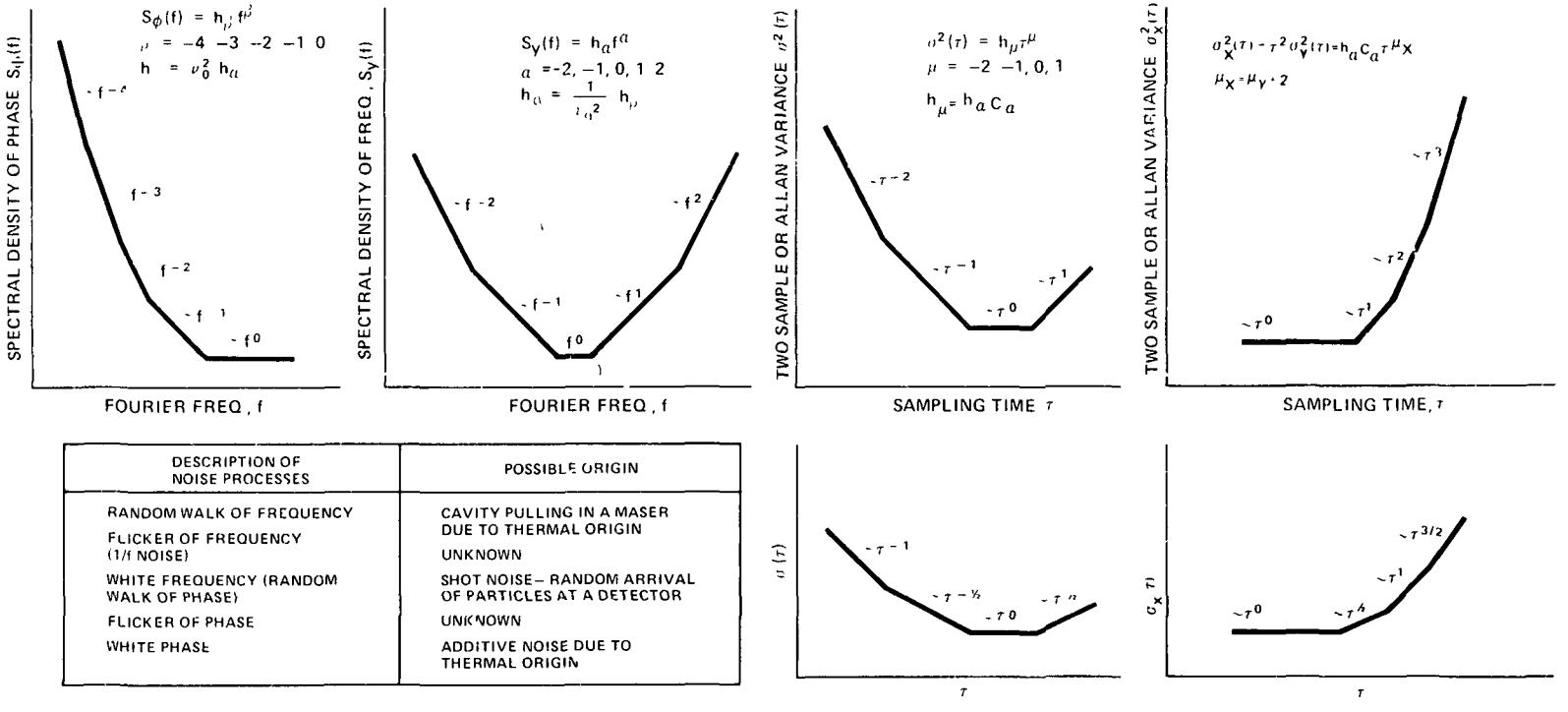
7.0 CONCLUSION

The mechanics of translation of frequency stability from frequency domain to time domain and vice versa have been shown. The procedure is simple and the translation relationships are given in Table 1. While the mechanics of translation are straight forward the same cannot be said for the preservation of the accuracy after translation. This is particularly true for the translation of the white phase and flicker phase noises from the time domain to the frequency domain. Additional errors may be introduced if the data

collection and data analysis are not on a common base. Those who are interested in the validity of translation and theoretical limitations of the power law model of frequency stability are referred to the original papers and review papers given in the reference.

8.0 ACKNOWLEDGEMENT

It is a pleasure to acknowledge the helpful discussions the author had with Mr. Michael C. Fischer of Hewlett-Packard Company, Mr. Hugh Fosque of the National Aeronautics and Space Administration, and Mr. David Allan of the National Bureau of Standards.



DESCRIPTION OF NOISE PROCESSES	POSSIBLE ORIGIN
RANDOM WALK OF FREQUENCY	CAVITY PULLING IN A MASER DUE TO THERMAL ORIGIN
FLICKER OF FREQUENCY (1/f NOISE)	UNKNOWN
WHITE FREQUENCY (RANDOM WALK OF PHASE)	SHOT NOISE– RANDOM ARRIVAL OF PARTICLES AT A DETECTOR
FLICKER OF PHASE	UNKNOWN
WHITE PHASE	ADDITIVE NOISE DUE TO THERMAL ORIGIN

Figure 1 Power law noise models that contribute to frequency instability in oscillators.

Table 1 Translation equations for frequency stability measured in frequency domain to time domain and vice versa

DESCRIPTION OF NOISE SOURCE	FREQUENCY DOMAIN TO TIME DOMAIN								TIME DOMAIN TO FREQUENCY DOMAIN			
	$\sigma_y^2(\tau)$						$\sigma_x^2(\tau)$		$S_y(f)$	$S_\phi(f)$	$S_x(f)$	$S_x(f)$
	α	FREQUENCY	μ_y	PHASE	β	PHASE–TIME	μ_x	PHASE–TIME	FREQUENCY	PHASE	PHASE–TIME	PHASE–TIME
GENERAL FORMULA	–	$C_\alpha \lvert f^{-\alpha} S_y(f) \rvert \tau^{\mu_y}$	–	$\frac{C_\alpha}{\nu_0^2} \lvert f^{-\beta} S_\phi(H) \rvert \tau^{\mu_y}$	~	$4\pi^2 C_\alpha \lvert f^{-\beta} S_x(f) \rvert \tau^{\mu_y}$	–	$4\pi^2 C_\alpha \lvert f^{-\beta} S_x(f) \rvert \tau^{\mu_x}$	$\frac{1}{C_\alpha} \lvert \tau^{-\mu_y} \sigma_y^2(\tau) \rvert f^\alpha$	$\frac{\nu_0^2}{C_\alpha} \lvert \tau^{-\mu_y} \sigma_y^2(\tau) \rvert f^\beta$	$\frac{1}{4\pi^2 C_\alpha} \lvert \tau^{-\mu_y} \sigma_y^2(\tau) \rvert f^\beta$	$\frac{1}{4\pi^2 C_\alpha} \lvert \tau^{-\mu_x} \sigma_x^2(\tau) \rvert f^\beta$
RANDOM WALK FREQ	–2	$C_{-2} \lvert f^{-2} S_y(f) \rvert \tau^1$	1	$\frac{C_{-2}}{\nu_0^2} \lvert f^{-2} S_\phi(f) \rvert \tau^1$	–4	$4\pi^2 C_{-2} \lvert f^{-2} S_x(f) \rvert \tau^3$	3	$4\pi^2 C_{-2} \lvert f^{-2} S_x(f) \rvert \tau^1$	$\frac{1}{C_{-2}} \lvert \tau^{-1} \sigma_y^2(\tau) \rvert f^{-2}$	$\frac{\nu_0^2}{C_{-2}} \lvert \tau^{-1} \sigma_y^2(\tau) \rvert f^{-4}$	$\frac{1}{4\pi^2 C_{-2}} \lvert \tau^{-1} \sigma_y^2(\tau) \rvert f^{-4}$	$\frac{1}{4\pi^2 C_{-2}} \lvert \tau^{-1} \sigma_x^2(\tau) \rvert f^{-4}$
FLICKER FREQUENCY	–1	$C_{-1} \lvert f^{-1} S_y(f) \rvert \tau^0$	0	$\frac{C_{-1}}{\nu_0^2} \lvert f^{-1} S_\phi(f) \rvert \tau^0$	–3	$4\pi^2 C_{-1} \lvert f^{-1} S_x(f) \rvert \tau^0$	2	$4\pi^2 C_{-1} \lvert f^{-1} S_x(f) \rvert \tau^2$	$\frac{1}{C_{-1}} \lvert \tau^0 \sigma_y^2(\tau) \rvert f^{-1}$	$\frac{\nu_0^2}{C_{-1}} \lvert \tau^0 \sigma_y^2(\tau) \rvert f^{-3}$	$\frac{1}{4\pi^2 C_{-1}} \lvert \tau^0 \sigma_y^2(\tau) \rvert f^{-3}$	$\frac{1}{4\pi^2 C_{-1}} \lvert \tau^{-2} \sigma_x^2(\tau) \rvert f^{-1}$
WHITE FREQUENCY	0	$C_0 \lvert f^0 S_y(f) \rvert \tau^{-1}$	–1	$\frac{C_0}{\nu_0^2} \lvert f^{-2} S_\phi(f) \rvert \tau^{-1}$	–2	$4\pi^2 C_0 \lvert f^{-2} S_x(f) \rvert \tau^{-1}$	1	$4\pi^2 C_0 \lvert f^{-2} S_x(f) \rvert \tau^1$	$\frac{1}{C_0} \lvert \tau^1 \sigma_y^2(\tau) \rvert f^0$	$\frac{\nu_0^2}{C_0} \lvert \tau^1 \sigma_y^2(\tau) \rvert f^{-2}$	$\frac{1}{4\pi^2 C_0} \lvert \tau^1 \sigma_y^2(\tau) \rvert f^{-2}$	$\frac{1}{4\pi^2 C_0} \lvert \tau^{-1} \sigma_x^2(\tau) \rvert f^{-2}$
FLICKER PHASE	1	$C_1 \lvert f^{-1} S_y(f) \rvert \tau^{-2}$	–2	$\frac{C_1}{\nu_0^2} \lvert f^{-1} S_\phi(f) \rvert \tau^{-2}$	–1	$4\pi^2 C_1 \lvert f^{-1} S_x(f) \rvert \tau^{-2}$	0	$4\pi^2 C_1 \lvert f^{-1} S_x(f) \rvert \tau^0$	$\frac{1}{C_1} \lvert \tau^2 \sigma_y^2(\tau) \rvert f^1$	$\frac{\nu_0^2}{C_1} \lvert \tau^2 \sigma_y^2(\tau) \rvert f^{-1}$	$\frac{1}{4\pi^2 C_1} \lvert \tau^2 \sigma_y^2(\tau) \rvert f^{-1}$	$\frac{1}{4\pi^2 C_1} \lvert \tau^0 \sigma_x^2(\tau) \rvert f^1$
WHITE PHASE	2	$C_2 \lvert f^{-2} S_y(f) \rvert \tau^{-2}$	–2	$\frac{C_2}{\nu_0^2} \lvert f^0 S_\phi(f) \rvert \tau^{-2}$	0	$4\pi^2 C_2 \lvert f^0 S_x(f) \rvert \tau^{-2}$	0	$4\pi^2 C_2 \lvert f^0 S_x(f) \rvert \tau^0$	$\frac{1}{C_2} \lvert \tau^2 \sigma_y^2(\tau) \rvert f^0$	$\frac{\nu_0^2}{C_2} \lvert \tau^2 \sigma_y^2(\tau) \rvert f^0$	$\frac{1}{4\pi^2 C_2} \lvert \tau^2 \sigma_y^2(\tau) \rvert f^0$	$\frac{1}{4\pi^2 C_2} \lvert \tau^0 \sigma_x^2(\tau) \rvert f^0$

EQUATIONS USED IN THE TABLE

$S_y(f) = h_\alpha f^\alpha$

$S_\phi(f) = (\nu_0^2/f^2) S_y(f) = \nu_0^2 h_\alpha f^{\alpha-2} \equiv h_\beta f^\beta$

$S_x(f) = (1/4\pi^2 f^2) S_y(f) = (1/4\pi^2) h_\alpha f^{\alpha-2} \equiv h_x f^\beta$

$\sigma_y^2(\tau) = h_\alpha C_\alpha \tau^{\mu_y}$

$\sigma_x^2(\tau) = \tau^2 \sigma_y^2(\tau) = h_\alpha C_\alpha \tau^{\mu_y+2} \equiv h_\alpha C_\alpha \mu^x$

$C_{-2} = 4\pi^2/6$

$C_{-1} = 2 \ln 2$

$C_0 = 1/2$

$C_1 = [1.038 + 3 \ln (2\pi f_h \tau)]/4\pi^2 \quad (2\pi f_h \tau \gg 1)$

$C_2 = 3f_h/4\pi^2$

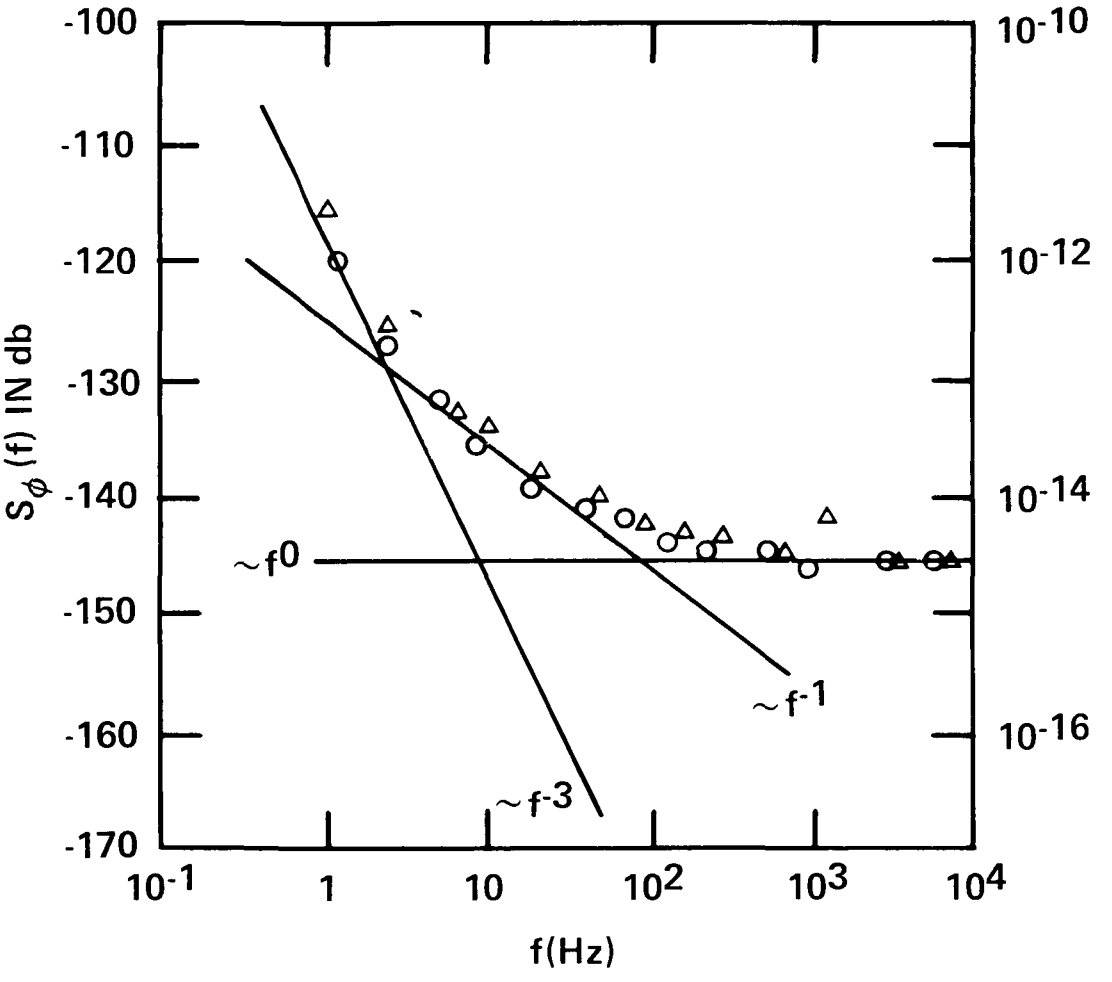


Figure 2. Spectral density of the phase of a very high quality 5 MHz quartz crystal oscillator.

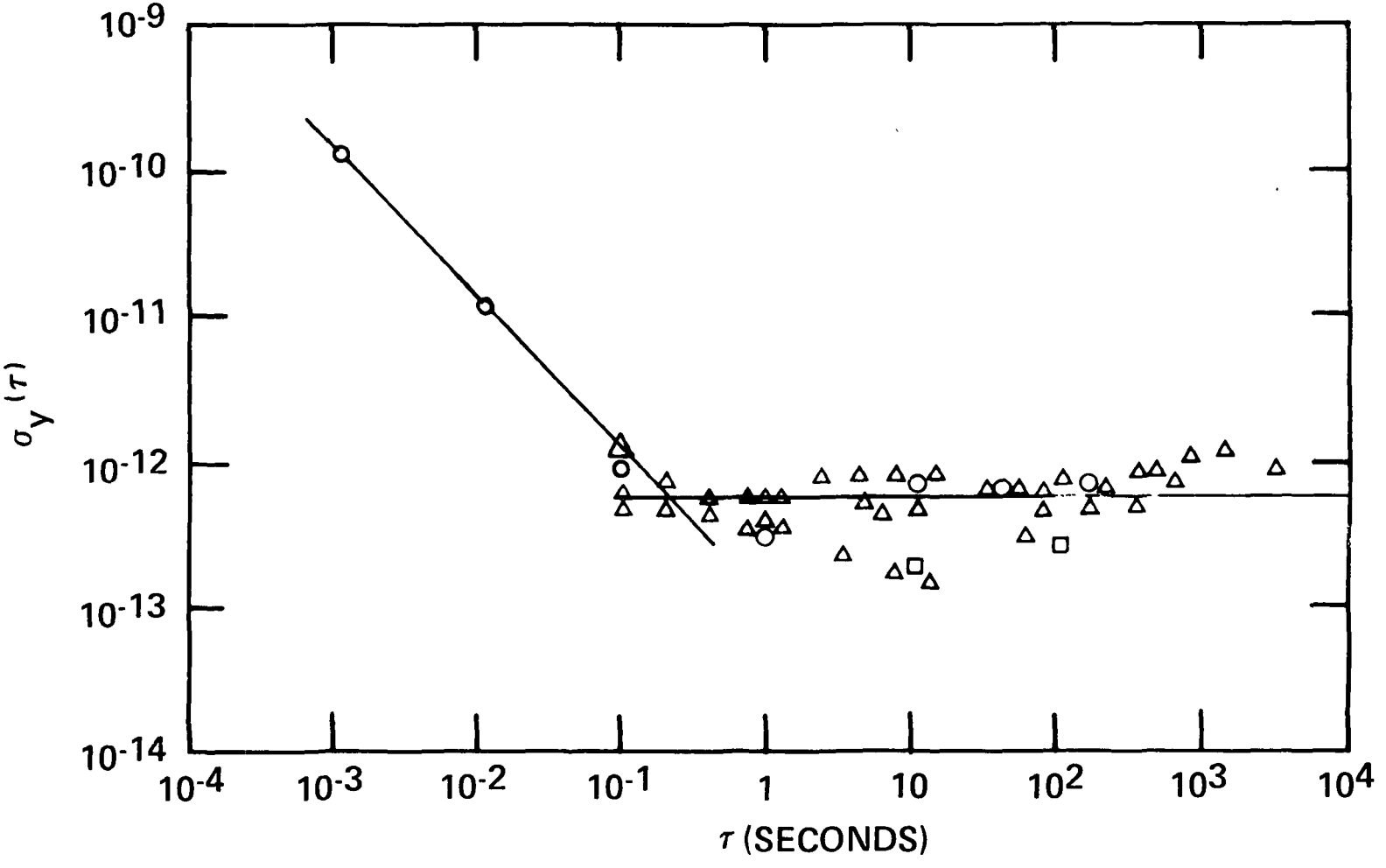


Figure 3. Frequency stability in time domain, $\sigma_y(\tau)$ vs τ, 5 MHz very high quality quartz crystal oscillator.

TABLE 2 DATA USED TO PLOT THE THEORETICAL NOISE SOURCES IN FIGURE 2

	FLICKER FREQ.		FLICKER PHASE		WHITE PHASE	
f	$S_\phi(f)$	$10\log S_\phi(f)$	$S_\phi(f)$	$10\log S_\phi(f)$	$S_\phi(f)$	$10\log S_\phi(f)$
10^0	1.58×10^{-12}	-118 db	3.16×10^{-13}	-125 db	3.98×10^{-15}	-144 db
10^1	1.58×10^{-15}	-148 db	-	-	3.98×10^{-15}	-144 db
10^2	-	-	3.16×10^{-15}	-145 db	3.98×10^{-15}	-144 db

TABLE 3 CALCULATED DATA FROM FREQUENCY DOMAIN TO TIME DOMAIN

	FLICKER PHASE		WHITE PHASE		FLICKER + WHITE	
τ	$\sigma^2(\tau)$	$\sigma(\tau)$	$\sigma^2(\tau)$	$\sigma(\tau)$	$\sigma^2(\tau)$	$\sigma(\tau)$
10^{-1}	6.52×10^{-25}	8.1×10^{-13}	1.21×10^{-24}	1.1×10^{-12}	1.86×10^{-24}	1.91×10^{-12}
10^{-2}	4.31×10^{-23}	6.6×10^{-12}	1.21×10^{-22}	1.1×10^{-11}	1.64×10^{-22}	1.76×10^{-11}
10^{-3}	2.10×10^{-21}	4.6×10^{-11}	1.21×10^{-20}	1.1×10^{-10}	1.42×10^{-21}	1.56×10^{-10}

TABLE 4 COMPARISON OF $\sigma(\tau)$ BETWEEN CALCULATED FROM FREQUENCY DOMAIN AND MEASURED IN TIME DOMAIN

	CALCULATED		MEASURED	
τ	FLICKER FREQUENCY	FLICKER PHASE + WHITE PHASE	FLICKER FREQUENCY	FLICKER PHASE + WHITE PHASE
-	2.96×10^{-13}	-	5×10^{-13}	-
10^{-1}	-	1.9×10^{-12}	-	1.6×10^{-12}
10^{-2}	-	1.8×10^{-11}	-	1.6×10^{-11}
10^{-3}	-	1.6×10^{-10}	-	1.6×10^{-10}

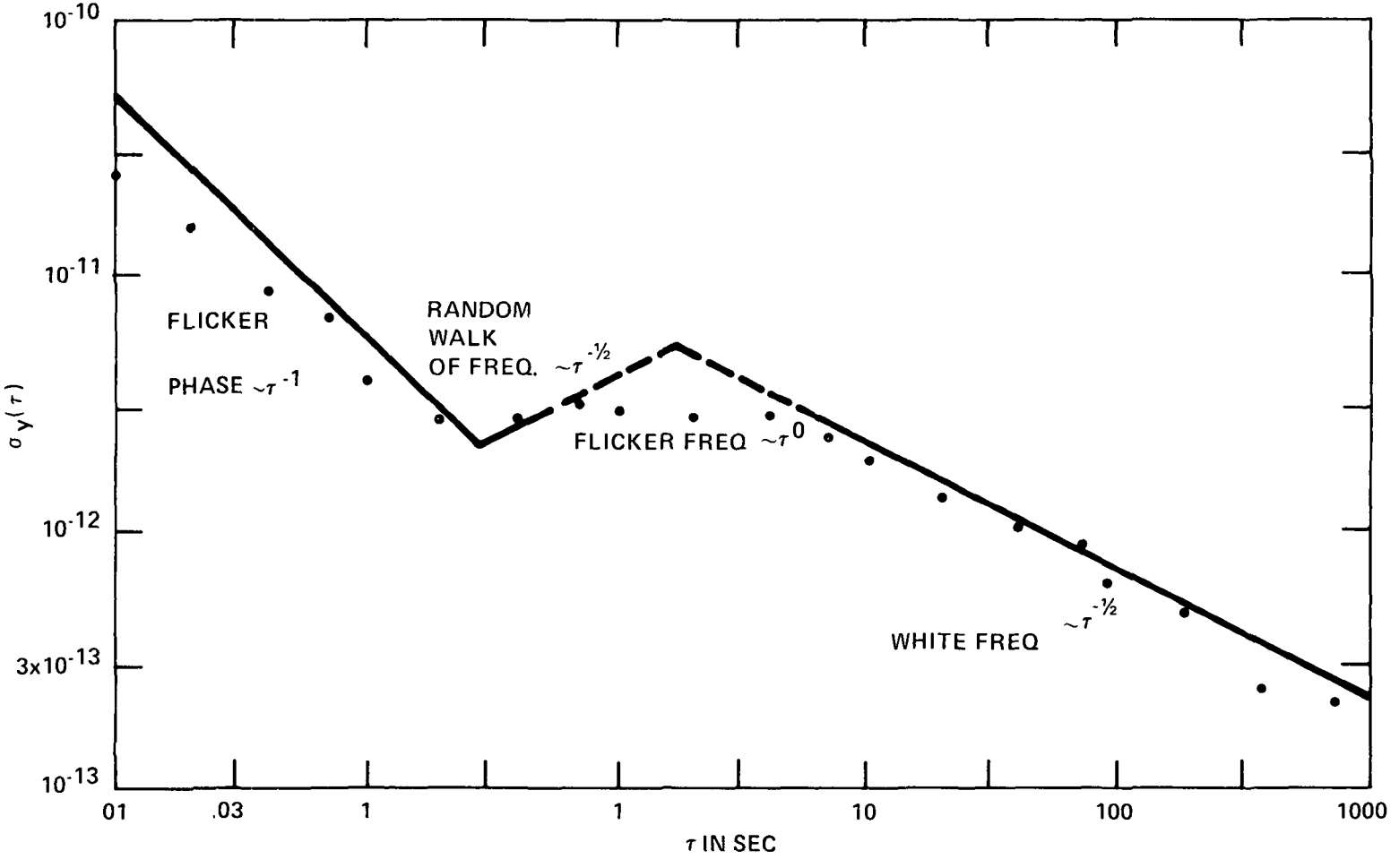


Figure 4. Frequency stability of a high performance cesium beam tube oscillator measured in the time domain

TABLE 5 CALCULATED DATA FROM TIME DOMAIN TO FREQUENCY DOMAIN

	DATA				CALCULATED RESULT			MEAS.
	$\mu^{1/2}$	τ	$\sigma(\tau)$	$S_\phi(f)$	f	$S_\phi(f)$	$10\log S_\phi(f)$	$10\log S_\phi(f)$
WHITE FREQ.	-1/2	10	2.3×10^{-12}	$2.64\times10^{-9}\, f^{-2}$	10^{-2}	2.64×10^{-5}	-45.7db	-46db
FLICKER FREQ.	0	1	3.0×10^{-12}	$1.62\times10^{-10} f^{-3}$	10^{-1}	1.62×10^{-7}	-67.9db	-68db
RANDOM WALK FREQUENCY	1/2	0.3	2.2×10^{-12}	$6.08\times10^{-11} f^{-4}$	1	6.08×10^{-11}	-102.2db	-102.4db
FLICKER PHASE	-1	10^{-1}	a 4.0×10^{-12}	$4.92\times10^{-12} f^{-1}$	10	4.92×10^{-13}	-123.1db	-129.6db
			a 2.5×10^{-11}	$2.45\times10^{-12} f^{-1}$		2.45×10^{-13}	-126.1db	
			b 5.6×10^{-12}	$9.64\times10^{-12} f^{-1}$		9.64×10^{-13}	-120.2db	
a = MEAS.			b 5.0×10^{-11}	$9.79\times10^{-12} f^{-1}$		9.79×10^{-13}	-120.1db	
b = TRANSL.		10^{-2}	a 4.0×10^{-12}		10^{2}	4.92×10^{-14}	-133.1db	-136.8db
			a 2.5×10^{-11}			2.45×10^{-14}	-136.1db	
			b 5.6×10^{-12}			9.64×10^{-14}	-130.2db	
			b 5.0×10^{-11}			9.79×10^{-14}	-130.1db	

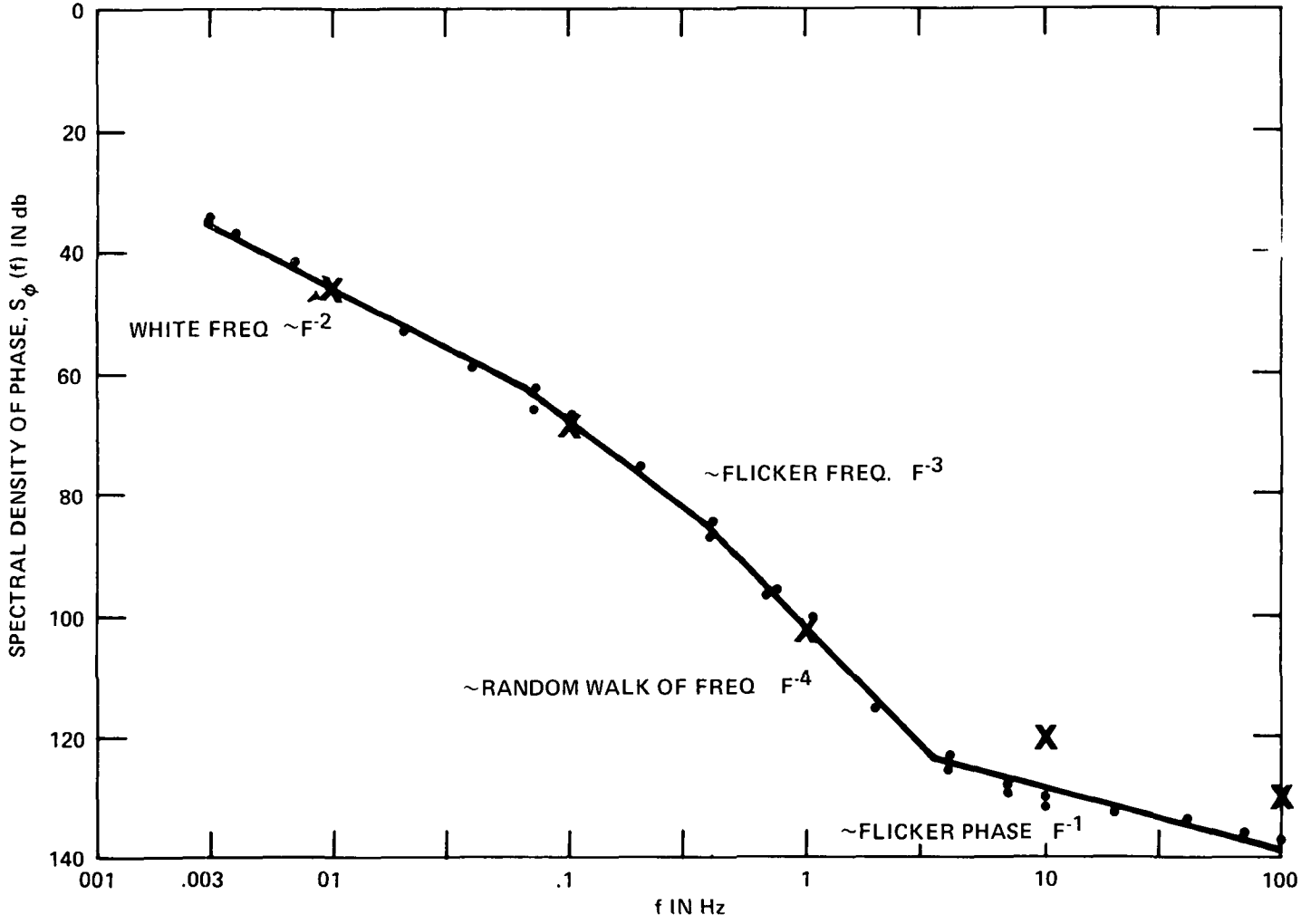
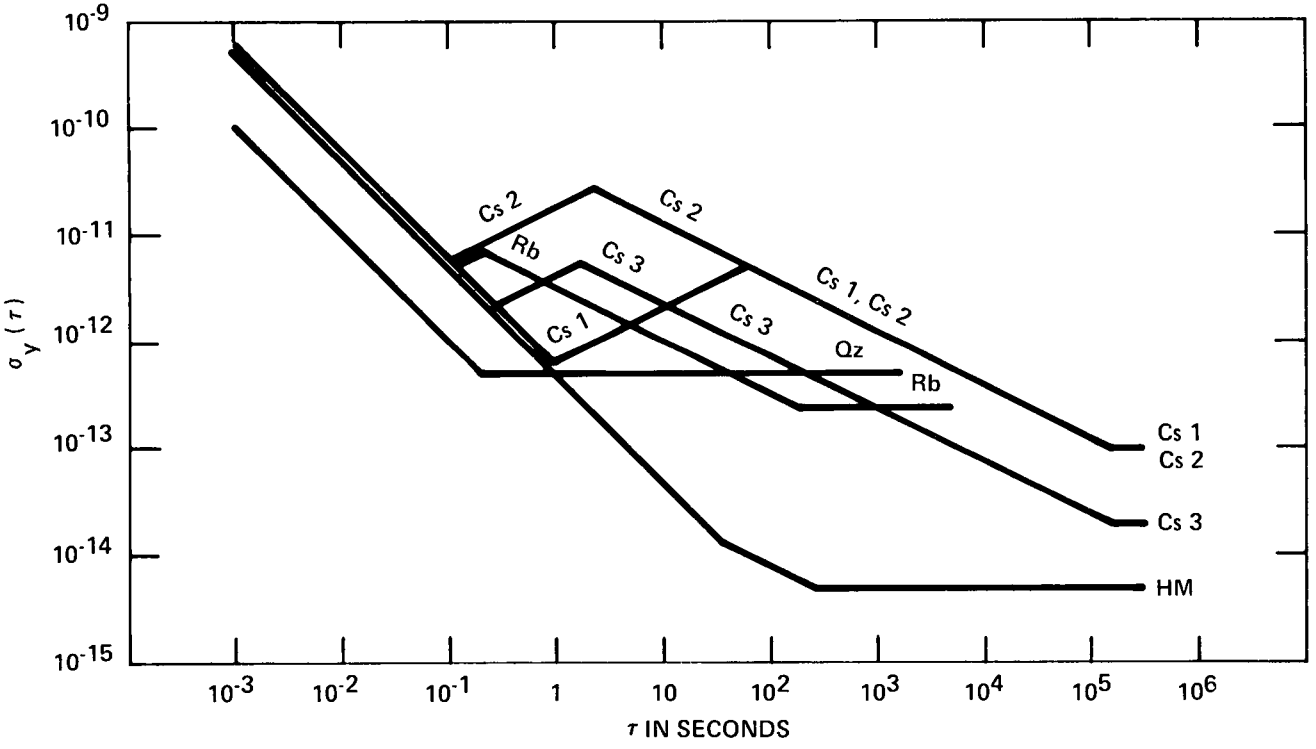
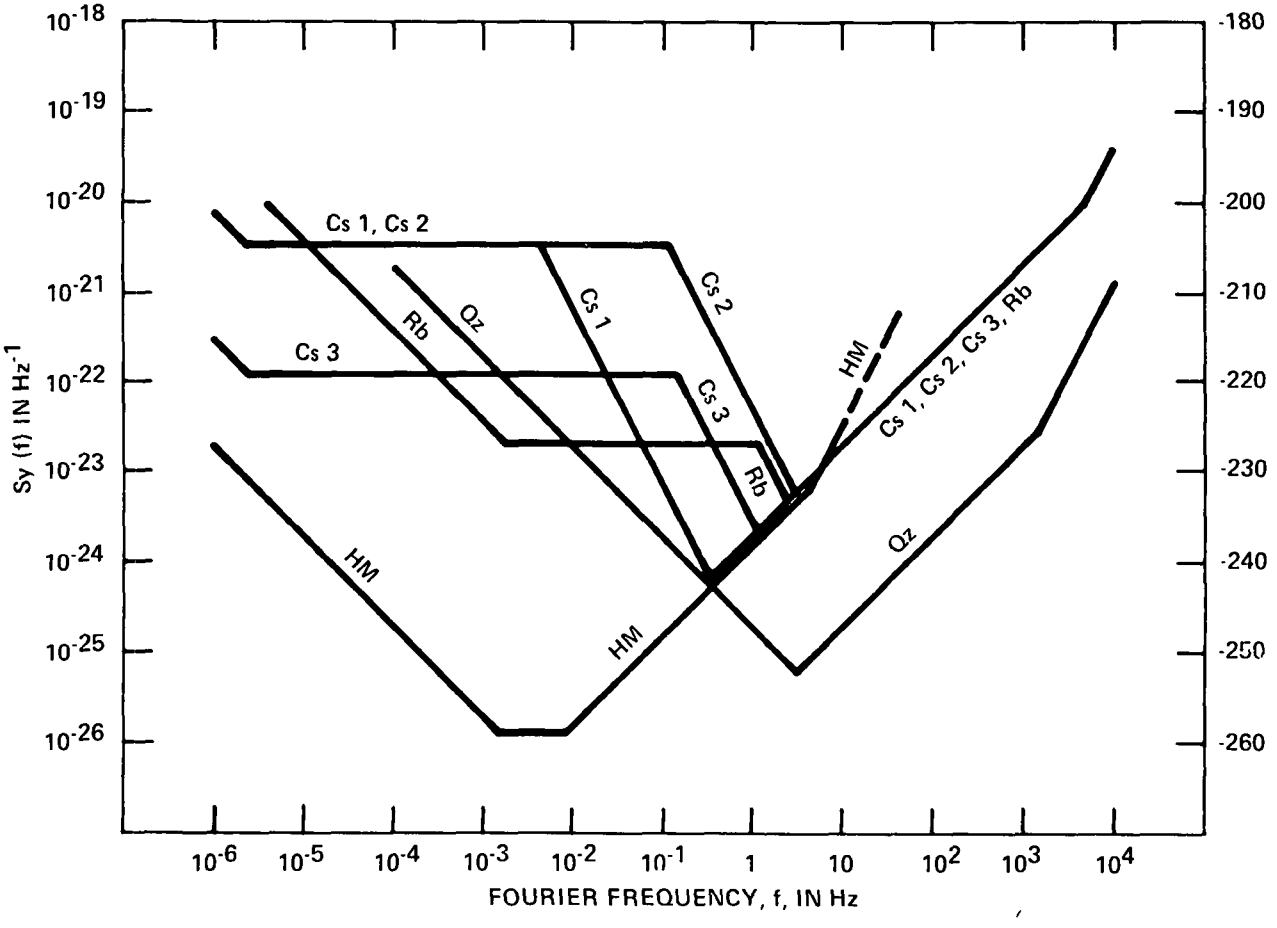


Figure 5 Spectral density of phase of a high performance cesium beam tube oscillator
The "Crosses" are points translated from the time domain for $f_h = 5 \times 10^4$ Hz $\nu_0 = 5$ MHz



OSC	SERVO LOOP TIME CONST (SEC)
Cs 1	60
Cs 2	2
Cs 3	2
Rb	0 3
Qz	—
HM	—

Figure 6 Frequency stability of typical atomic frequency standards and a selected quartz crystal controlled oscillator in the time domain (The positive slope portion of the curve is due to the electronic design of the frequency locked loop)



OCS	f_h (Hz)
Cs 1	10^4
Cs 2	10^4
Cs 3	10^4
Rb	10^4
Qz	10^4
HM	10

Figure 7 Spectral density of frequency of typical atomic frequency standards and a selected quartz crystal controlled oscillator in the frequency domain

REFERENCE

1. Audoin, C. and Vanier, J., "Atomic Frequency Standards and Clocks," J of Phys. E Scien. Instr., Vol. 9, PP 697-720, 1976.

2. Winkler, Gernot M.R., "A Brief Review of Frequency Stability Measures," Proc. 8th Ann. PTTI Applications and Planning Meeting, PP 489-528, December 1976.

3. Rutman, J., "Oscillator Specifications: A Review of Classical and New Ideas," Proc. 31st Ann. Sym. on Freq. Control, PP 291-301, June 1977.

4. Barnes, James A., "Review of Methods for Measuring and Specifying Frequency Stability," Proc. 9th Ann. PTTI Applications and Planning Meeting.

5. Barnes, James A., et al, "Characterization of Frequency Stability," IEEE Trans. in Instr. and Meas., Vol. IM-20, No. 2, PP 105-120, May 1971.

6. Brandenberger, H., Hadorn, F., Halford, D., and Shoaf, J.H., "High Quality Crystal Oscillators: Frequency Domain and Time Domain Stability," Proc. 25th Ann. Sym. Freq. Control," PP 226-230, April 1971.

7. Meeks, M. L., Editor, "Methods of Experimental Physics, Vol 12 - Part C, Astrophysics Radio Observatories," Chapter 5.4, "Frequency and Time Standards," by R.F.C. Vessot, PP 198-227, Academic Press 1976.

8. Babitch, D., and Oliverio, J., "Phase Noise of Various Oscillators at Very Low Fourier Frequencies," Proc. 28th Ann. Sym. on Freq. Control, PP 150-159, 1974.

9. Fischer, M.C., "Frequency Stability Measurement Procedures," Proc. 8th Ann. PTTI Applications and Planning Meeting, pp 575-677, December 1976.

DR. JACQUES VANIER, Laval University:

There is a question where you have the transition in the phase lock or frequency lock loop. There I think the table you have shown for transferring from the time to the frequency domain cannot be applied directly like that. And you cannot identify the kind of noise because you have a transition, and this may change the slope quite a lot. This also depends on the damping factor or the time constant in the servo loop.

MR. CHI: Correct.

DR. VANIER:

So, what I wanted to mention is that at some places we have a flat portion in the sigma-tau curve. This is not flicker noise of frequency, but just a question of the servo loop.

MR. CHI:

Within the servo loop, of course, it is partly a parameter for the manufacturers who are designing that system. He would have to tell what is the optimum for his own system.

DR. JAMES A. BARNES, National Bureau of Standards:

I would like to make one comment that is perhaps obvious, but I think it is worth mentioning anyway. One is using these examples, models, where you have super positions of noise. The noise laws that one talks about are the asyntotic behaviors. When you superimpose them, actually you don't make a sharp transition at a sharp corner from a slope minus 1, say, to a slope 0. It is a smooth transition, and when you actually go through the process of filling it in, you get smooth curves, not corners. And when you try to fit the sharp cornered curves, there is a tendency to put in more terms than necessary. The modeling can be done much more straightforward.

DR. GERNOT M. R. WINKLER, U. S. Naval Observatory:

My own opinion is that one really shouldn't make these conversions but that one should measure in that domain in which one needs to have the values.

COMPARISON OF THEORETICAL AND OBSERVED HYDROGEN MASER STABILITY LIMITATION DUE TO THERMAL NOISE AND THE PROSPECT FOR IMPROVEMENT BY LOW-TEMPERATURE OPERATION

R. F. C. Vessot, M. W. Levine, and E. M. Mattison
Center for Astrophysics
Harvard College Observatory and Smithsonian Astrophysical Observatory
Cambridge, Massachusetts 02138

ABSTRACT

Expressions describing the limitations to hydrogen maser stability due to random thermal noise are derived in terms of parameters that govern the operation of the maser oscillator. Possible effects from cavity pulling have been included by the ad hoc assumption of a random cavity resonance frequency variation characterized by a f^{-1} spectrum. The measured stability of the recently developed SAO VLG-11 masers is compared with the predicted stability limitations, and good agreement with theory is found for averaging times τ between 0.83 sec and 4.2×10^3 sec. The best observed Allan variance is $\sigma(2, 4.2 \times 10^3, 4.2 \times 10^3, 6) = 6 \times 10^{-16}$. For $\tau > 4.2 \times 10^3$ sec systematic variations appear to dominate the data, and the variance representation is no longer appropriate.

Using the stability limitation expressions we analyze the consequences of low temperature maser operation. We find that if the wall relaxation probability per collision remains at or below its room temperature value, there is a high likelihood of substantial improvement in maser performance from operation at cryogenic temperatures.

INTRODUCTION

The invention of the atomic hydrogen maser by Kleppner, Goldenberg and Ramsey in 1960[1] resulted from a search for means of reducing the resonance linewidth of an atomic clock by increasing the unperturbed interaction time of atoms in the microwave field that causes resonance transitions. An additional attractive feature that stimulated the search was the possibility of operating an atomic frequency standard as a microwave self-oscillator as had been done by Townes and by Basov in their pioneering work[2, 3] using the ammonia molecule as a maser oscillator.

Early results from the hydrogen maser indicated that storage times of about 1 sec could be realized by reflecting hydrogen atoms from surfaces coated with

This work is supported by NASA's George C. Marshall Space Flight Center and Jet Propulsion Laboratory and also by the Office of Naval Research.

alkylchloro-silanes (Dri-Film) or with Teflon. By using this type of wall coating in the maser storage bulb, oscillator line Q's on the order of 10^9 were achieved.

Predictions of the stability of such high Q oscillators were made using traditional methods[1] that assume that instability is due mainly to thermal noise within the oscillator linewidth. These predictions indicated that the stability should vary as $\tau^{-1/2}$, where τ is the averaging time interval, according to the expression

$$\frac{\Delta f}{f} = \frac{1}{Q_\ell} \sqrt{\frac{kT}{2 P_b \tau}} \quad . \tag{1}$$

Here Q_ℓ is the effective quality factor of the atomic resonance (the line Q), P_b is the power delivered by the radiating atoms to the resonant cavity, k is the Boltzmann constant, and T is the absolute temperature.

Early measurements of maser stability[4] indicated that other noise processes completely overwhelmed the noise source described by equation (1). Cross-correlation tests[5] of maser signals showed that the major source of maser instability was additive white phase noise within the bandwidth of the receiving or measuring system. In general, this noise could be described as due to an r.m.s. phase deviation, $\Delta\phi = \sqrt{(K kT B/P_o)}$, where F is the noise figure of the receiver, B is the effective noise bandwidth of the receiver, and P_o is the power input to the receiver. In terms of a frequency stability measurement over a time interval τ, we have

$$\frac{\Delta f}{f} = \frac{\Delta\phi}{2\pi f \tau} = \frac{1}{2\pi f \tau} \sqrt{\frac{F kT B}{P_o}} \quad . \tag{2}$$

The two noise processes, one identified with noise energy whose spectral components lie within the oscillator linewidth and the other with noise energy lying within the bandwidth of the receiver, can be combined as uncorrelated processes[6] to give

$$\frac{\Delta f}{f} = \left[\frac{kT}{2}\left(\frac{FB}{2\pi^2 f^2 P_o \tau^2} + \frac{1}{Q_\ell^2 P_b \tau}\right)\right]^{1/2} \quad . \tag{3}$$

Note that a distinction is made here between the oscillator power level P_b and the power delivered to the receiver system, P_o.

As the development, building, and testing of hydrogen masers continued, the stability data[7] agreed fairly well with equation (3), but the stability plot almost invariably flattened out for long averaging times, becoming proportional to τ^0. This behavior could be characterized by a spectral distribution known as flicker of frequency noise.[8] It appeared to be due to a combination of systematic effects chiefly associated with the maser's resonant cavity. Variations Δf_c in the cavity resonance frequency pull the maser output frequency by an amount

$$\Delta f_{out} = \frac{Q_L}{Q_\ell} \Delta f_c \quad , \tag{4}$$

where Q_L is the loaded cavity Q.

The statistical effect of such pulling can be included in the variance expression in equation (3) if we postulate that Δf_c can be assigned a spectral behavior to describe its frequency fluctuations. In view of the observed data the logical choice is to assume that Δf_c follows the 1/f spectral law, and write the power spectral density of cavity frequency variations as

$$S_{y_c} = \frac{h_c}{f} \quad , \tag{5}$$

where h_c is a proportionality constant. We can thus express the power spectral density of the output as

$$S_y(f) \equiv \frac{h_{-1}}{f} = \left(\frac{Q_L}{Q_\ell}\right)^2 \frac{h_c}{f} \quad . \tag{6}$$

If this spectral process is uncorrelated with the others, we can include it in expression (3) for the variance.

Before we do this it is appropriate to describe the variance in terms of the two-sample or Allan variance $\sigma(2, T, \tau, B)$, where τ is, as before, the averaging interval, T is the time between the beginning of one such interval and the beginning of the next in a time-ordered progression of data, and B is the noise bandwidth of the receiver. For the case where $T > \tau$, i.e., there is "dead time" between data samples, and for the two types of noise processes represented by equation (3), we have

$$\sigma(2, T, \tau, B) = \frac{\Delta f}{f} \quad .$$

Since we desire to continue using the two-sample variance when we include the cavity flicker effect, we must represent the flicker variance σ_f as

$$\sigma_f(2, T, \tau, B) = \frac{h_{-1}}{2} \left[-2\left(\frac{T}{\tau}\right)^2 \ell n \frac{T}{\tau} + \left(\frac{T}{\tau} + 1\right)^2 \ell n \left(\frac{T}{\tau} + 1\right) + \left(\frac{T}{\tau} - 1\right)^2 \ell n \left(\frac{T}{\tau} - 1\right) \right] \quad .$$

In our practice $(T - \tau)/\tau = 0.83/\tau$ so that $(T - \tau)/\tau < 0.01$ for $\tau > 83$ sec and we can write approximately

$$\sigma_f(2, T, \tau, B) \simeq h_{-1}\, 2\, \ell n 2 \quad .$$

Thus for $(T-\tau)/\tau \ll 1$ the total Allan variance is

$$\sigma(2,T,\tau,B) \simeq \left[\frac{kT}{2}\left(\frac{FB}{2\pi^2 f^2 P_o \tau^2}+\frac{1}{Q_\ell{}^2 P_b \tau}\right)+h_c \frac{Q_L{}^2}{Q_\ell{}^2}\, 2\,\ell n2\right]^{1/2} . \quad (7)$$

According to the above description, the $\tau^{-1/2}$ behavior of σ can be observed if the h_c factor describing the cavity resonance frequency variations is sufficiently small. An example of this is shown in Figure 1,[9] where we see that improving the power level P_b degrades the line Q owing to spin-exchange relaxation and, for a given level of cavity instability the flicker floor, or τ^0, data can combine with the τ^{-1} data in such a way as to obscure the $\tau^{-1/2}$ behavior.

STABILITY EXPRESSED IN TERMS OF THE MASER OPERATING PARAMETERS

The foregoing discussion has dealt with the operation of the hydrogen masers in terms of overall parameters. We now look more closely at the behavior of the hydrogen maser and seek to optimize its performance for various applications by considering its internal parameters.

Figure 2 (after Kleppner et al.[10]) shows the relation between oscillation power P_b and atomic flux I. The functional relationship between flux and power depends on a parameter, q, a threshold flux, I_{th}, and a critical power level, P_c. These three parameters are defined as follows:

$$q = \frac{\hbar}{8\pi \mu_o{}^2}\frac{I_{tot}}{I}\left(1+\frac{\gamma_w}{\gamma_b}\right)\frac{V_c}{\eta V_b}\frac{\sigma_{se}(T)\, v_r(T)}{Q_L} . \quad (8)$$

The value of q must be less than 0.172 for oscillation to occur.

$$P_b = \frac{\omega \hbar^2}{8\pi \mu_o{}^2}\frac{V_c}{\eta}\frac{1}{Q_L}(\gamma_b+\gamma_w)^2\left[-2q^2\left(\frac{I}{I_{th}}\right)^2+(1-3q)\frac{I}{I_{th}}-1\right] . \quad (9)$$

This assumes wall relaxation processes for which $\gamma_{1w} = \gamma_{2w}$.

$$I_{th} = \frac{\hbar V_c (\gamma_b+\gamma_w)^2}{4\pi \mu_o{}^2 Q_L \eta} . \quad (10)$$

In these equations,

ω = $2\pi f$, where f is the hydrogen hyperfine separation transition frequency.
$\hbar$ = Planck's constant/2π.
μ_o = the Bohr magneton.

I_{total} = the total flux entering the bulb.
I = the flux in the $F=1$, $m_F=0$ hyperfine sublevel of atomic hydrogen.
γ_w = the wall relaxation rate for loss of phase coherence.
γ_b = the loss rate of atoms from the bulb.
V_c = the resonant cavity volume.
V_b = the storage bulb volume.

$$\eta = \frac{(H_z \text{ averaged over bulb volume})^2}{H^2 \text{ averaged over the cavity volume}} = \text{"filling factor"}$$

where H is the rf magnetic field strength in the cavity and H_z is its component along the z axis.

$\sigma_{se}(T)$ = the spin exchange cross section, which depends on the speed of interatomic collisions and therefore on temperature.
$v_r(T)$ = the average relative velocity of the hydrogen atoms in the bulb.
Q_L = the loaded Q of the cavity resonator.

We have

$$\frac{1}{Q_L} = \frac{1}{Q_o} + \frac{1}{Q_{ext}}.$$

where Q_o is the unloaded Q of the resonator and Q_{ext} represents the loading due to the external circuitry coupled to the cavity.

We can express the line Q in terms of the parameter q and the beam flux as follows:

$$Q_\ell = \frac{\omega}{2\gamma} = \frac{\omega}{2(\gamma_b + \gamma_w + \gamma_{se})} = \frac{\omega}{2(\gamma_b + \gamma_w)\left(1 + q\frac{I}{I_{th}}\right)} . \qquad (11)$$

where γ_{se} is the relaxation rate due to spin exchange. If we substitute the above expressions for Q_ℓ, P_b, and I_{th} into the stability expressions given in equations (1), (2), and (3), we have for the noise limit due to noise within the oscillation linewidth

$$\sigma_o = \frac{\Delta f}{f} = \frac{1}{Q_\ell}\left(\frac{\frac{1}{2}kT}{P_b \tau}\right)^{1/2}$$

$$= \left[\frac{16\pi}{\omega^3} kT \frac{\mu_o \eta}{\hbar^2 V_c} \frac{Q_L}{\tau} \frac{\left(1 + q\frac{I}{I_{th}}\right)^2}{-1 + (1-3q)\frac{I}{I_{th}} - 2q^2\left(\frac{I}{I_{th}}\right)^2}\right]^{1/2} \qquad (12)$$

and for the additive noise limit

$$\sigma_a = \frac{1}{\omega\tau}\left(\frac{FkTB}{P_b}\frac{Q_{ext}}{Q_L}\right)^{1/2}$$

$$= \left\{\frac{8\pi}{\omega^3}\frac{FkTB\eta}{\hbar^2 V_c}\frac{Q_{ext}}{(\gamma_b+\gamma_w)^2}\frac{1}{\tau^2}\frac{1}{\left[-1+(1-3q)\frac{I}{I_{th}}-2q^2\left(\frac{I}{I_{th}}\right)^2\right]}\right\}^{1/2} \qquad (13)$$

These relations allow us to relate the stability limit to the operating conditions of the maser and to optimize the stability for a given averaging time interval τ.

In addition to the thermal noise terms we can, as before, include the systematic effect of cavity mistuning if we characterize the mistuning by a flicker-of-frequency behavior. Substituting for Q_ℓ in equation (6) we have

$$\sigma_f = \frac{2Q_L}{\omega}(\gamma_w+\gamma_b)(1+q\,I/I_{th})^2(h_c\,2\ell n2)^{1/2} \quad ,$$

and the complete expression for the stability is given by

$$\sigma(2,T,\tau,B) = \left\{\frac{Q_L^2}{\omega^2}4(\gamma_w+\gamma_b)^2(1+q\,I/I_{th})^2 h_c\,2\ell n2\,\tau^0\right.$$

$$+\frac{16\pi kT}{\omega^3\hbar^2 V_c}\frac{\mu_o\eta Q_L\left(1+q\frac{I}{I_{th}}\right)^2}{\left[-1+(1-3q)\frac{I}{I_{th}}-2q^2\left(\frac{I}{I_{th}}\right)^2\right]}\tau^{-1}$$

$$\left.+\frac{8\pi kT}{\omega^3\hbar^2 V_c}\frac{F\,Q_{ext}\,B}{(\gamma_b+\gamma_w)^2\left[-1+(1-3q)\frac{I}{I_{th}}-2q^2\left(\frac{I}{I_{th}}\right)^2\right]}\tau^{-2}\right\}^{1/2} \qquad (14)$$

This expression, which relates the statistical behavior of the maser's stability to its internal operating parameters, contains a great deal of information and gives a considerable amount of insight to the compromises and tradeoffs that must be considered in designing a device for a given application. For example if we choose an operating point by fixing q and I/I_{th}, we see that the value of $(\gamma_w+\gamma_b) \equiv \Gamma$ chosen for a particular design affects the τ^0 portion of σ as Γ, the $\tau^{-1/2}$ portion as Γ^0, and the τ^{-1} portion as Γ^{-1}. The tradeoff between short-term and long-term stability is very evident here.

The appearance in equation (14) of Q_{ext}, the external loading Q, and of Q_L, the loaded cavity Q, also is of considerable interest. At first glance it would appear that we should make Q_o, the intrinsic cavity Q, as high as possible, then make Q_L and Q_{ext} as low as possible by overcoupling. However, if we look more critically we see that heavy external loading can be harmful because the cavity resonance frequency (which necessarily depends on Q_{ext}) can be

shifted by such effects as line variations owing to temperature or by variations in the input impedance of the receiver. The fact that Q_L appears in the τ^0 portion of the stability function as Q_L^2 may tempt us to reduce Q_L by loading the cavity heavily, but systematic effects can negate any such benefits.

We have arbitrarily added the effect of cavity pulling in the stability equation to illustrate the effect of line Q in competition with the cavity Q; there is no physical reason that the cavity effect will have the assigned flicker-like behavior. Furthermore, if cavity perturbations can be reduced, it should be possible to see the underlying $\tau^{-1/2}$ behavior of σ due to thermal noise within the oscillator linewidth.

COMPARISON OF VLG-11 STABILITY DATA WITH THEORY

During the past summer we have had the opportunity to make measurements on the newly developed VLG-11 masers[11, 12] that were described at last year's P.T.T.I. conference. The sensitivity of the maser to magnetic, thermal, and barometric variations have been reported elsewhere;[13] there is no measurable barometric effect and the sensitivity to temperature and magnetic fields have been diminished by a factor of approximately 3 from the previous VLG-10A design used as ground station equipment for the 1976 gravitational redshift mission.

The stability data obtained from the VLG-11 tests are shown in Figure 3 along with the operating parameters for the test. The stability data closely follow the theoretical limit for averaging intervals from 0.83 sec to 1 hr. The best stability is $\sigma(2, 4.2 \times 10^3, 4.2 \times 10^3, 6) = 6 \times 10^{-16}$. For $\tau > 4.2 \times 10^3$ the statistical representation of the data shows the evidence of the slow drift that seemed to be the result of incomplete thermal stabilization of the masers and of variations in the laboratory temperature. Representing such systematic effects by a statistical variance is inappropriate.

The stability for $\tau < 1$ hr is limited by thermal noise. Perhaps it could be improved by operating the maser at more nearly optimum conditions, but we believe the improvement would not be a large one. Clearly, if a major improvement is to be made it will have to be the result of a substantial change in the parameters in equation (14) that describe the operating condition of the maser.

SPECULATION ON THE COLD HYDROGEN MASER

Recently the preliminary results of experiments on cold atomic hydrogen by Professor Daniel Kleppner and his co-workers at the Massachusetts Institute of Technology were brought to our attention by Professor Irwin Shapiro, who suggested that these data might offer new insights to hydrogen maser developments. Kleppner and his co-workers found that atomic hydrogen could be stored as a gas at 4 K even though molecular hydrogen freezes at 14 K.

It appears that the retention of atomic hydrogen is made possible by the presence of a coating of frozen molecular hydrogen on the walls of the storage vessel. If such a coating became contaminated with impurity atoms, atomic hydrogen would recombine on the impurity sites to form H_2, thus renewing the continuous hydrogen film. This would be an attractive property for a hydrogen maser storage bulb.

To illustrate the behavior of a cold hydrogen maser, we must establish a set of oscillation conditions. We can fix an operating point in Figure 2 by holding q and I/I_{th} constant as we lower the temperature. In this example we will also keep the cavity and bulb dimensions constant and assume that the wall relaxation probability remains unchanged.

The parameter q contains two temperature-dependent terms, the spin-exchange cross section, σ_{se}, and the average relative velocity, $\overline{v_r}$. The dependence of σ_{se} on temperature is given by Allison[14] and is shown in Figure 4.

If we lower the temperature from 322 K to 4 K, we see that σ_{se} decreases by a factor of about 22 and the velocity decreases by the factor $\sqrt{322/4} \approx 9$. The ratio $[\sigma_{se}(322)\ v_r(322)]/[\sigma_{se}(4)\ v_r(4)]$ is about 198, so in order to keep $q(322\ K) = q(4\ K)$, we can decrease Q_L by a factor of 198. In practice this would be done by overcoupling the cavity so that $Q_{ext}(4\ K) \ll Q_o(4\ K)$. If, for example, $Q_L(322\ K) = 3.5 \times 10^4$, we find that $Q_L(4\ K)$ should be made about $(3.5 \times 10^4)/198 \approx 177$, and $Q_{ext} \approx 177$. That the system should oscillate with such a remarkably low cavity Q is due to the long storage time produced by the low temperature.

Cooling the maser will also affect Q_ℓ and from the right-hand side of equation (11) we see that if we keep I/I_{th} unchanged Q_ℓ will increase by the ratio $\sqrt{322/4}$, since both γ_b and γ_w are proportional to velocity and, hence, to $T^{1/2}$.

The pulling effect $\Delta f_{out} = (Q_L\, \Delta f_c)/Q_\ell$, which is the chief source of systematic drift in the maser, is reduced by a factor of $1776 = 198 \times \sqrt{322/4}$, since Q_ℓ is improved and Q_L is reduced.

In order to maintain the operating point we must keep I/I_{th} constant. The quantity I_{th} depends on the ratio $(\gamma_b + \gamma_w)^2/Q_L$. At 4 K this quantity increases by a factor of $198/80 \approx 2.5$, which means that we must increase the atomic hydrogen flux by this amount in order to meet the conditions for our comparison.

Figure 5 shows the projected improvement in the stability limit under the above conditions. In this example we assume that the receiver noise figure F improves from 6 to 2 (7.8 db to 3 db) because the receiver's low noise preamplifier is considered to be at the same low temperature as the maser. The output power level depends on $(\gamma_b + \gamma_w)^2/Q_L$ and, under the assumptions of this example, is seen to increase by the factor $198/\sqrt{322/4} \simeq 22$ or 13 db. Based on the comparison with the actual SAO VLG-11 maser data,[12] we could expect an output power level of -85 dbm.

Maser operation at low temperatures leaves open other possibilities for improvement resulting from such phenomena as the reduction of thermal coefficients of expansion, the possibility of superconducting circuitry (including the cavity), and the use of superconducting magnetic shields.

As mentioned earlier, the big question is whether or not the hydrogen atom will successfully bounce off a frozen molecular hydrogen wall (or, if necessary, some other type of wall not yet specified). The wall relaxation term, $\gamma_w = \bar{v}/\lambda p$, contains p, the probability per collision of atomic relaxation by loss of phase coherence.

At present, the only data we know of that relate p to temperature are due to M. Desaintfuscien.[15] Figure 6 (from ref. 15) shows the relaxation probability per bounce for a F.E.P. Teflon-coated bulb. These data show a slight decrease in p as temperature is decreased to 76 K. Whether or not the probability stays reasonably low as we go from 76 K to 4 K is a very important question, as is the question of the magnitude and stability of the wall shift at these low temperatures.

To test the feasibility of low-temperature operation, we have begun a program to construct a maser that will operate at low temperatures. Figure 7 is a schematic view of our planned apparatus. The dewar that houses the TE 111 mode cavity assembly[16] has an inside diameter of 7" and is enclosed in a set of magnetic shields. The first tests will be made at the boiling point of liquid nitrogen (~77 K) to verify that we can reproduce Desaintfuscien's results for F.E.P. Teflon wall coatings.

We will then bring the dewar to liquid helium temperature while continuing pulsed operation and carefully monitoring the temperature of the cavity as it is cooled past 20 K, the condensing point of hydrogen, and 14 K, the freezing point of hydrogen. Successful pulsed operation below these temperatures will verify the storage of spin-aligned atomic hydrogen and will be a critical test of the device.

To prevent impurity atoms from reaching the interior of the cavity, a carefully located beam stop will be placed at the exit of the state selector magnet. At 4 K the cryostat itself becomes an extremely effective vacuum pump that will scavenge, by condensation and freezing, all stray gas other than helium in the system. The cavity assembly, by virtue of its thermal lag, will stay relatively clean until it, in turn, cools and condenses gas. It will then be possible to introduce in a controllable way gases such as argon or H_2 to serve as frozen-on wall coatings, and to observe the effect of these coatings on the relaxation rate of the hydrogen.

CONCLUSIONS

The relationship of the maser oscillation parameters to the ultimate stability of masers provides considerable insight into the behavior of masers. Further

work would be useful. A systematic parametrization of maser performance can be made using computer techniques, and a more general treatment of wall relaxation can be made by eliminating the requirement made here that $\gamma_{1w}=\gamma_{2w}$.

It must be recognized that our approach is valid only for stochastic processes such as thermal noise. Systematic limitations of known origin can be included if the perturbation has a reasonably well understood spectrum, even though the physical basis for the spectrum is in question.

Whether or not the cold maser will work can only be determined by experiment and we look forward to observing the behavior of the maser as temperature is decreased. The prospect for making relativity measurements such as tests for gravity waves using precise intersatellite doppler measurements would be very much improved if stability in the 10^{-17} level can be demonstrated.

We would like to thank Drs. D. Kleppner, S. Crampton, and I. Shapiro of M.I.T. for many useful and interesting discussions.

REFERENCES

[1]Kleppner, D., H.M. Goldenberg, and N.F. Ramsey. Phys. Rev., vol. 126, No. 2, pp. 603-615 (1962).
[2]Gordon, J.P., H.J. Zeiger, and C.H. Townes. Phys. Rev., vol. 95, p. 282, (1954).
[3]Basov, N.G. and A.M. Prokhorov. J. Expl. Theoret. Phys. (U.S.S.R.), vol. 27, p. 431 (1954).
[4]Vessot, R.F.C. Proc. 3rd International Conference on Quantum Electronics, (Paris), Grivet and Bloembergen, eds., Columbia University Press, N.Y., pp. 409-417 (1963).
[5]Vessot, R., L. Mueller, and J. Vanier. Proc. I.E.E.E., vol. 54, No. 2, pp. 199-207 (1966).
[6]Cutler, L.S., and C.L. Searle. Proc. I.E.E.E., vol. 54, No. 2, pp. 136-154 (1966).
[7]Finnie, C., R. Sydnor, and A. Sward. Proc. 25th Frequency Control Symposium, U.S. Army Electronics Command, Ft. Monmouth, New Jersey, pp. 348-351 (1971).
[8]Barnes, J.A. et al. IEEE Trans. Instr. Meas., vol. IM-20, No. 2, pp. 105-120 (1971).
[9]Vessot, R.F.C., M.W. Levine, P.W. Zitzewitz, P. Debely, and N.F. Ramsey. In Precision Measurement and Fundamental Constants, D.N. Langenberg, ed., N.B.S. Special Publication No. 343, pp. 27-37 (1971).
[10]Kleppner, D., S.B. Crampton, N.F. Ramsey, R.F.C. Vessot, H. Peters, and J. Vanier. Phys. Rev., vol. 138, No. 4A, pp. A972-A983 (1965).
[11]Levine, M.W., R. Vessot, E. Mattison, T. Hoffman, G. Nystrom, D. Graveline, R. Nicoll, C. Dovidio, and W. Brymer. In Proc. 8th Annual Precise Time and Time Interval (P.T.T.I.) Applications and Planning Meeting, U.S. Naval Research Laboratory, Wash., D.C., pp. 249-276 (1976).

[12]Levine, M.W., R. Vessot, E. Mattison, G. Nystrom, T. Hoffman, and E. Blomberg. A new generation of SAO hydrogen masers. Proc. 31st Annual Frequency Symposium on Frequency Control, U.S. Army Electronics Command, Ft. Monmouth, New Jersey, pp. 525-534 (1977).
[13]Vessot, R.F.C., M.W. Levine, and E.M. Mattison. A report on the evaluation of the performance of the Smithsonian Astrophysical Observatory VLG-11 atomic hydrogen masers. Smithsonian Astrophysical Observatory, Cambridge, Mass. (November 1977).
[14]Allison, A.C. Phys. Rev. A., vol. 5, No. 6, pp. 2695-2696 (1972).
[15]Desaintfuscien, M. Ph.D. Thesis, University of Paris (1975).
[16]Mattison, E.M., M.W. Levine, and R.F.C. Vessot. New TE 111 mode hydrogen maser. In Proc. 8th Annual Precise Time and Time Interval (P.T.T.I.) Applications and Planning Meeting, U.S. Naval Research Laboratory, Wash., D.C., pp. 355-367 (1976).

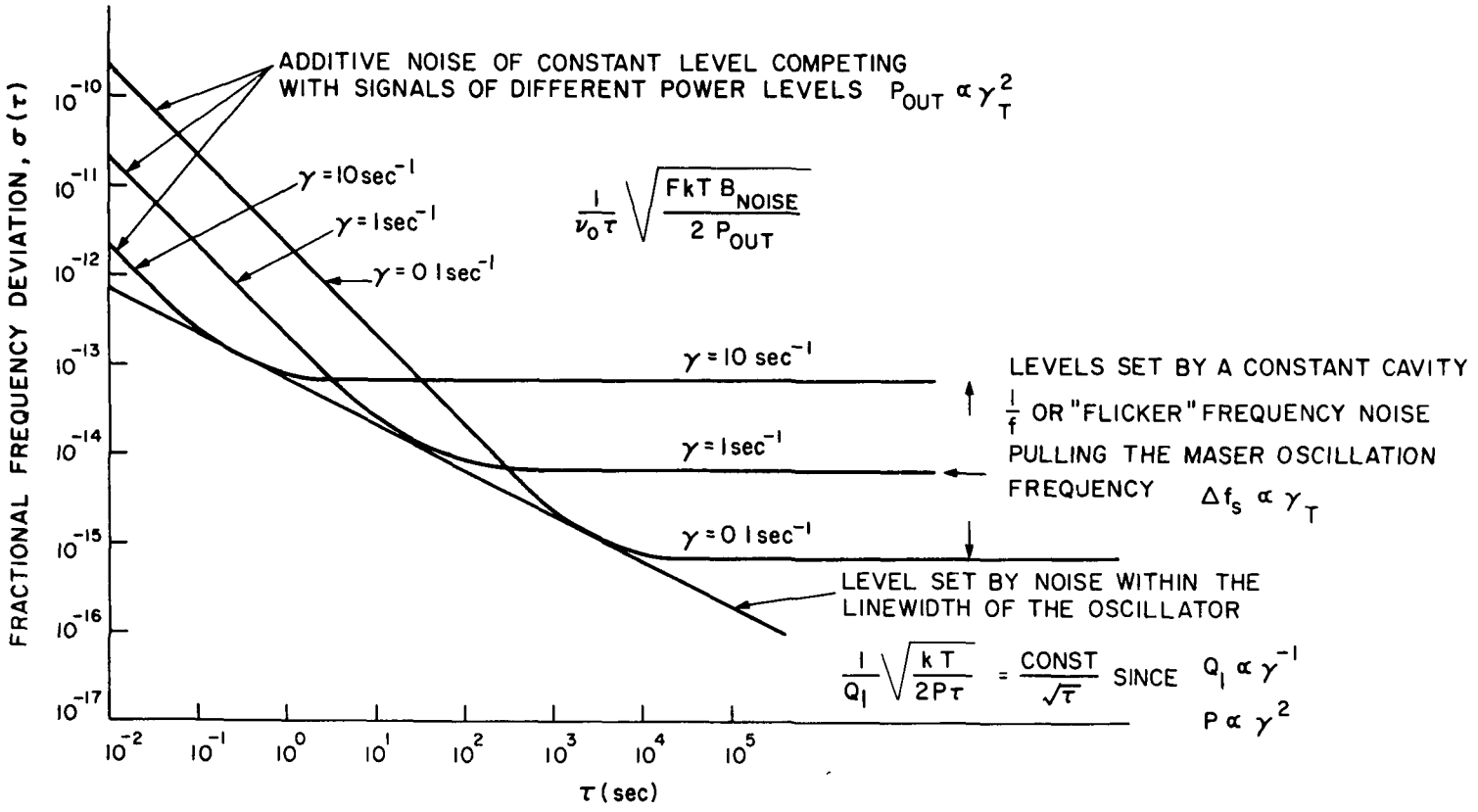


Fig. 1—Relationship of short- and long-term stability as storage parameter γ is varied in the hydrogen maser (from ref. 9).

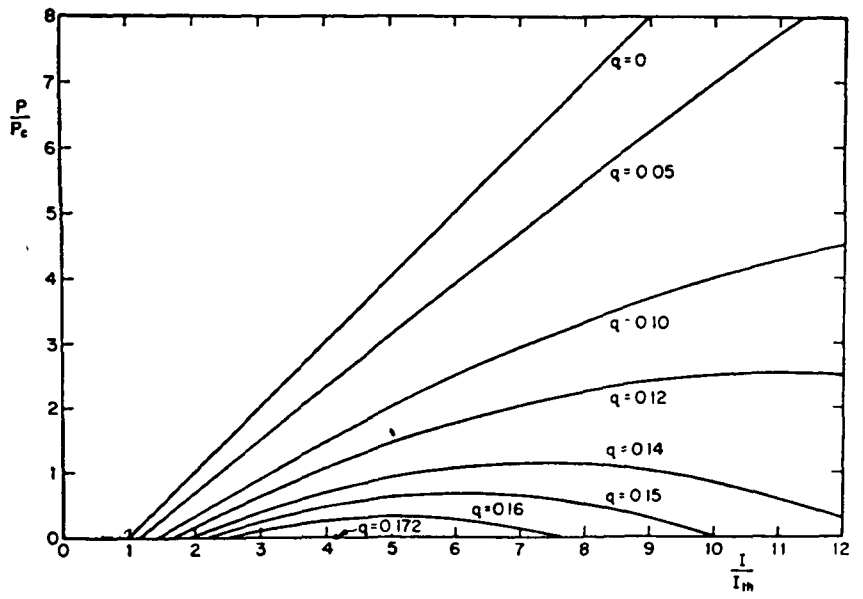


Fig. 2—P/P_c versus I/I_{th} for different values of the parameter q. This family of curves shows the strong influence of q on the operating conditions. If spin exchange is neglected, $q=0$ and radiated power increases monotonically with beam flux. For $q>0$ there is an upper limit to the flux for oscillation to occur and above a certain value ($q=0.172$) the maser cannot oscillate at any beam flux. q is defined in Eq. (8) (from ref. 10).

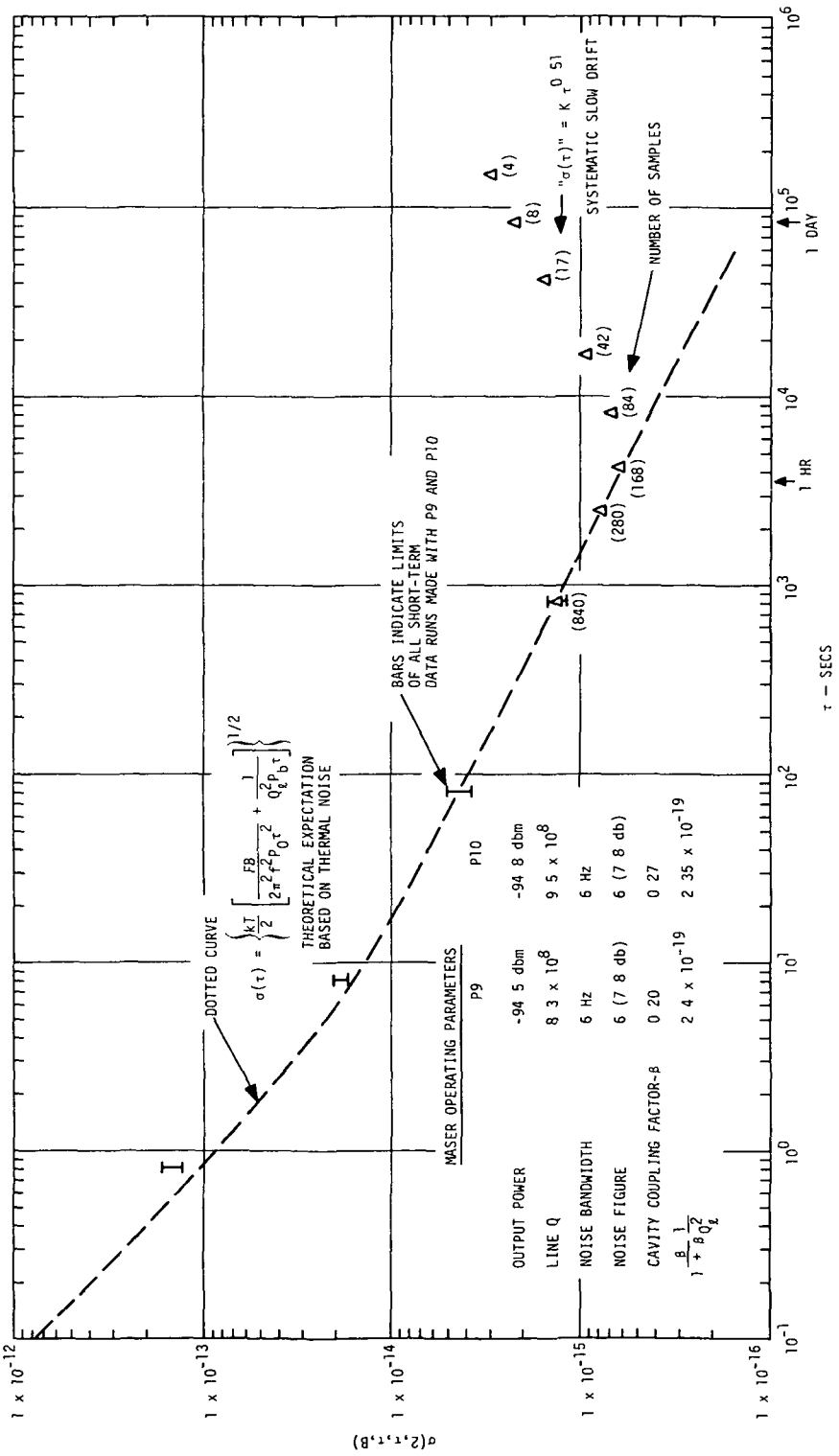


Fig. 3–VLG-11 stability data. $\sigma(2, \tau, \tau, B)$ vs τ for masers P9 and P10, October 9–17, 1977.

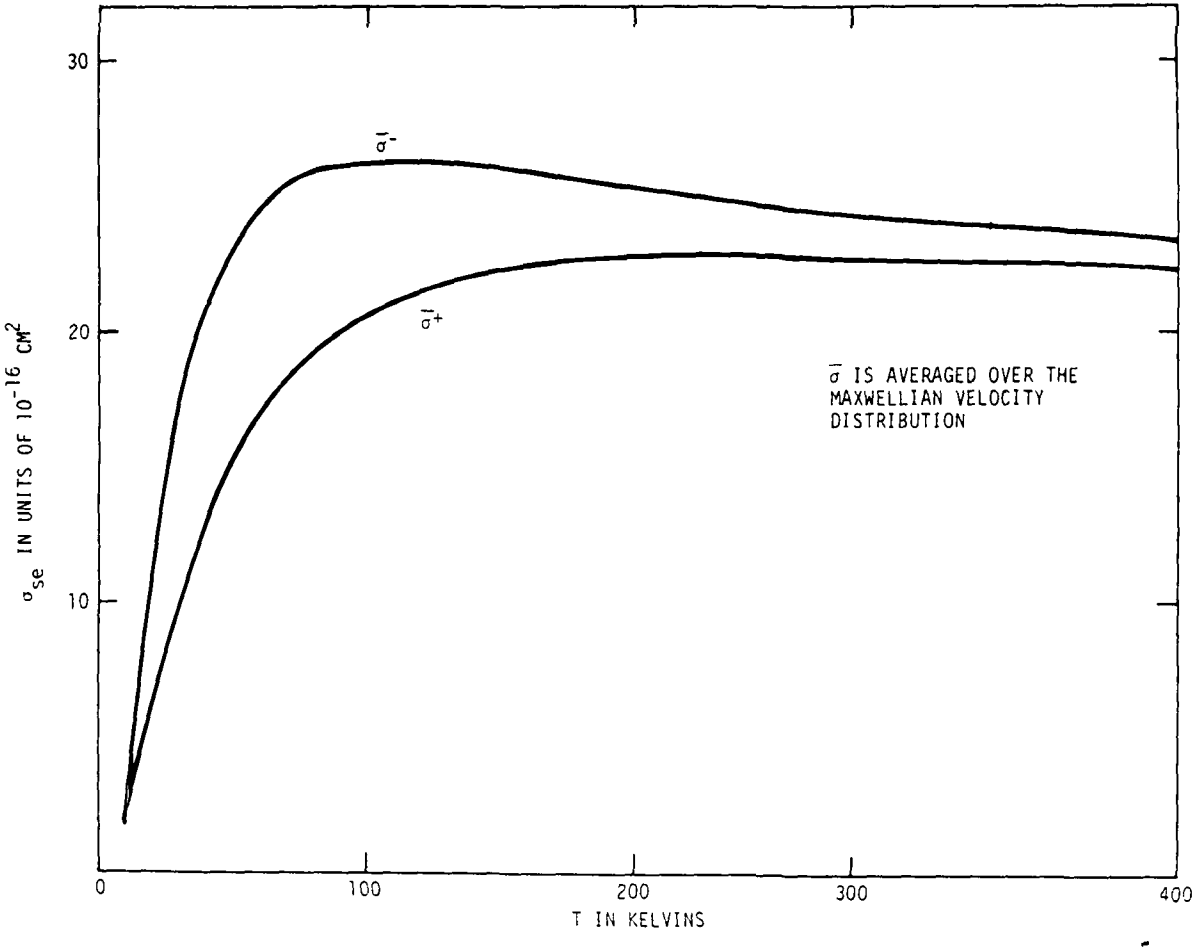


Fig. 4—Dependence of spin exchange cross section on temperature (from ref. 14).

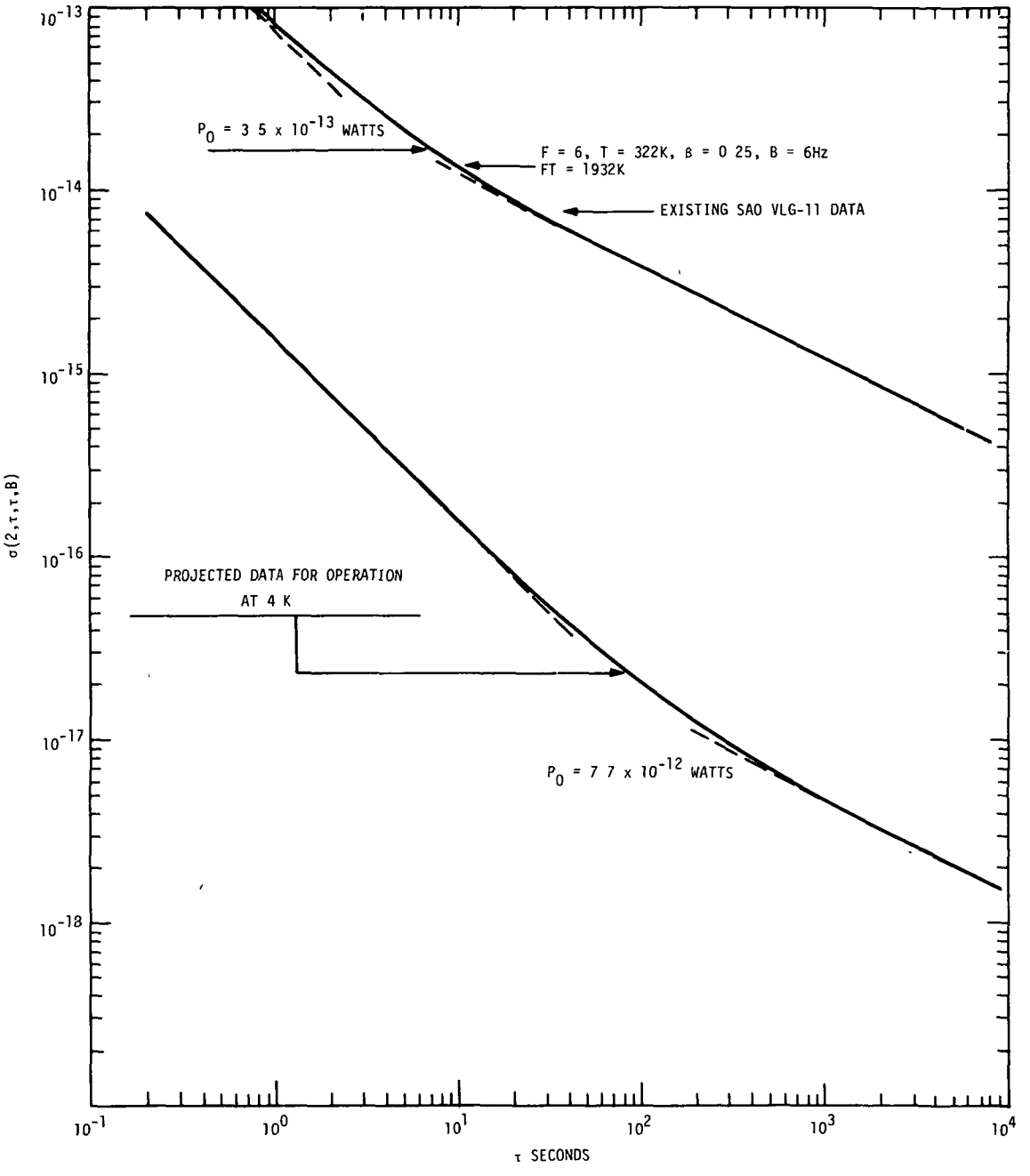


Fig. 5—Projected improvements in hydrogen-maser stability due to low-temperature operation.

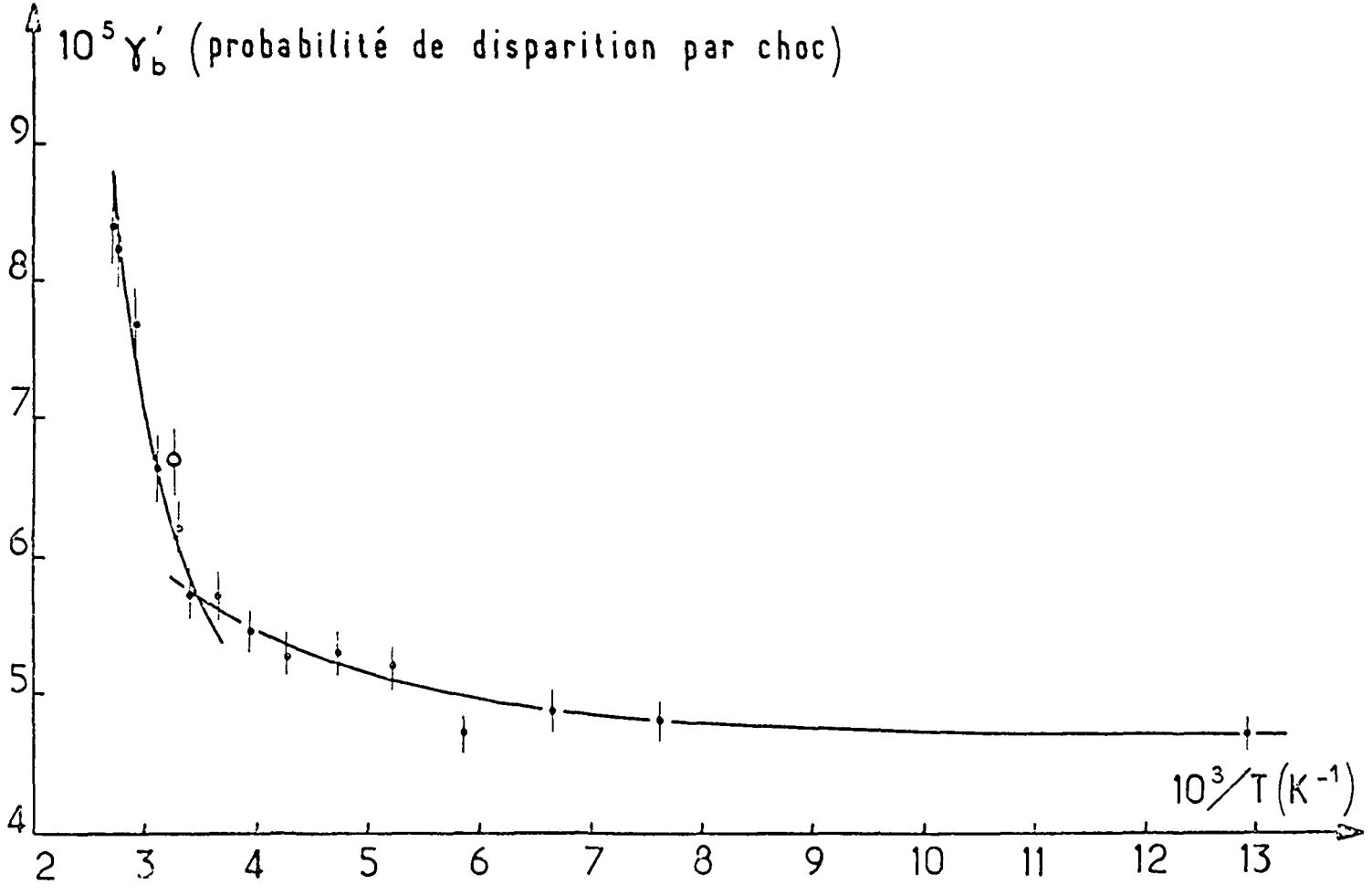


Fig. 6—Wall relaxation probability as a function of absolute temperature (from ref. 15).

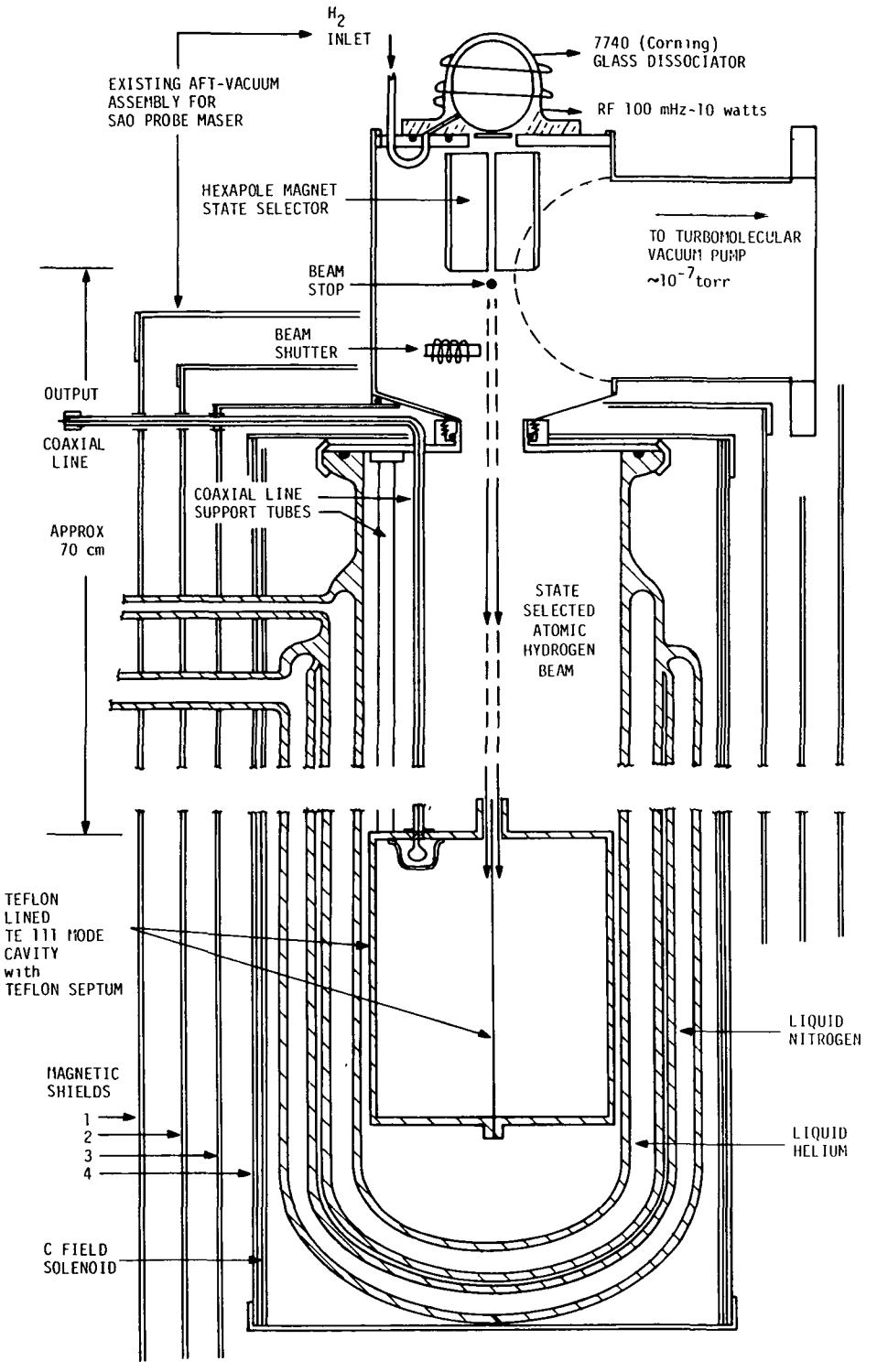


Fig. 7—Schematic view of low-temperature atomic hydrogen maser.

MR. HARRY PETERS:

Could you address the question of accuracy with respect to a constancy of the surfaces, the surface of hydrogen, the decrease in velocity, and so forth.

DR. VESSOT:

In this case, accuracy is a question of the wall shift. I didn't bring the plots that Desaintfuscien made of that, but there is substantial wall shift on Teflon as the Teflon gets colder. I don't know what happens with frozen molecular hydrogen. We can only measure it. I suspect that there will be a wall shift and it might be rather substantial.

I also would expect that it would be rather stable. First of all, we are running at 4° Kelvin and that temperature stability is usually pretty good. Secondly, the surface is, as I mentioned before, self-renewing. Whether or not the texture of the surface stays the same or whether you have frozen hydrogen icicles growing in this thing is a good question. I kind of doubt that. I think the vapor deposition will be very uniform. There is always the question of what might happen with the build-up of frozen molecular hydrogen within the cavity as time goes on. Will this bother us significantly? With the pulling factor reduced by 2,000, I think we might be able to relieve ourselves of some of those worries. I don't really know--that's why we are trying.

MR. HARRY WANG, Hughes Laboratory:

What is the probability of the hydrogen atom sticking to the surface?

DR. VESSOT:

It doesn't have to stick. It will thermalize, but I don't believe it has to stick. It will hit the surface and assume the surface energy and eventually reach the same level of energy as the surface. But I don't believe it has to stick necessarily.

MR. WANG:

In all these hydrogen masers running at different temperatures, we come down to the practical problem of the thermal electric current. It is entering all kinds of stray magnetic fields, and I wonder if you have considered that in your projection for stability. Of necessity, the way we have part of the maser at room temperature and not the other part, there is a difference and a probability of thermal electric current.

DR. VESSOT:

The cryostats were fine, made mostly of fiberglass. And we do recognize that the thermal electric currents are a problem. We have encountered them before in lasers. I assure you that this is one of the things we are watching out for, but as a fundamental limit I don't believe it ought to bother us.

The other things are that one can invoke the use of superconducting magnetic shields. The cavity in this case is going to be the copper cavity that we built for Roger Easton under previous contract. We are going to cut it down so that it will fit in a 7-inch pipe. Now that copper cavity may have thermal electric problems.

On the other hand, we are doing a very roughshod experiment here to look for a relaxation rate below or at 4° Kelvin. If we see anything that looks like a good relaxation rate, we are in business; and the next experiment is the one that is going to show whether it runs as a clock or not.

MR. V. J. FOLEN, Naval Research Laboratory:

The factor that you mentioned as a ratio of the Q's is really also a function of the relaxation time. Now, in the case where one normally runs the hydrogen maser, the relaxation time is changed by about a factor of two or three. However, when you go to 4° Kelvin, you have a radically different relaxation rate. In reality, you really have to look at it more closely and consider the relaxation times as well as the ratios of the Q to adequately determine the pulling factor.

DR. VESSOT:

That is correct. The relaxation time in question here is the same one that Harry Wang is questioning. It is relaxation time of the atom on the wall. In these conjectures here, we have taken the same relaxation time as exists at room temperature and said what

this obtains at 4° Kelvin. The relaxation number is contained in this term here (referring to slide), assuming that has not changed. In the geometry that we have, gamma wall is considered to be somewhat less than gamma bulb in all cases.

Why this optimism -- at least up to 76° Kelvin? The relaxation probability seems to improve as temperature drops. Now whether that will hold as this thing goes screaming up at 4° Kelvin is the main issue, I think, of the whole experiment. And all the things that happen as a result of this probability of relaxation is, in fact, the bottom line.

If we can show that that relaxation rate is acceptable, then we may be able to improve stability substantially.

Page intentionally left blank

Page intentionally left blank

A NEW METHOD TO ELIMINATE CAVITY PHASE SHIFT IN CESIUM BEAM STANDARDS

David J. Wineland, Stephen Jarvis, Jr.,
Helmut Hellwig, and R. Michael Garvey
National Bureau of Standards
Frequency & Time Standards Section
Boulder, Colorado 80302

Abstract

In our presently known laboratory and commercial cesium standards, the so-called Ramsey cavity is employed. The envelope of the associated Ramsey pattern is determined by the distribution of atomic velocities in the atomic beam. The wider the velocity distribution, the narrower will be the half-width of the envelope of the Ramsey pattern. The envelope of this Ramsey pattern is invariant against cavity phase shift. In other words, the center of the envelope - in contrast to the center of the main peak of the resonance - does not shift from cesium atomic resonance frequency when the cavity phase shift is varied.

Therefore, it is suggested that the systematic frequency shift due to an rf phase difference between the two interaction regions of a normal Ramsey cavity can be eliminated by using simultaneously two different frequencies around the cesium resonance applied to two separated interaction regions which are not part of the same cavity. To the atom this is equivalent to a time-varying cavity phase shift between the two interaction regions. A modulation of the frequencies ν_1 and ν_2 applied to cavities 1 and 2 will produce signals symmetrically spaced around true line center of the cesium resonance. This technique is briefly described and the advantages are noted.

An improvement in the achievable accuracy with laboratory type primary frequency standards appears possible. Commercially produced small beam tubes may realize accuracies presently achieved only with the much larger and more expensive laboratory units. In addition, long-term stability and clock performance should be enhanced significantly in both laboratory and commercial versions of this new technique. An experimental program aimed at realizing these advantages is presently under way.

INTRODUCTION

Atomic clocks of many configurations have been studied, used, and commercially produced. The most used and important example is the cesium beam atomic frequency standard or clock. Devices of this type form the basis for today's time services as well as for precision navigation and communication systems. They are also used as the primary standard for the unit of time. In addition to a number of laboratory built cesium beam clocks, a large number of commercial cesium atomic clocks is in existence in the world.

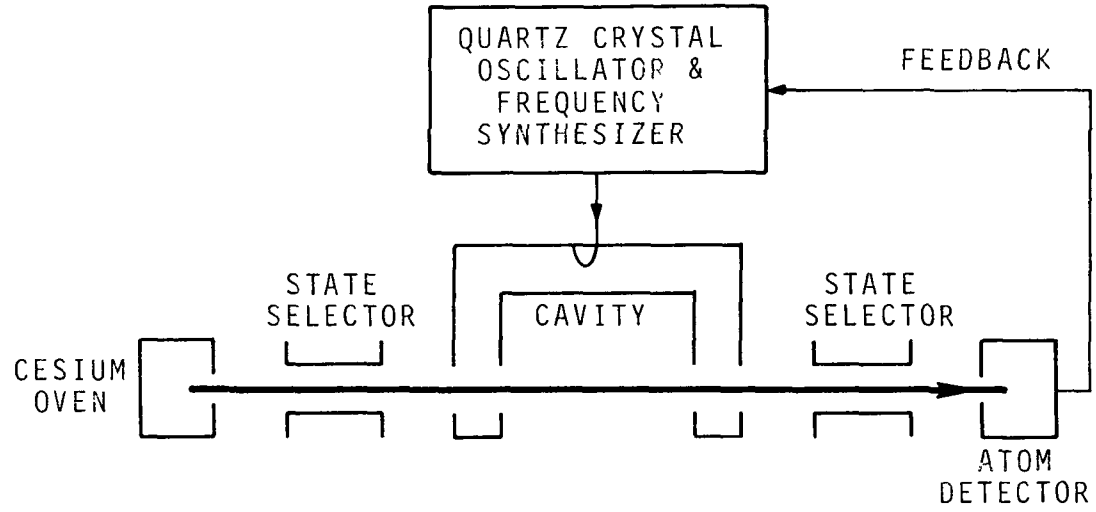


Figure 1. Schematic of a cesium beam frequency standard.

The basic configuration of a cesium standard is shown in Fig. 1. An oscillator (usually a crystal oscillator) is controlled via a servo loop by the cesium atomic resonator or beam tube. In order to lock the oscillator to the atomic resonance, the resonance has to be interrogated in order to produce an electronic signal at the detector which indicates how large the frequency offset from the atomic line center is and on which side of line center the frequency offset is located [1].

The properties of the microwave cavity to a high degree determine the performance of this device as a frequency standard or clock in terms of accuracy and long-term frequency stability. During the approximately twenty-five years of development of cesium beam devices, different cavity configurations and different modulation schemes have been tried. Most notably, cavities of the Ramsey type are being employed, i.e., two regions of interaction, spatially separated but part of the same microwave cavity as shown in Fig. 1 [2]. The modulation schemes for line-center lock which have been employed are generally of the frequency and phase modulation type, and sinewave or squarewave modulation has been used.

CAVITY PHASE SHIFT

The properties of the cavity affect the apparent frequency of the cesium resonance, i.e., the interaction of the cavity with the resonating cesium atoms may cause an apparent shift of the resonance frequency from the true resonant frequency of the atom. Cavity phase shift is caused by a non-uniform phase in the microwave cavity, either an end-to-end phase difference or a distribution of phases along and across the atomic beam trajectories in the cavity [3]. This cavity phase shift currently limits the absolute accuracy of the primary cesium standards to about 1×10^{-13} and the accuracy of commercial units to about 7×10^{-12}. There is also evidence that a time-varying cavity phase shift causes long-term frequency changes and instabilities (over the period of months to years) in such devices, limiting their usefulness as clocks in time generation.

In an atomic cesium standard using a Ramsey cavity there exists time dispersion between the two pulses (e.g., atomic beam with velocity spread which uses the separated oscillatory field technique) and one can observe the envelope of the resonance spectrum $g(\omega-\omega_o,\delta)$ (Ramsey pattern) as shown in Fig. 2. This envelope (dashed curve in Fig. 2) is symmetric

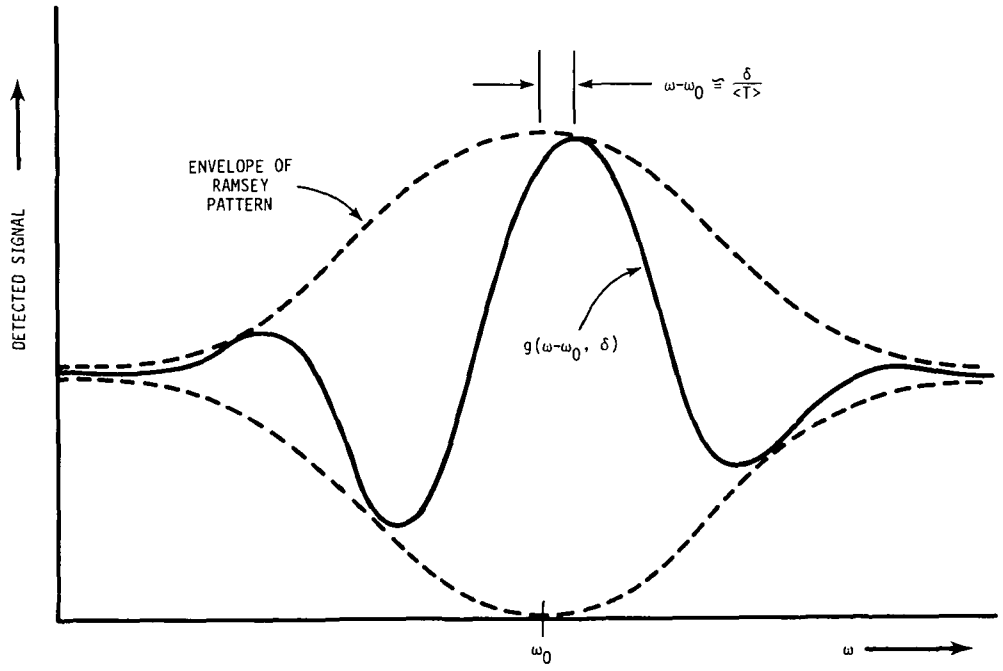


Figure 2. Microwave spectrum (Ramsey pattern) of a cesium tube using a Ramsey cavity.
ω_o = atomic (angular) resonance frequency,
δ = cavity phase difference,
<T> average time of flight between the two cavity regions.

with respect to rf phase shifts between the two interaction regions, while the Ramsey pattern itself, in general, is not, due to the cavity phase shift δ [4]. The central peak of the Ramsey pattern occurs approximately when $\omega - \omega_o \cong \delta/\langle T \rangle$ where $\langle T \rangle$ is the average transit time between interaction regions and where ω_o is the true atomic (angular) resonance frequency.

ELIMINATION OF THE CAVITY PHASE SHIFT

The purpose of this paper is to describe briefly a variation of Ramsey's separated oscillatory field technique. In the simplest form of this new technique, the resonance sample is interrogated by two time-delayed pulses of radiation as in the original technique [2]. It differs in that the rf phase of the second pulse is allowed to advance (or recede) at a constant rate; that is, the microwave frequency of the second pulse is offset from that of the first. In its practical realization, the two interrogation regions are not part of a single cavity (as in the traditional Ramsey cavity) but rather independent cavities driven by the frequencies ν_1 and ν_2 as shown in Fig. 3.

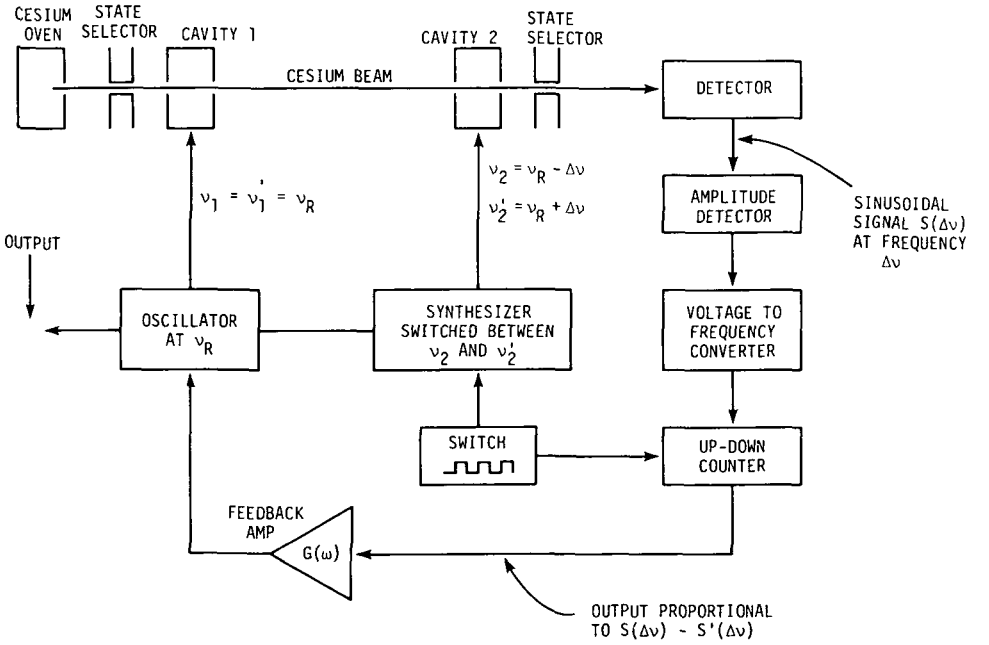


Figure 3. In this example; $\nu_1' = \nu_1 = \nu_R$, $\nu_2 = \nu_R - \Delta\nu$, $\nu_2' = \nu_R + \Delta\nu$ where $\Delta\nu \cong 1/T$ and where T is the approximate transit time of atoms between cavities. The servo finds the condition where $S(\Delta\nu) = S'(\Delta\nu)$ which is true only when $\nu_R = \nu_o$.

These two frequencies have a fixed frequency relationship to each other. The atoms are subjected to first the frequency ν_1 in the interaction region 1, then to the frequency ν_2 in the interaction region 2. To the atom, this is equivalent to a time-varying cavity phase shift between the two interaction regions; this cavity phase shift depends on the time-of-flight of the atoms between the two interaction regions and on the frequency difference $\nu_1 - \nu_2$.

At the detector there is a sinusoidally varying "signal" at frequency $\Delta\nu = \nu_1 - \nu_2$ whose amplitude depends on $\nu_1 - \nu_o$ and $\nu_2 - \nu_o$ where ν_o is the atomic resonance frequency. If frequencies ν_1' and ν_2' are now applied to cavities 1 and 2 respectively where $\nu_2' - \nu_1' = -(\nu_2 - \nu_1)$ then the signal at the detector has the same amplitude only when $(\nu_1 + \nu_1')/2 = \nu_o = (\nu_2 + \nu_2')/2$. For this "resonance" condition, any of the applied frequencies $(\nu_1, \nu_1', \nu_2, \nu_2')$ can be directly related to ν_o. One example is given in Fig. 3.

One slight disadvantage of this method, as compared to traditional cesium standards, is that the Ramsey envelope is broader than the central Ramsey peak obtained in the usual arrangement. However, this loss of resolution should not have to be more than a factor of two for a beam with a broad (e.g., Maxwellian) distribution.

CONCLUSIONS

The advantages of the above scheme are several:

(1) First-order phase-shift problems such as the cavity phase shift are eliminated in the two frequency separated oscillatory field method.
(2) Background pulling effects are greatly minimized in certain experiments. For example, in cesium clock operation systematic frequency pulling normally occurs due to overlap of the main line with (generally asymmetric) field-dependent transitions [5] ("Rabi" patterns). No signal content occurs at frequency $\Delta\nu$ from these overlapping transitions; this allows use of significantly reduced operating magnetic fields (which would normally increase this background pulling), thus greatly reducing magnetic field sensitivity of the clock transition, or alternatively reducing magnetic shielding requirements.

(3) Separate interaction regions can be constucted with low Q. This is an advantage because:
   (a) Cavity pulling [3] can be made negligible. For example, in a conventional atomic beam resonance apparatus using separated oscillatory fields the Q of the resonant cavity is made very high to make $|\delta|$ small. In the two-frequency method, two separate cavities of low Q can be made by terminating shorted pieces of waveguide at the input, thus making cavity pulling negligible. (We note that rf levels do not have to be the same in the two cavities.)
   (b) This may reduce fabrication complexity and cost. Moreover, superconducting cavities could be installed in laboratory standards such that only the end pieces were superconducting, thus simplifying the required cooling and eliminating distributed cavity phase shifts (see below).

(4) In high-accuracy frequency determinations, beam reversal [3] is no longer necessary, although it would provide a useful check of the method. Elimination of beam reversal would greatly simplify construction of laboratory standards and would give commercial cesium atomic clocks higher accuracy without increased complexity.

(5) Long-term frequency stability of devices using the two-frequency method should be increased. For example, in cesium beam frequency standards greater insensitivity to magnetic field, state selection, or cavity parameter changes should be obtained.

The above method does not completely eliminate systematic frequency offsets due to "distributed cavity phase shifts" [3,6]. This problem arises because the phase shift of the rf field may not be constant across the cross-section of the beam due to losses in the microwave cavity. However, the "distributed phase shift" problem may be more tractable with the two-frequency method. For example, the offset due to distributed cavity phase vanishes if the shape of the velocity distribution is the same on all the atomic trajectories through the cavities. Furthermore, as noted above, the distributed phase shift problem is completely eliminated by using superconducting cavities.

We have initiated an experimental program aimed at demonstrating this new technique. We are modifying an existing cesium beam tube to operate with this new cavity structure and a compatible electronic system along the principles depicted in Fig. 3.

REFERENCES

[1] H. Hellwig, IEEE Trans. Nucl. Sc. NS-23, 1629 (1976).

[2] N. F. Ramsey, Molecular Beams (Oxford University Press, London, England, 1956), p. 124.

[3] See, for example: D. J. Wineland, D. W. Allan, D. J. Glaze, H. Hellwig, S. Jarvis, Jr., IEEE Trans. Instrum. Meas. IM-23, 453 (1976), G. Becker, IEEE Trans. Instrum. Meas. IM-23, 458 (1976). A. G. Mungall, H. Daams, D. Morris, C. C. Costain, Metrologia 12, 129 (1976).

[4] S. Jarvis, Jr., D. J. Wineland, and H. Hellwig, Jour. Appl. Phys., to be published (Nov. 1977).

[5] N. F. Ramsey, op. cit., p. 132.

[6] S. Jarvis, Jr., NBS Tech. Note 660, (Jan. 1975).

DR. VICTOR REINHARDT, NASA Goddard Space Flight Center:

What does the asymmetry in the velocity distribution do to this, and also what happens to your frequency stability versus averaging time due to the fact that you now have effectively a smaller line Q?

DR. HELLWIG:

A smaller line Q, as most of you know, affects short-term stability. And a factor of two in line Q means that you need a factor of four more atoms to compensate for that. I think we have that leeway in most tubes. It is not a big sacrifice. It is less than the difference, say, between so-called standard tubes and super tubes right now.

I didn't quite understand your first question--asymmetry and velocity distribution?

DR. REINHARDT:

In your previous slide, you've shown that some of the velocity distributions coming out of some of the beam tubes have had double humps. At first glance, it would seem that that nice picture with the nice envelope could possibly be an asymmetrical one which might lead to some frequency shifts in that case?

DR. HELLWIG:

No, it will not. The asymmetries in the velocity distribution will not cause asymmetries in the envelope at all, except for the second-order Doppler effect, which you know is a basic asymmetry to that pattern anyway. With all present-day tubes, it is of the order of 10^{-13} or even less, because of the very heavy low-velocity selection we are entering. So that is not a limitation.

To just comment one step further, if you really want to apply that principle to so-called primary standard laboratory-type devices, and you really want to push to 1 part in 10^{14} in accuracy, then you have to watch those. If you use beam reversal, it allows you to

reduce an absolute knowledge of the velocity distributions to a symmetry argument. If you have basically similar velocity distributions with the two beams' directions, you are safe as far as the so-called distributed cavity phase shift is concerned, which is still a limitation.

MR. ANDREW CHI, NASA Goddard Space Flight Center:

The cavity phase shift of a cesium beam tube has a very gradual and slow change, which will stay put for a long time before you can observe it continuously. What is the relative gain when you don't shift the phase compared to when you do shift cavity phase? Also, when you try to do that, can you also control the relative amplitude of the side peak of the Ramsey resonance as a way to control its symmetry?

DR. HELLWIG:

I didn't quite get the second question. The first question was, what do you really gain by having rapidly changing phase shifts versus the rather steady and hardly varying phase shift which is present in present-day tubes?

First of all, the two animals are quite different. With the cavity phase shift built into the Ramsey-type cavities, you have a thing which causes you to be sensitive against other parameter variations. I agree with you that the phase shift itself doesn't vary much, but it makes you, for example, microwave power sensitive. It makes you sensitive against other things -- trajectory location effects and beam geometry effects under acceleration. These things transduce via a finite, even totally constant, cavity phase shift. And the electronic cavity phase shift which we are introducing certainly is varying. I just used that illustration as an example. The resonant spectrum of such a tube would be quite different. You will have no residual biases if you have the frequencies ν_1 and the sidebands ν_2 symmetric. Now, there is an easy way to do that: You create ν_2 by having sidebands on ν_1, and it is as symmetric as you want it.

DR. JACQUES VANIER, Laval University:

I did not quite understand this distribution. Is it not coming out to be the same thing as if you had simply one cavity after all?

DR. HELLWIG:

Your question relates back to why a Ramsey cavity is used. It is not equivalent because in a single cavity, you would have traveling waves going along the beam axis. The primary limitation of using a single cavity of a similar length is that you have residual losses and phase variations due to imperfections. You really have traveling waves along the whole interaction region which cause wild first-order Doppler effects. In fact, people have tried to build such things. They typically show parts in 10^{10} offsets because of them. This is the main advantage of two separate interaction regions. Additional advantages are the same whether you have it connected coherently or separately -- the averaging between the two regions as far as magnetic fields are concerned, for example. You are only sensitive to the average. Same here. It doesn't change.